VISIBLE-LIGHT METALLAPHOTOREDOX STRATEGIES FOR ORGANIC TRANSFORMATIONS THROUGH THE CLEAVAGE OF CSP3−CL BONDS

Jordi Aragón Artigas

UNIVERSITAT ROVIRA i VIRGILI

Visible-light metallaphotoredox strategies for organic transformations through the cleavage of Csp³–Cl bonds

JORDI ARAGÓN ARTIGAS

DOCTORAL THESIS
2022

UNIVERSITAT ROVIRA I VIRGILI

VISIBLE-LIGHT METALLAPHOTOREDOX STRATEGIES FOR ORGANIC TRANSFORMATIONS THROUGH THE CLEAVAGE OF CSP3-CL BONDS

Jordi Aragón Artigas

UNIVERSITAT ROVIRA I VIRGILI
VISIBLE-LIGHT METALLAPHOTOREDOX STRATEGIES FOR ORGANIC TRANSFORMATIONS THROUGH THE CLEAVAGE
OF CSP3-CL BONDS
Jordi Aragón Artigas

UNIVERSITAT ROVIRA I VIRGILI
VISIBLE-LIGHT METALLAPHOTOREDOX STRATEGIES FOR ORGANIC TRANSFORMATIONS THROUGH THE CLEAVAGE
OF CSP3-CL BONDS
Jordi Aragón Artigas

Jordi Aragón Artigas

Visible-light metallaphotoredox strategies for organic transformations through the cleavage of Csp³−Cl bonds

Doctoral thesis

Supervised by Prof. Dr. Julio Lloret Fillol

Tarragona, Catalunya

2022

UNIVERSITAT ROVIRA I VIRGILI
VISIBLE-LIGHT METALLAPHOTOREDOX STRATEGIES FOR ORGANIC TRANSFORMATIONS THROUGH THE CLEAVAGE
OF CSP3-CL BONDS
Jordi Aragón Artigas

UNIVERSITAT ROVIRA i VIRGILI

ICIQ
Institut
Català
d'Investigació
Química

Prof. Dr. Julio Lloret Fillol, Research Professor of the Catalan Institution for Research and Advanced Studies (ICREA) and Group Leader at the Institute of Chemical Research of Catalonia (ICIQ):

I STATE that the present study, entitled "Visible-light metallaphotoredox strategies for organic transformations through the cleavage of Csp³–Cl bonds", presented by Jordi Aragón Artigas for the award of the degree of Doctor, has been carried out under my supervision in my group at the Institute of Chemical Research of Catalonia (ICIQ) and fulfills all the requirements.

Tarragona, 14th April 2022

Doctoral Thesis Supervisor

Prof. Dr. Julio Lloret-Fillol

UNIVERSITAT ROVIRA I VIRGILI
VISIBLE-LIGHT METALLAPHOTOREDOX STRATEGIES FOR ORGANIC TRANSFORMATIONS THROUGH THE CLEAVAGE
OF CSP3-CL BONDS
Jordi Aragón Artigas

Als meus pares,
ja que no se'ns ha regalat mai res,
i aquest treball no podia ser la excepció.

~ Tot està per fer i tot és posible. ~

Miquel Martí i Pol

~ A mi la veritat sempre m'ha temptat de mala manera. ~

Mercè Rodoreda

~ In questioni di scienza, l'autorità di un migliaio di persone non vale tanto quanto l'umile ragionamento di un singolo individuo. ~

Galileo Galilei

UNIVERSITAT ROVIRA I VIRGILI
VISIBLE-LIGHT METALLAPHOTOREDOX STRATEGIES FOR ORGANIC TRANSFORMATIONS THROUGH THE CLEAVAGE
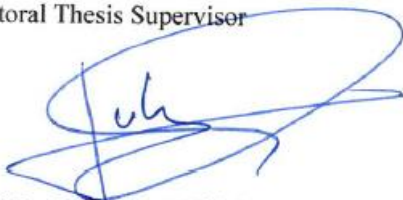OF CSP3-CL BONDS
Jordi Aragón Artigas

AGRAÏMENTS

M'agradaria expressar la meva gratitud amb unes humils paraules a totes aquelles persones que han fet possible el desenvolupament i finalització d'aquesta tesi.

Primer de tot, vull mostrar el més sincer agraïment al Prof. Julio Lloret, el meu director de tesi, per donar-me la gran oportunitat de créixer com a investigador i com a químic a un centre d'excel·lència com és el ICIQ. Tenint en compte que no ens coneixíem anteriorment, vas apostar per a mi després d'una sola entrevista i t'ho agraeixo, crec que no t'he fallat. Gràcies per haver confiat en mi des del principi. La teva multidisclipinitarietat és realment inspiradora.

En segon lloc, voldria donar les gràcies a la Dra. Alicia Casitas pel seu magnífic guiatge i supervisió durant els meus primers mesos de doctorat. Sento que tu també vas apostar fort per mi, tant escollint-me a mi com preparant-me, ensenyant-me i sobretot fent-me espavilar ràpidament al lab. Llàstima que els nostres camins es separessin abans del que pensàvem, tot i això, la petjada del teu mentoratge està present en aquesta tesi.

No voldria deixar-me als meus companys d'aventura durant aquesta etapa de més de 4 anys. Miguel, empiezo por ti y serás el único con el que cambiaré de idioma (a parte de Geyla). El resumen seria "gracias por aguantarme". Me has ayudado mucho en muchos aspectos durante estos años que hemos coincidido, tanto en química, como en el lab, como para sobrevivir en el ICIQ. También te quiero pedir disculpas por lo pesado que llegué a ser, en cuanto te fuiste me tocó sufrir en mis carnes lo que te hice pasar a ti, aunque creo que yo fui el menor de tus males. Fue un placer hacer equipo contigo. A en Sergi i la Geyla, els meus autèntics companys de viatge, començant junts, gràcies per acompanyar-me durant tot aquesta etapa. En especial tu Geylicita, compañela de lamentos y

flustaciones, pelo siemple con buen humol desde los paises de mielda. I bueno Sergi... qui diria que em quedaria de tu la part menys científica... les discrepàncies polítiques i el teu mal gust musical. Voldria fer una especial menció a en David i en Luis, fent-ho en català, ja que estic segur que ho entendran. Heu sigut les persones amb les quals millor he connectat durant aquesta etapa, permetent-me ser mentor, company, aprenent i amic. Que sapigueu que teniu algú en qui confiar a Barcelona. No voldria oblidar-me ni de la Laura, una madrilenya que fou important per a mi durant un curt període de temps i que espero que jo també li servís d'alguna cosa, ni dels estudiants que m'ha tocat guiar i supervisar (Sebastian, Suyun, Jingjing). Sebastian, ets l'aprenent perfecte, espero que tinguis un futur d'èxits. Jing, espavila, no et deixis trepitjar ni influenciar i treu el millor de tu, sense por, tens un gran cor i sovint no és compatible amb aquest món. No voldria deixar-me als postdocs que han anat passant pel lab, omplint-me de qualitat humana i de coneixements (Carla, Fede, Fèlix, Alberto, Noufal, Suvendu, Katia, Gonell...), m'emporto cosetes de tots. A partir d'aquí, també mostrar agraïment a tots els companys que han anat passant pel laboratori i que segur que algun em deixaré, així que prefereixo no especificar i que tothom es senti representat i estimat. També voldria agraïr en general a tota aquella gent de la comunitat ICIQ fora del grup que m'han fet la vida més fàcil durant aquests anys, en especial en Xisco, ja que la seva unitat m'ha salvat la tesi, però també en Xavi Asensio, en Xavi Blanch, Isra, Kermán, Simona, Marta, Maria, Irene, Bea, Cristina, Maria José... gràcies.

Ara toca agraïr a les persones "invisibles" o "intangibles" d'aquest treball. Aquelles persones que no s'han vist involucrades directament en el desenvolupament de la tesi, però que han estat necessàries per a la meva salut mental. En primer lloc, voldria agraïr a la meva principal font de desconnexió del doctorat entre setmana, la coral "The New Zombis". Tot i que no ha sigut fàcil compaginar els assaigs amb el doctorat, heu sigut vitals perquè pogués superar

mentalment les adversitats de la investigació, aportant-me una sortida artística i també espiritual que no sabia ni que tenia ni que era capaç de tenir-la. Òbviament, no em puc deixar els meus "Carapenes" i el "Noob Team", la família que un ha pogut escollir i que li donen sentit a la setmana, fent-me pujar a Barcelona per passar grans moments inoblidables. Mireia, no m'oblido de tu, has arribat a l'última etapa del doctorat i t'ha tocat aguantar-me en els pitjors moments. Gràcies pels ànims, la comprensió, i sobretot... l'ajuda amb la portada!

Finalment, voldria dedicar unes últimes paraules als meus pares. Sembla que fou començar aquesta etapa del doctorat i que tot se n'anés a la merda. Quan les coses van malament, sempre ens poden anar pitjor. Tot i això, igual que jo he pogut superar amb èxit aquesta etapa difícil, junts hem superat/superem/superarem tota la merda que ens vingui a sobre. Gràcies per estar sempre allà, pel vostre suport, per deixar-me fer el que volia amb plena llibertat, tot i que el món de la recerca sigui tan precària.

UNIVERSITAT ROVIRA I VIRGILI
VISIBLE-LIGHT METALLAPHOTOREDOX STRATEGIES FOR ORGANIC TRANSFORMATIONS THROUGH THE CLEAVAGE
OF CSP3-CL BONDS
Jordi Aragón Artigas

Financial support

UNIVERSITAT ROVIRA I VIRGILI
VISIBLE-LIGHT METALLAPHOTOREDOX STRATEGIES FOR ORGANIC TRANSFORMATIONS THROUGH THE CLEAVAGE
OF CSP3-CL BONDS
Jordi Aragón Artigas

Curriculum Vitae

Jordi Aragón Artigas was born on January 30th, 1994 in Barcelona (Catalonia). He studied chemistry at the University of Barcelona, obtaining his BSc degree in July 2016. During his undergraduate studies, he worked on the development of new water-in-water emulsion systems, in CSIC. In September of 2016, he started his MSc degree in "Organic Chemistry" at the University of Barcelona, under the supervision of Prof. Jaume Vilarrasa Llorenç and Prof. Anna Maria Costa Arnau. During his MSc studies, his research was focused on the "Ring-closing metathesis for the synthesis of trisubstituted double bonds from ω-diazo alkenes". He obtained his MSc degree in July 2017. After that, he moved to Tarragona for embarking on his PhD studies under the supervision of Professor Julio Lloret Fillol at the Institute of Chemical Research of Catalonia. His research was financially supported with FPI fellowship from the Spanish Ministry of Science (BES-2017-080107). The PhD results have been communicated at different national and international conferences, such as the the PhD Day of the ICIQ in Tarragona (2018, 2019 and 2020), the XI Marcial Moreno Mañas International School on Organometallic Chemistry in Oviedo (2018), the Photo4Future meeting in Eindhoven (Netherlands, 2018), the 4th EuCheMS conference on Green and Sustainable Chemistry in Tarragona (2019) and the ICIQ RedINTECAT school in Tarragona (2019). 1ª Jornada de Jóvenes Investigadores del GEQOR (2021, virtual), XXIV EuCOMC Conference on Organometallic Chemistry in Madrid (2021) and the 4th HC3A Meeting in Barcelona (2022).

UNIVERSITAT ROVIRA I VIRGILI
VISIBLE-LIGHT METALLAPHOTOREDOX STRATEGIES FOR ORGANIC TRANSFORMATIONS THROUGH THE CLEAVAGE
OF CSP3-CL BONDS
Jordi Aragón Artigas

LIST OF PUBLICATIONS

Jordi Aragón, Suyun Sun, David Pascual, Sebastian Jaworski and Julio Lloret-Fillol. "Photoredox activation of inert alkyl chlorides for the reductive cross-coupling with aromatic alkenes", *Angew. Chem. Int. Ed.* **2022**, e2024365, (DOI: 10.1002/anie.202114365).

Carla Casadevall**, Jordi Aragón**, Santiago Canyelles, Miquel Pericàs, Julio Lloret-Fillol and Xisco Caldentey."Development of Advanced High Throughput Experimentation Platforms for Photocatalytic Reactions"*, ACS ebook. In revision

Articles in preparation:

Jordi Aragón, Suyun Sun and Julio Lloret-Fillol. "Cyclopropanation of Alkenes Using Dichloromethane via Photoredox Catalysis"**. In preparation

Jordi Aragón, Suyun Sun and Julio Lloret-Fillol. "Iridium-catalyzed Photoactivation of chloroform for further Functionalization of Alkenes". In preparation.

Jordi Aragón, Alicia Casitas and Julio Lloret-Fillol. "A family of new tetradentate aminopyridine Co/Ni complexes for the cleavage of inert Csp^3-Cl bonds". In preparation.

Patents

Julio Lloret-Fillol, Alicia Casitas, Felix Ungeheuer, Miguel Claros and **Jordi Aragón**. *Photocatalytic C-Cl activation* (Pat-2018/115) Event for T: *Photocatalytic C-Cl activation* (Tech-2018/061)

Other publication related to other activities performed during this thesis which is not described in this doctoral dissertation:

Carla Casadevall, David Pascual, **Jordi Aragón**, Arnau Call, Alicia Casitas, Irene Casademont-Reig and Julio Lloret-Fillol. "Light-Driven Reduction of Aromatic Olefins in Aqueous Media Catalysed by Aminopyridine Cobalt Complexes", *Chem. Sci.,* **2022,** (DOI:10.1039/d1sc06608k)

PREFACE

The work presented in this dissertation has been performed at the Institut Català d'Investigació Química (ICIQ), during the period from September 2017 until April 2022 under the supervision of Professor Julio Lloret-Fillol. This thesis explored the development of metallaphotoredox dual systems for the implementation of unactivated alkyl chlorides as feasible and common starting materials in organic synthesis. The work is divided into six sections: a general introduction, the objectives of the thesis, three research chapters and a chapter in which the overall conclusions of the work are presented. Each of the research chapters includes a brief introduction on the topic, followed by the collected results and their discussion, the main conclusions, and finally a detailed experimental section. References and their numbering are independently organized by chapters.

UNIVERSITAT ROVIRA I VIRGILI
VISIBLE-LIGHT METALLAPHOTOREDOX STRATEGIES FOR ORGANIC TRANSFORMATIONS THROUGH THE CLEAVAGE
OF CSP3-CL BONDS
Jordi Aragón Artigas

TABLE OF CONTENTS

Chapter IV: Photoredox Reductive Cross-Coupling of Inert Alkyl Chlorides with Aromatic Alkenes

UNIVERSITAT ROVIRA I VIRGILI
VISIBLE-LIGHT METALLAPHOTOREDOX STRATEGIES FOR ORGANIC TRANSFORMATIONS THROUGH THE CLEAVAGE
OF CSP3-CL BONDS
Jordi Aragón Artigas

ABSTRACT

Recent photocatalytic methods based on the visible-light-induced generation of reactive radicals have allowed the construction of a large variety of C−C bonds. The inertness of chloroalkanes has precluded them as prevailing coupling partners in both conventional and photocatalytic cross-coupling reactions. In fact, few examples of using unactivated alkyl chlorides as building blocks have been developed, presenting limitations in their applicability for a general methodology. In the last years, our research group has been focused on the understanding of visible light photo-induced generation of radicals, using a dual bimetallic system based on earth-abundant metals.

In this line, this thesis describes the development of a new familiy of tetradentate aminopyridine Co and Ni complexes able to activate different chloroalkanes. The ligand availability, modularity and versatility let us the tune of the metal first coordination sphere by changing the electronic and structural features of the ligand. A collection of eighteen new Co and Ni complexes have been studied presenting a playground for synthetic methodology development.

As a main project, we disclosed a novel photoredox-catalyzed reductive cross-coupling reaction using inert chloroalkanes and alkenes as coupling partners. The general applicability of this methodology displays inert alkyl chlorides as interesting electrophiles for C−C bond formation in organic synthesis.

Finally, we went one step further, reporting the photoredox-catalyzed activation of inert and common chlorinated solvents (CH_2Cl_2 and $CHCl_3$) for the tuneable functionalization of aromatic olefins, affording a straightforward cyclopropanation method and/or a chloroalkanes synthesis.

The combination of spectroscopical (fluorescence quenching, UV-Vis, EPR, NMR) and electrochemical techniques (CV, SEC) with DFT studies and reactivity allowed us to shine light into the reaction mechanism, wherein a photogenerated

low-valent metal species reacts with the chloride substrate forming a carbon-centered radical. We also discussed the nucleophilic capacity of the low oxidation state metal center in relation with the Csp^3−Cl activation mechanism.

This thesis paves the way for a widespread extension of earth-abundant metallaphotoredox protocols for the implementing common and inert alkyl chlorides as feasible coupling partners.

RESUM

Recentment, la generació de radicals actius mitjançant metodologies fotocatalítiques amb llum visible ha permès la construcció d'una gran varietat d'enllaços C−C. La inèrcia dels cloroalcans ha impedit el seu ús com a socis d'acoblament predominants tant en reaccions d'acoblament creuat convencionals com fotocatalítiques. De fet, s'han desenvolupat escassos exemples que utilitzin clorurs d'alquil inactivats com a fragments de síntesi, els quals presenten limitacions a l'hora d'aplicar-se de manera general. En els últims anys, el nostre grup de recerca s'ha centrat en l'estudi de la formació de radicals a partir de la llum visible, utilitzant un sistema bimetàl·lic dual basat en metalls abundants.

En aquesta direcció, aquesta tesi descriu el desenvolupament d'una nova família de complexos tetradentats de Co i Ni capaços d'activar diferents clorurs d'alquil. La disponibilitat, versatilitat i modelatge d'aquests lligands ens permet la modificació controlada de la primera esfera de coordinació del metall a partir del canvi de les propietats electròniques i estructurals del lligand. La col·lecció de divuit nous complexos de Co i Ni significa un nou escenari per al desenvolupament de metodologies sintètiques.

Com a projecte principal, exposem una innovadora reacció d'acoblament fotocatalítica utilitzant cloroalcans inerts i alquens com a parelles d'acoblament. L'aplicació general d'aquesta metodologia mostra els clorurs d'alquil inerts com a interessants electròfils per a la formació d'enllaços C−C en síntesi orgànica.

Finalment anem més enllà, reportant l'activació fotocatalítica de dissolvents clorats comuns i inerts (CH_2Cl_2 i $CHCl_3$) per a la funcionalització modulable d'olefines aromàtiques, proporcionant un mètode senzill de ciclopropanació i/o de síntesi de cloroalcans.

La combinació de tècniques espectroscòpiques (fluorescència, UV-Vis, EPR, NMR) i electroquímiques (CV, SPEC) amb estudis de DFT i reactivitat ens ha permès posar llum al mecanisme, on una espècie metàl·lica de baixa valència

fotogenerada reacciona amb els clorurs d'alquil formant un intermedi radical centrat al carboni. Alhora, discutim la capacitat nucleofílica d'aquest baixos estats d'oxidació, conectant amb el mecanisme d'activació del enllaç Csp^3-Cl.

Aquesta tesi obre el camí per a una extensió generalitzada de protocols fotocatalítics utilitzant metalls abundants per a la implementació dels clorurs d'alquil comuns i inerts com a socis d'acoblament factibles.

LIST OF ABBREVIATIONS

In this doctoral thesis, the abbreviations and acronyms most commonly used in organic chemistry are based on the recommendations of the ACS "Guidelines for authors" which can be found at https://pubs.acs.org/doi/10.1021/bk-2006-STYG.ch010

General Abbreviations

[ ]	Concentration
°C	Degrees Celsius
Å	Angström(s)
A.U.	Arbitrary Units
aq	Aqueous
atm	Atmosphere(s)
br	Broad
Cal	Calorie
calcd	Calculated
cat	Catalyst
cm^{-1}	Wavenumber(s)
conv	Conversion
CV	Cyclic Voltammetry
D	Deuterium
d	Doublet
dd	Doublet of doublets
ddd	Double doublet of doublets
ddt	Double doublet of triplets
Emis	Emission

eq	Equation
equiv	Equivalent
Fc	Ferrocene
HIV	Human immunodeficiency viruses
HPLC	High-Performance Liquid Chromatography
HRMS	High-Resolution Mass Spectrometry
HTE	High-throughput experimentation
Hz	Hertz
IR	Infrared
J	Coupling Constant (in NMR spectrometry)
J	Joule(s)
LED	Light Emitting Diode
m	Multiplet
m/z	Mass-to-charge ratio
MALDI	Matrix-Assisted Laser Desorption Ionization
MEK	Mitogen-activated protein kinase
mp	Melting Point
MS	Mass Spectrometry
NMR	Nuclear Magnetic Resonance
ppm	Part(s) per million
q	Quartet
Redox	Reduction–Oxidation
s	Singlet
SCE	Saturated Calomel Electrode
SEC	Spectroelectrochemistry
t	Triplet
td	Triplet of doublets
tdd	Triplet doublet of doublets
TLC	Thin-Layer Chromatography
UV-Vis	Ultraviolet-Visible spectroscopy

Theoretical Calculations

AO   Atomic Orbital

B3LYP   3-parameter hybrid Becke exchange/ Lee–Yang–Parr correlation
          functional

BDE   Bond Dissociation Energy

DFT   Density Functional Theory

HOMO   Highest Occupied Molecular Orbital

LUMO   Lowest Unoccupied Molecular Orbital

MNL15   Molecular Orbital

MO   Molecular Orbital

SOMO   Single-Occupied Molecular Orbital

TS   Transition State

Mechanistic Considerations

CCHE   Cross-Coupling Hydrogen Evolution

CHAA   Concerted Halogen-Atom Abstraction

CT   Charge Transfer

EA   Electron Acceptor

ED   Electron Donor

EDA   Electron Donor-Acceptor

EDG   Electrondonating group

EnT   Electron Transfer

EWG   Electronwithdrawing group

HAA   Halogen Atom Abstraction

HAT   Hydrogen Atom Transfer

HC	Homolytic Cleavage
LMCT	Ligand to Metal Charge Transfer
MLCT	Metal-to-Ligand Charge Transfer
Nu	Nucleophile
OA	Oxidative Adition
PET	Photoinduced Electron Transfer
PCET	Proton-coupled Electron Transfer
RPKA	Reaction Progress Kinetic Analysis
SET	Single Electron Transfer
SMD	Solvation model based on density
S$_N$1	Unimolecular Nucleophilic Substitution
S$_N$2	Bimolecular Nucleophilic Substitution
TON	Turnover Number
VTNA	Variable Time Normalization Analysis

Organic Chemistry Abbreviations

Ac	Acetyl
AcOH	Acetic Acid
Acr-Mes	9-Mesityl-10-methylacridinium
AdoCbl	5'-Deoxy-5'-adenosylcobalamin
AIBN	2,2'-Azobisisobutyronitrile
Ar	Aryl
BNAH 1	Benzyl-1,4-dihydronicotinamide
Boc	*tert*-Butoxycarbonyl
Bpin	Bis(pinacolato)diboron
B$_2$cat$_2$	Bis(catecholato)diboron
Bu	Butyl
BuCN	Butyronitrile
***t*-Bu**	*tert*-Butyl

CHD	1,4-Cyclohexadiene
Cp	Cyclopropane, cyclopropil
DABCO	1,4-Diazabicyclo[2.2.2]octanedansyl
dba	Dibenzylideneacetone
DCM	Dichloromethane
DCE	Dichloroethane
DDD	1,1-Bis(4-chlorophenyl)-2,2-dichloroethane
DDE	Dichlorodiphenyldichloroethylene
DDT	1,1-Bis(4-chlorophenyl)-2,2,2-trichloroethane
DIBAL-H	Diisobutylaluminum Hydride
DIPEA	Diisopropyl ethyl amine
DMA	Dimethylacetamide
DMAP	4-(N,N-dimethylamino)pyridine
DME	1,2-dimethoxyethane
DMF	Dimethylformamide
DMM	Dimethylmethoxy
DMN	1,5-Dimethoxynaphthalene
DMSO	Dimethylsulfoxide
DPA	Di-(2-pyridyl)amine
DTC	Dithiocarbonyl
HE	Hantzsch ester
NMP	N-Methyl-2-pyrrolidone
EDC	N-(3-Dimethylaminopropyl)-N′-ethylcarbodiimide
EDTA	Ethylenediaminetetraacetic acid
Eos	Eosin
Et	Ethyl
Et$_2$O	Diethylether
Et$_3$N	Triethylamine
EtOAc	Ethyl acetate
EtOH	Ethanol

HCB	Hexachlorobenzene
HMPA	Hexamethylphosphoric Triamide (hexamethylphosphoramide)
LDA	Lithium Diisopropylamide
MCP	Dimethyl- bis(pyridinylmethyl)cyclohexane-1,2-diamine
Me	Methyl
MeCbl	Methylcobalamin
MeCN	Acetonitrile
MeOH	Methanol
MIDA	Methyliminodiacetic acid
MV	Methyl viologen
NBS	N-bromosuccinimide
NCS	N-chlorosuccinimide
NHC	N-heterocyclic Carbene
OTf	Triflate
Ph	Phenyl
Phen	1,10-Fenantroline
PMP	p-Metoxyphenyl
Phth	Phtalimide
iPr	Isopropyl
*i*PrOH	Isopropanol
PTFE	Polytetrafluoroethylene
Py	Pyridine
SLES	Sodium laureth sulfate
TBABr	Tetrabutylammonium Bromide
TBADT	Tetrabutylammonium decatungstate
TBS	Tert-Butyldimethylsilyl
TEA	Triethylamine
TEMPO	2,2,6,6-Tetramethylpiperidin-1-oxyl
THF	Tetrahydrofuran
TMG	Tetramethyl guanidine

TMS	Trimethylsilyl
Ts	p-Toluenesulfonyl (tosyl)
3DPA2FBN	2,4,6-Tris(diphenylamino)-3,5-difluorobenzonitrile
4CzIPN	1,2,3,5-Tetrakis(carbazol-9-yl)-4,6-dicyanobenzene

Ligands

acac	Acetylacetonate
bpy	1-Benzylimidazole
bpy	2,2'-Bipyridyl
cod	1,5-Cyclooctadiene
dap	2,9-Bis(*para*-anisyl)-1,10-phenanthroline
dtbbpy	Ditertbutylbipyridine
dMebpy	Dimethylbipyridine
dmabpy	Dimethylaminobipyridine
DPA	([2,2'-bipyridin]-6-yl)-N,N-bis(pyridin-2-ylmethyl)methanamine
glyme	1,2-Dimetoxyethane
MCP	N,N-Dimethyl-bis(pyridin-2-ylmethyl)cyclohexane-1,2-diamine
PDP	N,N-Dimethyl-bis(pyridin-2-ylmethyl)bipyrrolidine
ppy	Phenylpyridine
PyBCam[CN]	Pyridine-2,6-bis(N-cyanocarboxamidine)
tacn	Triazacyclononane
TPA	Tris(2-pyridylmethyl)amine

Structures and Abbreviations of the Catalysts
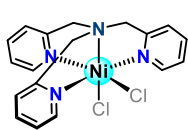
(^HTPA)NiCl₂
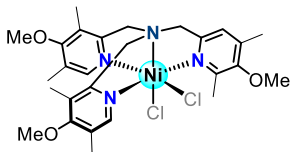
(^{DMM}TPA)NiCl₂
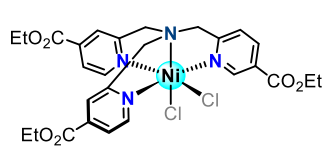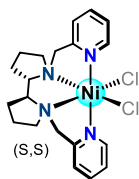
(^{CO2Et}TPA)NiCl₂

(^HPDP)NiCl₂
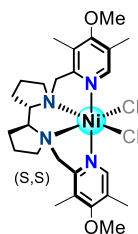
(^{DMM}PDP)NiCl₂
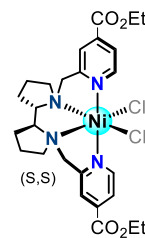
(^{CO2Et}PDP)NiCl₂
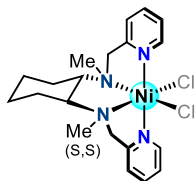
(^HMCP)NiCl₂
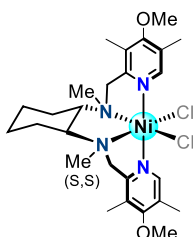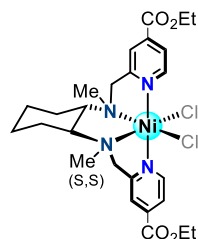
(^{DMM}MCP)NiCl₂

(^{CO2Et}MCP)NiCl₂
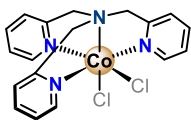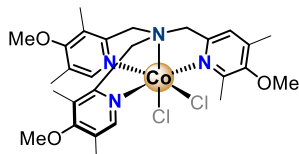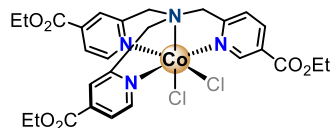
(^{H}TPA)CoCl$_2$ **(^{DMM}TPA)CoCl$_2$** **(^{CO2Et}TPA)CoCl$_2$**
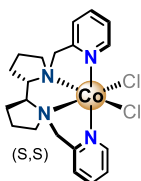
(^{H}PDP)CoCl$_2$ **(^{DMM}PDP)CoCl$_2$** **(^{CO2Et}PDP)CoCl$_2$**
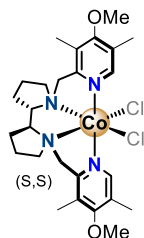
(^{H}MCP)CoCl$_2$ **(^{DMM}MCP)CoCl$_2$** **(^{CO2Et}MCP)CoCl$_2$**

$(Py_2{}^{Ts}tacn)Ni(OTf)_2$

$(^{DMM}Py_2{}^{Ts}tacn)Ni(OTf)_2$

$(^HDPA)Ni(OTf)_2$

$(Py_2{}^{Ts}tacn)Co(OTf)_2$

$[Ir(ppy)_2(^{COOEt}bpy)](PF_6)$
or
$PC_{Ir}{}^{COOEt}$

$[Ir(ppy)_2(bpy)](PF_6)$
or
$PC_{Ir}{}^{H}$

$[Ir(ppy)_2(^{tBu}py)](PF_6)$
or
$PC_{Ir}{}^{t-Bu}$

$[Ir(ppy)_2(^{NMe2}bpy)](PF_6)$
or
$PC_{Ir}{}^{NMe2}$

$[Cu(bathocuproine)(Xantphos)](PF_6)$
or
PC_{Cu}

4CzIPN

3DPA2FBN
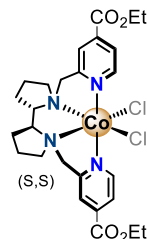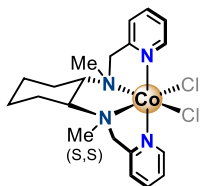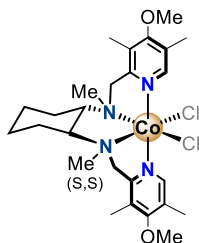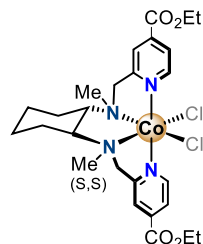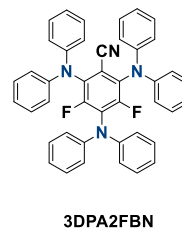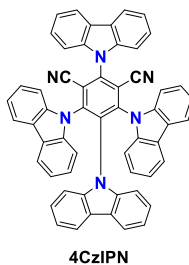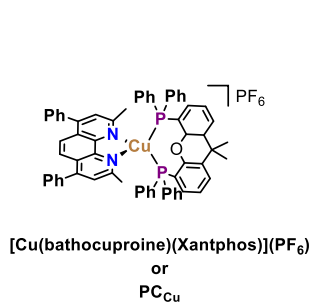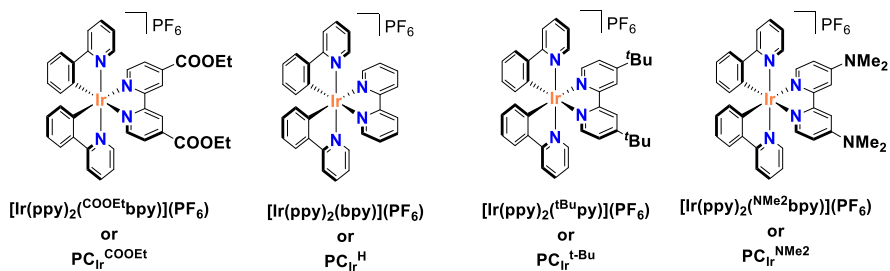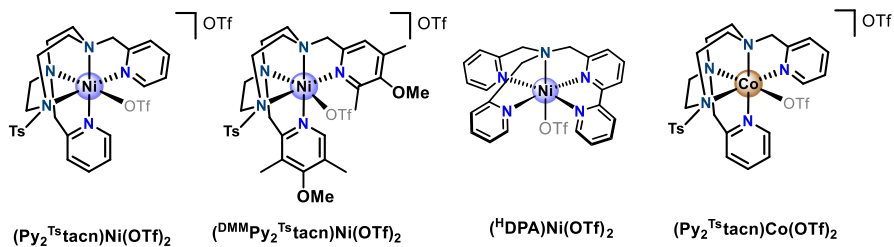
CHAPTER I:

General Introduction

UNIVERSITAT ROVIRA I VIRGILI
VISIBLE-LIGHT METALLAPHOTOREDOX STRATEGIES FOR ORGANIC TRANSFORMATIONS THROUGH THE CLEAVAGE
OF CSP3-CL BONDS
Jordi Aragón Artigas

1.1. Metallaphotoredox C−C bond transformations, an overview

Organic chemists have focused mainly on developing new methodologies for forming C−C bonds during the last decades. In this regard, the development of transition metal catalysis is considered one of the most relevant advances in chemistry over the last 70 years. Metal-mediated bond cleavage/formation has broaded the library of readily available precursors for synthesizing complex molecules, encompassing an extensive range of chemical reactivity. The award of three Nobel prizes for the developments in stereoselective catalysis,[1-3] olefin metathesis,[4-6] and palladium-catalyzed cross-coupling[7-9] is the cusp of transition metal catalysis.
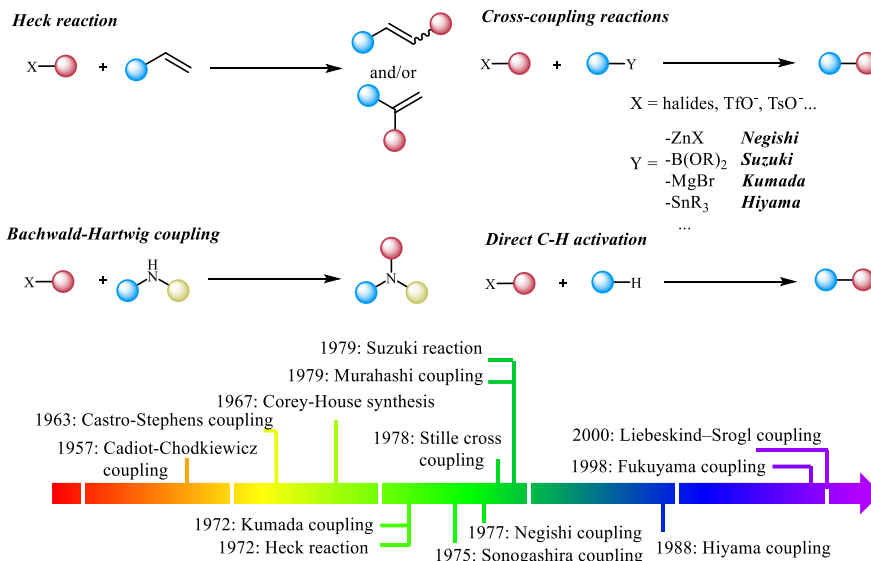
Scheme 1. 1. Selected examples of transition metal catalytic processes.

Nevertheless, the strategies employed to tune the reactivity of a transition metal have remained steady without significant upgrades for synthetic methodologies over the last years. Generally, the development of desired transformations by metal-based catalysis mainly proceeds by modulating either the metal's ligand field or oxidation state. However, while the oxidation state of metal catalysts has represented an important design parameter in discovering novel catalytic platforms, the tuning of this property has not been straightforward. Furthermore, since coordinative ligands can be highly selective in the binding of metal centers, modification of the oxidation state by either adding stoichiometric oxidants or reductants will inherently affect the overall reaction mixture. Therefore, a potential catalytic electron source capable of accurately modifying the electronic structure of transition metal was glimpsed as crucial for the upgrade of the catalysis field.

In this regard, the widespread adoption and growth of photochemistry could fill this huge strategic gap, where the understanding of the interaction between light and organometallic compounds or organic dyes extends the range of reactions enabled by single-electron transfer (SET) and energy transfer (EnT) processes.[10, 11] For example, the rationalization of the photophysical properties of photoredox catalysts contributed to the expansion of the field. Focusing on metal-based photocatalysts, usually, polypyridyl complexes of ruthenium, iridium or copper can be excited by visible light. The light irradiation provides a long-lived triplet excited state of the photocatalyst through a metal-to-ligand charge-transfer event (MLCT) followed by intersystem crossing. This excited species possesses both a metal-centered hole, capable of oxidizing a suitable electron donor (ED), and a π^*-centered unpaired spin, capable of reducing an adequate acceptor (EA). Afterward, the corresponding redox-modified ground state can perform the opposite SET event, rendering the complex a catalyst in the reduction and oxidation of substrates (Scheme 1. 2).[12] Then, the application of visible light as a reaction motor can be considered one of the most effective approaches for chemistry, pharma and other applied science. The excitation by low energy

enhances the selectivity of the catalyst over any organic and organometallic substrates in the mixture, enabling the development of precise chemoselective transformations.

Moreover, photocatalytic processes can usually be achieved at ambient temperature and under mild reaction conditions, enabling the use of versatile reagents containing many functional groups. Since photocatalytic reactions often proceed through a radical mechanism, they offer a complementary reactivity to that of transition-metal-catalyzed, two-electron processes. Remarkably, the rapid development of LED technology has rendered selective and intense light sources accessible, cost-efficient, and available for both batch- and flow-mode photoreactors.[13]
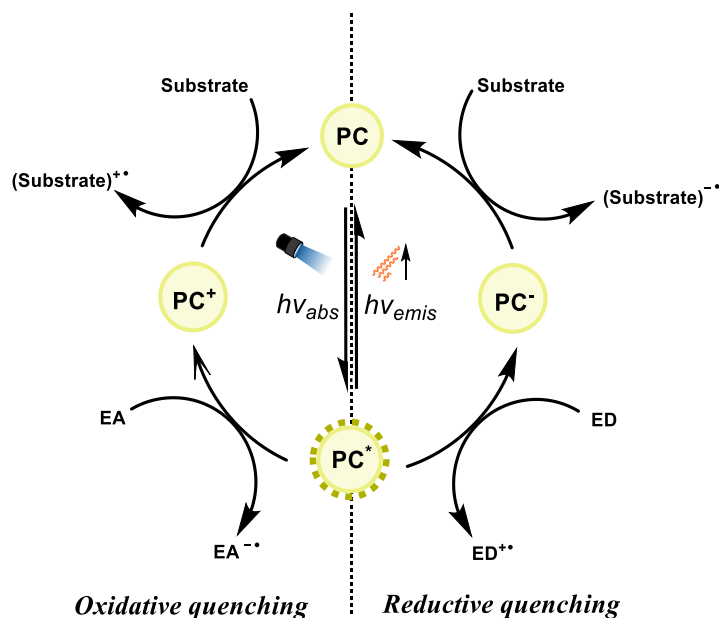
Scheme 1. 2. General photocatalytic cycle including reductive and oxidative electron-transfer quenching processes.

Although photoredox catalysis has been assimilated broadly for the activation and transformation of organic compounds, the merger with transition metals recently outbreaks the field of catalysis. The productive relationship of transition metal-mediated substrate activation with the excited-state chemistry of photocatalyst means a unique update of the catalysis field, combining two powerful disciplines for the lookout of unprecedented disconnections and novel reactivity (Scheme 1. 3). Furthermore, the application of photoinduced SET and EnT in the modification of metal catalyst electronic structure overcome the limitations of classical transition metal catalysis, reaching high-valent and excited state catalysis, notably in the absence of strong stoichiometric oxidants or high-energy light irradiation.[14]

Metallaphotoredox catalysis

expansion of the synthetic paradigm
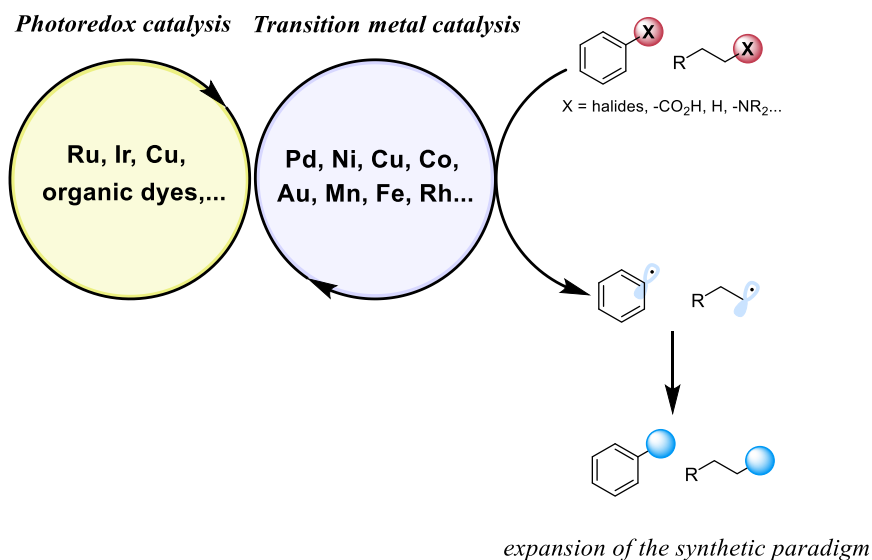
Scheme 1. 3. Metallaphotoredox catalysis activates inert functional groups towards transition metal catalysis *via* one-electron pathways.

1.1.1. Nickel-based metallaphotoredox catalysis

As mentioned before, the treasured work from Heck, Negishi, and Suzuki, among many others, for implementing palladium-catalyzed cross-coupling revolutionized the field of organic synthesis. Nevertheless, the widespread extension of palladium-catalyzed cross-couplings in building bonds to Csp^2 centers presents significant limitations regarding the coupling of Csp^3 centered synthons. In this sense, nickel catalysis has emerged as a substantial improvement toward this challenging aim. Although the use of palladium in Csp^2 couplings is more extended than other metals, nickel undergoes fastly oxidative addition into alkyl electrophiles and presents less β-hydride elimination with aliphatic ligands when compared with palladium.[15] The combination of nickel catalysis with photoredox catalysis is the most versatile and significant metallaphotoredox scenario, playing an integral role in novel bond disconnections.

The role of radical intermediates and the activation of alkyl electrophiles are well-established in nickel catalysis. In general, dual metal photocatalytic strategies using nickel are based on the interconnection between a photoredox cycle, which activates radical precursors, and a nickel catalytic cycle which undergoes the activation of electrophiles. We can find a vast collection of different radical precursors, which are latent nucleophiles for cooperative photocatalytic and nickel cycles. For example, carboxylic acids are one of the most abundant functional groups in nature, and their utility as radical precursors is well-exploited.[16-18] A collaboration between Macmillan and Doyle groups realized this merger for one of the first photoredox decarboxylation of carboxylic acid for the cross-coupling with aryl halides (Scheme 1. 4).[19]
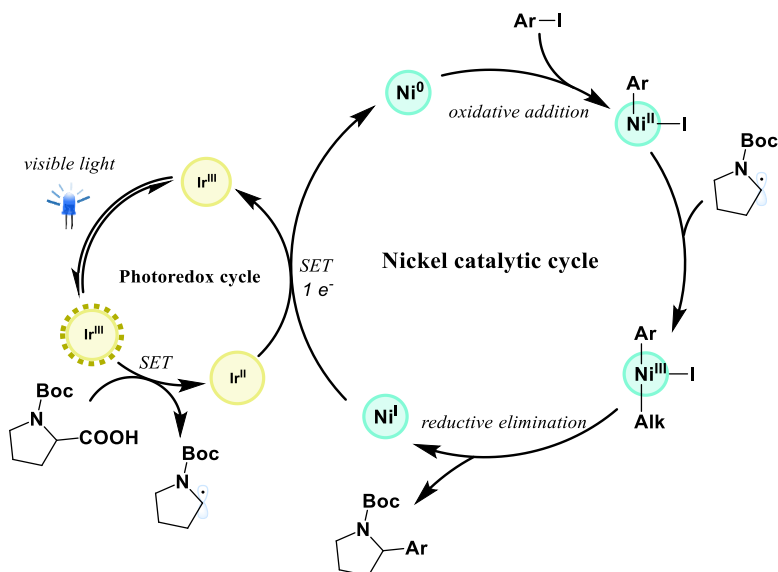
Scheme 1. 4. Metallaphotoredox nickel-catalyzed decarboxylative arylation.

Upon excitation of the photocatalyst, a SET event occurs between the triplet excited state and a carboxylate nucleophile, with the subsequent decarboxylation and formation of an alkyl radical. At the same time, after two sequential electron-transfers Ni^{II} precatalyst becomes Ni^{I} active species, which undergoes oxidative addition with an aryl halide. Then, the *aryl*−Ni^{II} intermediate captures the previous alkyl radical, affording *aryl*−Ni^{III}−*alkyl* complex. The fast reductive elimination recovers the Ni^{I} active species, releasing the Csp^2−Csp^3 coupling product. This mechanistic picture illustrates metallaphotoredox catalyzed C−C bond formation involving a Csp^2 electrophile, and it has been extended to multiple related reactions.[16-22] but also Csp^3−Csp^3 coupling wherein primary and secondary alkyl bromides are performed.[23] Following a similar mechanistic concept, Molander and co-workers introduced the use of alkylboron nucleophiles in photoredox cross-coupling reaction.[24] Alkyltrifluoroborates serve as C-centered radical precursors through a photocatalytic cycle such as previous carboxylic acids, interconnecting with a nickel catalytic cycle and settling in a Csp^2−Csp^3 coupling

with aryl halides. The implementation of enantioselectivity by employing a chiral ligand on the nickel catalyst, together with DFT calculation, suggests revising the proposed mechanism. In this update, the capture of C-centered radical by Ni^0 has lower energy, affording *Ni^I−alkyl* intermediate, which undergoes oxidative addition to form the *aryl−Ni^{III}−alkyl* intermediate, converging with the previous mechanism.[25] Thence, the use of borate salts with a large variety of electrophilic coupling partners has given rise to significant photocatalytic methodologies for building molecules.[26-31]

The value of carboxylic acids and alkylborates as C−centered radical precursors is reflected in an extensive number of elementary works in the field of metallaphotoredox transformations. Moreover, the extension of this approach to other radical precursors drives the development of novel strategies (Scheme 1. 5). Alcohols are among the most widely occurring, naturally abundant organic compounds known and are considered feedstock chemicals in many cases. Their easy functionalization into oxalate esters in a single step without purification results in another C−centered radical precursor using Csp^3−O bond photoactivation after losing two CO_2 molecules.[32, 33] Moreover, the relevance of alcohols as alkoxyl radical species for the remote C−C bond formation has to be considered. Rueping and co-workers developed a robust method for the remote site-specific arylation of ketones from easily accessible tertiary alcohols and aryl halides through a photoredox-enabled proton-coupled electron transfer (PCET) and nickel catalysis.[34] Martin and co-workers also recognized the utility of aliphatic alcohols as Csp^3 synthons, developing a general method for coupling alkyl and aryl halides *via* β-scission of N-phthalimide ethers as derivatized alcohols.[35] Afterwards, Zuo and co-workers disclosed the photocatalytic dehydroxymethylative arylation of free alcohols with aryl halides, enabled by the synergistic utilization of cerium and nickel catalysts.[36] Aldehydes can also be considered an indirect C−centered radicals, due to the expansion of strategies using dihydropyridines,[37-39] which could be synthesized in a single high-yielding

step from aldehydes. Other radical precursors have also been employed in nickel-based metallaphotoredox transformation, such as alkylsilicates[40] or sulfinates[41] showing less adoption in the field.
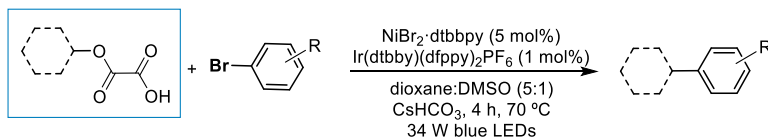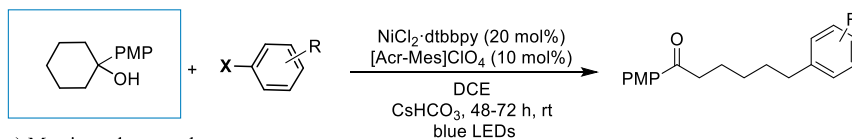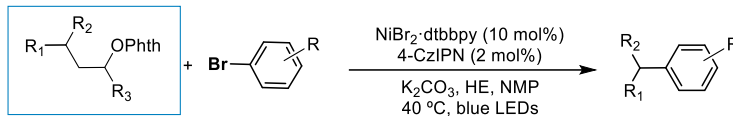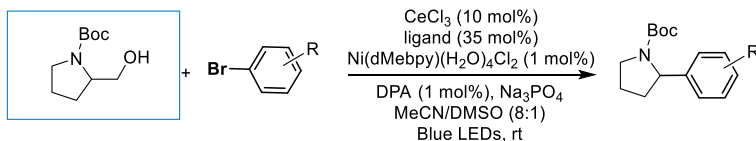
Scheme 1. 5. Metallaphotoredox deoxygenative cross-couplings.

The direct functionalization of C−H bonds in cross-coupling is another challenge in transition metal catalysis.[42] The C−H bond is the simplest organic fragment, remaining among the most sought-after transformations in synthetic chemistry, where metallaphotoredox catalysis has moved to the forefront of C−H functionalization strategies in recent years. The common use of tertiary amines such as electron donors in the reductive quenching of photocatalyst shows the basis of C−H photoactivation. Neutral amines are converted into radical cations via single-electron oxidation. After the generation of the radical cation, the C−H

bonds adjacent to the nitrogen atom are greatly acidified (pKa ca. 8), and deprotonation easily occurs to give α-aminoalkyl radicals and a proton.[43-45] This species should play as a competent open-shell nucleophile in a dual-catalytic cross-coupling. In this regard, Doyle and co-workers developed a cross-coupling of amines with aryl halides using a nickel-photoredox dual catalyst system, directly accessing benzylic radicals.[46] Additionally, this C−H functionalization manifold was extended to phenols, anhydrides, or thioesters as electrophiles.[47, 48] This oxidation−deprotonation has proved a valuable method for functionalizing redox-active amine substrates, but the redox properties of the substrate controls the scope of the methods.

With the aim of separing the redox properties of the substrate from the mode of activation, hydrogen atom transfer (HAT) became a strategy to activate a broader range of C−H bonds. In this context, amines give another possible C-H activation pathway through electron-deficient nitrogen-centered radicals. The hydridic α-amino C−H bond allows the polarity-matched HAT events by these heteroatom radicals.[49, 50] The mechanism relies on a favorable SET between excited photocatalyst and electron-rich amine, followed by a polarity-matched hydrogen atom abstraction by amine radical cation from the electron-rich α-amino C−H bond of protected amine. While the mechanism may be distinct from single-step, SET-mediated radical generations, the remaining components of the mechanism retain the same underlying elementary steps of previous nickel metallaphotocatalysis (Scheme 1. 6).
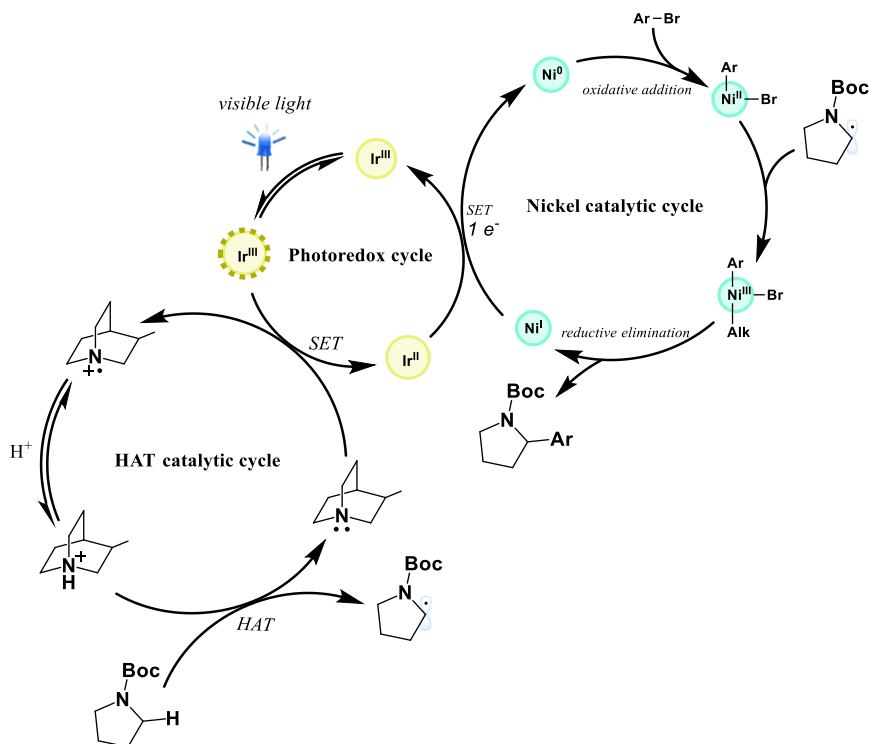
Scheme 1. 6. Metallaphotoredox nickel-catalyzed C-H activation with tertiary amines.

Halogen radicals have also been shown to engage productively in HAT events. Therefore, interfacing the capability of chlorine radicals to activate $Csp^3−H$ bonds with catalytic functionalization reactions of the resulting alkyl radicals could develop a wide range of elusive bond constructions.[51-53] Generally, the previous methods have been showing two main steps: HAT from photoredox cycle, Ni catalytic cycle merging alkyl radicals with the activation of aryl halides. In this context, Nocera and co-workers proposed a mechanism based on the integration of the Ni catalyst into the photoredox cycle:[54] the photolysis of a Ni^{III} aryl chloride intermediate, generated by single-electron oxidation, leads to elimination of a chlorine radical capable of activating $Csp^3−H$ bonds by abstraction (Scheme 1. 7).
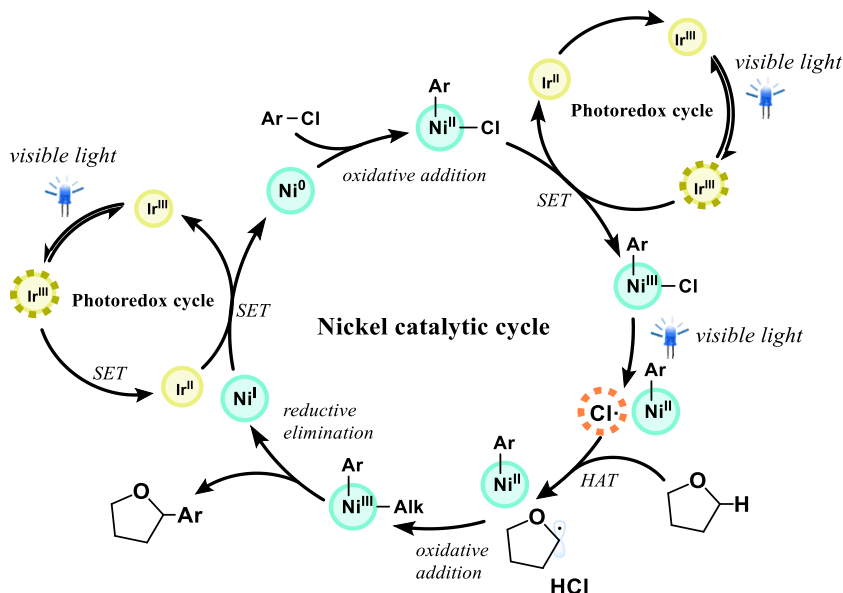
Scheme 1. 7. Metallaphotoredox nickel-catalyzed generation of chlorine radicals for C-H cross-coupling.

1.1.2. Cobalt-based metallaphotoredox catalysis

The relevance of cobalt in the field of inorganic photochemistry has kept chemical energy at the forefront of catalytic water splitting[55-59] and CO_2 reduction.[60-62] Recently, synthetic chemistry has shifted the focus toward engaging cobalt in light-enabled transformations of organic molecules, where the biological importance of B_{12}-dependent enzymes in several reactions such as dehalogenations, methyl transfers and group rearrangements serves as inspiration.[63, 64] While diverse transformations have been developed over the past decade, cobalt's well-established roots in hydrogen evolution have guided much of the developments in the area of cobalt and metallaphotoredox catalysis.

In this regard, a notable feature of this mechanism is the tendency for cobalt to oxidize intermediates in a SET, followed by proton reduction to hydrogen to carry

out transformations in the absence of sacrificial oxidants, affording a cobalt-catalyzed cross-coupling hydrogen evolution (CCHE). In 2014, Wu and co-workers showed the first Co-catalyzed CCHE to coupling indoles with tetrahydroisoquinolines.[65] As shown in Scheme 1. 8, the hypothesis starts with the photoexcitation of an organic dye (eosin Y) to a triplet excited state. Subsequently, tetrahydroisoquinoline suffers a SET, releasing a radical cation and reduced eosyn Y. The eosyn Y is regenerated by Co^{III} species, and the corresponding Co^{II} oxidizes the amine radical cation after the loss of a proton, forming Co^{I} hydride. Finally, the addition of indole into the resultant iminium cation, followed by rearomatization, affords the product. Afterward, the hydrogen formation through the protonation of Co^{I} closes the cobalt catalytic cycle.
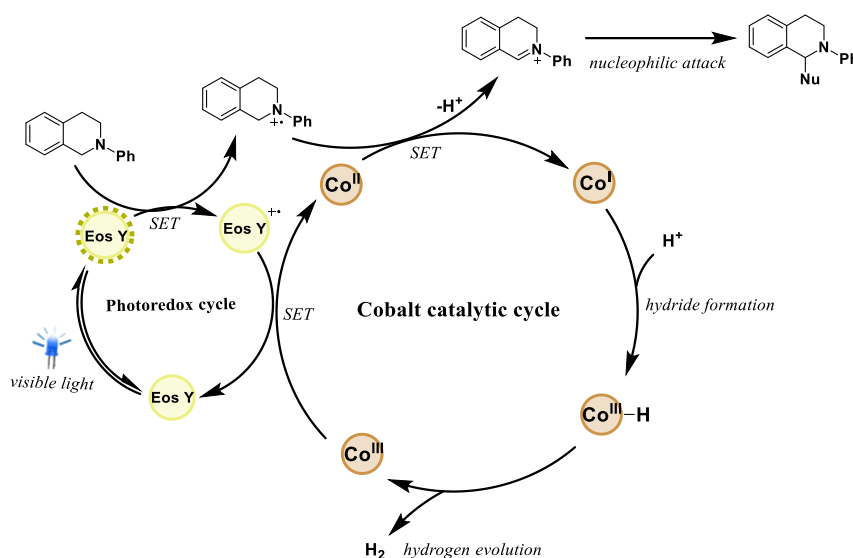
Scheme 1. 8. Mechanistic proposal for cobalt-catalyzed cross-dehydrogenative coupling.

Following this first example of CCHE, tetrahydroisoquinoline and isochromans have been involved in addition reactions with other nucleophiles (Scheme 1.9), such as β-ketoesters[66] or trialkylphosphites[67] under free oxidant

conditions. The potential merge of CCHE metallaphotoredox system with enamine catalytic cycle efforted the asymmetric functionalization of ketones with tetrahydroisoquinolines.[68]
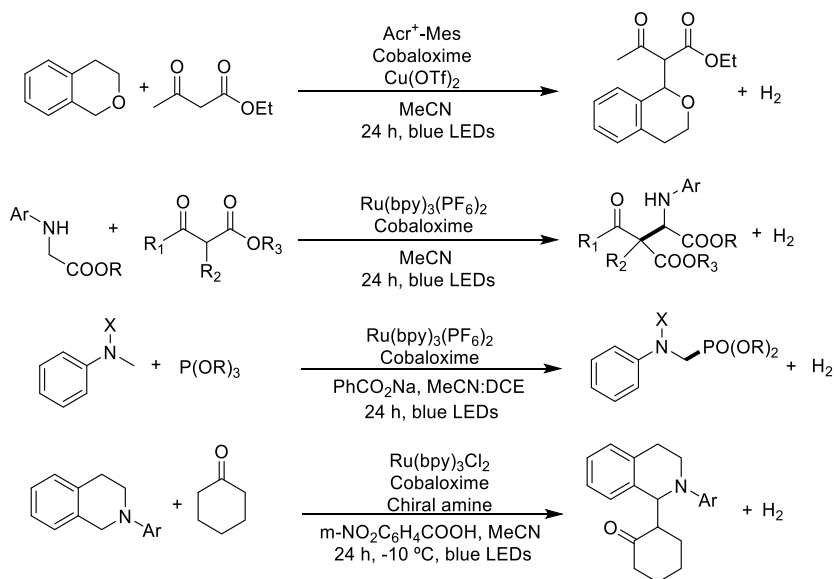
Scheme 1. 9. Metallaphotoredox cobalt-catalyzed cross-dehydrogenative couplings.

Outside the iminium and oxonium electrophiles generation, Co^{II} compounds can engage alkyl radicals, similarly to nickel catalysis, undergoing photoinduced Heck-type reactions (Scheme 1. 10).[66] A plausible mechanism starts with photoexcitation of photocatalyst and subsequent SET-induced decarboxylation of carboxylate. Then, this unstabilized alkyl radical attacks an activated alkene (styrenes,[66] vinyl silanes and boronates,[66] heterocycles[67]...), providing a stabilized C-centered radical intermediate. Co^{II} can capture this radical, and the abstraction of adjacent hydrogen atoms provides the desired olefin product and cobalt−hydride species. In a related way, Lei and co-workers introduced sulfur nucleophiles with activated alkenes.[68]
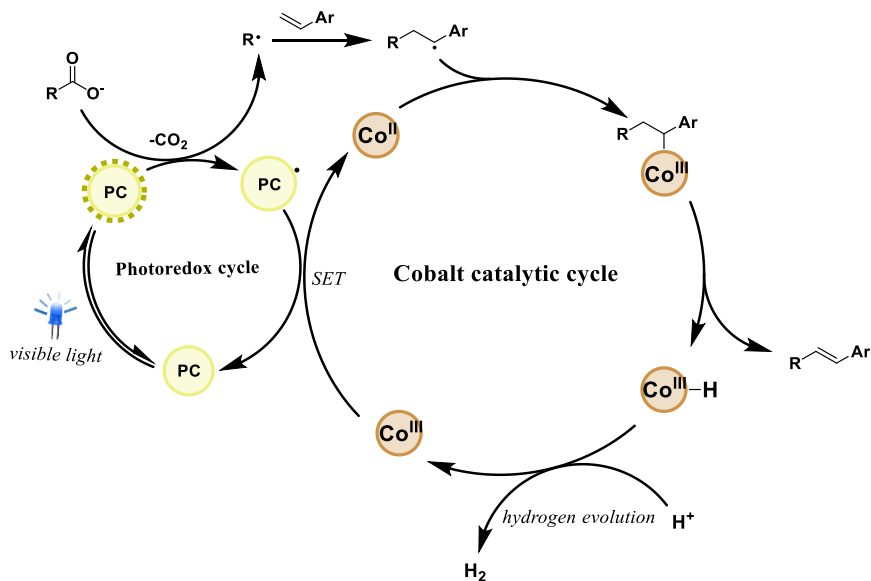
Scheme 1. 10. Metallaphotoredox cobalt-catalyzed Heck-type reaction.

The merge of cobalt's predilection for unactivated dienes rendering π-allyl complexes and the capacity to form catalytically active metal hydrides exposes another metallaphotoredox application: the hydrofunctionalization of unsaturated systems (Scheme 1. 11).[69] The oxidation and deprotonation of an amine by excited-state PC releases an α-amino alkyl radical. At the same time, a Co^{III} hydride complex is generated from the reduction of initial Co^{II} by the PC, and the sequential protonation of the Co^{I}. A migratory insertion with diene substrates forms π-allylcobalt intermediate, reduced by PC. This π-allyl−Co^{II} can trap the α-amino alkyl radical. A final reductive elimination affords the coupling product. Several groups expanded this catalytic approach to a range of different tertiary amines, but also in the isomerization of the terminal to internal olefins and the coupling of alkynes with activated alkenes.[70]
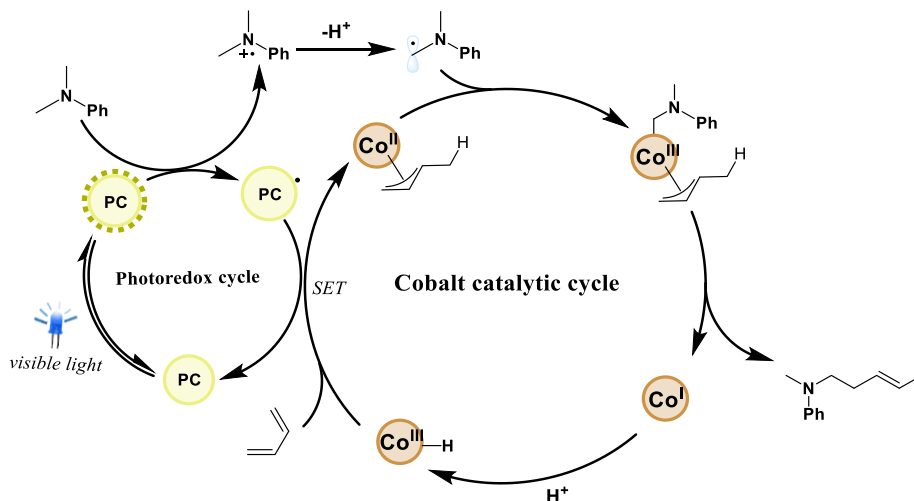
Scheme 1. 11. Metallaphotoredox cobalt-catalyzed hydrofunctionalization of dienes.

1.2. Photocatalytic activation of organic chlorides

As discussed above, visible light photoredox catalysis has opened a novel and moderate approaches for the C−C bond-forming *via* reactive free radical intermediates by photocatalytic activating strong σ-bonds,[28] including C−H bonds (~ 337 kJ/mol), C−C bonds (~ 370 kJ/mol), among others. In this regard, halide and pseudohalide electrophiles are among the most commonly employed reagents in synthetic organic chemistry. Their widespread adoption is based on their straightforward synthesis, bench stability, and ready commercial availability.[71-75] Actually, the deep exploitation of alkyl, aryl, and vinyl halides and pseudohalides especially emerges with the growth of photoredox cross-electrophile couplings. Upon light-induced reduction and subsequent C–X bond cleavage, they afford carbon-centered radicals, which can be engaged in many organic transformations.[76-79]

Despite the privileged role afforded to iodides and bromides coupling partners, limitations remain in using chlorides and fluorides electrophiles, especially their unactivated versions. However, the paradigm of unactivity of organic chlorides is now changing rapidly due to growing of photocatalytic methods. This challenging goal incites the development of new conceptual ideas behind each strategy based on how the catalytic system accumulates the light energy or reduces the bond dissociation energy (BDE) in the substrate.

1.2.1. Single-electron transfer methods
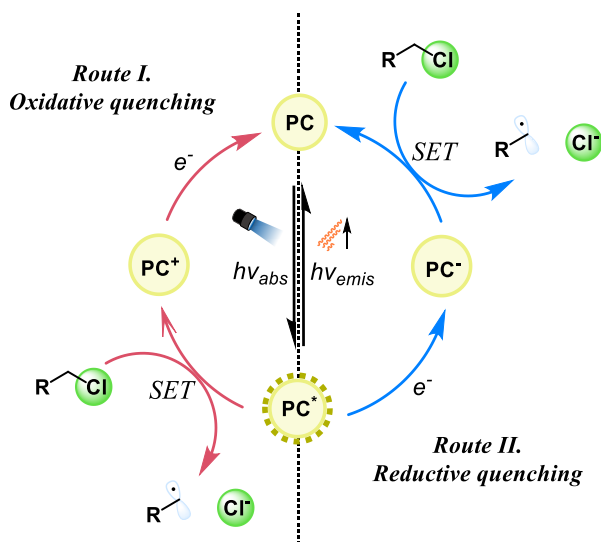
Scheme 1. 12. Mechanistic principles of SET-based activation of organic chlorides.

As seen in previous sections, a photocatalyst can undergo a SET through two different pathways depending on the energy match between the PC and the substrate (Scheme 1. 12): i) direct SET from the substrate can only arise if $\Delta G \leq 0$, considering the short lifetime of excited PCs (oxidative quenching), and ii) direct SET from one-electron-reduced form of the PC, with longer lifetimes (reductive quenching). All the approaches described here share the common

mechanistic step in which the C–Cl bond is weakened by SET, followed by homolytic cleavage and generation of the respective C-centered radical species.

The highly negative redox potentials of inert, unactivated organic chlorides (– 2.8 V *vs* SCE)[80] places them beyond the energetic limits, even though strongly reducing photoredox catalysts have been recently developed.[81-84] The stabilization of the target C-centered radical that forms upon SET and homolytic cleavage bond. In an adjacent π system, heteroatom or -in aryl radicals- the presence of electron-withdrawing substituents can diminish the energy barrier of the initial reduction step and make it thermodynamically feasible. Consequently, the exploitation of visible light direct SET activation of organic chlorides is exclusive to suitable activated compounds. Initially, the above-mentioned principle was applied in visible-light-induced dehalogenations.[85-87] In 2012, Reiser and co-workers reported a photocatalytic C−C bond formation *via* reductive allylation of α-chlorocarbonyl compounds catalyzed by Cu(dap)$_2$Cl (dap=2,9-bis(*para*-anisyl)-1,10-phenanthroline) as a photocatalyst, proved to be a more potent reducing agent than Ru(bpy)$_3^+$ (Scheme 1. 13).[88] Not until 7 years later α-chlorocarbonyl compounds were used as α-secondary stereocentres in enantioselective reactions with high yields with a dicyanopyrazine-based PC.[89] Alkenyl chlorides are more challenging feedstocks due to the relative unstability of vinyl radicals. The use of a powerful PC (*fac*-Ir(ppy)$_3$) beats this reaction barrier for the coupling of α-chloro cinnamates with enol acetates as a radical trap (Scheme 1. 13).[90] Moreover, the application of acyl radicals in organic synthesis has largely lagged behind that of simple alkyl and even vinyl radicals due to the strict conditions required for their generation. The group of Xu showed the potential of acyl chlorides as straightforward acyl radical precursors by using a visible light-excited *fac*-Ir(ppy)$_3$ in a cascade cyclization with 1,7 enynes.[91] This precedent underwent the expansion of SET activation of acyl chlorides with other coupling partners, involving them in Michael additions (Scheme 1. 13)[92] or Minisci acylation of heteroarenes,[93] among others. In the case of aryl chlorides,

the bond activation through SET requires lowering the reduction potential (Scheme 1. 13).[94-97] This requirement was clearly illustrated by Fu group, where electron-withdrawing groups into the aryl chloride and heteroaryl chlorides presented higher yields in less time (70-90%, 12 h), in contrast with electron-donating groups (40-50%, 24 h).[98] In 2015, Schelter and co-workers introduced the activation of benzyl chlorides for their homocoupling with a novel application of Ce^{III} complexes as photocatalyst (Scheme 1. 13). Returning to the initial idea, this work was a particular case using aliphatic derivatives as reagents, showing the limitation of SET strategies for the activation of organic chlorides.[99]
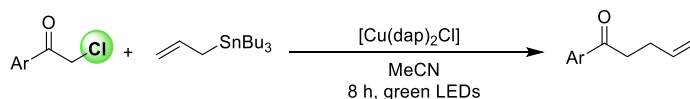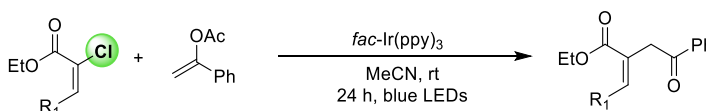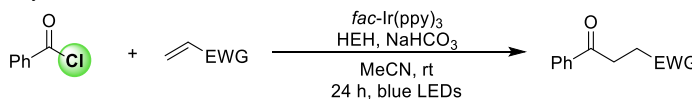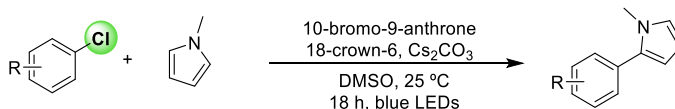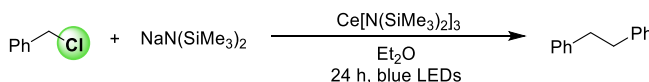
Scheme 1. 13. Visible light-induced SET activation of organic chlorides.

The implementation of synthetic protocols enhanced by visible light is one of the remarkable advantages of photoredox catalysis. However, the direct photolytic

cleavage of a chemical bond may occur under high-energy irradiation. For example, UV light can undergo the homolytic activation of aryl chlorides by a direct $\pi-\pi^*$ excitation.[100-103] In 1992, Yam and co-workers presented the first activation of aliphatic chlorides, based on a dinuclear gold complex under UV irradiation, affording the homocoupling of benzyl chlorides.[104] Almost 25 years later, the groups of Fu and Peters developed a general cyanation protocol of unactivated secondary alkyl chlorides.[105] They used CuCN from CuI as precatalyst and tetrabutylammonium cyanide, which under UV excitation (254 nm) furnishes a Cu^{II}–CN adduct and an alkyl radical.
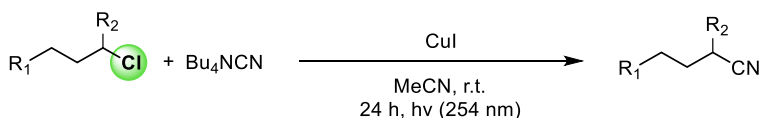
G. Fu, J. Peters and co-workers, *J. Am. Chem. Soc.*, **2015**, *137*, 13902-13907.

Scheme 1. 14. Photocatalytic cyanation of non-activated secondary alkyl chlorides under UV irradiation.

The continuous asking and revision of the phenomena are the basis of the science, and usually, the development of new chemical advances are based on going back to the origin and reformulating classical organic chemistry. One example is the application of solvated electrons to photocatalysis. Solvated electrons in an aqueous media show significant reductive potential (–3.15 V *vs* SCE) and a relatively long lifetime (1–2 μs).[106] The first example of a photocatalytic generation of hydrated electrons was in 2014, and shortly after, examples of activating C–Cl bonds using this methodology appeared.[107] This preliminary work included only dehalogenation of chloroacetate, 4-chlorobenzoic acid and 4-chlorophenyl acetic acid, without C–C coupling, and the irradiation of green low-energy had to be balanced by high-intensity sources. In 2018, Goez and co-workers optimized this challenge by employing micellar compartmentalization of the reagents in the aqueous media. The stabilization of the PC (Ru(bpy)₃) on

the micelle surface (negatively charged), together with sodium ascorbate as a sacrificial electron donor (ED), avoided the back-electron-transfer and increased the lifetime of the excited PC. Consequently, the PC may absorb a second photon, releasing hydrated electrons under low light intensity conditions (Scheme 1. 15).[108] The tune of the conditions with different anionic sacrificial electron donors or different micelles enhanced different C–C cross-coupling reactions through the activation of organic chlorides, such as α-chlorocarboxylates and benzyl chlorides.[108, 109] However, the preeminent application of this concept was achieved in 2020 by König and co-workers, implementing the first photocatalytic protocol of Csp^3−Cl bond activation of inert primary alkyl chlorides.[110]
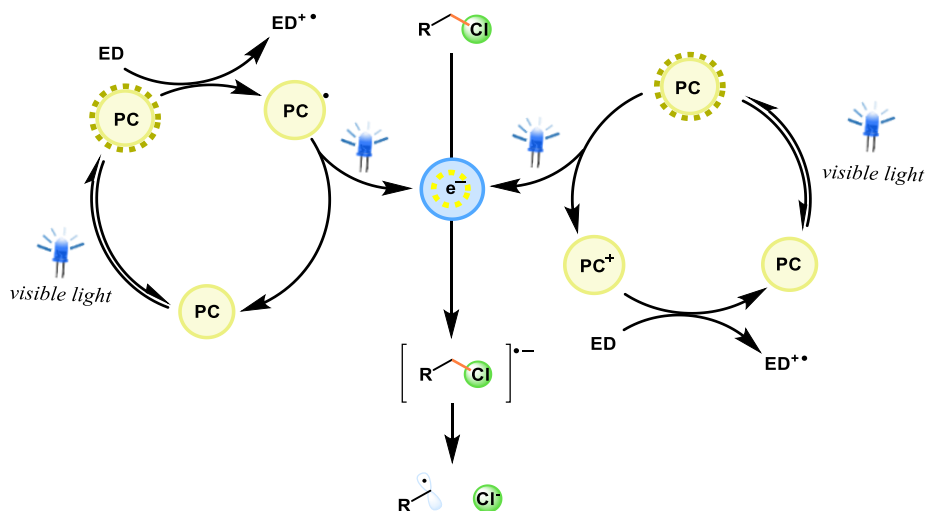
Scheme 1. 15. Photocatalytic solvated-electron mechanism for the activation of organic chlorides.

The merge of light irradiation with electrochemical was also raised as a feasible tool, considering the straightforward formation of colored radical anions and the requirement of extremely reducing conditions for the activation of unactivated organic. Electrophotocatalytic strategies are based on the cathodic single-electron reduction of PC and the consecutive photoexcitation, accessing to

highly reducing radical anions (< -3 V *vs* SCE).[111, 112] However, these tandem processes present chemoselectivity problems, and they are limited to reductive functionalization of aryl chlorides.
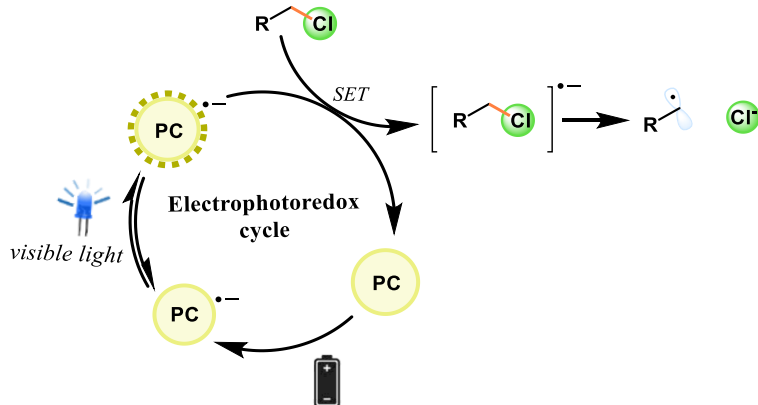
Scheme 1. 16. General electrophotoredox mechanism for the activation of organic chlorides.

1.2.2. Substitution/oxidative addition methods

On the other hand, an S_N2 or oxidative addition pathway can alternatively undergo the cleavage of the C–Cl bond by substituting the chloride, wherein dual catalysis and metallaphotoredox strategies are the main responsible.

Returning to the biological imitation, cobalt complexes has been successfully established in substitution protocols (Scheme 1. 17). The feasible achievement of Co^I species from Co^{III} and Co^{II} and their role, such as supernucleophiles enables nucleophilic substitution reactions with organic chlorides. Photoredox catalysis generally undergoes the in situ generations of the mentioned Co^I complexes, and also light-induced cleavage of Co–C bond can occur. Vitamin B_{12} derivatives were the first examples of cobalt catalysts in metallaphotoredox systems. For example, their implementation with Ru(bpy)$_3$Cl$_2$ as PC and triethanolamine as a sacrificial electron donor under visible-light irradiation achieved the dechlorination of the

insectiside and persistent pollutant 1,1-bis(4-chlorophenyl)-2,2,2-trichloroethane (DDT), obtaining 1,1-bis(4-chlorophenyl)-2,2-dichloroethane (DDD), as a starting point for other stratetigies of dechlorination.[113] However, Co-based metallaphotoredox systems are not limited to dechlorination reactions. In 2019, Hisaeda and co-workers proved the synthetic potential of vitamine B_{12} in a Sonogashira-type reaction between alkyl halides and alkynes, using some activated aliphatic chlorides as coupling partners and $Ir(dtbbpy)(ppy)_2PF_6$ as a PC.[114] A photogenerated nucleophilic Co^I species attacks the alkyl chloride, affording an organometallic intermediate. Then, upon the homolytic cleavage of the Co–C bond and addition of alkyl radical to the alkyne, a vinyl radical is generated. Subsequent oxidation from the excited PC forms a carbocation, prone to deprotonation, giving the final alkyne. Following a similar mechanism, a recent Heck-type coupling with olefins has also been reported.[115]
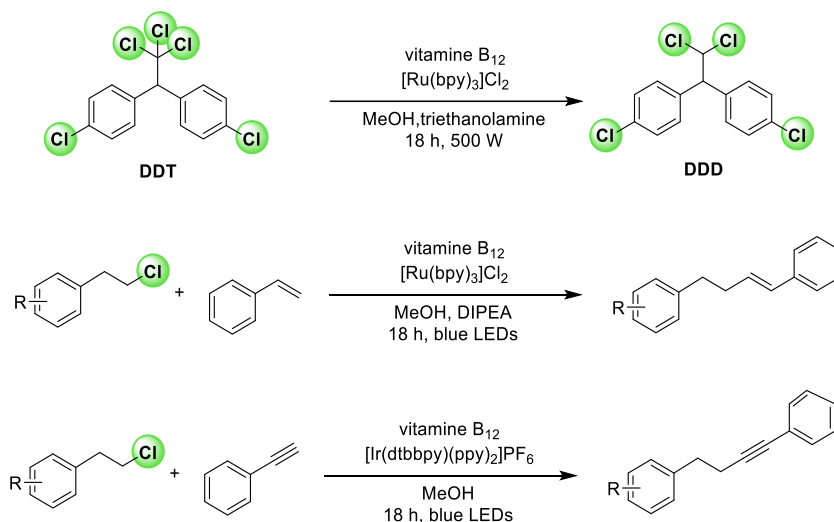
Scheme 1. 17. Cobalt-based metallaphotoredox strategies for the activation of aliphatic chlorides.

Nickel co-catalysts have also been extensively investigated, affording a versatile variety of cross-coupling reactions, combining the aforementioned mechanistic concepts (Scheme 1. 18). For example, Doyle and co-workers merged the generation of chlorine radicals as the product of aryl chloride activation with

their participation in HAT, affording the direct Csp^3-H functionalization of ethers with arylchlorides.[51] The catalytic system was based on $Ni(cod)_2$, dtbbpy as ligand, $Ir[dF(CF_3)ppy]_2(dtbbpy)PF_6$ as PC, K_3PO_4 and a blue light source. Following the Ni-based functionalization of aryl chlorides, one year later, Nielsen *et. al.* applied this metallaphotoredox system in the formylation of aryl chlorides.[53] The use of dual nickel photoredox catalysis was not limited only to the activation of aryl chlorides; the use of alkenyl,[116] carbamic[117] and acyl chlorides[118] has also been reported. Nevertheless, the real impact of Ni-based dual photocatalytic systems is the access to the employment of unactivated alkyl chlorides as coupling partners. In 2017, our group introduced the first step of this career, with an intramolecular cyclization of unactivated alkyl chlorides with pendant alkenes,[119] followed by a photoredox cross-coupling reaction between alkyl and aryl chlorides,[120] developed by Macmillan group in 2020 (both methodologies are further discussed in *Chapter III* and *Chapter IV*).
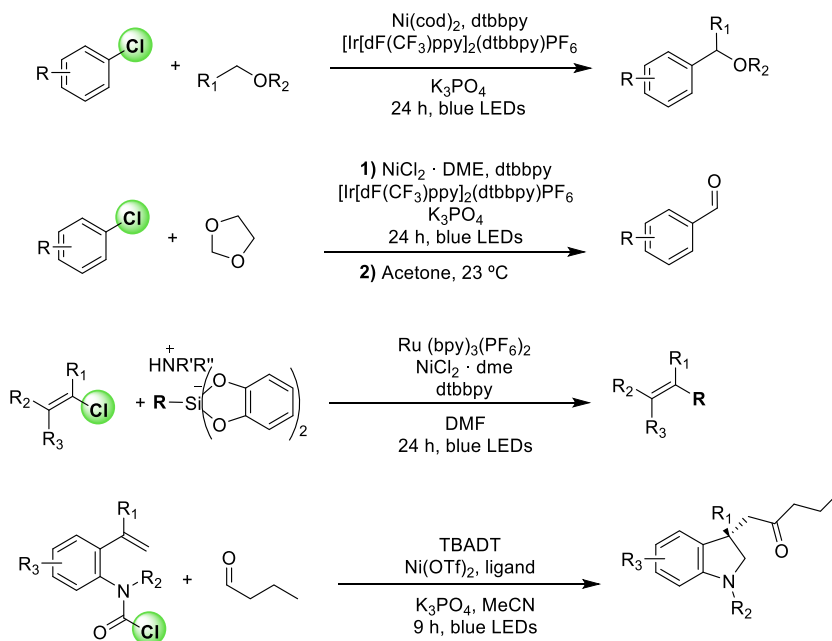
Scheme 1. 18. Nickel-based metallaphotoredox strategies for the activation of aliphatic chlorides.

Recently the combination of photo- and organocatalysis platforms for activating organic chlorides has received growing attention. In this field, the group of Prof. Melchiorre can be considered one of the pioneers of substitution/oxidative addition strategy in a strictly photoorganocatalytic version (Scheme 1. 19).[121] Dithiocarbonyl anions (DTC) are the catalysts, developing a two-step borylation of alkyl chlorides, bromides, and sulfonates. An S_N2 reaction followed by photoinduced C–S bond cleavage in species enabled the generation of radicals. Subsequently, carbon-centred radicals were trapped with bis(catecholato)diboron (B_2cat_2), affording the expected boronic esters. This methodology presented a wide range of substrates, including heterocyclic derivatives, using activated aliphatic chlorides such as benzyl chloride as coupling partners with high selectivity and good yields (54–83%).
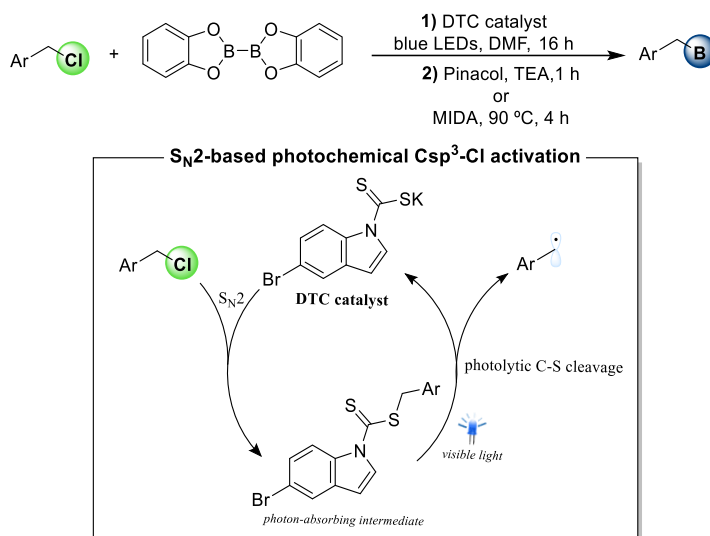
P. Melchiorre and co-workers, *ACS Catal.* **2019**, *9*, 5876−5880

Scheme 1. 19. Photochemical organocatalytic borylation of alkyl chlorides.

As presented here, the development of a general protocol for using unactivated aliphatic alkyl chlorides as cross-coupling partners is still missing in the field, being the main aim of the current thesis.

1.3. References

1.   Katsuki, T.; Sharpless, K. B., The first practical method for asymmetric epoxidation. *Journal of the American Chemical Society* **1980,** *102* (18), 5974-5976.

2.   Miyashita, A.; Takaya, H.; Souchi, T.; Noyori, R., 2, 2'-bis(diphenylphosphino)-1, 1'-binaphthyl(binap): A new atropisomeric bis(triaryl)phosphine. synthesis and its use in the rh(l)-catalyzed asymmetric hydrogenation of α-(acylamino)acrylic acids. *Tetrahedron* **1984,** *40* (8), 1245-1253.

3.   Knowles, W. S.; Sabacky, M. J., Catalytic asymmetric hydrogenation employing a soluble, optically active, rhodium complex. *Chemical Communications (London)* **1968,** (22), 1445-1446.

4.   Grubbs, R. H.; Brunck, T. K., Possible intermediate in the tungsten-catalyzed olefin metathesis reaction. *Journal of the American Chemical Society* **1972,** *94* (7), 2538-2540.

5.   Jean-Louis Hérisson, P.; Chauvin, Y., Catalyse de transformation des oléfines par les complexes du tungstène. II. Télomérisation des oléfines cycliques en présence d'oléfines acycliques. *Die Makromolekulare Chemie* **1971,** *141* (1), 161-176.

6.   Schrock, R. R., Alkylcarbene complex of tantalum by intramolecular .alpha.-hydrogen abstraction. *Journal of the American Chemical Society* **1974,** *96* (21), 6796-6797.

7.   Miyaura, N.; Yamada, K.; Suzuki, A., A new stereospecific cross-coupling by the palladium-catalyzed reaction of 1-alkenylboranes with 1-alkenyl or 1-alkynyl halides. *Tetrahedron Letters* **1979,** *20* (36), 3437-3440.

8.   Baba, S.; Negishi, E., A novel stereospecific alkenyl-alkenyl cross-coupling by a palladium- or nickel-catalyzed reaction of alkenylalanes with alkenyl halides. *Journal of the American Chemical Society* **1976,** *98* (21), 6729-6731.

9.   Heck, R. F., Acylation, methylation, and carboxyalkylation of olefins by Group VIII metal derivatives. *Journal of the American Chemical Society* **1968,** *90* (20), 5518-5526.

10.   Shaw, M. H.; Twilton, J.; MacMillan, D. W. C., Photoredox Catalysis in Organic Chemistry. *The Journal of Organic Chemistry* **2016,** *81* (16), 6898-6926.

11.   Romero, N. A.; Nicewicz, D. A., Organic Photoredox Catalysis. *Chemical Reviews* **2016,** *116* (17), 10075-10166.

12.   Capaldo, L.; Ravelli, D., The Dark Side of Photocatalysis: One Thousand Ways to Close the Cycle. *European Journal of Organic Chemistry* **2020,** *2020* (19), 2783-2806.

13.   Svejstrup, T. D.; Chatterjee, A.; Schekin, D.; Wagner, T.; Zach, J.; Johansson, M. J.; Bergonzini, G.; König, B., Effects of Light Intensity and Reaction Temperature on Photoreactions in Commercial Photoreactors. *ChemPhotoChem* **2021,** *5* (9), 808-814.

14.   Skubi, K. L.; Blum, T. R.; Yoon, T. P., Dual Catalysis Strategies in Photochemical Synthesis. *Chemical Reviews* **2016,** *116* (17), 10035-10074.

15.   Tasker, S. Z.; Standley, E. A.; Jamison, T. F., Recent advances in homogeneous nickel catalysis. *Nature* **2014,** *509* (7500), 299-309.

16.   Hu, X.-Q.; Liu, Z.-K.; Hou, Y.-X.; Gao, Y., Single Electron Activation of Aryl Carboxylic Acids. *iScience* **2020,** *23* (7), 101266.

17.   Chu, L.; Ohta, C.; Zuo, Z.; MacMillan, D. W. C., Carboxylic Acids as A Traceless Activation Group for Conjugate Additions: A Three-Step Synthesis of (±)-Pregabalin. *Journal of the American Chemical Society* **2014,** *136* (31), 10886-10889.

18.   Kölmel, D. K.; Meng, J.; Tsai, M.-H.; Que, J.; Loach, R. P.; Knauber, T.; Wan, J.; Flanagan, M. E., On-DNA Decarboxylative Arylation: Merging Photoredox with Nickel Catalysis in Water. *ACS Combinatorial Science* **2019,** *21* (8), 588-597.

19.   Zuo, Z.; Ahneman, D. T.; Chu, L.; Terrett, J. A.; Doyle, A. G.; MacMillan, D. W. C., Merging photoredox with nickel catalysis: Coupling of α-carboxyl sp^3-carbons with aryl halides. *Science* **2014,** *345* (6195), 437-440.

20.   Noble, A.; McCarver, S. J.; MacMillan, D. W. C., Merging Photoredox and Nickel Catalysis: Decarboxylative Cross-Coupling of Carboxylic Acids with Vinyl Halides. *Journal of the American Chemical Society* **2015,** *137* (2), 624-627.

21.   Zuo, Z.; Cong, H.; Li, W.; Choi, J.; Fu, G. C.; MacMillan, D. W. C., Enantioselective Decarboxylative Arylation of α-Amino Acids via the Merger of Photoredox and Nickel Catalysis. *Journal of the American Chemical Society* **2016,** *138* (6), 1832-1835.

22.   Chu, L.; Lipshultz, J. M.; MacMillan, D. W. C., Merging Photoredox and Nickel Catalysis: The Direct Synthesis of Ketones by the Decarboxylative Arylation of α-Oxo Acids. *Angewandte Chemie International Edition* **2015,** *54* (27), 7929-7933.

23.   Johnston, C. P.; Smith, R. T.; Allmendinger, S.; MacMillan, D. W. C., Metallaphotoredox-catalysed sp3–sp3 cross-coupling of carboxylic acids with alkyl halides. *Nature* **2016,** *536* (7616), 322-325.

24.   Tellis, J. C.; Primer, D. N.; Molander, G. A., Single-electron transmetalation in organoboron cross-coupling by photoredox/nickel dual catalysis. *Science* **2014,** *345* (6195), 433-436.

25.   Gutierrez, O.; Tellis, J. C.; Primer, D. N.; Molander, G. A.; Kozlowski, M. C., Nickel-Catalyzed Cross-Coupling of Photoredox-Generated Radicals: Uncovering a General Manifold for Stereoconvergence in Nickel-Catalyzed Cross-Couplings. *Journal of the American Chemical Society* **2015,** *137* (15), 4896-4899.

26.   El Khatib, M.; Serafim, R. A. M.; Molander, G. A., α-Arylation/Heteroarylation of Chiral α-Aminomethyltrifluoroborates by Synergistic Iridium Photoredox/Nickel Cross-Coupling Catalysis. *Angewandte Chemie International Edition* **2016,** *55* (1), 254-258.

27.   Karakaya, I.; Primer, D. N.; Molander, G. A., Photoredox Cross-Coupling: Ir/Ni Dual Catalysis for the Synthesis of Benzylic Ethers. *Organic Letters* **2015,** *17* (13), 3294-3297.

28.   Tellis, J. C.; Amani, J.; Molander, G. A., Single-Electron Transmetalation: Photoredox/Nickel Dual Catalytic Cross-Coupling of Secondary Alkyl β-Trifluoroboratoketones and -esters with Aryl Bromides. *Organic Letters* **2016,** *18* (12), 2994-2997.

29.   Lima, F.; Kabeshov, M. A.; Tran, D. N.; Battilocchio, C.; Sedelmeier, J.; Sedelmeier, G.; Schenkel, B.; Ley, S. V., Visible Light Activation of Boronic Esters Enables Efficient Photoredox C(sp2)–C(sp3) Cross-Couplings in Flow. *Angewandte Chemie International Edition* **2016,** *55* (45), 14085-14089.

30.   Stache, E. E.; Rovis, T.; Doyle, A. G., Dual Nickel- and Photoredox-Catalyzed Enantioselective Desymmetrization of Cyclic meso-Anhydrides. *Angewandte Chemie International Edition* **2017,** *56* (13), 3679-3683.

31.   Matsui, J. K.; Gutiérrez-Bonet, Á.; Rotella, M.; Alam, R.; Gutierrez, O.; Molander, G. A., Photoredox/Nickel-Catalyzed Single-Electron Tsuji–Trost Reaction: Development and Mechanistic Insights. *Angewandte Chemie International Edition* **2018,** *57* (48), 15847-15851.

32.   Nawrat, C. C.; Jamison, C. R.; Slutskyy, Y.; MacMillan, D. W. C.; Overman, L. E., Oxalates as Activating Groups for Alcohols in Visible Light Photoredox Catalysis: Formation of Quaternary Centers by Redox-Neutral Fragment Coupling. *Journal of the American Chemical Society* **2015,** *137* (35), 11270-11273.

33.   Zhang, X.; MacMillan, D. W. C., Alcohols as Latent Coupling Fragments for Metallaphotoredox Catalysis: sp3–sp2 Cross-Coupling of Oxalates with Aryl Halides. *Journal of the American Chemical Society* **2016,** *138* (42), 13862-13865.

34.   Huang, L.; Ji, T.; Rueping, M., Remote Nickel-Catalyzed Cross-Coupling Arylation via Proton-Coupled Electron Transfer-Enabled C–C Bond Cleavage. *Journal of the American Chemical Society* **2020,** *142* (7), 3532-3539.

35.   Cong, F.; Lv, X.-Y.; Day, C. S.; Martin, R., Dual Catalytic Strategy for Forging sp2–sp3 and sp3–sp3 Architectures via β-Scission of Aliphatic Alcohol Derivatives. *Journal of the American Chemical Society* **2020,** *142* (49), 20594-20599.

36.   Chen, Y.; Wang, X.; He, X.; An, Q.; Zuo, Z., Photocatalytic Dehydroxymethylative Arylation by Synergistic Cerium and Nickel Catalysis. *Journal of the American Chemical Society* **2021,** *143* (13), 4896-4902.

37.   Alandini, N.; Buzzetti, L.; Favi, G.; Schulte, T.; Candish, L.; Collins, K. D.; Melchiorre, P., Amide Synthesis by Nickel/Photoredox-Catalyzed Direct Carbamoylation of (Hetero)Aryl Bromides. *Angewandte Chemie International Edition* **2020,** *59* (13), 5248-5253.

38.   Gandolfo, E.; Tang, X.; Raha Roy, S.; Melchiorre, P., Photochemical Asymmetric Nickel-Catalyzed Acyl Cross-Coupling. *Angewandte Chemie International Edition* **2019,** *58* (47), 16854-16858.

39.   Gutiérrez-Bonet, Á.; Tellis, J. C.; Matsui, J. K.; Vara, B. A.; Molander, G. A., 1,4-Dihydropyridines as Alkyl Radical Precursors: Introducing the Aldehyde Feedstock to Nickel/Photoredox Dual Catalysis. *ACS Catalysis* **2016,** *6* (12), 8004-8008.

40.   Corcé, V.; Chamoreau, L.-M.; Derat, E.; Goddard, J.-P.; Ollivier, C.; Fensterbank, L., Silicates as Latent Alkyl Radical Precursors: Visible-Light Photocatalytic Oxidation of Hypervalent Bis-Catecholato Silicon Compounds. *Angewandte Chemie International Edition* **2015,** *54* (39), 11414-11418.

41.   Knauber, T.; Chandrasekaran, R.; Tucker, J. W.; Chen, J. M.; Reese, M.; Rankic, D. A.; Sach, N.; Helal, C., Ru/Ni Dual Catalytic Desulfinative Photoredox Csp2–

Csp3 Cross-Coupling of Alkyl Sulfinate Salts and Aryl Halides. *Organic Letters* **2017,** *19* (24), 6566-6569.

42.   Wencel-Delord, J.; Glorius, F., C–H bond activation enables the rapid construction and late-stage diversification of functional molecules. *Nature Chemistry* **2013,** *5* (5), 369-375.

43.   Dinnocenzo, J. P.; Banach, T. E., Deprotonation of tertiary amine cation radicals. A direct experimental approach. *Journal of the American Chemical Society* **1989,** *111* (23), 8646-8653.

44.   Su, Z.; Falvey, D. E.; Yoon, U. C.; Mariano, P. S., The Dynamics of α-Anilino Carboxylate and Related Cation Radical α-Heterolytic Fragmentations. *Journal of the American Chemical Society* **1997,** *119* (22), 5261-5262.

45.   McNally, A.; Prier, C. K.; MacMillan, D. W. C., Discovery of an alpha-Amino C-H Arylation Reaction Using the Strategy of Accelerated Serendipity. *Science* **2011,** *334* (6059), 1114-1117.

46.   Ahneman, D. T.; Doyle, A. G., C–H functionalization of amines with aryl halides by nickel-photoredox catalysis. *Chemical Science* **2016,** *7* (12), 7002-7006.

47.   Gui, Y.-Y.; Wang, Z.-X.; Zhou, W.-J.; Liao, L.-L.; Song, L.; Yin, Z.-B.; Li, J.; Yu, D.-G., Arylation of Aniline C(sp3)−H Bonds with Phenols via an In Situ Activation Strategy. *Asian Journal of Organic Chemistry* **2018,** *7* (3), 537-541.

48.   Joe, C. L.; Doyle, A. G., Direct Acylation of C(sp3)−H Bonds Enabled by Nickel and Photoredox Catalysis. *Angewandte Chemie International Edition* **2016,** *55* (12), 4040-4043.

49.   P. Roberts, B., Polarity-reversal catalysis of hydrogen-atom abstraction reactions: concepts and applications in organic chemistry. *Chemical Society Reviews* **1999,** *28* (1), 25-35.

50.   Maity, B.; Zhu, C.; Yue, H.; Huang, L.; Harb, M.; Minenkov, Y.; Rueping, M.; Cavallo, L., Mechanistic Insight into the Photoredox-Nickel-HAT Triple Catalyzed Arylation and Alkylation of α-Amino Csp3–H Bonds. *Journal of the American Chemical Society* **2020,** *142* (40), 16942-16952.

51.   Shields, B. J.; Doyle, A. G., Direct C(sp3)–H Cross Coupling Enabled by Catalytic Generation of Chlorine Radicals. *Journal of the American Chemical Society* **2016,** *138* (39), 12719-12722.

52.   Ackerman, L. K. G.; Martinez Alvarado, J. I.; Doyle, A. G., Direct C–C Bond Formation from Alkanes Using Ni-Photoredox Catalysis. *Journal of the American Chemical Society* **2018,** *140* (43), 14059-14063.

53.   Nielsen, M. K.; Shields, B. J.; Liu, J.; Williams, M. J.; Zacuto, M. J.; Doyle, A. G., Mild, Redox-Neutral Formylation of Aryl Chlorides through the Photocatalytic Generation of Chlorine Radicals. *Angewandte Chemie International Edition* **2017,** *56* (25), 7191-7194.

54.   Hwang, S. J.; Powers, D. C.; Maher, A. G.; Anderson, B. L.; Hadt, R. G.; Zheng, S.-L.; Chen, Y.-S.; Nocera, D. G., Trap-Free Halogen Photoelimination from Mononuclear Ni(III) Complexes. *Journal of the American Chemical Society* **2015,** *137* (20), 6472-6475.

55.   Call, A.; Codolà, Z.; Acuña-Parés, F.; Lloret-Fillol, J., Photo- and Electrocatalytic H2 Production by New First-Row Transition-Metal Complexes Based on an Aminopyridine Pentadentate Ligand. *Chemistry – A European Journal* **2014,** *20* (20), 6171-6183.

56.   Call, A.; Franco, F.; Kandoth, N.; Fernández, S.; González-Béjar, M.; Pérez-Prieto, J.; Luis, J. M.; Lloret-Fillol, J., Understanding light-driven H2 evolution through the electronic tuning of aminopyridine cobalt complexes. *Chemical Science* **2018,** *9* (9), 2609-2619.

57.   Call, A.; Lloret-Fillol, J., Enhancement and control of the selectivity in light-driven ketone versus water reduction using aminopyridine cobalt complexes. *Chemical Communications* **2018,** *54* (69), 9643-9646.

58.   Kärkäs, M. D.; Verho, O.; Johnston, E. V.; Åkermark, B., Artificial Photosynthesis: Molecular Systems for Catalytic Water Oxidation. *Chemical Reviews* **2014,** *114* (24), 11863-12001.

59.   Eckenhoff, W. T.; McNamara, W. R.; Du, P.; Eisenberg, R., Cobalt complexes as artificial hydrogenases for the reductive side of water splitting. *Biochimica et Biophysica Acta (BBA) - Bioenergetics* **2013,** *1827* (8), 958-973.

60.   Wang, F.; Cao, B.; To, W.-P.; Tse, C.-W.; Li, K.; Chang, X.-Y.; Zang, C.; Chan, S. L.-F.; Che, C.-M., The effects of chelating N4 ligand coordination on Co(ii)-catalysed photochemical conversion of CO2 to CO: reaction mechanism and DFT calculations. *Catalysis Science & Technology* **2016,** *6* (20), 7408-7420.

61.	Fernández, S.; Franco, F.; Casadevall, C.; Martin-Diaconescu, V.; Luis, J. M.; Lloret-Fillol, J., A Unified Electro- and Photocatalytic CO2 to CO Reduction Mechanism with Aminopyridine Cobalt Complexes. *Journal of the American Chemical Society* **2020,** *142* (1), 120-133.

62.	Fernández, S.; Cañellas, S.; Franco, F.; Luis, J. M.; Pericàs, M. À.; Lloret-Fillol, J., The Dual Effect of Coordinating −NH Groups and Light in the Electrochemical CO2 Reduction with Pyridylamino Co Complexes. *ChemElectroChem* **2021,** *8* (23), 4456-4465.

63.	Kräutler, B., Vitamin B12: chemistry and biochemistry. *Biochem Soc Trans* **2005,** *33* (Pt 4), 806-10.

64.	Hill, H. A. O.; Pratt, J. M.; O'Riordan, M. P.; Williams, F. R.; Williams, R. J. P., The chemistry of vitamin B12. Part XV. Catalysis of alkyl halide reduction by vitamin B12a: studies using controlled potential reduction. *Journal of the Chemical Society A: Inorganic, Physical, Theoretical* **1971,** (0), 1859-1862.

65.	Zhong, J.-J.; Meng, Q.-Y.; Liu, B.; Li, X.-B.; Gao, X.-W.; Lei, T.; Wu, C.-J.; Li, Z.-J.; Tung, C.-H.; Wu, L.-Z., Cross-Coupling Hydrogen Evolution Reaction in Homogeneous Solution without Noble Metals. *Organic Letters* **2014,** *16* (7), 1988-1991.

66.	Cao, H.; Jiang, H.; Feng, H.; Kwan, J. M. C.; Liu, X.; Wu, J., Photo-induced Decarboxylative Heck-Type Coupling of Unactivated Aliphatic Acids and Terminal Alkenes in the Absence of Sacrificial Hydrogen Acceptors. *Journal of the American Chemical Society* **2018,** *140* (47), 16360-16367.

67.	Tian, W.-F.; Hu, C.-H.; He, K.-H.; He, X.-Y.; Li, Y., Visible-Light Photoredox-Catalyzed Decarboxylative Alkylation of Heteroarenes Using Carboxylic Acids with Hydrogen Release. *Organic Letters* **2019,** *21* (17), 6930-6935.

68.	Zhang, G.; Zhang, L.; Yi, H.; Luo, Y.; Qi, X.; Tung, C.-H.; Wu, L.-Z.; Lei, A., Visible-light induced oxidant-free oxidative cross-coupling for constructing allylic sulfones from olefins and sulfinic acids. *Chemical Communications* **2016,** *52* (68), 10407-10410.

69.	Thullen, S. M.; Rovis, T., A Mild Hydroaminoalkylation of Conjugated Dienes Using a Unified Cobalt and Photoredox Catalytic System. *Journal of the American Chemical Society* **2017,** *139* (43), 15504-15508.

70.	Rai, P.; Maji, K.; Maji, B., Photoredox/Cobalt Dual Catalysis for Visible-Light-Mediated Alkene–Alkyne Coupling. *Organic Letters* **2019,** *21* (10), 3755-3759.

71.   Molander, G. A.; Traister, K. M.; O'Neill, B. T., Reductive Cross-Coupling of Nonaromatic, Heterocyclic Bromides with Aryl and Heteroaryl Bromides. *The Journal of Organic Chemistry* **2014,** *79* (12), 5771-5780.

72.   Bhonde, V. R.; O'Neill, B. T.; Buchwald, S. L., An Improved System for the Aqueous Lipshutz–Negishi Cross-Coupling of Alkyl Halides with Aryl Electrophiles. *Angewandte Chemie International Edition* **2016,** *55* (5), 1849-1853.

73.   Everson, D. A.; Weix, D. J., Cross-Electrophile Coupling: Principles of Reactivity and Selectivity. *The Journal of Organic Chemistry* **2014,** *79* (11), 4793-4798.

74.   Lekkala, R.; Lekkala, R.; Moku, B.; Rakesh, K. P.; Qin, H.-L., Recent Developments in Radical-Mediated Transformations of Organohalides. *European Journal of Organic Chemistry* **2019,** *2019* (17), 2769-2806.

75.   Studer, A.; Curran, D. P., Catalysis of Radical Reactions: A Radical Chemistry Perspective. *Angewandte Chemie International Edition* **2016,** *55* (1), 58-102.

76.   Zhang, P.; Le, C. C.; MacMillan, D. W. C., Silyl Radical Activation of Alkyl Halides in Metallaphotoredox Catalysis: A Unique Pathway for Cross-Electrophile Coupling. *Journal of the American Chemical Society* **2016,** *138* (26), 8084-8087.

77.   Smith, R. T.; Zhang, X.; Rincón, J. A.; Agejas, J.; Mateos, C.; Barberis, M.; García-Cerrada, S.; de Frutos, O.; MacMillan, D. W. C., Metallaphotoredox-Catalyzed Cross-Electrophile Csp3–Csp3 Coupling of Aliphatic Bromides. *Journal of the American Chemical Society* **2018,** *140* (50), 17433-17438.

78.   Constantin, T.; Zanini, M.; Regni, A.; Sheikh, N. S.; Juliá, F.; Leonori, D., Aminoalkyl radicals as halogen-atom transfer agents for activation of alkyl and aryl halides. *Science* **2020,** *367* (6481), 1021-1026.

79.   Ye, S.; Xiang, T.; Li, X.; Wu, J., Metal-catalyzed radical-type transformation of unactivated alkyl halides with C–C bond formation under photoinduced conditions. *Organic Chemistry Frontiers* **2019,** *6* (13), 2183-2199.

80.   Lambert, F. L.; Ingall, G. B., Voltammetry of organic halogen compounds. IV. The reduction of organic chlorides at the vitreous (glassy) carbon electrode. *Tetrahedron Letters* **1974,** *15* (36), 3231-3234.

81.   Connell, T. U.; Fraser, C. L.; Czyz, M. L.; Smith, Z. M.; Hayne, D. J.; Doeven, E. H.; Agugiaro, J.; Wilson, D. J. D.; Adcock, J. L.; Scully, A. D.; Gómez, D. E.; Barnett, N. W.; Polyzos, A.; Francis, P. S., The Tandem Photoredox Catalysis Mechanism

of [Ir(ppy)2(dtb-bpy)]+ Enabling Access to Energy Demanding Organic Substrates. *Journal of the American Chemical Society* **2019,** *141* (44), 17646-17658.

82.   Shon, J.-H.; Sittel, S.; Teets, T. S., Synthesis and Characterization of Strong Cyclometalated Iridium Photoreductants for Application in Photocatalytic Aryl Bromide Hydrodebromination. *ACS Catalysis* **2019,** *9* (9), 8646-8658.

83.   Lowry, M. S.; Bernhard, S., Synthetically Tailored Excited States: Phosphorescent, Cyclometalated Iridium(III) Complexes and Their Applications. *Chemistry – A European Journal* **2006,** *12* (31), 7970-7977.

84.   Askey, H. E.; Grayson, J. D.; Tibbetts, J. D.; Turner-Dore, J. C.; Holmes, J. M.; Kociok-Kohn, G.; Wrigley, G. L.; Cresswell, A. J., Photocatalytic Hydroaminoalkylation of Styrenes with Unprotected Primary Alkylamines. *Journal of the American Chemical Society* **2021,** *143* (39), 15936-15945.

85.   Maji, T.; Karmakar, A.; Reiser, O., Visible-Light Photoredox Catalysis: Dehalogenation of Vicinal Dibromo-, α-Halo-, and α,α-Dibromocarbonyl Compounds. *The Journal of Organic Chemistry* **2011,** *76* (2), 736-739.

86.   Neumann, M.; Füldner, S.; König, B.; Zeitler, K., Metal-Free, Cooperative Asymmetric Organophotoredox Catalysis with Visible Light. *Angewandte Chemie International Edition* **2011,** *50* (4), 951-954.

87.   Narayanam, J. M. R.; Tucker, J. W.; Stephenson, C. R. J., Electron-Transfer Photoredox Catalysis: Development of a Tin-Free Reductive Dehalogenation Reaction. *Journal of the American Chemical Society* **2009,** *131* (25), 8756-8757.

88.   Pirtsch, M.; Paria, S.; Matsuno, T.; Isobe, H.; Reiser, O., [Cu(dap)2Cl] As an Efficient Visible-Light-Driven Photoredox Catalyst in Carbon–Carbon Bond-Forming Reactions. *Chemistry – A European Journal* **2012,** *18* (24), 7336-7340.

89.   Zeng, G.; Li, Y.; Qiao, B.; Zhao, X.; Jiang, Z., Photoredox asymmetric catalytic enantioconvergent substitution of 3-chlorooxindoles. *Chemical Communications* **2019,** *55* (76), 11362-11365.

90.   Föll, T.; Rehbein, J.; Reiser, O., Ir(ppy)3-Catalyzed, Visible-Light-Mediated Reaction of α-Chloro Cinnamates with Enol Acetates: An Apparent Halogen Paradox. *Organic Letters* **2018,** *20* (18), 5794-5798.

91.   Li, C.-G.; Xu, G.-Q.; Xu, P.-F., Synthesis of Fused Pyran Derivatives via Visible-Light-Induced Cascade Cyclization of 1,7-Enynes with Acyl Chlorides. *Organic Letters* **2017,** *19* (3), 512-515.

92.   Wang, C.-M.; Song, D.; Xia, P.-J.; Wang, J.; Xiang, H.-Y.; Yang, H., Visible-Light-Promoted Synthesis of 1,4-Dicarbonyl Compounds via Conjugate Addition of Aroyl Chlorides. *Chemistry – An Asian Journal* **2018,** *13* (3), 271-274.

93.   Chang, R.; Fang, J.; Chen, J.-Q.; Liu, D.; Xu, G.-Q.; Xu, P.-F., Visible Light-Mediated Direct C–H Aroylation and Alkylation of Heteroarenes. *ACS Omega* **2019,** *4* (9), 14021-14031.

94.   Michelet, B.; Deldaele, C.; Kajouj, S.; Moucheron, C.; Evano, G., A General Copper Catalyst for Photoredox Transformations of Organic Halides. *Organic Letters* **2017,** *19* (13), 3576-3579.

95.   Liang, K.; Li, T.; Li, N.; Zhang, Y.; Shen, L.; Ma, Z.; Xia, C., Redox-neutral photochemical Heck-type arylation of vinylphenols activated by visible light. *Chemical Science* **2020,** *11* (8), 2130-2135.

96.   Senaweera, S.; Weaver, J. D., Dual C–F, C–H Functionalization via Photocatalysis: Access to Multifluorinated Biaryls. *Journal of the American Chemical Society* **2016,** *138* (8), 2520-2523.

97.   Schmalzbauer, M.; Ghosh, I.; König, B., Utilising excited state organic anions for photoredox catalysis: activation of (hetero)aryl chlorides by visible light-absorbing 9-anthrolate anions. *Faraday Discussions* **2019,** *215* (0), 364-378.

98.   Jiang, M.; Li, H.; Yang, H.; Fu, H., Room-Temperature Arylation of Thiols: Breakthrough with Aryl Chlorides. *Angewandte Chemie International Edition* **2017,** *56* (3), 874-879.

99.   Yin, H.; Carroll, P. J.; Anna, J. M.; Schelter, E. J., Luminescent Ce(III) Complexes as Stoichiometric and Catalytic Photoreductants for Halogen Atom Abstraction Reactions. *Journal of the American Chemical Society* **2015,** *137* (29), 9234-9237.

100.   Qiu, G.; Li, Y.; Wu, J., Recent developments for the photoinduced Ar–X bond dissociation reaction. *Organic Chemistry Frontiers* **2016,** *3* (8), 1011-1027.

101.   Steiner, A.; Williams, J. D.; Rincón, J. A.; de Frutos, O.; Mateos, C.; Kappe, C. O., Implementing Hydrogen Atom Transfer (HAT) Catalysis for Rapid and Selective Reductive Photoredox Transformations in Continuous Flow. *European Journal of Organic Chemistry* **2019,** *2019* (33), 5807-5811.

102.   Tyagi, A.; Yamamoto, A.; Yoshida, H., Photocatalytic Ullmann coupling of aryl halides by a novel blended catalyst consisting of a TiO2 photocatalyst and an Al2O3

supported Pd–Au bimetallic catalyst. *Catalysis Science & Technology* **2018,** *8* (23), 6196-6203.

103.	Ghosh, I.; Ghosh, T.; Bardagi, J. I.; König, B., Reduction of aryl halides by consecutive visible light-induced electron transfer processes. *Science* **2014,** *346* (6210), 725-728.

104.	Li, D.; Che, C.-M.; Kwong, H.-L.; Yam, V. W.-W., Photoinduced C–C bond formation from alkyl halides catalysed by luminescent dinuclear gold(I) and copper(I) complexes. *Journal of the Chemical Society, Dalton Transactions* **1992,** (23), 3325-3329.

105.	Ratani, T. S.; Bachman, S.; Fu, G. C.; Peters, J. C., Photoinduced, Copper-Catalyzed Carbon–Carbon Bond Formation with Alkyl Electrophiles: Cyanation of Unactivated Secondary Alkyl Chlorides at Room Temperature. *Journal of the American Chemical Society* **2015,** *137* (43), 13902-13907.

106.	Buxton, G. V.; Greenstock, C. L.; Helman, W. P.; Ross, A. B., Critical Review of rate constants for reactions of hydrated electrons, hydrogen atoms and hydroxyl radicals (·OH/·O− in Aqueous Solution. *Journal of Physical and Chemical Reference Data* **1988,** *17* (2), 513-886.

107.	Naumann, R.; Kerzig, C.; Goez, M., Laboratory-scale photoredox catalysis using hydrated electrons sustainably generated with a single green laser. *Chemical Science* **2017,** *8* (11), 7510-7520.

108.	Naumann, R.; Lehmann, F.; Goez, M., Generating Hydrated Electrons for Chemical Syntheses by Using a Green Light-Emitting Diode (LED). *Angewandte Chemie International Edition* **2018,** *57* (4), 1078-1081.

109.	Naumann, R.; Goez, M., A Green-LED Driven Source of Hydrated Electrons Characterized from Microseconds to Hours and Applied to Cross-Couplings. *Chemistry – A European Journal* **2018,** *24* (39), 9833-9840.

110.	Giedyk, M.; Narobe, R.; Weiß, S.; Touraud, D.; Kunz, W.; König, B., Photocatalytic activation of alkyl chlorides by assembly-promoted single electron transfer in microheterogeneous solutions. *Nature Catalysis* **2020,** *3* (1), 40-47.

111.	Kim, H.; Kim, H.; Lambert, T. H.; Lin, S., Reductive Electrophotocatalysis: Merging Electricity and Light To Achieve Extreme Reduction Potentials. *Journal of the American Chemical Society* **2020,** *142* (5), 2087-2092.

112. Cowper, N. G. W.; Chernowsky, C. P.; Williams, O. P.; Wickens, Z. K., Potent Reductants via Electron-Primed Photoredox Catalysis: Unlocking Aryl Chlorides for Radical Coupling. *Journal of the American Chemical Society* **2020,** *142* (5), 2093-2099.

113. Shimakoshi, H.; Tokunaga, M.; Baba, T.; Hisaeda, Y., Photochemical dechlorination of DDT catalyzed by a hydrophobic vitamin B12 and a photosensitizer under irradiation with visible light. *Chemical Communications* **2004,** (16), 1806-1807.

114. Chen, L.; Kametani, Y.; Imamura, K.; Abe, T.; Shiota, Y.; Yoshizawa, K.; Hisaeda, Y.; Shimakoshi, H., Visible light-driven cross-coupling reactions of alkyl halides with phenylacetylene derivatives for C(sp3)–C(sp) bond formation catalyzed by a B12 complex. *Chemical Communications* **2019,** *55* (87), 13070-13073.

115. Chen, L.; Hisaeda, Y.; Shimakoshi, H., Visible Light-Driven, Room Temperature Heck-Type Reaction of Alkyl Halides with Styrene Derivatives Catalyzed by B12 Complex. *Advanced Synthesis & Catalysis* **2019,** *361* (12), 2877-2884.

116. Patel, N. R.; Kelly, C. B.; Jouffroy, M.; Molander, G. A., Engaging Alkenyl Halides with Alkylsilicates via Photoredox Dual Catalysis. *Organic Letters* **2016,** *18* (4), 764-767.

117. Fan, P.; Lan, Y.; Zhang, C.; Wang, C., Nickel/Photo-Cocatalyzed Asymmetric Acyl-Carbamoylation of Alkenes. *Journal of the American Chemical Society* **2020,** *142* (5), 2180-2186.

118. Levernier, E.; Corcé, V.; Rakotoarison, L.-M.; Smith, A.; Zhang, M.; Ognier, S.; Tatoulian, M.; Ollivier, C.; Fensterbank, L., Cross coupling of alkylsilicates with acyl chlorides via photoredox/nickel dual catalysis: a new synthesis method for ketones. *Organic Chemistry Frontiers* **2019,** *6* (9), 1378-1382.

119. Claros, M.; Ungeheuer, F.; Franco, F.; Martin-Diaconescu, V.; Casitas, A.; Lloret-Fillol, J., Reductive Cyclization of Unactivated Alkyl Chlorides with Tethered Alkenes under Visible-Light Photoredox Catalysis. *Angewandte Chemie International Edition* **2019,** *58* (15), 4869-4874.

120. Sakai, H. A.; Liu, W.; Le, C. C.; MacMillan, D. W. C., Cross-Electrophile Coupling of Unactivated Alkyl Chlorides. *Journal of the American Chemical Society* **2020,** *142* (27), 11691-11697.

121. Mazzarella, D.; Magagnano, G.; Schweitzer-Chaput, B.; Melchiorre, P., Photochemical Organocatalytic Borylation of Alkyl Chlorides, Bromides, and Sulfonates. *ACS Catalysis* **2019,** *9* (7), 5876-5880.

CHAPTER II:

Main Objectives and Summary of Chapters

UNIVERSITAT ROVIRA I VIRGILI
VISIBLE-LIGHT METALLAPHOTOREDOX STRATEGIES FOR ORGANIC TRANSFORMATIONS THROUGH THE CLEAVAGE
OF CSP3-CL BONDS
Jordi Aragón Artigas

Organic chlorides are prevailing in both biologically active molecules and ready commercially available feedstocks in organic synthesis. The astonishing grown of photoredox protocols has expanded the library of bench-stable radical precursors for implementing new C−C and C−X strategies. However, the chemical inertness of chloroalkanes still hinders their extensive and broad use as electrophiles in cross-coupling methodologies. Previous studies of the group introduced the understanding of the reactivity of multidentate low-valent first row metal complexes against unactivated alkyl chlorides under photocatalytic conditions.

Based on these premises, the main aim of the current thesis are:

i) the development of new metallaphotoredox systems based on first row transition metals for the photocatalytic cleavage of Csp^3−Cl bonds,

ii) the implementation of new photoredox cross-coupling methodologies based on the activation of inert Csp^3−Cl bonds,

iii) understanding the reaction mechanism of the developed photoredox cross-coupling.

To this end, the rational design of the catalyst architecture and the study of the mechanism have played a crucial role in the development of novel organic transformations. The knowledge gained will aid in advancing the state-of-the-art of light-driven catalyzed cross-coupling reactions using apparently inert feedstocks.

Specifically, the tesis opens (*Chapter III*) with the synthesis and characterization of a family of eighteen tetradentate aminopyridine metal complexes: nine cobalt-based complexes and the corresponding nine nickel-based complexes. Then, we have studied their catalytic response in photoredox activation of different alkyl chlorides to stablish a rational relation between structure and catalytic activity.

M = Co, Ni R_1 = H, CO$_2$Et, MeO R_2 = H, Me
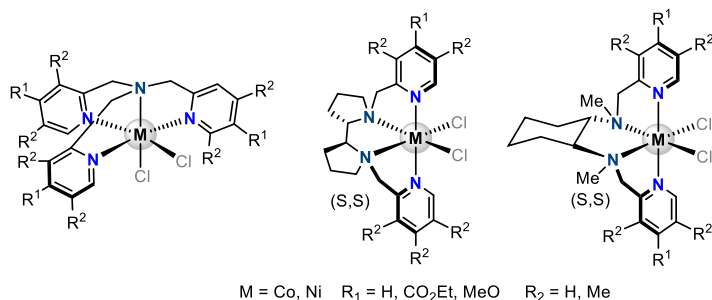
Figure 2. 1. Family of tetradentate N-based aminopyridine metal complexes, *Chapter III*.

The main project of this thesis is encompassed in *Chapter IV*, with the optimization and development of a new photoredox cross-coupling of unactivated alkyl chlorides with alkenes. This methodology may be considered as the first general protocol based on the use of inert primary chloroalkanes as coupling partners under mild conditions. We have performed an exhaustive study of the mechanism of this reaction, combining several techniques such as UV-Vis absorption and emission spectroscopy, electronic paramagnetic resonance (EPR), radical clock and deuterium labelling experiments. We envision that this study can be a significant upgrade in the field of photoredox catalysis.
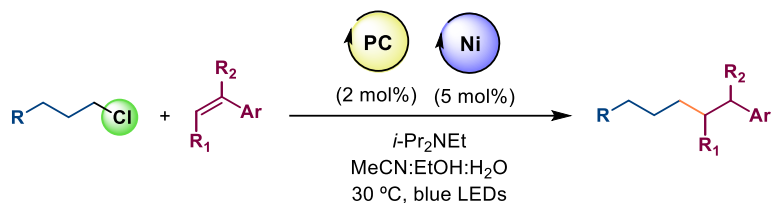
J. Aragón *et. al.*, *Angew. Chem. Int. Ed.* **2022**, e202114365 (DOI: 10.1002/anie.202114365)
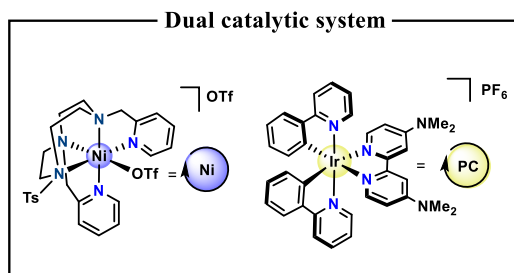
Figure 2. 2. Photoredox activation of inert alkyl chlorides for the reductive cross-coupling with alkenes, *Chapter IV*.

Chapter V takes the concepts showed in *Chapter III* and *Chapter IV*, developing a new metallaphotoredox strategy for the functionalization of olefins through the activation of common and inert chlorinated solvents. We have stablished a tuneable system capable of activate dichloromethane, serving as a C_1 synthon in the cyclopropanation of alkenes or as a chloromethyl units forming alkyl chlorides. Similarly, chloroform is also used as a substrate for the dichlorination of aromatic olefins. In that case we have performed UV-Vis absorption and emission spectroscopy, cyclic voltammetry, spectroelectrochemistry and deuterium labelling experiments to give insights into the reaction mechanism.
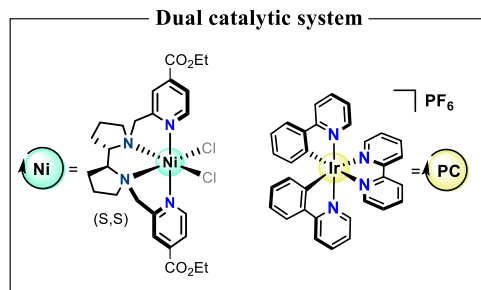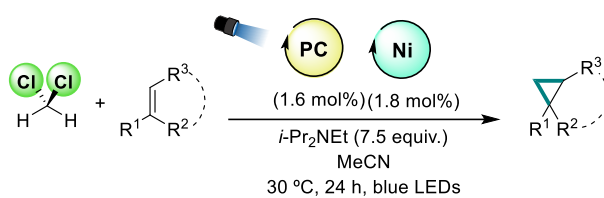
Figure 2. 3. Photoredox activation of CH_2Cl_2 for the cyclopropanation of alkenes, *Chapter V*.

Chapter III:

Development of a new family of N-based Ni and Co complexes for the activation of Csp^3-Cl bonds

UNIVERSITAT ROVIRA I VIRGILI
VISIBLE-LIGHT METALLAPHOTOREDOX STRATEGIES FOR ORGANIC TRANSFORMATIONS THROUGH THE CLEAVAGE
OF CSP3-CL BONDS
Jordi Aragón Artigas

3.1. State of the art

Chemistry and biological systems have a deep connection helping one each other to progress. For instance, chemistry served to understand how biological systems work by furnishing the needed chemical tools and the understanding of biological processes brings inspiration for new advances in chemistry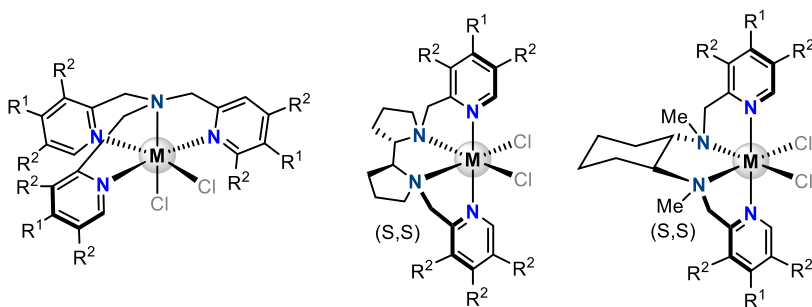. In this sense, biomimetic chemistry is defined as the development of new chemical approaches based on the principles used by nature.[1] Enzymes are a simple example in this transfer of knowledge, since many of the catalytic methodologies are mimicking them. The metal-carbon (M−C) bond in enzymatic processes was first revealed in 1948 with cofactor B_{12} (5'-deoxy-5'-adenosylcobalamin, *AdoCbl*), a cobalt complex with corrin ligand, a unique member of the natural tetrapyrroles.[2]

The biological importance of *B_{12}*-dependent enzymes resides in its involvement in reactions such as dehalogenations, methyl transfer and group rearrangements through the cleavage and formation of the M–C bond from the cobalt corrin cofactor. The unique environment offered by the corrin ligand reaches reduced cobalt species, acting such us "supernucleophiles", forming the Co–C bond, which can be cleaved under electrocatalytic, photocatalytic or thermal conditions in a controlled manner to furnish highly reactive radical carbon species. This property highlights their practicality as catalyst in the development of organic catalytic strategies (Scheme 3.1).[3, 4] In this regard, the nickel-based F_{430} from methyl coenzyme M reductase (MCR) is another biologically relevant cofactor. This Ni^I complex can activate alkyl halides by means of its high nucleophilicity.[5-7] The reactivity of these two cofactors is based on the same key concepts: i) reduced monovalent cobalt and nickel complexes bearing highly nucleophilic ligands activates potential electrophiles (alkyl halides, acyl halides, alkenes, epoxides…) forming M^{III}–C complexes, and ii) the homolytic cleavage

of this M^{III}-C bond under photo-, electro- or thermolytic conditions releases carbon-centered radicals.[7-10]
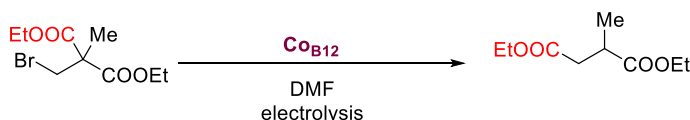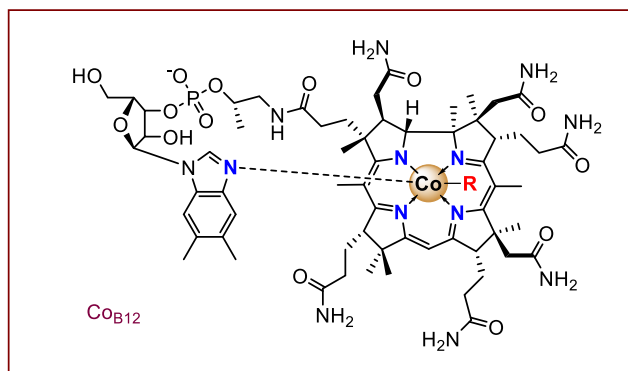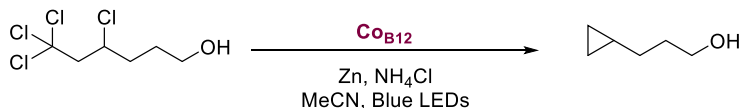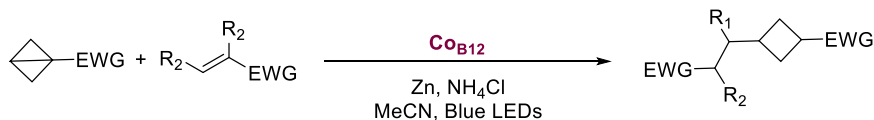
Scheme 3. 1. Synthetic and catalytic relevance of cofactor B_{12}.

The high impact of these biological systems in organometallic chemistry and catalysis aimed the community to further develop new first-row transition-metal complexes with a nucleophilic environment. In that direction, the development of

systems based on aminopyridine ligands emerged as versatile and tuneable versions of the mentioned cofactors, maintaining the same key concepts. Despite the first examples of aminopyridine cobalt complexes from Peters, Fujita and Fukuzumi among others were based on the reduction of protons to hydrogen (Figure 3. 1), they served as basis for next reaction approaches.[11-15]
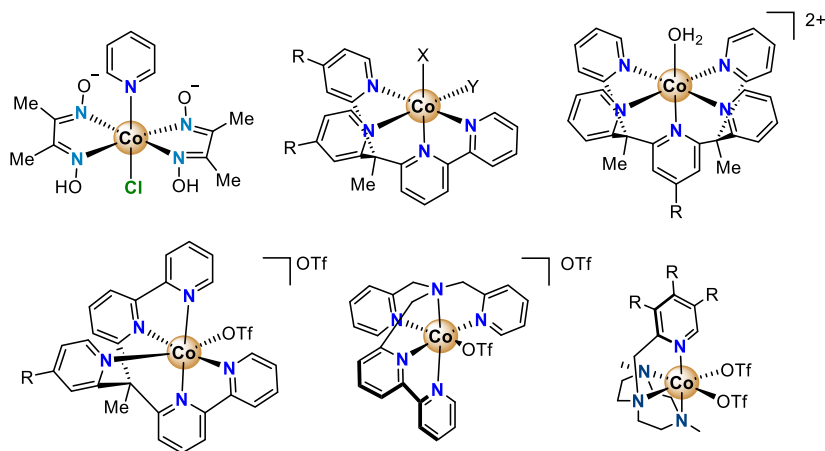
Figure 3. 1. Selected aminopyridine-cobalt complexes used in water reduction.

In 2014, our group contributed to the field with a photocatalytic reduction of water by cobalt complexes based on **Py_2^{Ts}tacn** (1,4-di(picolyl)-7-(*p*-toluenesulfonyl)-1,4,7-triazacyclononane) as aminopyridyl scaffold.[16, 17] The triazacyclononane (**tacn**) moiety stabilizes high oxidation states at metal center due to the reaction mechanism due to its highly electron-donating behavior. The addition of electron-withdrawing substituents (tosyl group) decreases the ligand stabilization and favor the low oxidation states but preserves the high chelating nature of the moiety. The merge of this Co catalyst with and iridium-based photocatalyst reaches a low-valent Co^I complex by a single-electron transfer (SET) from the reduced iridium photocatalyst (Scheme 3. 2). A subsequent protonation generates a Co^{III}–H intermediate and further reduction and protonation releases H_2 as product. The application of this rational system for the

selective photocatalytic reduction of organic substrates such as ketones, aldehydes and olefins show the effectivity of the aminopyridil cobalt complexes using light as a source of energy and water as the source of protons.[18, 19] The implementation of a copper photocatalyst instead of iridium and the tuneability of **Py$_2$^{Ts}tacn** moiety by the introduction of substituents in the pyridine ring showed the robustness and versatility of the system towards high value organic transformations. Returning to the initial concept of supernucleophilic species, this low-valent metal complex reached by **Py$_2$^{Ts}tacn** are active against electrophiles such alkyl halides, similarly than previous biological entities. In this regard, M. Claros *et. al.* developed the first photoredox activation of inert chloroalkanes for their reductive cyclization with pendant alkenes, using cobalt and nickel metal centers, been the nickel complex superior in terms of selectivity and yields.[20] The incapability of the photogenerated Ni^I to reduce protons to form Ni^{III}−H resulted beneficial to enhancement its reactivity as supernucleophile against alkyl chlorides, in comparison with its Co analog.
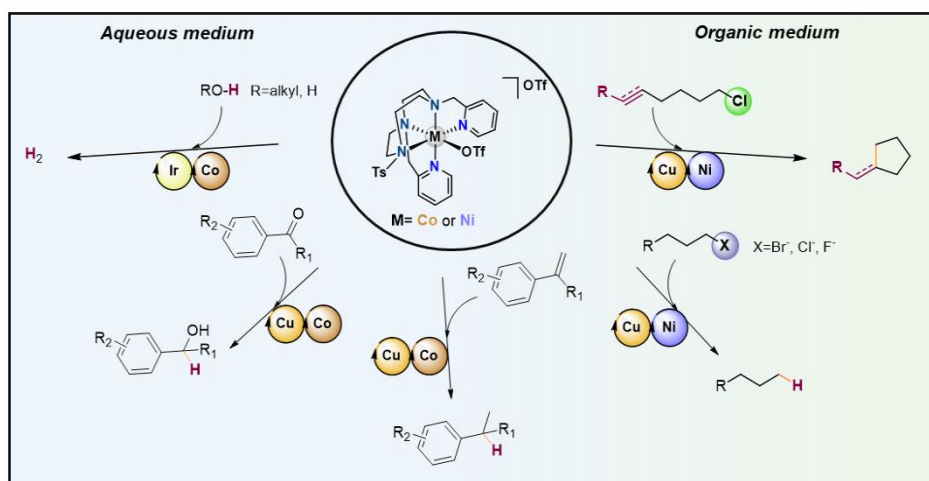
Scheme 3. 2. Photoredox catalytic methodologies developed by our research group using Py$_2$^{Ts}tacn ligand, before the current thesis.

The powerful of **Py$_2$^{Ts}tacn** as ligand and their corresponding first-row metal complexes was evidenced. Despite the excellent and versatile reactivity observed, the pentadentate ligand presents some challenges for the development of new and efficient organic methodologies: i) the synthesis of **Py$_2$^{Ts}tacn** is not efficient, following an expensive protocol of several steps with low atom economy ii) the complex presents only one free coordination position, limiting the reactivity, and iii) the discovery of enantiomeric reactions remains limited due to the chirality of the ligand environment.

In this chapter, we rationally design potential alternatives to the **Py$_2$^{Ts}tacn** moiety, trying to overcome its limitations without losing its reactive essence. We explored three different tetradentate scaffolds maintaining the combination of an amine backbone with pyridine moieties: tris(2-pyridylmethyl)amine (**TPA**), N,N-bispyridine-cyclohexyldiamine (**MCP**) and N,N-bispyridine-bispyrrolidine backbone (**PDP**). Up to now, these ligands are widely extend and used in oxidation chemistry, mainly with iron and manganese centers. The coordination chemistry of **TPA** with several metals was firstly reported in 1977.[21] For example, the iron complex served as synthetic model for the rationallization of some enzyme in alkene epoxidations.[22, 23] **PDP** was used first by C. White in 2007, reporting a tetradentate Fe^{II} catalyst capable of undergo C-H oxidations.[24] The relevance of this ligand resides in the stabilization of electrophilic high-valent metal-oxo intermediates, which together with the bulky environtment lead to stereoselective oxygen atom transfer. Regarding these properties, **PDP** and **tacn** shows similar effect to the metal center. Moreover, the tuning of the electronic properties of the ligand has a crucial effect into the metal center, as reported by M. Costas for epoxidation of alkenes[25] and C−H oxidations using high-valent Fe and Mn metal centers.[26, 27] These modifications are focused on the addition of substituents in the pyridine ring, revealing them as straightforward and versatile protocols for developing and controlling reactivity from different scaffolds by adding substituents in the pyridine ring (Figure 3. 2). They concluded that the

success of these ligands corresponds to both strong ligand−metal binding and resistance to oxidative degradation and (acid) hydrolysis.
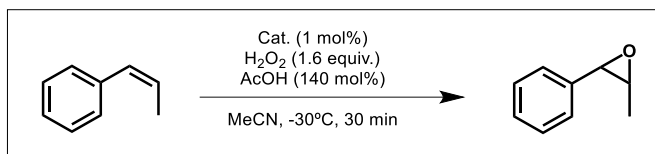
M. Costas and co-workers, *J. Am. Chem. Soc.* **2013**, 135, 14871−14878

	NMe₂	OMe	Me		Cl	CO₂Et
Conv. (%)	100	64	44	57	61	44
Yield (%)	85	37	27	33	38	27
ee (%)	61	39	31	15	21	19

Figure 3. 2. Asymmetric epoxidation by tuning of electronic properties of non-heme iron catalysts.

Although the use of these scaffolds for the stabilization of low-valent metal complexes is contraintuitive, the reactivity offered by **Py₂^{Ts}tacn** reaching Co^I and Ni^I glimpses a parallel reactivity with the proposed tetradentate scaffold. The application of inherent nucleophilicity of this Co^I and Ni^I complexes in photo- and electrocatalytic CO_2 reduction processes aims their use *versus* electrophiles and reductive transformations (Scheme 3. 3).[28-30] However, we still miss an exhaustive study of the electronic properties of the ligand and the exploitation of these tetradentate aminopyridine complexes for catalytic organic transformations such as activation of inert alkyl halides, mimicking the previously presented cofactors.
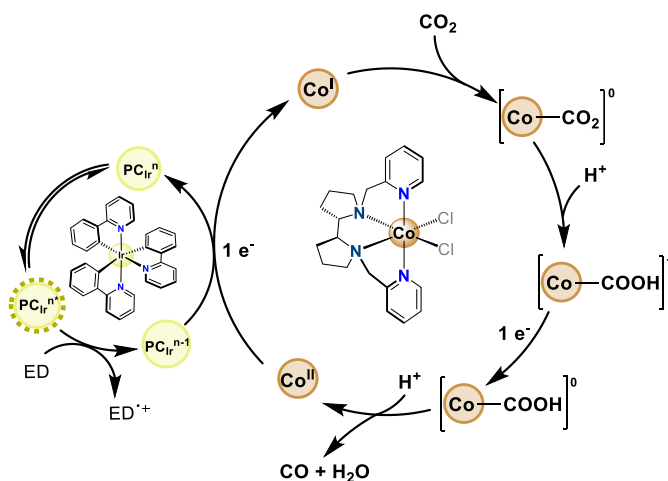
Scheme 3. 3. Selected example of photocatalytic CO_2 reduction by low valent state of (PDP)CoCl$_2$. Proposed mechanism under photochemical conditions.

3.2. Results and Discussion

We performed the synthesis and characterization of eighteen tetracoordinated N-based nickel and cobalt complexes. Then, we incorporated them in a photocatalytic dual system for undergoing different organic transformations involving the cleavage of inert $Csp^3−Cl$ bonds. To complete the study, we tried to stablish a structure/activity relationship by: i) evaluating their catalytic activity in a photocatalytic dual system involving the cleavage of inert $Csp^3−Cl$ bonds, ii) monitoring their catalytic activity in hydrogen evolution as main side reaction, and iii) study of the initial rates for **(^{X}PDP)NiCl$_2$**.

3.2.1. Synthesis and characterization of tetradentated N-based Cobalt complexes

We chose three different moieties as tetradentated N-based aminopyridine ligands (Scheme 3. 4): tris(2-pyridylmethyl)amine scaffold (**^{X}TPA**) and (S,S)-bis-pyridine ligands based on a (S,S)-cyclohexyldiamine (**^{X}MCP**) or bispyrrolidine backbone (**^{X}PDP**), where X refeered to the substituents in the pyridine ring (X= H, CO$_2$Et or DMM). The preparation of ligands **^{x}TPA** (X = H,[31] DMM[24]), **^{x}PDP** (H,[25] DMM,[22] CO$_2$Et[22]) and **^{x}MCP** (H, DMM)[22] was accomplished to a literature known procedures and ligands **^{CO2Et}TPA** and **^{CO2Et}PDP** were prepared following similar synthetic pathways.We have prepared a library of 9 well-defined coordination Co^{II} complexes. These complexes were synthesized by the equimolar reaction of tetradentate ligand (**^{x}TPA**, **^{x}PDP**, **^{x}MCP**) with CoCl$_2$ in a THF solution. Removal of the solvent under vacuum and recrystallization by Et$_2$O diffusion into dichloromethane or acetonitrile solutions yielded the targeted complexes as crystalline materials in good yields (40-96%) (Scheme 3. 4). Complexes (**^{H}TPA)CoCl$_2$**,[29] (**^{H}PDP)CoCl$_2$**,[30] (**^{H}MCP)CoCl$_2$**[32] have been previously described, while complexes (**^{CO2Et}TPA)CoCl$_2$**, (**^{DMM}TPA)CoCl$_2$**, (**^{DMM}PDP)CoCl$_2$**, (**^{CO2Et}PDP)CoCl$_2$**, (**^{DMM}MCP)CoCl$_2$**, (**^{CO2Et}MCP)CoCl$_2$** are described for the first time in this work.
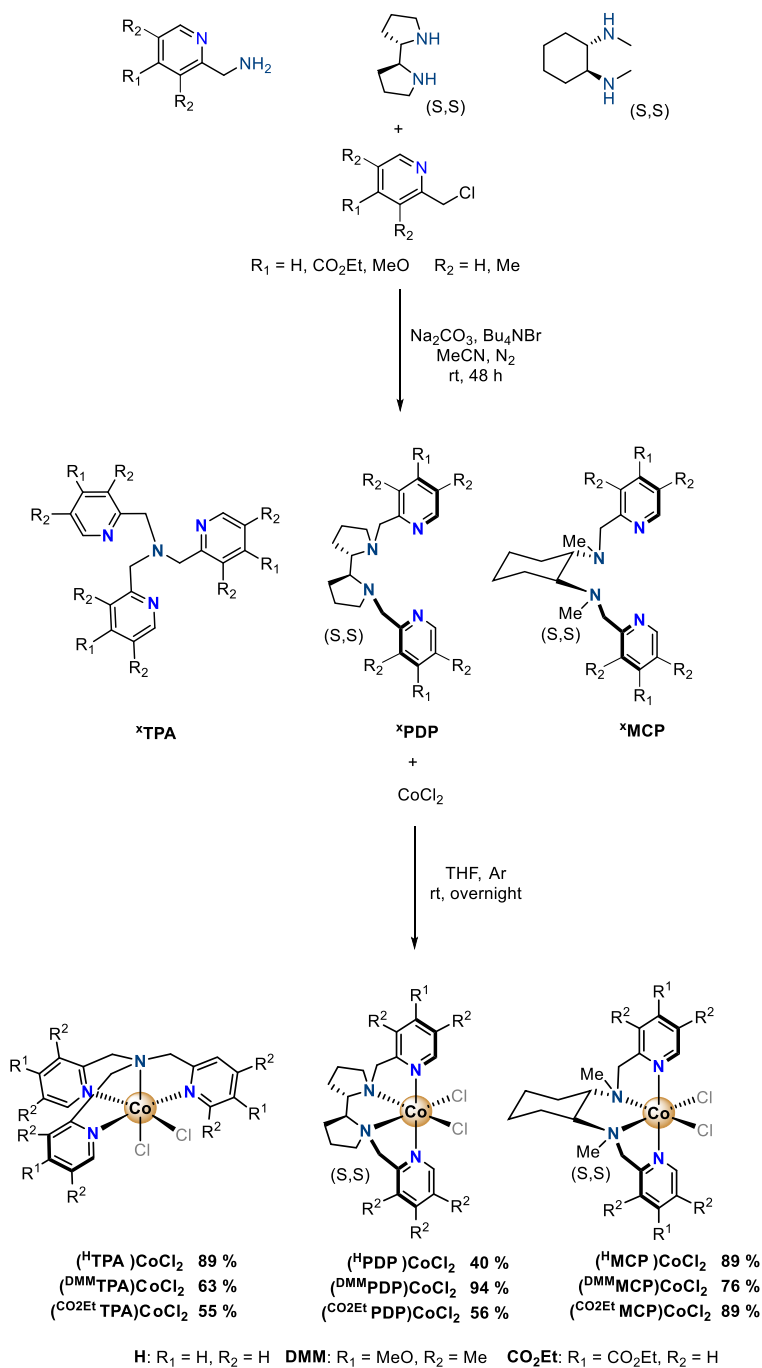
Scheme 3. 4. Synthesis of tetradentate N-based aminopyridine ligands and their corresponding Co complexes.

The use of chlorides as counteranions was not trivial. Generally our research group used labile counteranions such as triflates to minimize potential ligand exchange problems.[16, 18, 20] However, direct reaction of **PDP** or **MCP** ligand with metal triflates generally yielded the mixture of two topological isomers: *cis-α* and *cis-β* (Figure 3. 3). The rigid backbone of these ligands does not allow the formation of the trans isomer. This isomerization takes place during the reaction of coordination and depends on the metal salt source employed. Despite the expected lability of 1st row metal complex in low-valent states, like iron, cobalt and nickel, once the isomers are formed, the geometry exchange is not kinetically favor.[33] In this sense, chloride anions from the metal source present larger *trans* effect than triflates, locating themselves in *trans* position to amines, yielding the *cis-α* isomer. The obtention of pure and defined *cis-α* isomer, with C_2 symmetry, simplified the characterization and the understanding of their reactivity, avoiding different catalytic activity from the other isomer.[34]
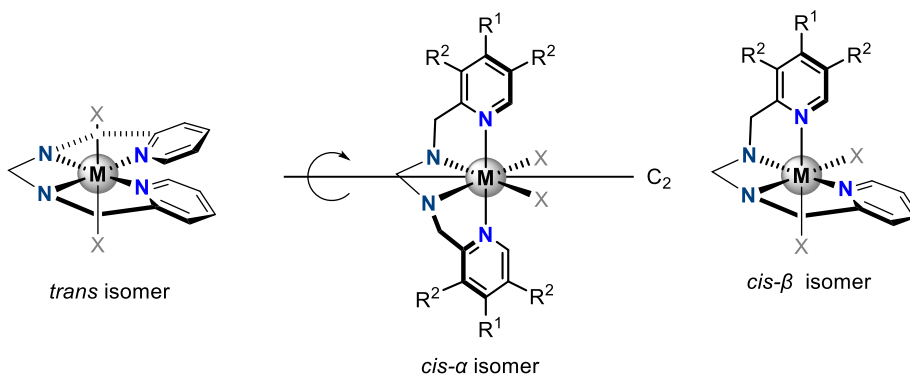

Figure 3. 3. Topological isomerism of PDP and MCP based metal complexes.

All complexes were fully characterized by ^{1}H-NMR spectroscopy, single crystal X-ray diffraction crystallography, FTIR spectroscopy, UV-Vis absorption spectroscopy, high-resolution mass spectrometry and elemental analysis.

3.2.1.1. Characterization in solution

The Co^{II} complexes were characterized in solution by means of ^{1}H-NMR spectroscopy. Since Co^{II} complexes are paramagnetic species, they present a fast nuclear relaxation (short T_1) with a line broadening around 2-50 Hz consistent with Co^{II} high spin complexes, larger than the spin-spin coupling constant. The ^{1}H-NMR spectra at room temperature of all the complexes are collected in the Experimental Section 3.4.4 and 3.4.5. The Co^{II} complexes exhibit spectra windows ranged from -14 to 240 ppm, which agrees with $t_{2g}^5 eg^2$ or $t_{2g}^6 e_g^1$ configuration of octahedral Co^{II} paramagnetic species. The unpaired electrons in d-orbitals of Co^{II} complexes are responsible of the paramagnetic behavior. Paramagnetism derives from atoms, molecules, or ions possessing a permanent magnetic moment associated with unpaired electron spins, acting as a magnetic dipoles which have random orientations without the influence of a magnetic field. The magnetic susceptibility is the measure of how a compound/material become magnetized in an applied magnetic field. The prevalence of paramagnetism against diamagnetism in front of a magnetic field is the paramagnetic susceptibility, where $\chi_m = \chi_{dia} + \chi_{para}$ is such that $\chi_{para} > |\chi_{dia}|$. In this sense, the Curie-Weiss law describes the dependance of the paramagnetic susceptibility with temperature. This phenomenon can be studied by ^{1}H NMR. The most shifted the signal the more affected the proton by the paramagnetic center of the complex. Therefore, considering the chemical shift, together with the different substitution pattern in the pyridine moiety, allowed us to propose the assignment of the H^α protons of the pyridine to this paramagnetic signal (Figure 3. 4).
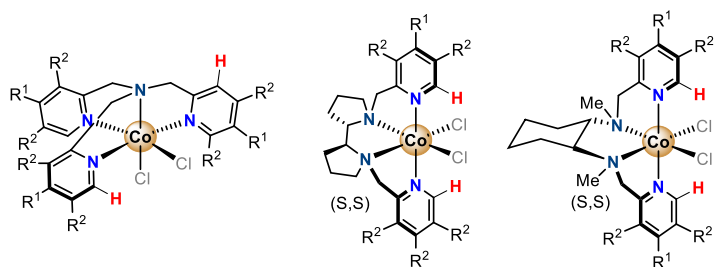
Figure 3. 4. Representation of the Hᵃ of the pyridine moiety of our complexes.

Then, the chemical shift of H^α should be linearly dependent on the 1/T, in concordance with Curie-Weiss law. We performed paramagnetic ^1H NMR at different temperature (243 – 293 K) for each complex for the study of their paramagnetic susceptibility (Figure 3.5 – Figure 3.13).
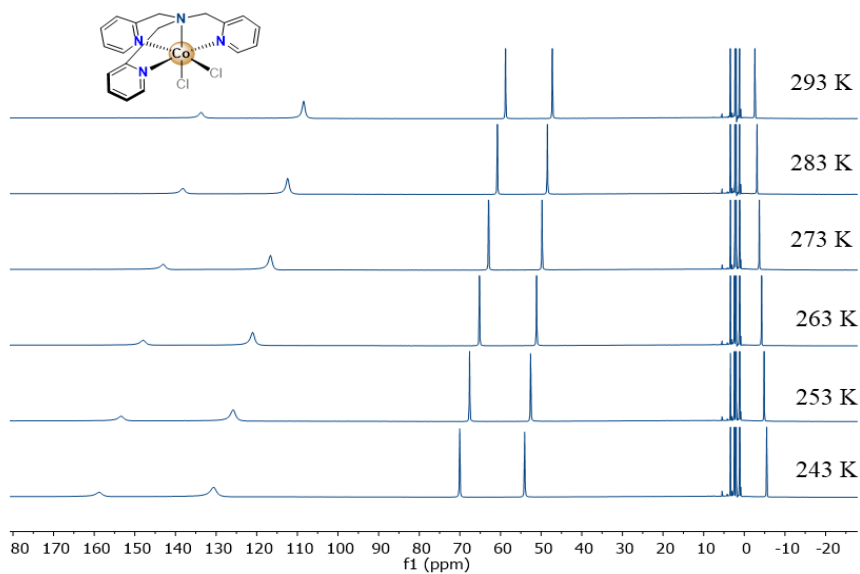
Figure 3. 5. ^{1}H-NMR spectrum of (**ᴴTPA**)**CoCl₂** in CD₃CN at variable temperatures.
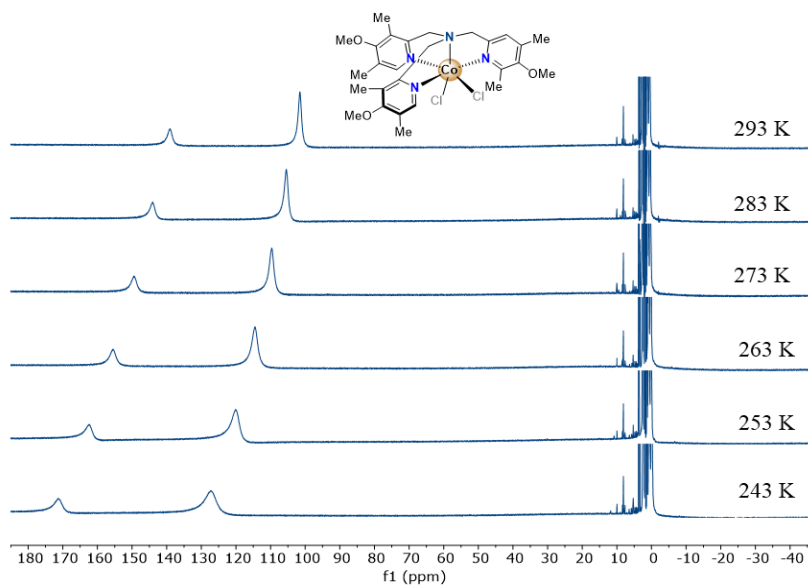
Figure 3. 6. ^{1}H-NMR spectrum of (^{DMM}**TPA**)**CoCl$_2$** in CD$_3$CN at variable temperatures.
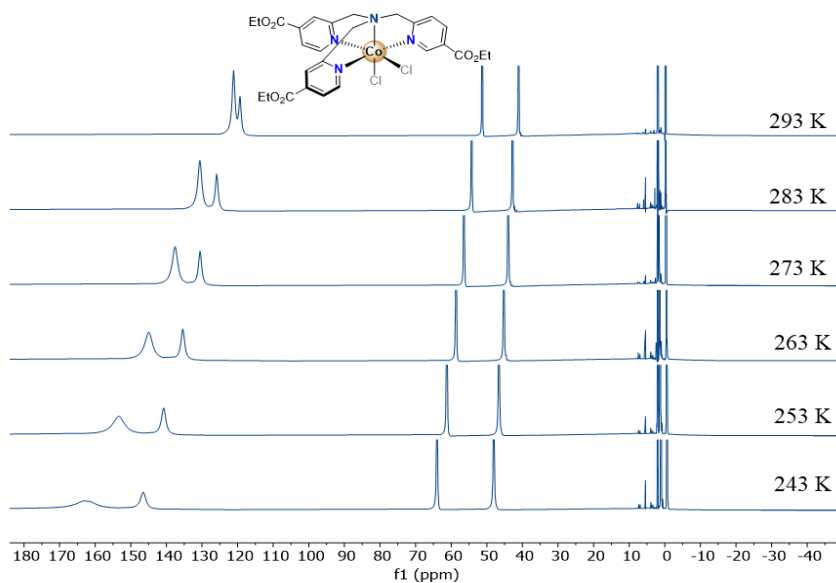
Figure 3. 7. ^{1}H-NMR spectrum of (^{CO2Et}**TPA**)**CoCl$_2$** in CD$_3$CN at variable temperatures.
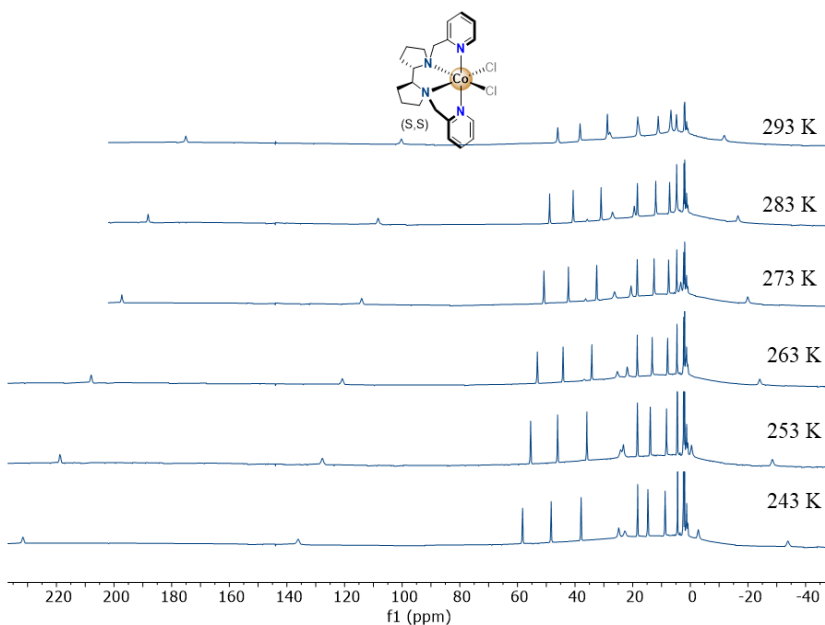
Figure 3. 8. ^{1}H-NMR spectrum of (**^{H}PDP)CoCl$_2$** in CD$_3$CN at variable temperatures.
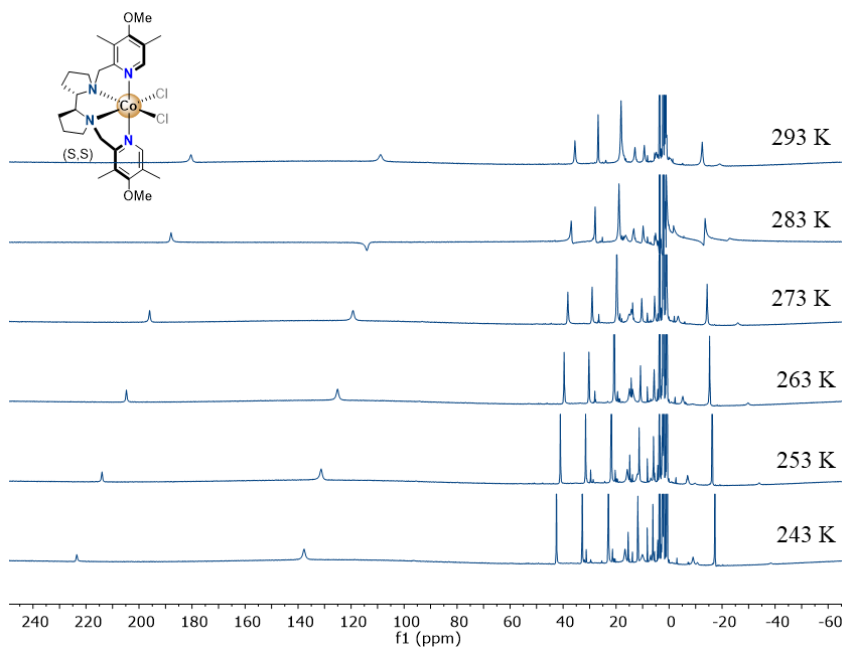
Figure 3. 9. ^{1}H-NMR spectrum of (**^{DMM}PDP)CoCl$_2$** in CD$_3$CN at variable temperatures.
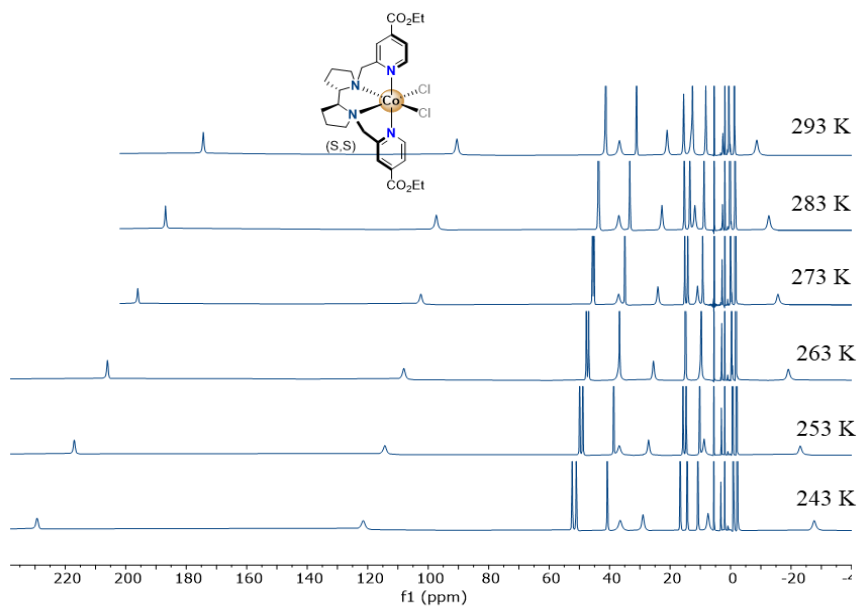
Figure 3. 10. ^{1}H-NMR spectrum of **(^{CO2Et}PDP)CoCl$_2$** in CD$_3$CN at variable temperatures.
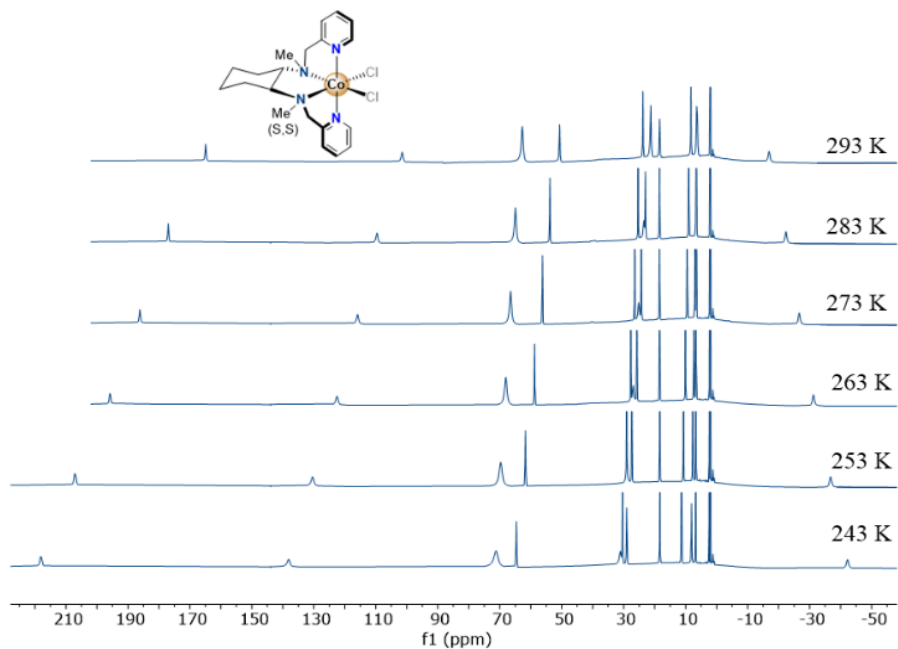
Figure 3. 11. ^{1}H-NMR spectrum of **(^{H}MCP)CoCl$_2$** in CD$_3$CN at variable temperatures.
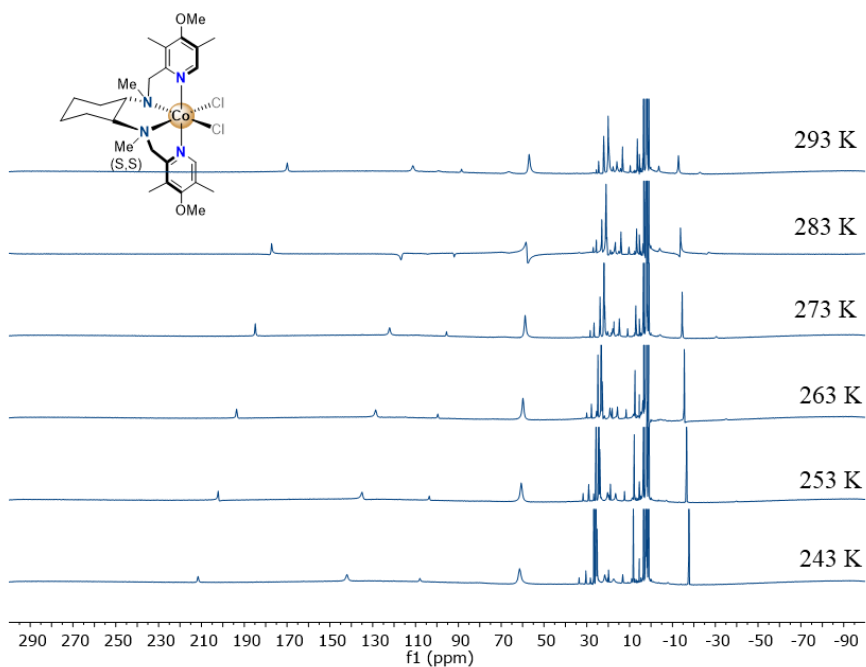
Figure 3. 12. ^{1}H-NMR spectrum of (^{DMM}**MCP**)**CoCl$_2$** in CD$_3$CN at variable temperatures.
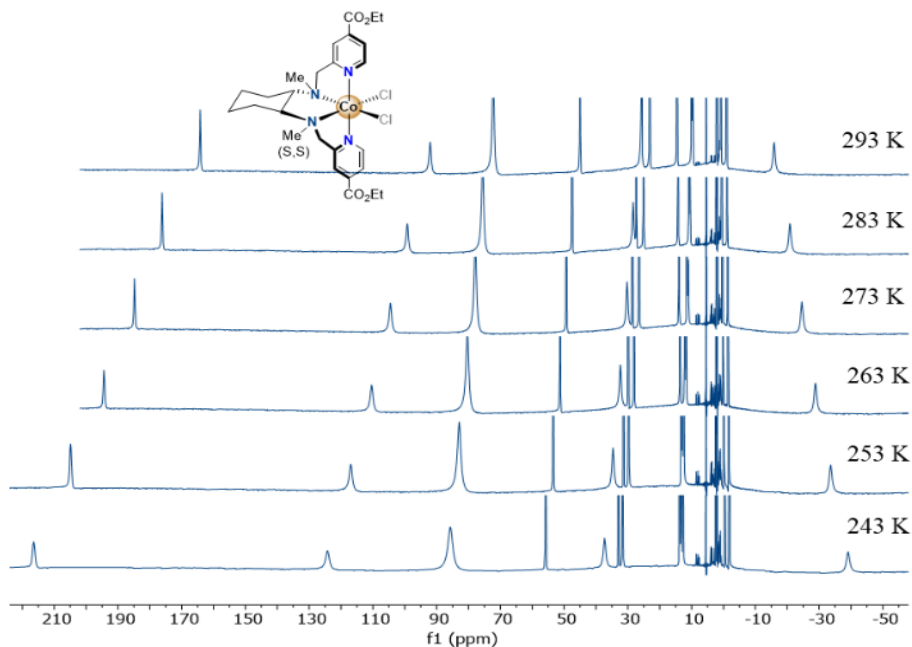
Figure 3. 13. ^{1}H-NMR spectrum of (^{CO2Et}**MCP**)**CoCl$_2$** in CD$_3$CN at variable temperatures.

In general terms, all protons found in the paramagnetic region of the spectrum exhibit a chemical shift linearly dependent on 1/T, consistent with Curie's law, which indicates that there is not a clear spin change in this temperature range (Figure 3. 14).[35]
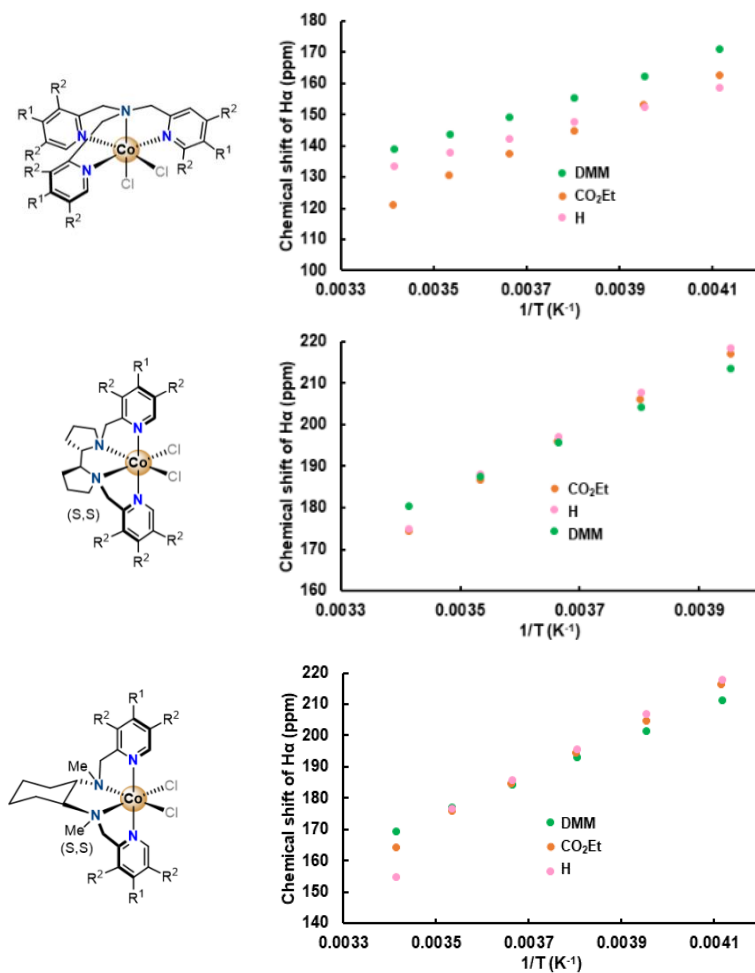
Figure 3. 14. Representation of the chemical shift of aromatic proton (Hᵃ) of tetradentated cobalt complexes in front of temperature in the ¹H-NMR spectrum in CD₃CN.

Although the previous procedure did not show a spin-crossover event between 293 K – 243 K, we could not determine the electronic configuration of octahedral Co^{II} paramagnetic complexes $(t_{2g}^5 e_g^2$ or $t_{2g}^6 e_g^1)$. Evans method is another appropriate and well-known procedure that allows the elucidation of the electronic configuration of paramagnetic compounds by NMR.[36, 37] The method is based on the fact that the resonance condition (magnetic field, frequency) in a NMR experiment for a given nucleus depends upon the volume susceptibility of the medium surrounding the nucleus. Inside a dry-box, a $CD_3CN:CH_2Cl_2$ (200:1) solution of precise amount of Co^{II} complex was prepared and placed in a NMR tube. A coaxial reference capillary filled with the same solvent system was then inserted inside the sample tube. Owing to the different volume susceptibility of the two solutions the protons of CH_2Cl_2 in the two compartments were differently shielded (Figure 3. 15).
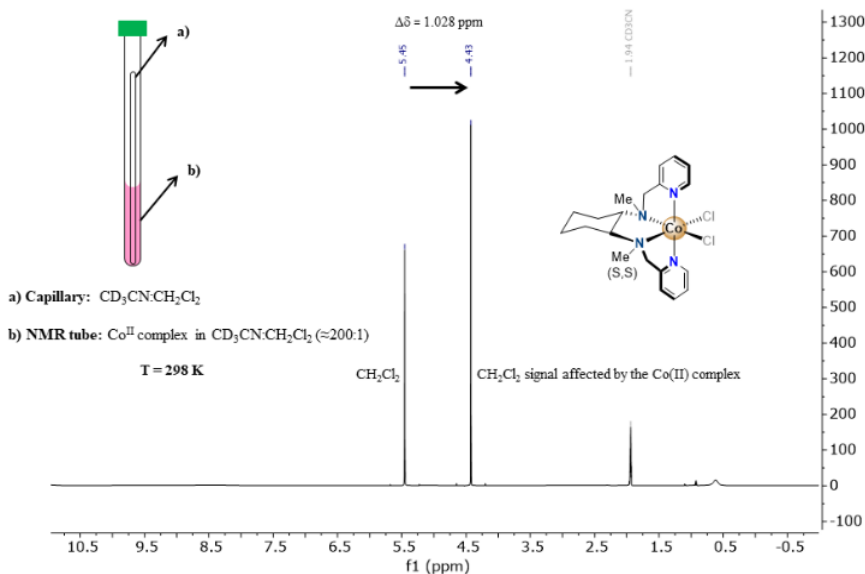
Figure 3. 15. Example of determination of magnetic moment by Evans method.

The magnetic susceptibility (χ_m) correlates with this paramagnetic shift by $\chi_m = (-3\Delta\delta \cdot 10^{-6})/(4\pi \cdot c)$ (where $\Delta\delta$ is the paramagnetic shift of the solvent in ppm and c is the concentration of the metal complex). Once we determined χ_m, the effective magnetic moment was calculated from the equation $\mu_{eff} = 2.828 (\chi_m T)^{1/2}$, where T is the temperature of the experiment. Finally, we aproximated the unpaired electron of the complex from $N = 1 + (1 + \mu_{eff}^2)^{1/2}$ (Table 3. 1).

Table 3. 1. Determination of unpaired electrons (N) for the Co^{II} complexes by Evans method.

Complex	$\Delta\delta$	mg	Cm	χ_m	μ_{eff}	N
(^{H}TPA)CoCl$_2$	0.9940	10.2	$3.4677 \cdot 10^{-5}$	$6.8432 \cdot 10^{-3}$	4.0385	**3.16**
(^{DMM}TPA)CoCl$_2$	0.7512	10.9	$2.6195 \cdot 10^{-5}$	$6.8463 \cdot 10^{-3}$	4.0394	**3.16**
(^{CO2Et}TPA)CoCl$_2$	0.657	10.3	$2.3121 \cdot 10^{-5}$	$6.7837 \cdot 10^{-3}$	4.0209	**3.14**
(^{H}PDP)CoCl$_2$	0.987	10.1	$3.1901 \cdot 10^{-5}$	$7.3863 \cdot 10^{-3}$	4.1956	**3.31**
(^{DMM}PDP)CoCl$_2$	0.7296	10.1	$2.5382 \cdot 10^{-5}$	$6.8623 \cdot 10^{-3}$	4.0441	**3.17**
(^{CO2Et}PDP)CoCl$_2$	0.7414	10.2	$2.4431 \cdot 10^{-5}$	$7.2447 \cdot 10^{-3}$	4.1552	**3.27**
(^{H}MCP)CoCl$_2$	1.0283	10.3	$3.2388 \cdot 10^{-5}$	$7.5796 \cdot 10^{-3}$	4.2502	**3.37**
(^{DMM}MCP)CoCl$_2$	0.8497	10.7	$2.6795 \cdot 10^{-5}$	$7.5701 \cdot 10^{-3}$	4.2476	**3.36**
(^{CO2Et}MCP)CoCl$_2$	0.6745	10.0	$2.3871 \cdot 10^{-5}$	$6.7455 \cdot 10^{-3}$	4.0095	**3.13**

Following this procedure, we estimated three unpaired electrons for all the tetradentated aminopyridine N-based Co^{II} complexes. This result corresponds to an electronic configuration of $t_{2g}^5 e_g^2$, remaining unaltered in the range of 243 – 293 K, without a spin-crossover event.
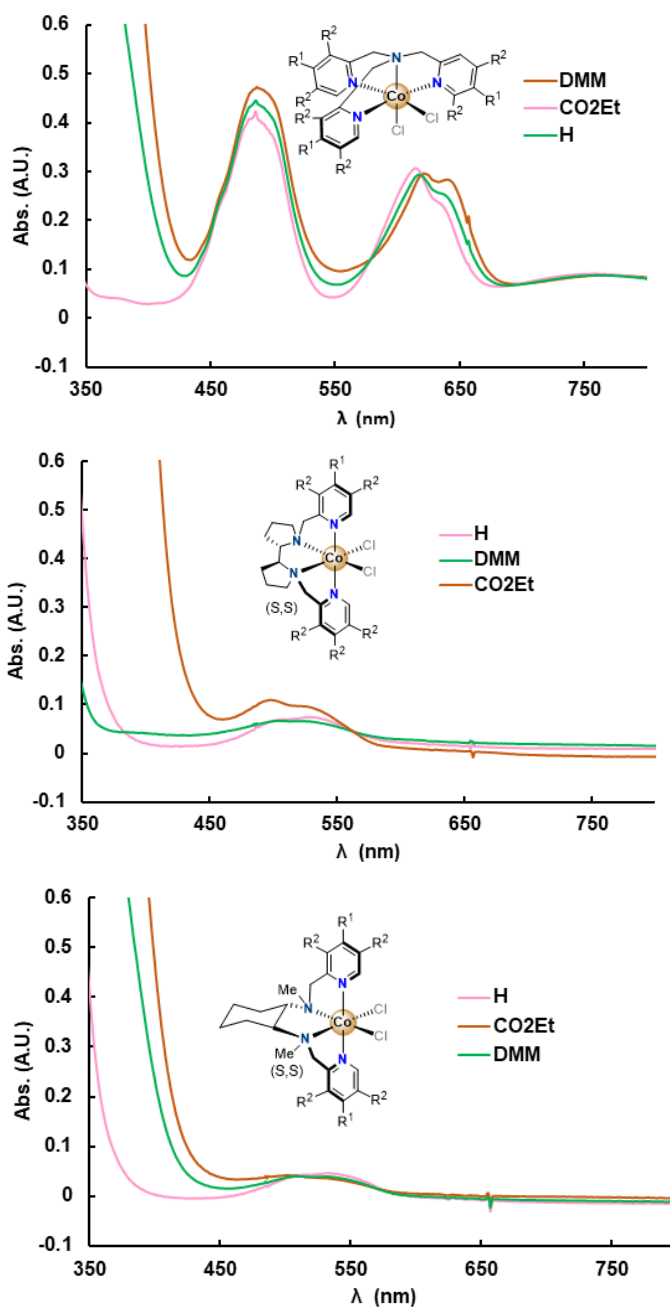
Figure 3. 16. UV-vis absorption spectra of Co^{II} complexes. (^{H}**TPA)CoCl$_2$** (2.1 mM, ε_{max} = 243 and 152 $M^{-1}cm^{-1}$), (^{DMM}**TPA)CoCl$_2$** (1.9 mM, ε_{max} = 240 and 149 $M^{-1}cm^{-1}$), (^{CO2Et}**TPA)CoCl$_2$** (2.3 mM, ε_{max} = 253 and 163 $M^{-1}cm^{-1}$), (^{H}**PDP)CoCl$_2$** (2.4 mM, ε_{max} = 28 $M^{-1}cm^{-1}$), (^{DMM}**PDP)CoCl$_2$** (2.1 mM, ε_{max} = 33 $M^{-1}cm^{-1}$), (^{CO2Et}**PDP)CoCl$_2$** (2.0 mM, ε_{max} = 46 $M^{-1}cm^{-1}$), (^{H}**MCP)CoCl$_2$** (2.1 mM, ε_{max} = 18 $M^{-1}cm^{-1}$), (^{DMM}**MCP)CoCl$_2$** (2.1 mM, ε_{max} = 21 $M^{-1}cm^{-1}$) and (^{CO2Et}**MCP)CoCl$_2$** (2.1 mM, ε_{max} = 21 $M^{-1}cm^{-1}$).

UV-vis spectroscopy complements the fully characterization of the family of cobalt complexes in solution (Figure 3. 16). All the complexes presented a higher intensive band in the UV region (200 to 350 nm) that can be assigned to a metal-ligand charge transfer (MLCT), ligand centered charge transfer (LLCT) or π-π^* transitions. The observed bands between 450-600 nm were characteristic for d-d electronic transitions and similar to the once reported for reported Co^{II} complexes (Figure 3. 16).[29, 30, 38, 39] ^{X}TPA based complexes presented two transition bands with similar: at 490 nm (ε_{max}~250 M^{-1} cm^{-1}) and at 630 nm (ε_{max}~173 M^{-1} cm^{-1}) with a shoulder at 645 nm. However, ^{x}**PDP** and ^{x}**MCP** based complexes presented only a poor intense transition band at 525 nm with very low extinction coefficients (ε_{max}~50 M^{-1} cm^{-1} and ε_{max}~30 M^{-1} cm^{-1}). The removal of one pyridine unit explains the different absorption pattern between both group of complexes, where an additional pyridine decreases the crystal field splitting Δ_O, enhancing d-d transition.

3.2.1.2. Characterization in solid state

The solid state structures of coordination cobalt chloride complexes bearing tetradentate N-donor ligand ^{x}**TPA, ^{x}PDP and ^{x}MCP** were determined by X-ray diffraction analysis. All single crystals suitable for X-Ray diffraction analysis were grown at room temperature by slow diffusion of diethyl ether into a dichloromethane or acetonitrile solution of the corresponding compound. Experimental details of their crystal structure are summarized in following tables. **(^{x}TPA)CoCl$_2$, (^{H}PDP)CoCl$_2$, (^{DMM}PDP)CoCl$_2$** and **(^{CO2Et}MCP)CoCl$_2$** crystallized in a monoclinic crystal system; **(^{CO2Et}PDP)CoCl$_2$** and **(^{H}MCP)CoCl$_2$** crystallized in a tetragonal crystal system and **(^{DMM}MCP)CoCl$_2$** in an orthorhombic crystal system.

The crystal structures for the family (**^{x}TPA)CoCl$_2$** presented a different Co^{II} coordination environment depending on the substitution in the pyridine moiety (Figure 3. 17, Table 3. 2). (**^{H}TPA)CoCl$_2$**[29] and (**^{CO2Et}TPA)CoCl$_2$** present a distorted octahedral coordination geometry for Co^{II} with the N atom from the alkylic moiety in axial coordination site, 1 chloride anion in the other axial position and 1 chloride in an equatorial position. However, (**^{DMM}TPA)CoCl$_2$** loses one chloride, having a distorted trigonal bipyramidal geometry, in concordance with an electrodonating behavior of the pyridine moieties which enriches the metal center crystal structures for (**^{x}TPA)CoCl$_2$** provide the first evidence of electronic properties of the pyridine moiety. The crystal structures of (**^{X}PDP)CoCl$_2$** and (**^{X}MCP)CoCl$_2$** (Figure 3. 18, Figure 3. 19) show the expected slightly distorted octahedral coordination geometries for Co^{II} with 2 axial coordination sites occupied by the N atoms of the pyridines, 2 equatorial coordination sites occupied by the N atoms from the backbone. This provides two accessible coordination sites in a relative *cis* configuration that are occupied by the two chloride anions. The Co–N bond lengths for all these complexes are 2.0-2.3 Å, typical for high-spin Co^{II} complexes with 3 unpaired electrons.[40, 41]

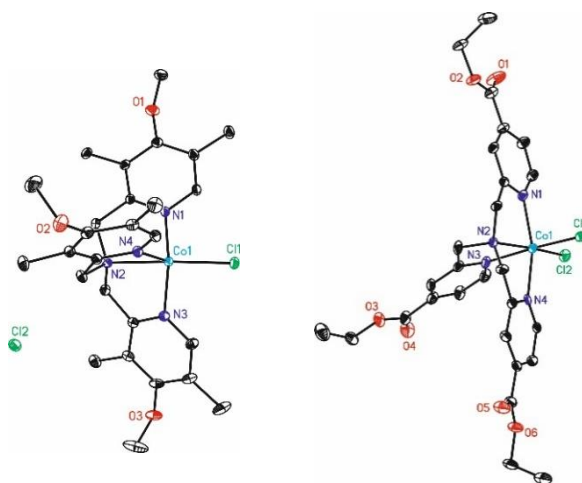**Figure 3. 17.** Solid state structures by single-crystal X-Ray diffraction of complexes (**^{X}TPA)CoCl$_2$**. The ellipsoid representation is at 50% probability. The hydrogen atoms and respective second halide counteranion are omitted for clarity.

Table 3. 2. Crystal and refinement data for complexes (^{X}TPA)CoCl$_2$.

	(^{H}TPA)CoCl$_2$[*]	(^{DMM}TPA)CoCl$_2$	(^{CO2Et}TPA)CoCl$_2$
empirical formula	C$_{20}$H$_{26}$Cl$_2$CoN$_4$	C$_{27}$H$_{36}$Cl$_2$CoN$_4$O$_3$	C$_{31}$H$_{40}$Cl$_2$CoN$_4$O$_7$
molecular weight	452.28	594.43	710.50
temperature (K)	100(2)	100(2)	100(2)
crystal system	monoclinic	monoclinic	monoclinic
space group	P2(1)	P21/c	P21/n
a (Å)	8.7071(3)	12.4193(4)	13.889(2)
b (Å)	14.3074(5)	11.9144(5)	12.081(2)
c (Å)	8.7686(3)	19.6320(8)	19.653(4)
α	90	90	90
β	115.7667(9)	104.9977(10)	98.267(6)
$\square$	90	90	90
volume (Å^3)	983.75(6)	2805.96(19)	3263.4(10)
Z	2	4	4
λ (Å)	0.71073	0.71073	0.71073
μ (mm^{-1})	1.157	0.837	0.742
nº reflections measured	9639	27242	26200
nº ind. reflections	5392	8787	9439
R$_{int}$	0.0161	0.0209	0.0499
restraints/parameters	1/245	2382/1495	18/421
R$_1$, wR$_2$ [$I > 2\sigma$(I)]	0.0231, 0.0524	0.0270, 0.0693	0.0545, 0.116
R$_1$ (all data)	0.0239	0.0321, 0.0722	0.0951, 0.142
GOF	1.113	1.027	1.045

[*]Reported data.[29]

Table 3. 3. Selected bond lengths (Å) and angles (deg) for complexes (^{X}TPA)CoCl$_2$.

	(^{H}TPA)CoCl$_2$[*]	(^{DMM}TPA)CoCl$_2$	(^{CO2Et}TPA)CoCl$_2$
Bond lengths (Å)			
M-N1	2.162(2)	2.0495(9)	2.141(2)
M-N2	2.2239(19)	2.1966(10)	2.199(2)
M-N3	2.1957(19)	2.0597(9)	2.228(3)
M-N4	2.160(2)	2.0696(10)	2.126(2)
M-Cl1	2.4045(6)	2.2695(3)	2.3385(8)
M-Cl2	2.4199(6)		2.4576(9)
Bond angles (deg)			
N1-M-N2	95.67(7)	78.70(4)	78.18(9)
N1-M-N4		122.22(4)	156.16(9)
N1-M-N3	77.16(7)	107.73(4)	80.86(9)
N4-M-N2	75.90(7)	77.97(4)	78.01(9)
N4-M-N3	97.43(7)	117.77(4)	95.29(9)
N1-M-Cl1	92.56(5)	103.03(3)	88.14(7)
N1-M-Cl2	92.99(6)		102.21(7)

[*]Reported data.[29]

Figure 3. 18. Solid state structures by single-crystal X-Ray diffraction of complexes (**^{X}PDP)CoCl$_2$**.The ellipsoid representation is at 50% probability. The hydrogen atoms and respective second halide counteranion are omitted for clarity.

Table 3. 4. Crystal and refinement data for complexes (**^{X}PDP)CoCl$_2$**.

	(**^{H}PDP)CoCl$_2$***	(**^{DMM}PDP)CoCl$_2$**	(**^{CO2Et}PDP)CoCl$_2$**
empirical formula	C$_{20}$H$_{26}$Cl$_2$CoN$_4$	C$_{108.75}$H$_{161.50}$Cl$_{17.50}$Co$_4$N$_{16}$O$_8$	C$_{27}$H$_{36}$Cl$_4$CoN$_4$O$_4$
molecular weight	452.28	677.12	681.33
temperature (K)	100(2)	100(2)	100(2)
crystal system	monoclinic	monoclinic	tetragonal
space group	P2(1)	P2(1)	P4(3)22
a (Å)	8.7071(3)	10.5920(4)	8.8516(12)
b (Å)	14.3074(5)	25.4091(11)	8.8516(12)
c (Å)	8.7686(3)	24.5740(11)Å	40.326(6)
α	90	90	90
β	115.7667(9)	92.2460(10)	90
□	90	90	90
volume (Å^3)	983.75(6)	6608.6(5)	3159.5(10)
Z	2	2	4
λ (Å)	0.71073	0.71073	0.71073
μ (mm^{-1})	1.157	0.903	0.920
nº reflections measured	9639	75735	21460
nº ind. reflections	5392	36897	5249
R$_{int}$	0.0161	0.0565	0.0294
restraints/parameters	1/245	2382/1495	95/244
R$_1$, wR$_2$ [$I > 2\sigma(I)$]	0.0231, 0.0524	0.0763, 0.2096	0.0454, 0.0991
R$_1$ (all data)	0.0239	0.0906	0.0510
GOF	1.113	1.027	1.185

Table 3. 5. Selected bond lengths (Å) and angles (deg) for complexes (**^{X}PDP)CoCl$_2$**.

	(**^{H}PDP)CoCl$_2$** *	(**^{DMM}PDP)CoCl$_2$**	(**^{CO2Et}PDP)CoCl$_2$** [a]
Bond lengths (Å)			
M-N1	2.162(2)	2.175(6)	2.168(2)
M-N2	2.2239(19)	2.197(6)	2.202(2)
M-N3	2.1957(19)	2.180(6)	
M-N4	2.160(2)	2.153(6)	
M-Cl1	2.4045(6)	2.449(2)	2.4250(8)
M-Cl2	2.4199(6)	2.3972(19)	
Bond angles (deg)			
N1-M-N2	95.67(7)	76.3(2)	76.94(9)
N1-M-N2'			101.66(9)
N1-M-N3	77.16(7)	99.7(2)	
N4-M-N2	75.90(7)	94.3(2)	
N4-M-N3	97.43(7)	75.8(2)	
N1-M-Cl1	92.56(5)	92.61(18)	91.96(6)
N1-M-Cl2	92.99(6)	90.12(18)	

[a](**^{CO2Et}PDP)CoCl$_2$** possesses a C$_2$ element of symmetry that generates the rest of the molecule.
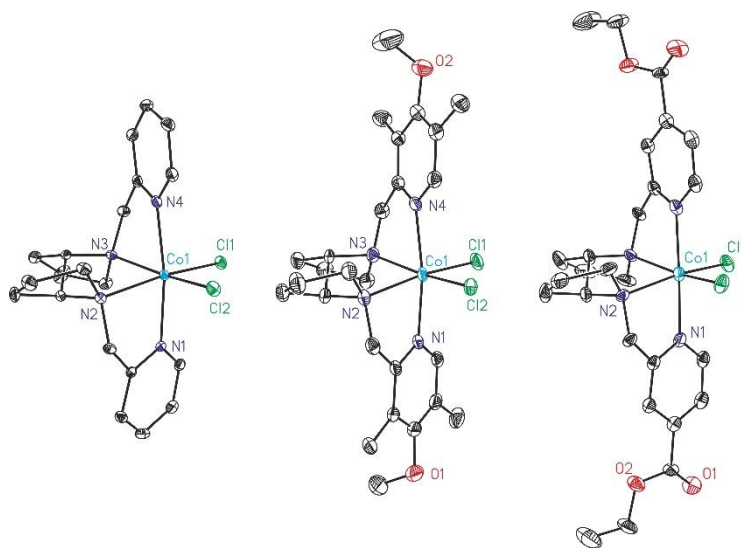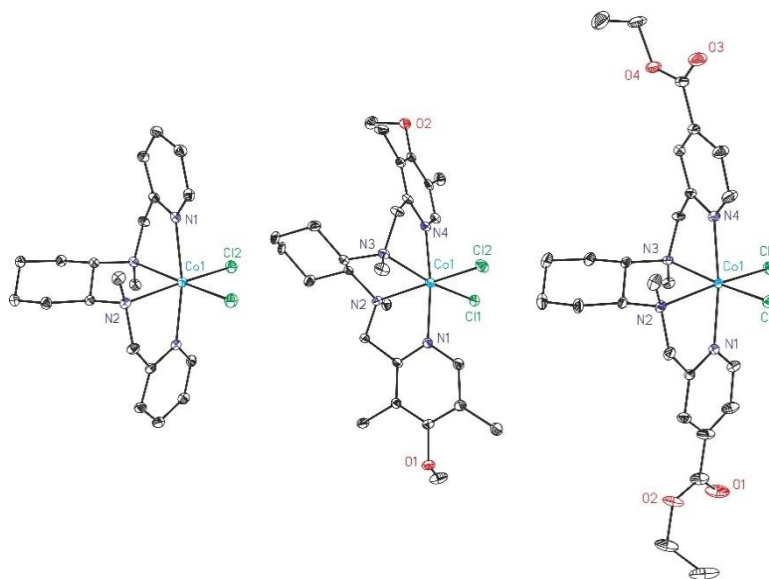

Figure 3. 19. Solid state structures by single-crystal X-Ray diffraction of complexes (**^{X}MCP)CoCl$_2$**. The ellipsoid representation is at 50% probability. The hydrogen atoms and respective second halide counteranion are omitted for clarity.

Table 3. 6. Crystal and refinement data for complexes **(^{X}MCP)CoCl$_2$**.

	(^{H}MCP)CoCl$_2$*	**(^{DMM}MCP)CoCl$_2$**	**(^{CO2Et}MCP)CoCl$_2$**
empirical formula	C$_{20}$H$_{28}$Cl$_2$CoN$_4$	C$_{54}$H$_{84}$Cl$_8$Co$_2$N$_8$O$_4$	C$_{27}$H$_{38}$Cl$_4$CoN$_4$O$_4$
molecular weight	454.29	1310.75	683.34
temperature (K)	100(2)	100(2)	100(2)
crystal system	Tetragonal	orthorhombic	monoclinic
space group	P4(3)2(1)2	P2(1)2(1)2(1)	P2(1)
a (Å)	9.1408(9)	11.6234(4)	11.4095(8)
b (Å)	9.1408(9)	14.6491(4)	10.3889(8)
c (Å)	23.552(3)	18.0766(6)	13.5987(10)
α	90	90	90
β	90	90	105.9722(18)
□	90	90	90
volume (Å^3)	1967.9(4)	3077.95(17)	1549.7(2)
Z	4	2	2
λ (Å)	0.71073	0.71073	0.71073
μ (mm^{-1})	1.157	0.936	0.938
n° reflections measured	16766	21983	11378
n° ind. reflections	3282	8887	7711
R$_{int}$	0.0298	0.0275	0.0144
restrains/parameters	0/124	99/ 379	214/412
R$_1$, wR$_2$ [$I > 2\sigma(I)$]	0.0223, 0.0548	0.0330, 0.0722	0.0260, 0.0625
R$_1$ (all data)	0.0240	0.0404	0.0268
GOF	1.087	1.037	1.040

Table 3. 7. Selected bond lengths (Å) and angles (deg) for complexes **(^{X}MCP)CoCl$_2$.**

	(^{H}MCP)CoCl$_2$^{a}	**(^{DMM}MCP)CoCl$_2$**	**(^{CO2Et}MCP)CoCl$_2$**
	Bond lengths (Å)		
M-N1	2.1644(13)	2.126(2)	2.1554(19)
M-N2	2.2421(14)	2.227(2)	2.2218(19)
M-N3		2.263(2)	2.2106(19)
M-N4		2.146(2)	2.1536(19)
M-Cl1	2.4138(5)	2.4299(7)	2.4043(6)
M-Cl2		2.4336(7)	2.3891(6)
	Bond angles (deg)		
N1-M-N2	95.06(5)	78.33(8)	76.80(7)
N1-M-N2'	76.32(5)		
N1-M-N3		103.64(8)	97.62(7)
N4-M-N2		91.80(8)	96.84(7)
N4-M-N3		76.78(8)	77.45(7)
N1-M-Cl1	90.69(4)	87.18(6)	90.54(5)
N1-M-Cl2		94.52(6)	94.01(5)

^{a}**(^{H}MCP)CoCl$_2$** possesses a C$_2$ element of symmetry that generates the rest of the molecule.

3.2.2. Synthesis and characterization of tetradentated N-based Nickel complexes

Similarly, we synthetized the corresponding well-defined Ni^{II} complexes, using $NiCl_2$ diglyme as metal source, obtaining crystalline compounds in good yields (40-89%) (Scheme 3. 5). Only complex (^{H}**TPA**)**NiCl$_2$**,[28, 29] have been previously described, and all the other compounds are described for the first time in this work.

H: R$_1$ = H, R$_2$ = H   **DMM**: R$_1$ = MeO, R$_2$ = Me   **CO$_2$Et**: R$_1$ = CO$_2$Et, R$_2$ = H
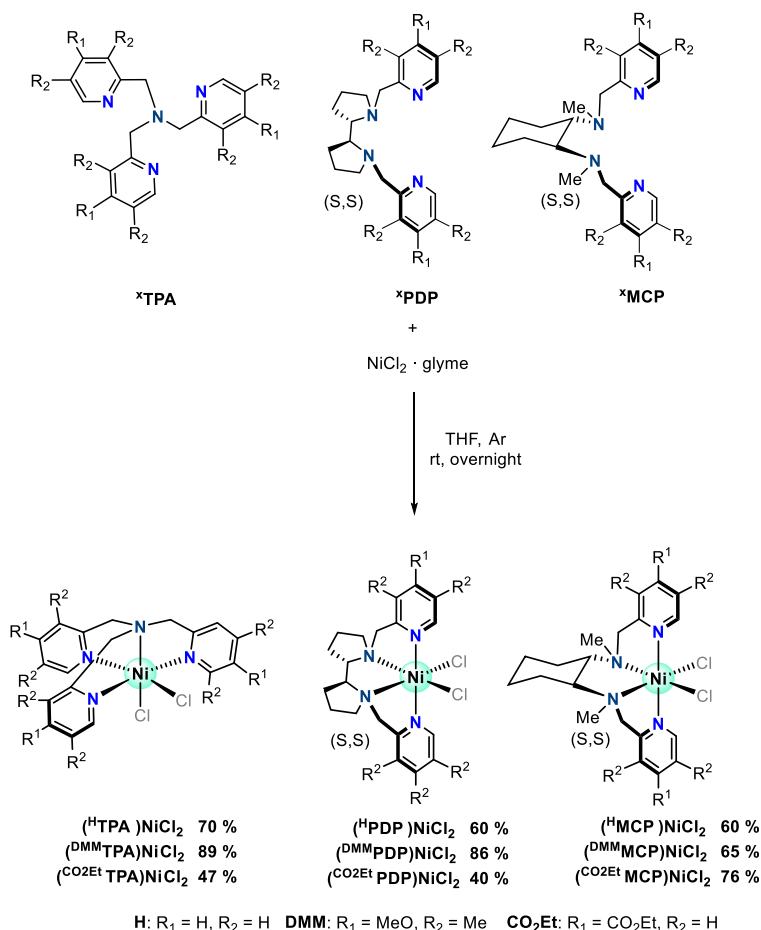
Scheme 3. 5. Synthesis of tetradentate N-based aminopyridine ligands and their corresponding Ni complexes.

All complexes were fully characterized by ^{1}H-NMR spectroscopy, single crystal X-ray diffraction crystallography, FTIR spectroscopy, UV-Vis absorption spectroscopy, high-resolution mass spectrometry and elemental analysis.

3.2.2.1. Characterization in solution

The Ni^{II} complexes were characterized in solution by means of ^{1}H-NMR spectroscopy. Ni^{II} presents a d^8 electronic configuration. The electronic structure, ligand-field spectroscopy and magnetism of Ni^{II} complexes depends on the geometry and the type of coordinated ligands. For example, square planar d^8 complexes are diamagnetic, but near tetrahedral d^8 complexes have temperature-dependent magnetic moments which are usually larger than the spin-only value. In the square-planar geometry, the ligands σ-interact strongly with the orbital d_{x2-y2} and the resulting σ* orbital is left unoccupied at the expense of pairing up of the eight d-electrons in the remaining four d-orbitals. The lack of σ* electrons lead to strong bonds. In near-tetrahedral complexes, the degeneracy of the highest energy d-orbitals means that single occupation is preferred. The square planar form is thus favored by stronger bonding whilst near-tetrahedral complexes are favored by lower pairing energy and reduced steric crowding.[42, 43] A similar behavior is observed in the case of octahedral complexes, where the degeneration of d-orbitals gives a configuration $t_{2g}^6 e_g^2$, with 2 unpaired electrons in two different molecular orbitals (d_{x2-y2} and d_{z2}) with slightly difference in energy, making them paramagnetic.[44]

As expected, the tetradentated N-based Ni^{II} complexes have less paramagnetic behavior than their Co^{II} analogs, exhibiting spectra windows ranged from -14 to 80 ppm. We performed paramagnetic ^{1}H NMR at different temperature for each complex for the study of their paramagnetic susceptibility (Figure 3. 20 – Figure 3. 28). In contrast with previous Co^{II} complexes, the most shifted signals were

broad and with less intensity, making difficult the study. Interestingly, (**DMMTPA)NiCl$_2$** (Figure 3. 21) did not show any signal in the paramagnetic region of 35-80 ppm, being the most diamagnetic compound of the family. Crystals of this compound revealed the formation of a dinuclear nickel complex containing two chlorides as bridging-ligands, which causes a distortion of the geometry, enhancing the diamagnetic behavior of the complex.[45, 46] All these facts difficult the assignation of H$^{\alpha}$ and the other protons. However, the chemical shift of protons influenced by the paramagnetic center should be linearly dependent on the 1/T, in concordance with Curie-Weiss law. So, in concordance with the previous section, we performed paramagnetic ^{1}H NMR at different temperature for each complex for the study of their paramagnetic susceptibility.
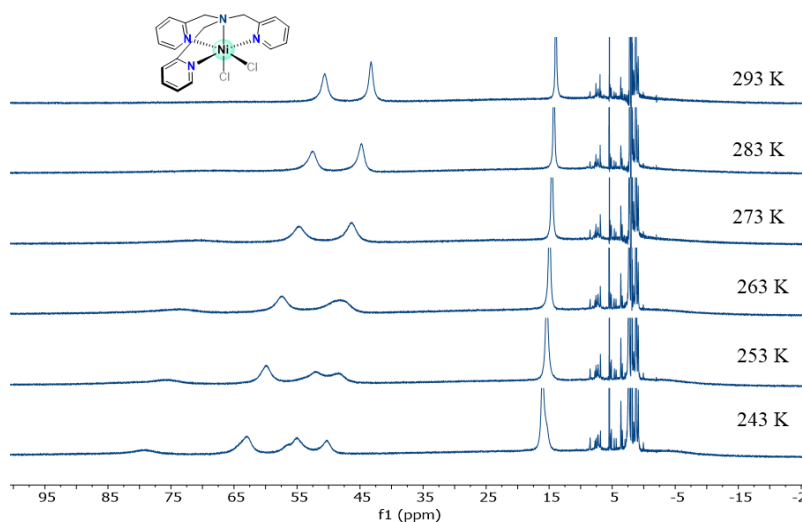

Figure 3. 20. ^{1}H-NMR spectrum of (**HTPA)NiCl$_2$** in CD$_3$CN at variable temperatures.
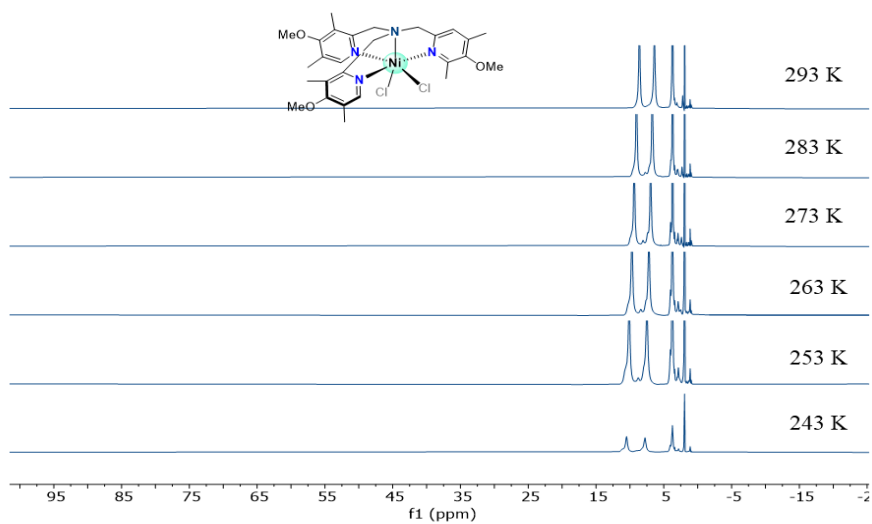
Figure 3. 21. ^{1}H-NMR spectrum of (**^{DMM}TPA)NiCl$_2$** in CD$_3$CN at variable temperatures.
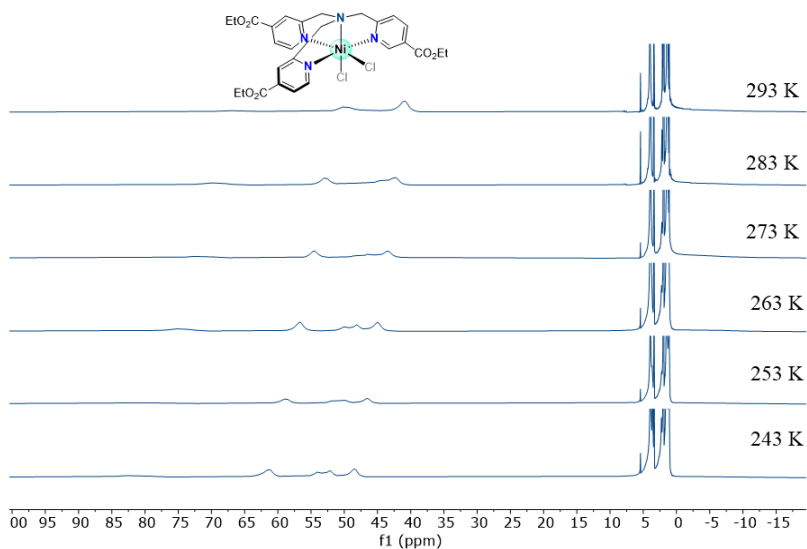
Figure 3. 22. ^{1}H-NMR spectrum of (**^{CO2Et}TPA)NiCl$_2$** in CD$_3$CN at variable temperatures.
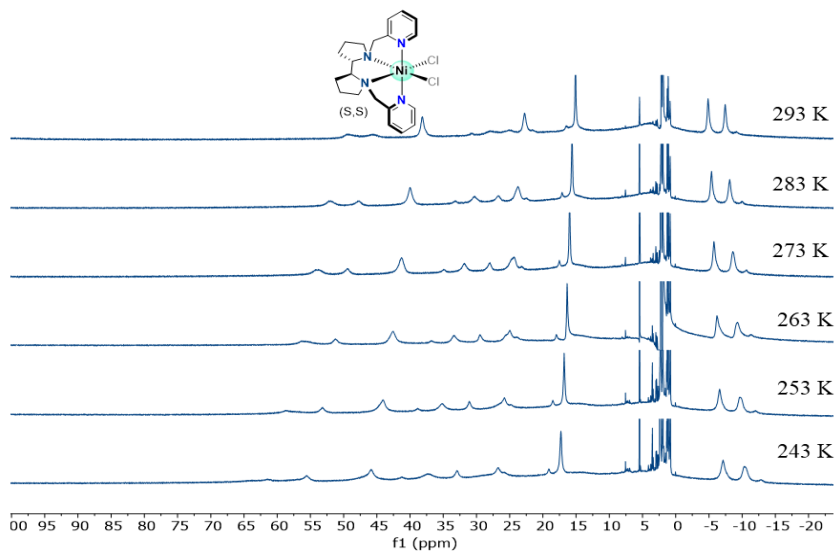
Figure 3. 23. ^{1}H-NMR spectrum of (**^{H}PDP)NiCl$_2$** in CD$_3$CN at variable temperatures.
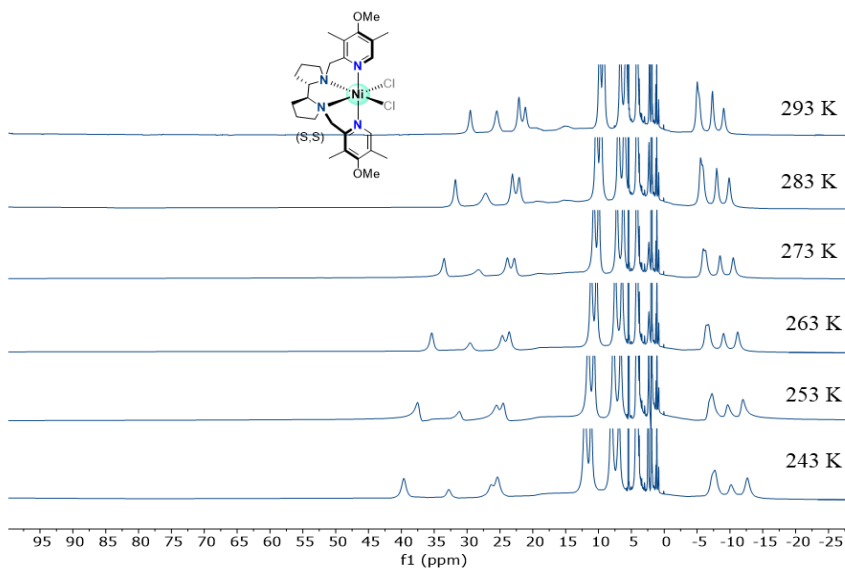
Figure 3. 24. ^{1}H-NMR spectrum of (**^{DMM}PDP)NiCl$_2$** in CD$_3$CN at variable temperatures.
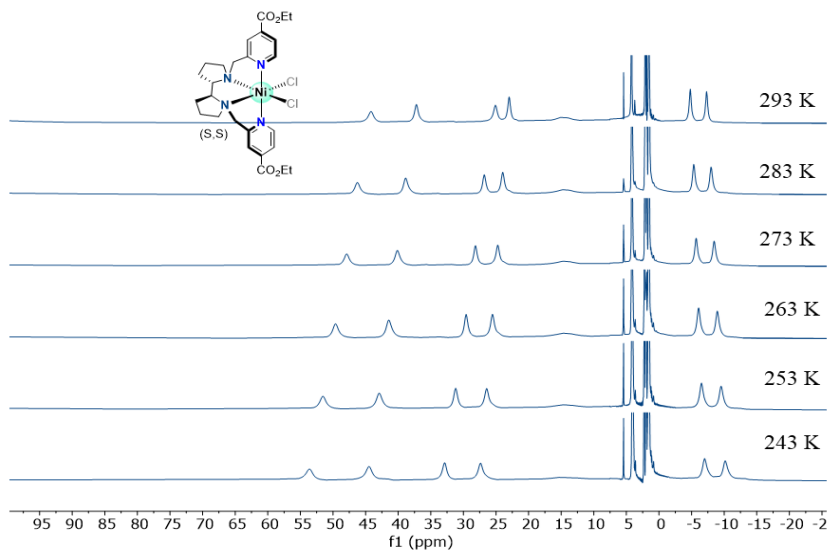
Figure 3. 25. ^{1}H-NMR spectrum of **(^{CO2Et}PDP)NiCl$_2$** in CD$_3$CN at variable temperatures.
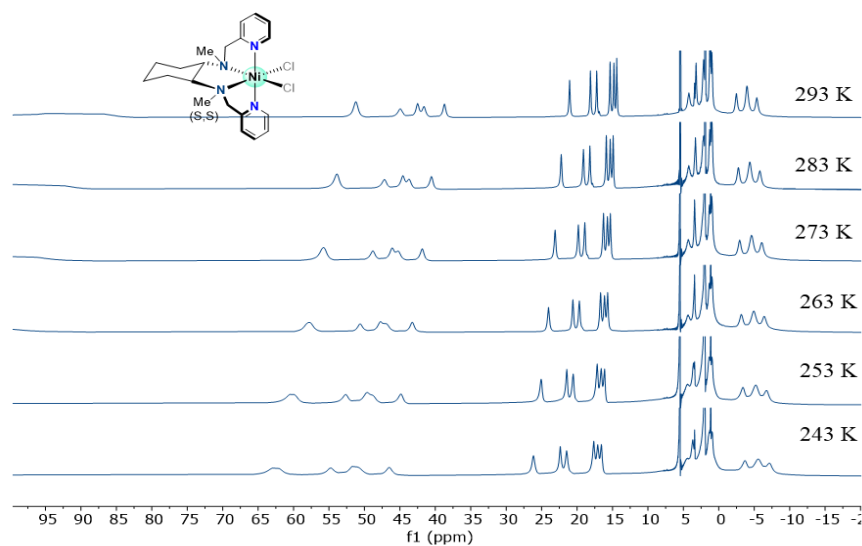
Figure 3. 26. ^{1}H-NMR spectrum of **(^{H}MCP)NiCl$_2$** in CD$_3$CN at variable temperatures.
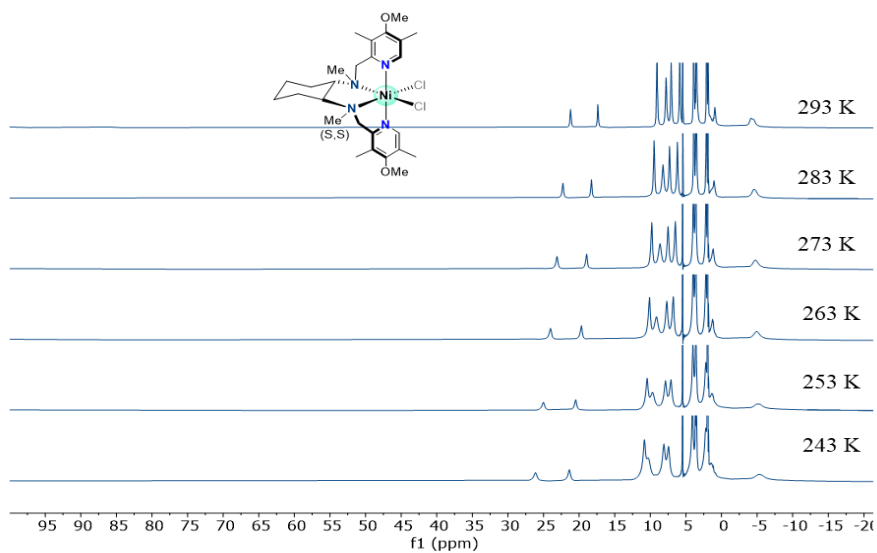
Figure 3. 27. ^{1}H-NMR spectrum of (^{DMM}MCP)NiCl$_2$ in CD$_3$CN at variable temperatures.
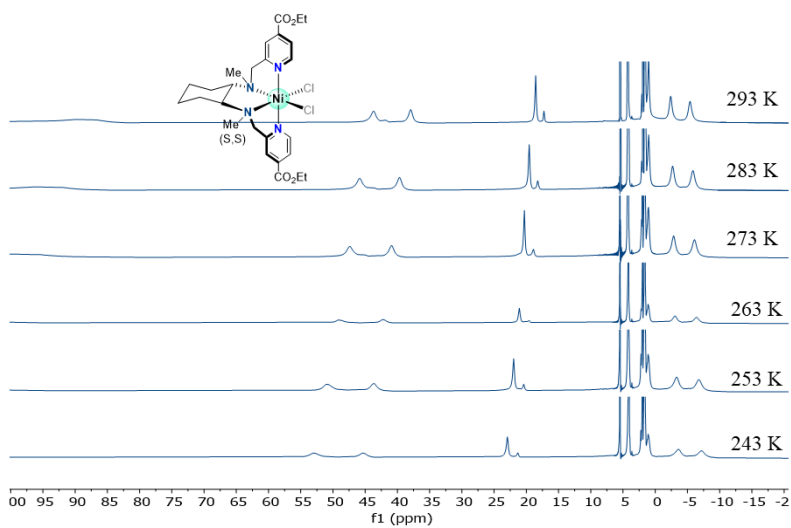
Figure 3. 28. ^{1}H-NMR spectrum of (^{CO2Et}MCP)NiCl$_2$ in CD$_3$CN at variable temperatures.

In general terms, all protons found in the paramagnetic region of the spectrum exhibit a chemical shift linearly dependent on 1/T, consistent with Curie's law, which indicates that there is not a spin change in this temperature range (Figure 3. 29).[35]
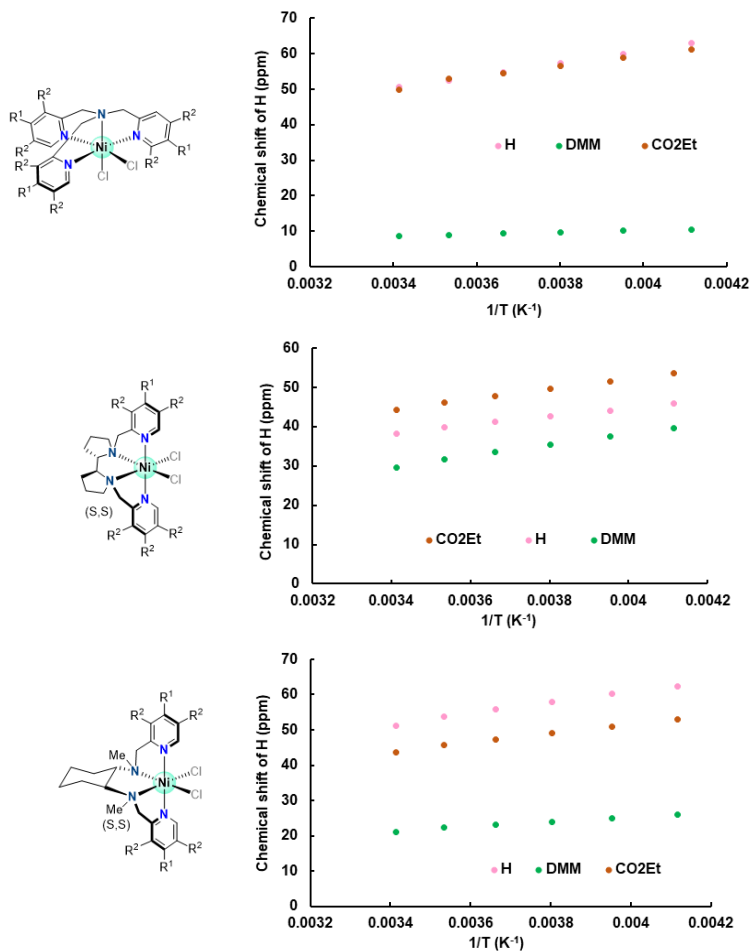
Figure 3. 29. Representation of the chemical shift of aromatic proton (Hα) of tetradentated Ni[II] complexes in front of temperature in the ^{1}H-NMR spectrum in CD3CN.
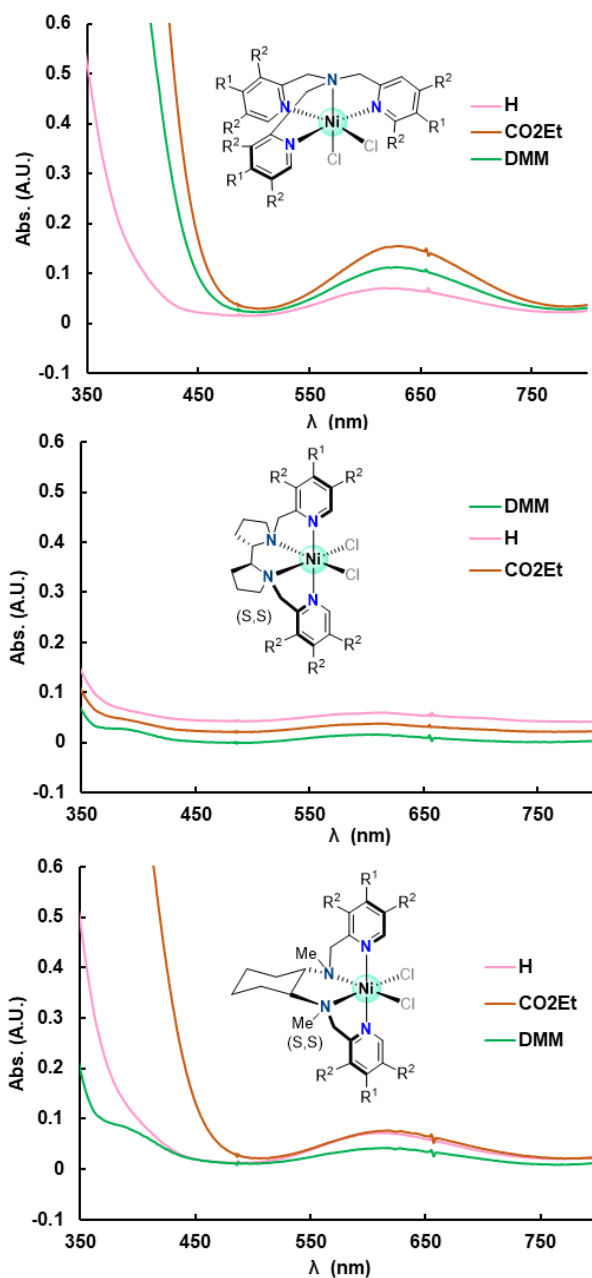
Figure 3. 30. UV-vis absorption spectra of Ni^{II} complexes. **(^{H}TPA)NiCl$_2$** (6.0 mM, ε_{max} = 12 M^{-1}cm^{-1}), **(^{DMM}TPA)NiCl$_2$** (5.7 mM, ε_{max} = 15 M^{-1}cm^{-1}), **(^{CO2Et}TPA)NiCl$_2$** (5.6 mM, ε_{max} = 28 M^{-1}cm^{-1}), **(^{H}PDP)NiCl$_2$** (5.5 mM, ε_{max} = 7 M^{-1}cm^{-1}), **(^{DMM}PDP)NiCl$_2$** (2.3 mM, ε_{max} = 5 M^{-1}cm^{-1}), **(^{CO2Et}PDP)NiCl$_2$** (4.3 mM, ε_{max} = 5 M^{-1}cm^{-1}), **(^{H}MCP)NiCl$_2$** (5.9 mM, ε_{max} = 13 M^{-1}cm^{-1}), **(^{DMM}MCP)NiCl$_2$** (5.4 mM, ε_{max} = 8 M^{-1}cm^{-1}) and **(^{CO2Et}MCP)NiCl$_2$** (6.1 mM, ε_{max} = 13 M^{-1}cm^{-1}).

UV-vis spectroscopy complements the fully characterization of the family of nickel complexes in solution. All the complexes presented a higher intensive bands in the UV region (200 to 350 nm) that can be assigned to a metal-ligand charge transfer (MLCT), ligand centered charge transfer (LLCT) or π-π^* transitions. All the complexes showed poor intense transition band near 640 nm (ε_{max}~5-12 M^{-1} cm^{-1}), which can be assigned to transitions between d_{x2-y2} and d_{z2} (Figure 3. 30).[47-49]

3.2.2.2. Characterization in solid state

The solid state structures of coordination nickel chloride complexes bearing tetradentate N-donor ligand **^{x}TPA, ^{x}PDP and ^{x}MCP** were determined by X-ray diffraction analysis. All single crystals suitable for X-Ray diffraction analysis were grown at room temperature by slow diffusion of diethyl ether into a dichloromethane or acetonitrile solution of the corresponding compound. Experimental details of their crystal structure are summarized in following tables. **(^{x}TPA)NiCl$_2$, (^{H}PDP)NiCl$_2$, (^{CO2Et}PDP)NiCl$_2$ and (^{CO2Et}MCP)NiCl$_2$** crystallized in a monoclinic crystal system; **(^{DMM}MCP)NiCl$_2$** crystallized in a triclinic crystal system; and **(^{DMM}PDP)NiCl$_2$ and (^{H}MCP)NiCl$_2$** in an orthorhombic crystal system.

The first evidence of electronic properties of the pyridine moiety arises with the crystal structures for **(^{x}TPA)NiCl$_2$** and their different Ni^{II} coordination environment (Figure 3. 31, Table 3. 8). **(^{H}TPA)NiCl$_2$** and **(^{CO2Et}TPA)NiCl$_2$** similarly behave as their analogous Co^{II}: they present a distorted octahedral coordination geometry for Ni^{II} with the N atom from the alkylic moiety in axial coordination site, 1 chloride anion in the other axial position and 1 chloride in an equatorial position. In contrast, crystals reveal that the synthesis of **(^{DMM}TPA)NiCl$_2$** did not bring the expected mononuclear nickel complex,

revealing the formation of a dinuclear Ni complex containing two chlorides as bridging-ligands, which causes a distortion of the geometry. This kind of dimeric nickel species have been already reported in the literature, behaving as diamagnetic compounds among other changes in their properties.[45, 46] We glimpse the electrodonating effect of the **DMMTPA** enriching the metal center as a key factor for the formation of dimeric compounds. The crystal structures of **(XPDP)NiCl₂** and **(XMCP)NiCl₂** (Figure 3. 32, Figure 3. 33,) show the expected slightly distorted octahedral coordination geometries for Ni[II] with 2 axial coordination sites occupied by the N atoms of the pyridines, 2 equatorial coordination sites occupied by the N atoms from the backbone. This provides two accessible coordination sites in a relative *cis* configuration that are occupied by the two chloride anions. In these cases, the removal of one pyridine unit in comparison with **XTPA** ligand directly avoid the formation of dinuclear side complexes.
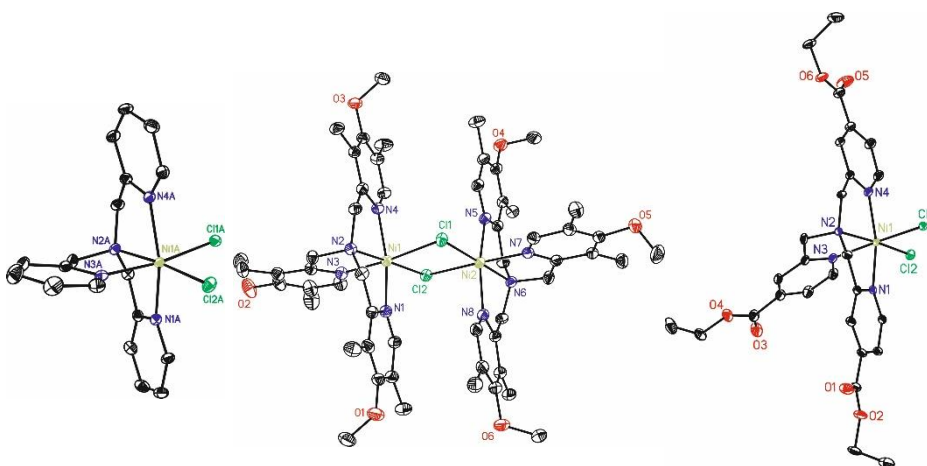

Figure 3. 31. Solid state structures by single-crystal X-Ray diffraction of complexes (**XTPA)NiCl₂**. The ellipsoid representation is at 50% probability. The hydrogen atoms are omitted for clarity.

Table 3. 8. Crystal and refinement data for complexes **(^{X}TPA)NiCl$_2$.**

	(^{H}TPA)NiCl$_2$	**(^{DMM}TPA)NiCl$_2$**	**(^{CO2Et}TPA)NiCl$_2$**
empirical formula	$C_{19.90}H_{20-20}Cl_{2.19}NiN_{4.90}$	$C_{59.60}H_{81.50}Cl_6Ni3N_4O_{6.50}$	$C_{31}H_{40}Cl_2NiN_4O_7$
molecular weight	465.24	1440.68	710.28
temperature (K)	100(2)	100(2)	100(2)
crystal system	monoclinic	monoclinic	monoclinic
space group	P21	P21/n	P21/n
a (Å)	8.7126(3)	18.9603(4)	13.8683(6)
b (Å)	15.6976(5)	18.8393(3)	12.0407(6)
c (Å)	30.6499(10)	20.6824(4)	19.5929(7)
α	90	90	90
β	91.2356(8)	112.4338(2)	98.8791(12)
□	90	90	90
volume (Å^3)	4190.9(2)	6828.4(2)	3232.5(2)
Z	8	4	4
λ (Å)	0.71073	0.71073	0.71073
μ (mm^{-1})	1.221	1.109	0.818
n° reflections measured	40034	79910	29255
n° ind. reflections	21125	27418	10530
R$_{int}$	0.0227	0.0320	0.0348
restraints/parameters	235/1055	198/873	18/421
R$_1$, wR$_2$ [$I > 2\sigma(I)$]	0.0283, 0.0593	0.0486, 0.1214	0.0426, 0.1062
R$_1$ (all data)	0.0318, 0.0606	0.0772, 0.1343	0.0554, 0.1130
GOF	0.907	1.037	1.030

Table 3. 9. Selected bond lengths (Å) and angles (deg) for complexes **(^{X}TPA)NiCl$_2$.**

|	**(^{H}TPA)NiCl$_2$**	**(^{DMM}TPA)NiCl$_2$**	**(^{CO2Et}TPA)NiCl$_2$**
	Bond lengths (Å)		
M-N1	2.0822(19)	2.0646(18)	2.0843(14)
M-N2	2.1124(19)	2.0811(17)	2.1264(14)
M-N3	2.1216(19)	2.0524(18)	2.1556(15)
M-N4	2.0703(19)	2.0586(18)	2.0736(15)
M-Cl1	2.4566(6)	2.5302(5)	2.44433(5)
M-Cl2	2.3571(6)	2.3821(5)	2.3572(4)
	Bond angles (deg)		
N1-M-N2	81.34(7)	80.90(7)	80.37(5)
N1-M-N4	160.99(8)	162.31(7)	160.44(6)
N1-M-N3	86.39(7)	89.65(7)	82.87(6)
N4-M-N2	79.73(7)	81.43(7)	80.14(6)
N4-M-N3	92.36(7)	89.23(7)	95.61(6)
N1-M-Cl1	88.02(6)	93.00(5)	90.45(4)
N1-M-Cl2	101.27(6)	96.69(5)	99.27(4)
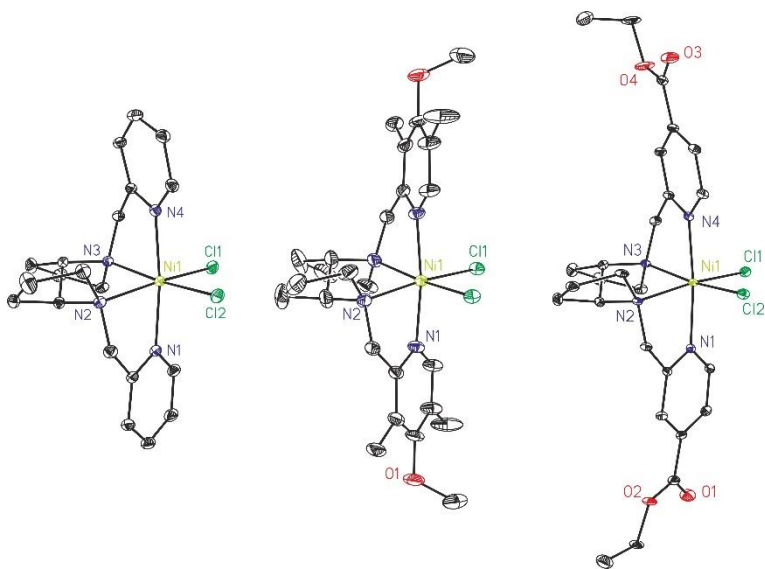
Figure 3. 32. Solid state structures by single-crystal X-Ray diffraction of complexes **(^{X}PDP)NiCl$_2$**. The ellipsoid representation is at 50% probability. The hydrogen atoms and respective second halide counteranion are omitted for clarity.

Table 3. 10. Crystal and refinement data for complexes **(^{X}PDP)NiCl$_2$**.

	(^{H}PDP)NiCl$_2$	**(^{DMM}PDP)NiCl$_2$**	**(^{CO2Et}PDP)NiCl$_2$**
empirical formula	C$_{20}$H$_{26}$Cl$_2$NiN$_4$	C$_{28}$H$_{42}$Cl$_6$NiN$_4$O$_2$	C$_{27}$H$_{36}$Cl$_4$CoN$_4$O$_4$
molecular weight	452.06	738.06	681.11
temperature (K)	100(2)	100(2)	100(2)
crystal system	monoclinic	orthorhombic	monoclinic
space group	P2(1)	C222(1)	P2(1)
a (Å)	8.65900(15)	12.2228(5)	8.6461(10)
b (Å)	14.30550(18)	13.8635(5)	14.7067(18)
c (Å)	8.71310(15)	19.6927(8)	11.9675(15)
α	90	90	90
β	115.731(2)	90	96.260(3)
☐	90	90	90
volume (Å^3)	972.28(3)	3336.9(2)	1512.7(3)
Z	2	4	2
λ (Å)	0.71073	0.71073	0.71073
μ (mm^{-1})	1.286	1.094	1.034
n^o reflections measured	16017	13033	12690
n^o ind. reflections	6422	5276	7306
R$_{int}$	0.0233	0.0338	0.0288
restraints/parameters	1/244	35/216	1/368
R$_1$, wR$_2$ [$I > 2\sigma(I)$]	0.0351, 0.0867	0.0340, 0.0827	0.0260, 0.0573
R$_1$ (all data)	0.0357	0.0400	0.0280
GOF	1.113	1.027	1.185

Table 3. 11. Selected bond lengths (Å) and angles (deg) for complexes **(^{X}PDP)NiCl$_2$**.

	(^{H}PDP)NiCl$_2$	(^{DMM}PDP)NiCl$_2$[a]	(^{CO2Et}PDP)NiCl$_2$
Bond lengths (Å)			
M-N1	2.104(3)	2.081(2)	2.1156(16)
M-N2	2.165(2)	2.126(2)	2.1408(18)
M-N3	2.133(2)		2.1493(18)
M-N4	2.098(3)		2.0999(17)
M-Cl1	2.4245(8)	2.4391(6)	2.4224(6)
M-Cl2	2.4124(8)		2.3858(6)
Bond angles (deg)			
N1-M-N2	77.82(10)	78.12(9)	78.52(6)
N1-M-N2'		96.14(8)	
N1-M-N3	97.32(10)		98.36(6)
N4-M-N2	95.68(10)		96.16(7)
N4-M-N3	79.14(10)		78.15(6)
N1-M-Cl1	94.48(7)	93.56(6)	90.75(5)
N1-M-Cl2	90.28(7)		92.78(5)

[a] Complex possesses a C$_2$ element of symmetry that generates the rest of the molecule.
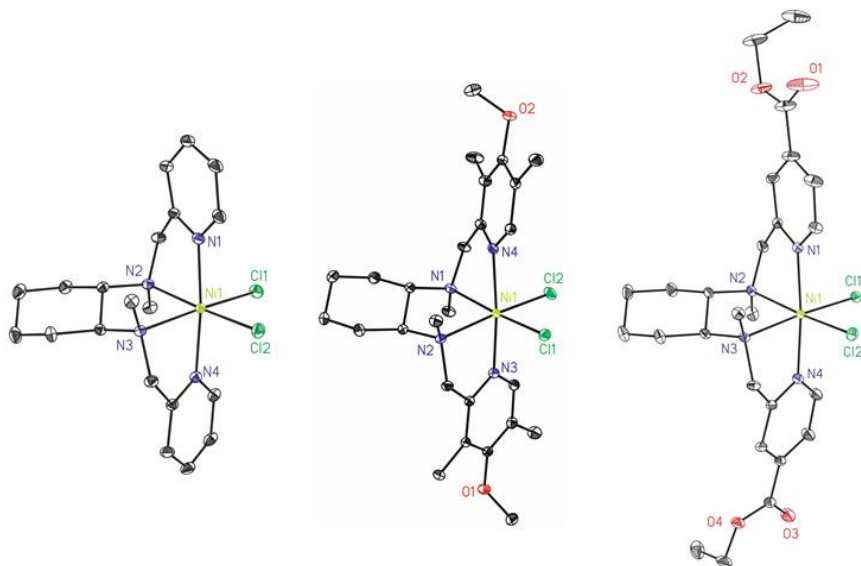

Figure 3. 33. Solid state structures by single-crystal X-Ray diffraction of complexes (**^{X}MCP)NiCl$_2$**. The ellipsoid representation is at 50% probability. The hydrogen atoms and respective second halide counteranion are omitted for clarity.

Table 3. 12. Crystal and refinement data for complexes **(^{X}MCP)NiCl$_2$.**

	(^{H}MCP)NiCl$_2$	**(^{DMM}MCP)NiCl$_2$[a]**	**(^{CO2Et}MCP)NiCl$_2$**
empirical formula	C$_{20}$H$_{28}$Cl$_2$NiN$_4$	C$_{8.67}$H$_{13.33}$Cl$_{0.67}$ Co$_0$N1.33 Ni$_{0.33}$ O$_{0.67}$	C$_{27}$H$_{38}$Cl$_4$NiN$_4$O$_4$
molecular weight	454.07	247.18	683.12
temperature (K)	100(2)	100(2)	100(2)
crystal system	orthorhombic	triclinic	Monoclinic
space group	P2(1)2(1)2(1)	P -1	P2(1)
a (Å)	9.3480(4)	9.4554(2)	11.35871(14)
b (Å)	14.7193(6)	12.5350(2)	10.30928(11)
c (Å)	14.7683(6)	13.1402(2)	13.55609(16)
α	90	95.6180(10)	90
β	90	103.2760(10)	105.4935(13)
□	90	95.419(2)	90
volume (Å^3)	2032.06(15)	1497.49(5)	1529.73(3)
Z	4	6	2
λ (Å)	0.71073	0.71073	0.71073
μ (mm^{-1})	1.231	0.802	1.023
nº reflections measured	27667	52837	26723
nº ind. reflections	8181	9993	9904
R$_{int}$	0.0249	0.0448	0.0172
restrains/parameters	0/246	0/423	70/411
R$_1$, wR$_2$ [$I > 2\sigma(I)$]	0.0226, 0.0528	0.0391, 0.1098	0.0251, 0.0643
R$_1$ (all data)	0.0244	0.0427, 0.1123	0.0254
GOF	1.044	1.041	1.039

[a]Contains 4 molecules in the unit cell.

Table 3. 13. Selected bond lengths (Å) and angles (deg) for complexes **(^{X}MCP)NiCl$_2$.**

	(^{H}MCP)NiCl$_2$[a]	**(^{DMM}MCP)NiCl$_2$**	**(^{CO2Et}MCP)NiCl$_2$**
Bond lengths (Å)			
M-N1	2.0755(12)	2.0571(11)	2.0971(16)
M-N2	2.1844(12)	2.1696(11)	2.1595(16)
M-N3	2.1650(12)	2.1135(11)	2.1480(16)
M-N4	2.0937(12)	2.0787(10)	2.0912(16)
M-Cl1	2.4345(4)		2.4061(5)
M-Cl2	2.4322(4)		2.3857(5)
Bond angles (deg)			
N1-M-N2	79.33(5)	78.19(4)	78.65(6)
N1-M-N2'			
N1-M-N3	95.98(4)	110.62(4)	97.55(6)
N4-M-N2	97.70(5)	127.90(4)	96.75(6)
N4-M-N3	78.25(5)	78.42(4)	79.24(6)
N1-M-Cl1	90.17(3)		89.45(5)
N1-M-Cl2	93.55(4)		93.75(5)

[a]Complex possesses a C$_2$ element of symmetry that generates the rest of the molecule.

3.2.3. Catalytic activity in dual photoredox Csp³-Cl activation

As discussed earlier, we envisioned the implementation of these family of complexes in dual photoredox systems for the development of organic transformations. We considered the replacement of **(Py₂ᵀˢtacn)Ni(OTf)₂** in the well-known photocatalytic activation of unactivated alkyl chlorides developed by the group,[20] using [Cu(bathocuproine)(xantphos)](PF₆)[50] (**PC_Cu**) as a photoredox catalyst. In that work, the system was able to reduce **(Py₂ᵀˢtacn)Ni(OTf)₂** forming Ni^I active species. Two mechanistic scenarios were proposed for the activation of Csp³−Cl bond: a concerted halogen atom abstraction (CHAA) by Ni^I forming an alkyl radical or a nucleophilic substitution/oxidative addition and the consequent homolytic cleavage. Finally, the second scenario was assumed as the main pathway based on DFT calculation. However, the use of different scaffolds and the direct modification of the electronic properties in this work do not allow to hide any route. Therefore, we started evaluating their capability for undergoing different kind of organic reactions involving the cleavage of Csp³−Cl bond.
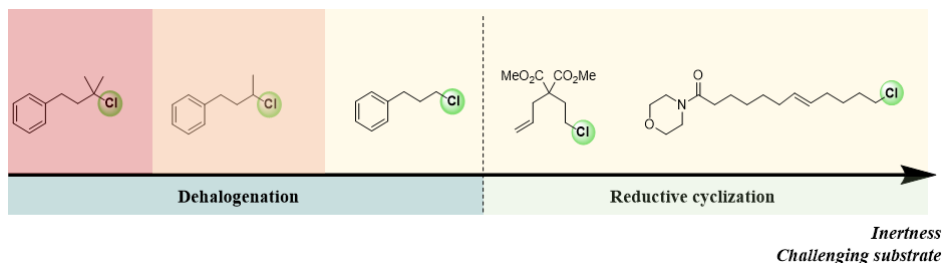

Figure 3. 34. Tested alkyl chlorides for the cleavage of inert Csp³-Cl bond using the family of tetradentated N-based complexes.

To define the reaction borders of the new family of complexes, we started with the simple activation of tertiary alkyl chlorides before targeting secondary and primary alkyl chlorides towards intramolecular cyclization with pendant alkenes (Figure 3. 34). We fixed the catalytic system under the reported reaction

conditions for the reductive cyclization of unactivated alkyl chlorides with tethered alkenes.

**Table 3. 14.** Screening of catalyst for the dechlorination of (3-chloro-3-methylbutyl)benzene.
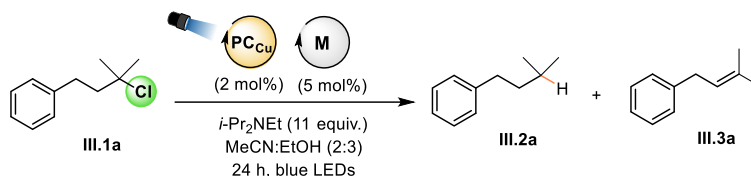
| | | 30ºC | | | 10ºC | | |
Catalyst	Conv. (%)	Yield III.2a (%)	Yield III.3a (%)	Conv. (%)	Yield III.2a (%)	Yield III.3a (%)
1	(CO2EtTPA)CoCl₂	90	18	55	83	18	59
2	(CO2EtTPA)NiCl₂	95	36	35	88	46	30
3	(HTPA)CoCl₂	93	20	39	84	21	48
4	(HTPA)NiCl₂	100	39	35	95	49	21
5	(DMMTPA)CoCl₂	94	37	22	67	29	30
6	(DMMTPA)NiCl₂	100	47	27	87	67	19
7	(CO2EtMCP)CoCl₂	100	53	25	100	77	15
8	(CO2EtMCP)NiCl₂	91	68	21	100	53	12
9	(HMCP)CoCl₂	100	40	35	100	39	38
10	(HMCP)NiCl₂	100	64	24	100	74	18
11	(DMMMCP)CoCl₂	100	35	45	99	28	69
12	(DMMMCP)NiCl₂	100	78	11	63	77	14
13	(CO2EtPDP)CoCl₂	100	54	27	100	62	17
14	(CO2EtPDP)NiCl₂	100	60	20	100	45	17
15	(HPDP)CoCl₂	100	51	22	100	41	39
16	(HPDP)NiCl₂	100	61	23	100	77	18
17	(DMMPDP)CoCl₂	100	49	31	79	26	68
18	(DMMPDP)NiCl₂	100	60	20	55	77	13

Reaction conditions: **III.1a** (10 mM), **PC_Cu** (2 mol%), catalyst (5 mol%), DIPEA (11.4 equiv.), EtOH/MeCN (3:2), visible-light irradiation with blue LEDs (1 W, 447 nm) for 24 h. Conversion and yield were determined by GC using biphenyl as an internal standard. Reactions run in triplicate.

(3-chloro-3-methylbutyl)benzene (**III.1a**) was chosen for the first screening. At 30ºC, full conversion was observed for all catalysts employed, which clearly illustrate the facility to activate tertiary alkyl chlorides. The reductive dechlorination yields (**III.2a**) were from moderate to good (18-78%), depending on the complex used (Table 3. 14. For example, TPA-based complexes presented the poorest yields, while nickel catalysts showed better catalytic performance, being the MCP ligand the best backbone. The identification of side reaction products was crucial to understand each metal reactivity. All the cases also presented significant amount of (3-methylbut-2-en-1-yl)benzene (**III.3a**), being the main product when using cobalt catalysts. We identified other minor products coming from the homocoupling reaction or the coupling with aminoalkyl radicals from DIPEA, which were not studied in more detail.

We can hypothesize that the first step of the reactions, independently of the product observed is the Csp^3-Cl bond activation, which could occur *via* concerted halogen atom abstraction (CHAA) or oxidative addition through an S_N2 (S_N2-OA) mechanisms. Nevertheless, the formation of the olefin indicates the potential formation of an organometallic intermediate which undergoes an β-hydride elimination (E2, bimolecular elimination, Scheme 3. 6). Previous studies with pentadentated complexes leaded to negligible amount of β-hydride elimination product, which suggests that the two vacancy coordination sites in the tetradentated complexes possibilities β-hydride elimination in agreement with the products observed.
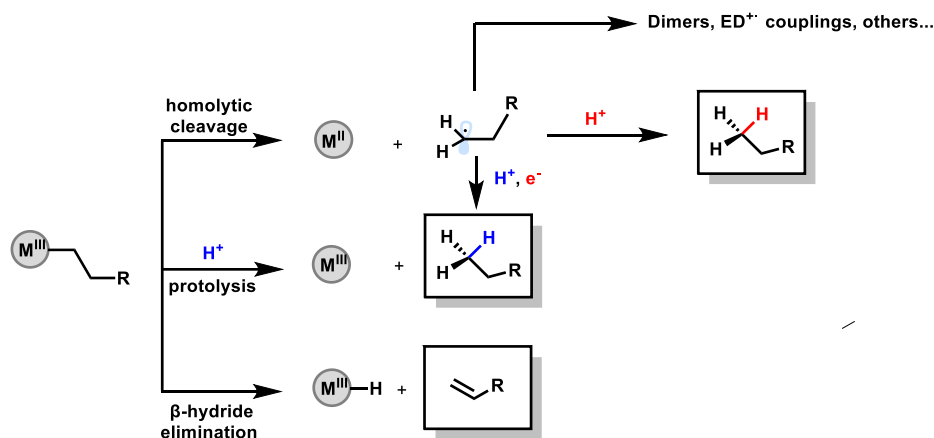
Scheme 3. 6. Csp^3-Cl bond activation: formation of a radical vs formation of an alkene.

In general, cobalt presents faster rates for β-hydride elimination than nickel and a good capability of being an hydride source, favoring the formation of the olefin in agreement with the observed results.[18, 51, 52,53] Moreover, the quantity of the β-hydride elimination product depended on the electronic effects of the ligand; electrodonating groups at the pyridines favored the olefin formation. Interestingly, in the case of the Ni complexes the reactivity was the opposite (Figure 3. 35.). The temperature of the reaction was a key parameter for the controlling of the selectivity of the system towards dehalogenation and we repeated the same screening at 10ºC (Table 3. 14.), to decrease/slow down the reactivity of the system. This temperature drop caused a clear improvement of the selectivity towards reductive dechlorination, increasing the yield of **III.2a** in most cases and decreasing the presence of **III.3a**. Despite electron rich complexes lost reactivity in terms of chloroalkane activation, alkene yield remained untouched. In conclusion, our family of complexes catalyzes the cleavage of Csp^3-Cl bond from tertiary alkyl chlorides, and the reaction was selectively drive to both the reductive dechlorination or the olefin formation by tuning the metal and the ligand. These results illustrate the potentiality of the system to develop a synthetic methodology, but more studies are needed. Nevertheless, since the aim of developing a synthetic

methodology for the formation of radicals from alkyl chlorides, we will focus on the reductive dechlorination product.
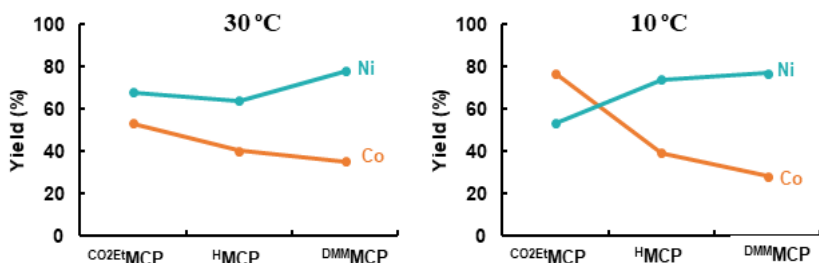

Figure 3. 35. Structure/Catalytic activity trend of (^{X}**MCP)MCl₂** in the photoactivation of **III.1a**.
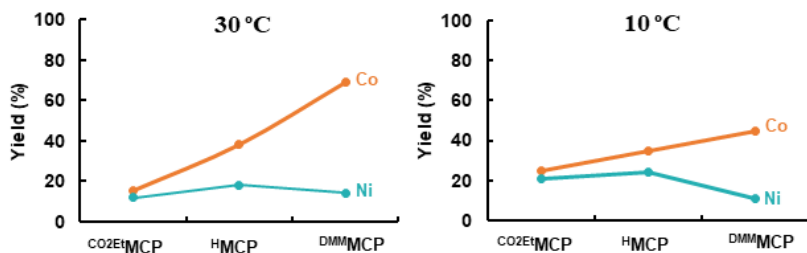

Figure 3. 36. Structure/Catalytic activity trend of (^{X}**MCP)MCl₂** in the formation of olefins from **III.1a**.

At this point, we evaluated the catalytic activity towards (3-chloro-butyl)benzene (**III.1b**) as a model secondary alkyl chloride (Table 3. 15). At 30ºC, the catalytic activation decreased compared to the tertiary alkyl chloride, with conversion within 29-100%. Now, β-hydride elimination occurred only with Co catalysts and in lower yields compared to the tertiary chloroalkane, showing a clear contrast between the different reactivity of Co and Ni complexes.

Table 3. 15. Screening of catalyst for reaction with (3-chloro-butyl)benzene.
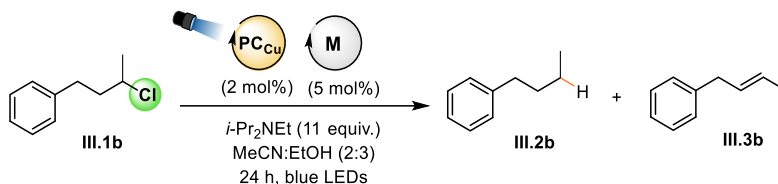
		30ºC			50ºC		
	Catalyst	Conv. (%)	Yield III.2b (%)	Yield III.3b (%)	Conv. (%)	Yield III.2b (%)	Yield III.3b (%)
1	(^{CO2Et}TPA)**CoCl$_2$**	45	**18**	20	88	**18**	25
2	(^{CO2Et}TPA)**NiCl$_2$**	61	**36**	0	75	**58**	0
3	(^{H}TPA)**CoCl$_2$**	63	**30**	13	79	**52**	20
4	(^{H}TPA)**NiCl$_2$**	33	**19**	0	85	**49**	0
5	(^{DMM}TPA)**CoCl$_2$**	29	**11**	14	77	**31**	15
6	(^{DMM}TPA)**NiCl$_2$**	65	**45**	0	87	**69**	0
7	(^{CO2Et}MCP)**CoCl$_2$**	100	**58**	8	100	**69**	12
8	(^{CO2Et}MCP)**NiCl$_2$**	64	**54**	0	96	**75**	0
9	(^{H}MCP)**CoCl$_2$**	73	**54**	15	92	**64**	14
10	(^{H}MCP)**NiCl$_2$**	74	**51**	0	92	**86**	0
11	(^{DMM}MCP)**CoCl$_2$**	64	**33**	10	96	**45**	32
12	(^{DMM}MCP)**NiCl$_2$**	57	**50**	0	100	**89**	0
13	(^{CO2Et}PDP)**CoCl$_2$**	77	**51**	10	97	**67**	14
14	(^{CO2Et}PDP)**NiCl$_2$**	61	**32**	0	88	**64**	0
15	(^{H}PDP)**CoCl$_2$**	73	**39**	18	97	**51**	16
16	(^{H}PDP)**NiCl$_2$**	34	**51**	0	77	**58**	0
17	(^{DMM}PDP)**CoCl$_2$**	36	**18**	0	80	**49**	10
18	(^{DMM}PDP)**NiCl$_2$**	81	**80**	0	100	**91**	0

Reaction conditions: **III.1b** (10 mM), **PC$_{Cu}$** (2 mol%), catalyst (5 mol%), DIPEA (11.4 equiv.), EtOH/MeCN (3:2), visible-light irradiation with blue LEDs (1 W, 447 nm) for 24 h. Conversion and yield were determined by GC using biphenyl as an internal standard. Reactions run in triplicate.

Regarding the ligand effect, again TPA-based complexes showed the worst scaffold for the desired reactivity. While MCP and PDP base catalysts showed better and similar reactivity. Now, the lower formation of olefin product prone us to increase the reaction temperature to 50ºC. This modification improved the reactivity of the catalysts towards dechlorination in most cases (Table 3. 15, 45-94% yield, close to full conversion), without a significant increment of the formation of the olefin. As previously observed, Ni catalysts presented better catalytic response, where the electron-rich substituents in the pyridine moiety showed a positive effect in dechlorination yields (Figure 3. 37). In the other cases only 10% yield separates the nickel catalysts from the cobalt catalysts, due to the formation of olefins.
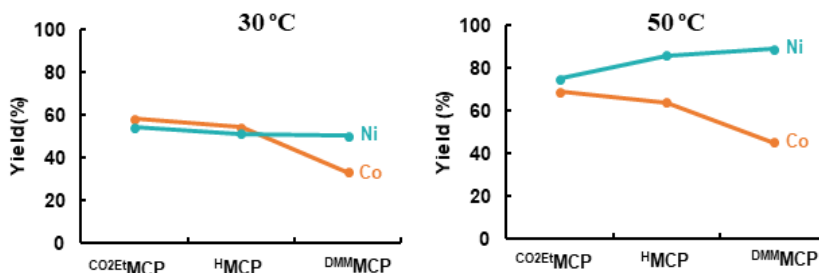

Figure 3. 37. Structure/Catalytic activity trend of (**ᵡMCP)MCl₂** in the photoactivation of **III.1b**.

Primary alkyl chlorides are the most inert compounds, therefore more remarkable for benchmarking the ability of developed tetradentate N-based complexes in the activation of Csp^3−Cl bond. To this end, we used (3-chloropropyl)benzene (**III.1c**) as model substrate. We observed a general drop in the catalytic activity of the complexes at 30ºC (Table 3. 16), with moderate conversions (27-77%) and poor yields of reductive dechlorination (5-53%). In this case, olefin was not detected, in agreement with the hypothesis of a substrate-dependent mechanism pathway. It can be rationalized that the β-hydride elimination is favored as followed tertiary > secondary > primary, while

considering that the metal alkyl complex is formed, presumably via a rebounding mechanism of the radical to the metal center. In principle, sterics should disfavored the rebounding with the tertiary, while it is the one that most efficiently forms the olefin. On the other hand, cannot be discarded a hydrogen abstraction mechanism (HAT) of a tertiary β-hydrogen to the radical producing the equivalent olefin product.

This first screening evidenced nickel as better metal center for the desired reactivity under these conditions, where certainly electrodonating groups at the pyridine benefited nickel catalysis and electrowithdrawing groups enhanced the catalytic activity of cobalt (Figure 3. 38.). Consequently, we increased the reaction temperature and although we obtained a general improvement of 10% yield at 50ºC, only 3 of the complexes presented a remarkable improvement of the reactivity (Table 3. 16, entries 7, 12 and 18). While (DMMMCP)NiCl$_2$ and (DMMPDP)NiCl$_2$ showed great dechlorination yield (~80%), (CO2EtMCP)CoCl$_2$ was the only Co complex capable to dehagenate (3-chloropropyl)benzene. Two different mechanisms may be attributed for each metal in cleavage of Csp^3-Cl bond; the different behavior of the metal related to their electronic properties is a clear key evidence of two different routes for the same reactivity. These results showed room for improvement, but at high temperatures (70ºC) the reactivity was poorer (Table 3. 16), suggesting that the catalytic system is sensible to temperature higher than 50 ºC.

Eventually, these family of complexes showed a capability of activate strong Csp^3−Cl bonds, with different catalytic activity depending on the substrate, the ligand and the metal center. However, this activation undergoes a manageable dehalogenation.

Table 3. 16. Screening of catalyst for the dechlorination of (3-chloro-propyl)benzene.
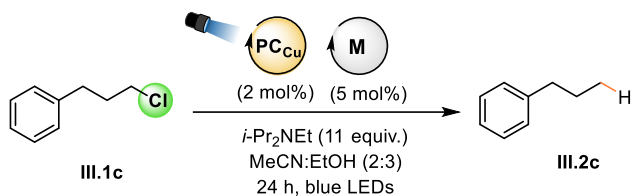
Catalyst	30°C		50°C		70°C	
	Conv. (%)	Yield III.2c (%)	Conv. (%)	Yield III.2c (%)	Conv. (%)	Yield III.3c (%)
1 $(^{CO2Et}TPA)CoCl_2$	59	34	73	45	71	44
2 $(^{CO2Et}TPA)NiCl_2$	31	18	35	19	39	23
3 $(^{H}TPA)CoCl_2$	39	23	39	30	38	27
4 $(^{H}TPA)NiCl_2$	23	9	35	16	35	11
5 $(^{DMM}TPA)CoCl_2$	25	10	30	15	33	19
6 $(^{DMM}TPA)NiCl_2$	55	29	75	49	69	51
7 $(^{CO2Et}MCP)CoCl_2$	70	39	89	74	92	70
8 $(^{CO2Et}MCP)NiCl_2$	34	13	35	33	48	28
9 $(^{H}MCP)CoCl_2$	60	37	58	37	54	36
10 $(^{H}MCP)NiCl_2$	50	27	49	47	60	43
11 $(^{DMM}MCP)CoCl_2$	32	16	43	32	85	64
12 $(^{DMM}MCP)NiCl_2$	92	73	85	78	69	57
13 $(^{CO2Et}PDP)CoCl_2$	35	12	57	47	45	21
14 $(^{CO2Et}PDP)NiCl_2$	49	27	35	34	22	12
15 $(^{H}PDP)CoCl_2$	31	8	35	33	65	43
16 $(^{H}PDP)NiCl_2$	38	18	32	25	47	36
17 $(^{DMM}PDP)CoCl_2$	27	5	42	23	50	37
18 $(^{DMM}PDP)NiCl_2$	72	49	86	80	82	64

Reaction conditions: **III.1c** (10 mM), **PC$_{Cu}$** (2 mol%), catalyst (5 mol%), DIPEA (11.4 equiv.), EtOH/MeCN (3:2), visible-light irradiation with blue LEDs (1 W, 447 nm) for 24 h. Conversion and yield were determined by GC using biphenyl as an internal standard. Reactions run in triplicate.
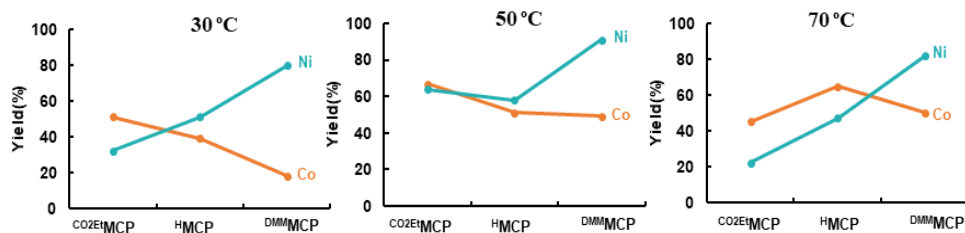
**Figure 3. 38.** Structure/Catalytic activity trend of (**ˣMCP)MCl₂** in the photoactivation of **III.1c**.

The next step consisted of the study of an intramolecular reductive cyclization, using the model reaction stablished in the work of M. Claros (Table 3. 17).[20] The model substrate (**III.3d**) contain two geminal substituents to favor the cyclization step by taking advantage of the *Thorpe-Ingold effect*.[54] The values of yield obtained were lower compared to the pentacoordinated Ni or Co catalyst, but our tetradentated catalysts showed good results without an exhaustive optimization of the conditions. We identified the same trends of reactivity: the effect of the electronic properties of the ligands (and the complex) effect on a different way depending on the metal. Ni complexes showed better results with electrondonating groups. However, Co complexes showed worse results with this kind of substituents.

We chose a second and more challenging substrate (**III.1e**) to better evaluate the performance of our system, without the *Thorpe-Ingold effect*. We started with some examples in the same conditions, obtaining few reactivity, so we increased the temperature of the system to 50ºC (Table 3. 18). Despite the general poor activity of all the catalysts against this compound, the reaction selectivity offered was high for the reductive cyclization.

Table 3. 17. Screening of catalyst for the reductive cyclization of dimethyl 2-allyl-2-(2-chloroethyl)malonate.
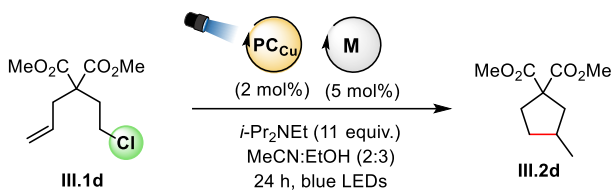
	Catalyst	50ºC	
		Conv. (%)	Yield III.2d (%)
1	(^{CO2Et}TPA)CoCl$_2$	33	18
2	(^{CO2Et}TPA)NiCl$_2$	88	46
3	(^{H}TPA)CoCl$_2$	13	10
4	(^{H}TPA)NiCl$_2$	95	49
5	(^{DMM}TPA)CoCl$_2$	67	57
6	(^{DMM}TPA)NiCl$_2$	87	67
7	(^{CO2Et}MCP)CoCl$_2$	100	78
8	(^{CO2Et}MCP)NiCl$_2$	92	65
9	(^{H}MCP)CoCl$_2$	90	75
10	(^{H}MCP)NiCl$_2$	98	46
11	(^{DMM}MCP)CoCl$_2$	69	68
12	(^{DMM}MCP)NiCl$_2$	100	71
13	(^{CO2Et}PDP)CoCl$_2$	98	76
14	(^{CO2Et}PDP)NiCl$_2$	86	70
15	(^{H}PDP)CoCl$_2$	100	81
16	(^{H}PDP)NiCl$_2$	91	32
17	(^{DMM}PDP)CoCl$_2$	52	46
18	(^{DMM}PDP)NiCl$_2$	100	78

Reaction conditions: **III.1d** (10 mM), **PC$_{Cu}$** (2 mol%), catalyst (5 mol%), DIPEA (11.4 equiv.), EtOH/MeCN (3:2), visible-light irradiation with blue LEDs (1 W, 447 nm) for 24 h. Conversion and yield were determined by GC using biphenyl as an internal standard. Reactions run in triplicate.

Table 3. 18. Screening of catalyst for the reductive cyclization of (E)-12-chloro-1-morpholinododec-7-en-1-one.
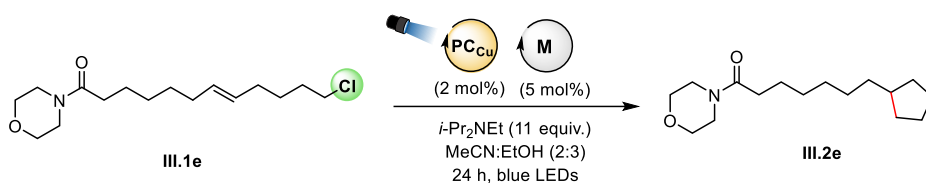
	Catalyst	30ºC	
		Conv. (%)	Yield III.2e (%)
1	(^{CO2Et}TPA)CoCl$_2$	25	6
2	(^{CO2Et}TPA)NiCl$_2$	28	5
3	(^{H}TPA)CoCl$_2$	22	5
4	(^{H}TPA)NiCl$_2$	11	5
5	(^{DMM}TPA)CoCl$_2$	25	15
6	(^{DMM}TPA)NiCl$_2$	36	8
7	(^{CO2Et}MCP)CoCl$_2$	79	75
8	(^{CO2Et}MCP)NiCl$_2$	41	18
9	(^{H}MCP)CoCl$_2$	26	21
10	(^{H}MCP)NiCl$_2$	63	32
11	(^{DMM}MCP)CoCl$_2$	31	19
12	(^{DMM}MCP)NiCl$_2$	49	33
13	(^{CO2Et}PDP)CoCl$_2$	26	17
14	(^{CO2Et}PDP)NiCl$_2$	25	11
15	(^{H}PDP)CoCl$_2$	19	15
16	(^{H}PDP)NiCl$_2$	20	13
17	(^{DMM}PDP)CoCl$_2$	22	13
18	(^{DMM}PDP)NiCl$_2$	65	43

Reaction conditions: **III.1e** (10 mM), **PC$_{Cu}$** (2 mol%), catalyst (5 mol%), DIPEA (11.4 equiv.), EtOH/MeCN (3:2), visible-light irradiation with blue LEDs (1 W, 447 nm) for 24 h. Conversion and yield were determined by GC using biphenyl as an internal standard. Reactions run in triplicate.

Remarkably, $(^{CO2Et}MCP)CoCl_2$ presented a promising result (75% yield), following the same observed trend in the previous experiments: electron-withdrawing ligands work better with Co complexes; electron-donating ligands present higher catalytic activity with Ni complexes. Ultimately, the tuning of the electronic properties of the ligand has an effect not only on the stability of low-valent metal intermediates, but also in their redox potentials and their interaction with the photocatalyst. These two aspects are modifying the reactivity against the activation of alkyl chlorides and other side reactions, at the same time.

Hydrogen evolution as side reaction

We can explain partially the different reactivity observed between nickel and cobalt by means of reaction selectivity towards side reactions. Aminopyridine cobalt complexes are well-known active catalysts for proton reduction and hydrogen production in aqueous conditions.[55, 56] Our group published a photo- and electrocatalytic hydrogen evolution strategy by first-row transition metal complexes based on pentacoordinated triazacyclononane ligand.[16, 17] Mechanistic investigations revealed the formation of a $Co^{III}-H$ hydride species from low-valent metal intermediates in presence of protic source, before undergoing the molecular hydrogen. In the case of nickel derivatives, no hydrogen production is observed due to the unfavorable formation of $Ni^{III}-H$ from low-valent nickel intermediate.

In this sense, we expected that the developed tetradentate N-based complexes in this thesis should similarly behave. Consequently, proton reduction could be an important side reaction that competes with the cleavage of Csp^3-Cl bond in protic solvents. For that reason, we carried out an exhaustive monitoring of the hydrogen evolution under optimized conditions (ethanol as protic solvent). We focused our attention on PDP and MCP based catalysts and their electronic properties, being

the most active catalysts from the synthetized family. In the case of employing cobalt complexes, considerable amounts of hydrogen were measured without adding substrate (Figure 3. 39, left). Turn-over-number (TON) allowed us to correlate the electronic properties of the ligand scaffold and the amount of hydrogen formation. In contrast with previous studies with **Py$_2$^{Ts}tacn** ligand, electrodonating groups in the pyridine moiety enhance the hydrogen generation, whereas the complexes with ester groups did not produce a significant amount of hydrogen. Regarding the ligand backbone, both skeletons presented similar trend in terms of electronic properties-hydrogen formation. However, PDP ligands showed higher TON of hydrogen formation in comparison with MCP ligands. The addition of model substrate **III.1d** for cyclization (Figure 3. 39, right) decreased the H$_2$ formation since the Co complex is also catalyzing the reductive cyclization through Csp^3−Cl activation.
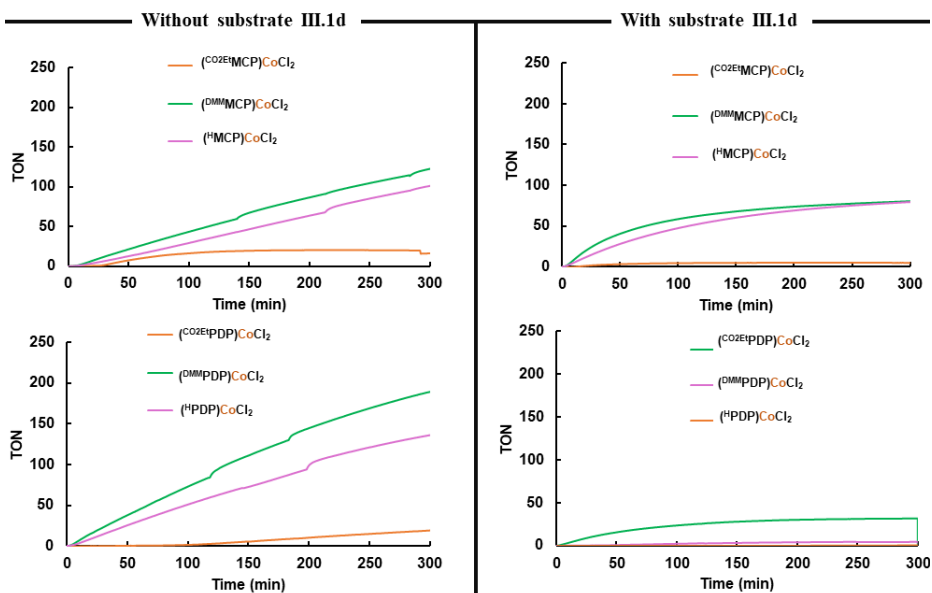
Figure 3. 39. Hydrogen evolution monitoring under optimized conditions for the cobalt catalysts. **PC$_{Cu}$** (2 mol%), catalyst (5 mol%), DIPEA (11.4 equiv.), EtOH/MeCN (3:2), visible-light irradiation with blue LEDs (1 W, 447 nm).

These evidences are in concordance with the previous results in catalysis, where (**^{CO2Et}MCP**)**CoCl$_2$** showed the best catalytic response in all the tested examples. In contrast, H$_2$ monitoring experiments indicate that Ni catalysts cannot undergo the photocatalytic proton reduction (Figure 3. 40). This capability of Co complexes to perform H$_2$ formation in contrast to Ni complexes might help to partially understand the higher efficiency of nickel catalysts towards the activation of Csp^3−Cl bonds under protic solvent conditions.
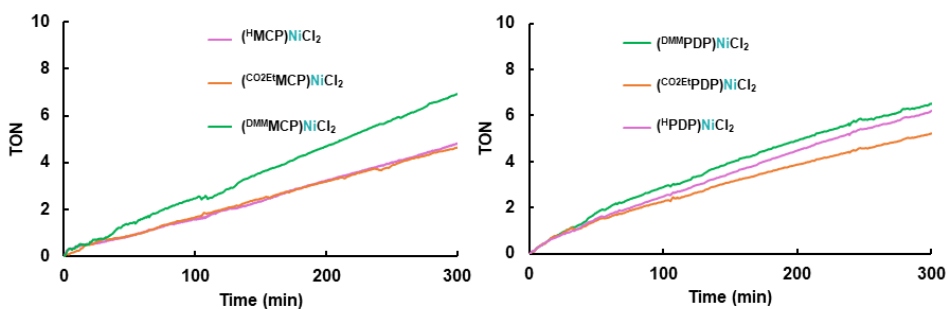
Figure 3. 40. Hydrogen evolution monitoring under optimized conditions for the nickel catalysts in absence of substrate. **PC$_{Cu}$** (2 mol%), catalyst (5 mol%), DIPEA (11.4 equiv.), EtOH/MeCN (3:2), visible-light irradiation with blue LEDs (1 W, 447 nm).

Monitoring of reductive cyclization reaction

Considering that the product yield after 24 h might besides reactivity could also involve stability issues of the coordination complexes, photocatalysts and other complex interferences, we inspected the evolution over time of selected reactions. In this sense, we monitored the reductive cyclization reaction of the model substrate **III.1d**, focusing on the (**^{X}PDP**)**MCl$_2$** family of complexes. These complexes present the most robust scaffold of the library, minimizing potential complications such as isomerization of the complex.

From initial monitoring tests, we identify 3 different kinetic regions in the profiles (Figure 3. 41): i) the first 10 minutes, ii) from minute 10 to minute 50, and iii) after 50 minutes until yield saturation.
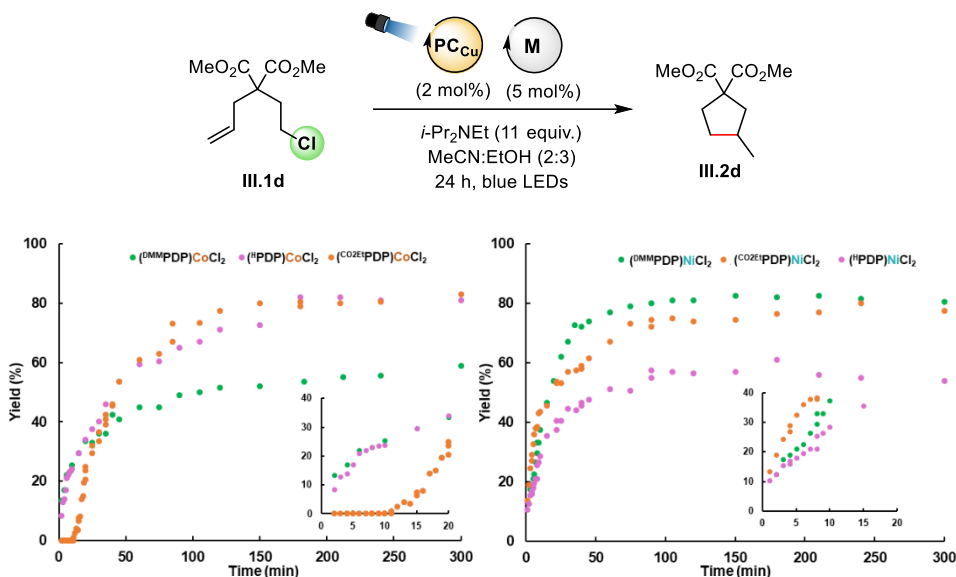

Figure 3. 41. Monitoring of reductive cyclization of **III.1d** and comparison of the catalytic response of $(^{X}\textbf{PDP})\textbf{MCl}_2$ over time. Each profile corresponds to the average of at least three reactions.

During the first minutes of reaction the catalytic system is cleaner and can better represent the electronic properties of the ligands. However, there is not a clear correlation between the reaction rate and the electronic effects of the ligand. Moreover, there is an induction period of 10 min in the case of the $(^{\textbf{CO2Et}}\textbf{PDP})\textbf{MCl}_2$, that deserves more work to understand the reason behind. Then, the reaction rate started to decrease in the second region time, where the stability of the species were compromised. Apparently, each ligand has a different effect to the stability of this intermediates, reaching to certain final yields depending on the stability of this species. In Figure 3. 41 (right), $(^{\textbf{DMM}}\textbf{PDP})\textbf{NiCl}_2$ presents the slowest initial rate. However, this ligand might stabilize the system, and therefore, the rate was maintained high in the second time region. On the other hand, the cobalt catalyst with the best catalytic response is $(^{\textbf{CO2Et}}\textbf{PDP})\textbf{CoCl}_2$, as seen

previously. After the time delay, $(^{CO2Et}PDP)CoCl_2$ the reaction rate was faster, obtaining the best final yield. This may indicate that the $(^{CO2Et}PDP)CoCl_2$ is a precatalyst that is *in-situ* transformed to the real catalyst in about 10 minutes.

Further studies of the kinetic profiles enables the elucidation of the reaction order for the important reaction components. This information is useful from a practical point of view, and it also allows discerning between different mechanistic proposals.[57] The growing of these technologies requires the development of new kinetic analyses. Classical treatments such as "initial rates method" is widely stablished, although the measurements are totally blind to the entire reaction.[58-63] The "reaction progress kinetic analysis" (RPKA) described by D. Blackmond in 2005 meant a breakthrough in kinetic methods.[63, 64] This procedure enables the elucidation of several events/parameters: catalyst deactivation, product inhibition, order in reagent… Nevertheless, RPKA requires rate data, which is obtained by isothermal calorimetry. In 2016 J. Burés designed a novel visual kinetic treatment called "variable time normalization analysis" (VTNA).[65-68] This graphical analysis plots **[A]** (where A can be substrate or product) against a normalized time scale, **$\Delta t \cdot [x]_o{}^{\alpha}$** (where x is the parameter to study and α its reaction order). The adjustment of the time scale for experiments with different **x** loadings makes the direct comparison of concentration profiles possible. The chosen normalization is theoretically because the **x** concentration is constant during the reaction. Therefore, **$\Delta t \cdot [x]_o{}^{\alpha}$** becomes one of the parameters of the function that describes the concentration of a product or reagent at each time point, independently of the complexity of the function. The time normalization is performed by multiplying each time point by the total concentration of catalyst used in each experiment raised to **α.** This value should be adjusted until all the corrected conversion curves overlay. This overlay occurs independently of the complexity of the reaction kinetics or changes in the kinetic regime.

We decided to apply VTNA for the study of $(^{X}\text{PDP})\text{NiCl}_2$ complexes, which showed similar kinetic profile and where the electronic properties showed an effect to the reaction rate. Specially, we took $(^{DMM}\text{PDP})\text{NiCl}_2,$ as the best catalyst, for the exhaustive VTNA of the kinetic profile. We determined by VTNA the reaction order in catalyst (Figure 3. 42) and in substrate (Figure 3. 43) for the reductive cyclization of the model compound **III.1d**.
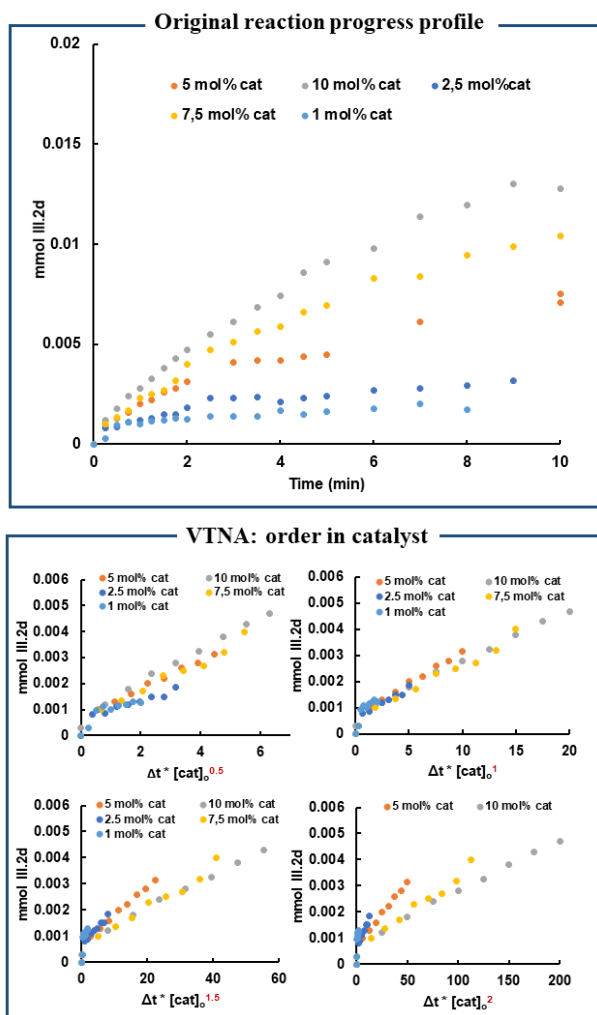

Figure 3. 42. Determination of order in catalyst for the reductive cyclization of **III.1d** using $(^{DMM}\text{PDP})\text{NiCl}_2$ as catalyst by VTNA.
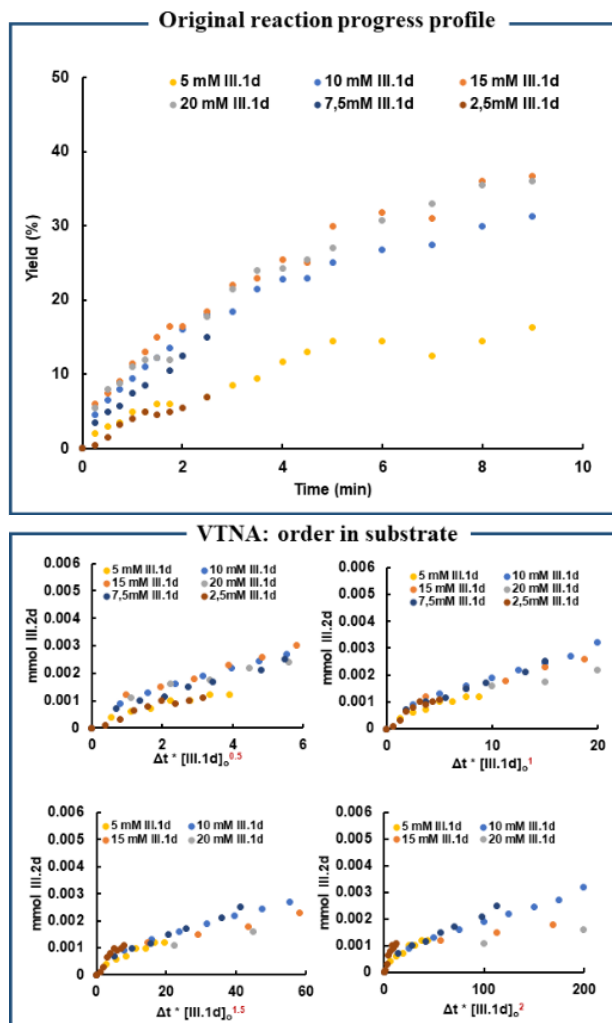
Figure 3. 43. Determination of order in substrate for the reductive cyclization of **III.1d** using (**DMMPDP**)**NiCl₂** as catalyst by VTNA.

Simplifying the rate law of this reaction to $v = k\,[III.1d]^x\,[cat]^y$, we determined from VTNA a first-order dependency on the catalyst concentration and also on the substrate concentration. To support this data treatment, we also determined the reaction orders by "initial rates method", studying the first 2 min of the reaction profile (Figure 3. 44). The initial rate of a reaction is equal to the slope of the

linear trend of formed product over time when substrate conversion remains below 15% (before 2 min in that case). Reaction orders close to 1 were obtained in each compound by the classical method, in concordance with VTNA results.
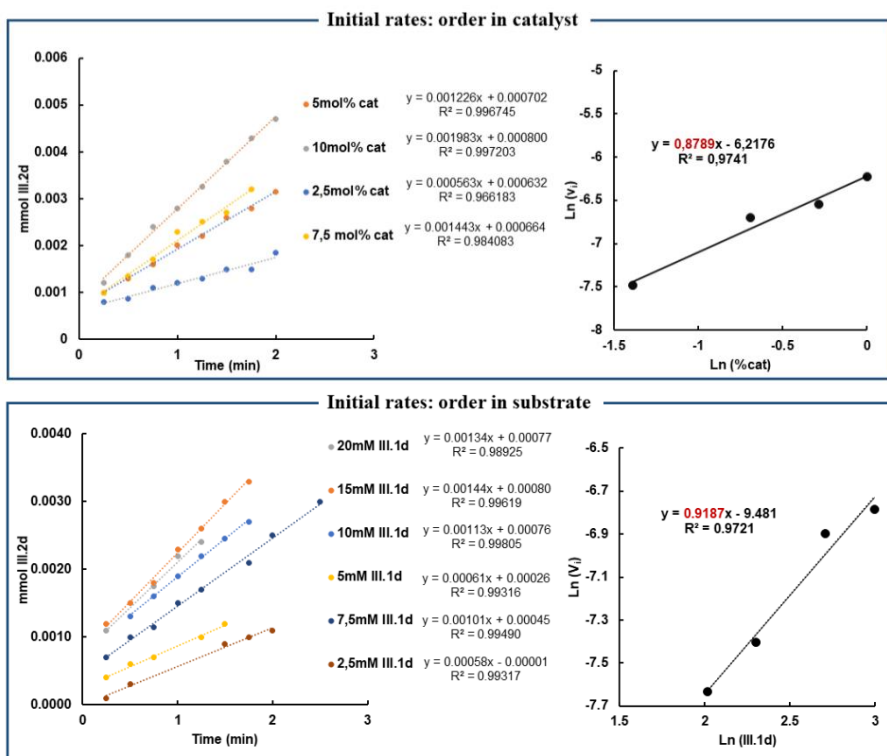
Figure 3. 44. Determination of order in substrate and in catalyst for the reductive cyclization of **III.1d** using (**DMM**PDP)NiCl$_2$ as catalyst by "initial rates method".

We envision the requirement of an exhaustive study of the kinetic profile of each catalyst and reaction, to stablish a rational structure/activity relationship together with a mechanistic proposal. Here we stablish the basis of the mentioned study.

3.3. Conclusions

In this chapter, we synthetized and fully characterized a family of 18 tetradentate N-based aminopyridine cobalt and nickel complexes. First we designed and synthetized 9 different ligands based on 3 different scaffolds: tris(2-pyridylmethyl)amine scaffold (**^{X}TPA**) and (S,S)-bis-pyridine ligands based on a (S,S)-cyclohexyldiamine (**^{X}MCP**) and bispyrrolidine backbone (**^{X}PDP**), where X refeered to the substituents in the pyridine ring (X= H, CO_2Et or DMM). The preparation of ligands **^{x}TPA** (X = H,[31] DMM[24]), **^{x}PDP** (H,[25] DMM,[22] CO_2Et[22]) and **^{x}MCP** (H, DMM)[22] was accomplished to a literature known procedures and ligands **^{CO2Et}TPA** and **^{CO2Et}PDP** were prepared following similar synthetic pathways. Then, we have prepared the corresponding library of 9 well-defined coordination Co^{II} complexes and 9 well-defined coordination Ni^{II} complexes, where (**^{CO2Et}TPA)CoCl$_2$**, (**^{DMM}TPA)CoCl$_2$**, (**^{DMM}PDP)CoCl$_2$**, (**^{CO2Et}PDP)CoCl$_2$**, (**^{DMM}MCP)CoCl$_2$**, (**^{CO2Et}MCP)CoCl$_2$**, (**^{CO2Et}TPA)NiCl$_2$**, (**^{DMM}TPA)NiCl$_2$**, (**^{H}PDP)NiCl$_2$**, (**^{CO2Et}PDP)NiCl$_2$**, (**^{DMM}PDP)NiCl$_2$**, (**^{H}MCP)NiCl$_2$** (**^{DMM}MCP)NiCl$_2$** and (**^{CO2Et}MCP)NiCl$_2$** have been described for the first time in this work. The complexes have been characterized by paramagnetic ^{1}H-NMR, elemental analysis, x-ray diffraction and UV-vis spectroscopy. The study of ^{1}H-NMR at different temperatures allowed us to determine the electronic configuration of the metal center and the paramagnetic behavior of the complexes.

Then, we have tested the efficiency of the library for the photoredox activation of inert alkyl chlorides in two different transformations: the reductive dechlorination of alkyl chlorides and the intramolecular cyclization of chloroalkanes with pendant alkenes. All the complexes were able to activate (3-chloro-3-methylbutyl)benzene, presenting a competition between reductive dechlorination and elimination products. Decreasing the temperature of the system allowed us to enhance the reductive dechlorination process using Ni

complexes. However, the selectivity of the Co complexes was not improved, presenting a considerable amount of olefin formation. In the case of (3-chloro-butyl)-benzene, the lower trend of chloride elimination allowed us to push the system by increasing the reaction temperature to 50ºC. This modification clearly improved the reactivity of the catalysts towards dechlorination in most cases, where the electron-rich substituents in the pyridine moiety ((**^{DMM}PDP)NiCl$_2$** and (**^{DMM}MCP)NiCl$_2$** showed a positive effect in dechlorination yields (89 and 94%). Except in these two cases, in all other cases only 10% yield separates the nickel catalysts from the cobalt catalysts. The library presented a general drop of the reactivity when 3-chloropropylbenzene was the model primary chloroalkane. While (**^{DMM}MCP)NiCl$_2$** and (**^{DMM}PDP)NiCl$_2$** showed great dechlorination yield (~80%), (**^{CO2Et}MCP)CoCl$_2$** was the only Co complex capable to activate (3-chloropropyl)benzene. The application of the library in challenging reductive cyclization of chloroalkanes with pendant alkenes confirmed these 3 complexes as the best candidates for explore further reactivity.

Considering these pieces of evidence, we have attributed two different mechanism for each metal in the cleavage of Csp^3−Cl bond where the different behavior of the metal related to their electronic properties plays a key role. The monitoring of hydrogen formation shows the capability of Co complexes to perform proton reduction, being one of the mains side reactions. This secondary reaction explains the lack of reactivity of Co complexes for the activation of primary alkyl chlorides, in contrast with Ni complexes. Moreover, (**^{CO2Et}MCP)CoCl$_2$** was not able to undergo hydrogen evolution, being the best Co catalyst of the library.

At last, we have monitored the model reductive cyclization catalyzed by (**^{X}PDP)MCl$_2$** to identify a structure/reactivity relationship. In general, the reactions presented a fast initial rate, and reflects a clear effect of the ligand into the stabilization of the catalytic system. In the case of Ni complexes,

electrodonating groups such as DMM keep the initial catalytic rate for longer periods. In contrast, electrodeficient ligands with CO_2Et are beneficial for Co complexes. We focused our attention on $(^XPDP)NiCl_2$, determining the reaction order in catalyst/substrate by two different analytic protocols: "initial rates" method and VTNA. We share the reproducibility of both protocols, obtaining comparable results, stablishing the basis for an exhaustive study of the kinetic profile of each catalyst and reaction to rationalize the mechanism and the structure/activity relationship.

3.4. Experimental section

3.4.1. Materials and reagents

Reagents and solvents were used as received from the commercial supplier unless otherwise stated. Triethylamine and diisopropylethylamine were distilled over potassium hydroxide and were stored under argon. Photocatalysts [Cu(bathocuproine)(xantphos)](PF$_6$) (**PC$_{Cu}$**)[69] were synthesized according to the literature procedures.

For the synthesis of reagents, the solvents (DMF, hexane, Et$_2$O, CH$_2$Cl$_2$, MeCN and toluene) were used from a SPS-400, Innovative Technology solvent purification system and stored under argon with activated 4 Å molecular sieves. Anhydrous acetonitrile was purchased from Sigma-Aldrich® and water was purified with a Milli-Q Millipore Gradient AIS system. Water, methanol, ethanol, trifluoroethanol, acetonitrile, dimethylformamide, dimethylacetamide and tetrahydrofurane used for photoreactions were degassed by freeze-pump-thaw method (repeated 3 cycles) and were stored under argon. All the alkeness were filtered by a pad of Celite (Hyflo Super Cel from Sigma-Aldrich, CAS: 68855-54-9) before running the photoreactions.

The synthesis of air-sensitive reagents as well as the preparation of visible light photocatalytic reactions were conducted inside a nitrogen-filled glove box (mBraun Unilab) with concentrations of O$_2$ and H$_2$O lower than 0.5 ppm and using Schlenk techniques under argon atmosphere.

3.4.2. Instruments

Nuclear magnetic resonance (NMR). NMR spectra were recorded on Bruker Fourier300, AV400, AV500 and AVIII500 spectrometers using standard conditions (300 K). All ^{1}H chemical shifts are reported in ppm and have been internally calibrated to the residual protons of the deuterated solvent. The ^{13}C chemical shifts have been internally calibrated to the carbon atoms of the deuterated solvent. The coupling constants were measured in Hz.

Mass Spectrometry. High resolution Mass Spectrometry (HRMS) data was collected on a HPLC-QqTOF (Maxis Impact, Bruker Daltonics) or HPLC-TOF (MicroTOF Focus, Bruker Daltonics) mass spectrometer using 1 mM solution of the analyzed compound.

UV-Vis spectroscopy. UV-Vis spectra were recorded on an Agilent 8453 diode array spectrophotometer (190-1100 nm range) in 1 cm quartz cells. A cryostat from Unisoku Scientific Instruments was used for the temperature control.

Gas chromatography analysis. The analysis and quantification of the starting materials and products were carried out on an Agilent 7820A gas chromatograph (HP5 column, 30m or Cyclosil-B column, 30m) and a flame ionization detector. GC-MS spectral analyses were performed on an Agilent 7890A gas chromatograph interfaced with an Agilent 5975c MS mass spectrometer.

3.4.3. In-house developed parallel photoreactor
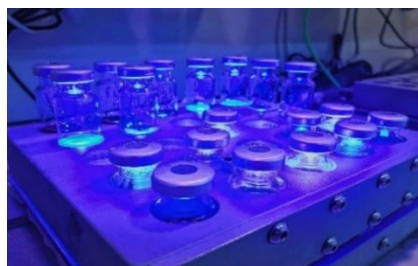
Figure 3. 45. In-house developed parallel photoreactors with 25 positions for vials of 10 or 21 mL.

Figure 3. 46. In-house developed parallel photoreactors with 48 positions for vials of 1 mL.

Light source: The reactions were performed using Royal-Blue ($\lambda = 447\pm20$ nm) LUXEON Rebel ES LED, mounted on a 20 mm Square Saber - 1030 mW @ 700mA as a light source.

Temperature Control: Reaction temperature was controlled by a high-precision thermoregulation Hubber K6 cryostat. Likewise, aiming at ensuring stable irradiation, the temperature of the LEDs was controlled and set at 22 ℃.

3.4.4. Synthesis and characterization of tetradentate aminopyridine ligands
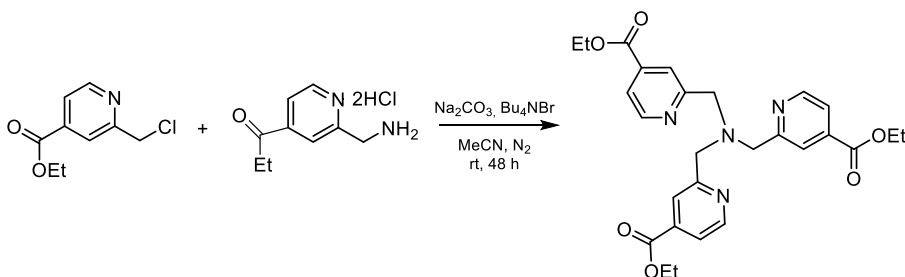
CO2Et TPA. 4-ethoxycarbonyl-2-chloromethylpyridine (0.99 g, 4.96 mmol), 4-ethoxycarbonyl-2-aminomethylpyridine (0.5 g, 2.31 mmol) and anhydrous MeCN (40 mL) were mixed in a 100 mL flask. Na2CO3 and tetrabutylammonium bromide (80 mg) were added directly as solids and the resulting mixture was heated at reflux under N2 for 22 h. After cooling to rt, the resulting orange mixture was filtered, and the filter cake was washed with CH2Cl2. The solvent was removed under reduced pressure and the resulting crude was treated with hexane (25 mL) and DCM (2 mL). This last procedure was repeated several times until the solid was clean. 0.91 g (78% yield). 1H NMR (400 MHz, CDCl3, 25 ºC): δ (ppm) = 8.59 (d, 1H), 8.10 (s, 1H), 7.65 (d, 1H), 4.45 (q, 2H), 4.06 (s, 2H), 1.47 (t, 3H).
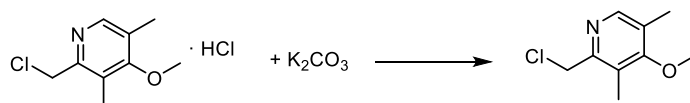
To a solution of 2-chloromethyl-3,5-dimethyl-4-methoxypyridine hydrochloride (3.00 g, 13.5 mmol) in water (3 mL) was added a solution of potassium carbonate prepared by mixing 2,43 g (17.6 mmol) of K2CO3 and 1.5 mL of water. The resulting mixture was stirred for 2-3 min and then extracted with DCM several times. The combined organic layers were dried over Na2SO4, and

the volatile components were removed under reduced pressure. 2.39 g (95% yield). 1H NMR (400 MHz, CDCl3, 25 °C): δ (ppm) = 8.21 (s, 1H), 4.69 (s, 2H), 3.78 (s, 3H), 2.34 (s, 3H), 2.26 (s, 3H).[70]
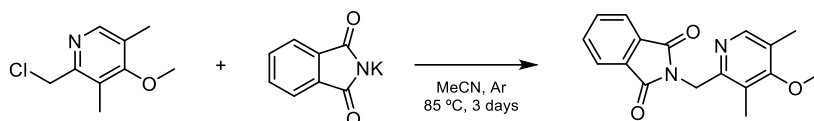
To a stirred solution of 2-chloromethyl-3,5-dimethyl-4-methoxypyridine (2.30 g, 12.4 mmol) in MeCN (40 mL) was added potassium phthalimide (2.32 g, 12.5 mmol). The mixture was vigorously stirred under Ar atmosphere at 85 °C for 3 days and then cooled to rt, followed by MeCN removal under reduced pressure. The remaining solid was dissolved in water and the aqueous solution was extracted with DCM several times. The organic extracts were dried over Na2SO4, and the volatile components were removed in vacuo. The resulting yellow solid was recrystallized from minimum volume of hot methanol. 2.47 g (67% yield). 1H NMR (400 MHz, CDCl3, 25 °C): δ (ppm) = 8.05 (s, 1H), 7.88 (m, 2H), 7.72 (m, 2H), 4.92 (s, 2H), 3.75 (s, 3H), 2.32 (s, 3H), 2.18 (s, 3H).[70]
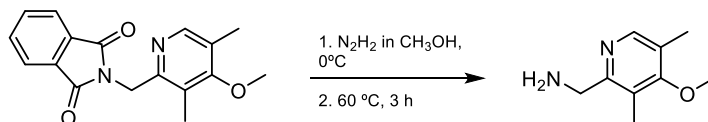
To a cooled (0 °C) stirred solution of 3,5-dimethyl-4-methoxy-2-phtalimidomethylpyridine (2.47 g, 8.34 mmol) in MeOH (27 mL) was added a solution of hydrazine hydrate (1.92 g, 19.17 mmol) in MeOH (6.8 mL) during 1 min. The resulting mixture was stirred at 60 °C for 3 h, and after cooling to rt, the volatile components were removed. The remaining solid was dissolved in 1.5 M NaOH aqueous solution, and the solution was extracted with DCM several times.

The organic extracts were dried over Na2SO4, and the solvent was removed under reduced pressure. 1.26 g (91% yield).1H NMR (400 MHz, CDCl3, 25 ºC): δ (ppm) = 8.20 (s, 1H), 3.92 (s, 2H), 3.75 (s, 3H), 2.24 (s, 3H), 2.20 (s, 3H).[70]
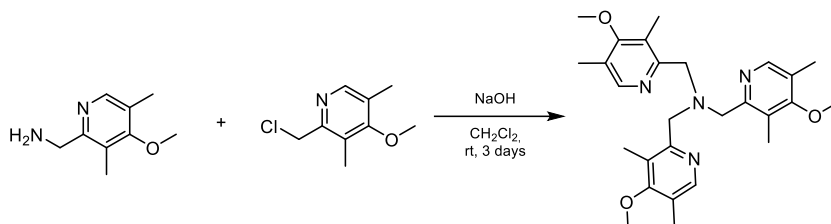

DMMTPA. To a stirred solution of 2-aminomethyl-3,5-dimethyl-4-methoxypyridine (1.26 g, 7.56 mmol) in DCM (42 mL) were added 2-chloromethyl-3,5-dimethyl-4-methoxypyridine hydrochloride (2.15 g, 16.26 mmol) and 1.11 M NaOH solution (29 mL, 31.8 mmol). The reaction mixture was vigorously stirred at rt for 3 days, after that the pH of the solution dropped to 8. The organic layer of the mixture was separated, and the aqueous layer was extracted with DCM. The combined organic layers were dried over Na2SO4, and the volatile components were removed under vacuum. The resulting crude was treated with hexane (25 mL) and DCM (2 mL). The supernatant was transferred to another flask and evaporated. This procedure was repeated several times until the solid was clean. 1.53 g (44% yield). 1H NMR (400 MHz, CDCl3, 25 °C): δ (ppm) = 8.19 (s, 1H), 3.75 (s, 2H), 3.66 (s, 3H), 2.23 (s, 3H), 1.62 (s, 3H). The spectroscopic characterization is in agreement with the reported literature.[70]
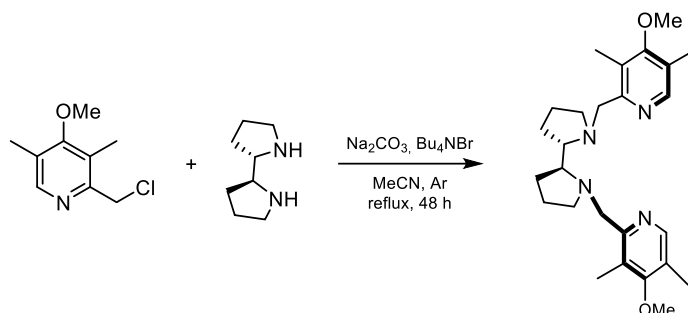
[DMM]**PDP**. 2-chloromethyl-3,5-dimethyl-4-methoxypyridine hydrochloride (1.74 g, 7.84 mmol), (2R,2'R)-2,2'-bipyrrolidine (0.5 g, 3.57 mmol) and anhydrous MeCN (45 mL) were mixed in a 100 mL flask. Na2CO3 and tetrabutylammonium bromide (0.115 g, 0.357 mmol) were added directly as solids and the resulting mixture was heated at reflux under N2 for 22 h. After cooling to rt, the resulting orange mixture was filtered, and the filter cake was washed with CH2Cl2. The solvent was removed under reduced pressure and the resulting crude was purified by flash chromatography (neutral Al2O3, DCM). 1.31 g (83 %). 1H NMR (400 MHz, CDCl3, 25 ºC): δ (ppm) = 8.14 (s, 2H), 7.95 (s, 1H), 4.05 (d, 2H), 3.75 (s, 6H), 3.39 (d, 2H), 2.75 (m, 2H), 2.68 (m, 2H), 2.31 (s, 6H), 2.26 (m, 2H), 2.24 (s, 6H), 1.69-1.53 (m, 8H). The spectroscopic characterization is in agreement with the reported in the literature.[71]
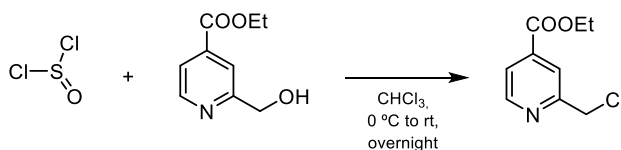
SOCl2 (8.86 g, 74.5 mmol) in chloroform (30 mL) was added dropwise to a degassed solution of 4-ethoxycarbonyl-2-hydroxymethylpyridine (2.70 g, 14.9 mmol) in chloroform (100 mL) at 0 ºC, stirred overnight at rt and then dried under vacuum. 1H NMR (400 MHz, CDCl3, 25 ºC): δ (ppm) = 8.89 (d, 1H), 8,41 (s, 1H), 8,24 (dd, 1H), 5.12 (s, 2H), 4.45 (q, 2H), 1.40 (t, 3H).
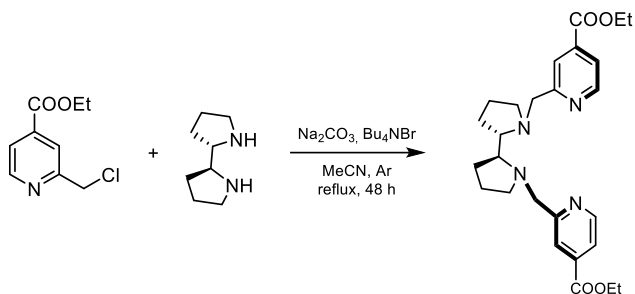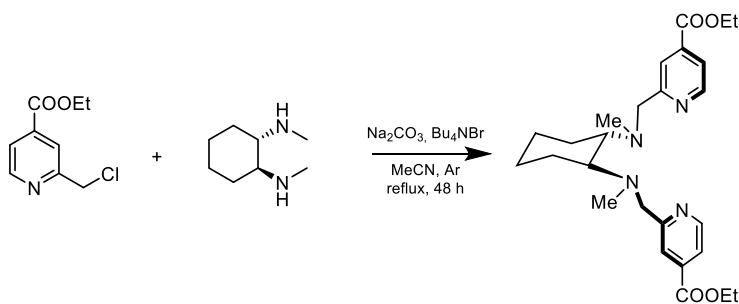
[CO2Et]**PDP**. 4-ethoxycarbonyl-2-chloromethylpyridine (1.9 g, 8.05 mmol), (2R,2'R)-2,2'-bipyrrolidine (0.508 g, 3.63 mmol) and anhydrous MeCN (45 mL) were mixed in a 100 mL flask. Na2CO3 and tetrabutylammonium bromide (80 mg) were added directly as solids and the resulting mixture was heated at reflux under N2 for 22 h. After cooling to rt, the resulting orange mixture was filtered and the filter cake was washed with CH2Cl2. The solvent was removed under reduced pressure and the resulting crude was purified by flash chromatography (neutral Al2O3, DCM). 1.46 g (39% yield). 1H NMR (400 MHz, CDCl3, 25 ºC): δ (ppm) = 8.75 (d, 1H),7.95 (s, 1H), 7.65 (dd, 1H), 4.45 (q, 2H), 4.30 (d, 1H), 3.65 (d, 1H), 3.0 (m, 1H), 2.85 (m, 1H), 2.33 (m, 1H), 1.75 (m, 2H), 1.70 (m, 2H), 1.66 (s, 2H), 1.45 (t, 3H). The spectroscopic characterization is in agreement with the literature reported.[71]
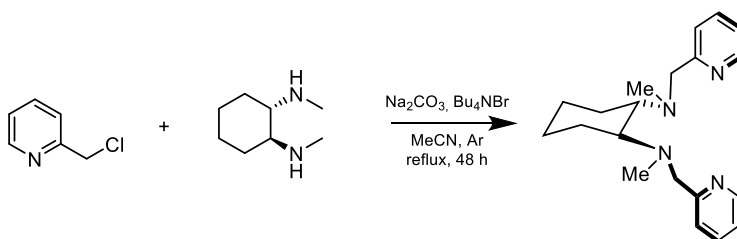

[H]**MCP**. 2-Pycolyl chloride hydrochloride (2.96 g, 23.2 mmol), (1S,2'S)-N,N'-dimethylcyclohexane-1,2-diamine (1,50 g, 10.6 mmol) and anhydrous MeCN (40 mL) were mixed in a 100 mL flask. Na2CO3 and tetrabutylammonium bromide (0.340 g, 1.055 mmol)) were added directly as solids and the resulting mixture was heated at reflux under N2 for 22 h. After cooling to rt, the resulting orange

mixture was filtered and the filter cake was washed with CH2Cl2. The solvent was removed under reduced pressure and the resulting crude was purified by flash chromatography (neutral Al2O3, DCM). 2.95 g (86% yield). 1H NMR (400 MHz, CDCl3, 25 ºC): δ (ppm) = 8.50 (d, 2H), 7.55 (d, 4H), 7.15 (m, 2H), 3.75 (m, 4H), 2.65 (m, 2H), 2.43 (d, 1H), 2.25 (s, 6H), 1.99 (m, 2H), 2.73 (m, 2H), 1.25 (m, 4H). The spectroscopic characterization is in agreement with the literature reported[72].

[CO2Et]**MCP**. 4-ethoxycarbonyl-2-chloromethylpyridine (1.544 g, 7.73 mmol), (1S,2'S)-N,N'-dimethylcyclohexane-1,2-diamine (0,50 g, 3.52 mmol) and anhydrous MeCN (20 mL) were mixed in a 100 mL flask. Na2CO3 and tetrabutylammonium bromide (0.113 g0.352 mmol)) were added directly as solids and the resulting mixture was heated at reflux under N2 for 22 h. After cooling to rt, the resulting orange mixture was filtered and the filter cake was washed with CH2Cl2. The solvent was removed under reduced pressure and the resulting crude was purified by flash chromatography (neutral Al2O3, hexanes/EtOAc). 1.05 g (64% yield). 1H NMR (400 MHz, CDCl3, 25 ºC): δ (ppm) = 8.73 (d, 2H), 8.35 (s, 2H), 7.65 (d, 2H), 4.25 (m, 4H), 3.96 (d, 2H), 3.83 (d, 2H), 2.69 (m, 2H), 2.28 (s, 6H), 2.13 (s, 2H), 2.10 (m, 4H), 1.78 (m, 2H), 1.25 (m, 8H). The spectroscopic characterization is in agreement with the literature reported[72].
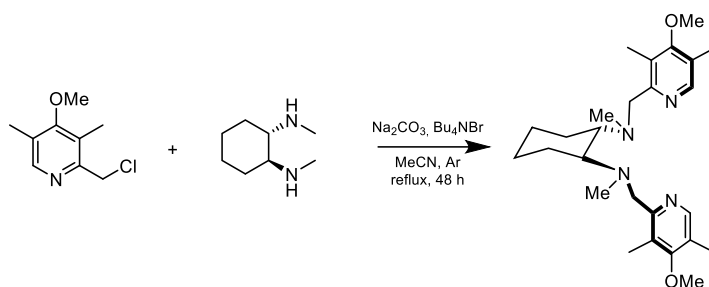
DMMMCP. 2-chloromethyl-3,5-dimethyl-4-methoxypyridine hydrochloride (2.58 g, 11.6 mmol), (1S,2'S)-N,N'-dimethylcyclohexane-1,2-diamine (0.75 g, 5.27 mmol) and anhydrous MeCN (45 mL) were mixed in a 100 mL flask. Na2CO3 and tetrabutylammonium bromide (0.170 g, 0.527 mmol)) were added directly as solids and the resulting mixture was heated at reflux under N2 for 22 h. After cooling to rt, the resulting orange mixture was filtered and the filter cake was washed with CH2Cl2. The solvent was removed under reduced pressure and the resulting crude was purified by flash chromatography (neutral Al2O3, DCM). 1.48 g (64% yield). 1H NMR (400 MHz, CDCl3, 25 ºC): δ (ppm) = 8.22 (s, 2H), 7.55 (d, 4H), 3.75 (m, 4H), 2.55 (m, 2H), 2.49 (s, 6H), 2.29 (s, 6H), 2.12 (s, 4H), 1.84 (m, 9H), 1.75 (m, 2H) (m, 2H), 1.25 (m, 4H), 1,19 (m, 4H). The spectroscopic characterization is in agreement with the literature reported[72].

3.4.5. Synthesis and characterization of tetradentate aminopyridine complexes

General procedure. In a glovebox, a solution of the ligand (1 eq) in THF (1ml) was added to a suspension of cobalt(II) chloride or Nickel(II) chloride ethylene glycol dimethyl ether complex (1 eq) in anhydrous THF (1ml). After few minutes, a colorful solution was obtained. After stirring overnight, Et2O was added and the solid was filtered. This solid was dissolved in DCM or MeCN and filtered through Celite. Removal of the solvent under vacuum and recrystallization by diethyl ether diffusion into dichloromethane or acetonitrile solutions yielded the targeted complexes as crystalline materials in good yields (60-94%).
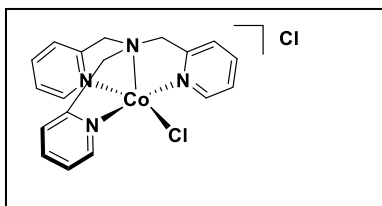
Prepared according to general procedure. 0.775 mmol scale. Isolated as a black solid in 0.289 g (89% yield). **^{1}H NMR** (500 in MHz, CD$_3$CN, 20 ºC): δ (ppm) = 131.0 (br), 106.1 (br), 58.4, 46.2, 2. In agreement with previously reported data.[73]
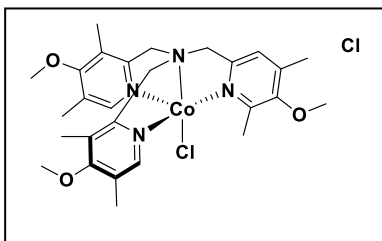
Prepared according to general procedure. 0.581 mmol scale. Isolated as a green crystalline solid in 0.300 g (73% yield).

**^{1}H NMR** (500 in MHz, CD$_3$CN, 20 ºC): δ (ppm) = 138.91 (br), 101.53 (br), 2.76, 1.17, 0.53. **IR** (film): 2946, 1600, 1571, 1479, 1421, 1401, 1273, 1248, 1078, 992, 883, 795 cm^{-1}. **MS:** m/z calcd for C$_{27}$H$_{36}$Cl$_2$CoN$_4$O$_3$ [M-Cl$^+$]: 558.1802, found

558.1791. **Anal. Calcd** (%) for $C_{27}H_{36}Cl_2CoN_4O_3 \cdot \frac{1}{4} CH_2Cl_2 \cdot \frac{1}{2} H_2O$: C 52.39, H 6.05, N: 8.97; found: C 52.12, H 6.18, N: 9.04.
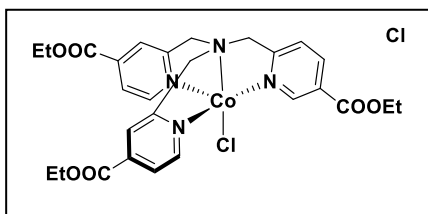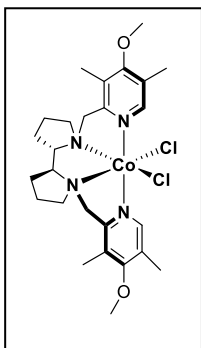

Prepared according to general procedure. 0.622 mmol scale. Isolated as a dark red crystalline solid in 0.296 g (75% yield).

^{1}H NMR (500 in MHz, CD$_3$CN, 20 ºC): δ (ppm) = 121.15 (br), 119.31 (br), 51.27, 41.10, 1.99, -0.20. **IR** (film): 2985, 1722, 1563, 1427, 1364, 1286, 1198, 1105, 1009, 767 cm^{-1}. **MS:** m/z calcd for $C_{27}H_{30}Cl_2CoN_4O_6$ [M-Cl$^+$]: 600.1164, found 600.1180. **Anal. Calcd** (%) for $C_{27}H_{30}Cl_2CoN_4O_6 \cdot \frac{1}{4} H_2O$: C 50.62, H 4.80, N: 8.75; found: C 50.62, H 4.68, N: 8.76.
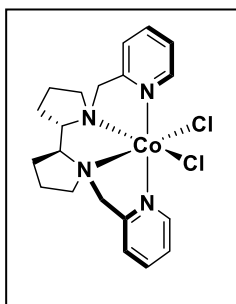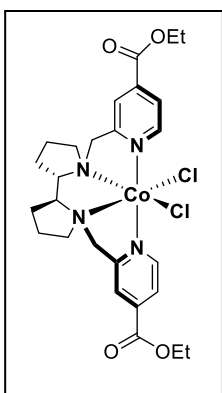

Prepared according to general procedure. 0.837 mmol scale. Isolated as a pink crystalline solid in 0.304 g (80% yield).

^{1}H NMR (500 in MHz, CD$_3$CN, 20 ºC): δ (ppm) = 175.07, 100.28, 45.99, 38.25, 2.78, 27.93, 18.26, 11.55, 6.71, 4.79, 2.12, 1.20, -11.78. **IR** (film): 3052, 2978, 2942, 2903, 1602, 1570, 1476, 1439, 1376, 1339, 1300, 1264, 1182, 1158, 1098, 1044, 1022, 996, 981, 896, 786, 641, 615, 566, 513, 427 cm^{-1}. **MS:** m/z calcd for $C_{20}H_{x26}OcoN_4$ [M-Cl$^+$]:416.1172, found 416.1160. **Anal. Calcd** (%) for $C_{20}H_{26}Cl_2CoN_4 \cdot \frac{1}{4} H_2O$: C 52.59, H 5.85, N: 12.27; found: C 52.67, H 5.67, N: 12.27.
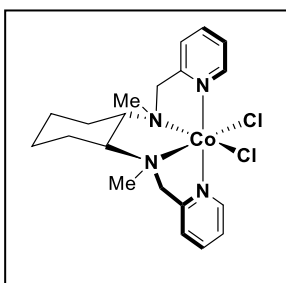
Prepared according to general procedure. 0.616 mmol scale. Isolated as a pink crystalline 0,328 g (94% yield).

¹H NMR (500 in MHz, CD3CN, 20 ºC): δ = 175.75, 105.96, 34.75, 26.22, 17.65, 12.32, 9.01, 5.45, 4.66, 1.34, -12.90, -17.85ppm. **IR** (film): 2946, 2881, 1599, 1573, 1475, 1402, 1359, 1268, 1226, 1089, 1063, 1034, 1002, 968, 938, 900, 871, 788, 513 cm⁻¹. **MS:** m/z calcd for $C_{26}H_{38}ClO_2CoN_4$ [M-Cl⁺]: 532.2010, found 532.2004. **Anal. Calcd** (%) for $C_{26}H_{38}Cl_2CoN_4O_2 \cdot \frac{3}{4} H_2O$: C 53.74, H 6.84, N: 9.64; found: C 53.67, H 6.66, N: 9.42.

Prepared according to general procedure. 0.579 mmol scale. Isolated as a brown crystalline solid in 0.302 g (88% yield).

¹H NMR (500 in MHz, CD₃CN, 20 ºC): δ (ppm) = 174.36, 90.49, 41.24, 36.72, 31-07, 20.96, 15.53, 12.59, 8.20, 5.44, 2.54, 0.53, -1.22, -8.66. **IR** (film): 2974, 2897, 1723, 1614, 1563, 1363, 1291, 1202, 1109, 1013, 918, 866, 767, 692 cm⁻¹. **Anal. Calcd** (%) for $C_{26}H_{34}Cl_2CoN_4O_4$: C 52.36, H 5.74, N: 9.39; found: C 52.12, H 5.67, N: 9.23.

Prepared according to general procedure. 1.109 mmol scale. Isolated as a pink crystalline solid in 0,447 g (89% yield).

¹H NMR (500 in MHz, CD₃CN, 20 ºC): δ (ppm) = 164.91, 101.2, 62.66, 50.65, 23.76, 21.23, 18.40, 8.23, 6.45, 2.14, 0.22, -16.95. **IR** (film): 2939, 1602, 1573, 1476, 1435, 1307, 1018, 955, 866, 766, 634, 580, 508 cm⁻¹. **MS:** m/z calcd for $C_{20}H_{28}ClCoN_4$ [M-Cl⁺]: 418.1329, found 418.1321. **Anal. Calcd** (%) for

$C_{20}H_{28}Cl_2CoN_4 \cdot \frac{1}{4} H_2O$: C 52.36, H 6.26, N: 12.21; found: C 52.37, H 4.68, N: 8.76.
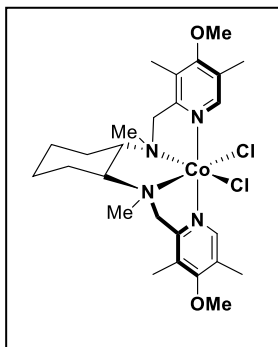
Prepared according to general procedure. 0.715 mmol scale. Isolated as a pink crystalline solid in 0.304 g (76% yield).

¹H NMR (500 in MHz, CD$_3$CN, 20 ºC): δ (ppm) = 164.17, 92.01, 72.22, 44.98, 25.64, 23.15, 14.56, 9.99, 9.70, 2.55, 2.25, 0.85, -15.9 **IR** (film): 2928, 2862, 1598, 1575, 1476, 1452, 1400, 1359, 1262, 1082, 1017, 867, 795 cm^{-1}. **Anal. Calcd** (%) for $C_{26}H_{40}Cl_2CoN_4O_2 \cdot \frac{1}{2} CH_2Cl_2$: C 51.93, H 6.74, N: 9.14; found: C 51.65, H 6.52, N: 8.85
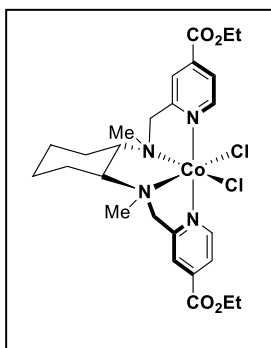
Prepared according to general procedure. 0.627 mmol scale. Isolated as a orange crystalline solid in 0.356 g (89% yield).

¹H NMR (500 in MHz, CD$_3$CN, 20 ºC): δ (ppm) = 98.03, 86.30, 68.52, 23.65, 16.70, 14.27, 12.53, 9.08, 5.45, 2.72, 2.22, -4.54. **IR** (film): 2931, 1720, 1614, 1561, 1289, 1201, 1103, 1012, 975, 865, 769, 716, 693 cm^{-1}.

MS: *m/z* calcd for $C_{26}H_{36}ClCoN_4O_4$ [M-Cl$^+$]: 562.1752, found 562.1753. **Anal. Calcd** (%) for $C_{26}H_{36}Cl_2CoN_4O_4 \cdot \frac{1}{2} H_2O \cdot CH_2Cl_2$: C 46.84 H 5.68, N: 8.09; found: C 47.07, H 5.54, N: 8.05.
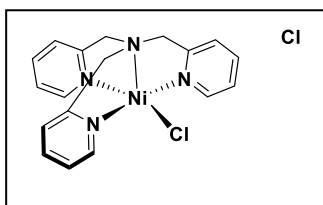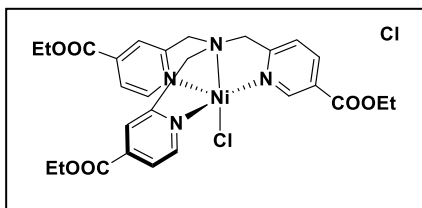
Prepared according to general procedure. 0.930 mmol scale. Isolated as a blue crystalline solid in 0.277 g (70% yield).

^{1}H NMR (500 in MHz, CD3CN, 20 ºC): δ = 50.53, 43.17, 13.94, 2.17 ppm. **IR** (film): 2916, 1603, 1572, 1477, 1473, 1286, 1099, 1049, 1022, 911, 769 cm^{-1}. **MS:** m/z calcd for $C_{18}H_{18}ClNiN_4$ [M-Cl$^+$]: 383.0568, found 383.0570. **Anal. Calcd** (%) for $C_{18}H_{18}Cl_2Ni \cdot \frac{1}{4} H_2O \cdot \frac{1}{4} CH_2Cl_2 \cdot \frac{1}{4}$ MeCN : C 50.62, H 4.80, N: 8.75; found: C 50.47, H 4.70, N: 8.74.
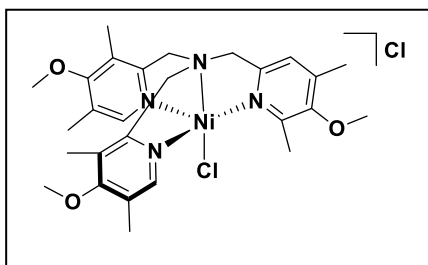
Prepared according to general procedure. 0.581 mmol scale. Isolated as a blue crystalline solid in 0.308 g (89% yield).

^{1}H NMR (500 in MHz, CD3CN, 20 ºC): δ = 58.97, 8.55, 6.33, 3.7 ppm. **IR** (film): 2945, 1598, 1570, 1475, 1420, 1261, 1072, 1036, 994, 959, 918, 877, 788, 521 cm^{-1}. **MS:** m/z calcd for $C_{27}H_{36}Cl_2NiN_4O_3$ [M-Cl$^+$]: 557.1824, found 557.1806. **Anal. Calcd** (%) for $C_{27}H_{36}Cl_2NiN_4O_3 \cdot \frac{1}{2}$ MeCN : C 53.73, H 6.15, N: 10.25; found: C 50.14, H 4.68, N: 9.39.

Prepared according to general procedure. 0.711 mmol scale. Isolated as a green crystalline solid in 0.347 g (77% yield).

^{1}H NMR (500 in MHz, CD3CN, 20 ºC): δ = 49.42, 40.63, 3.98, 1.35 ppm. **IR** (film): 2985, 1722, 1564, 1426, 1366, 1287, 1199, 1105, 1009, 767 cm^{-1}. **MS:** m/z calcd for $C_{27}H_{30}ClNiN_4O_6$ [M-Cl$^+$]:

599.1202, found 599.1203. **Anal. Calcd** (%) for $C_{27}H_{30}Cl_2NiN_4O_6 \cdot ¼ H_2O$: C 50.62, H 4.80, N: 8.75; found: C 50.47, H 4.70, N: 8.74.
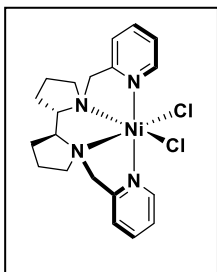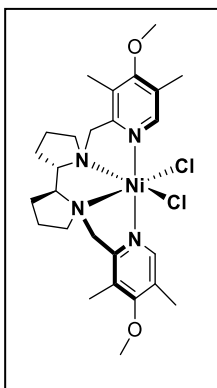

Prepared according to general procedure. 0.977 mmol scale. Isolated as a blue crystalline solid in 0,361 g (82% yield).

^{1}H NMR (500 in MHz, CD3CN, 20 ºC): δ = 49.10, 45.50, 38.14, 27.95, 25.07, 22.77, 14.98, 2.13, -4.96 ppm. **IR** (film): 2981, 1603, 1570, 1475, 1439, 1300, 1020, 900, 788 cm^{-1}. **MS:** m/z calcd for $C_{20}H_{38}ClNiN_4$ [M-Cl$^+$]: 415.1194, found 415.1195. **Anal. Calcd** (%) for $C_{20}H_{26}Cl_2NiN_4 \cdot 2 H_2O$: C 49.22, H 6.20, N: 11.48; found: C 49.40, H 5.54, N: 11.48.
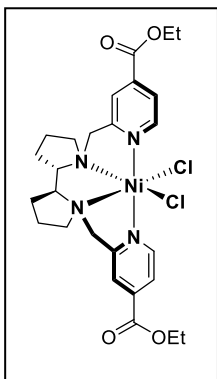

Prepared according to general procedure. 0.718 mmol scale. Isolated as a blue crystalline solid in 0,463 g (96% yield).

^{1}H NMR (500 in MHz, CD3CN, 20 ºC): δ = 39.54, 32.65, 26.38, 25.31, 12.03, 11.07, 7.94, 6.86, 4.17, -7.45, -7.96, -10.21, -12.75 ppm. **IR** (film): 2947, 1573, 1475, 1402, 1268, 1089, 1036, 1000, 900, 873 cm^{-1}. **MS:** m/z calcd for $C_{26}H_{38}ClNiN_4O_2$ [M-Cl$^+$]: 531.2031, found 531.2026. **Anal. Calcd** (%) for $C_{26}H_{38}Cl_2NiN_4O_2 \cdot ½ CH_2Cl_2$: C 52.12, H 6.44, N: 9.18; found: C 52.18, H 6.63, N: 9.26.
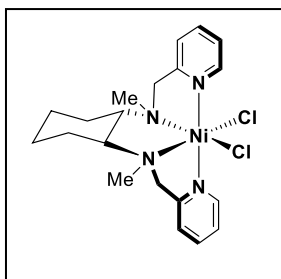
Prepared according to general procedure. 0.579 mmol scale. Isolated as a green crystalline solid in 0.244 g (70% yield).

^{1}H NMR (500 in MHz, CD3CN, 20 ºC): δ = 44.14, 37.22, 25.01, 22.93, 14.6, 4.20, 1.53, -4.82, -7.33 ppm. **IR** (film): 2979, 1727, 1615, 1566, 1471, 1417, 1364, 1290, 1201, 1098, 1016, 919, 863, 763, 720, 698, 687 cm^{-1}. **MS:** *m/z* calcd for $C_{26}H_{34}ClNiN_4O_4$ [M-Cl$^+$]: 559.1617, found 559.1623. **Anal. Calcd** (%) for $C_{26}H_{34}Cl_2NiN_4O_4 \cdot H_2O \cdot$ ½ MeCN : C 50.15, H 5.96, N: 9.93; found: C 50.31, H 5.78, N: 9.98.

Prepared according to general procedure. 1.109 mmol scale. Isolated as a blue crystalline solid in 0.302 g (60% yield).

^{1}H NMR (500 in MHz, CD3CN, 20 ºC): δ = 51.15, 44.87, 42.51, 41.51, 38.67, 21.03, 18.12, 17.24, 15.33, 14.81, 14.38, 2.16, 1.19, 0.9, -4.01, -5.43 ppm. **IR** (film): 2929, 1604, 1571, 1474, 1446, 1431, 1304, 1022, 976, 868, 770, 647, 583, 503 cm^{-1}. **MS:** *m/z* calcd for $C_{20}H_{28}ClNiN_4$ [M-Cl$^+$]: 417.1350, found 417.1332. **Anal. Calcd** (%) for $C_{20}H_{28}Cl_2NiN_4$: C 49.59, H 5.89, N: 11.28; found: C 50.33, H 5.90, N: 11.29.
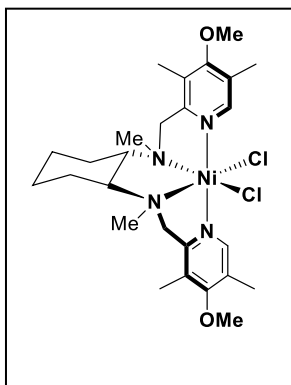
Prepared according to general procedure. 0.715 mmol scale. Isolated as a blue crystalline solid in 0.243 g (65% yield).

¹H NMR (500 in MHz, CD3CN, 20 ºC): δ = 26.08, 21.36, 10.77, 10.26, 8.07, 7.42, 4.07, 3.66, 3.54, 2.21, -5.34 ppm. **IR** (film): 2923, 1599, 1575, 1474, 1399, 1271, 1083, 1017, 993, 870, 794, 518 cm⁻¹. **MS:** m/z calcd for $C_{26}H_{40}ClNiN_4O_2$ [M-Cl⁺]: 533.2188, found 533.2195.
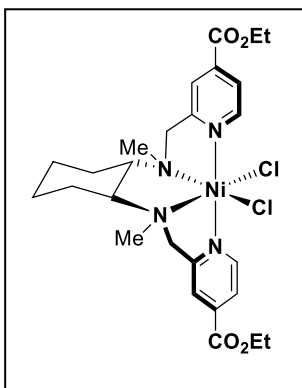
Prepared according to general procedure. 0.672 mmol scale. Isolated as a green crystalline solid in 0.339 g (76% yield).

¹H NMR (500 in MHz, CD3CN, 20 ºC): δ = 43.53, 41.76, 37.73, 18.43, 17.22, 4.21, 1.55, -2.41, -5.36 ppm. **IR** (film): 2935, 1716, 1613, 1562, 1291, 1194, 1108, 1020, 979, 863, 769, 716, 693 cm⁻¹. **MS:** m/z calcd for $C_{26}H_{36}ClNiN_4O_4$ [M-Cl⁺]: 561.1773, found 561.1746. **Anal. Calcd** (%) for $C_{26}H_{36}Cl_2NiN_4O_6 \cdot ¼ H_2O \cdot 1 CH_2Cl_2$: C 47.16, H 5.64, N: 8.15; found: C 47.01, H 5.45, N: 8.14.

3.4.6. Crystal preparation and X-Ray difraction analysis

Crystal preparation: Crystals of were grown by slow diffusion of Et2O in CH2Cl2 inside an anaerobic glovebox. The crystals for these samples were selected using a Zeiss stereomicroscope using polarized light and prepared under inert conditions immersed in perfluoropolyether as protecting oil for manipulation.

Data collection: Crystal structure determination for compound (^{DMM}TPA)NiCl$_2$ was carried out using a Rigaku diffractometer equipped with a Pilatus 200K area detector, a Rigaku MicroMax-007HF microfocus rotating anode with MoK$_\alpha$ radiation, Confocal Max Flux optics and an Oxford Cryosystems low temperature device Cryostream 700 plus (T = -173 $^\circ$C). Full-sphere data collection was used with ω and φ scans. *Programs used:* Data collection data reduction with CrysAlisPro and absorption correction with Scale3 Abspack scaling algorithm.

Crystal structure determinations for the other samples were carried out using a Apex DUO Kappa 4-axis goniometer equipped with an APPEX 2 4K CCD area detector, a Microfocus Source E025 IuS using MoK$_\alpha$ radiation, Quazar MX multilayer Optics as monochromator and an Oxford Cryosystems low temperature device Cryostream 700 plus (T = -173 $^\circ$C). *Programs used:* Bruker Device: Data collection APEX-2, data reduction Bruker Saint V/.60A and absorption correction SADABS or TWINABS.

Structure Solution and Refinement: Crystal structure solution was achieved using the computer program SHELXT. Visualization was performed with the program SHELXle. Missing atoms were subsequently located from difference Fourier synthesis and added to the atom list. Least-squares refinement on F using all measured intensities was carried out using the program SHELXL 2015. All non-hydrogen atoms were refined including anisotropic displacement parameters.

3.4.7. Photocatalytic experimental procedures

General procedure for catalytic tests of the library of complexes. Inside an anaerobic box, aliquots from stock solutions in MeCN of **alkyl chloride** 100 mM (0.2 mL, 0.02 mmol, 1.0 eq.), **complex** 5 mM (0.2 mL, 0.001 mmol, 5 mol %), **PC$_{Cu}$** 2 mM (0.2 mL, $4 \cdot 10^{-4}$ mmol, 2 mol %) and acetonitrile (0.2 mL) were equally distributed into a vial (10 mL of headspace) that contained glass beads. The vial was sealed with a septum and removed from the anaerobic box. Degassed ethanol was added to the vial to reach a total volume of 2 mL (total concentration of substrate 10 mM). iPr$_2$NEt (40 µL, 0.229 mmol, 11.4 equiv.) was added to each vial, which was placed in the photoreactor at the indicated temperature. After irradiating for 24h with blue LEDs ($\lambda = 447$ nm), the sample was diluted with ethyl acetate (2 mL). A solution of biphenyl in ethyl acetate was added as internal standard ($8.7 \cdot 10^{-3}$ mmol in 0.25 mL). Then, addition of 1 mL of H$_2$O formed a biphasic solution and an aliquot of the organic phase was passed through a plug of MgSO$_4$ and eluted with EtOAc. The resulting solution was analyzed by gas chromatography. The yields reported for each reaction are given as an average of at least two runs.

General procedure for the H2 evolution monitoring. Inside an anaerobic box, aliquots from stock solutions in MeCN of **dimethyl allyl chloroethylmalonate** 100 mM (1 mL, 0.15 mmol, 1.0 equiv.), **complex** 5 mM (1 mL, $7.5 \cdot 10^{-3}$ mmol, 5 mol%), **PC$_{Cu}$** 2 mM (1 mL, $3 \cdot 10^{-3}$ mmol, 2 mol%) and acetonitrile (1 mL) were equally distributed into 2 vials (22 mL of headspace) that contained glass beads. The vials were sealed with a septum and removed from the anaerobic box. Degassed ethanol was added to each vial to reach a total volume of 10 mL (total concentration of substrate 10 mM). iPr$_2$NEt (200 µL, 1.72 mmol,

11.4 equiv.) was added to each vial, which was placed in the photoreactor at 30 ºC. Each reaction vial was connected to a differential pressure transducer sensor (Honeywell-ASCX15DN) with a reference vial that contains only PC_{Cu}, electron donor and solvents. The reaction and reference vials were kept under the same experimental conditions to compensate the noise due to temperature-pressure fluctuations. The dihydrogen generated in the reaction vessels were monitored by recording the increase of pressure in the headspace, which is measured as the difference in pressure between the reaction and the reference vial. Also, blank experiments in order to monitor the dihydrogen evolution in the absence of substrate were performed at the same reaction conditions.

General procedure for reaction monitoring. Inside an anaerobic box, aliquots from stock solutions in MeCN of **dimethyl allyl chloroethylmalonate** 100 mM (0.2 mL, 0.02 mmol, 1.0 equiv.), **complex (^{X}PDP)MCl$_2$** 5 mM (0.2 mL, 0.002 mmol, 5 mol%), PC_{Cu} 2 mM (0.2 mL, $4 \cdot 10^{-4}$ mmol, 2 mol%) and acetonitrile (0.2 mL) were equally distributed into 8 vials (10 mL of headspace) that contained glass beads. The vials were sealed with a septum and removed from the anaerobic box. Degassed ethanol was added to each vial to reach a total volume of 2 mL (total concentration of substrate 10 mM). i-Pr$_2$NEt (40 µL, 0.23 mmol, 11.4 equiv.) was added to each vial, which was placed in the photoreactor at the indicated temperature (30 ºC). At specific points of time (see plot), aliquots of 100 µL were taken from the sealed vials and mixed with 29 µL of solution of biphenyl in EtOAc (34.8 mM) and the resulting mixture was analyzed by GC-FID. Light irradiation was switched off and on at specific points of the single-point monitoring experiment, which indicates that the reaction stops when the vial is not irradiated with visible light.

3.5. References

1. Xu, R., Chapter 1 - Introduction - Frontiers in Modern Inorganic Synthetic Chemistry. In *Modern Inorganic Synthetic Chemistry*, Xu, R.; Pang, W.; Huo, Q., Eds. Elsevier: Amsterdam, 2011; pp 1-7.

2. Kräutler, B., Vitamin B12: chemistry and biochemistry. *Biochem Soc Trans* **2005,** *33* (Pt 4), 806-10.

3. Giedyk, M.; Goliszewska, K.; Gryko, D., Vitamin B12 catalysed reactions. *Chemical Society Reviews* **2015,** *44* (11), 3391-3404.

4. Ociepa, M.; Wierzba, A. J.; Turkowska, J.; Gryko, D., Polarity-Reversal Strategy for the Functionalization of Electrophilic Strained Molecules via Light-Driven Cobalt Catalysis. *Journal of the American Chemical Society* **2020,** *142* (11), 5355-5361.

5. Jaun, B.; Thauer, R. K., Nickel-alkyl bond formation in the active site of methyl-coenzyme m reductase. *Met Ions Life Sci* **2009,** *6*, 115-32.

6. Helvenston, M. C.; Castro, C. E., Nickel(I) octaethylisobacteriochlorin anion. An exceptional nucleophile. Reduction and coupling of alkyl halides by anionic and radical processes. A model for factor F-430. *Journal of the American Chemical Society* **1992,** *114*, 8490-8496.

7. Dey, M.; Li, X.; Kunz, R. C.; Ragsdale, S. W., Detection of Organometallic and Radical Intermediates in the Catalytic Mechanism of Methyl-Coenzyme M Reductase Using the Natural Substrate Methyl-Coenzyme M and a Coenzyme B Substrate Analogue. *Biochemistry* **2010,** *49* (51), 10902-10911.

8. Hill, H. A. O.; Pratt, J. M.; O'Riordan, M. P.; Williams, F. R.; Williams, R. J. P., The chemistry of vitamin B12. Part XV. Catalysis of alkyl halide reduction by vitamin B12a: studies using controlled potential reduction. *Journal of the Chemical Society A: Inorganic, Physical, Theoretical* **1971,** (0), 1859-1862.

9. Schrauzer, G. N.; Lee, L.-P.; Sibert, J. W., Alkylcobalamins and alkylcobaloximes. Electronic structure, spectra, and mechanism of photodealkylation. *Journal of the American Chemical Society* **1970,** *92* (10), 2997-3005.

10. Schrauzer, G. N.; Sibert, J. W.; Windgassen, R. J., Photochemical and thermal cobalt-carbon bond cleavage in alkylcobalamins and related organometallic compounds. Comparative study. *Journal of the American Chemical Society* **1968,** *90* (24), 6681-6688.

11. Lewandowska-Andralojc, A.; Baine, T.; Zhao, X.; Muckerman, J. T.; Fujita, E.; Polyansky, D. E., Mechanistic Studies of Hydrogen Evolution in Aqueous Solution Catalyzed by a Tertpyridine–Amine Cobalt Complex. *Inorganic Chemistry* **2015,** *54* (9), 4310-4321.

12. Mandal, S.; Shikano, S.; Yamada, Y.; Lee, Y.-M.; Nam, W.; Llobet, A.; Fukuzumi, S., Protonation Equilibrium and Hydrogen Production by a Dinuclear Cobalt–Hydride Complex Reduced by Cobaltocene with Trifluoroacetic Acid. *Journal of the American Chemical Society* **2013,** *135* (41), 15294-15297.

13. Lacy, D. C.; Roberts, G. M.; Peters, J. C., The Cobalt Hydride that Never Was: Revisiting Schrauzer's "Hydridocobaloxime". *Journal of the American Chemical Society* **2015,** *137* (14), 4860-4864.

14. Bachmann, C.; Guttentag, M.; Spingler, B.; Alberto, R., 3d Element Complexes of Pentadentate Bipyridine-Pyridine-Based Ligand Scaffolds: Structures and Photocatalytic Activities. *Inorganic Chemistry* **2013,** *52* (10), 6055-6061.

15. Singh, W. M.; Mirmohades, M.; Jane, R. T.; White, T. A.; Hammarström, L.; Thapper, A.; Lomoth, R.; Ott, S., Voltammetric and spectroscopic characterization of early intermediates in the Co(II)–polypyridyl-catalyzed reduction of water. *Chemical Communications* **2013,** *49* (77), 8638-8640.

16. Call, A.; Codolà, Z.; Acuña-Parés, F.; Lloret-Fillol, J., Photo- and Electrocatalytic H2 Production by New First-Row Transition-Metal Complexes Based on an Aminopyridine Pentadentate Ligand. *Chemistry – A European Journal* **2014,** *20* (20), 6171-6183.

17. Call, A.; Franco, F.; Kandoth, N.; Fernández, S.; González-Béjar, M.; Pérez-Prieto, J.; Luis, J. M.; Lloret-Fillol, J., Understanding light-driven H2 evolution through the electronic tuning of aminopyridine cobalt complexes. *Chemical Science* **2018,** *9* (9), 2609-2619.

18. Call, A.; Casadevall, C.; Acuña-Parés, F.; Casitas, A.; Lloret-Fillol, J., Dual cobalt–copper light-driven catalytic reduction of aldehydes and aromatic ketones in aqueous media. *Chemical Science* **2017,** *8* (7), 4739-4749.

19. Call, A.; Lloret-Fillol, J., Enhancement and control of the selectivity in light-driven ketone versus water reduction using aminopyridine cobalt complexes. *Chemical Communications* **2018,** *54* (69), 9643-9646.

20. Claros, M.; Ungeheuer, F.; Franco, F.; Martin-Diaconescu, V.; Casitas, A.; Lloret-Fillol, J., Reductive Cyclization of Unactivated Alkyl Chlorides with Tethered Alkenes under Visible-Light Photoredox Catalysis. *Angewandte Chemie International Edition* **2019,** *58* (15), 4869-4874.

21. Anderegg, G.; Hubmann, E.; Podder, N. G.; Wenk, F., Pyridinderivate als Komplexbildner. XI. Die Thermodynamik der Metallkomplexbildung mit Bis-, Tris- und Tetrakis[(2-pyridyl)methyl]-aminen. *Helvetica Chimica Acta* **1977,** *60* (1), 123-140.

22. Chen, K.; Costas, M.; Kim, J.; Tipton, A. K.; Que, L., Olefin Cis-Dihydroxylation versus Epoxidation by Non-Heme Iron Catalysts: Two Faces of an FeIII−OOH Coin. *Journal of the American Chemical Society* **2002,** *124* (12), 3026-3035.

23. Xue, G.; Wang, D.; Hont, R. D.; Fiedler, A. T.; Shan, X.; Münck, E.; Que, L., A synthetic precedent for the $[Fe^{IV}_2(\mu\text{-}O)_2]$ diamond core proposed for methane monooxygenase intermediate Q. *Proceedings of the National Academy of Sciences* **2007,** *104* (52), 20713-20718.

24. Chen, M. S.; White, M. C., A Predictably Selective Aliphatic C - H Oxidation Reaction for Complex Molecule Synthesis. *Science* **2007,** *318* (5851), 783-787.

25. Cussó, O.; Garcia-Bosch, I.; Ribas, X.; Lloret-Fillol, J.; Costas, M., Asymmetric Epoxidation with H2O2 by Manipulating the Electronic Properties of Non-heme Iron Catalysts. *Journal of the American Chemical Society* **2013,** *135* (39), 14871-14878.

26. Vicens, L.; Bietti, M.; Costas, M., General Access to Modified α-Amino Acids by Bioinspired Stereoselective γ-C−H Bond Lactonization. *Angewandte Chemie International Edition* **2021,** *60* (9), 4740-4746.

27. Vicens, L.; Olivo, G.; Costas, M., Rational Design of Bioinspired Catalysts for Selective Oxidations. *ACS Catalysis* **2020,** *10* (15), 8611-8631.

28. Rebolledo-Chávez, J. P. F.; Cruz-Ramírez, M.; Ramírez-Palma, D. I.; Ocampo-Hernández, J.; Mendoza, A.; Cortés-Guzmán, F.; Ortiz-Frade, L., Electrochemical mechanism of CO2 reduction mediated by Ni^{II}(tpa) (tpa = tris(2-pyridylmethyl)amine) complexes: An integral view. *Electrochimica Acta* **2021,** *400*, 139465.

29. Chan, S. L.-F.; Lam, T. L.; Yang, C.; Lai, J.; Cao, B.; Zhou, Z.; Zhu, Q., Cobalt(II) tris(2-pyridylmethyl)amine complexes [Co(TPA)X]+ bearing coordinating anion (X=Cl−, Br−, I− and NCS−): synthesis and application for carbon dioxide reduction. *Polyhedron* **2017,** *125*, 156-163.

30. Wang, F.; Cao, B.; To, W.-P.; Tse, C.-W.; Li, K.; Chang, X.-Y.; Zang, C.; Chan, S. L.-F.; Che, C.-M., The effects of chelating N4 ligand coordination on Co(ii)-catalysed photochemical conversion of CO2 to CO: reaction mechanism and DFT calculations. *Catalysis Science & Technology* **2016,** *6* (20), 7408-7420.

31. Xue, G.; Wang, D.; De Hont, R.; Fiedler, A. T.; Shan, X.; Münck, E.; Que, L., Jr., A synthetic precedent for the $[Fe^{IV}_2(\mu\text{-}O)_2]$ diamond core proposed for methane monooxygenase intermediate Q. *Proc Natl Acad Sci U S A* **2007,** *104* (52), 20713-8.

32. Kooistra, T. M.; Hekking, Koen F. W.; Knijnenburg, Q.; de Bruin, B.; Budzelaar, Peter H. M.; de Gelder, R.; Smits, Jan M. M.; Gal, Anton W., Cobalt Chloride Complexes of N3 and N4 Donor Ligands. *European Journal of Inorganic Chemistry* **2003,** *2003* (4), 648-655.

33. Costas, M.; Que, J., Lawrence, Ligand Topology Tuning of Iron-Catalyzed Hydrocarbon Oxidations. *Angewandte Chemie International Edition* **2002,** *41* (12), 2179-2181.

34. Codolà, Z.; Gamba, I.; Acuña-Parés, F.; Casadevall, C.; Clémancey, M.; Latour, J.-M.; Luis, J. M.; Lloret-Fillol, J.; Costas, M., Design of Iron Coordination Complexes as Highly Active Homogenous Water Oxidation Catalysts by Deuteration of Oxidation-Sensitive Sites. *Journal of the American Chemical Society* **2019,** *141* (1), 323-333.

35. Fryzuk, M. D.; Leznoff, D. B.; Thompson, R. C.; Rettig, S. J., One-Electron Transformations of Paramagnetic Cobalt Complexes. Synthesis and Structure of Cobalt(II) Amidodiphosphine Halide and Alkyl Complexes and Their Reaction with Alkyl Halides. *Journal of the American Chemical Society* **1998,** *120* (39), 10126-10135.

36. Evans, D. F., 400. The determination of the paramagnetic susceptibility of substances in solution by nuclear magnetic resonance. *Journal of the Chemical Society (Resumed)* **1959,** (0), 2003-2005.

37. Loliger, J.; Scheffold, R., Paramagnetic moment measurements by nmr. A micro technique. *Journal of Chemical Education* **1972,** *49* (9), 646.

38. Kochem, A.; Kanso, H.; Baptiste, B.; Arora, H.; Philouze, C.; Jarjayes, O.; Vezin, H.; Luneau, D.; Orio, M.; Thomas, F., Ligand Contributions to the Electronic Structures of the Oxidized Cobalt(II) salen Complexes. *Inorganic Chemistry* **2012,** *51* (20), 10557-10571.

39. Dhanaraj, C. J.; Nair, M. S., Synthesis and characterization of cobalt(II) and zinc(II) complexes of poly(3-nitrobenzyli dene-1-naphthylamine-co-succinic anhydride). *Journal of Saudi Chemical Society* **2014,** *18* (5), 479-485.

40. Khnayzer, R. S.; Thoi, V. S.; Nippe, M.; King, A. E.; Jurss, J. W.; El Roz, K. A.; Long, J. R.; Chang, C. J.; Castellano, F. N., Towards a comprehensive understanding of visible-light photogeneration of hydrogen from water using cobalt(ii) polypyridyl catalysts. *Energy & Environmental Science* **2014,** *7* (4), 1477-1488.

41. Newkome, G. R.; Gupta, V. K.; Fronczek, F. R.; Pappalardo, S., Multidentate ligands containing 2,2'-bipyridine and/or pyridine moieties: structural aspects of their octahedral and pentagonal-bipyramidal complexes. *Inorganic Chemistry* **1984,** *23* (16), 2400-2408.

42. Bridgeman, A. J., On the origin of paramagnetism in planar nickel(ii) complexes. *Dalton Transactions* **2008,** (15), 1989-1992.

43. Belle, C.; Bougault, C.; Averbuch, M.-T.; Durif, A.; Pierre, J.-L.; Latour, J.-M.; Le Pape, L., Paramagnetic NMR Investigations of High-Spin Nickel(II) Complexes. Controlled Synthesis, Structural, Electronic, and Magnetic Properties of Dinuclear vs Mononuclear Species. *Journal of the American Chemical Society* **2001,** *123* (33), 8053-8066.

44. Braun, J. D.; Lozada, I. B.; Shepit, M.; van Lierop, J.; Herbert, D. E., Pseudo-octahedral nickel(ii) complexes of strongly absorbing benzannulated pincer-type amido ligands: ligand-based redox and non-Aufbau electronic behaviour. *RSC Advances* **2021,** *11* (6), 3547-3555.

45. Tong, B.; Norman, R. E.; Chang, S.-C., Di-μ-chloro-bis{[tris(2-pyridylmethyl)amine-κ4N]nickel(II)} bis(triethylammonium) tetraperchlorate. *Acta Crystallographica Section C* **1999,** *55* (8), 1236-1238.

46. Xu, W.-y.; Tian, X.-z.; Sun, G.-m.; Song, Y.-m.; Yuan, Z.-z.; Liao, Z.-w.; Huang, H.-x.; Luo, M.-b.; Liu, S.-j.; Luo, F., One 2D Ni(II)-based compound showing diamagnetic-paramagnetic transition. *Inorganic Chemistry Communications* **2012,** *17*, 68-70.

47. Novoa, N.; Manzur, C.; Roisnel, T.; Dorcet, V.; Cabon, N.; Robin-Le Guen, F.; Ledoux-Rak, I.; Kahlal, S.; Saillard, J.-Y.; Carrillo, D.; Hamon, J.-R., Redox-switching of ternary Ni(ii) and Cu(ii) complexes: synthesis, experimental and theoretical studies along with second-order nonlinear optical properties. *New Journal of Chemistry* **2019,** *43* (26), 10468-10481.

48. Arion, V. B.; Rapta, P.; Telser, J.; Shova, S. S.; Breza, M.; Lušpai, K.; Kožišek, J., Syntheses, Electronic Structures, and EPR/UV−Vis−NIR Spectroelectrochemistry of Nickel(II), Copper(II), and Zinc(II) Complexes with a Tetradentate Ligand Based on S-Methylisothiosemicarbazide. *Inorganic Chemistry* **2011,** *50* (7), 2918-2931.

49. Goldcamp, M. J.; Edison, S. E.; Squires, L. N.; Rosa, D. T.; Vowels, N. K.; Coker, N. L.; Krause Bauer, J. A.; Baldwin, M. J., Structural and Spectroscopic Studies of Nickel(II) Complexes with a Library of Bis(oxime)amine-Containing Ligands. *Inorganic Chemistry* **2003,** *42* (3), 717-728.

50. Luo, S. P.; Mejia, E.; Friedrich, A.; Pazidis, A.; Junge, H.; Surkus, A. E.; Jackstell, R.; Denurra, S.; Gladiali, S.; Lochbrunner, S.; Beller, M., Photocatalytic water reduction with copper-based photosensitizers: a noble-metal-free system. *Angew. Chem. Int. Ed.* **2013,** *52* (1), 419-23.

51. Léonard, N. G.; Palmer, W. N.; Friedfeld, M. R.; Bezdek, M. J.; Chirik, P. J., Remote, Diastereoselective Cobalt-Catalyzed Alkene Isomerization–Hydroboration: Access to Stereodefined 1,3-Difunctionalized Indanes. *ACS Catalysis* **2019,** *9* (10), 9034-9044.

52. Ibrahim, A. D.; Entsminger, S. W.; Fout, A. R., Insights into a Chemoselective Cobalt Catalyst for the Hydroboration of Alkenes and Nitriles. *ACS Catalysis* **2017,** *7* (5), 3730-3734.

53. Zhao, H.; McMillan, A. J.; Constantin, T.; Mykura, R. C.; Juliá, F.; Leonori, D., Merging Halogen-Atom Transfer (XAT) and Cobalt Catalysis to Override E2-Selectivity in the Elimination of Alkyl Halides: A Mild Route toward contra-Thermodynamic Olefins. *Journal of the American Chemical Society* **2021,** *143* (36), 14806-14813.

54. Beesley, R. M.; Ingold, C. K.; Thorpe, J. F., CXIX.—The formation and stability of spiro-compounds. Part I. spiro-Compounds from cyclohexane. *Journal of the Chemical Society, Transactions* **1915,** *107* (0), 1080-1106.

55. Queyriaux, N.; Jane, R. T.; Massin, J.; Artero, V.; Chavarot-Kerlidou, M., Recent developments in hydrogen evolving molecular cobalt(II)–polypyridyl catalysts. *Coordination Chemistry Reviews* **2015,** *304-305*, 3-19.

56. Artero, V.; Chavarot-Kerlidou, M.; Fontecave, M., Splitting Water with Cobalt. *Angewandte Chemie International Edition* **2011,** *50* (32), 7238-7266.

57. Burés, J., What is the Order of a Reaction? *Topics in Catalysis* **2017,** *60* (8), 631-633.

58. Cook, A. K.; Sanford, M. S., Mechanism of the Palladium-Catalyzed Arene C–H Acetoxylation: A Comparison of Catalysts and Ligand Effects. *Journal of the American Chemical Society* **2015,** *137* (8), 3109-3118.

59. Avidan-Shlomovich, S.; Ghosh, H.; Szpilman, A. M., Synthetic and Mechanistic Study of the Catalytic Enantioselective Preparation of Primary β-Amino Ketones from Enones and a Fluorinated Gabriel Reagent. *ACS Catalysis* **2015,** *5* (1), 336-342.

60. Chatelet, B.; Joucla, L.; Dutasta, J.-P.; Martinez, A.; Szeto, K. C.; Dufaud, V., Azaphosphatranes as Structurally Tunable Organocatalysts for Carbonate Synthesis from CO2 and Epoxides. *Journal of the American Chemical Society* **2013,** *135* (14), 5348-5351.

61. Liu, B.; Roisnel, T.; Carpentier, J.-F.; Sarazin, Y., When Bigger Is Better: Intermolecular Hydrofunctionalizations of Activated Alkenes Catalyzed by Heteroleptic Alkaline Earth Complexes. *Angewandte Chemie International Edition* **2012,** *51* (20), 4943-4946.

62. Mahy, W.; Plucinski, P.; Jover, J.; Frost, C. G., Ruthenium-Catalyzed O- to S-Alkyl Migration: A Pseudoreversible Barton–McCombie Pathway. *Angewandte Chemie International Edition* **2015,** *54* (37), 10944-10948.

63. Guimond, N.; MacDonald, M. J.; Lemieux, V.; Beauchemin, A. M., Catalysis through Temporary Intramolecularity: Mechanistic Investigations on Aldehyde-Catalyzed Cope-type Hydroamination Lead to the Discovery of a More Efficient Tethering Catalyst. *Journal of the American Chemical Society* **2012,** *134* (40), 16571-16577.

64. Mathew, J. S.; Klussmann, M.; Iwamura, H.; Valera, F.; Futran, A.; Emanuelsson, E. A. C.; Blackmond, D. G., Investigations of Pd-Catalyzed ArX Coupling Reactions Informed by Reaction Progress Kinetic Analysis. *The Journal of Organic Chemistry* **2006,** *71* (13), 4711-4722.

65. Nielsen, C. D. T.; Burés, J., Visual kinetic analysis. *Chemical Science* **2019,** *10* (2), 348-353.

66. Burés, J., Variable Time Normalization Analysis: General Graphical Elucidation of Reaction Orders from Concentration Profiles. *Angewandte Chemie International Edition* **2016,** *55* (52), 16084-16087.

67. Martínez-Carrión, A.; Howlett, M. G.; Alamillo-Ferrer, C.; Clayton, A. D.; Bourne, R. A.; Codina, A.; Vidal-Ferran, A.; Adams, R. W.; Burés, J., Kinetic Treatments for Catalyst Activation and Deactivation Processes based on Variable Time Normalization Analysis. *Angewandte Chemie International Edition* **2019,** *58* (30), 10189-10193.

68. Burés, J., A Simple Graphical Method to Determine the Order in Catalyst. *Angewandte Chemie International Edition* **2016,** *55* (6), 2028-2031.

69. Luo, S.-P.; Mejía, E.; Friedrich, A.; Pazidis, A.; Junge, H.; Surkus, A.-E.; Jackstell, R.; Denurra, S.; Gladiali, S.; Lochbrunner, S.; Beller, M., Photocatalytic Water Reduction with Copper-Based Photosensitizers: A Noble-Metal-Free System. *Angewandte Chemie International Edition* **2013,** *52* (1), 419-423.

70. O. Y. Lyakin, A. M. Z., D. G. Samsonenko, K. P. Bryliakov, E. P. Talsi*, *ACS Catal.* **2015,** *5* (5), 2702.

71. O. Cussó, I. G.-B., X. Ribas, J. Lloret-Fillol, M. Costas, *J. Am. Chem. Soc.* **2013,** *135*, 14871-14878.

72. White, M. C., Base-Metal Catalysis:Embrace the Wild Side. *Adv.Synth. Catal.* **2016,** *358*, 2364-2365.

73. Davies, C. J.; Solan, G. A.; Fawcett, J., Synthesis and structural characterisation of cobalt(II) and iron(II) chloride complexes containing bis(2-pyridylmethyl)amine and tris(2-pyridylmethyl)amine ligands. *Polyhedron* **2004,** *23* (18), 3105-3114.

UNIVERSITAT ROVIRA I VIRGILI
VISIBLE-LIGHT METALLAPHOTOREDOX STRATEGIES FOR ORGANIC TRANSFORMATIONS THROUGH THE CLEAVAGE
OF CSP3-CL BONDS
Jordi Aragón Artigas

CHAPTER IV:

Photoredox Reductive Cross-Coupling of Inert Alkyl Chlorides with Aromatic Alkenes
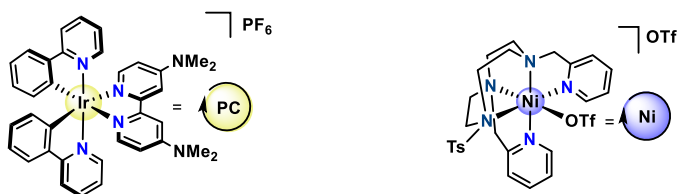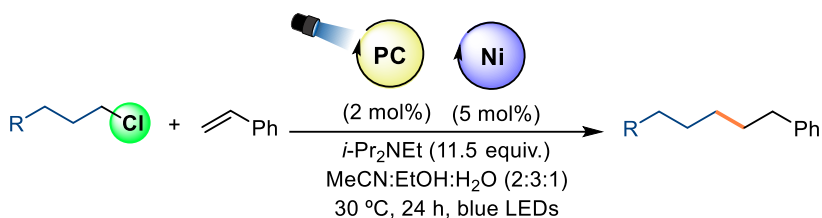
All this chapter corresponds to the following publication:

4.1. State of the art

Alkyl chlorides are remarkable feedstocks in organic synthesis. They are economical, ready commercially available, stable, and easy to synthesize by common synthetic routes. Moreover, organic chlorides are present in natural products and biologically active compounds, making them an interesting functional group for late-stage postmodification in drug discovery.[1]

Nevertheless, their chemical inertness hinders their use as electrophilic partners in transition metal-catalyzed reactions.[2-6] Albeit organic bromides and organic iodides are widely used as electrophiles from their activation through visible light-mediated single-electron transfer (SET) reactions,[7, 8] alkyl chlorides present higher bond strengths (397 kJ mol^{-1}) compared to their analogs (Scheme 4.1).[9-11]
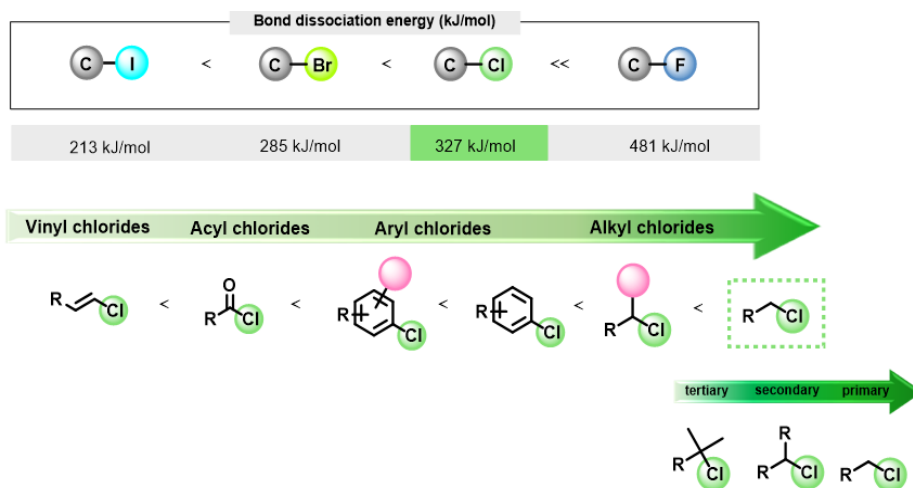
Scheme 4. 1. Comparition of BDE for alkyl halides.

Thereby, the cleavage of Csp^3−Cl bond requires arduous reaction conditions (Scheme 4.2),[12-18] in which the utility of the reaction is constrained to dehalogenation and the chemoselectivity towards the final product is often compromised.
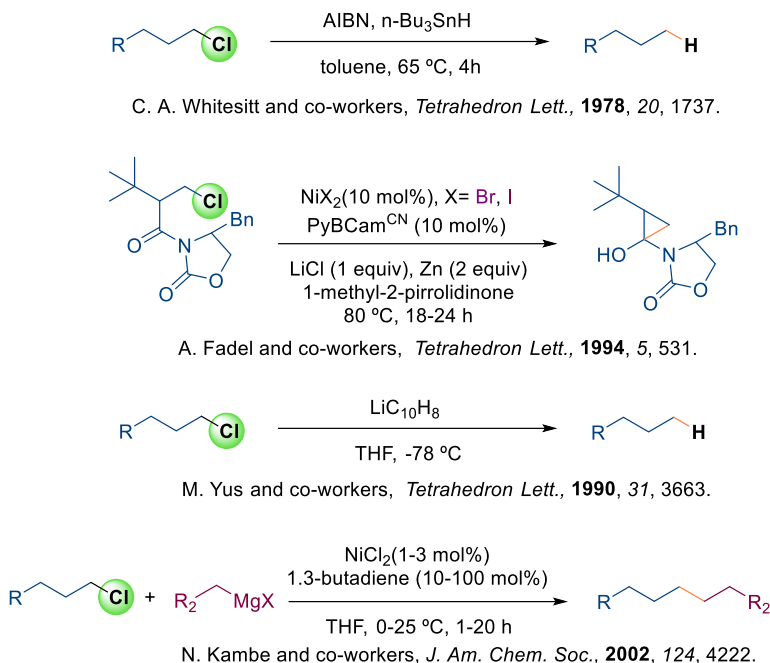
Scheme 4. 2. Classical methods for activation of alkyl chlorides.

Alternatively to the direct activation of alkyl chlorides, the use of alkyl chlorides as coupling partners under mild conditions has been displayed by halide exchange strategies, forming *in-situ* an alkyl bromide/iodide from the alkyl chloride to obtain the activable electrophile. This pre-functionalization also requires an excess of Zn or Mn as metallic reductant (Scheme 4.3).[19-21]

R. Martin and co-workers, *J. Am. Chem. Soc.,* **2016**, *138* (24), 7504-7507.

D. J. Weix and co-workers, *J. Am. Chem. Soc.,* **2020**, *142* (22), 9902-9907.
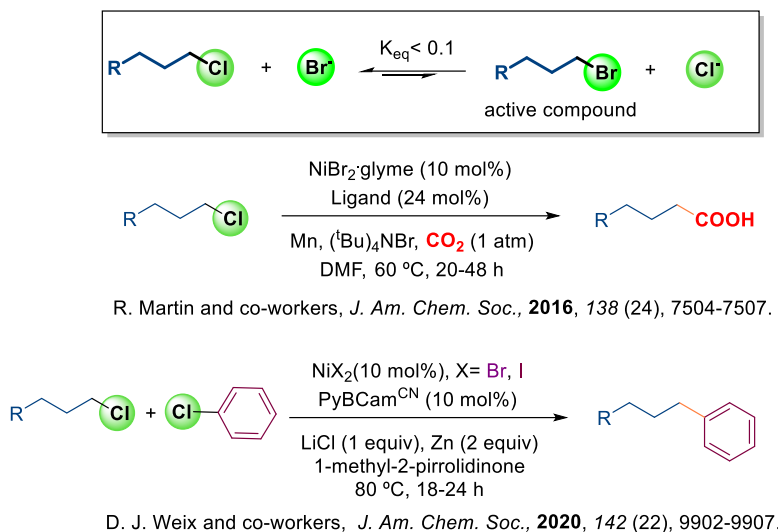
Scheme 4. 3. Halide exchange strategies for using alkyl chlorides as coupling partners.

In this regard, visible-light photocatalysis has shown potential to transform unactivated alkyl chlorides without prefunctionalization.[22] The continuous development of photocatalysts (PCs) has contributed to the expansion of the redox potential window beyond −3 V *vs* SCE and, consequently, the expansion of the alkyl halides scope by single-electron transfer strategies.[23-25] Still, most of the reported methods used only activated alkyl chlorides (arylic,[26-31] benzylic,[32-37] alkenyl[38] or α-carbonyl chlorides[39-43]) as electrophiles, while the fate of unactivated alkyl chlorides remained limited to dehalogenation processes.[44] In order to build more complex and valuable compounds from inert alkyl chlorides, more sophisticated strategies are required. In 2020, König, Kunz and Giedyk published an elegant strategy that promoted the activation of chloroalkanes under visible-light conditions (Scheme 4.4).[45] In their proposal, a micellar aqueous solution stabilizes the photogenerated [Ir(dtbby)(ppy)2]- radical anion *via* non-covalent interactions and compartmentation of the reacting compounds. The excitation of this radical anion by a second photon promotes an electron transfer to the alkyl chloride, reaching the formation of the C-centered radical, meaning

the first activation of alkyl chlorides by a photocatalyst. The potential of this approach was demonstrated in dehalogenation, intramolecular cyclizations and few examples of Giese-type radical addition to electrodeficient olefins by tuning the reaction conditions. However, its broad synthetic application is still limited, using only 4 primary alkyl chlorides as coupling partners.
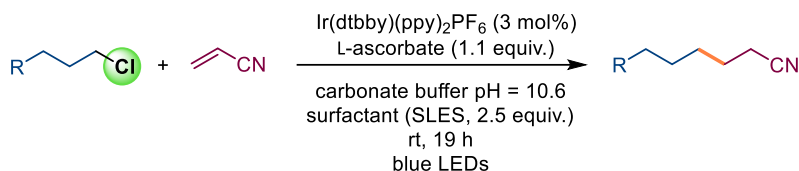
B. König and co-workers, *Nat. Catal.*, **2020**, *3* (1), 40-47.

Scheme 4. 4. Photocatalytic activation of alkyl chlorides by APSET.

Considering the use of the same photocatalyst [Ir(dtbby)(ppy)₂]PF₆, in the same year MacMillan reported a different approach for the activation of alkyl chlorides and their engagement in a cross-coupling reaction. They developed the photogeneration of silyl radicals by SET from the photocatalyst to a novel organosilane reagent, which can perform chlorine atom abstraction under mild photocatalytic conditions. The merging of such a photoredox step with a dual Ir/Ni metallaphotoredox system capable of activating aryl chlorides resulted in one of the first $Csp^2–Csp^3$ couplings between secondary alkyl chlorides and aryl chlorides (Scheme 4.5),[46] including six examples of primary unactivated chloroalkanes.
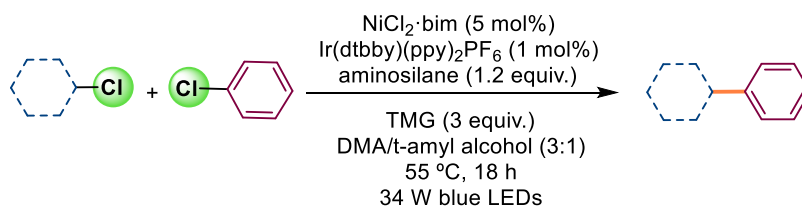
D. W. C. MacMillan and coworkers, *J. Am. Chem. Soc.*, **2020**, *142*, 11691−11697

Scheme 4. 5. Cross-electrophile coupling of unactivated alkyl chlorides with aryl chlorides.

These relevant advances highlight the importance of finding a general protocol to exploit inert alkyl chlorides as coupling partners, being the main objective of this chapter. We target the intermolecular version of the cyclization implemented in 2019 by our group,[47] following the same key concepts: the photogeneration of low-valent Ni/Co species for the cleavage of primary alkyl chlorides (Scheme 4.6).
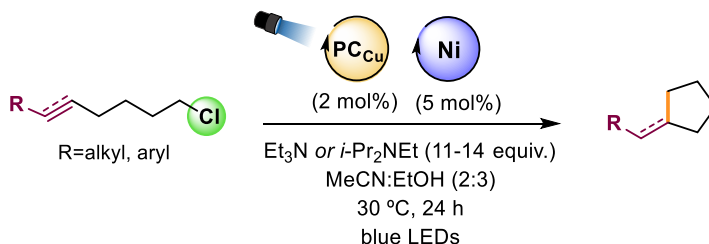
M. Claros *et. al., Angew. Chem. Int. Ed.*, **2019**, *58*, 4869 –4874

- 36 unactivated alkyl chlorides (up to 85% yield)
- 14 aromatic olefins (up to 79% yield)
- 3 examples of cascade reactivity (70-78% yield)
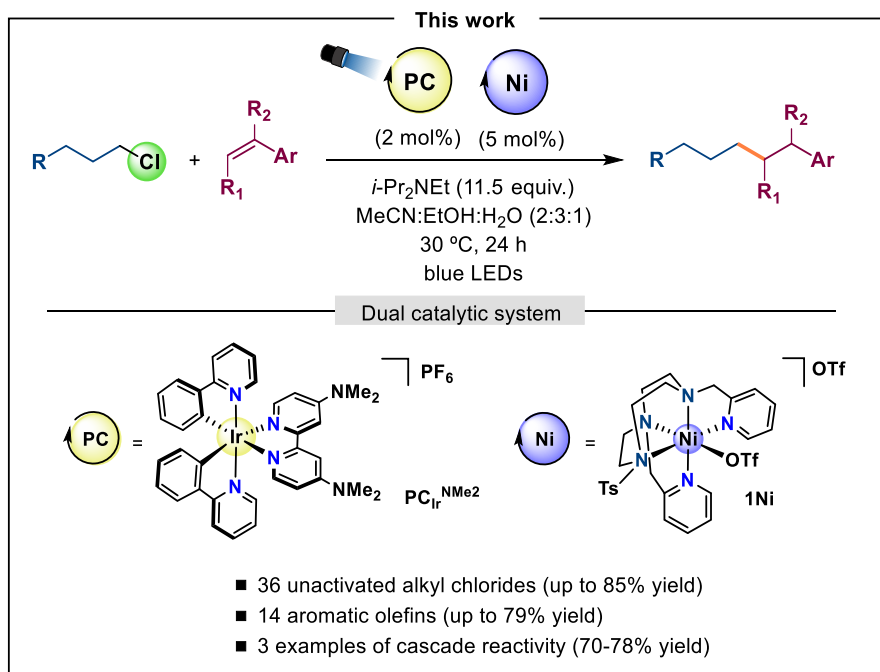
Scheme 4. 6. Photoredox reductive cross-coupling of inert alkyl chlorides with aromatic alkenes.

4.2. Results and Discussion

4.2.1. Optimization of the reaction by high throughput techniques

High-throughput experimentation is an extremely useful and successful approach to deal with reaction discovery and optimization processes in photoredox catalyzed transformations since the number of variables to optimize is usually large. For instance, catalyst, co-catalyst and substrate loadings, additives, solvent, temperature, light source and intensity all influence the catalytic outcome and performance, leading to a typical amount of 1000 – 5000 different experiments per study. In this regard, visible-light photoredox catalysis has had a high impact on the community, expanding the scope of reactivity, such as SET-based organic methodologies.[48-53] This prevailing paradigm promotes the photogeneration of highly reactive species (organic radicals, excited states, reactive oxidation states in metals…) under mild conditions, paving the way towards more general and efficient transformations. However, slight changes in the reaction mixture can have a considerable effect on the catalytic response. Therefore, a precise and reproducible high-throughput experimentation (HTE) system is essential for an exhaustive study and development of new photoredox organic methodology, where light intensity and reaction temperature control arise as the main responsible for the lack of reproducibility in photoredox setups for HTE. In this respect, our group has devoted efforts to develop HTE platforms that allow tight control of the light irradiation intensity as well as the reaction temperature while providing high-intensity modular LEDs (up to 1.5 W of irradiation, 447 nm) as irradiation source (see the experimental section for details).

With these facilities in hand, we proceeded with an exhaustive process of HTE for the development and optimization of a cross-coupling reaction using unactivated alkyl chlorides as coupling partners. We selected (3-chloropropyl)-1-benzene (**iv.1a**) as a model alkyl chloride and styrene (**iv.2a**) as coupling partners

(Scheme 4.7.), seeking a Giese-type radical addition to an olefin through blue LED irradiation.
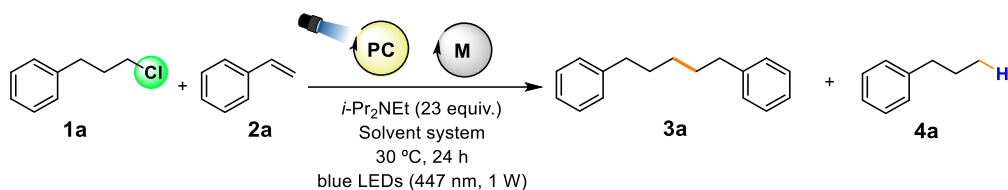
Scheme 4. 7. Model cross-coupling reaction for optimization.

Election of a suitable dual catalytic system

The first step of the discovery and optimization of the reaction consisted of identifying the appropriate catalytic system. Considering our previous expertise, we expected the requirement of a dual catalytic system similar to the one used before in reductive cyclization. To start the discovery of the reactivity, we chose **PC$_{Cu}$** as the initial photocatalyst and both Ni and Co complexes bearing **Py$_2$^{Ts}tacn** as pentacoordinated ligand. In addition to these well-known active catalysts, we also evaluated the family of tetracoordinated N-based complexes [(**^{X}PDP)MCl$_2$** and (**^{X}MCP)MCl$_2$**, M= Ni, Co, X= H, DMM, CO$_2$Et] developed in *Chapter III*, due to their potential against activation of alkylchlorides. At the same time, we studied the effect of the solvent on the catalytic response, starting with the same mixture from the previous methodologies (MeCN:EtOH, 2:3), and trying to substitute ethanol for tetrahydrofuran in order to diminish the amount of protons in the medium and consequently, dehalogenation. Moreover, THF is a common polar aprotic solvent used in organometallic chemistry due to its capacity to favor the solvation of intermediates.

**Table 4. 1.** Screening of catalysts using **PC_{Cu}** and solvent system.
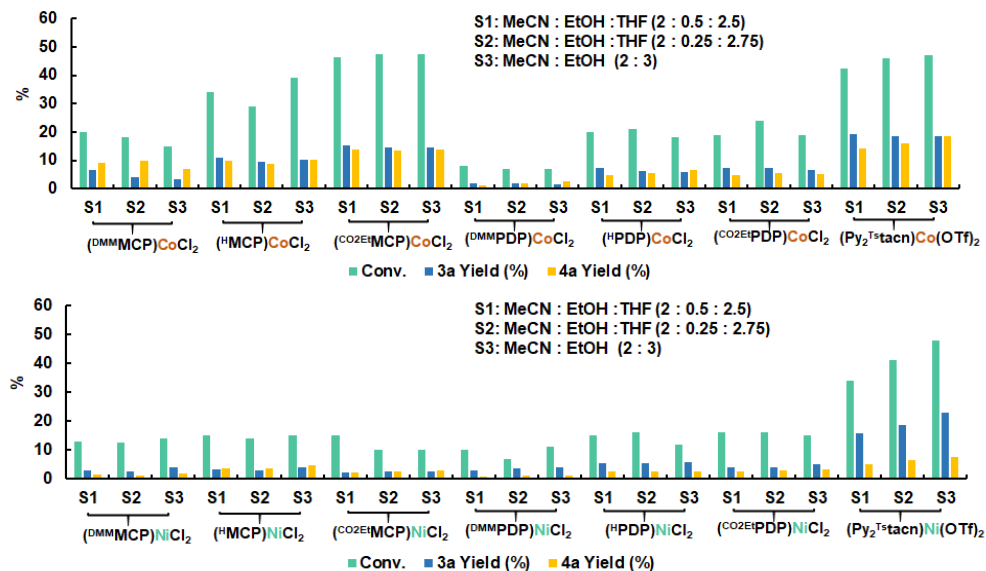
General procedure **A**: **iv.1a** (10 mM), **iv.2a** (5 equiv.), **PC_{Ir}^{NMe2}** (2 mol %), **catalyst** (5 mol %) **DIPEA** (23 equiv.). Total volume = **300 µl**. Visible-light irradiation with blue LEDs (1 W, 447 nm) for 24 h at 30ºC. Conversion and yield were determined by GC-FID using biphenyl as an internal standard. Reactions run in duplicate.

This first conditions screening did not reveal an effective catalytic system for the desired reactivity (Table 4.1). Unexpectedly, (**X**PDP)NiCl_2 and (**X**MCP)NiCl_2 showed poor reactivity against the activation of (3-chloropropyl)-1-benzene, in comparison with their cobalt analogs. In this sense, **X**MCP ligands presented significant substrate conversion (close to 40%) using Co as a metal center, and we obtained similar results with both well-known (Py_2^{Ts}tacn)Co(OTf)_2 and (Py_2^{Ts}tacn)Ni(OTf)_2. However, cobalt complexes also clearly enhanced the dehalogenation of the starting compound, in concordance with their ability to form hydrides from protic solvents. These preliminary results did not allow to extract conclusions from the effect of the solvent system since the addition of THF instead of EtOH did not cause a remarkable effect on the catalytic response. Nevertheless, we put into value these preliminary results, considering the versatility and capability of these catalysts. At this point, we focused on dealing with the lack of

substrate conversion, trying to increment the number of reactive species in the catalytic mixture. To do that, we repeated the previous screening but replacing the photocatalyst with a more reducing one: $Ir(^{NMe2}bpy)(ppy)_2PF_6$, (**PC$_{Ir}$^{NMe2}**) with $E_{1/2}^{+/0}$ of -1.80 V *vs* SCE.

Table 4. 2. Screening of catalysts usinc **PC$_{Ir}$^{NMe2}** and solvent system.
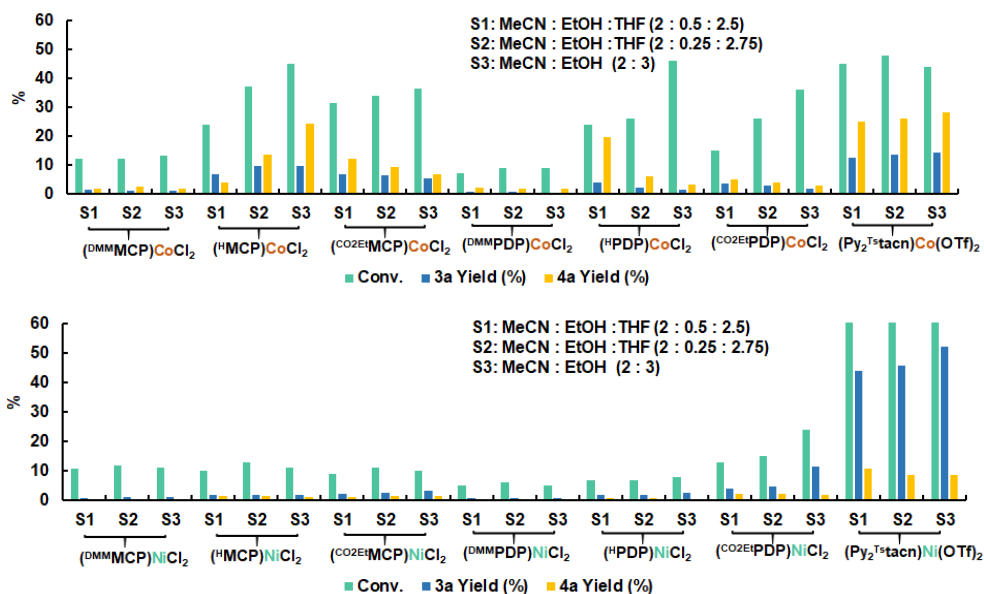
General procedure **A**: **iv.1a** (10 mM), **iv.2a** (10 equiv.), **PC$_{Ir}$^{NMe2}** (2 mol %), **catalyst** (5 mol %) **DIPEA** (23 equiv.). Total volume = **300 μl**. Visible-light irradiation with blue LEDs (1 W, 447 nm) for 24 h at 30°C. Conversion and yield were determined by GC-FID using biphenyl as an internal standard. Reactions run in duplicate.

The use of **PC$_{Ir}$^{NMe2}** as photocatalyst meant a remarkable turning point in the process of optimization (Table 4.2). While tetradentate N-based complexes presented had low reactivity, **(Py$_2$^{Ts}tacn)M(OTf)$_2$** catalysts showed a notable improvement of the catalytic response. Nevetheless, the reactivity presented by each metal center was significantly different: **(Py$_2$^{Ts}tacn)Ni(OTf)$_2$** presented higher substrate conversions (close to 60%) with a 50% yield of the desired product. On the other hand, conversions from **(Py$_2$^{Ts}tacn)Co(OTf)$_2$** were lower

(close to 50%) with a higher contribution of dehalogenation. With these results in hand, we focused on **Py$_2$^{Ts}tacn** ligand-based complexes and **PC$_{Ir}$^{NMe2}** as the most promising dual catalytic system. Regarding the solvent system, the addition of THF did not improve the final result therefore we kept it out of the optimization process. In the next step, we optimized the ratio of the chosen catalytic system by modifying the % of **PC$_{Ir}$^{NMe2}** (0.1 – 4 mol%) together with the substrate concentration (10 mM, 50 mM, 100 mM), to maximize the catalytic response of the system (Table 4.3).

Table 4. 3. Screening of substrate concentration and % PC.
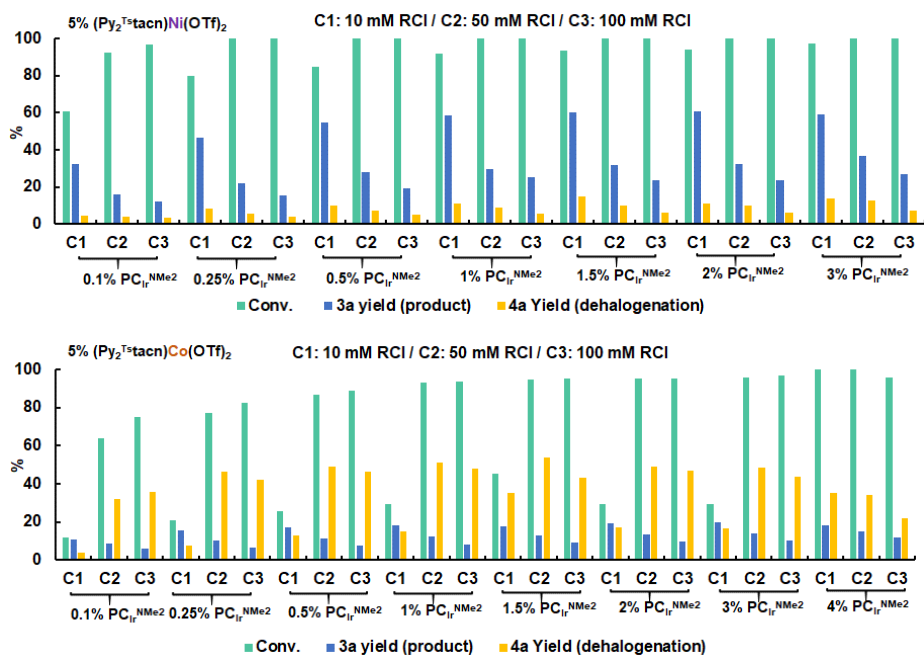
General procedure **A**: **iv.1a** (10-100 mM), **iv.2a** (10 equiv.), **PC$_{Ir}$^{NMe2}** (0.1 - 3 mol %), **catalyst** (5 mol %) **DIPEA** (23 equiv.). Total volume = **300 µl**. Visible-light irradiation with blue LEDs (1 W, 447 nm) for 24 h at 30ºC. Conversion and yield were determined by GC-FID using biphenyl as an internal standard. Reactions run in duplicate.

In this second screening of parameters, the different selectivity offered by the metal center resolved into the final choosing of **(Py$_2$^{Ts}tacn)Ni(OTf)$_2$** as the desired

catalyst. Despite these Co complexes having shown a promising catalytic activity towards the cleavage of Csp^3−Cl bonds, we concluded that their high activity towards proton reduction is their major limitation, favoring dehalogenation and restricting their use in coupling reactions. Regarding substrate concentration, our dual catalytic system presents a better catalytic response under diluted conditions (10 mM), in contrast with the common conditions used in photoredox transformations (50 mM, 100 mM). To select the suitable catalytic system ratio, we observed a maximum yield (Table 4.3) at 1.5-2 mol% of photocatalyst. Therefore, we set 2 mol% of **PC$_{Ir}^{NMe2}$** and 5 mol% of **(Py$_2^{Ts}$tacn)Ni(OTf)$_2$** as the dual catalytic system for exploring the scope of the cross-coupling reaction.

Mitigation of side reactivity

After fixing the dual catalytic system, the exhaustive analysis of the reaction crudes was crucial to understand the lack of efficiency of the system towards cross-coupling reaction. As discussed before, the use of nickel as metal center reduced the dehalogenation process, and the homocoupling after activation of (3-chloropropyl)-1-benzene remained minor. However, the large excess of styrene and DIPEA formed *N,N*-diisopropyl-4-phenylbutan-2-amine as the major subproduct. The formation of this product occurs presumably from the reaction between the olefin and aminoalkyl radicals derived from reductive quenching of the **PC$_{Ir}^{NMe2}$** excited state.[54] Another minor side reaction was the photodimerization of styrene transformed into a mixture of two diastereomeric cyclobutanes.[55-57] In this sense, we rationalized the mitigation of side reactions, especially the coupling of styrene with DIPEA, as the key point for enhancing a distinguished cross-coupling reactivity. The diminution of styrene's secondary reactions should increase the available styrene for the desired process, increasing the final yield.

In this regard, we initially considered the use of other well-known electron donors, such as different tertiary amines (such as triethylamine, 1,4-diazabicyclo[2.2.2.]octane, 1,4-dimethylpiperazane, 1-phenylpiperidine…), ascorbic acid, oxalates… together with decreasing amounts of the corresponding electron donors to avoid this undesired coupling (Table 4.4).
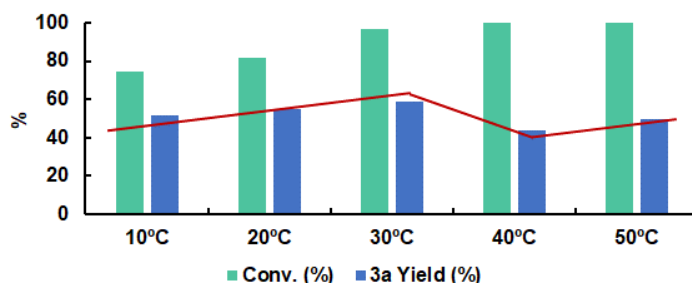
Table 4. 4. Screening of electron donors.
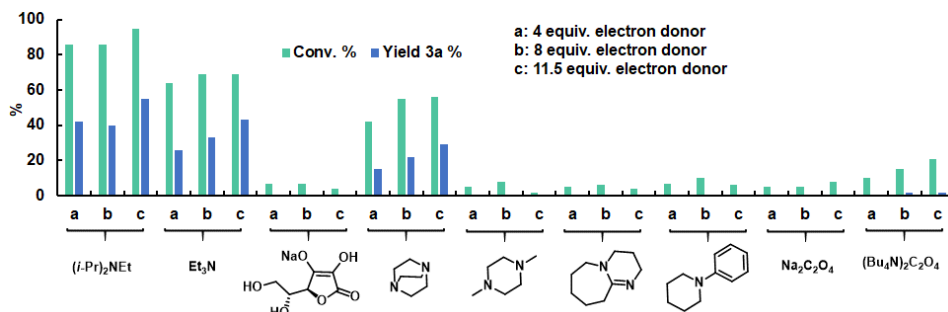
General procedure **A**: **iv.1a** (10 mM), **iv.2a** (10 equiv.), **PC$_{Ir}^{NMe2}$** (2 mol %), **(Py$_2^{Ts}$tacn)Ni(OTf)$_2$** (5 mol %) **electron donor** (x equiv.). Total volume = **300 µl**. Visible-light irradiation with blue LEDs (1 W, 447 nm) during 24 h at 30ºC. Conversion and yield were determined by GC-FID using biphenyl as an internal standard. Reactions run in duplicate.

Regarding the electron donors, most of them mismatched with the catalytic system, presenting poor reactivity. Only triethylamine and 1,4-diazabicyclo[2.2.2.]octane could reach at least poor catalytic activity. Anyhow, this screening allowed us to decrease the amount of DIPEA, presenting little decay in the final result when using 11.5 equiv. of the ED. Fewer equivalents of DIPEA (4 or 8) resulted in a loss of 15% of the final product.

Another parameter to be considered for decreasing the reactivity of the system is the temperature. Our in-house photoreactors allow us to control this variable with the maximum reproducibility between the different reaction spots. At this point, we also started to run the reactions on a bigger scale (V$_{total}$= 2 mL), trying to evaluate the scalability of the methodology for the next procedures. Surprisingly, the new reaction scale increased the desired product (Table 4.5, up

to 10% of increased yield). We presume that small reaction scales are highly sensitive to oxygen, impurities or little changes in the mixture, which are neglected by increasing the reaction scale. Regarding the optimal temperature, the initial 30 ºC was still the best one. Higher temperatures (40 ºC and 50 ºC) increased the formation of the aforementioned side products, damaging the cross-coupling reactivity of the system. In contrast, lower temperatures (10 ºC and 20 ºC) resulted in general mitigation of the reactivity of the catalytic system, decreasing at the same time the formation of side products and the activation of (3-chloropropyl)-1-benzene.

Table 4. 5. Screening of temperatures.

General procedure **B**: **iv.1a** (10 mM), **iv.2a** (10 equiv.), **PC$_{Ir}^{NMe2}$** (2 mol %), **(Py$_2$^{Ts}tacn)Ni(OTf)$_2$** (5 mol %) **DIPEA** (11.5 equiv.). Total volume = **2 ml**. Visible-light irradiation with blue LEDs (1 W, 447 nm) for 24 h at 30ºC. Conversion and yield were determined by GC-FID using biphenyl as an internal standard. Reactions run in duplicate.

In summary, we fixed an optimal dual catalytic system, the best electron donor and the suitable reaction temperature, but the study of the solvent system was still missing in this process. We extracted from previous screenings and the previous intramolecular strategy[47] that the solvent system should be formed by a polar aprotic solvent (MeCN) and a protic solvent (EtOH), because we are dealing with organometallic ionic intermediates and radical species. Dimethylacetamide (DMA) and dimethylformamide (DMF) were tested as an alternative to acetonitrile and trifluoroethanol (CF$_3$CH$_2$OH) as protic solvent (Table 4.6). Together with the reoptimization of the solvent system, we studied the effect of

the substrate concentration, centering the screening at diluted concentrations close to 10 mM. The use of DMA and DMF did not improve the catalytic response of the system in MeCN and the change of ethanol by CF_3CH_2OH resulted in a totally loss of the reactivity. All the proposed modifications failed for ameliorating the catalytic approach. However, we raised the yield barrier up to 60% by increasing the substrate concentration to 15 and 20 mM (Table 4.6).

Table 4. 6. Screening of solvent system and substrate concentration.
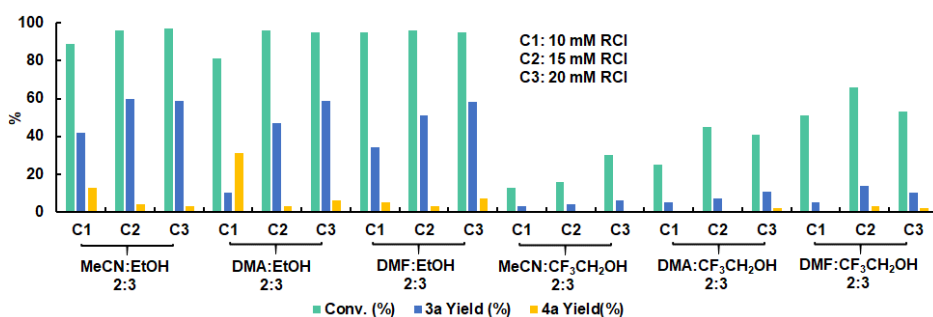
General procedure **A**: **iv.1a** (x mM), **iv.2a** (10 equiv.), $\textbf{PC}_{\textbf{Ir}}^{\textbf{NMe2}}$ (2 mol %), $(\textbf{Py}_2{}^{\textbf{Ts}}\textbf{tacn})\textbf{Ni(OTf)}_2$ (5 mol %) **DIPEA** (11.5 equiv.). Total volume = **300 μl**. Visible-light irradiation with blue LEDs (1 W, 447 nm) for 24 h at 30ºC. Conversion and yield were determined by GC-FID using biphenyl as an internal standard. Reactions run in duplicate.

Returning to the initial idea of diminishing side reactivity of the coupling partner, we had been dealing with the mitigation of side reaction, trying to favor our desired reaction, failing in almost all the attempts. Considering olefin-DIPEA coupling was the major side product, we realized about a new hypothesis: the quenching of the subproducts coming from DIPEA. The idea consisted of adding a compound able to react with these side products, avoiding their engagement by styrene. We quickly considered water as the best additive for committing this purpose. Under equilibrium conditions of species, the addition of water should favor the hydrolysis of the iminium ion intermediate, leading to the formation of N,N-diisopropylamine and acetaldehyde. Therefore, turning the hydrolysis irreversible and diminishing the coupling between the α-aminoalkyl radical and styrene (Scheme 4.8).
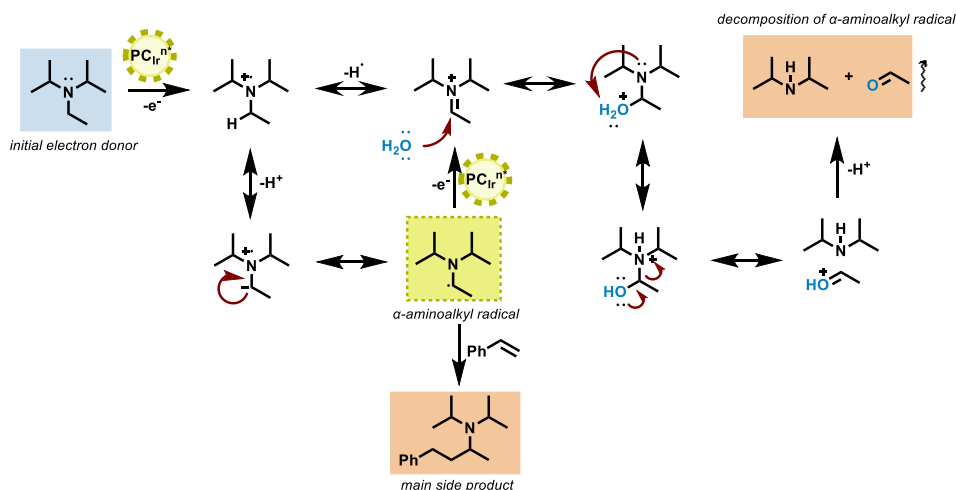
Scheme 4. 8. Photogeneration of α-aminoalkyl radicals and their side reactivity.

The results in Table 4.7 confirmed this hypothesis, obtaining a 70% yield of the cross-coupling product by adding only 8% of water. At this point, the system was very sensitive to tiny changes of added water and substrate concentration, where 17% of water and 20 mM of (3-chloropropyl)-1-benzene showed the best catalytic response (82% yield, see Table 4.7).

Table 4. 7. Screening of water as an additive and substrate concentration.
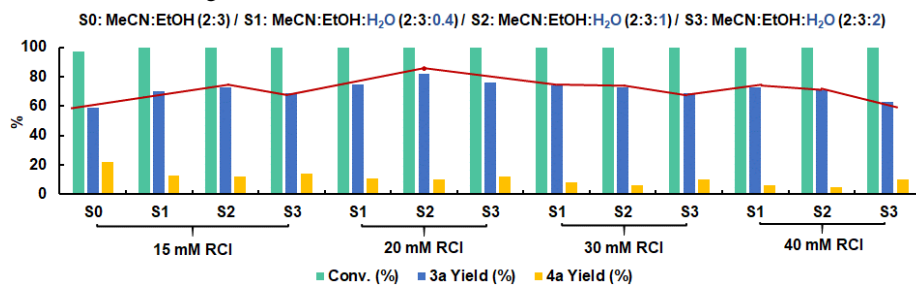
General procedure **B**: **iv.1a** (x mM), **iv.2a** (10 equiv.), **PCIr^{NMe2}** (2 mol %), (**Py2^{Ts}tacn)Ni(OTf)2** (5 mol %) **DIPEA** (11.5 equiv.). Total volume = **2 ml**. Visible-light irradiation with blue LEDs (1 W, 447 nm) for 24 h at 30°C. Conversion and yield were determined by GC-FID using biphenyl as an internal standard. Reactions run in duplicate.

After these screenings of variables, we define PC_{Ir}^{NMe2} (2 mol%), $(Py_2{}^{Ts}tacn)Ni(OTf)_2$ (5 mol%), iPr$_2$NEt (DIPEA) and **iv.1a** concentration (20 mM) in MeCN/EtOH/H$_2$O 2:3:1 as the optimal conditions for the reductive cross-coupling of the model compounds.

Delimitation of the reaction borders

For an initial understanding of the reaction mechanism and the reaction borders, we interrogated the system by performing control experiments (Table 4.8) and monitoring the reaction (Figures 4.1).

Table 4. 8. Control experiments .

Entry	Deviation from standard conditions	% Yield (Conv.)
1	**none**	**82 (100)**
2	no H$_2$O	59 (97)
3[a]	no $(Py_2{}^{Ts}tacn)Ni(OTf)_2$	0 (9)
4	no PC_{Ir}^{NMe2}	0 (3)
5[b]	no DIPEA	0 (3)
6	no Blue LED irradiation	0 (0)
7	under air	64 (74)
8	**1Co** instead of $(Py_2{}^{Ts}tacn)Ni(OTf)_2$	23 (50)
9	(dtbbpy)NiCl$_2$ instead of $(Py_2{}^{Ts}tacn)Ni(OTf)_2$	0 (14)
10	(bpy)NiCl$_2$ instead of $(Py_2{}^{Ts}tacn)Ni(OTf)_2$	0 (6)
11	(phen)NiCl$_2$ instead of $(Py_2{}^{Ts}tacn)Ni(OTf)_2$	0 (8)
12	Ni(OTf)$_2$(MeCN)$_2$ instead of $(Py_2{}^{Ts}tacn)Ni(OTf)_2$	0 (2)

General procedure **B**: **1a** (20 mM), **2a** (10 equiv.), PC_{Ir}^{NMe2} (2 mol %), $(Py_2{}^{Ts}tacn)Ni(OTf)_2$ (5 mol %), **DIPEA** (11.5 equiv.). Total volume = **2 ml**. Visible-light irradiation with blue LEDs (1 W, 447 nm) for 24 h at 30ºC. Conversion and yield were determined by GC-FID using biphenyl as an internal standard. Reactions run in duplicate.

Control experiments demonstrated that every component of the catalytic system (($Py_2^{Ts}tacn$)Ni(OTf)$_2$, PC_{Ir}^{NMe2}, DIPEA and blue LED) was required to yield the desired product (Table 4.8, entries 3-6). When ($Py_2^{Ts}tacn$)Ni(OTf)$_2$ was excluded from the standard optimized conditions (**iv.1a**, **iv.2a**, PC_{Ir}^{NMe2}, DIPEA and blue LED), the alkyl chloride was recovered unreacted. In that case, the olefin reacted with aminoalkyl radicals, yielding *N,N*-diisopropyl-4-phenylbutan-2-amine as the major product.[54] Moreover, when DIPEA was also excluded from the reaction mixture, the alkyl chloride was fully recovered, while the olefin was transformed into a mixture of two diastereomeric cyclobutanes.[55-57] This indicates an energy transfer (EnT) process from the PC_{Ir}^{NMe2} excited state to the olefin, interfering with catalysis. However, the formation of cyclobutanes was practically inhibited when all components of the catalytic system were present, suggesting that the potential PC-olefin EnT interference with the catalysis is negligible. On the other hand, the olefin-DIPEA coupling product was still formed, although to a minor extent. These results revealed the capacity of PC_{Ir}^{NMe2} to engage in both SET and EnT reactions.

We also evaluated the kinetic profile of the reaction through single-point monitoring experiments, where the reaction was fully accomplished after 7 h of continuous blue LED irradiation. Moreover, we performed the same monitoring through light-dark cycles, showing no evolution of the reaction under dark periods, agreeing with a light-mediated transformation (Figure 4.1).

As the last step of this optimization section, we discuss the selection of the suitable photocatalyst and its importance in the catalytic system. Although the reduced ($Py_2^{Ts}tacn$)Ni(OTf)$_2$ was the main character for activating the Csp^3−Cl bond, the choice of a suitable photocatalyst emerged as crucial for the development of the desired cross-coupling reaction. Different metallic photocatalysts and organic dyes were tested (Table 4.8) to understand the different parameters required for successful reactivity.
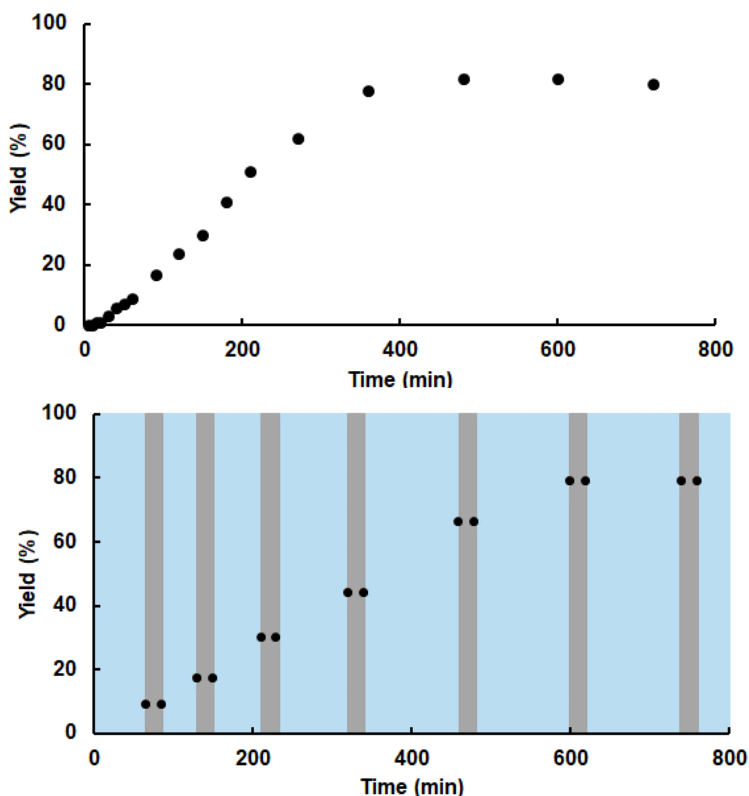
Figure 4. 1. *Top:* Single-point monitoring of the reductive cross-coupling reaction. *Bottom:* Single-point monitoring under light-dark cycles.

In this sense, the redox potential of the excited PC (*PC$^+$) of all the tested compounds matched with DIPEA as electron donor (0.50 V *vs* SCE). Then, the metallic photocatalysts presented a correlation between their redox potential and the catalytic activity: **PC$_{Ir}$^{NMe2}** presented the strongest reducing power (-1.80 V *vs* SCE) and the best catalytic response. Following this trend, **3DPA2FBN** should improve the final results considering its redox potential (-1.92 V vs SCE). However, the lifetime of its excited version was considerably shorter (4.3 ns) compared to the previous metallic photocatalyst, showing that a suitable redox potential and longer lifetimes of the excited catalyst were required for a successful

reactivity. We further discuss the role of both metal catalysts and their mechanistic pathway in section 4.2.4. (Mechanistic investigations).

Table 4. 9. Comparison of the redox potentials and lifetime of some photocatalysts and their catalytic response against the reductive cross-coupling reaction.

	PC	$E^o(PC^+ / PC^0)$	$E^o(*PC^+ / PC^0)$	*Lifetime (ns)*	% Yield (Conv.)
1	PC_{Ir}^{NMe2}	**-1.80**	**+0.77**	**2430[58]**	**82 (100)**
2	PC_{Ir}^{COOEt}	-1.01	+0.84	39.7[59]	0 (20)
3	PC_{Ir}^{H}	-1.42	+0.67	338[60]	5 (33)
4	PC_{Ir}^{tBu}	-1.51	+0.66	550[61]	38 (80)
5	PC_{Cu}	-1.64	+0.93	280[62]	64 (100)
6	4CzIPN	-1.21	+1.35	12.7[63]	10 (49)
7	3DPA2FBN	-1.92	+0.92	4.2[63]	51 (100)

General procedure **B**. Redox potentials in V vs SCE. To compare with the redox potential of DIPEA (0.50 V vs SCE).

4.2.2. Scope of the reaction

With the optimized conditions for the cross-coupling in hand (Table 4.8, entry 1), we explored the generality of our methodology for a radical hydroalkylation of styrene using various unactivated alkyl chlorides as alkylation agents (Table 4.10). The mild reaction conditions allowed a broad functional group tolerance, including alkyl chains (**iv.3a, iv.3b**), alkenes (**iv.3c, iv.3d**), ketones (**iv.3i, iv.3ab**), esters (**iv.3j- iv.3l**), ethers (**iv.3h, iv.3m**), silyl ethers (**iv.3g**), nitriles (**iv.3m**) and acetals (**iv.3h**). Remarkably, free aliphatic alcohols (**iv.3e, iv.3f**) worked without previous functional group protection, thus providing an additional handle for further functionalization. In a first instance, substrates bearing a basic nitrogen

atom were expected to be challenging under radical and reducing conditions; however, amides (**iv.3n- iv.3q**) showed excellent results, giving versatility to the methodology to one of the most widely present functional groups in pharmaceuticals, natural products or polymers.[64, 65] In the same direction, the methodology presented interesting results against different aromatic heterocyclic rings (**iv.3r- iv.3w**). Moreover, we were able to modify biologically active molecules such as ibuprofen (**iv.3aa**) or estrone (**iv.3ab**), which, together with the good tolerance of the reaction conditions to some heterocyclic compounds, illustrate the potential of using the methodology in drug discovery or final stage functionalization by installing an inert alkyl chloride at the target molecule.

Particularly, other atypical functional groups tested in organic methodologies such as tioethers (**iv.3x**), phosphine oxide (**iv.3y**) and alkyl selenides (**iv.3z**) also survived the reaction conditions, considering that they might be active functionalities under radical conditions. The model reaction was also scaled up to gram scale using 0.7 g of **iv.1a,** 4.4 g of **iv.2a** and irradiation for 24 h (KESSIL lamp, λ = 467 nm, separated 7 cm to maintain a temperature close to 30ºC (Table 4.10 and experimental section). Finally, secondary alkyl chlorides (**iv.3ac- iv.3ag**) also presented high yields, in agreement with their lower BDE compared to primary chloroalkanes. However, we found tertiary alkyl chlorides as a limitation, most probably due to their high intrinsic reactivity towards elimination and dehalogenated products.[66] Together with tertiary chloroalkanes, the other main border of this methodology were benzylic carbonyls, which produced ketyl radicals under these reductive conditions.[67]

Table 4. 10. Scope of the reductive cross-coupling of inert alkyl chlorides with styrene.
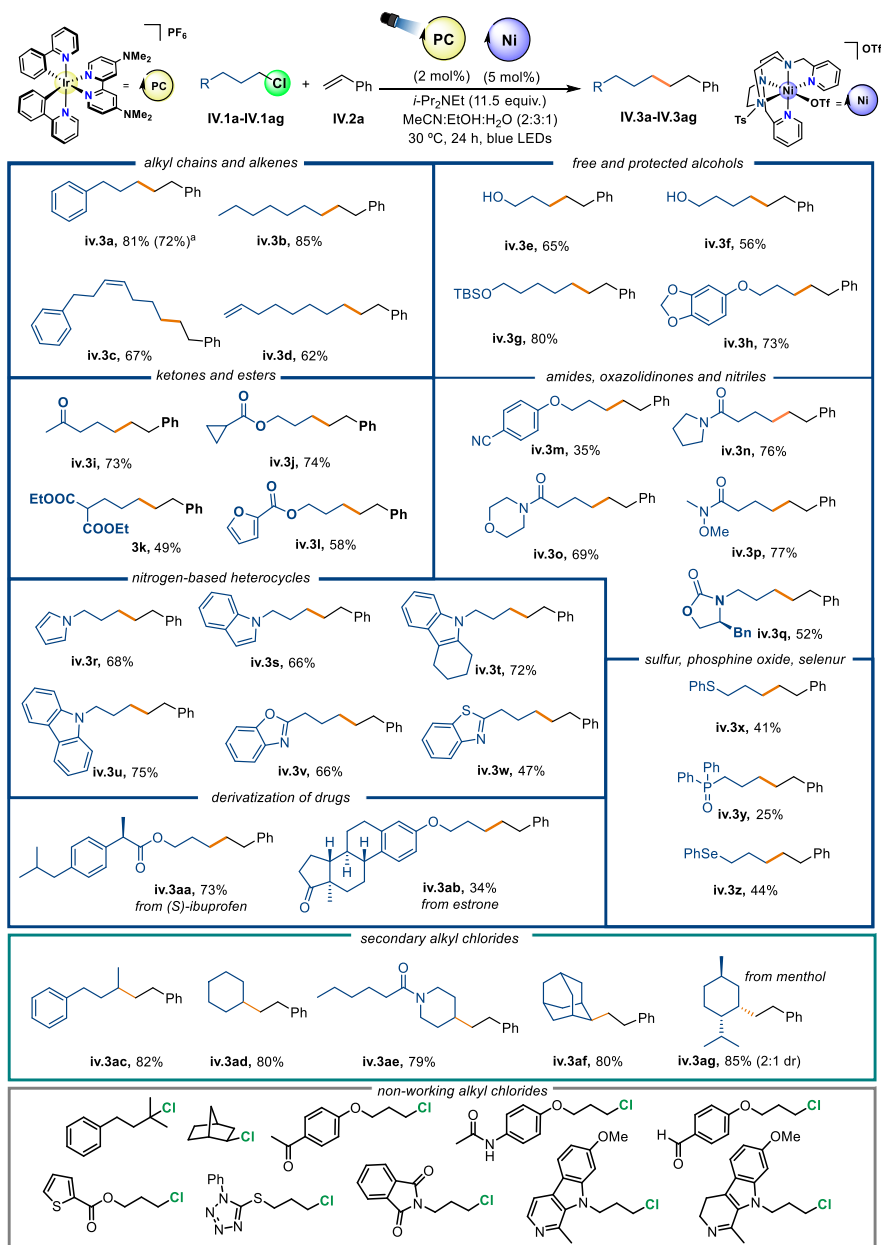
Standard reaction conditions: **iv.3a-ag** (20 mM), **iv.2a** (10 equiv.), **PC$_{Ir}$ ^{NMe2}** (2 mol %), **(Py$_2$^{Ts}tacn)Ni(OTf)$_2$** (5 mol %), DIPEA (230 mM), MeCN:EtOH:H$_2$O (2:3:1), V$_T$ = 2 mL. Blue LED irradiation (1 W, 447 nm). All of those are isolated products and averages of at least eight reactions. [a] Reaction performed at gram scale (4.3 mmol), visible-light irradiation with a KESSIL lamp (467 nm), separated 7 cm to maintain the temperature at 30ºC, for 24 h.

Table 4. 11. Scope of the cross-coupling of **iv.1h** with aromatic alkenes.
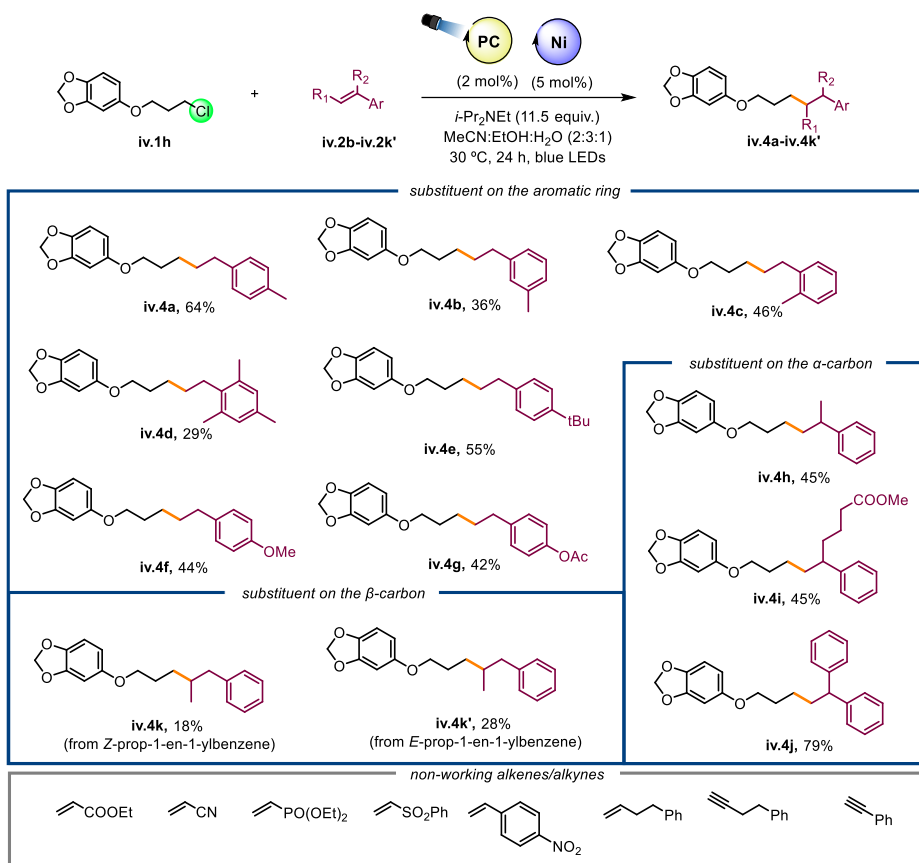
Standard reaction conditions: **iv.1h** (20 mM), **iv.2b-k'** (10 equiv.), **PC$_{Ir}$ ^{NMe2}** (2 mol %), **(Py$_2$^{Ts}tacn)Ni(OTf)$_2$** (5 mol %), DIPEA (230 mM), MeCN:EtOH:H$_2$O (2:3:1), V$_T$ = 2 mL. Blue LED irradiation (1 W, 447 nm). All of those are isolated products and averages of at least eight reactions.

We also evaluated the expansion of the methodology against aromatic alkenes (Table 4.11). We established **iv.1h,** such as a model substrate, to facilitate the identification and purification of the final product. Different substituted aryl olefins were viable coupling partners: alkyl chains in *para* position (**iv.4a, iv.4e**) presented good yields, although adding an alkyl substituent in *ortho* or *meta* position diminished the alkene reactivity (**iv.4b, iv.4c**) largely. The role of the

electronic properties of the aryl ring in the alkene reactivity was proven by the introduction of electron-donating groups in *para* position (**iv.4f, iv.4g**), showing a mitigated reactivity. Furthermore, the reactivity is consistent with a Giese-type radical addition to an olefin: the attack of the radical to the alkene was restricted by the addition of a substituent in the *β*-carbon of the olefin (**iv.4k, iv.4k'**); different alkyl chains in the *α*-carbon (**iv.4h, iv.4i**) did not show any significant change in the behavior of the olefin. However, a phenyl group at this position (**iv.4j**) enhanced the yield.

Nevertheless, the current reaction conditions present a restriction regarding alkene type. Our attempts to expand the reactivity to other substituted alkenes (Table 4.11) yielded the homocoupling of the alkyl chloride as the main reaction product (together with dehalogenation) without the formation of cross-coupling products. We hypothesized that the highly reducing reaction conditions led to the direct transformation of olefins triggered by a SET from the reduced PC or an EnT from the excited PC to the olefin. Moreover, it is known that these olefins are highly reactive against radicals, leading to secondary reactions. In this regard, low oxidation state metal complexes, formed under less reducing conditions but keeping their supernucleophilic character, could be a way to deliver the desired reactivity in a broader olefin scope.

4.2.3. Expansion of the reactivity: cascade radical reaction

Based on the observed reactivity, we hypothesized that the dual catalytic system generates a carbon-centered radical through the cleavage of the Csp^3−Cl bond, engaging the intermolecular cross-coupling with the olefin in the following step. However, if an intramolecular radical addition is possible, it should be kinetically more favored than an intermolecular one.[68] Therefore, we should trap the radical intermediate under appropriate reaction conditions, thus opening the

opportunity for cascade Csp^3-Csp^3 bond-forming reactions. To this end, we evaluated the catalytic system against alkyl chlorides with pendant alkenes. In our previous work,[47] a 5-*exo-trig* cyclic product was promoted after activating the Csp^3-Cl bond, generating a highly reactive radical intermediate that engaged a hydrogen-atom transfer (HAT) from the solvent. However, previous reaction conditions failed to elaborate the reactivity further and did not successfully produce the intermolecular cross-coupling product.
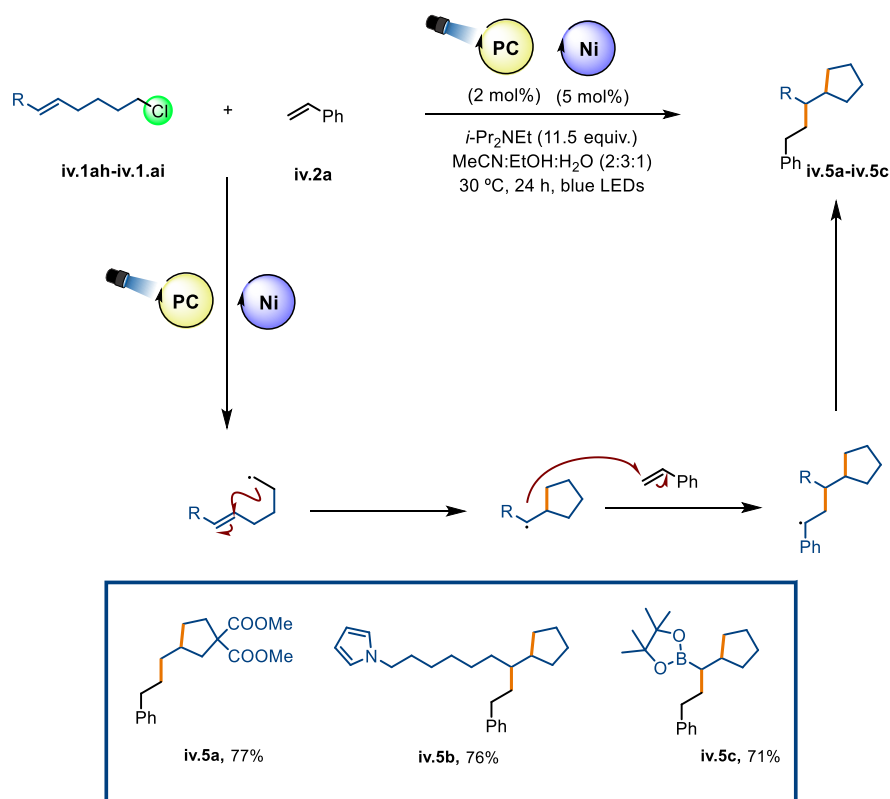
Scheme 4.9. Cascade intramolecular cyclization and reductive cross-coupling reactions. Standard reaction conditions: **iv.1ah-ai** (20 mM), **iv.2a** (10 equiv.), **PC$_{Ir}^{NMe2}$** (2 mol %), **(Py$_2^{Ts}$tacn)Ni(OTf)$_2$** (5 mol %), DIPEA (230 mM), MeCN:EtOH:H2O (2:3:1), total volume = 2 mL. Visible-light irradiation with blue LEDs (1 W, 447 nm). All of those are isolated products and averages of at least eight reactions.

The conditions reported herein produced excellent results (Scheme 4.9, **iv.5a-iv.5c**, 71-77% yield). The products formed can be explained by a *5-exo-trig* cyclization followed by addition of the intermediate radical to styrene, which increases the molecular complexity, but keeping intact a heterocycle such as pyrrole (**iv.5b**), and versatile functional groups such as malonate (**iv.5a**) or boronic ester (**iv.5c**), allowing post-modification of the products. Noticeably, the boronic ester located at the vinylic position in the starting substrate remains untouched after the attack of the radical and the reduction step. The methodology produced exceptional chemoselectivity in synthesizing more complex molecular scaffolds after the formation of two consecutive Csp^3-Csp^3 bonds (Scheme 4.9).

4.2.4. Mechanistic investigations

The reductive cross-coupling of alkyl chlorides with aromatic olefins is proposed to proceed through carbon-centered radicals generated by the reaction of an *in-situ* photogenerated low-valent Ni intermediate with the corresponding chloroalkane (Scheme 4.10). In this section, we would shed some light on the reaction mechanism, with the elucidation of a plausible and detailed catalytic cycle as the main goal.
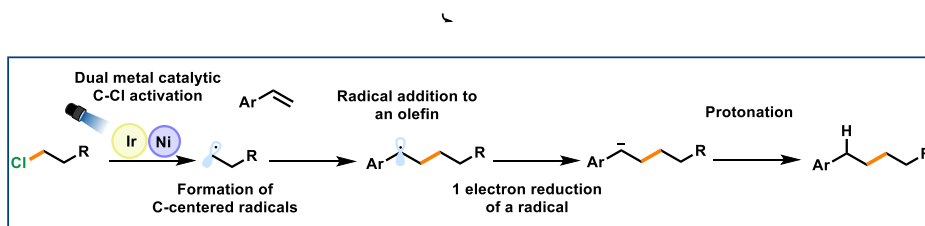
Scheme 4.10. General proposed cross-coupling pathway between alkyl chlorides and styrene.

4.2.4.1. Study of the dual metal catalytic system by spectroscopy
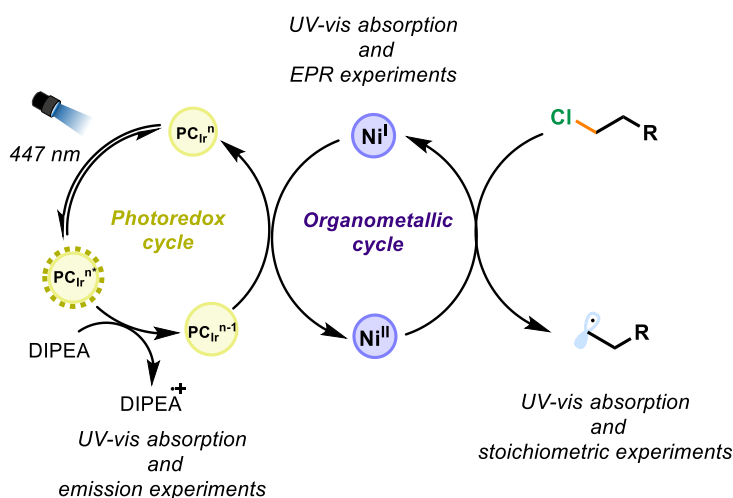
Scheme 4. 11. Proposed mechanism for the photoactivation of alkyl chlorides.

Previous works from our group on the photocatalytic hydrogenation of ketones and the intramolecular cyclization of alkenes, as well as previous sections in the current thesis, suggested the formation of low valent Ni^I or Co^I intermediates by SET pathway from reduced $\mathbf{PC_{Cu}^{n-1}}$ (E = -1.64 V vs SCE).[47, 67, 69] These low valent metal species can undergo the cleavage of Csp^3−Cl bonds, with similar pathways studied for coenzyme B_{12} derivates and macrocyclic nickel complexes.[70-73] We envisioned an analog reactivity for the present catalytic system, using $\mathbf{PC_{Ir}^{NMe2}}$ as photocatalyst and $\mathbf{(Py_2^{Ts}tacn)Ni(OTf)_2}$ as the catalyst (Scheme 4.11). For that, spectroscopic techniques were used to detect and monitor the reactivity of the active species in the catalytic system.

Reactivity of Iridium Photocatalyst: UV-Vis emission experiments
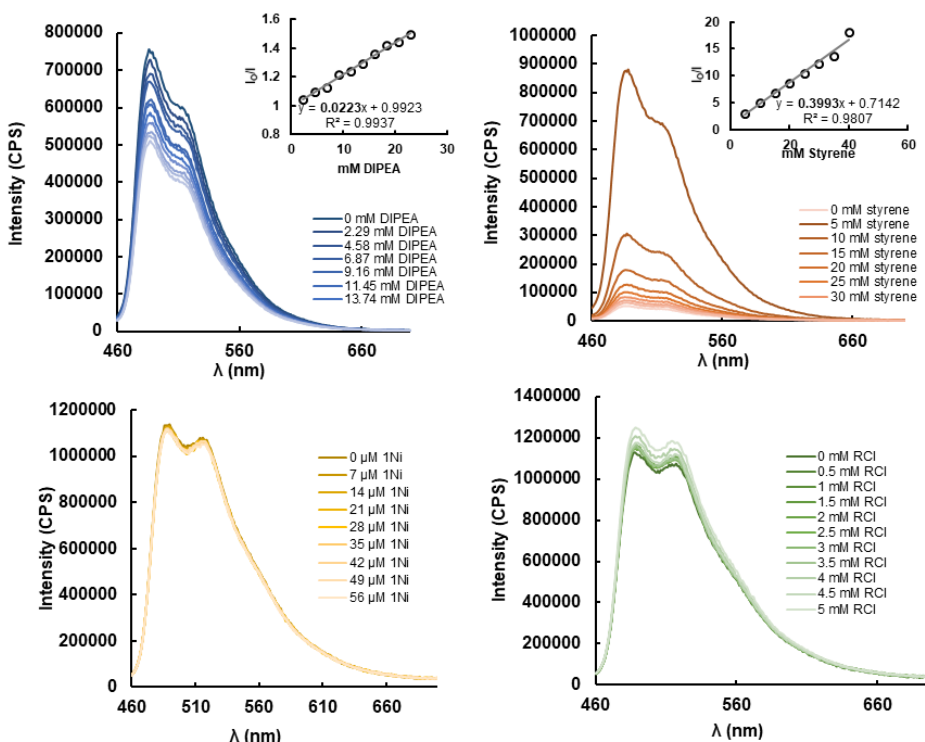
Figure 4. 2. Emission spectra of $\mathbf{PC_{Ir}^{NMe2}}$ in presence of varying concentrations of different compounds. . [$\mathbf{PC_{Ir}^{NMe2}}$]= 10 µM in MeCN:EtOH:H₂O (400 µL/1200 µL / 300 µL); cell path b = 1 cm; 25ºC, λ_{ex}= 450 nm. *Top-left*: Consecutive additions of 20 µL of a stock solution of **DIPEA** (229 mM). Top-right: Consecutive additions of 20 µL of a stock solution of **styrene** (500 mM). *Bottom-left*: Consecutive additions of 20 µL of a stock solution of **(Py₂^{Ts}tacn)Ni(OTf)₂** (700 µM). *Bottom-right*: Consecutive additions of 20 µL of a stock solution of **(3-chloropropil)-1-benzene** (50 mM).

We performed fluorescence quenching experiments of the $\mathbf{PC_{Ir}^{NMe2}}$ against the different compounds of the reaction mixture to ensure that, upon visible-light irradiation, a long-lived excited [$\mathbf{PC_{Ir}^{NMe2}}$]* is formed, which is then reductively quenched only by N-diisopropylethylamine, in consonance with our previous mechanistic proposal (Figure 4.2).

Fluorescence spectra of **PC_{Ir}^{NMe2}** showed an emission band at 485 nm, which DIPEA quenched with a K_{SV} of 22.3 M^{-1} through a Stern-Volmer analysis. As expected, **$(Py_2^{Ts}tacn)Ni(OTf)_2$** and (3-chloropropil)-1-benzene did not have a qualitative effect on the emission of the **PC_{Ir}^{NMe2}** . However, styrene caused a clear quenching of the excited state of the photocatalyst, showing a K_{SV} of 399.3 M^{-1}. Considering the reactivity observed in blank experiments (see previous section 4.2.1), the two compounds differ in the quenching pathway of the PC. Removing DIPEA from the reaction mixture resulted in maintaining untouched the alkyl chloride, with the detection of cyclobutane products from the homocoupling of the styrene. While DIPEA could reduce the excited state of **PC_{Ir}^{NMe2}** into the reduced **$[PC_{Ir}^{NMe2}]^0$** and promote the subsequent reactivity with **$(Py_2^{Ts}tacn)Ni(OTf)_2$** and the alkyl chloride, styrene follows an energy transfer process with the **$[PC_{Ir}^{NMe2}]^*$**, resulting in an inefficient active quenching for the dual catalytic system, obtaining a parallel secondary reaction.[55] The estimation of the excited state redox potential from the reductive quenching pathway is crucial for the understanding of the distinct reactivity and is given by the following equations:[74]

$$E^o(*PC / PC^0) = E^o(PC^+ / PC^0) + E_{00}$$

$$E^o(PC^{2+} / {}^*PC) = E^o(PC^{2+} / PC^+) - E_{00}$$

where $E^o(PC^+ / PC^0)$ and $E^o(PC^{2+} / PC)$ are the redox potentials in the ground state and E_{00} is the difference between the zero vibrational levels of the ground and excited electronic states. The E_{00} energy can be estimated as the wavelength corresponding to the first emission peak, the 0-0 transition.

This, together with the $E^o(PC^+ / PC^0)$ and $E^o(PC^{2+} / PC^+)$ measured by CV (-1.80 and 1.08 V *vs* SCE)[69] led us to determine the excited state redox potentials **$E^o(*PC^+ / PC^0)$** and **$E^o(PC^{2+} / {}^*PC^+)$** (**0.77** and **-1,49 V** *vs* SCE, respectively). Thus, **$[PC_{Ir}^{NMe2}]^*$** could be reductively quenched by the DIPEA (0.50 V *vs* SCE)[75] to form the reduced **$[PC_{Ir}^{NMe2}]^0$** under the reaction conditions. However, styrene

(1.97 V *vs* SCE)[76] could not be oxidized by **[PC$_{Ir}^{NMe2}$]***, confirming our previous hypothesis of the energy transfer between the PC and the olefin.

Photogeneration and detection of Ni^i active species
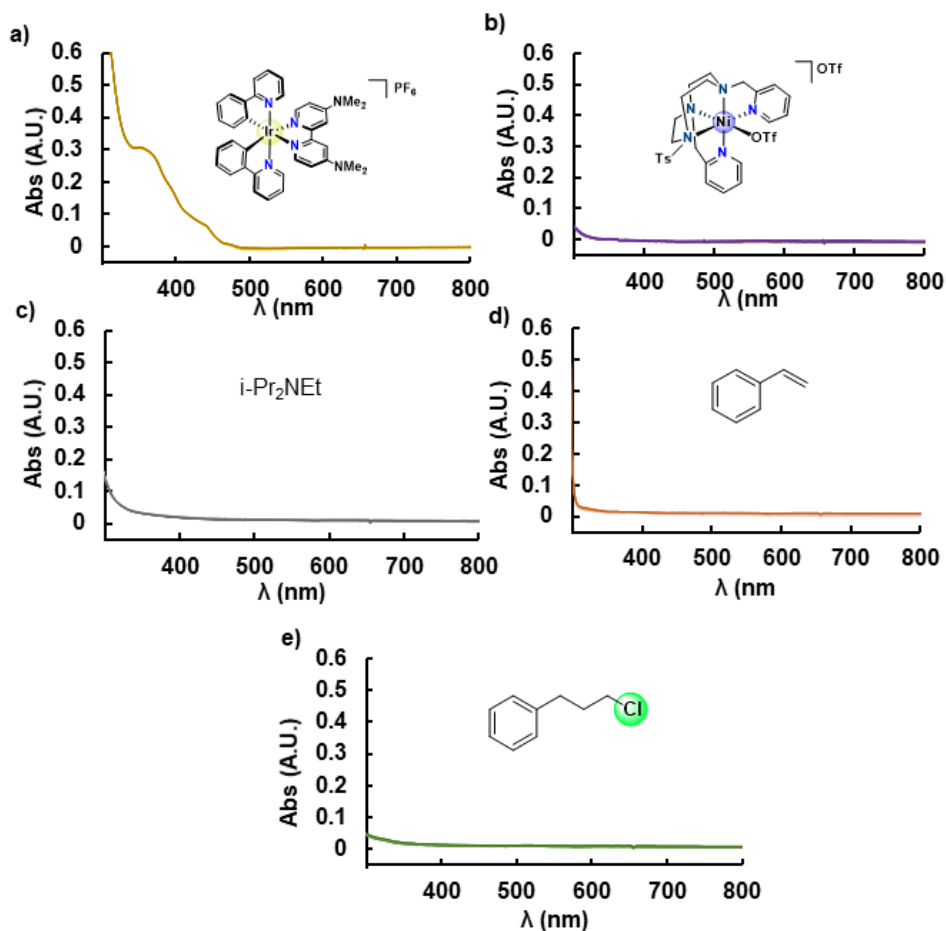
Figure 4.3. Blanks UV-Vis spectrum in MeCN:EtOH:H$_2$O (2:3:1) of: a) **PC$_{Ir}^{NMe2}$** (40 µM), b) **(Py$_2^{Ts}$tacn)Ni(OTf)$_2$** (100 µM), c) DIPEA (2 mM), d) styrene (2 mM), e) (3-chloropropyl)-1-benzene (2 mM).

Once the quenching of the excited state of PC was elucidated, the dual catalytic system was interrogated through UV-Vis absorption spectroscopy. The organic compounds did not present an absorption band in the visible range, enabling the

scrutiny of the metal species, whose d-d transitions can absorb in the visible range (Figure 4.4).

Then, time-dependent UV-Vis absorption experiments were performed in order to monitor the evolution of $(\mathbf{Py_2^{Ts}tacn})\mathbf{Ni(OTf)_2}$, $\mathbf{PC_{Ir}^{NMe2}}$ and DIPEA under relevant catalytic conditions while irradiating the sample with an LED lamp (λ 447 nm). Interestingly, a new absorption band appeared at λ 520 nm once the blue irradiation started (Figure 4.4, left). The reduced species of some iridium photocatalysts also tipically presented an absorption band near 500 nm,[69] caused by the spin density delocalization into the ligand instead of the metal center. However, $\mathbf{PC_{Ir}^{NMe2}}$ in the presence of DIPEA did not show any formation of a new band in the mentioned region (Figure 4.4, right).
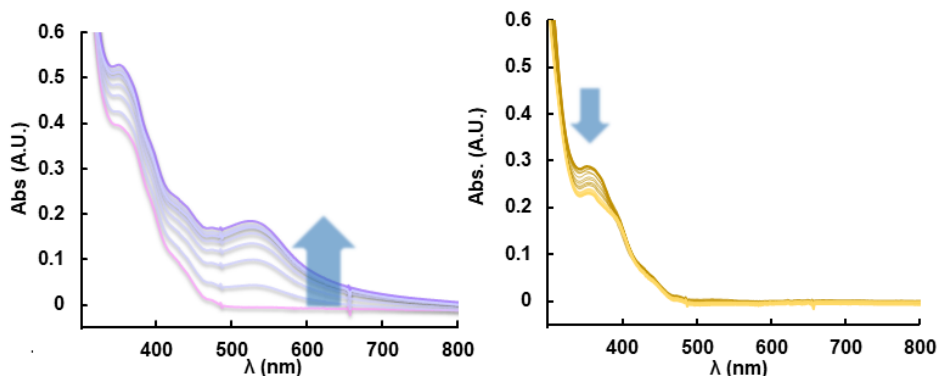
Figure 4. 4. *Left:* Changes in UV-Vis spectrum of a reaction mixture containing $\mathbf{PC_{Ir}^{NMe2}}$ (40 µM), $(\mathbf{Py_2^{Ts}tacn})\mathbf{Ni(OTf)_2}$ (100 µM) and DIPEA (10 µL) in MeCN:EtOH:H$_2$O (2:3:1) during 25 s of irradiation (blue LED, 447 nm) at 30ºC. In this period, a band at 520 nm appears, corresponding to the formation of Ni^I species. *Right:* . Changes in UV-Vis spectrum of a reaction mixture containing $\mathbf{PC_{Ir}^{NMe2}}$ (40 µM) and DIPEA (10 µL) in MeCN:EtOH:H$_2$O (2:3:1) during 10 min of irradiation (blue LED, 447 nm) at 30ºC.

The same experiments performed in an EPR tube were also resolutive in the same direction. Control experiments were performed in the absence of the **(Py$_2$^{Ts}tacn)Ni(OTf)$_2$** complex (**PC$_{Ir}$^{NMe2}**, 2 mol% in *n*-BuCN:EtOH:*i*-PrNEt$_2$, 2:3:0.1) before and after irradiation, without any EPR signal (Figure 4.6). However, 1 min of irradiation (LED λ_{max} 447 nm) of an EPR tube containing **(Py$_2$^{Ts}tacn)Ni(OTf)$_2$** (5 mol%) and **PC$_{Ir}$^{NMe2}** (2 mol%) gave an EPR signal with an almost axial symmetry (g-values centered at 2.06, 2.08 and 2.29) consistent with an unpaired electron predominantly localized in the $d_{x^2-y^2}$ orbital (Figure 4.5). The obtained g-values combined with the appearance of an absorption band at λ 520 nm in the UV-Vis are consistent with the photogeneration of a square pyramidal **Ni^I** with a spin 1/2 and equivalent to previously reported **Ni^I** complexes with similar ligand environment.[47, 77]
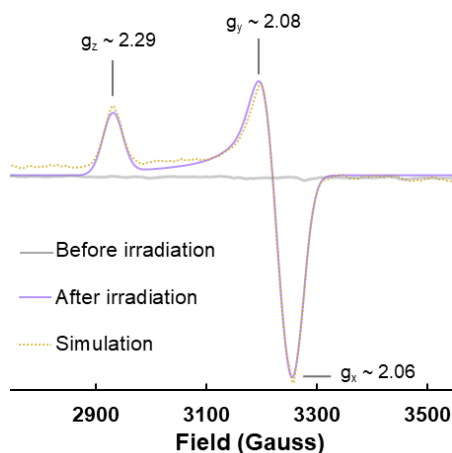
Figure 4.5. EPR spectra and simulation of reaction mixture of Ni^I spin ½ species formed by irradiation (LED λ_{max} 447 nm, room temperature). Reaction conditions: **PC$_{Ir}$^{NMe2}** (40 µM) and **(Py$_2$^{Ts}tacn)Ni(OTf)$_2$** (100 µM) in n-BuCN:EtOH (2:3) with DIPEA (11.4 mM).
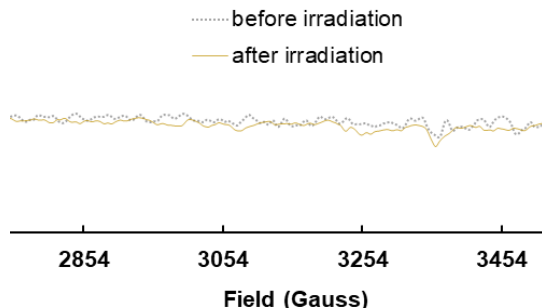
Figure 4. 6. EPR spectra of $\mathbf{PC_{Ir}^{NMe2}}$ (40 µM) in n-BuCN:EtOH (2:3) with DIPEA (11.4 mM).

Revealing the $(Py_2{}^{Ts}tacn)Ni^i(OTf)_2$ as key species for the activation of Csp^3- Cl bonds

Following that recognition of $\mathbf{Ni^I}$ intermediate *in situ* photogenerated upon the reaction of the $\mathbf{(Py_2{}^{Ts}tacn)Ni(OTf)_2}$ precatalyst with the $\mathbf{[PC_{Ir}^{NMe2}]^0}$, the catalytic activation of alkyl chlorides by this species was examined in the same way by time-dependent UV-Vis spectroscopy: the catalytic system was monitored $(\mathbf{(Py_2{}^{Ts}tacn)Ni(OTf)_2}, \mathbf{PC_{Ir}^{NMe2}}$ and DIPEA) and on-line irradiation (LED, Royal blue, 447 nm) enhanced the formation of the absorption band at 520 nm. Switching off the LED and adding concurrently 20 equivalents of (3-chloropropyl)-1-benzene (Figure 4.7, green line) resulted in a drastic decay of the 520 nm signal. We assigned this phenomenon to the reaction of the *in situ* formed $\mathbf{Ni^I}$ intermediate and the chloroalkane. A control experiment by adding styrene (same volume, 200 equiv.) instead of the chloroalkane resulted in a smooth signal decrease (Figure 4.7, orange line). The faster kinetic decay of the absorption signal yielded by the photogenerated $\mathbf{Ni^I}$ intermediate upon addition of the chloroalkane *versus* addition of styrene evidence the $\mathbf{(Py_2{}^{Ts}tacn)Ni^I(OTf)_2}$ as key species for the activation of Csp^3-Cl bonds, without presenting an additional reactivity with styrene.
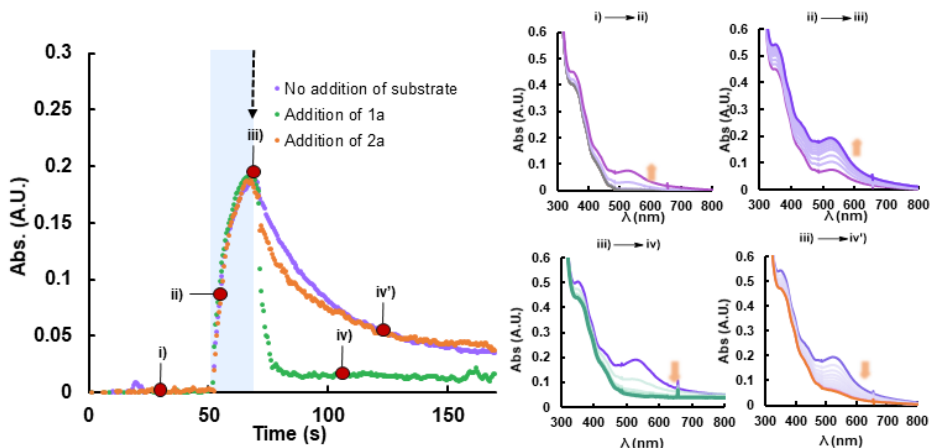
Figure 4. 7. Absorbance monitored at 520 nm of a solution containing **PC_{Ir}^{NMe2}** (40 µM) and **($Py_2^{Ts}tacn$)Ni(OTf)₂** (100 µM) in MeCN:EtOH:H₂O (2:3:1) with DIPEA (11.4 mM) at 30ºC. After 50 s the light is switch on (LED λ_{max} 447 nm). After 25 s the light is switch off. At this point, the addition of 20 equiv. of **1a** (2 mM) triggers a rapid drop of the **Ni^I** band (green line). In contrast, in the absence of **1a**, the decay in the dark of the **Ni^I** band (purple line) is significantly slower. The same slow decay is observed when adding 200 equiv. of **2a** (orange line) instead of **1a**.

Nevertheless, the role of styrene does not remain innocent in the photoredox system. At the beginning of the experiment, the presence of styrene produced a substantial drop in the formation rate of **Ni^I** intermediate together with halved Abs_max for 520 nm band (Figure 4.8). This observation correlates with the previously observed emission quenching of the excited PC by the styrene (Figure 4.2) and can be assigned to an energy transfer process. This pathway would not directly interfere with neither the photogeneration of the **Ni^I** intermediate nor the activation of the alkyl chloride. The energy transfer would diminish the population of PC available for the **($Py_2^{Ts}tacn$)Ni(OTf)₂** reduction, rendering a slower formation rate of **Ni^I**. However, the energy transfer may not consume the PC, and the slower formation of **Ni^I** could enhance the endurance of the catalytic system.
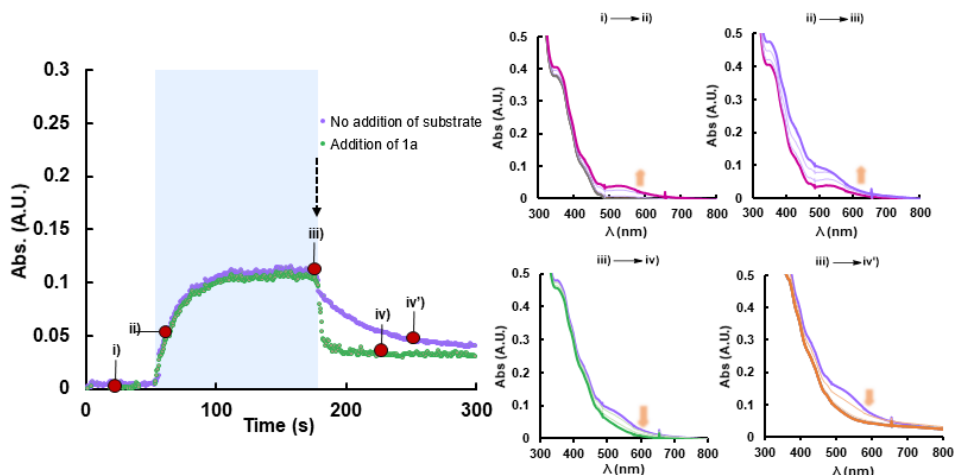
Figure 4. 8. Absorbance monitored at 520 nm of a solution containing PC_{Ir}^{NMe2} (40 µM) and $(Py_2^{Ts}tacn)Ni(OTf)_2$ (100 µM) in MeCN:EtOH:H$_2$O (2:3:1) with DIPEA (11.4 mM) at 30ºC. After 50 s the light is switched on (LED λ_{max} 447 nm). After 25 s the light is switched off. At this point, the addition of 20 equiv. of **iv.1a** (2 mM) triggers a rapid drop of the Ni^I band (green line). In contrast, in the absence of **iv.1a**, the decay in the dark of the Ni^I band (purple line) is significantly slower. The same slow decay is observed when adding 200 equiv. of **iv.2a** (orange line) instead of **iv.1a**.

This revealing UV-Vis monitoring approach allowed us to go one step further, designing an experiment to estimate the amount of the *in situ* photochemically generated Ni^I by analyzing its reactivity against two reactive compounds: the model alkyl chloride **iv.1a** and methyl viologen (Scheme 4.12).
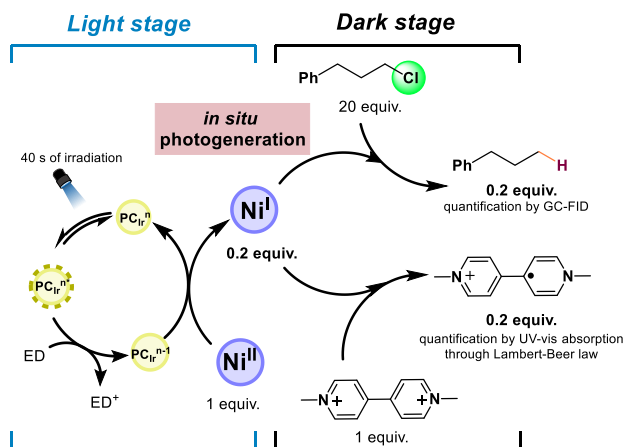
Scheme 4. 12. Summary of the stoichiometric reactivity of the in situ photogenerated Ni^I with methyl viologen and (3-chloropropyl)benzene.

The low concentration conditions used in previous UV-Vis spectroscopic experiments did not allow us to quantify the organic compounds obtained after irradiation. To solve this problem, we repeated the same experiment developed in Figure 4.8, changing the concentrations to the standard reaction conditions (1 mM **(Py₂Tstacn)Ni(OTf)₂**, 0.4 mM of **PCIr^NMe2**, 20 mM of **iv.1a**). A concentration of 200 µM of dehalogenated **iv.1a** was determined by GC-FID (Figure 4.9), obtaining 1% yield (GC-yield, see calibration in Figure 4.10) related to **iv.1a** and 20 % yield related to **(Py₂Tstacn)Ni(OTf)₂**.
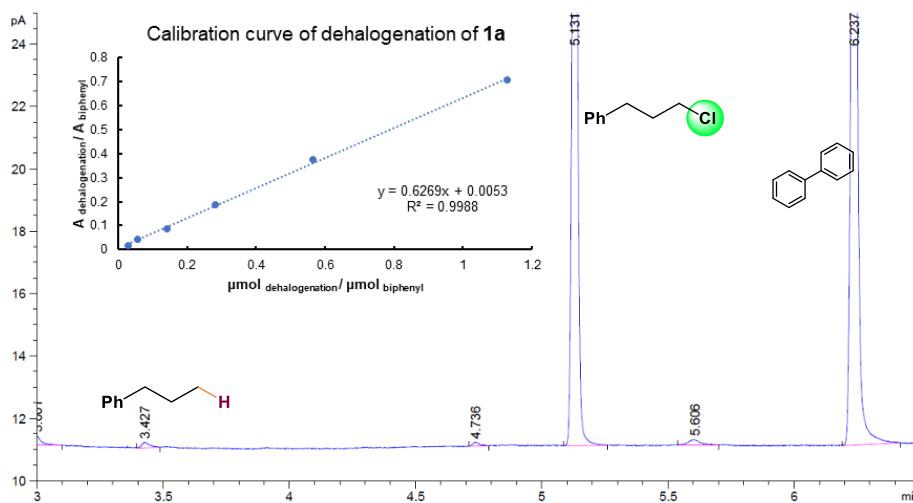
Figure 4.9. GC-FID chromatogram of the reaction crude of a solution containing **PCIr^NMe2** (400 µM) and **(Py₂Tstacn)Ni(OTf)₂** (1000 µM) in MeCN:EtOH:H₂O (2:3:1) with DIPEA (11.4 mM), after 40 s of light irradiation (LED λmax 447 nm). **iv.1a** (20 mM) was added after irradiation. Calibration curve of the response of dehalogenated **iv.1a** using biphenyl as internal standard in GC-FID for the determination of the GC-Yield.

The second estimation of the amount of photochemically-generated **Ni^I** (**(Py₂Tstacn)Ni^I(OTf)₂**) with **PCIr^NMe2** was accomplished by analyzing the extent of the reduction of methyl viologen when it reacts with the *in situ* formed **Ni^I**. The reduction of methyl viologen is a well-known reaction that presents two consecutive reduction processes at -0.69 V (MV²⁺/MV⁺·) and -1.04 V (MV⁺·/MV⁰)

vs SCE.[78] The first reduction can be monitored by UV-Vis following the formation of its band at 600 nm.[79] In this spectral region, the PC or the nickel complex signals do not significantly interfere with the signal. In comparison, the second reduction implies the disappearance of the band at 600 nm.
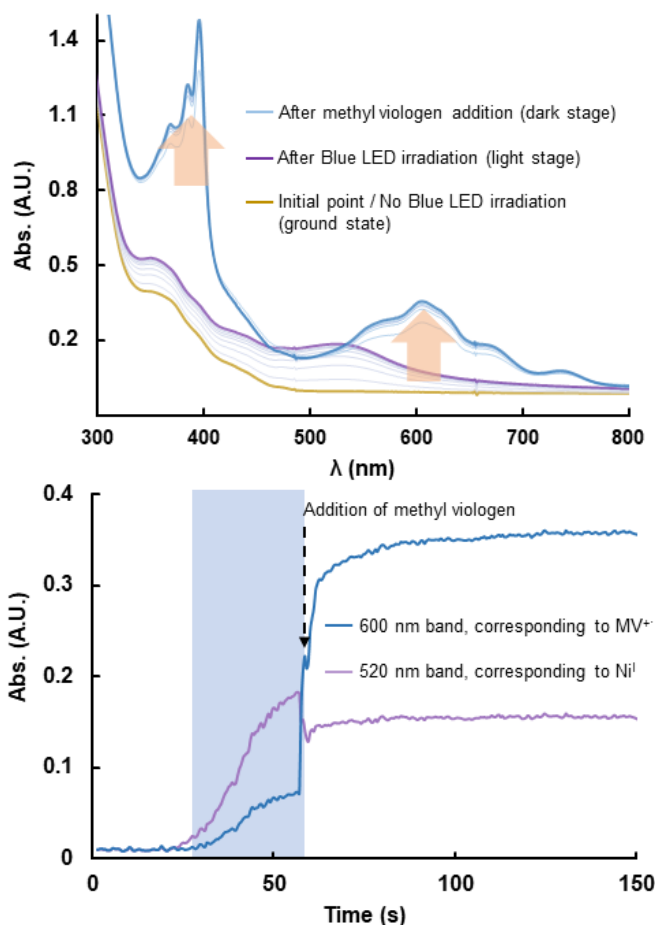
Figure 4.10. *Top:* Changes in UV-vis spectrum of a reaction mixture containing **PC$_{Ir}$^{NMe2}** (40 µM), **(Py$_2$^{Ts}tacn)Ni(OTf)$_2$** (100 µM) and DIPEA (10 µL) in MeCN:EtOH:H$_2$O (2:3:1) during 40 s of irradiation (blue LED, 447 nm) at 30°C. After 25 s the light is switch on (LED λ_{max} 447 nm). After 40 s the light is switch off. At this point, the addition of 1 equiv. of **iv.1a** (100 µM) triggers a rapid drop of the **Ni^I** band (purple line). In contrast, a new band appears at 600 nm, corresponding to the formation of reduced methyl viologen species, which is stabilized after few seconds. *Bottom:* Comparition of the evolution of the absorption band at 600 nm (corresponding to MV$^{+•}$) and 520 nm (corresponding to **Ni^I**).

In the experiment, a solution containing the **(Py$_2$^{Ts}tacn)Ni^I(OTf)$_2$** (*in-situ* photochemically-generated after 40 s of irradiation) reacted fast with an added solution of MV^{2+} (1 equiv. respect to the initial concentration of **(Py$_2$^{Ts}tacn)Ni(OTf)$_2$** added in the dark), inducing the evolution of a new band at 600 nm, corresponding to MV$^+$ (Figure 4.10)'. This band reached a *plateau* after few seconds of the addition of the MV^{2+}, allowing the quantification of MV$^+$.
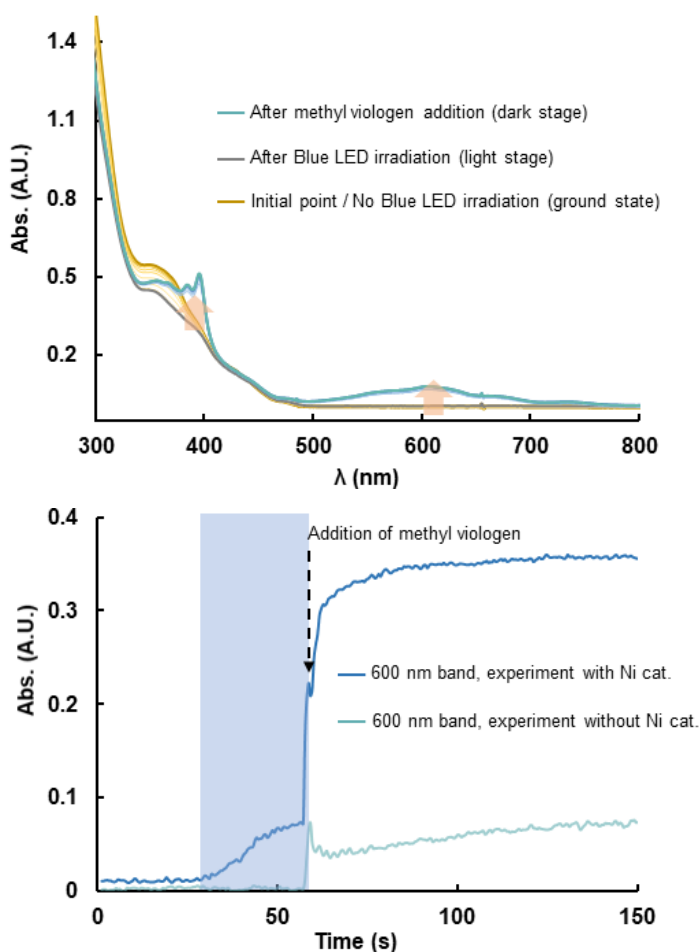
Figure 4.11. *Top:* Changes in UV-Vis spectrum of a reaction mixture containing **PC$_{Ir}$^{NMe2}** (40 µM) and DIPEA (10 µL) in MeCN:EtOH:H$_2$O (2:3:1) during 40 s of irradiation (blue LED, 447 nm) at 30ºC. After 40 s the light is switch off. Concurrently 1 equiv. of methyl viologen (100 µM) was added. *Bottom:* Comparition of the evolution of the absorption band at 600 nm with/without **(Py$_2$^{Ts}tacn)Ni(OTf)$_2$** in the reaction mixture.

Then, we performed blank experiments without $(\mathbf{Py_2^{Ts}tacn})\mathbf{Ni(OTf)_2}$ to obtain purely the amount of $MV^{+\cdot}$ reduced entirely by $\mathbf{Ni^I}$, removing the contribution of other species in the mixture (Figure 4.11). In this case, an appeased band at 600 nm arose after adding MV^{2+}, quickly reaching a *plateau* and allowing us to exclude the contribution of other compounds from the reaction mixture.

At this point, a concentration of reduced methyl viologen of 20.34 μM was determined (Table 4.12) through the Lambert-Beer equation, revealing a 20 % of $\mathbf{Ni^I}$ formation after 40 s of blue LED irradiation under UV-Vis conditions, which agrees with the result obtained previously using (3-chloropropil)-1-benzene.

Table 4. 12. Determination of reduced methyl viologen by Lamber-Beer law.

$$\text{Abs} = \varepsilon_{max} \cdot c \cdot l \qquad c = \frac{\text{Abs}}{l \cdot \varepsilon}$$

where $l = 1$ cm and $\varepsilon_{max} = 13900$ M^{-1}cm^{-1}

Experiment	Mesured absorbance at 600 nm	Determined concentration (Lamber-Beer Law)	
With $\mathbf{1_{Ni}}$ (no correction)	0.35653	$c = \dfrac{0.3565}{1 \cdot 13900} =$	25.6 μM
Without $\mathbf{1_{Ni}}$ (correction)	0.07378	$c = \dfrac{0.0738}{1 \cdot 13900} =$	5.3 μM
With $\mathbf{1_{Ni}}$ – Without $\mathbf{1_{Ni}}$ (corrected)	0.2827	$c = \dfrac{0.2827}{1 \cdot 13900} =$	**20.3 μM**

Experiment 1: Containing $\mathbf{PC_{Ir}^{NMe2}}$ (40 μM), $(\mathbf{Py_2^{Ts}tacn})\mathbf{Ni(OTf)_2}$ (100 μM) and DIPEA (10 μL) in MeCN:EtOH:H$_2$O (2:3:1). Experiment 2: Containing $\mathbf{PC_{Ir}^{NMe2}}$ (40 μM) and DIPEA (10 μL) in MeCN:EtOH:H$_2$O (2:3:1). 1 equiv. of methyl viologen (100 μM) was added as described. l = 1 cm. The molar extinction coefficient for the reduced methyl viologen species at 600 nm is approximately $\varepsilon_{max} = 13900$ M^{-1}cm^{-1}.[79] The mesured absorbance corresponded to an average of 3 samples.

4.2.4.2. Study of the radical formation and its reactivity: radical clock experiment

The preceding spectroscopic studies allow us to demonstrate the photogeneration of $\mathbf{Ni^I}$ and its catalytic activity against alkyl chlorides. However, these experiments do not shed light on the catalyst-substrate interaction or the

result of this interaction. The mechanistic pathway for the cleavage of Csp^3−Cl bonds is discussed in the following section 4.2.4.4. Computational studies.

Considering the previous cascade reactivity (section 4.2.3.), the formation of free radicals through homolytic cleavage of Csp^3−Cl bond seems feasible. Radical clocks are another classical method to test the likelihood of free radicals being formed during a reaction. Olefin **iv.2l'** contains a 2-aryl-cyclopropyl moiety at the α-position, which can be used as a radical clock coupling partner (Scheme 4.13). If **iv.2l'** is transformed into a benzylic radical, the aryl cyclopropyl radical will ring-open with a rate of ≈10^8 s^{-1}.[80-82] Therefore, the formation of ring-opening products is diagnostic of the formation of radical species. Under our catalytic conditions, the coupling of **iv.1a** with (1-(2-phenylcyclopropyl)vinyl)benzene (**iv.2l'**) gave the ring-opened product (**iv.5d**) as a single cross-coupling product, endorsing the photogeneration of highly reactive alkyl radicals.
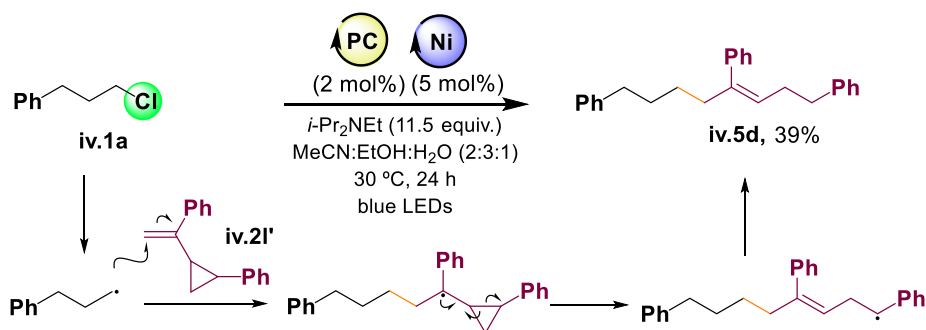
Scheme 4. 13. Radical clock experiment.

4.2.4.3. Study of the last step of the reaction: deuterium labelling experiments

The cascade reaction and the radical clock illustrate perfectly how the free radical attacks the less substituted carbon of the alkene, forming a more stable carbon radical at the adjacent position due to induction and hyperconjugation of the phenyl ring. However, a chain termination process is required to obtain the

final desired product instead of other secondary reactions from the polymerization of the generated radicals with the alkenes present in the solution.

To understand how the final product is formed from benzylic radicals, we carried out deuterium labeling experiments using different deuterated solvent systems (Figure 4.12).
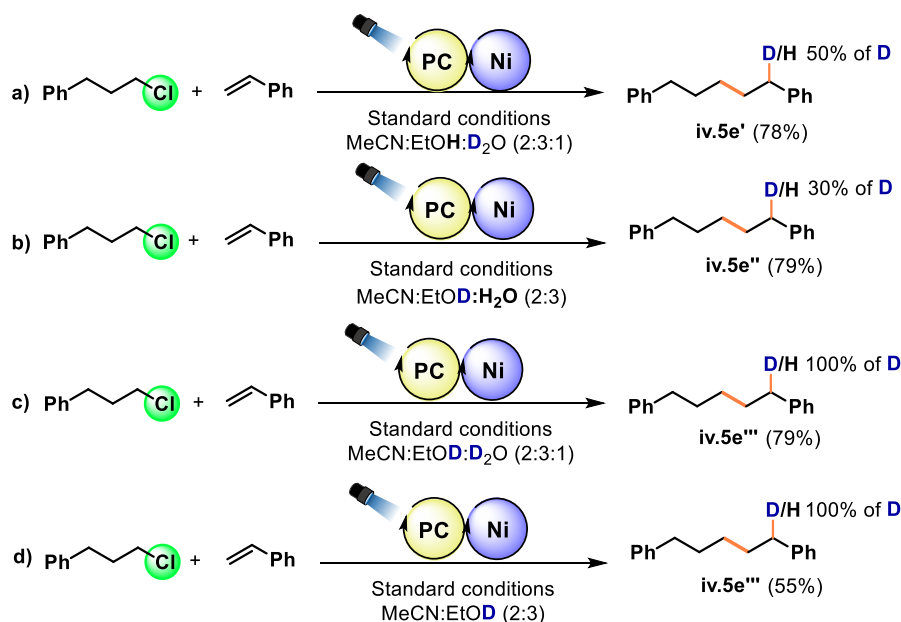
Figure 4.12. Deuterium labelling experiments.

Mixtures of deuterated and protic solvents (Figure 4.12, a and b) gave partial deuterium incorporation into the benzylic position, implying both protic solvents finally protonate the product. Furthermore, when using MeCN:EtOD (2:3) and MeCN:EtOD:D_2O (2:3:1) solvent mixtures, the reductive cross-coupling product incorporated 100% of deuterium in the α-carbon of the styrene (Figure 4.12, c and d), excluding MeCN and DIPEA as proton sources.

Nevertheless, deuterated water and deuterated ethanol are well-known sources of deuterium cations and weak deuterium atom donors. We hypothesized that the benzylic radical formed should be reduced by PC_{Ir}^{NMe2} (-1.80 V *vs* SCE) to the corresponding radical anion, which is then protonated by the [D]-solvent. DFT calculations correctly confirmed this final pathway, finding the redox potential for the benzyl alkyl radicals in the -0.9 to -1.7 V range vs SCE (Table 4.13).

Table 4. 13. Calculated and experimental redox potentials of substituted benzyl radicals.
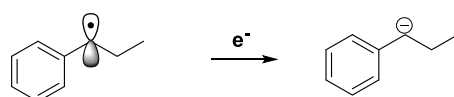
Theoretical $E_{(1/2)}$ = -1.65 V vs SCE

$$R\cdot + e^- \;\rightarrow\; R\cdot$$

Entry	R·	$E_{1/2}^{(0/-I)}$ exp.[a]	$E_{1/2}^{(0/-I)}$ theo.[b]
1	[*p*-MeO-PhCH$_2$]•	-1.75	-1.71
2	[*p*-Me-PhCH$_2$]•	-1.62	-1.56
3	[*p*-F-PhCH$_2$]•	-1.50	-1.55
4	[PhCH$_2$]•	-1.43	-1.45
5	[*p*-Cl-PhCH$_2$]•	-1.40	-1.40
6	[*p*-NC-PhCH$_2$]•	-0.77	-0.92
7	[*p*-C(O)CH$_3$-PhCH$_2$]•	-0.71	-0.97
8	[PhCHCH$_2$CH$_3$]•		-1.65

All redox potentials are given in V vs SCE. a) Redox potentials obtained from reference: *J. Am. Chem. Soc.* **1989**, *111*, 755-757. b) Theoretical redox potentials calculated at MNL15/6-31+g* level including solvent effects (SMD, MeCN).

4.2.4.4. Computational Studies

In the previous section, we identified **Ni^I** species as reactive intermediate against alkyl chlorides, without information about the reaction pathway. The computational modelling allowed us to understand the exceptional reactivity of the **Ni^I** intermediate with (3-chloropropyl)benzene (**iv.1a**). Starting from the **Ni^I** intermediate, we compared two different potential reaction pathways with **1a** as a representative and challenging unactivated model substrate:

    i)   the oxidative addition by an S_N2 mechanism (**OA-S$_N$2**)

    ii)   the concerted halogen atom abstraction (**CHAA**).

The **OA-S$_N$2** mechanism involves the oxidative addition of the Ni^I complex to the Csp^3−Cl bond generating the Ni^{III}−alkyl organometallic intermediate **I3$_{Ni(III)-C···Cl-}$**.[71, 83-85] The low energy barrier ($\Delta G^{\ddagger} = 10.8$ kcal·mol^{-1}) shows the capacity of the **Ni^I** species to nucleophilic attack *via* an S_N2 mechanism (Figure 4.13). DFT calculations also agree with favorable thermodynamics for the process ($\Delta G = -5.5$ kcal·mol^{-1}). The spin density calculated for **I3$_{Ni(III)-C···Cl-}$** shows the formation of the free chloride anion and the nickel center in oxidation state III (Figure 4.14). The one-electron reduction of the Ni^{III}−(3-phenylpropyl) organometallic complex occurs at -0.6 V. Then, homolytic cleavage of the weak M−C bond by excitation-induced elimination initiated by light or energy transfer from the photocatalysts could regenerate the divalent metal complex while forming the C-centered 3-phenylpropyl radical.[86-90] Additionally, DFT calculations indicated that the bond homolysis is also thermally accessible ($\Delta G = 19.3$ kcal·mol^{-1}). The catalytic cycle is closed with a driving force of -15.5 kcal·mol^{-1}.
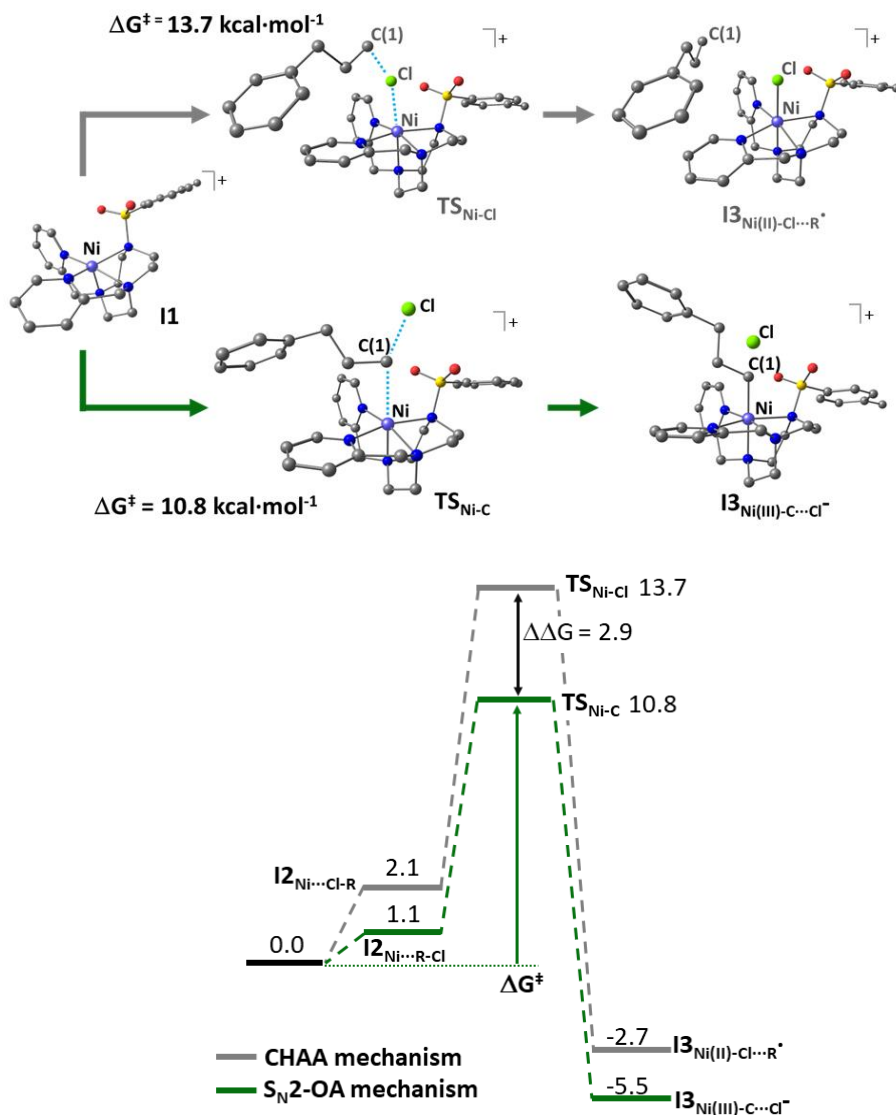
Figure 4.13. Summary of computed mechanisms. *Top:* Energy profile for the Csp−Cl cleavage by (**Py$_2$^{Ts}tacn)Ni(OTf)$_2$** in oxidation state I. Numbers in the energy profile represent the Gibbs energies given in kcal·mol^{-1}. *Bottom:* Representation of (**Py$_2$^{Ts}tacn)Ni^I(OTf)$_2$** transition states and final products for reaction pathways **OA-S$_N$2** and **CHAA.**

The alternative pathway studied was activating the Csp^3−Cl bond *via* **CHAA**, forming directly a Ni^{II} chloride complex and the corresponding 3-propylphenyl radical (Figure 4.13, $\Delta G^‡$ = 13.7 and ΔG = -2.7 kcal·mol^{-1}). For **I3$_{Ni(II)-Cl\cdots R}$$^•$** the

flat geometry of the terminal aliphatic carbon together with the spin density of about -1 e$^-$ for the 3-propylphenyl radical shows the formation of the carbon-centered radical and the consistency with a Ni center in oxidation state II (Figure 4.14).
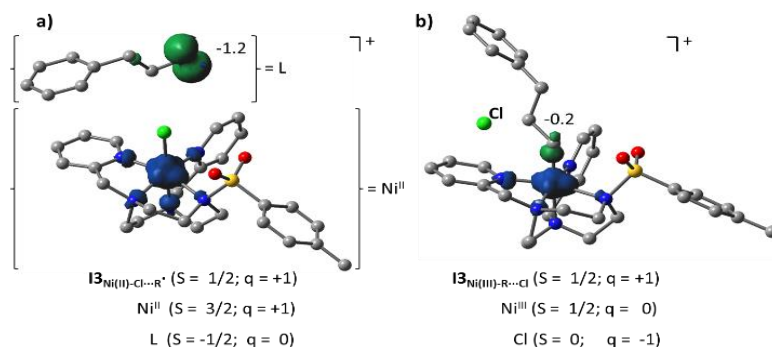
Figure 4. 14. Spin densities calculated for the optimized geometries of intermediates a) **I3$_{Ni(II)}$-Cl···R·** and b) **I3$_{Ni(III)}$-C···Cl-.**

In both cases, the energy barriers are low, indicating that regarding the mechanism, the **Ni^I** intermediate derived from **(Py$_2$^{Ts}tacn)Ni(OTf)$_2$** is highly reactive towards aliphatic alkyl chlorides. Nevertheless, the barrier for **OA-S$_N$2** was lower in energy than for **CHAA**. Therefore, based on the computational data, the **OA-S$_N$2** is proposed as the main pathway for substrates similar to de model **1a**. Furthermore, it is interesting to discuss that the **OA-S$_N$2** mechanism was previously considered for activating alkyl chlorides with nickel complexes but presented larger energy barriers than the **CHAA**.[91] Previous studied nickel complexes involved mainly monophosphines,[92, 93] diphosphines[94] and dichelating nitrogen ligands,[87, 95-98] while our system has a multidentate character. This difference in coordination index and the strong basicity of the ligand may explain their differences in reactivity. Thermodynamics discard a potential outer-sphere SET from the reduced **[PC$_{Ir}$^{NMe2}]^0** or its excited state (-1.80 V and -1.49 V *vs* SCE, respectively) to a Csp^3−Cl bond (< - 3 V *vs* SCE).[10]

4.2.4.5. Mechanistic proposal

Based on these results, we have proposed a plausible catalytic pathway for the photoredox reductive cross-coupling of alkyl chlorides with aromatic alkenes using **PC_{Ir}^{NMe2}/(Py$_2^{Ts}$tacn)Ni(OTf)$_2$** as dual catalytic system (Scheme 4.14). Under catalytic conditions, the **$[PC_{Ir}^{NMe2}]*$** excited state ($E°(*PC^+ / PC^0) = 0.77$ V *vs* SCE) could be reductively quenched by the DIPEA (0.50 V *vs* SCE)[75] to form the reduced **$[PC_{Ir}^{NMe2}]^0$** under the reaction conditions. Then, this **$[PC_{Ir}^{NMe2}]^0$** ($E°(PC^+ / PC^0) = -1.80$ V vs SCE) reduces **(Py$_2^{Ts}$tacn)Ni(OTf)$_2$** ($E°(Ni^{II} / Ni^{I}) = -1.08$ V vs SCE) by one electron forming the key **Ni^I** intermediate, characterized by UV-Vis and EPR techniques. UV-Vis monitoring experiments suggest that the in situ photogenerated **Ni^I** species is highly reactive in front of alkyl chlorides. Based on DFT studies (Figure 4.13), we hypothesize two different scenarios for the activation of Csp^3-Cl bonds.

First, the cleavage of the Csp^3−Cl bond *via* an oxidative addition by an S$_N$2 mechanism (OA-S$_N$2) that generates an organometallic nickel intermediate (Figure 4.13., $\Delta G^{\ddagger} = 10.8$ kcal·mol^{-1}) as a favorable thermodynamic process ($\Delta G = -5.5$ kcal·mol^{-1}, see Figure 4.14). Then, homolytic cleavage of the weak M-C bond by excitation-induced elimination initiated by light or energy transfer from the photocatalysts could regenerate the divalent metal complex while forming the C-centered alkyl radical, resulting in a total driving force of -15.5 kcal·mol^{-1} for the catalytic cycle. On second thought, the activation of the Csp^3−Cl bond can take place *via* concerted halogen atom abstraction (CHAA), forming directly a Ni^{II} chloride complex and the corresponding 3-propylphenyl radical (Figure 4.13, $\Delta G^{\ddagger} = 13.7$ and $\Delta G = -2.7$ kcal·mol^{-1}). Both pathways present feasible energy barriers, implying that the mechanism most probably is substrate-dependent. Cascade reaction and radical clock confirm the generation of free radicals from alkyl chlorides, which engage the styrene. The final benzylic radical (ca. -1.65 V *vs* SCE, see Table 4.13) is reduced by the photocatalyst to the corresponding

radical anion, allowing the termination of the reaction by protonation from the solvent.
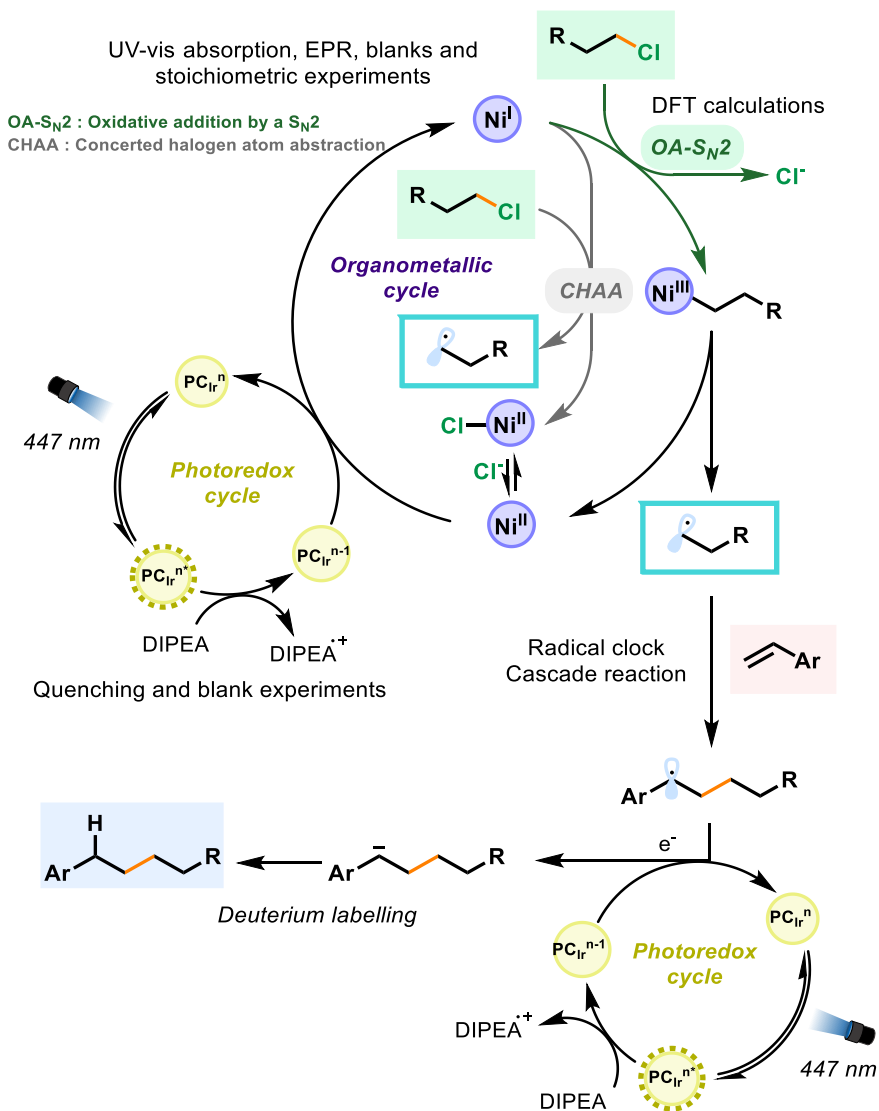
Scheme 4. 14. Hypothetical catalytic cycle for the visible-light cross-coupling reaction of inert alkyl chlorides with aromatic olefins.

4.3. Conclusions

In this chapter, we have developed a dual catalyst system for the reductive cross-coupling reaction of unactivated alkyl chlorides with aromatic alkenes. We determined as the best system for the reaction the combination of **(Py$_2$^{Ts}tacn)Ni(OTf)$_2$** as the catalyst and [Ir(dmabpy)(ppy)$_2$](PF$_6$) **(PC$_{Ir}$^{NMe2})** as photocatalyst using *i*Pr$_2$NEt as an electron donor. The combination of ethanol as protic solvent and acetonitrile as an aprotic solvent was necessary to accomplish the reactivity. Moreover, the introduction of water and its role in the hydrolysis of aminoalkyl intermediates played a crucial role in obtaining high yields. Blank experiments together with single-point monitoring reactions under light-dark cycles revealed that the presence of all components (photocatalyst, catalyst, electron-donor and light) is required for the reaction to manifest. Once we established the optimal conditions for the cross-coupling strategy, a broad substrate scope was tested, reaching up to 85% yield for 36 different alkyl chlorides and 14 different aromatic olefins, exhibiting an excellent group tolerance. We consider this methodology one of the first strategies for a general cross-coupling reaction using inert alkyl chlorides as coupling partners.

Regarding the mechanism, we proposed the photogeneration of a **Ni^I** intermediate from **(Py$_2$^{Ts}tacn)Ni(OTf)$_2$**, as well as its role as active specie against alkyl chlorides, based on spectroscopic techniques. According to DFT studies, the most feasible pathway consists of an oxidative addition/S$_N$2 step in which the formation of a **Ni^{III}**-alkyl compound from the photogenerated **Ni^I**, is followed by the release of the carbon-centered radical. However, we cannot discard the concerted halogen atom abstraction by **Ni^I**, forming directly the free organic radical, since this alternative pathway presents an energy difference of only 1.8 kcal/mol versus the OA-S$_N$2. Such a carbon-centered radical intermediate can attack a radical acceptor forming a new C-C bond. The final radical is then

reduced and subsequently protonated from the solvent, obtaining the final reductive cross-coupling product.

4.4. Experimental section

4.4.1. Materials and reagents

Reagents and solvents were used as received from the commercial supplier unless otherwise stated. Triethylamine and diisopropylethylamine were distilled over potassium hydroxide and were stored under argon. Photocatalysts [Ir(dmabpy)(ppy)$_2$](PF$_6$) (**PC$_{Ir}^{NMe2}$**),[99, 100] [Cu(bathocuproine)(xantphos)](PF$_6$) (**PC$_{Cu}$**)[101] and complexes (**Py$_2$^{Ts}tacn)Ni(OTf)$_2$**,[47] (**Py$_2$^{Ts}tacn)Co(OTf)$_2$**[102] were synthesized according to the literature procedures. Tetradentate aminopyridine complexes were synthetized according to *Chapter III* procedures.

For the synthesis of reagents, the solvents (DMF, hexane, Et$_2$O, CH$_2$Cl$_2$, MeCN and toluene) were used from a SPS-400, Innovative Technology solvent purification system and stored under argon with activated 4 Å molecular sieves. Anhydrous acetonitrile was purchased from Sigma-Aldrich® and water was purified with a Milli-Q Millipore Gradient AIS system. Water, methanol, ethanol, trifluoroethanol, acetonitrile, dimethylformamide, dimethylacetamide and tetrahydrofurane used for photoreactions were degassed by freeze-pump-thaw method (repeated 3 cycles) and were stored under argon. All the alkeness were filtered by a pad of Celite (Hyflo Super Cel from Sigma-Aldrich, CAS: 68855-54-9) before running the photoreactions.

The synthesis of air-sensitive reagents as well as the preparation of visible light photocatalytic reactions were conducted inside a nitrogen-filled glove box

(mBraun Unilab) with concentrations of O_2 and H_2O lower than 0.5 ppm and using Schlenk techniques under argon atmosphere.

4.4.2. Instruments

Nuclear magnetic resonance (NMR). NMR spectra were recorded on Bruker Fourier300, AV400, AV500 and AVIII500 spectrometers using standard conditions (300 K). All ^1H chemical shifts are reported in ppm and have been internally calibrated to the residual protons of the deuterated solvent. The ^{13}C chemical shifts have been internally calibrated to the carbon atoms of the deuterated solvent. The coupling constants were measured in Hz.

Electronic paramagnetic resonance (EPR). An EMX Micro X-band EPR spectrometer from Bruker was used to collect the data using a finger dewar for measurements at 77 K. Data was acquired in perpendicular mode with a modulation frequency of 100 KHz, a modulation amplitude of 10 G, a 5.1 ms time constant and 21.4 ms conversion time and a microwave power of 0.18 mW. Spectra was simulated using the EasySpin software package.

Mass Spectrometry. High resolution Mass Spectrometry (HRMS) data was collected on a HPLC-QqTOF (Maxis Impact, Bruker Daltonics) or HPLC-TOF (MicroTOF Focus, Bruker Daltonics) mass spectrometer using 1 mM solution of the analyzed compound.

Electrochemistry. All the electrochemical experiments were performed with a VSP potentiostat from BioLogic, equipped with the EC-Lab software. CV measurements were carried out under Ar atmosphere using 1 mM solutions of nickel complex or Ir photoredox catalysts in MeCN, with tetrabutylammonium hexafluorophosphate (TBAPF$_6$) as supporting electrolyte (0.1 M). A single-

compartment cell was employed, with glassy carbon (GC) working electrodes (3 mm and 1 mm diameter). Additionally, a Pt wire was used as a counter electrode and a Ag/AgCl wire as pseudo-reference, immersed in a bridge tube containing the same electrolyte solution (0.1 M $TBAPF_6$/MeCN) and separated from the working solution by a porous tip. Ferrocene (Fc) was added to the solution as an internal standard and all the potentials are first referenced vs. the $Fc^{+/0}$ redox couple and then vs. SCE. The working electrodes were polished by using 0.05 µm alumina powder (CHInstruments) on a polishing pad wet with distilled H_2O, followed by rinsing with distilled water/acetone and sonication to remove the residues of alumina over the electrode.

UV-Vis spectroscopy. UV-Vis spectra were recorded on an Agilent 8453 diode array spectrophotometer (190-1100 nm range) in 1 cm quartz cells. A cryostat from Unisoku Scientific Instruments was used for the temperature control.

Fluorescence spectroscopy. Fluorescence measurements were carried out on a Fluorolog Horiba Jobin Yvon spectrofluorimeter equipped with photomultiplier [or InGaAs if using the nitrogen cooled detector] detector, double monochromator and Xenon light source. Sample preparation was the same as that of absorption experiments in 1 cm quartz cells.

Gas chromatography analysis. The analysis and quantification of the starting materials and products were carried out on an Agilent 7820A gas chromatograph (HP5 column, 30m or Cyclosil-B column, 30m) and a flame ionization detector. GC-MS spectral analyses were performed on an Agilent 7890A gas chromatograph interfaced with an Agilent 5975c MS mass spectrometer.

4.4.3. In-house developed parallel photoreactor

Light source: The reactions were performed using Royal-Blue ($\lambda = 447\pm20$ nm) LUXEON Rebel ES LED, mounted on a 20 mm Square Saber - 1030 mW @ 700mA as a light source.

Temperature Control: Reaction temperature was controlled by a high-precision thermoregulation Hubber K6 cryostat. Likewise, aiming at ensuring stable irradiation, the temperature of the LEDs was controlled and set at 22 ºC.
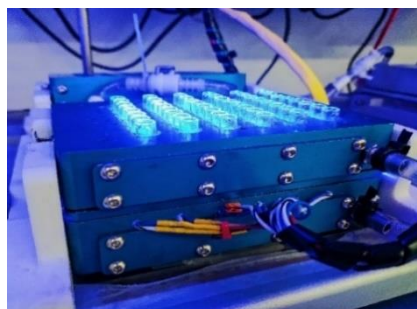
Figure 4. 16. In-house developed parallel photoreactors with 48 positions for vials of 1 mL.
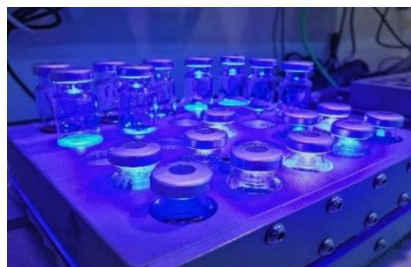
Figure 4. 15. In-house developed parallel photoreactors with 25 positions for vials of 10 or 21 mL.

4.4.4. Experimental procedures

General procedure A for optimization screening: Inside an anaerobic box, aliquots from stock solutions of (3-chloropropyl)benzene (30 µL, 0.003 mmol, 1.0 equiv.) in MeCN, styrene (30 µL, 0.03 mmol, 10 equiv.) in MeCN, **(Py₂ᵀˢtacn)Ni(OTf)₂** or **(Py₂ᵀˢtacn)Co(OTf)₂** catalyst (30 µL, 0.15-0.3 µmol, 5-10 mol %) in MeCN, **PC_Cu** or **PC_Ir^NMe2** (30 µL, 0.06-0.12 µmol, 2 mol %) in MeCN were equally distributed into vial (1 mL of headspace) that contained glass beads. Then degassed protic solvents were added to the vial to reach a total volume of 300 µL total concentration of substrate 10 mM). Electron donor (in general *i*-Pr₂NEt) (6 µL, 0.034 mmol, 11.5 equiv. These vials were located in the small-scale in-house parallel photoreactor (Figure SI 2). All the photoreactor was sealed with a septum and removed from the anaerobic box, which was placed in the photoreactor at the indicated temperature (30 ºC). After irradiating for 24 h with blue LEDs ($\lambda = 447$ nm), each sample was diluted with ethyl acetate (0.2 mL) and a solution of biphenyl in ethyl acetate was added as internal standard (1.4×10^{-3} mmol in 0.20 mL). The organic phase was passed through a plug of $MgSO_4 + SiO_2$ and eluted with EtOAc. The resulting solution was analyzed by gas chromatography. The yield reported for each reaction is given as an average of at least two runs.

General procedure B for optimization screening: Inside an anaerobic box, aliquots from stock solutions of (3-chloropropyl)benzene (200 µL, 0.02 mmol, 1.0 equiv.) in MeCN, styrene (200 µL, 0.2 mmol, 10 equiv.) in MeCN, **(Py₂ᵀˢtacn)Ni(OTf)₂** or **(Py₂ᵀˢtacn)Co(OTf)₂** catalyst (200 µL, 0.1-0.2 µmol, 5-10 mol %) in MeCN, **PC_Cu** or **PC_Ir^NMe2** (200 µL, 0.4-0.8 µmol, 2 mol %) in MeCN were equally distributed into vial (10 mL of headspace) that contained glass beads. All the vials were sealed with a septum and removed from the anaerobic box, and Schlenk techniques were used to add to the vial degassed protic solvents and

electron donor (in general i-Pr$_2$NEt, 40 µL, 0.22 mmol, 11.5 equiv.), reaching a total volume of 2 mL and total concentration of substrate 10 mM. The vial was placed in the photoreactor at the indicated temperature (30 ºC). After irradiating for 24h with blue LEDs (λ = 447 nm), the sample was diluted with ethyl acetate (2 mL). A solution of biphenyl in ethyl acetate was added as internal standard (8.7×10^{-3} mmol in 0.25 mL). Then, the addition of 1 mL of H$_2$O formed a biphasic solution and an aliquot of the organic phase was passed through a plug of MgSO$_4$ and eluted with EtOAc. The resulting solution was analyzed by gas chromatography. The yield reported for each reaction is given as an average of at least two runs.

General procedure for photoredox cross-coupling reaction: Inside an anaerobic box, aliquots from stock solutions of chloroalkane (200 µL, 0.04 mmol, 1.0 equiv.) in MeCN, styrene analogue (200 µL, 0.4 mmol, 10 equiv.) in MeCN, **(Py$_2$^{Ts}tacn)Ni(OTf)$_2$** (200 µL, 2 µmol, 5 mol %) in MeCN, **PC$_{Ir}$^{NMe2}** (200 µL, 0.8 µmol, 2 mol %) in MeCN were equally distributed into 8 vials (10 mL of headspace) that contained glass beads. Then degassed protic solvents were added to each vial to reach a total volume of 2 mL total (concentration of substrate 20 mM). *i*-Pr$_2$NEt (80 µL, 0.46 mmol, 11.5 equiv.) was added to these vials and they were placed in the photoreactor at the indicated temperature (30 ºC) under orbital stirring. After irradiating the vials for 24 h with visible light (blue LED, 447 nm), they were opened and the content was combined in a separatory funnel. H$_2$O (15 mL) and Et$_2$O (15 mL) were added and the organic layer was separated. The aqueous layer was extracted with Et$_2$O (3 x 15 mL), and the combined organic extracts were washed with HCl 10% (15 mL) and dried over MgSO$_4$. The solvent was removed under reduced pressure and the crude material was purified *via* column chromatography.

Procedure for the gram scale version of photoredox cross-coupling reaction: Inside an anaerobic box, 0.663 g of **1a** (4.2 mmol, 1.0 equiv.), 4.4 g of **2a** (42 mmol, 10 equiv.), **(Py₂^{Ts}tacn)Ni(OTf)₂** catalyst (210 mg, 0.21 mmol, 5 mol %), **PC_{Ir}^{NMe2}** (117 mg, 0.08 mmol, 2 mol %) and acetonitrile (84 mL) were distributed into into a 1 L 2-necked round bottom flask. Degassed ethanol (126 mL) was added (out of the anaerobic box) to the flask (total concentration of substrate 20 mM). i-Pr₂NEt (8 mL, 48.3 mmol, 11.5 equiv.) was finally added to the solution flask, which was irradiated by a KESSIL lamp ($\lambda = 467$ nm), separated 7 cm (to maintain a temperature close to 30 ºC). After irradiating for 24 h, H_2O (150 mL) and Et_2O (150 mL) were added and the organic layer was separated. The aqueous layer was extracted with Et_2O (3 x 100 mL), and the combined organic extracts were washed with brine (150 mL) and dried over $MgSO_4$. The solvent was removed under reduced pressure and the crude material was purified *via* column chromatography yielding 0.69 g (73% yield) of the pure cross-coupling product.

Figure 4. 17. Gram scale set up.

Procedure for reaction monitoring: Inside an anaerobic box, aliquots from stock solutions of **1a** (100 µL, 0.02 mmol, 1.0 equiv.) in MeCN, **2a** (100 µL, 0.2 mmol, 10 equiv.) in MeCN, (**Py$_2$^{Ts}tacn)Ni(OTf)$_2$** (100 µL, 1 µmol, 5 mol %) in MeCN, **PC$_{Ir}$^{NMe2}**(100 µL, 0.4 µmol, 2 mol %) in MeCN were equally distributed into 8 vials (10 mL of headspace) that contained glass beads. Then degassed protic solvents were added to the vial to reach a total volume of 1 mL total (concentration of substrate 20 mM). To these vials i-Pr$_2$NEt(40 µL, 0.23 mmol, 11.5 equiv.) was added and the vials were placed in the photoreactor at the indicated temperature (30 °C) and stirring was switched on. At specific points of time (see plot), aliquots of 100 µL were taken from the sealed vials and mixed with 29 µL of solution of biphenyl in EtOAc (34.8 mM) and the resulting mixture was analyzed by GC-FID. Light irradiation was switched off and on at specific points of the single-point monitoring experiment, which indicates that the reaction stops when the vial is not irradiated with visible light.

Procedure for EPR studies: Control experiments were performed in the absence of the (**Py$_2$^{Ts}tacn)Ni(OTf)$_2$** complex (**PC$_{Ir}$^{NMe2}**, 2 mol% in n-BuCN:EtOH:i-PrNEt$_2$ (2:3:0.1) before and after irradiation did not yield any EPR signal. However, 1 min of irradiation (LED λ_{max} 447 nm) of an EPR tube containing the (**Py$_2$^{Ts}tacn)Ni(OTf)$_2$** complex (5 mol%) and the photoredox catalyst **PC$_{Ir}$^{NMe2}** (2 mol%) in the reaction mixture of n-BuCN:EtOH:i-PrNEt$_2$ (2:3:0.1) gave an EPR signal with an almost axial symmetry consistent with an unpaired electron predominantly localized in the d$_{x^2-y^2}$ orbital.

4.4.5. Synthesis and characterization of substrates
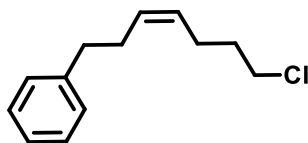
Substrate (**iv.1c**): Lindlar catalyst (0.600 g) and quinoline (58 uL) to a solution of (7-chlorohept-3-yn-1-yl)benzene (1 g, 4.84 mmol) in cyclohexene were added to a solution of (7-chlorohept-3-yn-1-yl)benzene (1 g, 4.84 mmol) in cyclohexene. The mixture was stirred under hydrogen gas (3 atm) until the reaction was complete. Then the mixture was filtered throught celite and washed with cyclohexene (150 mL). The organic phase was washed with KHSO$_4$ (aq) (1%, 30 mL), neutralized with NaHCO$_3$ (aq) (sat, 30 mL), then with NaCl (aq) (sat, 50 mL) and dried over Na$_2$SO$_4$. Removal of solvent in vacuum afforded the crude product which was purified by column chromatography (95:5 Hexane:AcOEt), to obtain 600 mg of the desired product (60 % yield). **^{1}H NMR** (400 MHz, Chloroform-d) δ 7.33 – 7.29 (m, 2H), 7.24 – 7.20 (m, 3H), 5.55 – 5.47 (m, 1H), 5.40 – 5.32 (m, 1H), 3.49 (t, J = 6.6, 6.6 Hz, 2H), 2.73 – 2.67 (m, 2H), 2.45 – 2.37 (m, 2H), 2.20 – 2.13 (m, 2H), 1.80 – 1.72 (m, 2H). **^{13}C NMR** (126 MHz, Chloroform-d) δ 130.38, 128.51, 128.43, 128.28, 125.83, 44.46, 35.92, 32.29, 29.20, 24.36. **GC-MS** (m/z): 208.1.
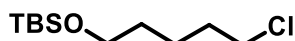
Substrate (**iv.1g**): Triphosgene (0.10 g, 0.343 mmol, 0.5 equiv.) was added to a mixture of alcohol (0.15g, 0.68 mmol, 1.0 equiv.) and Et$_3$N (0.24 mL, 1.72 mmol, 2.5 equiv.) in CH$_2$Cl$_2$ (5 mL) at 0 °C. The mixture was stirred for 2 h at ambient temperature and the reaction was quenched by the addition of sat. aq. NaHCO$_3$ (5 mL). The org. layer was separated and the aq. layer was extracted with CH$_2$Cl$_2$ (2*10 mL). The combined org. extracts were washed with H$_2$O (10 mL) and dried over MgSO$_4$. The solvent was removed under reduced pressure and the crude mixture was purified by FCC (5% Et$_2$O --> 10% --> 20% Et$_2$O in hexane) to yield 132 mg of title compound as a colorless oil. **^{1}H**

NMR (400 MHz, Chloroform-d) δ 3.64 (t, J = 6.2, 6.2 Hz, 2H), 3.56 (t, J = 6.7, 6.7 Hz, 2H), 1.87 – 1.77 (m, 2H), 1.60 – 1.46 (m, 4H), 0.92 (s, 9H), 0.07 (s, 6H). **^{13}C NMR** (126 MHz, Chloroform-d) δ 62.89, 45.05, 32.44, 32.04, 25.96, 23.29, 18.35, -5.29. **GC-MS** (m/z): 236.2.
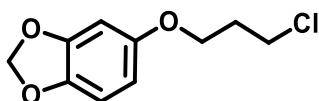
Substrate (**iv.1h**): Sesamol (1 equiv., 1.5 g, 10.9 mmol) was added together with 1-bromo-3-chloropropane (5 equiv., 3.6 ml, 54.5 mmol) and K$_2$CO$_3$ (1.5 equiv., 1.5 g, 54.3 mmol) in 15 ml of dry acetonitrile. The reaction mixture was then heated to 80 ºC and left to stir under reflux overnight. After cooling the reaction mixture was filtered through a pad of celite, concentrated and purified by column chromatography (9:1 Hexane:AcOEt). The product was obtained as a colourless solid 0.99 g (42.5 % yield). **^{1}H NMR** (400 MHz, Chloroform-d) δ = 6.70 (d, J = 8.4 Hz, 1 H), 6.50 (d, J = 2.5 Hz, 1 H), 6.33 (dd, J = 2.5 Hz, J = 8.5 Hz, 1 H), 5.91 (s, 2 H), 4.04 (t, J = 6.0 Hz, 2 H), 3.73 (t, J = 6.3 Hz, 2 H), 2.20 (q, J = 6.0 Hz, 2 H) ppm. **^{13}C NMR** (126 MHz, Chloroform-d) δ = 154.7, 148.7, 142.6, 108.4, 106.2, 101.6, 98.6, 66.8, 42.0, 32.8 ppm. **GC-MS** (m/z): 214.1.
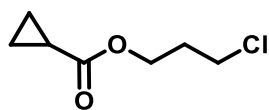
Substrate (**iv.1j**): 3-Chloro-1-Propanol (1.5 equiv., 1.19 ml, 14.4 mmol), DMAP (0.1 equiv., 0.117 g, 0.96 mmol) and Et$_3$N (3 equiv., 3.98 ml, 28.70 mmol) were added together in 18 ml of DCM at 0 ºC and left to stir for 10 minutes. Then cyclopropanecarbonyl chloride (1 equiv., 1 g, 9.57 mmol) was added and the reaction mixture was left to stir for 4 h. The reaction was then quenched by adding aqueous conc. NH$_4$Cl solution. The aqueous phase was extracted with DCM three times and the combined organic phases were dried using Na$_2$SO$_4$ and concentrated in vaccum. The residue was then purified by column chromatography (5:1 Hexane:AcOEt) to obtain the

product as a colorless liquid (1.39 g, 89% yield). **¹H NMR** (400 MHz, Chloroform-d) δ 4.24 (t, J = 6.1, 6.1 Hz, 2H), 3.65 (t, J = 6.5, 6.5 Hz, 2H), 2.12 (p, J = 6.3, 6.3, 6.3, 6.3 Hz, 2H), 1.66 – 1.58 (m, 1H), 1.04 – 0.99 (m, 2H), 0.92 – 0.84 (m, 2H). **¹³C NMR** (126 MHz, Chloroform-d) δ 174.75, 61.16, 61.14, 41.26, 31.70, 12.79, 8.52. **GC-MS** (m/z): 162.0.
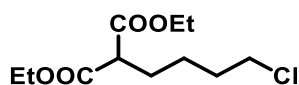
Substrate (**iv.1k**): K₂CO₃ (1.3 mmol, 179.7 mg) and a solution of diethyl malonate (1.0 mmol, 160.2 mg) and 1-bromo-3-chlorobutane (1.1 mmol, 173.2 mg) in absolute ethanol (5 mL) was added to a roundbottomed flask provided with a water-cooled reflux condenser and a thermometer. The mixture was heated to 65 ºC on oil bath and stirred for 8 h. The mixture was filtered and then purified by column chromatography (5:1 Hexane:AcOEt) distilled to collect the product 205.9 mg (87.5% yield). **¹H NMR** (500 MHz, Chloroform-d) δ 4.21 – 4.15 (m, 4H), 3.51 (td, J = 6.6, 6.6, 0.9 Hz, 2H), 3.30 (td, J = 7.5, 7.5, 0.9 Hz, 1H), 1.92 – 1.84 (m, 2H), 1.83 – 1.71 (m, 2H), 1.52 – 1.43 (m, 2H), 1.25 (td, J = 7.1, 7.1, 0.9 Hz, 6H). **¹³C NMR** (101 MHz, Chloroform-d) δ 169.59, 169.56, 61.23, 52.07, 33.39 , 29.18, 28.77, 27.34, 14.18, 14.09. **GC-MS** (m/z): 177.1.
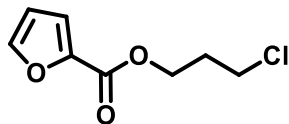
Substrate (**iv.1l**): 3-chloro-1-propanol (1.1 equiv., 0.70 ml, 8.43 mmol), DMAP (0.1 equiv., 0.094 g, 0.77 mmol) and Et₃N (3 equiv., 3.20 ml, 22.98 mmol) were added together in 19.2 ml of DCM at 0 ºC and left to stir for 10 minutes. Then furan-2-carbonyl chloride (1 equiv., 1 g, 6.82 mmol) was added and the reaction mixture was left to stir for 4 h. The reaction was then quenched by adding aqueous conc. NH₄Cl solution. The aqueous phase was extracted with DCM three times and the combined organic phases were dried using Na₂SO₄ and

concentrated in vaccum. The residue was then purified by column chromatography (5:1 Hexane:AcOEt) to obtain the product as a colourless oil (1.12 g, 69.2 %). **¹H NMR** (400 MHz, Chloroform-d) δ 7.58 (dd, *J* = 1.8 Hz, 0.9 Hz, *J* = Hz, 1 H), 7.18 (dd, *J* = 3.5 Hz, 0.9 Hz, 1 H), 6.51 (q, *J* = 1.8 Hz, 1 H), 4.46 (t, *J* = 6.1 Hz, 2 H), 3.86 (t, *J* = 6.4 Hz, 2 H), 2.22 (q, *J* = 6.3 Hz, 2 H). **¹³C NMR** (126 MHz, Chloroform-d) δ 159.0, 146.9, 145.0, 118.6, 111.5, 62.1, 41.6, 32.2. **GC-MS** (m/z): 188.1.
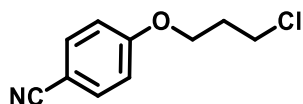
Substrate (**iv.1m**): 4-hydroxy-benzonitril (1 equiv., 1.5 g, 12.59 mmol), 1-bromo-3-chloropropane (1.1 equiv., 1.38 ml, 13.85 mmol) and K_2CO_3 (1.5 equiv., 2.61 g, 18.89 mmol) were added together in 20 ml of dry MeCN and heated to 80 ºC and left to stir overnight. After cooling the reaction mixture was filtered through a pad of celite and concentrated in vaccum to afford the product as a colourless solid (2.23 g, 91%). **¹H NMR** (400 MHz, Chloroform-d) δ 7.59 (dt, *J* = 9.0, 2 H), 6.96 (dt, *J* = 9.0, 2 H), 4.17 (t, *J* = 5.9 Hz, 2H), 3.75 (t, *J* = 6.2 Hz, 2 H), 2.27 (q, *J* = 6.0 Hz, 2 H). **¹³C NMR** (126 MHz, Chloroform-d) δ 162.1, 134.2 (2C), 119.3, 115.3 (2C), 104.4, 64.8, 41.3, 32.1. **GC-MS** (m/z): 195.0.
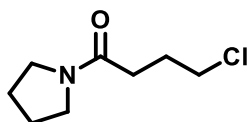
Substrate (**iv.1n**): To a solution of pyrrolidine (1 g, 14.1 mmol, 1.0 equiv.) in 20 mL of dichloromethane containing triethylamine (1.57 g, 14.5 mmol, 1.10 equiv.) was added 4-chlorobutyryl chloride (2.02 g, 14.3 mmol, 1.02 equiv.) dropwise at 0 °C under argon atmosphere. The mixture was allowed to warm to room temperature and was stirred for another 4 h. The solution was washed twice with 450 mL of saturated aqueous NH_4Cl and once with 450 mL of saturated aqueous $NaHCO_3$, and then 450 mL of saturated aqueous NaCl. The organic phase was dried over 20 g of Na_2SO_4 and filtered. The solid

was washed with 50 mL of dichloromethane. The crude residue was obtained after removing solvent under vaccum, then purified by flash chromatography (SiO$_2$, 1:0→100:1 hexane:EtOAc) to afford compound 1n (2.94 g, 93 %) as a colorless oil. **^{1}H NMR** (500 MHz, Chloroform-d): δ 3.66 – 3.62 (m, 2H), 3.44 (dtd, J = 13.7, 6.8, 1.6 Hz, 4H), 2.44 (td, J = 7.0, 1.6 Hz, 2H), 2.16 – 2.09 (m, 2H), 1.95 (qd, J = 6.7, 1.4 Hz, 2H), 1.88 – 1.81 (m, 2H). **^{13}C NMR** (126 MHz, Chloroform-d): δ 170.34, 46.67, 45.78, 45.12, 31.35, 27.72, 26.20, 24.51. **HRMS** (ESI): m/z found for C8H14NO [M-Cl]$^+$: 140.1067. Spectroscopic data match those previously reported in the literature.[103]
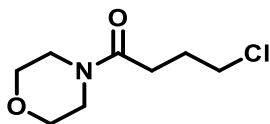
Substrate (**iv.1o**): The previous procedure (**iv.1n**) was followed. To a solution of morpholine (1.01 g, 11.6 mmol, 1.0 equiv.) in 20 mL of dichloromethane containing triethylamine (1.29 g, 12.8 mmol, 1.10 equiv.) was added 4-chlorobutyryl chloride (1.67 g, 11.8 mmol, 1.02 equiv.) dropwise at 0 °C under argon atmosphere. The mixture was allowed to warm to room temperature and was stirred for another 4 h. The solution was washed twice with 450 mL of saturated aqueous NH$_4$Cl and once with 450 mL of saturated aqueous NaHCO$_3$, and then 450 mL of saturated aqueous NaCl. The organic phase was dried over 20 g of Na$_2$SO$_4$ and filtered. The solid was washed with 50 mL of dichloromethane. After evaporation of solvent under vaccum, compound 1o was obtained as a yellow liquid (1.97 g, 90 %) without further purification. **^{1}H NMR** (300 MHz, Chloroform-d): δ 3.70 – 3.58 (m, 8H), 3.52 – 3.44 (m, 2H), 2.49 (t, J = 7.1 Hz, 2H), 2.13 (p, J = 6.5 Hz, 2H). **^{13}C NMR** (75 MHz, Chloroform-d): δ 170.48, 66.97, 66.71, 45.93, 44.94, 42.06, 29.64, 27.84. **HRMS** (ESI): m/z found for C8H14O2N [M-Cl]$^+$: 156.1095. Spectroscopic data match those previously reported in the literature.[103]
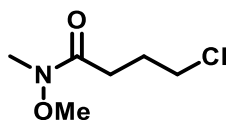
Substrate (**iv.1p**): The previous procedure (**iv.1n**) was followed. To a solution of N,O-dimethylhydroxylamine hydrochloride (1.26 g, 8.9 mmol, 1.0 equiv.) in 20 mL of dichloromethane containing triethylamine (2.26 g, 22.4 mmol, 2.5 equiv.) was added 4-chlorobutyryl chloride (1.04 g, 10.7 mmol, 1.1 equiv.) dropwise at 0 °C under argon atmosphere. The mixture was allowed to warm to room temperature and was stirred for another 4 h. The solution was washed twice with 450 mL of saturated aqueous NH_4Cl and once with 450 mL of saturated aqueous $NaHCO_3$, and then 450 mL of saturated aqueous NaCl. The organic phase was dried over 20 g of Na_2SO_4 and filtered. The solid was washed with 50 mL of dichloromethane. After evaporation of solvent under vaccum, compound 1p was obtained as a yellow liquid (1.23 g, 83%) without further purification. **^{1}H NMR** (500 MHz, Chloroform-d): δ 3.69 (s, 3H), 3.63 (t, J = 6.3 Hz, 2H), 3.17 (s, 3H), 2.61 (t, J = 7.1 Hz, 2H), 2.15 – 2.06 (m, 2H). **^{13}C NMR** (126 MHz, Chloroform-d): δ 173.40, 61.38, 44.84, 32.30, 28.85, 27.37. **GC-MS** (m/z): 165.1. Spectroscopic data match those previously reported in the literature.[103]
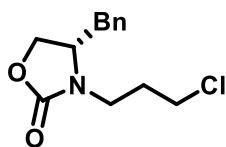
Substrate (**iv.1q**): The previous procedure (**iv.1n**) was followed. A flame-dried flask was charged with DMF (20 mL), NaH (279 mg, 11.6 mmol, 2 equiv.), and 1-bromo-3-chloropropane (1.2 g, 7.6 mmol, 1.3 equiv.) at 0 °C, the solution of carbazole (0.5 g, 5.8 mmol) was added dropwise and the mixture was allowed to warm to room temperature. The mixture was stirred for 2 hours, then quenched by aqueous NH_4Cl and extracted with hexane (50 mL×3 times). The combine organic phase was washed with water, brine and dried with anhydrous Na2SO4, concentrated in vaccum to afford crude product as a yellowish oil. The crude residue was purified by flash chromatography (SiO_2,

hexane:EtOAc, 3:0→1:1) to afford compound 1q (0.98 g, 67 %) as a colorless oil.
¹H NMR (500 MHz, Chloroform-d): δ 7.34 (dd, *J* = 8.2, 6.6 Hz, 2H), 7.30 – 7.26 (m, 1H), 7.17 (dd, *J* = 7.0, 1.8 Hz, 2H), 4.23 – 4.14 (m, 1H), 4.08 – 3.99 (m, 2H), 3.64 – 3.56 (m, 3H), 3.31 (ddd, *J* = 14.1, 7.6, 6.1 Hz, 1H), 3.17 (dd, *J* = 13.4, 4.0 Hz, 1H), 2.69 (dd, *J* = 13.6, 8.6 Hz, 1H), 2.19 – 2.00 (m, 2H). **¹³C NMR** (126 MHz, Chloroform-d): δ 158.31, 135.44, 129.17, 127.47, 67.03, 57.06, 42.29, 39.99, 38.81, 30.59. **HRMS** (ESI): m/z calcd for C13H17ClNO2 [M+H]⁺ : 254.0942, found 254.0945.
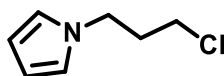

Substrate (**iv.1r**): A flame-dried flask was charged with DMF (100 mL), NaH (379 mh, 15.8 mmol, 1.1 equiv.), and 1-bromo-3-chloropropane (4.53 g, 28.8 mmol, 1.9 equiv.) at 0 ºC, the solution of pyrrole (0.967 g, 14.4 mmol) was added dropwise and the mixture was allowed to warm to room temperature. The mixture was stirred for 2 hours, then quenched by aqueous NH4Cl and extracted with hexane (50 mL×3 times). The combine organic phase was washed with water, brine and dried with anhydrous Na₂SO₄, concentrated in vacuum to afford crude product as a yellowish oil. The crude residue was purified by flash chromatography (SiO₂, hexane:EtOAc, 1:0→100:1) to afford compound 1r (1.736 g, 83.1%) as a colorless oil. **¹H NMR** (500 MHz, Chloroform-d): δ 6.68 (q, *J* = 2.0 Hz, 1H), 6.17 (q, *J* = 2.0 Hz, 1H), 4.10 (t, *J* = 6.4 Hz, 1H), 3.47 (t, *J* = 6.1 Hz, 1H), 2.19 (p, *J* = 6.3 Hz, 1H). **¹³C NMR** (126 MHz, Chloroform-d): δ 120.79, 108.52, 46.10, 41.78, 34.21. **GC-MS** (m/z): 143.1.
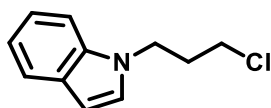
Substrate (**iv.1s**): A flame-dried flask was charged with DMF (100 mL), NaH (410 mg, 17 mmol, 2 equiv.), and 1-bromo-3-chloropropane (1.75 g, 11.1

mmol, 1.3 equiv.) at 0 °C, the solution of indole (1 g, 8.54 mmol) was added dropwise and the mixture was allowed to warm to room temperature. The mixture was stirred for 2 hours, then quenched by aqueous NH₄Cl and extracted with hexane (50 mL×3 times). The combine organic phase was washed with water, brine and dried with anhydrous Na₂SO₄, concentrated in vaccum to afford crude product as a yellowish oil. The crude residue was purified by flash chromatography (SiO₂, 15:1→10:1 hexane:EtOAc) to afford compound 1s (1.02 g, 61 %) as a colorless oil. **¹H NMR** (500 MHz, Chloroform-d): δ 7.78 (dt, J = 7.9, 1.1 Hz, 1H), 7.50 (dt, J = 8.3, 1.0 Hz, 1H), 7.36 (ddd, J = 8.2, 7.0, 1.2 Hz, 1H), 7.26 – 7.23 (m, 1H), 6.65 (dd, J = 3.1, 1.1 Hz, 1H), 4.46 (t, J = 6.4 Hz, 2H), 3.57 (t, J = 6.0 Hz, 2H), 2.39 (p, J = 6.2 Hz, 2H). **¹³C NMR** (75 MHz, Chloroform-d): δ 135.94, 128.82, 128.14, 121.75, 121.19, 119.60, 109.36, 101.61, 42.94, 41.98, 32.72. **HRMS** (APCI): m/z calcd for C11H13ClN [M-H]⁺ : 194.0731, 194.0729.
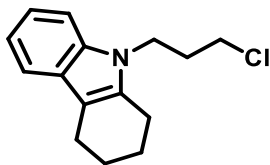
Substrate (**iv.1t**): A flame-dried flask was charged with DMF (25 mL), NaH (140 mg, 5.8 mmol, 2 equiv.), and 1-bromo-3-chloropropane (0.6 g, 3.8 mmol, 1.3 equiv.) at 0 °C, the solution of carbazole (0.5 g, 2.92 mmol) was added dropwise and the mixture was allowed to warm to room temperature. The mixture was stirred for 2 hours, then quenched by aqueous NH₄Cl and extracted with hexane (50 mL×3 times). The combine organic phase was washed with water, brine and dried with anhydrous Na₂SO₄, concentrated in vaccum to afford crude product as a yellowish oil. The crude residue was purified by flash chromatography (SiO₂, 1:0→100:1 hexane:EtOAc) to afford compound 1t (560 mg, 77 %) as a colorless oil. **¹H NMR** (500 MHz, Chloroform-d): δ 7.46 (dd, J = 7.7, 1.2 Hz, 1H), 7.29 (d, J = 8.1 Hz, 1H), 7.13 (ddd, J = 8.2, 7.0, 1.3 Hz, 1H), 7.08 – 7.04 (m, 1H), 4.19 (t, J = 6.7 Hz,

2H), 3.52 – 3.47 (m, 2H), 2.75 – 2.69 (m, 4H), 2.20 (p, J = 6.6 Hz, 2H), 1.94 (qd, J = 6.1, 5.2, 1.7 Hz, 2H), 1.88 – 1.83 (m, 2H). **13C NMR** (126 MHz, Chloroform-d): δ 136.31, 135.39, 127.66, 120.88, 118.98, 118.01, 109.94, 108.78, 42.31, 39.87, 33.16, 23.48, 23.33, 22.37, 21.20. **HRMS** (APCI): m/z calcd for C15H19ClN [M+H]$^+$: 248.1201, found 248.1206.
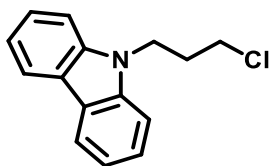
Substrate (**iv.1u**): A flame-dried flask was charged with DMF (100 mL), NaH (287 mg, 12 mmol, 2 equiv.), and 1-bromo-3-chloropropane (1.22 g, 7.78 mmol, 1.3 equiv.) at 0 °C, the solution of carbazole (1 g, 5.98 mmol) was added dropwise and the mixture was allowed to warm to room temperature. The mixture was stirred for 2 hours, then quenched by aqueous NH4Cl and extracted with hexane (50 mL×3 times). The combine organic phase was washed with water, brine and dried with anhydrous Na2SO4, concentrated in vaccum to afford crude product as a yellowish oil. The crude residue was purified by flash chromatography (SiO2, 1:0→100:1 hexane:EtOAc) to afford compound 1u (1.27 g, 91 %) as a colorless oil. **1H NMR** (500 MHz, Chloroform-d): δ 8.11 (dt, J = 7.8, 1.0 Hz, 2H), 7.51 – 7.46 (m, 4H), 7.29 – 7.26 (m, 1H), 7.26 – 7.23 (m, 1H), 4.53 (t, J = 6.5 Hz, 2H), 3.55 – 3.52 (m, 2H), 2.36 (p, J = 6.4 Hz, 2H). **13C NMR** (75 MHz, Chloroform-d): δ 140.55, 125.98, 123.16, 120.56, 119.29, 108.70, 42.44, 39.94, 31.95. **HRMS** (APCI): m/z calcd for C15H15ClN [M+H]$^+$: 244.0888, found 244.0888.
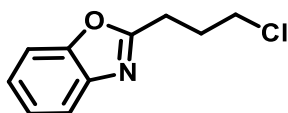
Substrate (**iv.1v**): To a solution of 2-aminophenol (1 g, 9.16 mmol, 1.0 equiv.), 4-chlorobutanoyl chloride (1.55 g, 1.23 mmol, 1.2 equiv.), and triethylamine (1.11 g, 1.46 mmol, 1.2 equiv.) in

EtOAc (25 mL) was heated to reflux for 10 hours. After allowing to cool to r.t., EtOAc (100 mL) was added and the solution was washed once with 10% aq. HCl (100 mL). The aqueous layer was extracted with EtOAc 3 times and the combined organic phase was dried over anhydrous Na_2SO_4 and concentrated under reduced pressure to afford intermediate crude. Then polyphosphoric acid (8.56 g, 0.6 mmol) was added to the crude, and the mixture was heated with magnetic stirring at 130 ℃ for 4 hours. The reaction mixture was diluted by ice-water (50 mL) and neutralized with saturated aq. $NaHCO_3$, and extracted with EtOAc twice. The combined organic phase was washed with brine, dried over Na_2SO_4, and concentrated under reduced pressure. The crude was purified by column chromatography (SiO_2, hexane/EtOAc=10:1→5/1) to afford compound 1v (1.47 g, 75%) as a light yellow oil. **^{1}H NMR** (500 MHz, Chloroform-d): δ 7.70 – 7.65 (m, 1H), 7.51 – 7.46 (m, 1H), 7.33 – 7.29 (m, 2H), 3.71 (t, J = 6.3 Hz, 2H), 3.13 (t, J = 7.3 Hz, 2H), 2.38 (ddd, J = 13.6, 7.3, 6.3 Hz, 2H). **^{13C} NMR** (126 MHz, Chloroform-d): δ 165.84, 150.97, 141.43, 124.83, 124.36, 119.79, 110.49, 43.91, 29.47, 25.91. **HRMS** (ESI): m/z calcd for C10H1ClNO [M+H]$^{+}$: 196.0524, found 196.0519. Spectroscopic data match those previously reported in the literature.[104]
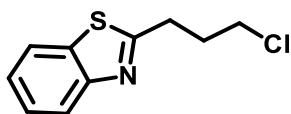
Substrate (**iv.1w**): To a solution of 2-aminothiophenol (1.17 g, 9.4 mmol, 1.0 equiv.), 4-chlorobutyryl chloride (1.62 g, 11.5 mmol, 1.25 equiv.) in toluene (10 mL) was stirred for 48 hours at r.t. The mixture was diluted with EtOAc (30 mL) and washed with sat. aq. $NaHCO_3$ (50 mL) for twice. The organic phase was combined and washed with brine, dried with Na_2SO_4, concentrated under reduced pressure, followed by column chromatography (SiO_2, hexane/ EtOAc =40:1→10:1→5:1) to afford compound 1w (1.63 g, 82.4%) as colorless oil. **^{1}H NMR** (500 MHz, Chloroform-d): δ 7.97 (dt, J = 8.2, 0.9 Hz, 1H), 7.85 (ddd, J = 7.9, 1.2, 0.6 Hz, 1H), 7.46 (ddd,

J = 8.2, 7.2, 1.2 Hz, 1H), 7.36 (ddd, J = 8.2, 7.2, 1.2 Hz, 1H), 3.68 (t, J = 6.4 Hz, 2H), 3.33 – 3.26 (m, 2H), 2.38 (tt, J = 7.3, 6.3 Hz, 2H). 13C-NMR (126 MHz, Chloroform-d): δ 170.09, 153.47, 135.27, 126.17, 125.03, 122.80, 121.67, 43.95, 31.98, 31.36. **HRMS** (ESI): m/z calcd for C10H11ClNS [M+H]$^+$: 212.0295, found 212.0295. Spectroscopic data match those previously reported in the literature.[105]
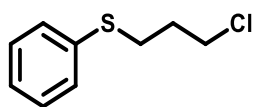
Substrate (**iv.1x**): 1-Bromo-3-chloropropane (785.6 mg, 4.99 mmol, 1.1 equiv.) was added dropwise to a suspension of benzenethiol (500 mg, 4.54 mmol, 1.0 equiv.) and K_2CO_3 (815 mg, 5.9 mmol, 1.3 equiv.) in DMF (10 mL) at room temperature. The resulting mixture was stirred for 1.5 h, then diluted with water (10 mL) and extracted with hexane (15 mL×3 times). The combine organic phase was washed with water, brine and dried with anhydrous Na_2SO_4, concentrated in vaccum to afford crude product as a yellowish oil. The crude residue was purified by flash chromatography (SiO$_2$, 20:1→15:1 hexane:EtOAc) to provide compound 1x (719 mg, 84.9%) as a colourless oil. **^{1}H-NMR**(500 MHz, Chloroform-d): δ 7.40 – 7.34 (m, 2H), 7.33 – 7.27 (m, 2H), 7.23 – 7.18 (m, 1H), 3.67 (t, J = 6.3 Hz, 2H), 3.08 (t, J = 7.0 Hz, 2H), 2.12 – 2.04 (m, 2H). **^{13}C-NMR** (126 MHz, Chloroform-d): δ 135.78, 129.64, 129.11, 126.37, 43.45, 31.80, 30.84. **GC-MS** (m/z): 186.1.
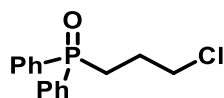
Substrate (**iv.1y**): A mixture of 3-bromo-1-propanol (1.54 g, 11.1 mmol, 1 equiv.) and NaI (3.32 g, 22.2 mmol, 2 equiv.) in acetone (10 mL) was refluxed overnight. The solution was filtered and the solvent was removed by evaporation. The residue was dissolved in CH_2Cl_2, filtered and the

solvent removed. The resulting red-orange oil was dissolved again in CH_2Cl_2 (25 mL), filtered through a silica plug and the solvent was removed under vacuum, obtaining a red oil crude. Then triphenylphosphine (2.9 g, 11.1 mmol, 1 equiv.) and toluene (10 mL) were added into the crude. The reaction mixture was refluxed for 24 h. The solid was filtered, washed with diethyl ether (10 mL) twice, dried, and recrystallized from ethanol to give a white solid. Then the solid was dissolved in ethanol (8 mL) in a one-necked flask, and a 50% wt aqueous NaOH solution (great excess, 10 mL) was added. The mixture was concentrated under vacuum under vaccum at 50-60 °C to about one-third of the original volume and extracted with DCM (30 mL X 3) after addition of water (50 mL). The organic layers were washed with water (30 mL X 3), dried over anhydrous Na_2SO_4, and concentrated under reduced pressure. Then thionyl chloride (1.4 g, 11.7 mmol, 1.05 equiv.) was added dropwise to a stirred solution of the crude in pyridine (2.22 g, 2.8 mmol, 2.5 equiv.) and THF (30 mL), with the temperature maintained below 5 °C. After the addition was complete, the mixture was stirred for a further 3 hours. Chloroform (20 mL) and water (10 mL) were added, and the chloroform layer was separated, washed with hydrochloric acid (10% w/v; 3 x 30 ml.) and with sat. aq. $NaHCO_3$ (10 ml.), dried over Na_2SO_4, and evaporated, to give a semisolid residue which was purified by column chromatography (SiO_2, hexane/ EtOAc /MeOH=10/1/1) to afford compound 1y (1.92 g, 62%, 4 steps) as white solid. **^{1}H NMR** (300 MHz, Chloroform-d): δ 7.74 (ddd, J = 11.6, 7.8, 1.8 Hz, 4H), 7.48 (tdd, J = 8.9, 5.5, 2.0 Hz, 6H), 3.60 (t, J = 6.1 Hz, 2H), 2.50 – 2.36 (m, 2H), 2.09 (tq, J = 8.2, 6.0 Hz, 2H). **^{13}C NMR** (75 MHz, Chloroform-d): δ 132.03, 130.90, 130.78, 128.95, 128.80, 45.71, 45.49, 27.79, 24.97. **HRMS** (ESI): m/z calcd for C15H17ClOP [M+H]$^+$: 279.0700, found 279.0706.
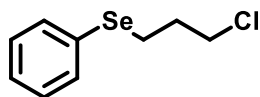
Substrate (**iv.1z**): Diphenyl diselenide(476mg, 1.5 mmol, 1 equiv.) was stirred in absolute ethanol (25 mL) at r.t. under nitrogen and NaBH$_4$ (152 mg, 4.5 mmol, 3 equiv.) was added. After 30 min, ethyl 1-bromo-3-chloropropane (152 mg, 3.4 mmol, 2.2 equiv.) dissolved in ethanol (5 mL) was added and the mixture was stirred for 16h. Quenched by 2M HCl and the solution extracted with diethyl ether, then washed with sat. NaHCO$_3$ and brine, dried over Na$_2$SO$_4$, and concentrate under reduced pressure. The residue was purified by dry flash chromatography (SiO$_2$, hexane/ EtOAc =20:1→10:1→7:1) to yield compound 1z (274 mg, 76.9%) as colorless oil. **^{1}H NMR** (500 MHz, Chloroform-d): δ 7.55 – 7.47 (m, 2H), 7.28 (d, J = 9.0 Hz, 2H), 3.64 (t, J = 6.2 Hz, 2H), 3.03 (t, J = 6.8 Hz, 2H), 2.12 (p, J = 6.8 Hz, 2H). **^{13}C NMR** (75 MHz, Chloroform-d): δ 132.87, 129.17, 127.12, 77.45, 77.02, 76.60, 44.29, 32.60, 24.55. **GC-MS** (m/z):: 243.0. Spectroscopic data match those previously reported in the literature.[8]
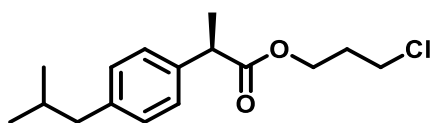
Substrate (**iv.1aa**):): 3-chloropropan-1-ol (0.7 g, 7 mmol, 1.5 equiv.) was added dropwise to a suspension of 2-(4-isobutylphenyl)propanoic acid (1 g, 5 mmol, 1.0 equiv.) and K$_2$CO$_3$ (1 g, 10 mmol, 2 equiv.) in DMF (50 mL) at reflux. The resulting mixture was stirred overnight, then diluted with water (10 mL) and extracted with hexane (15 mL×3 times). The combine organic phase was washed with water, brine and dried with anhydrous Na$_2$SO$_4$, concentrated in vaccum to afford crude product as a yellowish oil. The crude residue was purified by flash chromatography (SiO$_2$, 9:1 hexane: EtOAc) to provide compound 1aa (600 mg, 40%) as a white solid. **^{1}H NMR** (500 MHz, Chloroform-d): δ 7.22 – 7.17 (m, 2H), 7.14 – 7.09 (m, 2H), 4.30 – 4.16 (m, 2H), 3.75 – 3.68 (m, 1H), 3.45 (t, J = 6.5, 6.5

Hz, 2H), 2.47 (d, J = 7.2 Hz, 2H), 2.03 (p, J = 6.2, 6.2, 6.2, 6.2 Hz, 2H), 1.90 – 1.82 (m, 1H), 1.51 (d, J = 7.2 Hz, 3H), 0.91 (d, J = 6.6 Hz, 6H). **^{13}C NMR** (126 MHz, Chloroform-d): δ 174.71, 140.49, 138.01, 129.29, 128.39, 65.10, 46.31, 45.05, 35.76, 30.96, 25.44, 22.39, 18.45. **GC-MS** (m/z): 282.1.
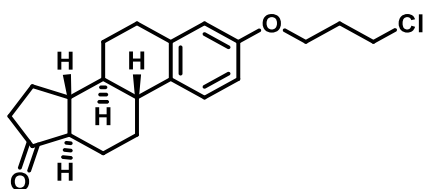
Substrate (**iv.1z**): To a solution of estrone (0.5 g, 1.85 mmol, 1 equiv.) in MeCN (100 mL) were added K_2CO_3 (307 mg, 2.22 mmol, 1.2 equiv.) and 1-bromo-3-chloropropane (1.46 g, 9.25 mmol, 5 equiv.), and the mixture was stirred at 80 °C for 7 h. After cooling at room temperature, the mixture was concentrated in vaccum. The residue was taken with CHCl$_3$ and the CHCl$_3$ layer was washed with 0.2 M NaOH (aq), dried over Na$_2$SO$_4$, filtered and concentrated in vaccum. The residue was purified by silica gel column chromatography (hexane/AcOEt=9/1) to give 1z (234 mg, 37%) as colorless solid. **^{1}H NMR** (500 MHz, Chloroform-d) δ 7.20 (dd, J = 8.6, 1.0 Hz, 1H), 6.72 (dd, J = 8.6, 2.8 Hz, 1H), 6.65 (d, J = 2.8 Hz, 1H), 4.09 (t, J = 5.8, 5.8 Hz, 2H), 3.74 (t, J = 6.4, 6.4 Hz, 2H), 2.89 (dt, J = 10.0, 6.4, 6.4 Hz, 2H), 2.50 (ddd, J = 18.9, 8.7, 0.9 Hz, 1H), 2.44 – 2.37 (m, 1H), 2.24 – 2.20 (m, 2H), 2.18 – 2.08 (m, 1H), 2.07 – 1.98 (m, 2H), 1.98 – 1.92 (m, 1H), 1.67 – 1.54 (m, 4H), 1.54 – 1.39 (m, 4H). **^{13}C NMR** (126 MHz, Chloroform-d) δ 157.11, 138.17, 132.70, 126.71, 114.96, 112.54, 64.63, 50.82, 48.36, 44.36, 41.91, 38.76, 36.21, 32.73, 31.97, 30.00, 26.91, 26.30, 21.95, 14.22. **GC-MS** (m/z): 332.2.
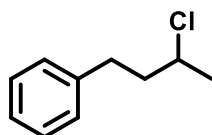
Substrate (**iv.1ac**): To a 20 mL closed tube was added 4-phenylbutan-2-yl methanesulfonate (1.6 g, 7.0 mmol, 1 equiv.) and 1-butyl-3-methylimidazolium chloride (1.4 g, 7.7 mmol, 1.2 equiv.), then the mixture was stirred under Argon in the preheated oil bath. After 24 h, the mixture was distributed in water (10 mL) and diethyl ether (10 mL). The organic layer was separated and washed with brine (10 mL), dried over anhydrous $MgSO_4$ and concentrated to give the desired product as colorless oil (985 mg, 5.8 mmol, 83% yield). **^{1}H NMR** (400 MHz, Chloroform-d) δ 7.36 – 7.29 (m, 2H), 7.26 – 7.21 (m, 3H), 4.07 – 3.97 (m, 1H), 2.88 (ddd, J = 14.2, 8.2, 6.1 Hz, 1H), 2.83 – 2.73 (m, 1H), 2.09 – 2.00 (m, 2H), 1.56 (dd, J = 6.6, 1.3 Hz, 3H). **^{13}C NMR** (101 MHz, Chloroform-d) δ 141.09, 128.51, 128.46, 128.40, 126.04, 57.91, 41.92, 32.88, 25.42. **GC-MS** (m/z): 168.2.
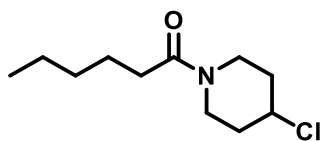
Substrate (**iv.1ae**): A flame-dried flask with a magnetic stir bar was added 4-chloropiperidine hydrochloride (200 mg, 1.28 mmol, 1.0 equiv.) and dry THF under nitrogen. The solution was cooled to 0 °C, followed by the addition of DIPEA (364 mg, 2.8 mmol, 2.2 equiv.) with stirring. Then hexanoyl chloride (207 mg, 1.54 mmol, 1.2 equiv.) Was added dropwise to the reaction. The reaction was warmed up to room temperature and stir under nitrogen for 4 hours. Afterwards, the reaction was quenched with 20 mL H2O and the aqueous layer was extracted with EtOAc three times. The combined organic layers were dried over anhydrous NaSO4, filtered and concentrated under vacuum. The crude was purified by column chromatography (SiO2, hexane/EtOAc=10/1→7/1) to afford the title compound 1ae as a yellowish oil (204 mg, 73% yield). **^{1}H NMR** (500 MHz, Chloroform-d): δ 4.27 (tt, J = 7.3, 3.7 Hz, 1H), 3.84 (ddd, J = 12.1, 7.7, 3.7 Hz, 1H), 3.71 (ddd, J = 14.0, 7.6, 3.4 Hz, 1H), 3.56 (ddd, J = 13.7, 7.6, 3.9 Hz, 1H), 3.37 (ddd, J = 13.8, 7.4, 3.6 Hz, 1H), 2.32 (td, J = 7.3, 1.9 Hz, 2H), 2.05 (tdd, J = 12.6, 8.0, 3.9 Hz, 2H), 1.89 – 1.77

(m, 2H), 1.62 (dq, $J = 13.1$, 7.6 Hz, 2H), 1.37 – 1.29 (m, 4H), 0.93 – 0.88 (m, 3H). ^{13}**C-NMR** (126 MHz, Chloroform-d): δ 171.77, 56.70, 43.02, 38.98, 35.69, 34.83, 33.45, 31.82, 25.22, 22.62, 14.09. **HRMS** (ESI): m/z calcd for C11H20ClNONa[M+Na]$^+$: 240.1131, found 240.125. **GC-MS** (m/z): 217.1.
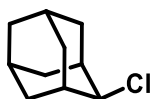
Substrate (**iv.1af**): To mixture of 2-adamantanol (0.5 g, 3.28 mmol, 1.0 equiv.) and diethyl ether (10 mL) at to 0 ℃, PCl$_5$ (1.03 g, 4.93 mmol, 1.5 equiv.) was added slowly and then reflux for 30 min. The resulting mixture was allowed to cool to rt, and solvent was removed under reduced pressure to give compound 1af (370 mg, 66%) as white solid without further purification. ^{1}**H NMR** (500 MHz, Chloroform-d): δ 4.40 (dt, $J = 3.4$, 1.7 Hz, 1H), 2.30 – 2.24 (m, 2H), 2.08 (q, $J = 3.2$ Hz, 2H), 1.98 – 1.92 (m, 2H), 1.86 (hept, $J = 3.0$ Hz, 2H), 1.82 – 1.74 (m, 4H), 1.57 (ddq, $J = 12.9$, 3.4, 1.6 Hz, 2H). ^{13}**C-NMR** (126 MHz, Chloroform-d): δ 68.40, 38.28, 37.84, 35.94, 31.10, 27.57, 26.98. **GC-MS** (m/z): 135.1.
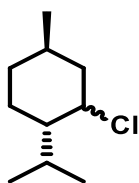
Substrate (**iv.1ag**): To mixture of (-)-menthol (0.1 g, 3.2 mmol, 1.0 equiv.) and diethyl ether (15 mL) at to 0 ℃, PCl$_5$ (200 mg, 4.8 mmol, 1.5 equiv.) was added slowly and then stir at rt for 30 min. The resulting mixture was quenched by water, then extracted with diethylether. Combined organic phase was washed with sat. aq. NaHCO$_3$, brine, dried under Na$_2$SO$_4$, concentrated under reduced pressure to afford crude. Then purified by column chromatography (SiO$_2$, hexane) to give compound 1ag (76 mg, 68%) as a colorless liquid. ^{1}**H NMR** (500 MHz, Chloroform-d): δ 3.78 (tdd, $J = 11.0$, 4.2, 1.7 Hz, 1H), 2.41 – 2.16 (m, 2H), 1.71 (dq, $J = 11.0$, 2.0 Hz, 2H), 1.51 – 1.30 (m, 3H), 1.10 – 0.86 (m, 8H), 0.77

(dd, J = 7.0, 1.8 Hz, 3H). **^{13}C NMR** (75 MHz, Chloroform-d): δ 63.59, 49.11, 43.43, 34.90, 30.21, 26.02, 24.41, 22.02, 20.94, 20.33. **GC-MS** (m/z): 139.2.
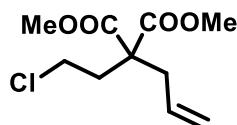
Substrate (**iv.1ah**): To a suspension of NaH (176 mg, 7.32 mmol, 1.1 equiv.) in DMF (10 mL) was added at 0 °C a solution of dimethyl allylmalonate (1.2 g, 6.97 mmol, 1.0 equiv.) in THF (5 mL). The mixture was stirred at room temperature for 30 min in which it became a clear solution. To this solution was added dropwise a solution of freshly distilled 1-bromo-2-chloroethane (1.5 g, 10.45 mmol, 1.5 equiv.) in THF (2 mL). The solution was stirred overnight at room temperature. The reaction was quenched by addition of H_2O (15 mL) and extracted with Et_2O (3 × 15 mL). The combined organic extracts were dried over $MgSO_4$ and the solvent was removed under reduced pressure. The crude material was purified by flash chromatography (SiO_2, 10 % diethyl ether in hexane) to yield 1.05 g (64 %) of the title compound as colorless oil. **^{1}H NMR** (400 MHz, Chloroform-d): δ = 5.73 - 5.52 (m, 1H), 5.23 - 5.02 (m, 2H), 3.74 (s, 6H), 3.53 (t, J = 7.6 Hz, 2H), 2.68 (dt, J = 7.4, 1.2 Hz, 2H), 2.37 (d, J = 7.6 Hz, 2H) ppm. **^{13}C NMR** (101 MHz, Chloroform-d): δ = 170.9 (2C), 131.8, 119.9, 56.7, 52.8 (2C), 39.9, 38.0, 36.0 23 ppm. **HRMS**: m/z calcd for C10H15ClNaO4 [M + Na]+ : 257.0551, found 257.0549.
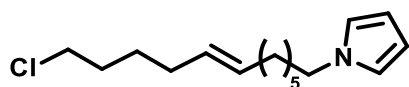
Substrate (**iv.1ai**): Isolated as pale yellow liquid in 66 % yield (383 mg, 1.4 mmol). **^{1}H NMR** (400 MHz, Chloroform-d): δ = 6.55 (t, J = 2.1 Hz, 2H), 6.03 (t, J = 2.1 Hz, 2H), 5.35 - 5.22 (m, 2H), 3.76 (t, J = 7.2 Hz, 2H), 3.43 (t, J = 6.7 Hz, 2H), 1.98 - 1.82 (m, 4H), 1.74 - 1.59 (m, 4H), 1.45 - 1.35 (m, 2H), 1.28 - 1.12 (m, 6H) ppm. **^{13}C NMR** (101

MHz, Chloroform-d) δ = 131.1, 129.7, 120.6, 107.9, 49.7, 45.2, 32.6, 32.2, 31.9, 31.7, 29.5, 28.8, 26.9, 26.8 ppm. **HRMS**: m/z calcd for C16H27ClN: [M + H]+ : 268.1827, found 268.1838.
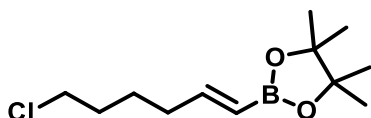
Substrate (**iv.1aj**): A Schlenk flask was charged with dicyclohexylborane (0.274 g, 1.54 mmol, 7 mol%) and to this flask was added pinacolborane (3.35 mL, 23.10 mmol, 1.05 equiv.) and 6-chlorohex-1-yne (2.67 mL, 22 mmol, 1.0.equiv.) at 0 ºC. The mixture was stirred for 24 h at room temperature, diluted hexane (25 mL) followed by bubbling air through the solution for 2 h. The organic layer was washed with H₂O (3 × 20 mL) and the solvent was removed under reduced pressure to yield 5.01 g (93 %) of title compound as a colorless oil. **¹H NMR** (400 MHz, Chloroform-d): δ = 6.60 (dt, *J* = 18.0, 6.4 Hz, 1H), 5.45 (dt, *J* = 18.0, 1.7 Hz, 1H), 3.52 (t, *J* = 6.7 Hz, 2H), 2.28 - 2.08 (m, 2H), 1.89 - 1.70 (m, 2H), 1.64 - 1.51 (m, 2H), 1.26 (s, 12H) ppm. **¹³C NMR** (101 MHz, Chloroform-d): δ = 153.6, 83.2 (2C), 45.0, 35.0, 32.1, 25.5, 24.9 (4C) ppm. **HRMS**: m/z calcd for C12H22NaO2BCl [M + Na] + : 266.1330, found 266.1325.
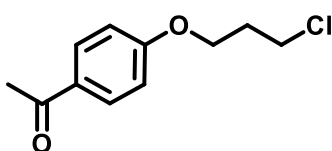
1-(4-Hydroxyphenyl)-ethanone (1 equiv., 1 g, 7.3 mmol) was added together with 1-bromo3-chloropropane (2 equiv., 1.5 ml, 14.7 mmol) and K₂CO₃ (3 equiv., 3.05 g, 22.0 mmol) in 20 ml of dry Acetone. The reaction mixture was heated to 65 ºC and left to stir under reflux overnight. After cooling the reaction mixture was filtered through a pad of celite and concentrated in vaccum. The residue was then dissolved in Diethyl ether and washed with

concentrated aqueous NaHCO$_3$ and brine. After concentrating the product was dried in vaccum to afford the product. (1.17 g, 74.9 %). **^{1}H NMR** (400 MHz, Chloroform-d) δ = 7.94 (dt, *J* = 8.9 Hz, 2 H), 6.94 (dt, *J* = 9.0 Hz, 2 H), 4.19 (t, *J* = 5.6 Hz, 2 H), 3.75 (t, *J* = 6.0 Hz, 2 H), 2.56 (s, 3 H), 2.27 (q, *J* = 6.1 Hz, 2 H) ppm. **^{13}C NMR** (126 MHz, Chloroform-d) δ = 197.2, 163.1, 131.1 (2C), 131.0, 114.6 (2C), 64.9, 41.7, 32.5, 26.8 ppm. **GC-MS** (m/z): 212.1.
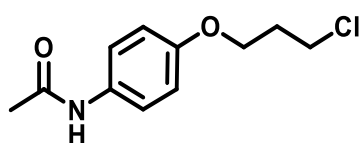
N-(4-hydroxyphenyl)acetamide (1 equiv., 1 g, 6.62 mmol) was added together with 1-bromo-3-chloropropane (1.9 equiv., 1.26 ml, 12.64 mmol) and K$_2$CO$_3$ (3.3 equiv., 3.02 g, 21.83 mmol) in 20 ml of dry Acetone. The reaction mixture was heated to 65 ºC and left to stir under reflux overnight. After cooling the reaction mixture was filtered through a pad of celite and concentrated in vaccum to afford the product. (1.03 g, 68.4 %). **^{1}H NMR** (400 MHz, Chloroform-d) δ = 7.38 (dt, *J* = 9.0, 2 H), 7.06 (s, 1 H, br), 6.86 (dt, *J* = 9.0, 2 H), 4.09 (t, *J* = 5.9 Hz, 2H), 3.74 (t, *J* = 6.3 Hz, 2 H), 2.22 (q, *J* = 6.1 Hz, 2 H), 2.16 (s, 3 H) ppm. **^{13}C NMR** (126 MHz, Chloroform-d) δ = 168.2, 155.8, 131.3, 122.0 (2C), 115.0 (2C), 64.7, 41.7, 32.4, 24.6 ppm. **GC-MS** (m/z): 227.1.
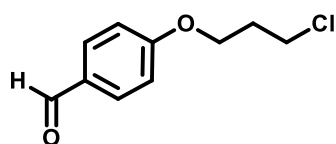
4-hydroxybenzaldehyde (1 equiv., 1 g, 8.19 mmol) was added together with 1-bromo-3-chloropropane (2 equiv., 1.6 ml, 16.38 mmol) and K$_2$CO$_3$ (3 equiv., 3.4 g, 24.57 mmol) in 11 ml of dry acetone. The reaction mixture was heated to 65 ºC and left to stir under reflux overnight. After cooling the reaction mixture was filtered through a pad of celite and concentrated in vaccum. The residue was purified using column chromatography (5:1 Hexane:AcOEt) to obtain the product as colourless liquid (0.94 g, 57.8 %). **^{1}H NMR** (400 MHz, Chloroform-d) δ = 7.48 (m, 2 H), 6.91 (dt,

J = 8.8 Hz, 2 H), 6.60 (d, J = 16.2 Hz, 1 H), 4.14 (t, J = 5.9 Hz, 2 H), 3.74 (t, J = 6.3 Hz, 2 H) 2.35 (s, 3 H), 2.24 (q, J = 6 Hz, 2 H). **GC-MS** (m/z): 198.1.
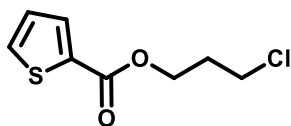
3-Chloro-1-Propanol (1.1 equiv., 0.62 ml, 7.50 mmol), DMAP (1 equiv., 0.833 g, 6.82 mmol) and trimethylamine (3 equiv., 2.85 ml, 20.47 mmol) were added together in 18 ml of DCM at 0 ºC and left to stir for 10 minutes. Then, thiophene-2-carbonyl chloride (1 equiv., 1 g, 6.82 mmol) was added and the reaction mixture was left to stir over night. For workup aqueous saturated NH_4Cl solution was added and the aqueous phase was extracted with DCM three times. It was then dried with Na_2SO_4 and concentrated in vaccum. The residue was then purified using column chromatography (9:1 Hexane:AcOEt) to obtain the product as a colourless liquid (1.15 g, 82.4 %). **¹H NMR** (400 MHz, Chloroform-d) δ = 7.81 (dd, J = 5.0 Hz, J = 1.3 Hz, 1 H), 7.56 (dd, J = 5.0 Hz, J = 1.3 Hz,1 H), 7.11 (dd, J = 4.4 Hz, J = 1.2 Hz, 1 H), 4.46 (t, J = 6.1 Hz, 2 H), 3.69 (t, J = 6.4 Hz, 2 H), 2.22 (q, J = 6.2 Hz, 2 H) ppm. **¹³C NMR** (126 MHz, Chloroform-d) δ = 162.2, 133.7, 132.7, 128.0, 62.0, 41.3, 31.9 ppm. **GC-MS** (m/z): 204.8.
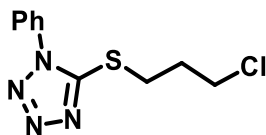
1-Bromo-3-chloropropane (583.1 mg, 3.7 mmol, 1.1 equiv.) was added dropwise to a suspension of 1-phenyl-1H-tetrazole-5-thiol (600 mg, 3.37 mmol, 1.0 equiv.) and K_2CO_3 (930 mg, 3.7 mmol, 2.0 equiv.) in acetone (50 mL) at room temperature. The resulting mixture was stirred for 1 h, then filter and concentrated in vaccum to afford crude product as a yellowish oil. The crude residue was purified by flash chromatography (SiO$_2$, 12:1→10:1 hexane:EA) to provide the compound (719 mg, 83.9%) as a colourless oil. **¹H NMR** (300 MHz, Chloroform-d): δ 7.56 (d, J = 1.9 Hz, 5H), 3.68 (t, J = 6.1 Hz, 2H), 3.53 (t, J = 6.9 Hz, 2H), 2.35 (qd, J = 6.8, 6.0 Hz, 2H). **¹³C NMR** (75 MHz,

Chloroform-d): δ 153.94, 133.67, 130.34, 129.97, 123.90, 42.20, 31.62, 30.34. **GC-MS** (m/z): 254.8.
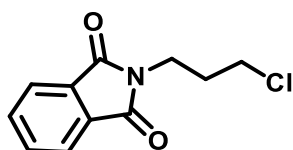
1-Bromo-3-chloropropane (823 mg, 5.23 mmol, 1.1 equiv.) was added dropwise to a suspension of phthalimide (700 mg, 3.7 mmol, 1.0 equiv.) and K_2CO_3 (1.32 g, 9.53 mmol, 2.0 equiv.) in acetone (20 mL) at room temperature. The resulting mixture was stirred for 1 h, then filter and concentrated in vaccum to afford product (1.04 g, 97.7%) as a white soild, which was not further purified. **¹H NMR** (300 MHz, Chloroform-d): δ 7.89 – 7.81 (m, 1H), 7.73 (td, J = 5.3, 2.1 Hz, 1H), 3.85 (t, J = 6.9 Hz, 1H), 3.58 (t, J = 6.5 Hz, 1H), 2.17 (p, J = 6.8 Hz, 1H). **¹³C NMR** (75 MHz, Chloroform-d): δ 168.38, 134.20, 132.17, 123.47, 42.14, 35.80, 31.60. **GC-MS** (m/z): 223.7.
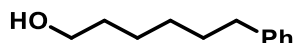
4.4.6. Characterization of products
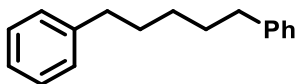
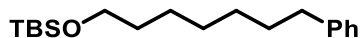Product (**iv.3a**): Cross-coupling according to general procedure: scale 0.32 mmol, flash chromatography (SiO₂, 100% hexane) yielded 0.32 mg (81 %) of the title compound as a colorless liquid. **¹H NMR** (500 MHz, Chloroform-d) δ 7.33 – 7.28 (m, 4H), 7.24 – 7.16 (m, 6H), 2.66 – 2.60 (m, 4H), 1.73 – 1.64 (m, 4H), 1.47 – 1.38 (m, 2H). **¹³C NMR** (101 MHz, Chloroform-d) δ 142.78, 128.40, 128.26, 125.61, 35.91, 31.40, 28.99. **GC-MS** (m/z) : 224.1
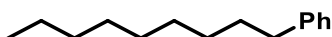
Product (**iv.3b**): Cross-coupling according to general procedure: scale 0.32 mmol, flash chromatography (SiO₂, 100% hexane) yielded 55 mg (85 %) of the title compound as a colorless liquid. **¹H NMR** (500 MHz, Chloroform-d) δ 7.31 (t, J = 7.5, 7.5

Hz, 2H), 7.21 (d, J = 7.3 Hz, 3H), 2.67 – 2.58 (m, 2H), 1.65 (p, J = 7.3, 7.3, 7.2, 7.2 Hz, 2H), 1.39 – 1.32 (m, 6H), 1.30 (s, 6H), 0.92 (t, J = 6.7, 6.7 Hz, 3H). **¹³C NMR** (101 MHz, Chloroform-d) δ 142.97, 128.40, 128.21, 125.53, 36.01, 31.92, 31.55, 29.57, 29.54, 29.37, 29.35, 22.69, 14.12. **GC-MS** (m/z) : 204.2.
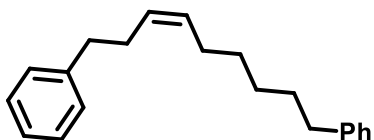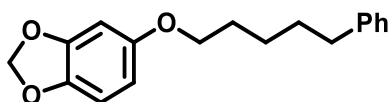

Product (**iv.3c**): Cross-coupling according to general procedure: scale 0.32 mmol, flash chromatography (SiO_2, 100% hexane) yielded 45 mg (67 %) of the title compound as a colorless liquid. **¹H NMR** (500 MHz, Chloroform-d) δ 7.31 – 7.25 (m, 4H), 7.21 – 7.14 (m, 6H), 5.46 – 5.34 (m, 2H), 2.70 – 2.62 (m, 2H), 2.62 – 2.57 (m, 2H), 2.39 – 2.31 (m, 2H), 2.03 – 1.94 (m, 2H), 1.66 – 1.58 (m, 2H), 1.35 – 1.29 (m, 4H). **¹³C NMR** (126 MHz, Chloroform-d) δ 143.19, 142.49, 130.92, 129.10, 128.81, 128.74, 128.60, 128.58, 126.11, 125.93, 36.39, 36.31, 31.76, 29.83, 29.54, 29.32, 27.51. **HRMS** (APCI): m/z calcd for C21H27 [M+H]⁺ : 279.2107, found 279.2098.
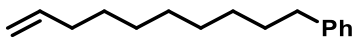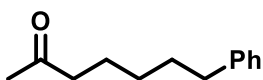

Product (**iv.3d**): Cross-coupling according to general procedure: scale 0.32 mmol, flash chromatography (SiO_2, 100% hexane) yielded 32 mg (62 %) of the title compound as a colorless liquid. **¹H NMR** (500 MHz, Chloroform-d) δ 7.34 – 7.28 (m, 2H), 7.23 – 7.17 (m, 3H), 5.90 – 5.78 (m, 1H), 5.06 – 4.98 (m, 1H), 4.98 – 4.93 (m, 1H), 2.66 – 2.59 (m, 2H), 2.12 – 2.03 (m, 2H), 1.69 – 1.59 (m, 2H), 1.44 – 1.27 (m, 10H).**¹³C NMR** (126 MHz, Chloroform-d) δ 142.94, 139.23, 128.39, 128.21, 128.09, 125.54, 114.11, 36.00, 33.82, 31.52, 29.46, 29.43, 29.33, 29.14, 28.94. **HRMS** (APCI): m/z calcd for C16H23 [M+H]⁺ : 215.1794, found 215.1786.
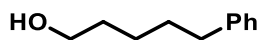
HO ⌒⌒⌒ Ph   Product (**iv.3e**): Cross-coupling according to general procedure: scale 0.32 mmol, flash chromatography (SiO$_2$, 100% hexane) yielded 0.32 mg (88 %) of the title compound as a colorless liquid. **^{1}H NMR** (500 MHz, Chloroform-d) δ 7.25 (d, *J* = 7.9 Hz, 2H), 7.16 (dt, *J* = 8.0, 3.0, 3.0 Hz, 3H), 3.63 (q, *J* = 6.2, 6.2, 6.2 Hz, 2H), 2.61 (t, *J* = 7.7, 7.7 Hz, 2H), 1.68 – 1.61 (m, 2H), 1.60 – 1.55 (m, 2H), 1.43 – 1.36 (m, 2H), 1.20 (t, *J* = 5.4, 5.4 Hz, 1H). **^{13}C NMR** (126 MHz, Chloroform-d) δ 142.91, 128.74, 128.63, 126.02, 63.30, 36.27, 33.02, 31.62, 25.77. **HRMS** (ESI): m/z calcd for C11H13 [M-H2O]$^+$: 146.1095, found 146.1092.

HO ⌒⌒⌒ Ph   Product (**iv.3f**): Cross-coupling according to general procedure: scale 0.32 mmol, flash chromatography (SiO$_2$, 100% hexane) yielded 0.32 mg (88 %) of the title compound as a colorless liquid. **^{1}H NMR** (500 MHz, Chloroform-d) δ 7.32 – 7.29 (m, 2H), 7.22 – 7.18 (m, 3H), 3.66 (t, *J* = 6.6, 6.6 Hz, 2H), 2.68 – 2.58 (m, 2H), 1.70 – 1.63 (m, 2H), 1.62 – 1.56 (m, 2H), 1.42 – 1.38 (m, 4H). **^{13}C NMR** (126 MHz, Chloroform-d) δ 142.73, 128.39, 128.25, 125.62, 63.01, 35.89, 32.72, 31.44, 29.07, 25.62. **HRMS** (ESI): m/z calcd for C12H18 [M-H2O]$^+$: 178.1095, found 178.1099.

TBSO ⌒⌒⌒ Ph   Product (**iv.3g**): Cross-coupling according to general procedure: scale 0.32 mmol, flash chromatography (SiO$_2$, 100% hexane) yielded 78.5 mg (80 %) of the title compound as a colorless liquid. **^{1}H NMR** (500 MHz, Chloroform-d) δ 7.28 – 7.25 (m, 2H), 7.18 – 7.15 (m, 3H), 3.58 (t, *J* = 6.6, 6.6 Hz, 2H), 2.62 – 2.56 (m, 2H), 1.64 – 1.57 (m, 2H), 1.49 (q, *J* = 6.8, 6.8, 6.7 Hz, 2H), 0.98 – 0.89 (m, 6H), 0.88 (s, 9H), 0.04 (s, 6H). **^{13}C NMR** (126 MHz, Chloroform-d) δ 143.25, 128.73,

128.56, 125.90, 63.66, 36.32, 33.23, 31.79, 29.65, 26.35, 26.11, 18.73, -4.90. **HRMS** (APCI): m/z calcd for C19H35OSi [M+H]$^+$: 307.2452, found 307.2446.

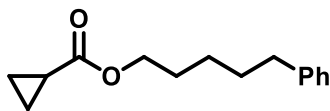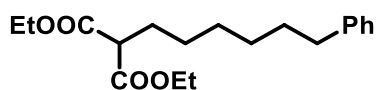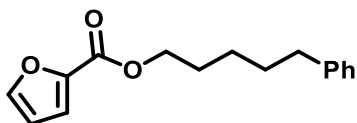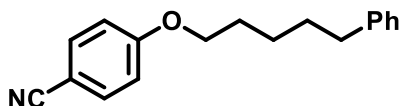Product (**iv.3h**): Cross-coupling according to general procedure: scale 0.32 mmol, flash chromatography (SiO$_2$, 100% hexane) yielded 66 mg (73 %) of the title compound as a colorless liquid. **^{1}H NMR** (500 MHz, Chloroform-d) δ 7.30 – 7.25 (m, 2H), 7.19 – 7.14 (m, 3H), 6.70 – 6.66 (m, 1H), 6.47 (d, *J* = 2.5 Hz, 1H), 6.29 (dd, J = 8.5, 2.5 Hz, 1H), 5.89 (s, 2H), 3.86 (t, *J* = 6.5, 6.5 Hz, 2H), 2.66 – 2.59 (m, 2H), 1.81 – 1.73 (m, 2H), 1.71 – 1.64 (m, 2H), 1.51 – 1.45 (m, 2H). **^{13}C NMR** (126 MHz, Chloroform-d) δ 154.99, 148.56, 142.88, 141.82, 128.76, 128.71, 128.63, 126.04, 108.28, 106.05, 101.41, 98.43, 69.19, 36.22, 31.58, 29.55, 26.08. **HRMS** (APCI): m/z calcd for C18H21O3 [M+H]$^+$: 285.1485, found 285.1484.

Product (**iv.3i**): Cross-coupling according to general procedure: scale 0.32 mmol, flash chromatography (SiO$_2$, 100% hexane) yielded 58 mg (73 %) of the title compound as as a colorless liquid. **^{1}H NMR** colorless liquid. **^{1}H NMR** (500 MHz, Chloroform-d) δ 7.35 – 7.27 (m, 3H), 7.20 – 7.10 (m, 2H), 2.64 (t, *J* = 7.7, 7.7 Hz, 2H), 2.44 (t, *J* = 7.4, 7.4 Hz, 2H), 2.15 (s, 3H), 1.69 – 1.59 (m, 4H). **^{13}C NMR** (126 MHz, Chloroform-d) δ 209.15, 142.53, 128.39, 128.28, 125.68, 43.68, 35.75, 31.24, 29.89, 28.80, 23.67. **HRMS** (APCI): m/z calcd for C13H18NaO [M+Na]$^+$: 213.1250, found 213.1258.
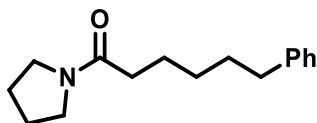
Product (**iv.3j**): Cross-coupling according to general procedure: scale 0.32 mmol, flash chromatography (SiO₂, 100% hexane) yielded 66 mg (73 %) of the title compound as a colorless liquid. **¹H NMR** (500 MHz, Chloroform-d) δ 7.34 – 7.30 (m, 2H), 7.23 – 7.19 (m, 4H), 4.10 (t, J = 6.7, 6.7 Hz, 2H), 2.69 – 2.63 (m, 2H), 1.73 – 1.67 (m, 4H), 1.47 – 1.42 (m, 2H), 1.03 – 0.99 (m, 3H), 0.88 – 0.85 (m, 2H). **¹³C NMR** (101 MHz, Chloroform-d) δ 174.93, 142.42, 128.38, 128.35, 128.28, 128.25, 128.22, 125.70, 64.46, 35.79, 31.05, 28.57, 25.57, 12.91, 12.89, 12.84, 8.29, 8.25, 8.19. **HRMS** (ESI): m/z calcd for C15H20NaO2 [M+Na]⁺ : 255.1356, found 255.1361.
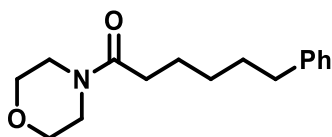
Product (**iv.3k**): Cross-coupling according to general procedure: scale 0.32 mmol, flash chromatography (SiO₂, 100% hexane) yielded 49 mg (49 %) of the title compound as a colorless liquid. **¹H NMR** (500 MHz, Chloroform-d) δ 7.30 – 7.25 (m, 2H), 7.18 – 7.14 (m, 3H), 4.21 – 4.16 (m, 4H), 3.30 (t, J = 7.6, 7.6 Hz, 1H), 2.62 – 2.56 (m, 2H), 1.90 – 1.85 (m, 2H), 1.64 – 1.57 (m, 2H), 1.35 – 1.32 (m, 4H), 1.27 – 1.24 (m, 6H), 0.94 – 0.90 (m, 2H). **¹³C NMR** (126 MHz, Chloroform-d) δ 169.59, 169.55, 142.71, 128.36, 128.22, 125.59, 52.07, 35.89, 31.32, 29.08, 28.96, 28.72, 27.25, 14.08, 13.79. **HRMS** (ESI): m/z calcd for C19H28NaO4 [M+Na]⁺ : 343.1886, found 343.1881.
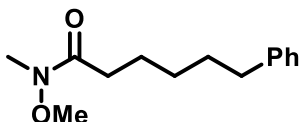
Product (**iv.3l**): Cross-coupling according to general procedure: scale 0.32 mmol, flash chromatography (SiO₂, 100% hexane) yielded 48 mg (58 %) of the title compound as a colorless liquid. **¹H NMR** (500 MHz, Chloroform-d) δ 7.60 (dd, J = 1.8, 0.8 Hz, 1H), 7.32 – 7.30 (m, 1H), 7.22 – 7.18 (m, 5H), 6.53 (dd, J = 3.5, 1.8 Hz, 1H),

4.33 (t, J = 6.7, 6.7 Hz, 2H), 3.17 (p, J = 6.7, 6.7, 6.7, 6.7 Hz, 1H), 2.69 – 2.62 (m, 2H), 1.81 (dq, J = 9.0, 6.9, 6.9, 6.8 Hz, 2H), 1.74 – 1.68 (m, 2H), 1.53 – 1.47 (m, 2H). **¹³C NMR** (126 MHz, Chloroform-d) δ 159.17, 146.52, 145.23, 142.72, 128.74, 128.64, 126.06, 118.07, 112.12, 65.29, 36.11, 31.39, 28.92, 25.89. **HRMS** (APCI): m/z calcd for C16H18NaO3 [M+Na]⁺ : 281.1148, found 281.1141.

Product (**iv.3m**): Cross-coupling according to general procedure: scale 0.32 mmol, flash chromatography (SiO$_2$, 100% hexane) yielded 30 mg (35 %) of the title compound as a colorless liquid. **¹H NMR** (500 MHz, Chloroform-d) δ 7.62 – 7.56 (m, 2H), 7.33 – 7.29 (m, 2H), 7.24 – 7.17 (m, 3H), 6.98 – 6.91 (m, 2H), 4.01 (t, J = 6.5, 6.5 Hz, 2H), 2.67 (t, J = 7.7, 7.7 Hz, 2H), 1.89 – 1.81 (m, 2H), 1.73 (p, J = 7.7, 7.7, 7.6, 7.6 Hz, 3H), 1.54 (d, J = 7.2 Hz, 2H). **¹³C NMR** (126 MHz, Chloroform-d) δ 157.94, 132.18, 129.34, 123.80, 123.09, 121.50, 110.50, 109.09, 59.92, 36.40, 27.20. **HRMS** (APCI): m/z calcd for C18H20NO [M+H]⁺ : 266.1539, found 266.1535.

Product (**iv.3n**): Cross-coupling according to general procedure: scale 0.32 mmol, flash chromatography (SiO$_2$, 100% hexane) yielded 60 mg (76 %) of the title compound as a colorless liquid. **¹H NMR** (500 MHz, Chloroform-d) δ 7.29 – 7.23 (m, 2H), 7.18 – 7.12 (m, 3H), 3.44 (t, J = 6.9, 6.9 Hz, 2H), 3.37 (t, J = 6.8, 6.8 Hz, 2H), 2.63 – 2.57 (m, 2H), 2.26 – 2.20 (m, 2H), 1.96 – 1.89 (m, 2H), 1.86 – 1.79 (m, 2H), 1.70 – 1.60 (m, 4H), 1.41 – 1.33 (m, 2H).**¹³C NMR** (126 MHz, Chloroform-d) δ 143.03, 128.76, 128.59, 125.96, 46.96, 45.94, 36.17, 35.08, 31.66, 29.52, 26.49, 25.15,
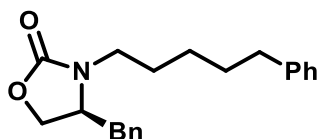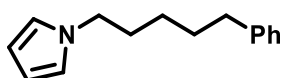
24.77. **HRMS** (ESI): m/z calcd for C16H24NO [M+H]$^+$: 246.1852, found 246.1848.

Product (**iv.3o**): Cross-coupling according to general procedure: scale 0.32 mmol, flash chromatography (SiO$_2$, 100% hexane) yielded 57 mg (68 %) of the title compound as a colorless liquid. **^{1}H NMR** (500 MHz, Chloroform-d) δ 7.31 – 7.24 (m, 2H), 7.18 – 7.13 (m, 3H), 3.65 – 3.61 (m, 4H), 3.61 – 3.57 (m, 2H), 3.47 – 3.39 (m, 2H), 2.64 – 2.56 (m, 2H), 2.31 – 2.25 (m, 2H), 1.69 – 1.59 (m, 6H), 1.41 – 1.32 (m, 2H). **^{13}C NMR** (126 MHz, Chloroform-d) δ 172.09, 142.88, 128.75, 128.62, 126.03, 67.31, 67.03, 46.39, 42.24, 36.13, 33.35, 31.59, 29.42, 25.45. **HRMS** (ESI): m/z calcd for C16H24NO2 [M+H]$^+$: 262.1802, found 262.1790.

Product (**iv.3p**): Cross-coupling according to general procedure: scale 0.32 mmol, flash chromatography (SiO$_2$, 100% hexane) yielded 58 mg (77 %) of the title compound as a colorless liquid. **^{1}H NMR** (500 MHz, Chloroform-d) δ 7.28 – 7.24 (m, 2H), 7.19 – 7.13 (m, 3H), 3.65 (s, 3H), 3.16 (s, 3H), 2.65 – 2.56 (m, 2H), 2.40 (t, *J* = 7.7, 7.7 Hz, 2H), 1.68 – 1.61 (m, 4H), 1.41 – 1.35 (m, 2H). **^{13}C NMR** (126 MHz, Chloroform-d) δ 143.01, 128.75, 128.60, 125.97, 61.55, 36.15, 31.62, 29.45, 24.84. **HRMS** (ESI): m/z calcd for C14H22NO2 [M+H]$^+$: 236.1645, found 236.1648.
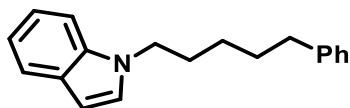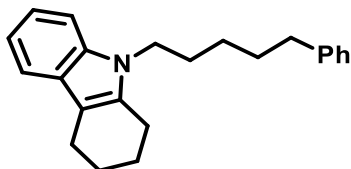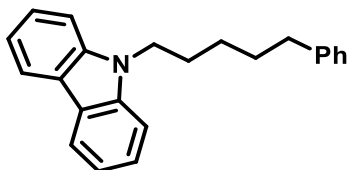
Product (**iv.3q**): Cross-coupling according to general procedure: scale 0.32 mmol, flash chromatography (SiO$_2$, 100% hexane) yielded 43 mg (52 %) of the title compound as a colorless liquid. **^{1}H NMR** (500 MHz, Chloroform-d) δ 7.32 – 7.25 (m, 5H), 7.18 – 7.13 (m, 5H), 4.14 – 4.10 (m, 1H), 4.00 – 3.94 (m, 2H), 3.53 – 3.44 (m, 1H), 3.09 – 3.00 (m, 2H), 2.66 – 2.57 (m, 3H), 1.66 – 1.56 (m, 4H), 1.37 – 1.29 (m, 2H). **^{13}C NMR** (126 MHz, Chloroform-d) δ 158.43, 142.65, 135.92, 129.37, 129.31, 128.76, 128.67, 127.58, 126.11, 67.04, 56.38, 42.39, 38.88, 36.12, 31.33, 27.66, 26.62. **GC-MS** (m/z): 346.2.

Product (**iv.3r**): Cross-coupling according to general procedure: scale 0.32 mmol, flash chromatography (SiO$_2$, 100% hexane) yielded 46 mg (68 %) of the title compound as a colorless liquid. **^{1}H NMR** (500 MHz, Chloroform-d) δ 7.29 – 7.25 (m, 2H), 7.18 – 7.13 (m, 3H), 6.62 (t, J = 2.1, 2.1 Hz, 2H), 6.13 (t, J = 2.1, 2.1 Hz, 2H), 3.85 (t, J = 7.2, 7.2 Hz, 2H), 2.61 – 2.56 (m, 2H), 1.82 – 1.76 (m, 2H), 1.63 (tt, J = 9.4, 9.4, 6.9, 6.9 Hz, 2H), 1.37 – 1.30 (m, 2H). **^{13}C NMR** (126 MHz, Chloroform-d) δ 142.73, 128.71, 128.66, 126.08, 120.79, 108.19, 49.88, 36.14, 31.82, 31.41, 26.79. **HRMS** (APCI): m/z calcd for C15H20N [M+H]$^+$: 214.1590, found 214.1588.

Product (**iv.3s**): Cross-coupling according to general procedure: scale 0.32 mmol, flash chromatography (SiO$_2$, 100% hexane) yielded 55 mg (63 %) of the title compound as a colorless liquid. **^{1}H NMR** (500 MHz, Chloroform-d) δ 7.66 (dt, J = 7.9, 1.1, 1.1 Hz, 1H), 7.36 (dq, J = 8.2, 0.9, 0.9, 0.9 Hz, 1H), 7.32 – 7.28 (m, 2H), 7.26 – 7.19 (m, 2H), 7.19 – 7.15 (m, 2H), 7.15 – 7.09 (m, 2H), 6.51 (dd, J = 3.1, 0.9 Hz,

1H), 4.14 (t, J = 7.1, 7.1 Hz, 2H), 2.65 – 2.56 (m, 2H), 1.96 – 1.84 (m, 2H), 1.73 – 1.64 (m, 2H), 1.46 – 1.35 (m, 2H). **^{13}C NMR** (126 MHz, Chloroform-d) δ 142.32, 128.58, 128.36, 128.30, 127.74, 125.73, 121.31, 120.94, 119.16, 109.33, 100.89, 46.31, 35.77, 31.09, 30.10, 26.63. **HRMS** (ESI): m/z calcd for C19H22N [M+H]$^+$: 264.1747, found 262.1737.
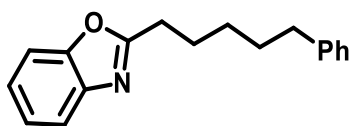
Product (**iv.3t**): Cross-coupling according to general procedure: scale 0.32 mmol, flash chromatography (SiO$_2$, 100% hexane) yielded 72 mg (72 %) of the title compound as a colorless liquid. **^{1}H NMR** (500 MHz, Chloroform-d) δ 7.49 – 7.45 (m, 1H), 7.30 – 7.25 (m, 2H), 7.21 – 7.10 (m, 4H), 7.08 – 7.03 (m, 1H), 4.02 – 3.94 (m, 2H), 2.77 – 2.71 (m, 2H), 2.71 – 2.66 (m, 2H), 2.62 – 2.57 (m, 2H), 2.17 (d, J = 3.0 Hz, 1H), 1.97 – 1.90 (m, 2H), 1.90 – 1.83 (m, 2H), 1.80 – 1.72 (m, 2H), 1.65 (qd, J = 7.9, 7.9, 7.7, 4.2 Hz, 2H), 1.40 (qd, J = 8.7, 8.5, 8.5, 3.5 Hz, 2H).**^{13}C NMR** (126 MHz, Chloroform-d) δ 142.74, 136.39, 135.56, 128.76, 128.66, 127.67, 126.09, 120.77, 118.84, 118.11, 109.56, 109.09, 43.18, 36.20, 31.62, 30.60, 27.13, 23.72, 23.62, 22.66, 21.47. **HRMS** (ESI): m/z calcd for C23H27NNa [M+Na]$^+$: 340.2036, found 340.2041.
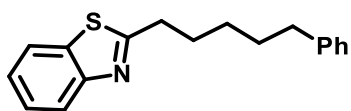
Product (**iv.3u**): Cross-coupling according to general procedure: scale 0.32 mmol, flash chromatography (SiO$_2$, 100% hexane) yielded 68 mg (75 %) of the title compound as a colorless liquid. **^{1}H NMR** (500 MHz, Chloroform-d) δ 8.12 – 8.08 (m, 2H), 7.49 – 7.43 (m, 2H), 7.40 – 7.36 (m, 2H), 7.28 – 7.20 (m, 5H), 7.14 – 7.10 (m, 2H), 4.29 (t, J = 7.3, 7.3 Hz, 2H), 2.60 – 2.52

(m, 2H), 1.90 (p, J = 7.5, 7.5, 7.4, 7.4 Hz, 2H), 1.69 – 1.59 (m, 2H), 1.48 – 1.39 (m, 2H). **¹³C NMR** (126 MHz, Chloroform-d) δ 142.69, 140.78, 128.72, 128.65, 126.08, 125.94, 123.22, 120.70, 119.09, 119.05, 108.98, 43.34, 36.16, 31.62, 29.16, 27.33. **HRMS** (ESI): m/z calcd for C23H23NNa [M+Na]⁺ : 336.1723, found 336.1716.
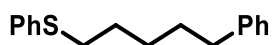
Product (**iv.3v**): Cross-coupling according to general procedure: scale 0.32 mmol, flash chromatography (SiO₂, 100% hexane) yielded 56 mg (66 %) of the title compound as a colorless liquid. **¹H NMR** (500 MHz, Chloroform-d) δ 7.68 – 7.65 (m, 1H), 7.48 – 7.45 (m, 1H), 7.30 – 7.28 (m, 2H), 7.26 – 7.23 (m, 2H), 7.18 – 7.14 (m, 3H), 2.94 – 2.90 (m, 2H), 2.65 – 2.59 (m, 2H), 1.96 – 1.88 (m, 2H), 1.73 – 1.65 (m, 2H), 1.52 – 1.43 (m, 2H). **¹³C NMR** (126 MHz, Chloroform-d) δ 151.14, 142.77, 141.66, 128.74, 128.63, 126.05, 124.80, 124.44, 119.88, 110.63, 36.04, 31.39, 29.12, 28.94, 26.97. **HRMS** (ESI): m/z calcd for C18H20NO [M+H]⁺ : 266.1539, found 266.1541.

Product (**iv.3w**): Cross-coupling according to general procedure: scale 0.32 mmol, flash chromatography (SiO₂, 100% hexane) yielded 43 mg (47 %) of the title compound as a colorless liquid. **¹H NMR** (500 MHz, Chloroform-d) δ 7.98 – 7.94 (m, 1H), 7.85 – 7.81 (m, 1H), 7.47 – 7.40 (m, 1H), 7.36 – 7.31 (m, 1H), 7.29 – 7.23 (m, 3H), 7.18 – 7.12 (m, 3H), 3.14 – 3.07 (m, 2H), 2.64 – 2.58 (m, 2H), 1.91 (p, J = 7.7, 7.7, 7.7, 7.7 Hz, 2H), 1.73 – 1.64 (m, 2H), 1.52 – 1.44 (m, 2H). **¹³C NMR** (126 MHz, Chloroform-d) δ 142.80, 128.74, 128.63, 126.26, 126.04, 125.02, 122.86,

121.84, 36.08, 34.60, 31.45, 29.90, 29.12. **HRMS** (ESI): m/z calcd for C18H20NS [M+H]$^+$: 282.1311, found 282.1311.
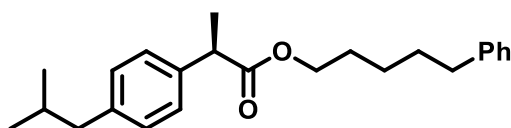
Product (**iv.3x**): Cross-coupling according to general procedure: scale 0.32 mmol, flash chromatography (SiO$_2$, 100% hexane) yielded 24 mg (41 %) of the title compound as a colorless liquid. **^{1}H NMR** (500 MHz, Chloroform-d) δ 7.32 – 7.25 (m, 6H), 7.18 – 7.14 (m, 4H), 2.92 – 2.86 (m, 2H), 2.59 (t, J = 7.7, 7.7 Hz, 2H), 1.70 – 1.59 (m, 4H), 1.50 – 1.41 (m, 2H). **^{13}C NMR** (101 MHz, Chloroform-d) δ 142.81, 137.27, 129.34, 129.17, 128.73, 128.62, 126.06, 126.03, 36.13, 33.93, 31.33, 29.41, 28.80. **HRMS** (APCI): m/z calcd for C17H21S [M+Na]$^+$: 257.1358, found 257.1357.

Product (**iv.3y**): Cross-coupling according to general procedure: scale 0.32 mmol, flash chromatography (SiO$_2$, 100% hexane) yielded 28 mg (25 %) of the title compound as a colorless liquid. **^{1}H NMR** (500 MHz, Chloroform-d) δ 7.78 – 7.71 (m, 4H), 7.56 – 7.45 (m, 7H), 7.28 – 7.25 (m, 2H), 7.22 – 7.07 (m, 4H), 2.58 (t, J = 7.6, 7.6 Hz, 2H), 2.32 – 2.21 (m, 2H), 1.69 – 1.57 (m, 5H), 1.51 – 1.42 (m, 3H). **^{13}C NMR** (101 MHz, Chloroform-d) δ 142.32, 131.72, 130.84, 130.75, 128.70, 128.59, 128.36, 128.32, 128.25, 125.68, 36.65, 35.59, 30.85, 30.58, 30.43, 24.69, 23.36, 21.30. **HRMS** (ESI): m/z calcd for C23H25NaOP [M+Na]$^+$: 371.1535, found 371.1542.
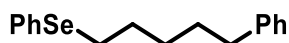
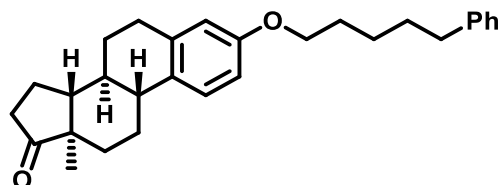Product (**iv.3z**): Cross-coupling according to general procedure: scale 0.32 mmol, flash chromatography (SiO$_2$, 100% hexane) yielded 43 mg (44 %) of the title compound as a colorless liquid. **^{1}H NMR** (500 MHz,

Chloroform-d) δ 7.53 – 7.48 (m, 2H), 7.33 – 7.24 (m, 6H), 7.22 – 7.15 (m, 3H), 2.96 – 2.90 (m, 2H), 2.65 – 2.58 (m, 2H), 1.81 – 1.71 (m, 2H), 1.69 – 1.60 (m, 2H), 1.53 – 1.42 (m, 2H). **^{13}C NMR** (101 MHz, Chloroform-d) δ 142.48, 132.45, 128.98, 128.38, 128.26, 126.64, 125.66, 35.77, 30.90, 30.05, 29.44, 27.81. **HRMS** (APCI): m/z calcd for C17H21Se [M+H]$^+$: 305.0804, found 305.0799.
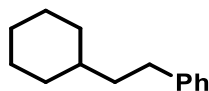

Product (**iv.3aa**): Cross-coupling according to general procedure: scale 0.32 mmol, flash chromatography (SiO$_2$, 100% hexane) yielded 62 mg (73 %) of the title compound as a white solid. **^{1}H NMR** (400 MHz, Chloroform-d) δ 7.34 – 7.27 (m, 2H), 7.25 – 7.19 (m, 3H), 7.19 – 7.16 (m, 2H), 7.14 – 7.09 (m, 2H), 4.08 (q, *J* = 6.1, 6.1, 5.6 Hz, 2H), 3.70 (q, *J* = 7.2, 7.1, 7.1 Hz, 1H), 2.62 – 2.56 (m, 2H), 2.48 (d, *J* = 7.2 Hz, 2H), 1.91 – 1.83 (m, 1H), 1.67 – 1.56 (m, 5H), 1.51 (d, *J* = 7.2 Hz, 3H), 1.37 – 1.28 (m, 2H), 0.93 (d, *J* = 6.6 Hz, 6H). **^{13}C NMR** (126 MHz, Chloroform-d) δ 174.79, 142.43, 140.44, 137.89, 129.26, 128.36, 128.26, 127.15, 125.68, 64.60, 45.21, 45.05, 35.76, 30.96, 30.19, 28.41, 25.44, 22.39, 18.45. **HRMS** (ESI): m/z calcd for C24H32NaO2 [M+Na]$^+$: 375.2295, found 375.2281.

Product (**iv.3ab**): Cross-coupling according to general procedure: scale 0.32 mmol, flash chromatography (SiO$_2$, 100% hexane) yielded 33 mg (34 %) of the title compound as a white solid. **^{1}H NMR** (500 MHz, Chloroform-d) δ 7.28 – 7.25 (m, 1H), 7.16 (td, J = 4.9, 4.7, 2.3 Hz, 3H), 6.69 (dd, *J* = 8.6, 2.8 Hz, 1H),

6.62 (d, J = 2.8 Hz, 1H), 3.91 (t, J = 6.6, 6.6 Hz, 2H), 2.88 (dd, J = 9.8, 6.2 Hz, 2H), 2.65 – 2.60 (m, 2H), 2.49 (dd, J = 18.9, 8.8 Hz, 1H), 2.41 – 2.35 (m, 1H), 2.23 (t, J = 10.7, 10.7 Hz, 1H), 2.12 (dd, J = 19.0, 9.0 Hz, 1H), 2.06 – 2.02 (m, 1H), 1.99 (ddd, J = 13.0, 5.7, 3.1 Hz, 1H), 1.96 – 1.90 (m, 1H), 1.78 (dt, J = 14.4, 6.7, 6.7 Hz, 2H), 1.72 – 1.65 (m, 2H), 1.52 (d, J = 5.0 Hz, 4H), 1.50 – 1.46 (m, 4H). ^{13}**C NMR** (126 MHz, Chloroform-d) δ 157.49, 142.90, 138.04, 132.24, 128.75, 128.62, 126.62, 126.02, 114.93, 112.50, 68.15, 50.82, 48.38, 44.37, 38.78, 36.23, 31.98, 31.57, 30.01, 29.57, 26.94, 26.30, 26.12, 21.95, 14.22. **HRMS** (ESI): m/z calcd for C29H36NaO2 [M+Na]$^+$: 439.260, found 439.2597.
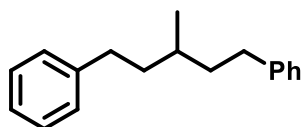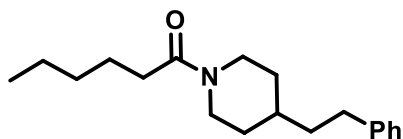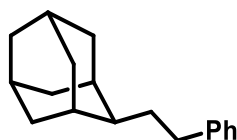
Product (**iv.3ac**): Cross-coupling according to general procedure: scale 0.32 mmol, flash chromatography (SiO$_2$, 100% hexane) yielded 82 mg (82 %) of the title compound as a colorless liquid. ^{1}**H NMR** (500 MHz, Chloroform-d) δ 7.32 – 7.27 (m, 4H), 7.20 – 7.16 (m, 6H), 2.71 – 2.62 (m, 2H), 2.62 – 2.54 (m, 2H), 1.76 – 1.66 (m, 2H), 1.55 – 1.47 (m, 3H), 1.02 (d, J = 6.1 Hz, 3H). ^{13}**C NMR** (126 MHz, Chloroform-d) δ 143.44, 128.73, 128.66, 125.96, 39.22, 33.79, 32.57, 19.94. **HRMS** (APCI): m/z calcd for C18H23 [M+H]$^+$: 239.1794, found 239.1788.

Product (**iv.3ad**): Cross-coupling according to general procedure: scale 0.32 mmol, flash chromatography (SiO$_2$, 100% hexane) yielded 48 mg (80 %) of the title compound as a colorless liquid. ^{1}**H NMR** (500 MHz, Chloroform-d) δ 7.26 (t, J = 7.6, 7.6 Hz, 2H), 7.18 – 7.13 (m, 3H), 2.63 – 2.57 (m, 2H), 1.80 – 1.73 (m, 2H), 1.69 (dt, J = 12.4, 3.1, 3.1 Hz, 2H), 1.66 – 1.61 (m, 1H), 1.53 – 1.46 (m, 2H), 1.29 – 1.13 (m, 4H), 0.93 (qd, J = 11.9, 11.9, 11.9, 3.3 Hz, 2H). ^{13}**C NMR** (126 MHz,

Chloroform-d) δ 143.61, 128.69, 128.58, 125.83, 39.74, 37.70, 33.68, 33.63, 27.07, 26.70. **GC-MS** (m/z): 181.2.
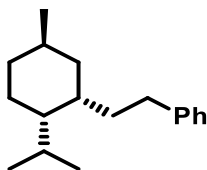
Product (**iv.3ae**): Cross-coupling according to general procedure: scale 0.32 mmol, flash chromatography (SiO$_2$, 100% hexane) yielded 76 mg (79 %) of the title compound as a colorless liquid. **^{1}H NMR** (500 MHz, Chloroform-d) δ 7.30 – 7.26 (m, 2H), 7.20 – 7.15 (m, 3H), 4.61 (ddt, *J* = 13.2, 4.6, 2.4, 2.4 Hz, 1H), 3.83 (ddt, *J* = 13.5, 4.7, 2.5, 2.5 Hz, 1H), 2.96 (td, *J* = 13.2, 13.0, 2.7 Hz, 1H), 2.63 (td, *J* = 7.2, 7.2, 1.5 Hz, 2H), 2.50 (td, *J* = 12.9, 12.9, 2.9 Hz, 1H), 2.34 – 2.26 (m, 2H), 1.81 – 1.74 (m, 2H), 1.66 – 1.55 (m, 4H), 1.53 – 1.47 (m, 1H), 1.37 – 1.28 (m, 4H), 1.17 – 1.05 (m, 2H), 0.93 – 0.86 (m, 3H).**^{13}C NMR** (126 MHz, Chloroform-d) δ 171.88, 142.67, 128.73, 128.64, 126.14, 46.31, 42.26, 38.49, 36.00, 33.85, 33.29, 33.26, 32.25, 32.09, 25.55, 22.85, 14.33. **GC-MS** (m/z): 288.2.
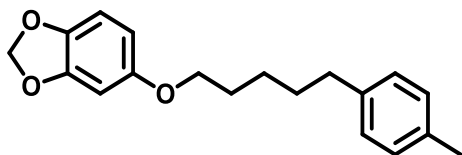
Product (**iv.3af**): Cross-coupling according to general procedure: scale 0.32 mmol, flash chromatography (SiO$_2$, 100% hexane) yielded 62 mg (80 %) of the title compound as a colorles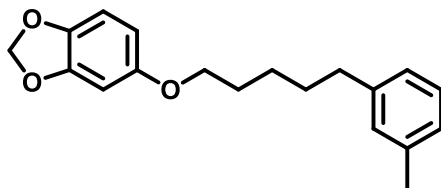s liquid. **^{1}H NMR** (500 MHz, Chloroform-d) δ 7.34 – 7.28 (m, 2H), 7.25 – 7.17 (m, 3H), 2.64 – 2.58 (m, 2H), 1.96 – 1.83 (m, 6H), 1.80 – 1.71 (m, 9H), 1.55 (d, *J* = 12.1 Hz, 2H). **^{13}C NMR** (126 MHz, Chloroform-d) δ 143.32, 128.37, 128.26, 125.52, 44.14, 39.27, 38.47, 34.95, 34.04, 31.87, 31.70, 28.38, 28.15. **HRMS** (APCI): m/z calcd for C18H25 [M+H]$^+$: 241.1951, found 241.1947.

Product (**iv.3ag**): Cross-coupling according to general procedure: scale 0.32 mmol, flash chromatography (SiO$_2$, 100% hexane) yielded 78 mg (85 %) of the title compound as a colorless liquid. **^{1}H NMR** (500 MHz, Chloroform-d) δ 7.33 – 7.29 (m, 2H), 7.24 – 7.16 (m, 4H), 2.79 – 2.67 (m, 1H), 2.54 – 2.43 (m, 1H), 2.10 – 1.99 (m, 1H), 1.91 – 1.84 (m, 2H), 1.77 – 1.72 (m, 1H), 1.68 – 1.60 (m, 2H), 1.47 – 1.27 (m, 4H), 1.02 – 0.96 (m, 2H), 0.94 – 0.90 (m, 6H), 0.73 – 0.68 (m, 3H).**^{13}C NMR** (126 MHz, Chloroform-d) δ 143.49, 143.27, 128.37, 128.31, 128.25, 125.56, 125.50, 48.39, 46.51, 41.30, 38.72, 38.20, 35.94, 35.42, 34.92, 34.89, 34.28, 32.88, 32.37, 29.25, 27.31, 26.42, 26.02, 25.32, 24.35, 22.92, 22.88, 21.69, 21.63, 20.68, 15.25. **HRMS** (APCI): m/z calcd for C18H29 [M+H]$^+$: 245.2264, found 245.2260.
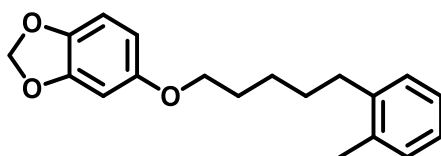

Product (**iv.4a**): Cross-coupling according to general procedure: scale 0.32 mmol, flash chromatography (SiO$_2$, 100% hexane) yielded 46 mg (64 %) of the title compound as a colorless liquid. **^{1}H NMR** (500 MHz, Chloroform-d) δ 7.07 (d, J = 3.0 Hz, 2H), 6.68 (d, J = 8.5 Hz, 1H), 6.47 (d, J = 2.5 Hz, 1H), 6.31 – 6.27 (m, 1H), 5.90 – 5.88 (m, 2H), 3.85 (t, J = 6.5, 6.5 Hz, 2H), 2.63 – 2.56 (m, 2H), 2.33 – 2.30 (m, 4H), 1.81 – 1.72 (m, 2H), 1.69 – 1.62 (m, 3H), 1.50 – 1.45 (m, 2H), 1.27 – 1.24 (m, 2H). **^{13}C NMR** (126 MHz, Chloroform-d) δ 155.01, 148.56, 141.82, 139.79, 135.44, 129.32, 128.63, 127.98, 108.27, 106.06, 101.41, 101.39, 98.44, 69.21, 35.76, 31.69, 29.55, 26.06, 21.35. **HRMS** (APCI): m/z calcd for C19H23O3 [M+H]$^+$: 299.1642, found 299.1640.
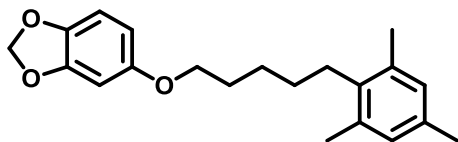
Product (**iv.4b**): Cross-coupling according to general procedure: scale 0.32 mmol, flash chromatography (SiO$_2$, 100% hexane) yielded 26 mg (36 %) of the title compound as a colorless liquid. **^{1}H NMR** (500 MHz, Chloroform-d) δ 7.28 – 7.20 (m, 1H), 7.19 – 7.13 (m, 1H), 6.98 (d, J = 6.3 Hz, 3H), 6.68 (d, J = 8.5 Hz, 1H), 6.51 – 6.42 (m, 1H), 6.34 – 6.24 (m, 1H), 5.89 (s, 2H), 3.86 (t, J = 6.6, 6.6 Hz, 2H), 2.64 – 2.57 (m, 2H), 2.36 – 2.30 (m, 4H), 1.80 – 1.74 (m, 2H), 1.70 – 1.64 (m, 2H), 1.52 – 1.44 (m, 2H). **^{13}C NMR** (126 MHz, Chloroform-d) δ 155.00, 148.56, 142.83, 141.82, 138.16, 129.58, 128.52, 126.77, 125.75, 108.27, 106.06, 101.41, 98.44, 69.20, 36.15, 31.61, 26.12, 21.76. **HRMS** (APCI): m/z calcd for C19H23O3 [M+H]$^+$: 299.1642, found 299.1637.
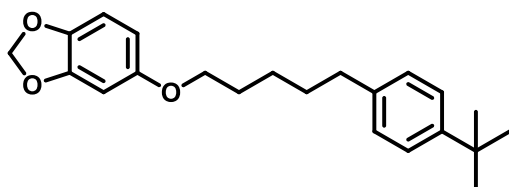

Product (**iv.4c**): Cross-coupling according to general procedure: scale 0.32 mmol, flash chromatography (SiO$_2$, 100% hexane) yielded 33 mg (46 %) of the title compound as a colorless liquid. **^{1}H NMR** (500 MHz, Chloroform-d) δ 7.13 – 7.10 (m, 3H), 6.68 (d, J = 8.5 Hz, 1H), 6.47 (d, J = 2.5 Hz, 1H), 6.33 – 6.28 (m, 1H), 5.89 (d, J = 0.9 Hz, 2H), 3.87 (t, J = 6.5, 6.5 Hz, 2H), 2.63 – 2.59 (m, 2H), 2.30 (s, 3H), 1.82 – 1.75 (m, 2H), 1.66 – 1.59 (m, 3H), 1.56 – 1.49 (m, 2H). **^{13}C NMR** (126 MHz, Chloroform-d) δ 155.01, 148.57, 141.84, 141.05, 136.16, 130.48, 129.14, 126.22, 126.18, 108.28, 106.07, 101.41, 98.44, 69.23, 33.58, 30.37, 29.62, 26.47, 19.65. **HRMS** (APCI): m/z calcd for C19H23O3 [M+H]$^+$: 299.1642, found 299.1644.
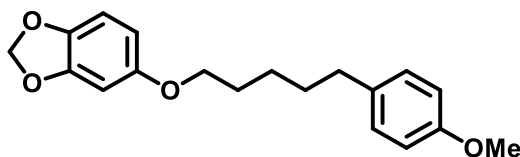
Product (**iv.4d**): Cross-coupling according to general procedure: scale 0.32 mmol, flash chromatography (SiO$_2$, 100% hexane) yielded 23 mg (29 %) of the title compound as a colorless liquid. **^{1}H NMR** (400 MHz, Chloroform-d) δ 6.85 (s, 2H), 6.72 (d, J = 8.5 Hz, 1H), 6.52 (d, *J* = 2.5 Hz, 1H), 6.35 (dd, *J* = 8.5, 2.5 Hz, 1H), 5.93 (d, *J* = 4.4 Hz, 2H), 3.92 (t, *J* = 6.5, 6.5 Hz, 2H), 2.67 – 2.58 (m, 2H), 1.87 – 1.79 (m, 2H), 1.61 (dd, *J* = 6.6, 2.5 Hz, 2H), 1.56 – 1.49 (m, 2H). **^{13}C NMR** (101 MHz, Chloroform-d) δ 157.68, 154.63, 148.19, 141.45, 134.62, 129.25, 128.89, 113.71, 113.11, 107.91, 105.68, 101.05, 98.06, 68.84, 55.26, 55.11, 44.60, 34.91, 31.45, 29.18, 25.64, 24.51. **GC-MS** (m/z): 326.3.
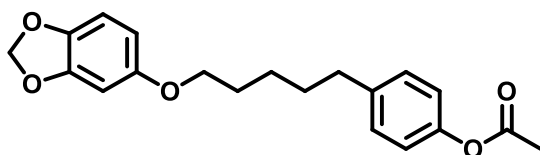

Product (**iv.4e**): Cross-coupling according to general procedure: scale 0.32 mmol, flash chromatography (SiO$_2$, 100% hexane) yielded 45 mg (55 %) of the title compound as a colorless liquid. **^{1}H NMR** (400 MHz, Chloroform-d) δ 7.36 – 7.31 (m, 2H), 7.17 – 7.12 (m, 2H), 6.74 – 6.70 (m, 1H), 6.51 (d, *J* = 2.5 Hz, 1H), 6.33 (dt, *J* = 8.4, 2.7, 2.7 Hz, 1H), 5.93 (s, 2H), 3.90 (t, *J* = 6.5, 6.5 Hz, 2H), 2.66 – 2.59 (m, 2H), 1.81 (dt, *J* = 14.2, 6.8, 6.8 Hz, 2H), 1.73 – 1.66 (m, 3H), 1.56 – 1.50 (m, 2H), 1.34 (s, 9H). **^{13}C NMR** (101 MHz, Chloroform-d) δ 154.65, 148.45, 148.20, 141.45, 139.44, 128.02, 126.98, 125.15, 107.92, 105.69, 101.05, 98.07, 68.85, 35.30, 31.42, 31.20, 29.20, 25.80. **HRMS** (ESI): m/z calcd for C22H28NaO3 [M+Na]$^+$: 363.1928, found 363.1931.
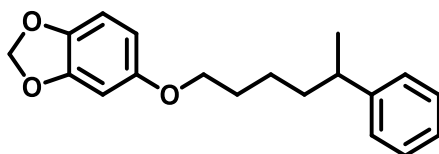
Product (**iv.4f**): Cross-coupling according to general procedure: scale 0.32 mmol, flash chromatography (SiO$_2$, 100% hexane) yielded 33 mg (43 %) of the title compound as a colorless liquid. **^{1}H NMR** (400 MHz, Chloroform-d) δ 7.18 – 7.07 (m, 2H), 6.88 – 6.83 (m, 2H), 6.72 – 6.66 (m, 1H), 6.50 (d, J = 2.5 Hz, 1H), 6.33 (dd, J = 8.5, 2.5 Hz, 1H), 5.93 (s, 2H), 3.89 (t, J = 6.5, 6.5 Hz, 2H), 2.64 – 2.55 (m, 2H), 1.79 (dt, J = 14.8, 6.6, 6.6 Hz, 2H), 1.72 – 1.63 (m, 2H), 1.54 – 1.45 (m, 2H). **^{13}C NMR** (101 MHz, Chloroform-d) δ 157.68, 154.63, 148.19, 141.45, 134.62, 129.25, 128.89, 113.71, 113.11, 107.91, 105.68, 101.05, 98.06, 68.84, 55.26, 55.11, 44.60, 34.91, 31.45, 29.18, 25.64, 24.51. **HRMS** (APCI): m/z calcd for C19H23O4 [M+H]$^+$: 315.1591, found 315.1588.
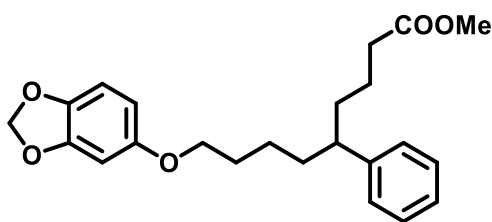

Product (**iv.4g**): Cross-coupling according to general procedure: scale 0.32 mmol, flash chromatography (SiO$_2$, 100% hexane) yielded 34 mg (42 %) of the title compound as a colorless liquid. **^{1}H NMR** (400 MHz, Chloroform-d) δ 7.23 – 7.17 (m, 2H), 7.04 – 6.99 (m, 2H), 6.72 (d, J = 8.5 Hz, 1H), 6.50 (d, J = 2.5 Hz, 1H), 6.33 (dd, J = 8.5, 2.5 Hz, 1H), 5.93 (s, 2H), 3.90 (t, J = 6.5, 6.5 Hz, 2H), 2.68 – 2.61 (m, 2H), 2.31 (s, 3H), 1.80 (dt, J = 14.8, 6.7, 6.7 Hz, 2H), 1.75 – 1.64 (m, 3H), 1.56 – 1.47 (m, 2H). **^{13}C NMR** (101 MHz, Chloroform-d) δ 169.67, 154.61, 148.66, 148.20, 141.46, 140.05, 129.27, 121.25, 107.92, 105.68, 101.05, 98.06, 68.78, 35.23, 31.15, 29.16, 25.69, 21.14. **HRMS** (ESI): m/z calcd for C20H22NaO5 [M+Na]$^+$: 365.1356, found 365.1359.

Product (**iv.4h**): Cross-coupling according to general procedure: scale 0.32 mmol, flash chromatography (SiO$_2$, 100% hexane) yielded 33 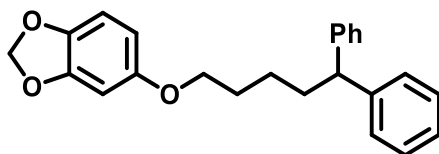mg (45 %) of the title compound as a colorless liquid. **^{1}H NMR** (500 MHz, Chloroform-d) δ 7.28 (dd, *J* = 8.2, 7.0 Hz, 2H), 7.19 – 7.15 (m, 3H), 6.67 (d, *J* = 8.4 Hz, 1H), 6.44 (d, J = 2.5 Hz, 1H), 6.26 (dd, *J* = 8.5, 2.5 Hz, 1H), 5.88 (s, 2H), 3.83 – 3.79 (m, 2H), 2.73 – 2.65 (m, 1H), 1.73 – 1.67 (m, 2H), 1.64 – 1.59 (m, 2H), 1.33 – 1.26 (m, 2H), 1.24 (d, *J* = 6.9 Hz, 3H). **^{13}C NMR** (126 MHz, Chloroform-d) δ 154.98, 148.54, 147.90, 141.80, 128.67, 127.33, 126.22, 108.28, 108.25, 106.06, 101.40, 98.43, 69.19, 40.26, 38.46, 29.70, 24.52, 22.66. **HRMS** (APCI): m/z calcd for C19H23O3 [M+H]$^+$: 299.1642, found 299.1639.

Product (**iv.4i**): Cross-coupling according to general procedure: scale 0.32 mmol, flash chromatography (SiO$_2$, 100% hexane) yield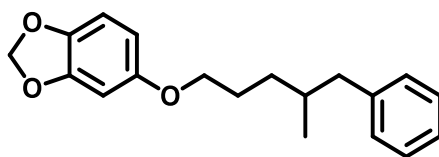ed 41 mg (45 %) of the title compound as a colorless liquid. **^{1}H NMR** (400 MHz, Chloroform-d) δ 7.38 – 7.26 (m, 2H), 7.26 – 7.16 (m, 1H), 7.19 – 7.11 (m, 2H), 6.70 (d, *J* = 8.4 Hz, 1H), 6.46 (d, *J* = 2.5 Hz, 1H), 6.33 – 6.24 (m, 1H), 5.94 (d, *J* = 7.4 Hz, 0H), 5.92 (s, 2H), 3.90 – 3.75 (m, 2H), 3.65 (s, 3H), 2.60 – 2.48 (m, 1H), 2.35 – 2.19 (m, 2H), 1.80 – 1.68 (m, 1H), 1.73 – 1.61 (m, 2H), 1.65 – 1.50 (m, 1H), 1.54 – 1.41 (m, 1H), 1.44 – 1.18 (m, 2H). **^{13}C NMR** (101 MHz, Chloroform-d) δ 174.04, 154.57, 148.16, 145.19, 141.42, 128.36, 127.60, 126.08, 107.89, 105.66, 101.04, 98.06, 68.76, 51.44, 45.77, 36.57,

36.27, 34.07, 29.29, 24.00, 23.03. **HRMS** (ESI): m/z calcd for C24H36N [M+H]$^+$: 407.1829, found 407.1831.

Product (**iv.4j**): Cross-coupling according to general procedure: scale 0.32 mmol, flash chromatography (SiO$_2$, 100% hexane) yielded 69 mg (79 %) of the title compound as a colorless liquid. **^{1}H NMR** (400 MHz, Chloroform-d) δ 7.34 – 7.19 (m, 6H), 7.23 – 7.13 (m, 2H), 6.69 (dd, J = 8.5, 1.1 Hz, 1H), 6.46 (dd, J = 2.5, 1.2 Hz, 1H), 6.32 – 6.24 (m, 1H), 5.90 (d, J = 0.7 Hz, 2H), 3.93 (t, J = 7.8, 7.8 Hz, 1H), 3.84 (t, J = 6.5, 6.5 Hz, 2H), 2.17 – 2.06 (m, 2H), 1.79 (p, J = 6.8, 6.8, 6.7, 6.7 Hz, 2H), 1.50 – 1.37 (m, 2H). **^{13}C NMR** (101 MHz, Chloroform-d) δ 154.56, 148.19, 145.03, 141.47, 128.44, 127.85, 126.12, 107.91, 105.67, 101.06, 98.08, 68.69, 51.31, 35.42, 29.25, 24.53. **HRMS** (ESI): m/z calcd for C24H24NaO3 [M+Na]$^+$: 383.1618, found 383.1617.

Product (**iv.4k**): Cross-coupling according to general procedure: scale 0.32 mmol, flash chromatography (SiO$_2$, 100% hexane) yiel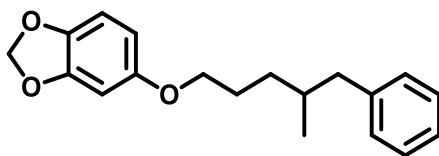ded 13 mg (18 %) of the title compound as a colorless liquid. **^{1}H NMR** (400 MHz, Chloroform-d) δ 7.33 – 7.29 (m, 2H), 7.23 – 7.16 (m, 3H), 6.72 (d, J = 8.5 Hz, 1H), 6.50 (d, J = 2.5 Hz, 1H), 6.32 (dd, J = 8.5, 2.5 Hz, 1H), 5.93 (s, 2H), 3.90 – 3.86 (m, 2H), 2.74 – 2.64 (m, 2H), 2.48 – 2.39 (m, 2H), 1.86 – 1.73 (m, 4H), 1.55 – 1.49 (m, 2H), 0.92 (d, J = 6.6 Hz, 3H). **^{13}C NMR** (101 MHz, Chloroform-d) δ 129.17, 128.12, 125.69, 107.92, 105.71,

101.06, 98.08, 69.19, 43.58, 34.85, 32.83, 26.93, 19.36. **HRMS** (APCI): m/z calcd for C19H23O3 [M+H]$^+$: 299.1642, found 299.1646.

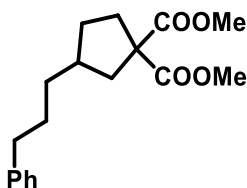Product (**iv.4k'**): Cross-coupling according to general procedure: scale 0.32 mmol, flash chromatography (SiO$_2$, 100% hexane) yielded 19 mg (26 %) of the title compound as a colorless liquid. **^{1}H NMR** (400 MHz, Chloroform-d) δ 7.33 – 7.29 (m, 2H), 7.23 – 7.16 (m, 3H), 6.72 (d, J = 8.5 Hz, 1H), 6.50 (d, J = 2.5 Hz, 1H), 6.32 (dd, J = 8.5, 2.5 Hz, 1H), 5.93 (s, 2H), 3.90 – 3.86 (m, 2H), 2.74 – 2.64 (m, 2H), 2.48 – 2.39 (m, 2H), 1.86 – 1.73 (m, 4H), 1.55 – 1.49 (m, 2H), 0.92 (d, J = 6.6 Hz, 3H). **^{13}C NMR** (101 MHz, Chloroform-d) δ 129.17, 128.12, 125.69, 107.92, 105.71, 101.06, 98.08, 69.19, 43.58, 34.85, 32.83, 26.93, 19.36. **HRMS** (APCI): m/z calcd for C19H23O3 [M+H]$^+$: 299.1642, found 299.1648.
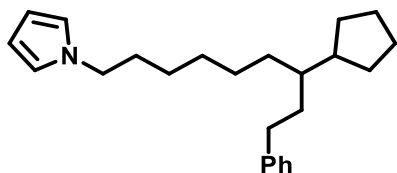
Product (**iv.5a**): Cross-coupling according to general procedure: scale 0.32 mmol, flash chromatography (SiO$_2$, 100% hexane) yielded 61 mg (77 %) of the title compound as a colorless liquid. **^{1}H NMR** (400 MHz, Chloroform-d) δ 7.34 – 7.28 (m, 2H), 7.22 – 7.16 (m, 3H), 3.74 (s, 3H), 3.73 (s, 3H), 2.65 – 2.59 (m, 2H), 2.52 – 2.46 (m, 1H), 2.36 – 2.29 (m, 1H), 2.21 – 2.12 (m, 1H), 2.04 – 1.93 (m, 1H), 1.93 – 1.86 (m, 1H), 1.74 – 1.64 (m, 2H), 1.46 – 1.35 (m, 2H), 1.32 – 1.24 (m, 1H). **^{13}C NMR** (101 MHz, Chloroform-d) δ 173.20, 142.55, 128.36, 128.26, 125.65, 59.92, 52.62, 52.60, 40.87, 39.72, 36.08, 34.88, 33.91, 32.04, 30.37. **HRMS** (ESI): m/z calcd for C18H24NaO4 [M+Na]$^+$: 327.1567, found 327.1553.
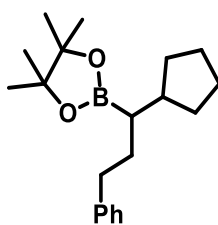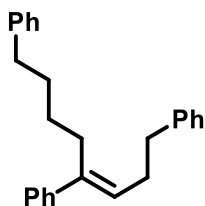
Product (**iv.5b**): Cross-coupling according to general procedure: scale 0.32 mmol, flash chromatography (SiO$_2$, 100% hexane) yielded 62 mg (76 %) of the title compound as a colorless liquid.

^{1}H NMR (400 MHz, Chloroform-d) δ 7.35 – 7.28 (m, 3H), 7.21 (d, *J* = 7.1 Hz, 3H), 6.68 (q, *J* = 2.3, 2.2, 2.2 Hz, 2H), 6.17 (q, *J* = 2.1, 2.1, 2.1 Hz, 2H), 3.93 – 3.83 (m, 2H), 2.70 – 2.46 (m, 2H), 1.83 – 1.73 (m, 4H), 1.68 (ddd, *J* = 10.5, 5.8, 4.1 Hz, 2H), 1.65 – 1.50 (m, 6H), 1.38 – 1.24 (m, 8H), 1.14 (ddt, *J* = 11.6, 5.4, 2.7, 2.7 Hz, 2H). **^{13}C NMR** (101 MHz, Chloroform-d) δ 143.36, 128.31, 128.27, 126.62, 125.54, 120.46, 107.77, 49.66, 43.54, 42.36, 33.74, 32.97, 31.64, 31.44, 30.52, 30.47, 29.81, 26.86, 26.31, 25.35. **HRMS** (ESI): m/z calcd for C24H36N [M+H]$^+$: 338.2842, found 338.2831.

Product (**iv.5c**): Cross-coupling according to general procedure: scale 0.32 mmol, flash chromatography (SiO$_2$, 100% hexane) yielded 51 mg (72 %) of the title compound as a colorless liquid. **^{1}H NMR** (500 MHz, Chloroform-d) δ 7.25 (t, J = 7.5, 7.5 Hz, 2H), 7.21 – 7.09 (m, 3H), 2.68 – 2.60 (m, 1H), 2.54 – 2.46 (m, 1H), 1.89 – 1.78 (m, 2H), 1.75 – 1.70 (m, 2H), 1.59 – 1.52 (m, 4H), 1.50 – 1.42 (m, 2H), 1.27 (s, 12H), 1.15 – 1.03 (m, 2H), 0.97 – 0.90 (m, 1H).**^{13}C NMR** (126 MHz, Chloroform-d) δ 143.56, 128.70, 128.56, 125.88, 83.27, 42.17, 36.42, 33.36, 32.84, 32.45, 30.06, 25.66, 25.47, 25.34, 25.24. **HRMS** (ESI): m/z calcd for C20H31NaO2^{10}B [M+Na]$^+$: 336.2346, found 336.2348.

Product (**iv.5d**): Cross-coupling according to general procedure: scale 0.32 mmol, flash chromatography (SiO$_2$, 100% hexane) yielded 51 mg (72 %) of the title compound as a colorless liquid. **^{1}H NMR** (500 MHz, Chloroform-d) δ 7.33 – 7.27 (m, 7H), 7.21 – 7.16 (m, 4H), 7.13 – 7.10 (m, 2H), 7.05 – 7.01 (m, 2H), 5.51 – 5.47 (m, 1H), 2.66 (dd, J = 8.6, 6.8 Hz, 2H), 2.61 – 2.56 (m, 2H), 2.38 (t, J = 7.5, 7.5 Hz, 2H), 2.26 (q, J = 7.5, 7.5, 7.4 Hz, 2H), 1.63 – 1.58 (m, 2H), 1.40 – 1.33 (m, 3H). **^{13}C NMR** (126 MHz, Chloroform-d) δ 142.80, 141.98, 141.62, 141.18, 128.53, 128.39, 128.32, 128.23, 128.19, 127.97, 126.37, 125.70, 125.58, 39.06, 36.38, 35.77, 30.94, 30.78, 27.63. **HRMS** (APCI): m/z calcd for C26H25[M+H]$^+$: 341.2251, found 341.2214.

4.4.7. Computational details

DFT calculations have been performed with the *Gaussian16* software package. Geometry optimizations and frequency calculations of ground state structures and transition states have been performed at the MNL15/6-31+G* level of theory which includes dispersion correction. Solvent effects (CH$_3$CN) are considered through the SMD model. Redox potentials (E°) have been evaluated through the Nernst equation in standard state conditions using the Standard Hydrogen Electrode (*SHE*) as reference following the equation, where n is the number of electrons involved in the reduction step, F is the Faraday constant, $\Delta G°_{SHE}$ = -4.24 eV.

$$E°(V) = -\left(\frac{\Delta G°}{nF} - \frac{\Delta G°_{SHE}}{F}\right)$$

Bond dissociation energy/enthalpy (BDE) is defined as the enthalpy change of the dissociation reaction of homolytic bonds at 298.15 K, 1 atm, where H(R·) and H(X·) and H(R—X) are enthalpies of the radicals and the molecule. The experimental data was obtained from bibliography.

$$R–X \quad \rightarrow \quad R· \quad + \quad X·$$

$$BDE(R–X) = H(R·) + H(X·) - H(R–X)$$

For the molecules involved in reaction mechanism modeling, the energy of the geometry optimized molecules at MNL15/6-31+G* was refined by single point calculation at MNL15/6-311+G** level of theory. Spin correction was applied when for errors higher than 3% and accounted for less than 0.3 kcal·mol^{-1} in the energy barriers.

4.5. References

1. Gál, B.; Bucher, C.; Burns, N. Z., Chiral Alkyl Halides: Underexplored Motifs in Medicine. *Marine Drugs* **2016,** *14* (11), 206.

2. Sun, S.-Z.; Börjesson, M.; Martin-Montero, R.; Martin, R., Site-Selective Ni-Catalyzed Reductive Coupling of α-Haloboranes with Unactivated Olefins. *Journal of the American Chemical Society* **2018,** *140* (40), 12765-12769.

3. Xu, H.; Zhao, C.; Qian, Q.; Deng, W.; Gong, H., Nickel-catalyzed cross-coupling of unactivated alkyl halides using bis(pinacolato)diboron as reductant. *Chemical Science* **2013,** *4* (10), 4022-4029.

4. Ziegler, D. T.; Choi, J.; Muñoz-Molina, J. M.; Bissember, A. C.; Peters, J. C.; Fu, G. C., A Versatile Approach to Ullmann C–N Couplings at Room Temperature: New Families of Nucleophiles and Electrophiles for Photoinduced, Copper-Catalyzed Processes. *Journal of the American Chemical Society* **2013,** *135* (35), 13107-13112.

5. Alonso, F.; Beletskaya, I. P.; Yus, M., Metal-Mediated Reductive Hydrodehalogenation of Organic Halides. *Chemical Reviews* **2002,** *102* (11), 4009-4092.

6. Choi, J.; Fu, G. C., Transition metal–catalyzed alkyl-alkyl bond formation: Another dimension in cross-coupling chemistry. *Science* **2017,** *356* (6334), eaaf7230.

7. Lekkala, R.; Lekkala, R.; Moku, B.; Rakesh, K. P.; Qin, H.-L., Recent Developments in Radical-Mediated Transformations of Organohalides. *European Journal of Organic Chemistry* **2019,** *2019* (17), 2769-2806.

8. Martin, E. T.; McGuire, C. M.; Mubarak, M. S.; Peters, D. G., Electroreductive Remediation of Halogenated Environmental Pollutants. *Chemical Reviews* **2016,** *116* (24), 15198-15234.

9. Handbook of Bond Dissociation Energies in Organic Compounds By Yu-Ran Luo (University of South Florida, St. Petersburg). CRC Press LLC: Boca Raton. 2003. xii + 380 pp. $159.95. ISBN 0-8493-1589-1. *Journal of the American Chemical Society* **2004,** *126* (3), 982-982.

10. Lambert, F. L.; Ingall, G. B., Voltammetry of organic halogen compounds. IV. The reduction of organic chlorides at the vitreous (glassy) carbon electrode. *Tetrahedron Lett.* **1974,** *15* (36), 3231-3234.

11. Hammerich, O. S., B., *Organic Electrochemistry: Revised and Expanded* CRC Press: 2015.

12. Jefford, C. W.; Kirkpatrick, D.; Delay, F., Reductive dehalogenation of alkyl halides with lithium aluminum hydride. Reappraisal of the scope of the reaction. *Journal of the American Chemical Society* **1972,** *94* (25), 8905-8907.

13. Carraro, M.; Pisano, L.; Azzena, U., Silica Gel Stabilized Na and Na/K Alloys: Highly Effective, Versatile and Environmentally Friendly Reducing Agents. *Synthesis* **2017,** *49* (09), 1931-1937.

14. Krief, A.; Laval, A.-M., Coupling of Organic Halides with Carbonyl Compounds Promoted by SmI2, the Kagan Reagent. *Chemical Reviews* **1999,** *99* (3), 745-778.

15. Whitesitt, C. A.; Herron, D. K., Reactions of 4-chloroazetidinones with tributyl tin hydride. *Tetrahedron Letters* **1978,** *19* (20), 1737-1740.

16. Terao, J.; Watanabe, H.; Ikumi, A.; Kuniyasu, H.; Kambe, N., Nickel-Catalyzed Cross-Coupling Reaction of Grignard Reagents with Alkyl Halides and Tosylates: Remarkable Effect of 1,3-Butadienes. *Journal of the American Chemical Society* **2002,** *124* (16), 4222-4223.

17. Clayden, J., Greeves, N. & Warren, S. , *Organic Chemistry* Oxford Univ. Press: 2012.

18. Vechorkin, O.; Barmaz, D.; Proust, V.; Hu, X., Ni-Catalyzed Sonogashira Coupling of Nonactivated Alkyl Halides: Orthogonal Functionalization of Alkyl Iodides, Bromides, and Chlorides. *Journal of the American Chemical Society* **2009,** *131* (34), 12078-12079.

19. Wu, X.; Hao, W.; Ye, K.-Y.; Jiang, B.; Pombar, G.; Song, Z.; Lin, S., Ti-Catalyzed Radical Alkylation of Secondary and Tertiary Alkyl Chlorides Using Michael Acceptors. *J. Am. Chem. Soc.* **2018,** *140* (44), 14836-14843.

20. Börjesson, M.; Moragas, T.; Martin, R., Ni-Catalyzed Carboxylation of Unactivated Alkyl Chlorides with CO2. *J. Am. Chem. Soc.* **2016,** *138* (24), 7504-7507.

21. Kim, S.; Goldfogel, M. J.; Gilbert, M. M.; Weix, D. J., Nickel-Catalyzed Cross-Electrophile Coupling of Aryl Chlorides with Primary Alkyl Chlorides. *Journal of the American Chemical Society* **2020,** *142* (22), 9902-9907.

22. Cybularczyk-Cecotka, M.; Szczepanik, J.; Giedyk, M., Photocatalytic strategies for the activation of organic chlorides. *Nature Catalysis* **2020,** *3* (11), 872-886.

23. Meyer, A. U.; Slanina, T.; Heckel, A.; König, B., Lanthanide Ions Coupled with Photoinduced Electron Transfer Generate Strong Reduction Potentials from Visible Light. *Chemistry – A European Journal* **2017,** *23* (33), 7900-7904.

24. Michelet, B.; Deldaele, C.; Kajouj, S.; Moucheron, C.; Evano, G., A General Copper Catalyst for Photoredox Transformations of Organic Halides. *Organic Letters* **2017,** *19* (13), 3576-3579.

25. Discekici, E. H.; Treat, N. J.; Poelma, S. O.; Mattson, K. M.; Hudson, Z. M.; Luo, Y.; Hawker, C. J.; de Alaniz, J. R., A highly reducing metal-free photoredox catalyst: design and application in radical dehalogenations. *Chem. Commun.* **2015,** *51* (58), 11705-11708.

26. Ghosh, I.; Ghosh, T.; Bardagi, J. I.; König, B., Reduction of aryl halides by consecutive visible light-induced electron transfer processes. *Science* **2014,** *346* (6210), 725.

27. Jiang, M.; Li, H.; Yang, H.; Fu, H., Room-Temperature Arylation of Thiols: Breakthrough with Aryl Chlorides. *Angew. Chem. Int. Ed.* **2017,** *56* (3), 874-879.

28. Schmalzbauer, M.; Ghosh, I.; König, B., Utilising excited state organic anions for photoredox catalysis: activation of (hetero)aryl chlorides by visible light-absorbing 9-anthrolate anions. *Faraday Discussions* **2019,** *215* (0), 364-378.

29. Zhang, L.; Jiao, L., Visible-Light-Induced Organocatalytic Borylation of Aryl Chlorides. *Journal of the American Chemical Society* **2019,** *141* (23), 9124-9128.

30. Liang, K.; Li, T.; Li, N.; Zhang, Y.; Shen, L.; Ma, Z.; Xia, C., Redox-neutral photochemical Heck-type arylation of vinylphenols activated by visible light. *Chemical Science* **2020,** *11* (8), 2130-2135.

31. Connell, T. U.; Fraser, C. L.; Czyz, M. L.; Smith, Z. M.; Hayne, D. J.; Doeven, E. H.; Agugiaro, J.; Wilson, D. J. D.; Adcock, J. L.; Scully, A. D.; Gómez, D. E.; Barnett, N. W.; Polyzos, A.; Francis, P. S., The Tandem Photoredox Catalysis Mechanism of [Ir(ppy)2(dtb-bpy)]+ Enabling Access to Energy Demanding Organic Substrates. *Journal of the American Chemical Society* **2019,** *141* (44), 17646-17658.

32. Li, D.; Che, C.-M.; Kwong, H.-L.; Yam, V. W., Photoinduced C–C bond formation from alkyl halides catalysed by luminescent dinuclear gold(I) and copper(I) complexes. *J. Chem. Soc., Dalton Trans.* **1992,** (23), 3325-3329.

33. Su, Y.; Zhang, L.; Jiao, N., Utilization of Natural Sunlight and Air in the Aerobic Oxidation of Benzyl Halides. *Organic Letters* **2011,** *13* (9), 2168-2171.

34. Yin, H.; Carroll, P. J.; Anna, J. M.; Schelter, E. J., Luminescent Ce(III) Complexes as Stoichiometric and Catalytic Photoreductants for Halogen Atom Abstraction Reactions. *Journal of the American Chemical Society* **2015,** *137* (29), 9234-9237.

35. Revol, G.; McCallum, T.; Morin, M.; Gagosz, F.; Barriault, L., Photoredox Transformations with Dimeric Gold Complexes. *Angew. Chem. Int. Ed.* **2013,** *52* (50), 13342-13345.

36. Chow, P.-K.; Cheng, G.; Tong, G. S. M.; To, W.-P.; Kwong, W.-L.; Low, K.-H.; Kwok, C.-C.; Ma, C.; Che, C.-M., Luminescent Pincer Platinum(II) Complexes with Emission Quantum Yields up to Almost Unity: Photophysics, Photoreductive C-C Bond Formation, and Materials Applications. *Angew. Chem. Int. Ed.* **2015,** *54* (7), 2084-2089.

37. Mazzarella, D.; Magagnano, G.; Schweitzer-Chaput, B.; Melchiorre, P., Photochemical Organocatalytic Borylation of Alkyl Chlorides, Bromides, and Sulfonates. *ACS Catalysis* **2019,** *9* (7), 5876-5880.

38. Patel, N. R.; Kelly, C. B.; Jouffroy, M.; Molander, G. A., Engaging Alkenyl Halides with Alkylsilicates via Photoredox Dual Catalysis. *Organic Letters* **2016,** *18* (4), 764-767.

39. Narayanam, J. M. R.; Tucker, J. W.; Stephenson, C. R. J., Electron-Transfer Photoredox Catalysis: Development of a Tin-Free Reductive Dehalogenation Reaction. *Journal of the American Chemical Society* **2009,** *131* (25), 8756-8757.

40. Maji, T.; Karmakar, A.; Reiser, O., Visible-Light Photoredox Catalysis: Dehalogenation of Vicinal Dibromo-, α-Halo-, and α,α-Dibromocarbonyl Compounds. *The Journal of Organic Chemistry* **2011,** *76* (2), 736-739.

41. Föll, T.; Rehbein, J.; Reiser, O., Ir(ppy)3-Catalyzed, Visible-Light-Mediated Reaction of α-Chloro Cinnamates with Enol Acetates: An Apparent Halogen Paradox. *Organic Letters* **2018,** *20* (18), 5794-5798.

42. Hou, M.; Lin, L.; Chai, X.; Zhao, X.; Qiao, B.; Jiang, Z., Enantioselective photoredox dehalogenative protonation. *Chemical Science* **2019,** *10* (27), 6629-6634.

43. Zeng, G.; Li, Y.; Qiao, B.; Zhao, X.; Jiang, Z., Photoredox asymmetric catalytic enantioconvergent substitution of 3-chlorooxindoles. *Chemical Communications* **2019,** *55* (76), 11362-11365.

44. Matsubara, R.; Yabuta, T.; Md Idros, U.; Hayashi, M.; Ema, F.; Kobori, Y.; Sakata, K., UVA- and Visible-Light-Mediated Generation of Carbon Radicals from Organochlorides Using Nonmetal Photocatalyst. *The Journal of Organic Chemistry* **2018,** *83* (16), 9381-9390.

45. Giedyk, M.; Narobe, R.; Weiß, S.; Touraud, D.; Kunz, W.; König, B., Photocatalytic activation of alkyl chlorides by assembly-promoted single electron transfer in microheterogeneous solutions. *Nature Catalysis* **2020,** *3* (1), 40-47.

46. Sakai, H. A.; Liu, W.; Le, C. C.; MacMillan, D. W. C., Cross-Electrophile Coupling of Unactivated Alkyl Chlorides. *Journal of the American Chemical Society* **2020,** *142* (27), 11691-11697.

47. Claros, M.; Ungeheuer, F.; Franco, F.; Martin-Diaconescu, V.; Casitas, A.; Lloret-Fillol, J., Reductive Cyclization of Unactivated Alkyl Chlorides with Tethered Alkenes under Visible-Light Photoredox Catalysis. *Angewandte Chemie International Edition* **2019,** *58* (15), 4869-4874.

48. Shaw, M. H.; Twilton, J.; MacMillan, D. W. C., Photoredox Catalysis in Organic Chemistry. *The Journal of Organic Chemistry* **2016,** *81* (16), 6898-6926.

49. Prier, C. K.; Rankic, D. A.; MacMillan, D. W. C., Visible Light Photoredox Catalysis with Transition Metal Complexes: Applications in Organic Synthesis. *Chemical Reviews* **2013,** *113* (7), 5322-5363.

50. Crisenza, G. E. M.; Melchiorre, P., Chemistry glows green with photoredox catalysis. *Nature Communications* **2020,** *11* (1), 803.

51. McAtee, R. C.; McClain, E. J.; Stephenson, C. R. J., Illuminating Photoredox Catalysis. *Trends in Chemistry* **2019,** *1* (1), 111-125.

52. Wills, A. G.; Charvet, S.; Battilocchio, C.; Scarborough, C. C.; Wheelhouse, K. M. P.; Poole, D. L.; Carson, N.; Vantourout, J. C., High-Throughput Electrochemistry: State of the Art, Challenges, and Perspective. *Organic Process Research & Development* **2021,** *25* (12), 2587-2600.

53. Biyani, S. A.; Moriuchi, Y. W.; Thompson, D. H., Advancement in Organic Synthesis Through High Throughput Experimentation. *Chemistry–Methods* **2021,** *1* (7), 323-339.

54. Czyz, M. L.; Taylor, M. S.; Horngren, T. H.; Polyzos, A., Reductive Activation and Hydrofunctionalization of Olefins by Multiphoton Tandem Photoredox Catalysis. *ACS Catalysis* **2021,** *11* (9), 5472-5480.

55. Pagire, S. K.; Hossain, A.; Traub, L.; Kerres, S.; Reiser, O., Photosensitised regioselective [2+2]-cycloaddition of cinnamates and related alkenes. *Chemical Communications* **2017,** *53* (89), 12072-12075.

56. Li, R.; Ma, B. C.; Huang, W.; Wang, L.; Wang, D.; Lu, H.; Landfester, K.; Zhang, K. A. I., Photocatalytic Regioselective and Stereoselective [2 + 2] Cycloaddition of Styrene Derivatives Using a Heterogeneous Organic Photocatalyst. *ACS Catalysis* **2017,** *7* (5), 3097-3101.

57. Wu, Q.-A.; Ren, C.-C.; Chen, F.; Wang, T.-Q.; Zhang, Y.; Liu, X.-F.; Chen, J.-B.; Luo, S.-P., Heteroleptic copper(I) complexes as energy transfer photocatalysts for the intermolecular [2 + 2] photodimerization of chalcones, cinnamates and cinnamamides. *Tetrahedron Letters* **2021,** *72*, 153091.

58. De Angelis, F.; Fantacci, S.; Evans, N.; Klein, C.; Zakeeruddin, S. M.; Moser, J.-E.; Kalyanasundaram, K.; Bolink, H. J.; Grätzel, M.; Nazeeruddin, M. K., Controlling Phosphorescence Color and Quantum Yields in Cationic Iridium Complexes: A Combined Experimental and Theoretical Study. *Inorganic Chemistry* **2007,** *46* (15), 5989-6001.

59. Wang, F.-X.; Chen, M.-H.; Hu, X.-Y.; Ye, R.-R.; Tan, C.-P.; Ji, L.-N.; Mao, Z.-W., Ester-Modified Cyclometalated Iridium(III) Complexes as Mitochondria-Targeting Anticancer Agents. *Scientific Reports* **2016,** *6* (1), 38954.

60. Garces, F. O.; King, K. A.; Watts, R. J., Synthesis, structure, electrochemistry, and photophysics of methyl-substituted phenylpyridine ortho-metalated iridium(III) complexes. *Inorganic Chemistry* **1988,** *27* (20), 3464-3471.

61. Tordera, D.; Delgado, M.; Ortí, E.; Bolink, H. J.; Frey, J.; Nazeeruddin, M. K.; Baranoff, E., Stable Green Electroluminescence from an Iridium Tris-Heteroleptic Ionic Complex. *Chemistry of Materials* **2012,** *24* (10), 1896-1903.

62. Friedrich, A.; Bokareva, O. S.; Luo, S.-P.; Junge, H.; Beller, M.; Kühn, O.; Lochbrunner, S., Effective quenching and excited-state relaxation of a Cu(I) photosensitizer addressed by time-resolved spectroscopy and TDDFT calculations. *Chemical Physics* **2018,** *515*, 557-563.

63. Askey, H. E.; Grayson, J. D.; Tibbetts, J. D.; Turner-Dore, J. C.; Holmes, J. M.; Kociok-Kohn, G.; Wrigley, G. L.; Cresswell, A. J., Photocatalytic Hydroaminoalkylation of Styrenes with Unprotected Primary Alkylamines. *Journal of the American Chemical Society* **2021,** *143* (39), 15936-15945.

64. Bray, B. L., Large-scale manufacture of peptide therapeutics by chemical synthesis. *Nature Reviews Drug Discovery* **2003,** *2* (7), 587-593.

65. Wang, X., Challenges and outlook for catalytic direct amidation reactions. *Nature Catalysis* **2019,** *2* (2), 98-102.

66. Rablen, P. R.; McLarney, B. D.; Karlow, B. J.; Schneider, J. E., How Alkyl Halide Structure Affects E2 and SN2 Reaction Barriers: E2 Reactions Are as Sensitive as SN2 Reactions. *The Journal of Organic Chemistry* **2014,** *79* (3), 867-879.

67. Call, A.; Casadevall, C.; Acuña-Parés, F.; Casitas, A.; Lloret-Fillol, J., Dual cobalt–copper light-driven catalytic reduction of aldehydes and aromatic ketones in aqueous media. *Chemical Science* **2017,** *8* (7), 4739-4749.

68. Liao, J.; Yang, X.; Ouyang, L.; Lai, Y.; Huang, J.; Luo, R., Recent advances in cascade radical cyclization of radical acceptors for the synthesis of carbo- and heterocycles. *Organic Chemistry Frontiers* **2021,** *8* (6), 1345-1363.

69. Casadevall, C.; Pascual, D.; Aragón, J.; Call, A.; Casitas, A.; Casademont-Reig, I.; Lloret-Fillol, J., Light-driven reduction of aromatic olefins in aqueous media catalysed by aminopyridine cobalt complexes. *Chemical Science* **2022**.

70. Thauer, R. K., Methyl (Alkyl)-Coenzyme M Reductases: Nickel F-430-Containing Enzymes Involved in Anaerobic Methane Formation and in Anaerobic Oxidation of Methane or of Short Chain Alkanes. *Biochemistry* **2019,** *58* (52), 5198-5220.

71. Helvenston, M. C.; Castro, C. E., Nickel(I) octaethylisobacteriochlorin anion. An exceptional nucleophile. Reduction and coupling of alkyl halides by anionic and radical processes. A model for factor F-430. *Journal of the American Chemical Society* **1992,** *114* (22), 8490-8496.

72. Dey, M.; Kunz, R. C.; Lyons, D. M.; Ragsdale, S. W., Characterization of Alkyl-Nickel Adducts Generated by Reaction of Methyl-Coenzyme M Reductase with Brominated Acids. *Biochemistry* **2007,** *46* (42), 11969-11978.

73. Giedyk, M.; Goliszewska, K.; Gryko, D., Vitamin B12 catalysed reactions. *Chemical Society Reviews* **2015,** *44* (11), 3391-3404.

74. Buzzetti, L.; Crisenza, G. E. M.; Melchiorre, P., Mechanistic Studies in Photocatalysis. *Angewandte Chemie International Edition* **2019,** *58* (12), 3730-3747.

75. McTiernan, C. D.; Morin, M.; McCallum, T.; Scaiano, J. C.; Barriault, L., Polynuclear gold(i) complexes in photoredox catalysis: understanding their reactivity through characterization and kinetic analysis. *Catalysis Science & Technology* **2016,** *6* (1), 201-207.

76. Tanaka, K.; Iwama, Y.; Kishimoto, M.; Ohtsuka, N.; Hoshino, Y.; Honda, K., Redox Potential Controlled Selective Oxidation of Styrenes for Regio- and Stereoselective Crossed Intermolecular [2 + 2] Cycloaddition via Organophotoredox Catalysis. *Organic Letters* **2020,** *22* (13), 5207-5211.

77. Mishra, V.; Mishra, H.; Mukherjee, R., Generation and Properties of CoI/NiI Species Stabilized by a Tetradentate Pyridylpyrazole Ligand: Crystal Structures of Dialkyl-CoIII Complexes. *European Journal of Inorganic Chemistry* **2009,** *2009* (20), 2973-2980.

78. Heyrovský, M., The electroreduction of methyl viologen. *Journal of the Chemical Society, Chemical Communications* **1987,** (24), 1856-1857.

79. Watanabe, T.; Honda, K., Measurement of the extinction coefficient of the methyl viologen cation radical and the efficiency of its formation by semiconductor photocatalysis. *The Journal of Physical Chemistry* **1982,** *86* (14), 2617-2619.

80. Walborsky, H. M., The cyclopropyl radical. *Tetrahedron* **1981,** *37* (9), 1625-1651.

81. Mann, D. J.; Halls, M. D., Ring-opening of the cyclopropyl radical in the condensed phase: A combined density functional theory/molecular mechanics quasiclassical trajectory study. *Physical Chemistry Chemical Physics* **2002,** *4* (20), 5066-5071.

82. Tanko, J. M.; Drumright, R. E., Radical ion probes. 2. Evidence for the reversible ring opening of arylcyclopropylketyl anions. Implications for mechanistic studies. *Journal of the American Chemical Society* **1992,** *114* (5), 1844-1854.

83. Schrauzer, G. N.; Deutsch, E., Reactions of cobalt(I) supernucleophiles. The alkylation of vitamin B12s, cobaloximes(I), and related compounds. *J. Am. Chem. Soc.* **1969,** *91* (12), 3341-3350.

84. Dey, M.; Li, X.; Kunz, R. C.; Ragsdale, S. W., Detection of Organometallic and Radical Intermediates in the Catalytic Mechanism of Methyl-Coenzyme M Reductase Using the Natural Substrate Methyl-Coenzyme M and a Coenzyme B Substrate Analogue. *Biochemistry* **2010,** *49* (51), 10902-10911.

85. Anderson, T. J.; Jones, G. D.; Vicic, D. A., Evidence for a NiI Active Species in the Catalytic Cross-Coupling of Alkyl Electrophiles. *Journal of the American Chemical Society* **2004,** *126* (26), 8100-8101.

86. Tian, L.; Till, N. A.; Kudisch, B.; MacMillan, D. W. C.; Scholes, G. D., Transient Absorption Spectroscopy Offers Mechanistic Insights for an Iridium/Nickel-Catalyzed C–O Coupling. *Journal of the American Chemical Society* **2020,** *142* (10), 4555-4559.

87. Lin, Q.; Fu, Y.; Liu, P.; Diao, T., Monovalent Nickel-Mediated Radical Formation: A Concerted Halogen-Atom Dissociation Pathway Determined by Electroanalytical Studies. *J. Am. Chem. Soc.* **2021,** *143* (35), 14196-14206.

88. Ting, S. I.; Garakyaraghi, S.; Taliaferro, C. M.; Shields, B. J.; Scholes, G. D.; Castellano, F. N.; Doyle, A. G., 3d-d Excited States of Ni(II) Complexes Relevant to Photoredox Catalysis: Spectroscopic Identification and Mechanistic Implications. *Journal of the American Chemical Society* **2020,** *142* (12), 5800-5810.

89. Strieth-Kalthoff, F.; Glorius, F., Triplet Energy Transfer Photocatalysis: Unlocking the Next Level. *Chem* **2020,** *6* (8), 1888-1903.

90. Kandoth, N.; Pérez Hernández, J.; Palomares, E.; Lloret-Fillol, J., Mechanisms of photoredox catalysts: the role of optical spectroscopy. *Sustainable Energy & Fuels* **2021,** *5* (3), 638-665.

91. Greaves, M. E.; Johnson Humphrey, E. L. B.; Nelson, D. J., Reactions of nickel(0) with organochlorides, organobromides, and organoiodides: mechanisms and structure/reactivity relationships. *Catalysis Science & Technology* **2021,** *11* (9), 2980-2996.

92. Entz, E. D.; Russell, J. E. A.; Hooker, L. V.; Neufeldt, S. R., Small Phosphine Ligands Enable Selective Oxidative Addition of Ar–O over Ar–Cl Bonds at Nickel(0). *J. Am. Chem. Soc.* **2020,** *142* (36), 15454-15463.

93. Funes-Ardoiz, I.; Nelson, D. J.; Maseras, F., Halide Abstraction Competes with Oxidative Addition in the Reactions of Aryl Halides with [Ni(PMenPh(3−n))4]. *Chemistry – A European Journal* **2017,** *23* (66), 16728-16733.

94. Diccianni, J. B.; Katigbak, J.; Hu, C.; Diao, T., Mechanistic Characterization of (Xantphos)Ni(I)-Mediated Alkyl Bromide Activation: Oxidative Addition, Electron Transfer, or Halogen-Atom Abstraction. *Journal of the American Chemical Society* **2019,** *141* (4), 1788-1796.

95. Poremba, K. E.; Dibrell, S. E.; Reisman, S. E., Nickel-Catalyzed Enantioselective Reductive Cross-Coupling Reactions. *ACS Catalysis* **2020,** *10* (15), 8237-8246.

96. Diccianni, J.; Lin, Q.; Diao, T., Mechanisms of Nickel-Catalyzed Coupling Reactions and Applications in Alkene Functionalization. *Accounts of Chemical Research* **2020,** *53* (4), 906-919.

97. Kolahdouzan, K.; Khalaf, R.; Grandner, J. M.; Chen, Y.; Terrett, J. A.; Huestis, M. P., Dual Photoredox/Nickel-Catalyzed Conversion of Aryl Halides to Aryl Aminooxetanes: Computational Evidence for a Substrate-Dependent Switch in Mechanism. *ACS Catalysis* **2020,** *10* (1), 405-411.

98. Reeves, E. K.; Entz, E. D.; Neufeldt, S. R., Chemodivergence between Electrophiles in Cross-Coupling Reactions. *Chemistry – A European Journal* **2021,** *27* (20), 6161-6177.

99. Monos, T. M.; Sun, A. C.; McAtee, R. C.; Devery, J. J.; Stephenson, C. R. J., Microwave-Assisted Synthesis of Heteroleptic Ir(III)+ Polypyridyl Complexes. *The Journal of Organic Chemistry* **2016,** *81* (16), 6988-6994.

100.   Pannwitz, A.; Prescimone, A.; Wenger, O. S., Ruthenium(II)–Pyridylimidazole Complexes as Photoreductants and PCET Reagents. *European Journal of Inorganic Chemistry* **2017,** *2017* (3), 609-615.

101.   Luo, S.-P.; Mejía, E.; Friedrich, A.; Pazidis, A.; Junge, H.; Surkus, A.-E.; Jackstell, R.; Denurra, S.; Gladiali, S.; Lochbrunner, S.; Beller, M., Photocatalytic Water Reduction with Copper-Based Photosensitizers: A Noble-Metal-Free System. *Angewandte Chemie International Edition* **2013,** *52* (1), 419-423.

102.   Call, A.; Codolà, Z.; Acuña-Parés, F.; Lloret-Fillol, J., Photo- and Electrocatalytic H2 Production by New First-Row Transition-Metal Complexes Based on an Aminopyridine Pentadentate Ligand. *Chemistry – A European Journal* **2014,** *20* (20), 6171-6183.

103.   Peters, R.; Waldmeier, P.; Joncour, A., Efficient Synthesis of a 5-HT2C Receptor Agonist Precursor. *Organic Process Research & Development* **2005,** *9* (4), 508-512.

104.   Misiti, D.; Rimatori, V.; Gatta, F., The schmidt reaction with oxa- and azabenzocycloalkenones. *Journal of Heterocyclic Chemistry* **1973,** *10* (5), 689-696.

105.   Peprah, K.; Zhu, X. Y.; Eyunni, S. V. K.; Etukala, J. R.; Setola, V.; Roth, B. L.; Ablordeppey, S. Y., Structure–activity relationship studies of SYA 013, a homopiperazine analog of haloperidol. *Bioorganic & Medicinal Chemistry* **2012,** *20* (5), 1671-1678.

UNIVERSITAT ROVIRA I VIRGILI
VISIBLE-LIGHT METALLAPHOTOREDOX STRATEGIES FOR ORGANIC TRANSFORMATIONS THROUGH THE CLEAVAGE
OF CSP3-CL BONDS
Jordi Aragón Artigas

CHAPTER V:

Cyclopropanation of Alkenes Using Dichloromethane *via* Photoredox Catalysis
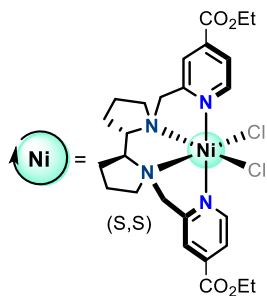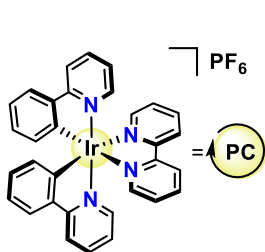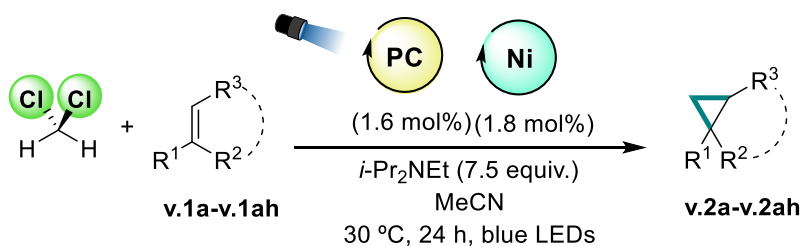
UNIVERSITAT ROVIRA I VIRGILI
VISIBLE-LIGHT METALLAPHOTOREDOX STRATEGIES FOR ORGANIC TRANSFORMATIONS THROUGH THE CLEAVAGE
OF CSP3-CL BONDS
Jordi Aragón Artigas

5.1. State of the art

The cyclopropane ring displays a crucial role in medicinal chemistry and drug discovery, as one of the prevalent groups present in small biologically active molecules.[1-3] Its structure presents uncommon features: three coplanar carbon atoms with shorter C−C bonds (1.51 Å), a more intense π-character of the C−C bonds, and stronger C−H bonds (106 kcal/mol) compared to those in alkanes (100 kcal/mol).[3] Due to this exceptional architecture, cyclopropane ring serves an important function in nature as 1,2-disubstituted aromatic ring bioisostere,[1] enhancing the metabolic stability, bioactivity, and target specificity of the molecule.
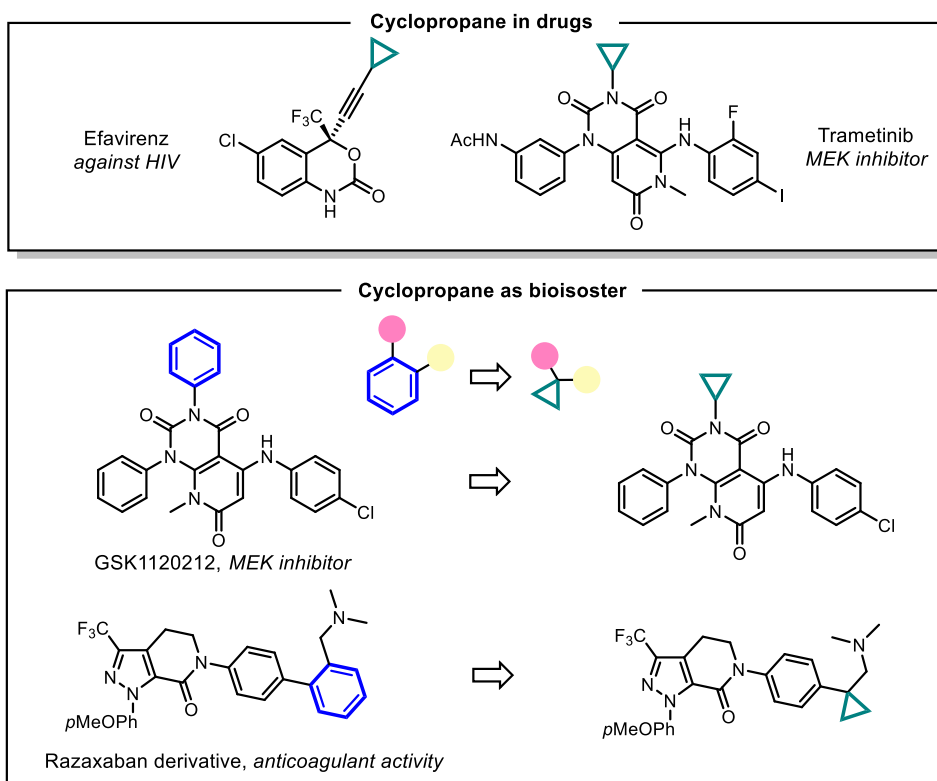
Figure 5. 1. Biological relevance of cyclopropane group.

At the same time, because of its unusual chemical skeleton structure of the cyclopropanes, the 3-membered rings strain (27 kcal/mol) limits their manipulation, presenting synthetic challenges[4] faced since the first synthesis of the cyclopropane ring by August Freund in 1882.[5]

In this sense, the Simmons-Smith reaction emerged as the most exploited method for the addition of a methylene or other simple alkylidene groups to alkenes in cyclopropanation synthetic strategies. The originally method employed diiodomethane with a copper-zinc in the presence of an alkene to give a cyclopropane (Scheme 5. 1, a), in which an α-iodomethylmetal species (ICH_2ZnI) is generally regarded as key intermediate. [6-8]

From here, a large variety of modifications (including the use of other halomethanes or diazo compounds as C_1 source together with a transition metal catalyst) were developed with the aim of expanding the scope of this strategy (Scheme 5. 1, b).[9, 10] The lack of general applicability can be assigned to the use of carbenoid intermediates, which rarely work under mild conditions, but also the requirement of considerable excess of reagents and the presence of toxic and hard to handle precursors (diazoalkane reagents are inherently unstable in the absence of electron-withdrawing substituents). Alternatively, under alkaline conditions in an organic solvent, promoted by an alchoxide, chloroform undergoes decomposition to give a free carbene. Doering and Hoffman proved that a solution of ^{t}BuOK in ^{t}BuOH with chloroform and in the presence of an alkene generates a vigorously exothermic reaction to generate cyclopropane ring. However, this route also presents low practicability in common synthetic routes, limited to the formation of 1,1-dichlorocyclopropil derivates (Scheme 5. 1, c).[11-13] Therefore, establishing new and readily available C_1 synthons is key for the advance in broadly applicable cyclopropanation methods.

Compared to previous halomethanes, dichloromethane (CH_2Cl_2) is one of the most readily commercially available, cheap and accessible. CH_2Cl_2 is commonly

used as a common solvent in a plethora of synthetic methodologies and purification protocols due to its inertness. However, if the innerness is overcome, could be for the same reasons and excellent C_1 synthon in synthetic chemistry. Indeed, the use of CH_2Cl_2 as substrate remains challenging in current synthetic methodologies, with only a few examples of success.[14] In 2016, Uyeda and coworkers reported a cyclopropanation of alkenes based on a dinuclear nickel catalytic system, in which a low-valent nickel complex promotes an oxidative addition of a 1,1-dichloroalkane reagent, forming an organometallic intermediate. Methylene transfer to an organic substrate yields an oxidized $NiCl_2$ complex, which then undergoes two-electron reduction to close the catalytic cycle, using an excess of zinc as stoichiometric reductant (3 equiv.) (Scheme 5. 1, d).[15]
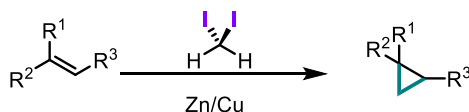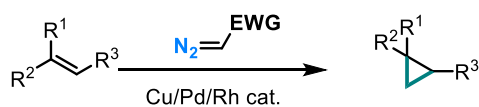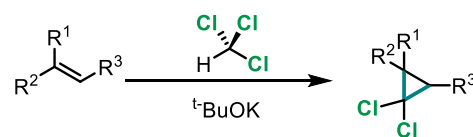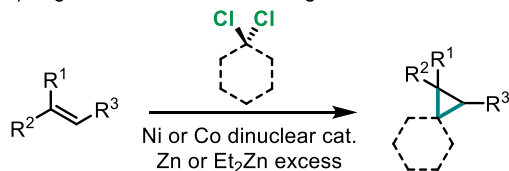
Scheme 5. 1. Carbene-based strategies for cyclopropanation.

At this point, SET strategies by photoredox catalysis enabled the use of mild conditions through the generation of radicals, expanding the window of potential possibilities. In 2017, Suero and coworkers presented the first stereoconvergent cyclopropanation of styrenes using CH_2I_2 as a triplet carbene equivalent under white LED irradiation (Scheme 5. 2).[16] The irradiation of the ruthenium catalyst $[Ru(bpy)_3]^{2+}$ with visible light in the presence of DIPEA triggers a well-established SET process promoting the iodomethyl radical formation. The subsequent radical addition to aromatic alkenes leads to the formation of benzylic radical species, which can undergo a homolytic substitution for the final cyclization.
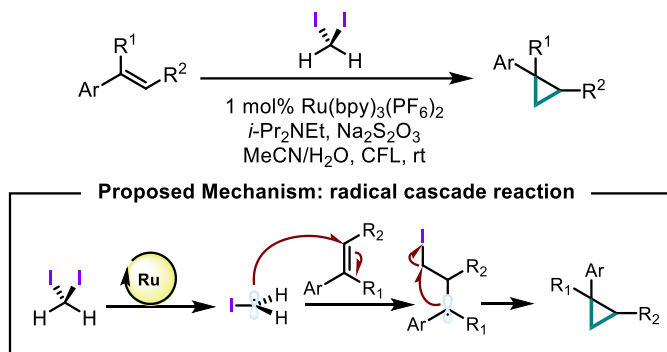
M. Suero and co-workers, *Angew. Chem. Int. Ed.,* **2016**, *55*, 1-5.

Scheme 5. 2. Triplet carbene equivalent photogeneration strategy for cyclopropanation of aromatic olefins.

In 2018, Molander and coworkers, evolved the methodology of using CH_2I_2 under photochemical conditions, and developed a photoredox cyclopropanation of 1-aryl-1-trifluoromethyl alkenes using a iodomethylsilicate as C_1 synthon (Scheme 5. 3.).[17] In this example, they introduced the concept of radical/polar crossover *via* a photogenerated iodomethyl radical addition to an electrodeficient alkene followed by radical SET reduction, undergoing an anionic 3-*exo-tet* cyclization, under mild conditions. They supported this hypothesis by an

exhaustive theoretical study of the anionic 3-exo-tet cyclization *versus* the radical pathway, together with experimental evidences.
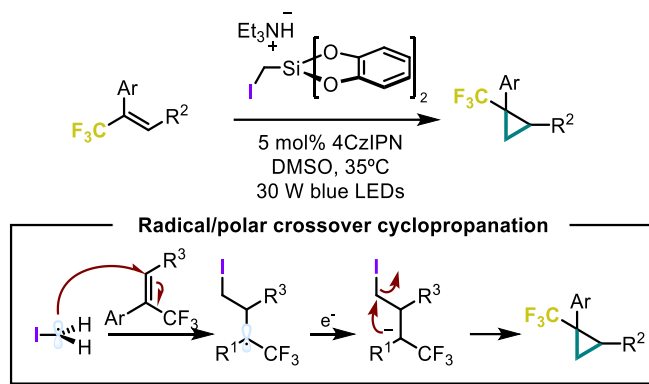

G. Molander and co-workers, *J. Am. Chem. Soc.*, **2018**, *140*, 8037-8047.

Scheme 5. 3. Redox-neutral photocatalytic cyclopropanation via radical/polar crossover.

It should be noted that Rusling introduced the radical/polar crossover concept for cyclopropanation of styrene in 2001.[18] In his work, vitamin B_{12} (a cobalt corrin complex) activated the Csp^3−Cl bond from dichloromethane forming the corresponding 1-chloromethyl radical under electrochemical conditions, followed by an analogous radical/polar crossover cyclopropanation. Notwithstanding, this work lacked of synthetic application, and focused on the mechanistic study of the electrochemical activation of CH_2Cl_2 with Co^I−L from vitamin B_{12} and the proof of concept for the cyclopropanation of styrene.

In this sense, merging a photoredox SET strategy with the use of CH_2Cl_2 as C_1 synthon is pivotal for an efficient cyclopropanation under mild conditions. At this point, our background in the field of photoredox transformations and the activation of Csp^3−Cl bonds was crucial. In the previous Chapters, we have brought to light a catalytically active family of tetradentated *N*-based Ni/Co complexes (*Chapter III*) towards the cleavage of inert Csp^3−Cl bonds, together

with a well-studied dual metal Ir/Ni system capable of performing the photoredox activation of primary alkyl chlorides towards a cross-coupling reaction (*Chapter IV*). In this chapter, we target the activation of dichloromethane in a equivalent approach. Even though CH_2Cl_2 is a stable compound used as a common solvent in chemical research and manufacturing, its Csp^3−Cl bond dissociation energy (272 kJ mol-1) should be accessible for our developed dual-catalytic photoredox systems. Consequently, we plan to fill this gap in synthetic methodology by using a dual metallaphotoredox system which generates radicals from CH_2Cl_2, trapping them by an alkene, and after a radical / polar crossover step, a 3-*exo-tet* cyclization would achieve the cyclopropanation (Scheme 5. 4).
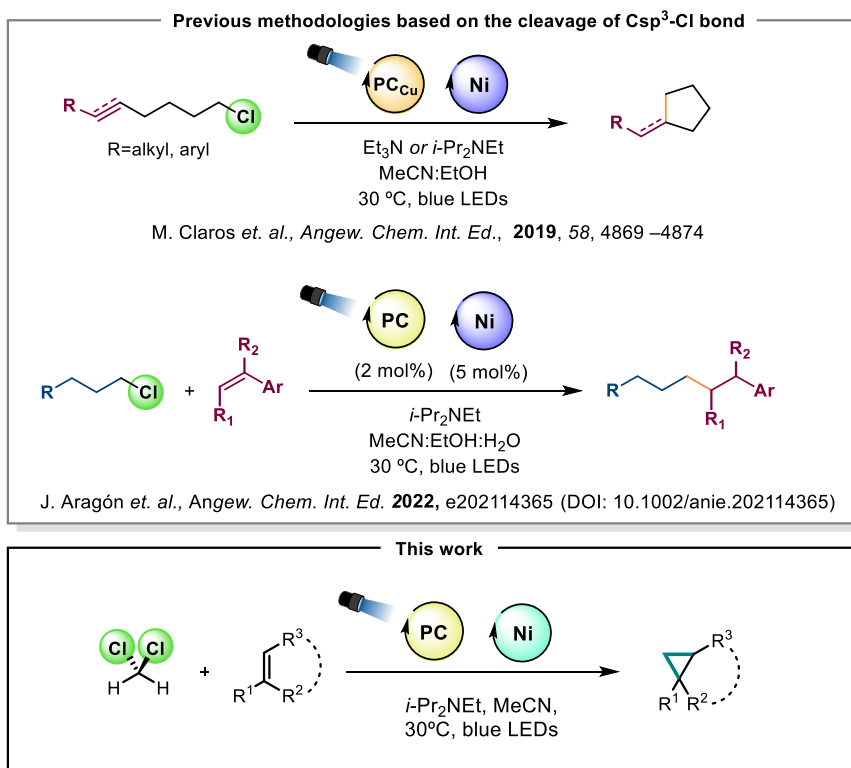
Scheme 5. 4. Evolution of the developed methodologies in our group based on Csp3-Cl bond activation.

5.2. Results and Discussion

5.2.1. Development of the reaction by high throughput techniques

Preliminary studies of reactivity using styrene

Chapter IV shows that HTE is an outstanding procedure for the discovery and development of new photoredox methodologies. Continuing with this approach, we proceeded with the discovery and the development of a new cyclopropanation of olefins. Initially, we selected styrene (**iv.2a**) as model olefin (Scheme 5. 5), due to its proved reactivity against radicals coming from alkyl chlorides.
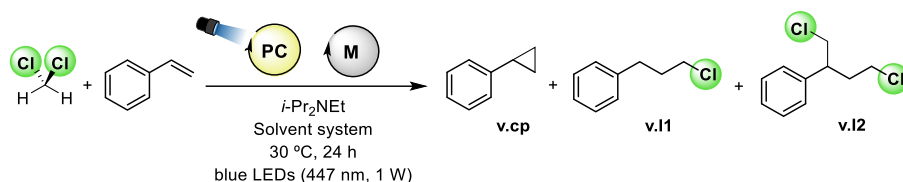
Scheme 5. 5. Initial model cyclopropanation reaction for optimization.

We focused our efforts on searching for an appropriate catalytic system able to reach our desired cyclopropane product (**v.cp**). We started with the dual catalytic system developed in *Chapter IV* (**PC$_{Ir}$^{NMe2}** and **[Py$_2$^{Ts}tacn)Ni](OTf)$_2$** in MeCN/CH$_2$Cl$_2$ (1:1) (Table 5. 1). We excluded protic solvents from the reaction mixture to avoid the protonation of the benzylic anion and promote the 3-*exo-tet* cyclization. We started using CH$_2$Cl$_2$ as solvent, in a large excess, to favor the desired reactivity.

Despite obtaining full conversion of the olefin, we did not achieve the cyclopropanation. Instead, we identified (3-chloropropyl)-1-benzene (**v.I1**) and (1,4-dichlorobutan-2-yl)benzene (**v.I2**) as minor products, proving that our previous system could successfully activate the Csp^3−Cl bond from CH_2Cl_2. The other products were mainly the coupling product between the alkene and the electron donor, and the homocoupling products coming from the benzylic radical after the addition of the chloromethyl radical to the olefin. Moreover, the formation of **v.I2** came from a double insertion of chloromethyl radicals to the olefin, indicating that we were not promoting the reduction of the benzylic radical. However, the formation of **v.I1** and **v.I2** encouraged us to further optimize the process. In particular, we did not observe drastic changes in the catalytic outcome by changing the % and ratio of catalyst / PC, highlighting the potential of the reaction under low % of the dual metal system.

Table 5. 1. Evaluation of the previous catalytic system against cyclopropanation.
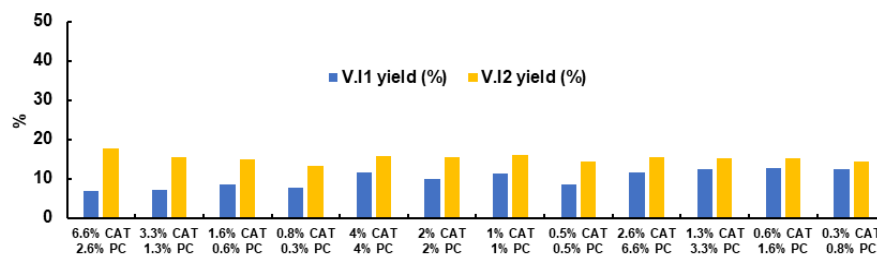
General procedure A: Styrene (24 mM), **PC_{Ir}^{NMe2}** (x mol %), (**$Py_2^{Ts}tacn$)Ni(OTf)$_2$** (x mol %), DIPEA (7.5 equiv.) in MeCN: **CH_2Cl_2** 1:1 (80 equiv.), $V_T = 300$ μL. Blue LED irradiation (1 W, 447 nm). GC-FID yields.

With these preliminary results in hand, we hypothesized that decreasing the catalytic activity of the system should result in a mitigation of the generation of chloromethyl radicals, minimizing **v.I2** formation. Consequently, we tested a library of 22 Ni and Co catalysts and 4 photocatalysts (**PC_{Ir}^{COOEt}**, **PC_{Ir}^{H}**, **PC_{Ir}^{NMe2}** and **PC_{Cu}**) as potential candidates to tune the catalytic activity. In particular, we

used as catalysts: the family of complexes from *Chapter III* **[(^{X}TPA)MCl$_2$,** **(^{X}PDP)MCl$_2$ and (^{X}MCP)MCl$_2$**, M= Ni, Co, X= H, DMM, CO$_2$Et], the well-known pentacoordinated catalyst from *Chapter IV* [**(Py$_2$^{Ts}tacn)M(OTf)$_2$**, M=Ni, Co], also **(^{DMM}Py$_2$^{Ts}tacn)Ni(OTf)$_2$**, and an alternative pentacoordinated N-based Ni catalyst [**(^{H}DPA)Ni(OTf)$_2$**, DPA=([2,2'-bipyridin]-6-yl)-N,N-bis(pyridin-2-ylmethyl)methanamine].

We organized the data by the PC to have a general view of the results (Table 5.2). Within the photocatalysts a pattern started to appear, higher the redox potential higher the **v.I2** yield, including the blanks without including the Ni, or Co complexes.

In contrast, for the less reducing ones, (**PC$_{Ir}$^{COOEt}** and **PC$_{Cu}$**) the reactivity decreased in almost all of cases with the exception of when using (**^{CO2Et}PDP)NiCl$_2$** and (**^{CO2Et}MCP)NiCl$_2$** as catalysts. At this point we summarize that the CH$_2$Cl$_2$ can be directly activated with strongly reducing photocatalysts like **PC$_{Ir}$^{NMe2}**, and that could be possible that the CH$_2$Cl$_2$ activation is facilitated in the presence of (**^{CO2Et}PDP)NiCl$_2$** and (**^{CO2Et}MCP)NiCl$_2$** opening a door to further control the reactivity. However, their catalytic activity was 10% lower in combination with the powerful **PC$_{Ir}$^{NMe2}**. We assigned this counterintuitive event to over reactivity mentioned before. **PC$_{Ir}$^{NMe2}** caused more side reactions than the other PCs. Consequently, we selected (**^{CO2Et}PDP)NiCl$_2$** and (**^{CO2Et}MCP)NiCl$_2$** as potential candidates for further reaction development and **PC$_{Ir}$^{H}** as the optimal photocatalyst.

Table 5.2. Screening of catalyst and photocatalysts.
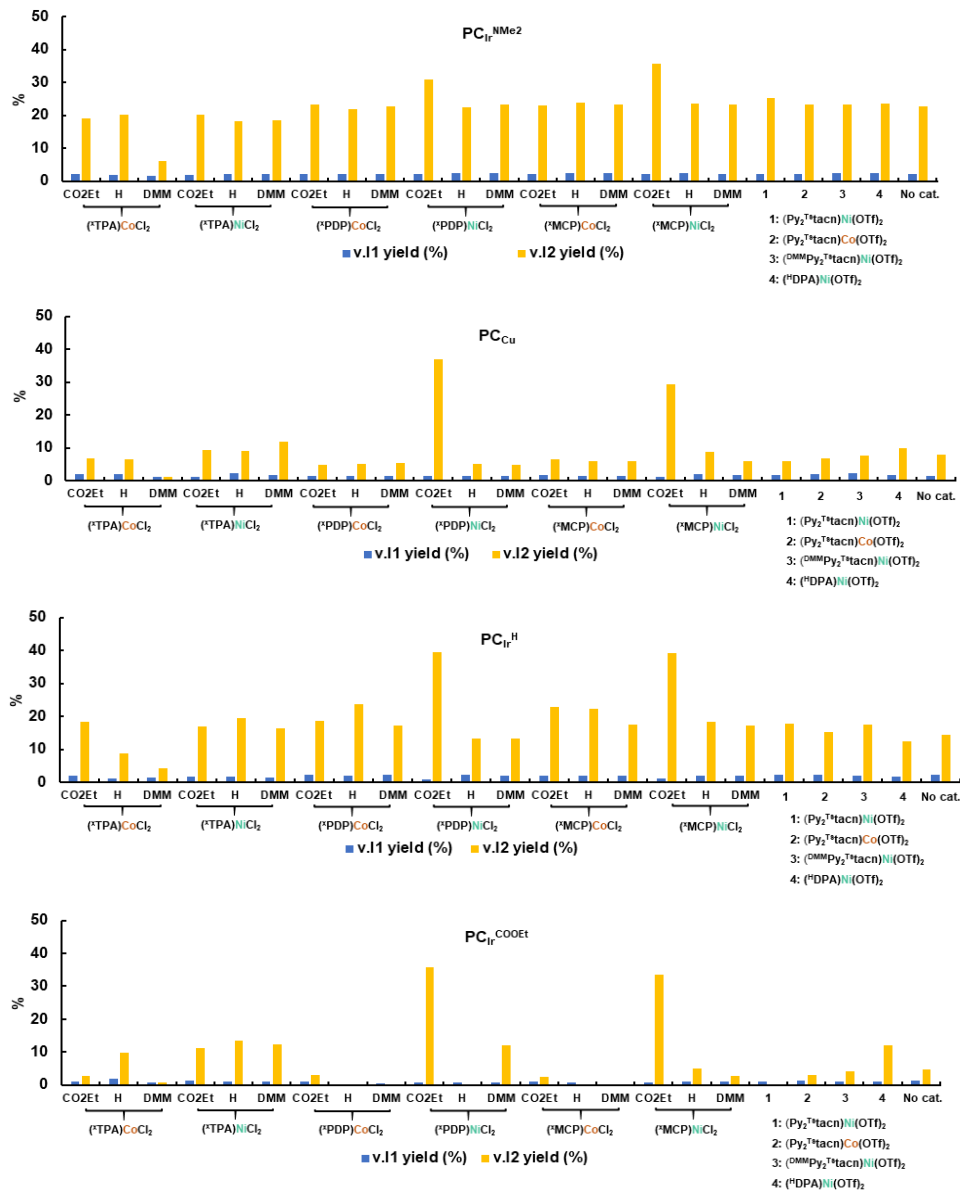
General procedure A: Styrene (24 mM), PC (1 mol %), catalyst (1 mol %), DIPEA (7.5 equiv.) in MeCN: **CH₂Cl₂** 1:1 (80 equiv.), V_T = 300 μL. Blue LED irradiation (1 W, 447 nm). GC-FID yields.

Then, different amounts of CH_2Cl_2 were tested to diminish side reactivity by increasing the number of available chloromethyl radicals in the reaction mixture (Table 5.3). When using a 1:1 CH_2Cl_2:CH_3CN solvent mixture , (**CO2EtPDP**)**NiCl₂** showed better catalytic activity towards **v.I2**. However, the increment of CH_2Cl_2 resulted in a proportional increase of **v.I2** but also the side products, with a total mitigation of **v.I1**.

Table 5.3. Screening of % of CH_2Cl_2 using (CO2EtPDP)NiCl₂ and (CO2EtMCP)NiCl₂ .
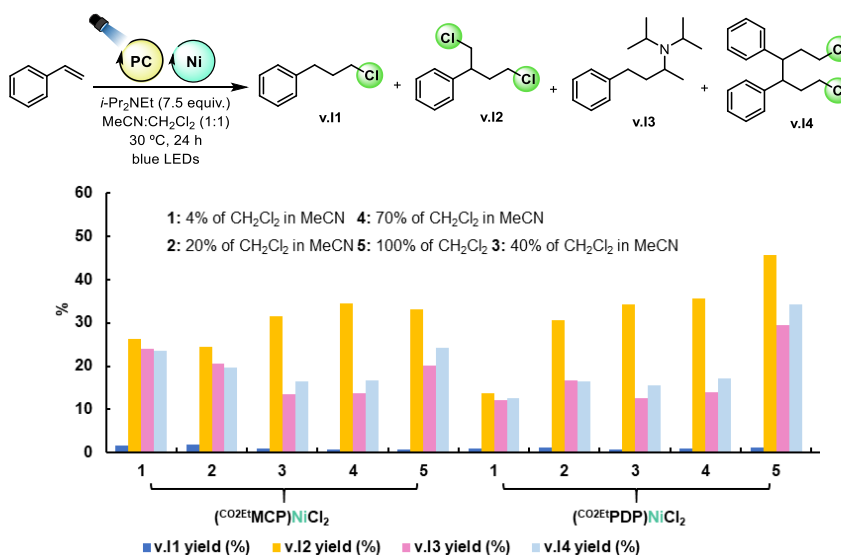
General procedure A: Styrene (24 mM), **PC_Ir^H** (1 mol %), (**CO2EtPDP**)**NiCl₂** or (**CO2EtMCP**)**NiCl₂** (1 mol %), DIPEA (7.5 equiv.) in MeCN: **CH₂Cl₂** 1:1 (80 equiv.), V_T = 300 µL. Blue LED irradiation (1 W, 447 nm). GC-FID yields.

Up to that moment, we were able to activate dichloromethane efficiently, but a cyclopropanation protocol was still missing. The high/fast reactivity of chloromethyl radicals in comparison with the reduction of the benzylic anions seemed to be the main barrier for the desired reactivity. Therefore, we employed olefins with less reducing potential of the corresponding benzylic radical, to facilitate the radical/polar crossover formation of the radical anion. In that direction, 1,1-diphenylethylene (**v.1a**) presented promising results when using the best catalytic conditions, with cyclopropanation being the principal outcome (55%

yield, Scheme 5.6). This result encouraged us to change the model substrate for **v.1a**, resuming the process of optimization.
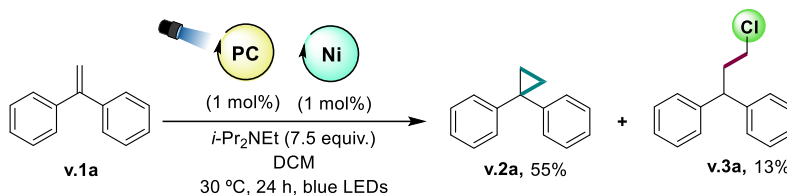
Scheme 5. 6. Preliminar cyclopropanation of ,1-diphenylethylene. Styrene (24 mM), **PC$_{Ir}^H$** (1 mol %), (**^{CO2Et}PDP)NiCl$_2$** (1 mol %), DIPEA (7.5 equiv.) in MeCN: CH$_2$Cl$_2$ 1:1 (80 equiv.), V$_T$ = 300 µL. Blue LED irradiation (1 W, 447 nm). GC-FID yields.

Optimization of photoredox cyclopropanation reaction

Preliminary results showed that the selected catalytic system has high efficiency for the catalytic conversion of CH$_2$Cl$_2$ and reaction with the alkene. Testing different ratios of catalyst:photocatalyst increase the **v.1a** yield up to 65%. (Table 5.4). The following optimization steps targeted the **v.2a** yield, with the most cost-effective conditions. Then, we decreased considerably the amount of CH$_2$Cl$_2$ to 10 equiv. in MeCN, obtaining an improvement of the reactivity with an 84% yield of cyclopropanation (Table 5.5). Albeit a excess of CH$_2$Cl$_2$ is required, its ready availability and low price.

Table 5.4. Screening of the optimal % of catalyst and photocatalyst.
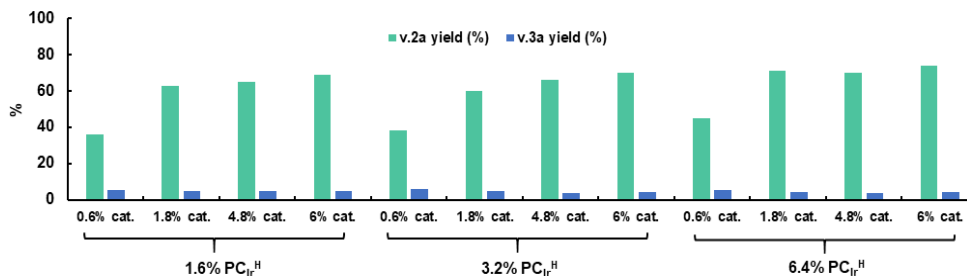
General procedure A: **v.2a** (24 mM), **PC$_{Ir}^{H}$** (x mol %), (**^{CO2Et}PDP)NiCl$_2$** (x mol %), DIPEA (7.5 equiv.) in **CH$_2$Cl$_2$**, V$_T$ = 300 μL. Blue LED irradiation (1 W, 447 nm). GC-FID yields.

Table 5. 5. Optimization of the required amount of dichloromethane.
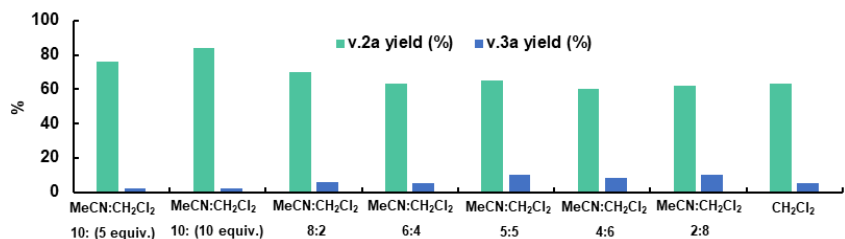
General procedure A: **v.2a** (24 mM), **PC$_{Ir}^{H}$** (1.6 mol %), (**^{CO2Et}PDP)NiCl$_2$** (1.8 mol %), DIPEA (7.5 equiv.) in different mixtures of **MeCN:CH$_2$Cl$_2$**, V$_T$ = 300 μL. Blue LED irradiation (1 W, 447 nm). GC-FID yields.

As the last step of this process of optimization, we wondered if this 84% yield of **v.2a** could be improved by reducing the DIPEA side reactivity. With this intention, we followed the same reasoning from *Chapter IV*, adding water to the solvent system (Table 5.6). Interestingly, the increment of water in the solvent system resulted in a clear exchange of the selectivity of the reaction, where **v.3a** was the main product. The presence of a protic source in the reaction mixture clearly protonated the benzylic radical anion intermediate, confirming our mechanistic hypothesis. This evidence potentially unlocks a different

methodology by activating dichloromethane, and we further explore it in next section 5.2.3.

Table 5. 6. The effect of water in the catalytic response of the system.
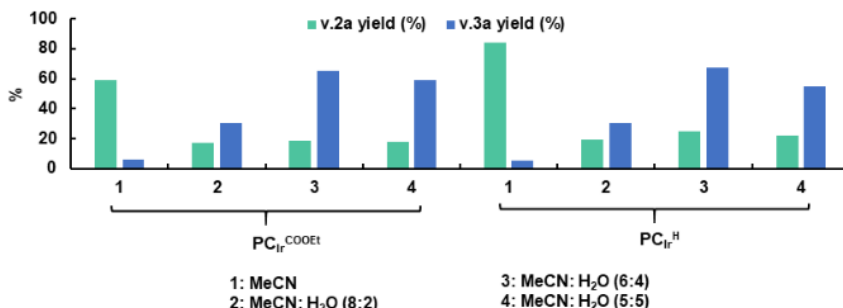
General procedure A: **v.2a** (24 mM), **PC** (1.6 mol %), **(^{CO2Et}PDP)NiCl$_2$** (1.8 mol %), CH$_2$Cl$_2$ (10 equiv.), DIPEA (7.5 equiv.) in different MeCN, V_T = 300 μL. Blue LED irradiation (1 W, 447 nm). GC-FID yields.

PC$_{Ir}$^{COOEt} was also tested, considering its high catalytic response and few side products (Table 5.2). However, **PC$_{Ir}$^{H}** still presented higher yields against cyclopropanation (Table 5.6). Then, we focused on the **(^{CO2Et}PDP)NiCl$_2$** and **PC$_{Ir}$^{H}** system, even though the selection was based on the previous reactivity with styrene.

Finally, we reevaluated the other catalytic system under the optimized conditions (Table 5.7). Noticeably, the whole family of tetracoordinated complexes from *Chapter III* presented relevant catalytic behaviour for cyclopropanation of **v.1a**. In general, cobalt catalysts presented lower **v.2a** yields than their nickel analogues, with less conversion of the alkene **v.1a**. Electrodeficient groups at the ligands of the nickel catalysts enhanced the

cyclopropanation and the highly reducing photocatalysts as PC_{Cu} and PC_{Ir}^{NMe2} clearly limited the reactivity of the system.

Table 5.7. Evaluation of the catalytic response of different catalysts and photocatalysts.
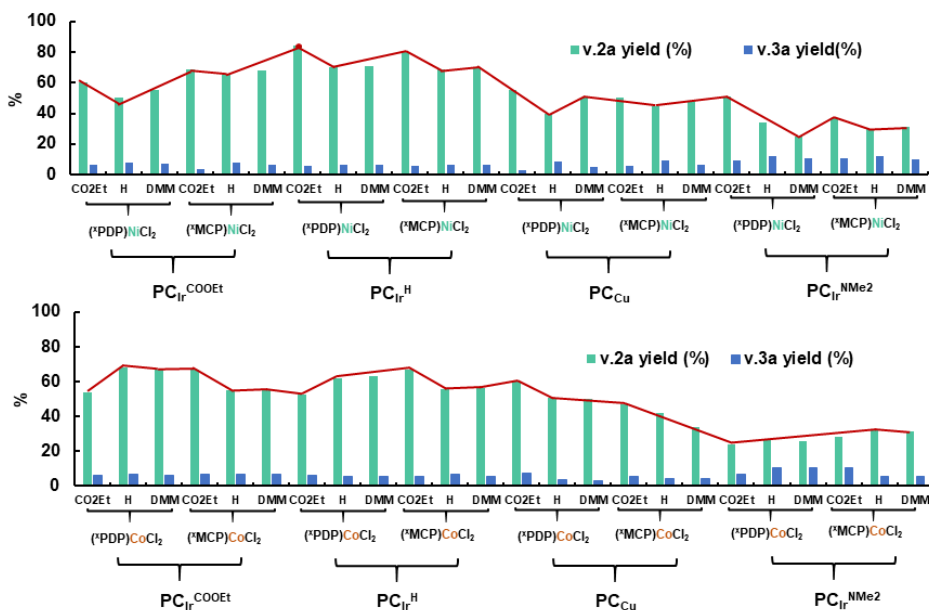
General procedure A: **v.2a** (24 mM), **PC** (1.6 mol %), **catalyst** (1.8 mol %), **CH₂Cl₂** (10 equiv.), DIPEA (7.5 equiv.) in MeCN, V_T = 300 μL. Blue LED irradiation (1 W, 447 nm). GC-FID yields.

As a consequence of this comprehensive high-throughput procedure, the system was really pushed and optimized for the efficient activation of dichloromethane under mild and diluted catalyst conditions, involving: only 10 equiv. of CH₂Cl₂, 24 mM concentration of **v.1a**, 1.6% of PC_{Ir}^{H} and 1.8% (^{CO2Et}**PDP)NiCl₂** in MeCN, under blue LED irradiation (447 nm) at 30ºC.

Delimitation of the reaction borders

For an initial understanding of the reaction mechanism and the reaction borders, we interrogated the system by performing control experiments (Table 5. 8). A rational ligand design and catalyst screening allowed us to find **(^{COOEt}PDP)NiCl$_2$** as the best candidate, giving 84% yield for the cyclopropanation of 1,1-diphenylethylene. We had already highlighted the importance of pentacoordinated nitrogen-based ligands, and specially Py$_2$^{Ts}tacn, for the activation of chloroalkanes. However, in this case the optimal formation of chloromethyl radicals from CH$_2$Cl$_2$ was not found using pentacoordinated complexes, obtaining moderated selectivity towards our desired reaction (

Table 5. 8, entries 2, 5 and 6), where nickel still presented better reactivity than cobalt or iron (

Table 5. 8, entries 3 and 4). We also tested NiCl$_2$ glyme or other Ni(II) catalysts based on commercially available ligands such as 2,2'-dipyridyl (bpy), 4,4'di-tert-butyl-2,2'-dipyridyl (dtbbpy) or phenanthroline (phen) and all of them presented poor reactivity (

Table 5. 8, entries 7-10). In contrast, the tetracoordinated N-based nickel catalyst **(^{COOEt}PDP)NiCl$_2$** gave an excellent balance between reactivity and selectivity to the catalytic system, becoming the definitive catalyst.

Control experiments demonstrated that every component of the catalytic system (**(^{CO2Et}PDP)NiCl$_2$, PC$_{Ir}$^{H}**, DIPEA and blue LED) was required to yield the desired product (

Table 5. 8, entries 12-16). No reactivity was found when $\textbf{PC}_{\textbf{Ir}}{}^{\textbf{H}}$ or blue irradiation were excluded, confirming a light-mediated transformation. When DIPEA was also excluded from the reaction mixture, the alkene was not fully recovered (20% conv.) due to EnT process from the $\textbf{PC}_{\textbf{Ir}}{}^{\textbf{H}}$ excited state to the olefin. This process was avoided by the efficiency of the system in presence of $(^{\textbf{CO2Et}}\textbf{PDP})\textbf{NiCl}_2$ and DIPEA.

Table 5. 8. Screening of catalysts and control experiments.
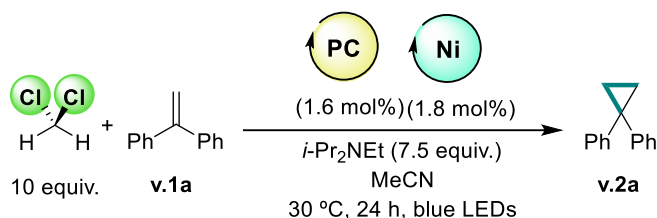
Entry	Deviation from standard conditions	% Yield (Conv.)
1	none	84 (100)
2	$[\textbf{Ni(Py}_2{}^{\textbf{Ts}}\textbf{tacn)(OTf)}_2]$ instead of $(^{\textbf{CO2Et}}\textbf{PDP})\textbf{NiCl}_2$	73 (100)
3	$[\textbf{Co(Py}_2{}^{\textbf{Ts}}\textbf{tacn)(OTf)}_2]$ instead of $(^{\textbf{CO2Et}}\textbf{PDP})\textbf{NiCl}_2$	64 (100)
4	$[\textbf{Fe(Py}_2{}^{\textbf{Ts}}\textbf{tacn)(OTf)}_2]$ instead of $(^{\textbf{CO2Et}}\textbf{PDP})\textbf{NiCl}_2$	13 (41)
5	$[\textbf{Ni(dpa-bpy)(OTf)}_2]$ instead of $(^{\textbf{CO2Et}}\textbf{PDP})\textbf{NiCl}_2$	66 (100)
6	$[\textbf{Ni(Me}_3\textbf{tacn)(OTf)}_2]$ instead of $(^{\textbf{CO2Et}}\textbf{PDP})\textbf{NiCl}_2$	33 (100)
7	$\textbf{NiCl}_2 \textbf{. glyme}$ instead of $(^{\textbf{CO2Et}}\textbf{PDP})\textbf{NiCl}_2$	12 (30)
8	$(\textbf{bpy})\textbf{NiCl}_2$ instead of $(^{\textbf{CO2Et}}\textbf{PDP})\textbf{NiCl}_2$	30 (66)
9	$(\textbf{phen})\textbf{NiCl}_2$ instead of $(^{\textbf{CO2Et}}\textbf{PDP})\textbf{NiCl}_2$	22 (51)
10	$(\textbf{dtbbpy})\textbf{NiCl}_2$ instead of $(^{\textbf{CO2Et}}\textbf{PDP})\textbf{NiCl}_2$	30 (42)
11	$(\textbf{py})_2\textbf{NiCl}_2$ instead of $(^{\textbf{CO2Et}}\textbf{PDP})\textbf{NiCl}_2$	14 (28)
12	no $\textbf{1}_{\textbf{Ni}}$	13 (51)

13	no **PC$_{Ir}^{H}$**	0 (7)
14	no DIPEA	0 (20)
15	no CH$_2$Cl$_2$	0 (27)
16	no Blue LED irradiation	0 (4)

General procedure B: **v.2a** (24 mM), **PC** (1.6 mol %), **catalyst** (1.8 mol %), **CH$_2$Cl$_2$** (10 equiv.), DIPEA (7.5 equiv.) in MeCN, $V_T = 2$ mL. Blue LED irradiation (1 W, 447 nm). Conversion and yield of screening reactions were determined by GC-FID using biphenyl as an internal standard. GC-FID yield averages of at least three reactions.

5.2.2. Scope of the reaction

Encouraged by these results and in collaboration with Suyun Sun, we explored the generality of the use of dichloromethane as C$_1$ synthon for the cyclopropanation of olefins (Table 5.9). We found that the reaction conditions were rather general, with notable high chemoselectivity, obtaining in most of the cases over 70% and up to 89% yield. The mild reaction conditions allowed a broad functional group tolerance, including ethers (**v.2b-v.2g**), acetal (**v.2h**), nitriles (**v.2j-v.2m**), alkyl chains (**v.2e, v2.m**), amines (**v.2l**) and fused rings (**v.2z-v.2aa**). Initially, we considered a possible electronic effect of the aromatic ring to the reactivity of the alkene. However, no appreciable differences were observed in the reactivity when the substituent was located in *ortho*, *meta* or *para* positions, as shown in cases **v.2b-v.2d** and **v.2j-v.2l**, using a methoxy or a cyanide group as substituents. Furthermore, this methodology gave excellent chemoselectivity in presence of aryl iodides (**v.2e**), aryl bromides (**v.2r, v.2ad**), aryl chlorides (**v.2q, v.2ac**), alkyl/aryl fluorides (**v.2m-v.2p**) and pseudohalogens (**v.2t**), illustrating the compatibility of the current strategy with other classical cross-coupling reactions and serving as an additional tool for further functionalization in the synthesis of complex molecules. In this regard the use of a tetradentated N-based Ni catalyst

together with low mol% of the catalytic system instead of the previous **[Ni(OTf)(Py₂ᵀˢtacn)](OTf)** catalyst is key for keeping haloalkanes unaltered.

**Table 5. 9.** Scope of the photoredox cyclopropanation of alkenes using dichloromethane.
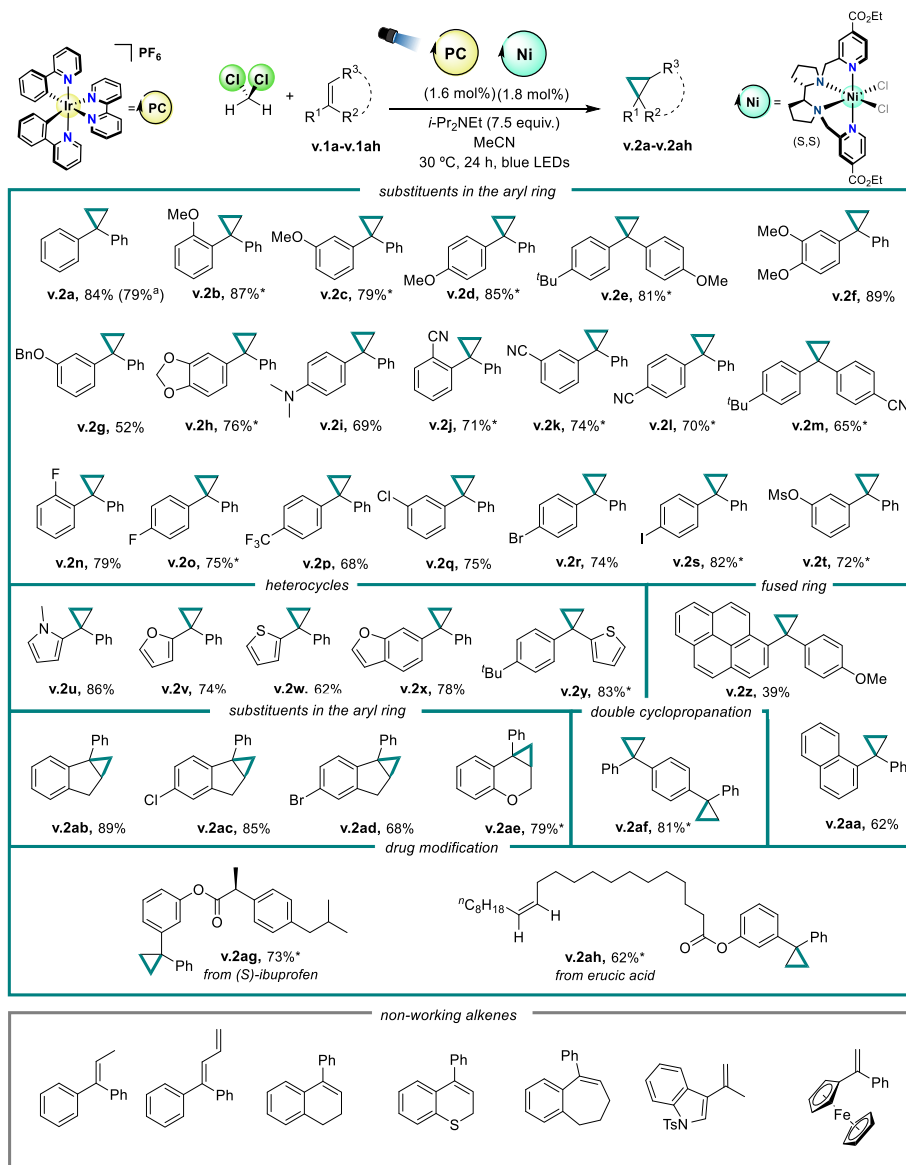
Standard reaction conditions: **v.1a-ah** (24 mM), **CH₂Cl₂** (10 equiv.), **PC_Ir** [H] (1.6 mol %), (^CO2Et**PDP)NiCl₂** (1.8 mol %), DIPEA (8.7 equiv.) in MeCN, V_T = 2 mL. Blue LED irradiation (1

W, 447 nm). All of those are isolated products and averages of at least eight reactions. [*]Reaction and isolation performed by Suyun Sun. [a] Reaction performed at gram scale.

Remarkably, the scope of the reaction was not restricted to 1,1-diaryl olefins: the replacement of one aryl ring by a heterocyclic moiety such as pyrrole (**v.2u**), furan (**v.2v**) or thiophene (**v.2w-v.2y**) showed outstanding cyclopropanation, providing an added value to the methodology. The excellent chemoselectivity allowed us to implement this strategy in drug modification, getting notable incorporation of the cyclopropane moiety into biologically active derivates from ibuprofen (**v.2ag**) and erucic acid (**v.2ah**), as examples. Initial attempts to expand the reactivity to tri- and tetrasubstituted alkenes failed, in agreement with a typical radical addition to an electrodeficient olefin.[19, 20] However, trisubstituted cyclopentenes were well tolerated, obtaining an excellent catalytic response (**v.2ab-v.2ae**). Other endocyclic alkenes presented low conversions, where only the flavanoid analogue 1-phenyl-phenylchromane (**v.2ae**) gave a successful 79% yield.

We also attempted the introduction of challenging moieties such as a tosylated amine, which mainly decomposed, and ferrocene, presenting no conversion. Then, we attempted the expansion of the reaction to other alkenes with substituents like nitro-, ester or CF_3 instead of an aryl group failed. However, the reactivity of these olefins enlightened us about the mechanistic pathway and the understanding of the reaction boundary, and we discuss it in next section 5.2.5.3.

The great yields obtained with the dual photoredox system, along with the use of CH_2Cl_2 as a stoichiometric C_1 synthon, prompted the exploration of deuterium-labelling in the compounds using CD_2Cl_2 (Table 5. 10). Without any reoptimization of the conditions, we achieved in all the cases 100% of deuterium incorporation to the β-carbon of the olefin. Interestingly, yields slightly decreased if we compare with the previous results using CH_2Cl_2. We attributed this

difference to a secondary isotope effect, where the replacement of a proton by a deuterium should affect the internal vibration of the system.

**Table 5. 10.** Examples of deuterium-labelled cyclopropanes.
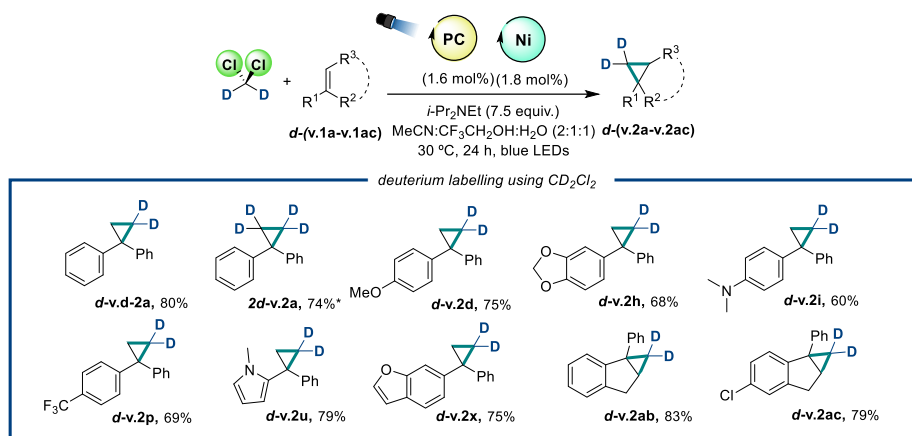
Standard reaction conditions: **v.1a-ah** (24 mM), **CH₂Cl₂** (10 equiv.), **PC_Ir ^H** (1.6 mol %), (**^CO2EtPDP)NiCl₂** (1.8 mol %), DIPEA (8.7 equiv.) in MeCN, V_T = 2 mL. Blue LED irradiation (1 W, 447 nm). All of those are isolated products and averages of at least eight reactions.

5.2.3. Divergent reactivity towards 1-chloromethyl insertion

The last steps of optimization (Table 5.6) showed the possibility to develop a versatile catalytic system by tuning only the solvent mixture. In this sense, the addition of protons to the system should stop the reaction by quenching the radical anion, giving the chloroalkane **v.3a** as the main product. However, the selectivity of the system towards the formation of the chloroalkane was not ideal, yielding 62% of **v.3a** and 24% of **v.2a**, when using MeCN:H₂O (6:4) as solvent mixture. This result highlights the competition between the protonation of the benzylic radical anion, and its intramolecular nucleophilic attack to the Csp³−Cl bond. We envisioned that acidic conditions should favor the protonation step, increasing the selectivity of the system towards the 1-insertion product. On the other hand, the

use of 7.5 equivalents of DIPEA restricted the acidification of the mixture without losing reactivity. In this regard, the introduction of alcohols with low pKa, such as trifluoroethanol (pKa ~ 12.5) or phenol (pKa ~ 9.9), could assist the protonation step. Moreover, we should consider the redox potential of the benzylic radical. The electronic properties of the aromatic ring have an effect to the formation of the radical anion, modifying the rate of the reactions and consequently, the selectivity towards one product. Preliminary results with different alkenes showed huge differences in terms of reaction selectivity, so we performed the optimization

Table 5. 11. Optimization of 1-chlormethyl insertion in some alkenes.
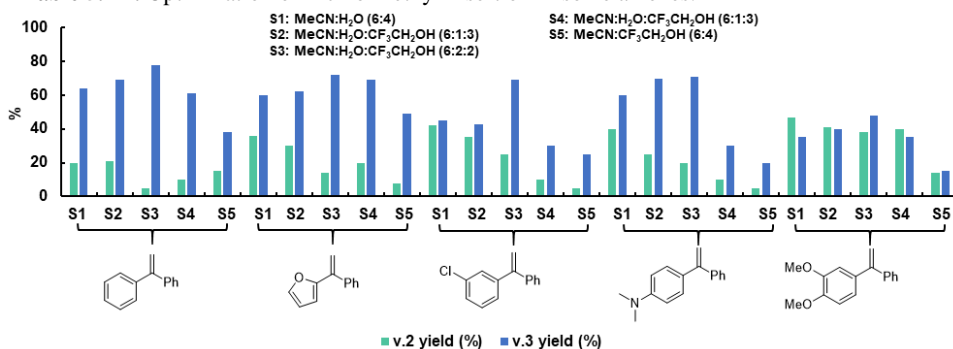
with several and representative alkenes, to find the most general protocol (Table 5.11).

General procedure B: **v.2**(24 mM), **PC** (1.6 mol %), (**CO2EtPDP)NiCl₂** (1.8 mol %), **CH₂Cl₂** (10 equiv.), DIPEA (7.5 equiv.) in MeCN,V_T = 2 mL. Blue LED irradiation (1 W, 447 nm). Conversion and yield of screening reactions were determined by GC-FID using biphenyl as an internal standard. GC-FID yield averages of at least three reactions.

The introduction of certain amount of CF₃CH₂OH was propitious for the selectivity of the reaction. We selected MeCN:H₂O:CF₃CH₂OH (3:1:1) as the most general and efficient solvent system for a high selectivity towards 1-chloromethyl addition product. Under these conditions, several examples presented notable yields towards the addition of 1-chloromethyl unit (Table 5.12), proving the well-controlled versatility of the catalytic system: the adjustment of the solvent system allowed us to change the selectivity of the reaction towards the

formation of alkyl chlorides instead of cyclopropanes without altering the catalytic response, providing a new tool for further derivatization of molecules.

Table 5. 12. Scope of the photoredox 1-chloromethyl addition to alkenes using CH_2Cl_2.
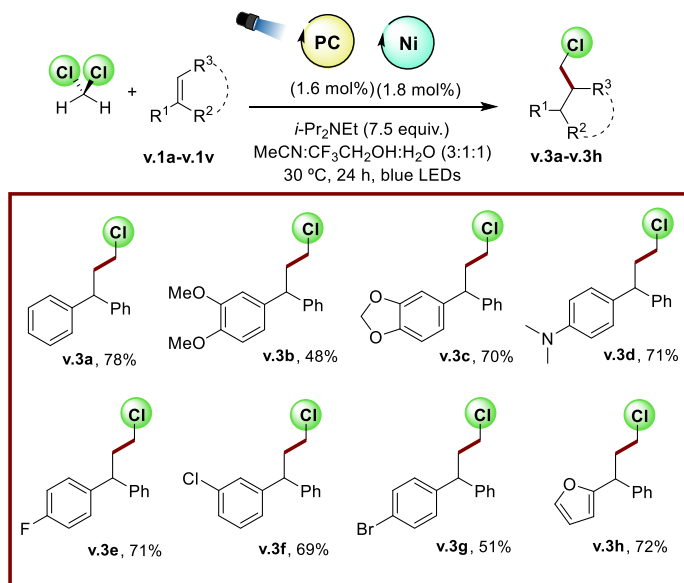
Standard reaction conditions: **v.1a-v** (24 mM), **CH₂Cl₂** (10 equiv.), **PC$_{Ir}^H$** (1.6 mol %), (**^{CO2Et}PDP)NiCl₂** (1.8 mol %), DIPEA (8.7 equiv.) in MeCN:CH₃CH₂OH:H₂O (3:1:1), $V_T = 2$ mL. Blue LED irradiation (1 W, 447 nm). All of those are isolated products and averages of at least eight reactions.

5.2.4. Expansion of the reactivity: activation of chloroform

Encouraged by these results and the tunability of the system reactivity, we explored the implementation of chloroform as a ready commercially available C_1 synthon following the same strategy. Traditionally, the treatment of chloroform under alkaline conditions with an alkene undergoes the formation of 1,1-chlorocarbene for the subsequent cyclopropanation.[11, 12] Considering its BDE (252 kJ·mol⁻¹), the homolytic activation of chloroform by the system was feasible. First attempts and blank experiments presented good catalytic response by using none

other catalyst than PC_{Ir}^{H}, where the presence of $(^{CO2Et}PDP)NiCl_2$ caused only an increment of 15-20% in the yield. A process of optimization without the nickel catalyst, was sufficient to form the cyclopropanation and the 1-insertion products (Scheme 5.7).
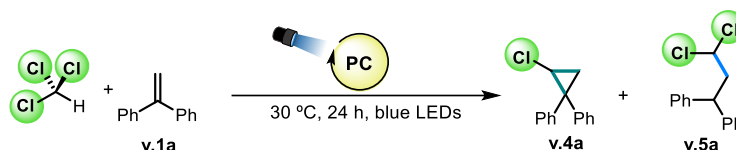
Scheme 5. 7. Model reaction through the photoactivation of $CHCl_3$.

We focused on 3 parameters for further reaction improvement: photocatalyst, substrate concentration and solvent system (Table 5.13). The best PCs for previous CH_2Cl_2 activation (PC_{Ir}^{H} and PC_{Ir}^{COOEt}) gave similar catalytic response for the new protocol. However, diluted conditions benefited the reactivity of the system, stablishing 10 mM of the olefin as a new modification.

Table 5. 13. Optimization of the photoredox activation of $CHCl_3$ for further functionalization of olefins.
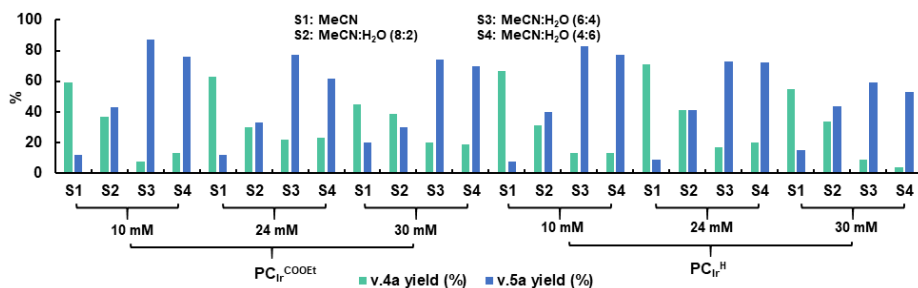
Reaction conditions: **v.1a**, **CHCl₃** (10 equiv.), **PC** (1.6 mol %), (DIPEA (8.7 equiv.) in solvent mixtures, $V_T = 300$ μL. Blue LED irradiation (1 W, 447 nm). GC-FID yield.

The reaction behaved similarly to the previous methodology, where the addition of water protonated the benzylic radical anion, obtaining the product of the first radical insertion **v.5a** as main product with MeCN:H₂O (6:4). Although the system

offered notable reactivity and selectivity with the model alkene, its lack of a general selective chlorocyclopropanation with other olefins hindered the development of the strategy (Table 5.14).

Table 5. 14. Evaluation of the protocol against different alkenes.
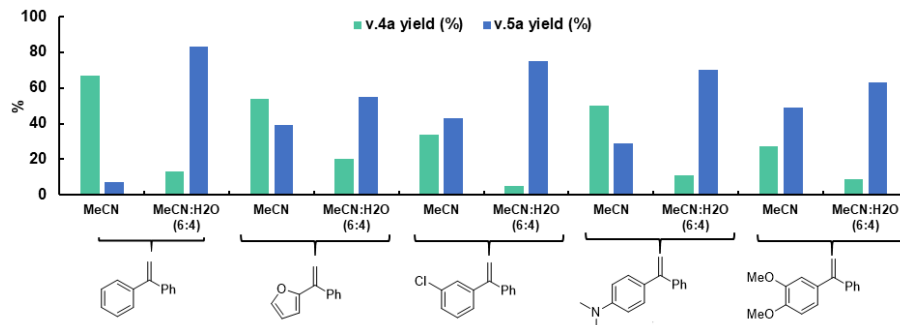
Standard reaction conditions: alkene (10 mM), **CHCl₃** (10 equiv.), **PC$_{Ir}$ ^{H}** (1.6 mol %), (DIPEA (8.7 equiv.) in solvent mixtures, $V_T = 1$ mL. Blue LED irradiation (1 W, 447 nm). GC-FID yield.

The poor selectivity towards one product under acetonitrile conditions can be rationallized due to the acidic behaviour of CHCl₃ (pKa~ 15.7), which protonates the benzylic radical anion in a similar way than H₂O (further discussion in following section 5.2.5.3). Hence, the use of CHCl₃ itself avoids the applicability of the protocol for the obtention of chlorinated cyclopropanes from other alkenes. In the other hand, the first addition of 1,1-dichloromethyl radical was rather successful and general, allowing us to exploit chloroform for the synthesis of geminal dichloroalkanes (Table 5.15). Despite not having as great results as those obtained previously with CH₂Cl₂, the expansion of the reaction scope showed that we are in front of a general methodology with a great tolerance to diverse functional groups, obtaining mostly yields between 55% to 77%. Thus, we demonstrate the power and tunability of the catalytic approach in the activation of chlorinated compounds and its applicability.

Table 5. 15. Scope of the photoredox 1,1-dichloromethyl addition to alkenes using CHCl₃.
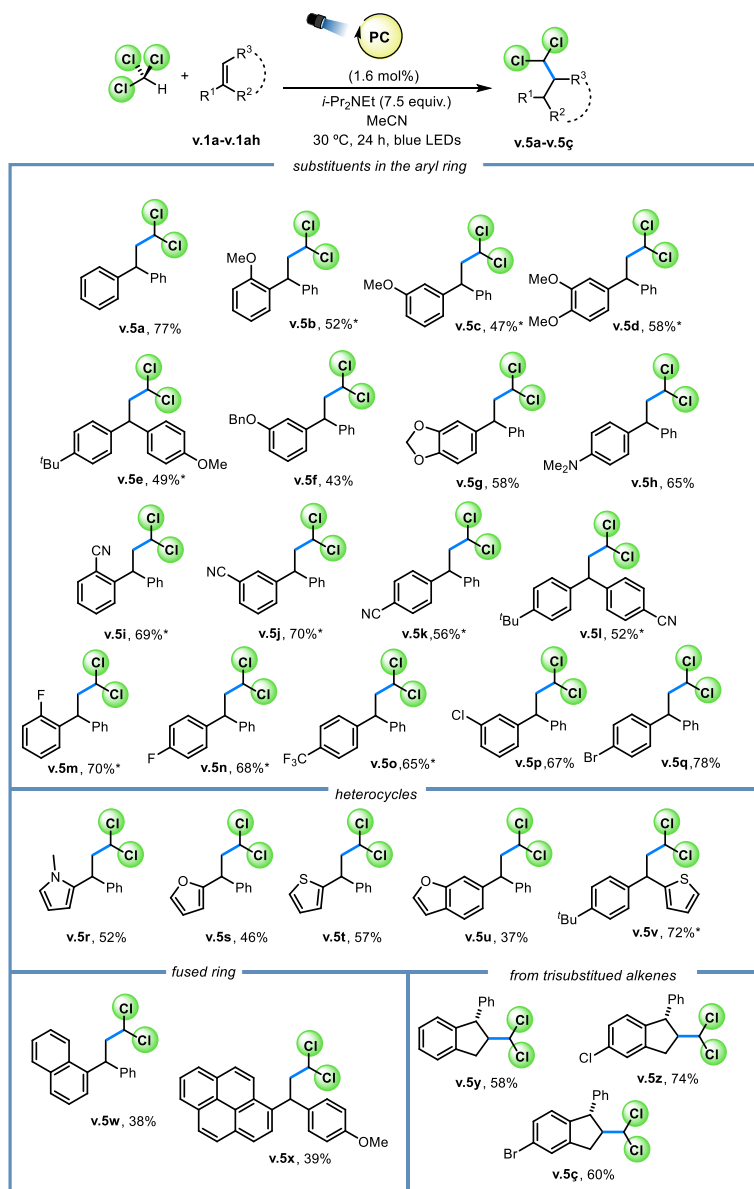
Standard reaction conditions: **v.1a-ç** (10 mM), **CH₂Cl₂** (10 equiv.), **PC_Ir H** (1.6 mol %), (DIPEA (8.7 equiv.) in MeCN::H₂O (3:2), V_T = 2 mL. Blue LED irradiation (1 W, 447 nm). All of those are isolated products and averages of at least eight reactions. *Reaction and isolation performed by Suyun Sun.

5.2.5. Mechanistic investigations

After the exhaustive elucidation of the photoredox activation of chloroalkanes and the subsequent cross-coupling reaction with alkenes, we were in front of a similar hypothesis for the mechanistic pathway of the photocatalytic cyclopropanation protocol (Scheme 5.8). The dual catalytic system breaks homolytically a Csp^3−Cl bond of dichloromethane molecule under photocatalytic conditions, generating 1-chloromethyl radicals. The engagement of the radical with an alkene led to the formation of a new benzylic C−centered radical, which undergoes a radical/polar crossover reactivity. We are able to control the final reactivity by tuning the reactions conditions. We discuss in more details the reaction mechanism in this section.
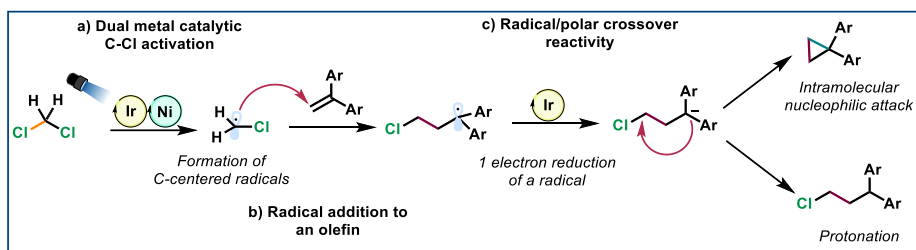
Scheme 5. 8. General proposed photoredox cyclopropanation of olefins route between using CH_2Cl_2 as C_1 synthon.

5.2.5.1. Study of the dual metal catalytic system by electro- and spectroelectrochemistry

Having explored the synthetic paradigm of the methodology, elucidating the selectivity of the system through a rational radical-polar crossover reaction, we next turned our attention on the activation of dichloromethane. Based on our previous works,[21] the dual metal system is able to reach Ni^I species, which activates homolitically Csp^3−Cl bonds. In this sense, **(^{COOEt}PDP)NiCl$_2$** was

evaluated by electrochemistry and spectroelectrochemistry, in collaboration with Sergio Fernandez.
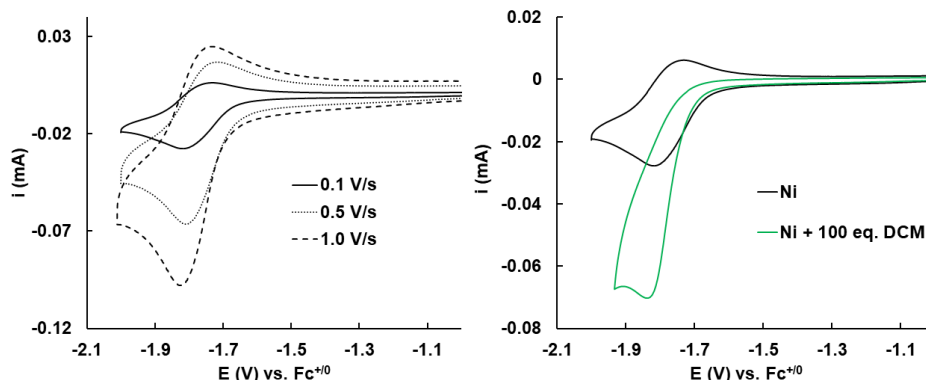
Figure 5. 2. *Left*: Cyclic voltammetry under Ar atmosphere of (**CO2EtPDP)NiCl₂** (2 mM) in MeCN/TBAPF₆ (0.2 M) electrolyte at 0.1, 0.5 and 1.0 V/s. $E_{1/2}$ (Ni$^{II/I}$) = -1.78 V vs. Fc$^{+/0}$. *Right*: CV under Ar atmosphere of (**CO2EtPDP)NiCl₂** (2 mM) with (green) and without (black) added CH₂Cl₂ (100 equiv.) in MeCN/TBAPF₆ (0.2 M) electrolyte at 0.1 V/s.
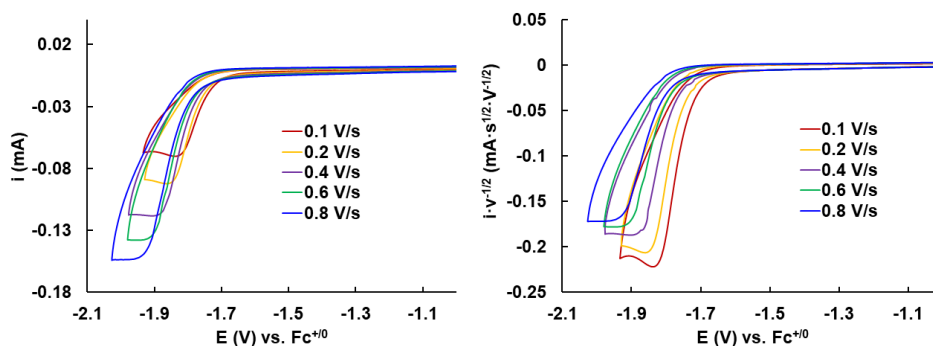
Figure 5. 3. *Left*: Cyclic voltammetry under Ar atmosphere of (**CO2EtPDP)NiCl₂** (2 mM) with added CH₂Cl₂ (100 equiv.) in MeCN/TBAPF₆ (0.2 M) electrolyte at increasing scan rates (0.1 – 0.8 V/s). *Right:* Cyclic voltammetry plot of the normalized current by the square root of the scan rate.

The cyclic voltammetry of complex **Ni^{COOEt}** showed a reversible Ni$^{II/I}$ wave at -1.78 V (Figure 5.2, left). After the addition of 100 equivalents of CH₂Cl₂, the Ni$^{II/I}$ wave loses its reversibility while the current is increased suggesting a catalytic reaction between CH₂Cl₂ and the electrogenerated Ni^{I} species (Figure

5.2, right). The catalytic peak shaped voltammogram observed at 0.1 V/s becomes an S-shaped voltammogram at higher scan rates (Figure 5.3, left). Moreover, the normalized current by the square root of scan rate behaves according to the Randles–Sevcik equation (the higher is the scan rate, the lower is the normalized current, Figure 5.3, right). These two features are consistent with a catalytic process.[22]

Moreover, the addition of 1,1-diphenylethylene (10 equiv.) did not produce remarkable changes in the cyclic voltammetry of $(^{COOEt}PDP)NiCl_2$ in the presence of CH_2Cl_2 (Figure 5.4). This is consistent with a rate determining activation of CH_2Cl_2. After the addition of a large excess of 1,1-diphenylethylene (30 equiv.), a subtle change in the shape of the voltammogram going from a peak shape to an S-shape is observed.
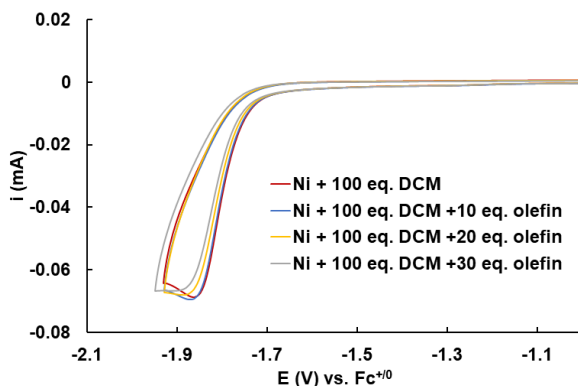
Figure 5. 4. Cyclic voltammetry under Ar atmosphere of complex $(^{CO2Et}PDP)NiCl_2$ (2 mM) with added CH_2Cl_2 (100 equiv.) in $MeCN/TBAPF_6$ (0.2 M) electrolyte at 0.1 V/s in the absence (red) and in the presence of added alkene (10 – 30 equiv. of 1,1-diphenylethylene).

UV-Vis spectroelectrochemistry (SEC) of $(^{COOEt}PDP)NiCl_2$ in neat electrolyte reveals the formation of a new species with features at 325 and 420 nm as well as a broad absorption in between 700 and 1000 nm (Figure 5.5, left).
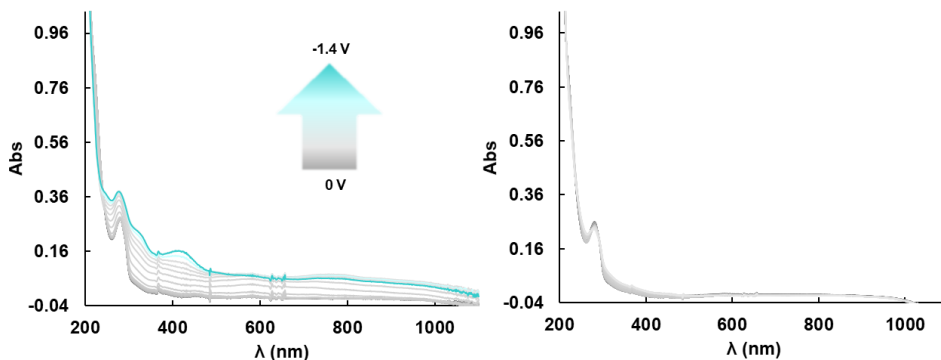
Figure 5. 5. UV-Vis SEC under Ar atmosphere of **(^{CO2Et}PDP)NiCl$_2$** (4 mM) from 0 to -1.4 V vs. Ag (pseudo)RE in MeCN/TBAPF$_6$ (0.2 M) electrolyte at 2 V/s. *Top*: Without added CH$_2$Cl$_2$. *Right:* With added CH$_2$Cl$_2$ (100 equivalents). Au/Pt/Ag Ottle cell.

We assigned this new species to the catalytically active Ni^I intermediate. However, a different spectroelectrochemical behaviour is observed for **(^{COOEt}PDP)NiCl$_2$** in the presence of CH$_2$Cl$_2$ (100 equiv.) is drastically different (Figure 5.5, right). In this case, we did not observe the formation of the new Ni^I species, suggesting that the reaction between Ni^I and CH$_2$Cl$_2$ is fast and do not allow for the accumulation of Ni^I. Moreover, the lack of remarkable spectral changes suggests that the resting state for the catalytic activation of CH$_2$Cl$_2$ is a Ni^{II} species that should be very similar to starting catalyst **(^{COOEt}PDP)NiCl$_2$** or even the same(Scheme 5.9).
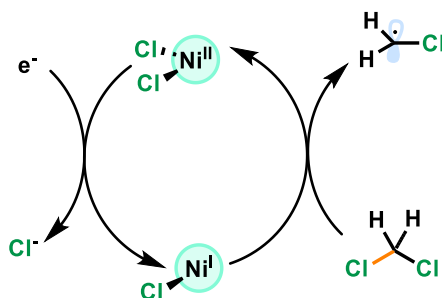
Scheme 5. 9. Electrochemical activation of CH$_2$Cl$_2$ catalyzed by (^{COOEt}PDP)NiCl$_2$.

In this sense, we build up an analogy from this electrochemical activation of CH_2Cl_2 and our dual metal photocatalytic protocol. Our mechanistic elucidation in *Chapter IV* presented the iridium PC as a reducing agent of **(Py$_2$^{Ts}tacn)Ni(OTf)$_2$** after its excitation by light and its reductive quenching by DIPEA. In other words, the PC reaches the 1 electron reduction of the nickel catalyst, which is the active intermediate in front of chloroalkanes. Here, we hypothesized that the dual catalytic system should behave in a similar manner, where the **(^{COOEt}PDP)Ni^{I}Cl$_2$** is active towards CH_2Cl_2 dehalogenation, using electrochemistry instead of PC for the accumulation of this intermediate.

5.2.5.2. Identification of the formed 1-chloromethyl radical

The preceding electrochemical and SEC studies show a catalytic process between the Ni^I intermediate and CH_2Cl_2. To prove our proposed mechanism, the identification of the dechlorinated radical from CH_2Cl_2 is a missing link. The aforementioned reactivity correlates with a formal homolytic cleavage of one Csp^3−Cl bond, followed by a Giese type radical addition to an electrodeficient olefin. We wondered if this C-centered radical could be trapped, having a alternative mechanistic probe of radical species. In this regard, we designed the capture of this key intermediate by substitution of the alkene for (2,2,6,6-tetramethylpiperidin-1-yl)oxyl (TEMPO) (Scheme 5.10). The success of the strategy with the formation of **v.6a** confirms the identity of the intermediate as a C-centered radical. Remarkably, the system was not active enough for the second Csp^3−Cl bond activation, allowing us to clearly identify the 1-chloromethyl radical. Moreover, these results show the potential expansion of this protocol towards the development of new reactivity between CH_2Cl_2 and other kind of radicals.
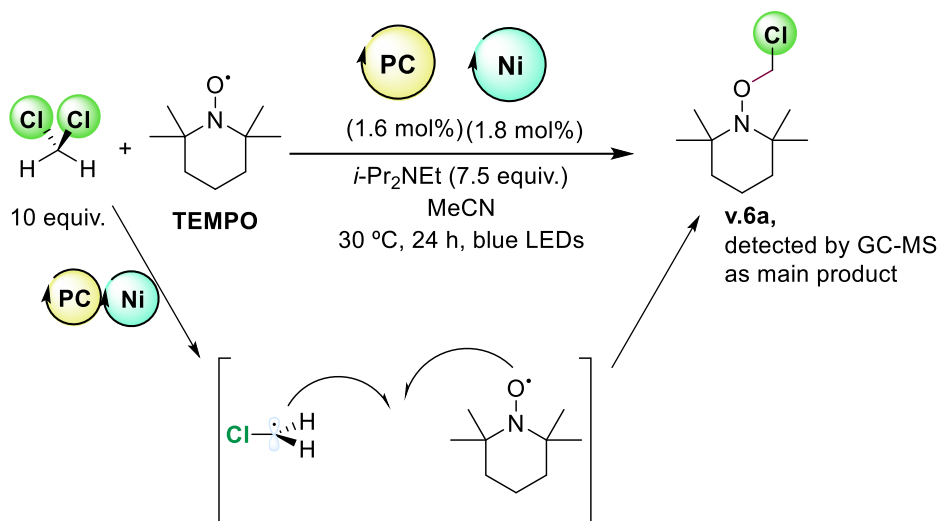
Scheme 5.10. Capture of the photogenerated 1-chloromethyl radical by TEMPO.

The presence of free 1-chloromethyl radicals under photocatalytic conditions was also confirmed by an indirect reasoning. It is relatively well-known that N-centered radicals from tertiary amines can react with 1-chloromethyl radicals, forming cyanine dyes. In 2016, Bach and coworkers monitored the formation of these cyanine dyes from DIPEA and CH_2Cl_2, assigning an intense absorption band at 415 nm.[23] Our system combines both compounds under radical conditions, so we envisioned UV-vis monitoring of the catalytic system and the identification of the organic dye as an extra prove of free 1-chloromethyl radicals.

The apparent lack of $[PC_{Ir}^{H}]^0$ in presence of dichloromethane under blue LED irradiation (Figure 5. 6, top-right) explains the 13% of **v.2a** yield obtained in previous blank experiments (Table 5.8, entry 12). The system without a Ni catalyst is able to activate CH_2Cl_2 to a lesser extent, observing a tiny band at 415 nm assigned to the cyanine dyes. Seemingly $[PC_{Ir}^{H}]^0$ is also not formed when $(^{CO2Et}PDP)NiCl_2$ is present in the mixture, covered by the tenuous formation of Ni^I intermediate (Figure 5. 6, bottom-left). By contrast, a significant absorption

band at 415 nm is generated when having CH_2Cl_2 in the mixture under blue LED irradiation (Figure 5. 6, bottom-right). The high intensity of the band is indicative of large generation of cyanine dyes, from the reaction between aminoalkyl radicals and 1-chloromethyl radicals. Indirectly, we are confirming the generation of 1-chloromethyl radicals by **(^{CO2Et}PDP)Ni^{I}Cl$_2$** under photocatalytic conditions.
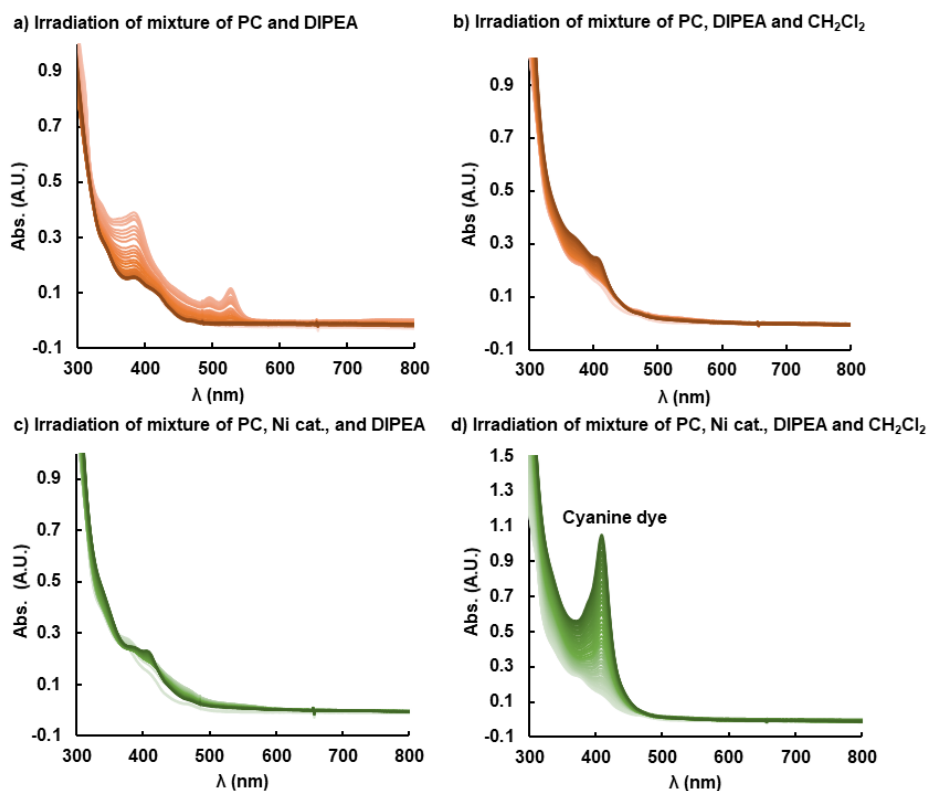
Figure 5. 6. Changes in UV-Vis spectrum of a reaction mixture in MeCN during 8 min of irradiation (blue LED, 447 nm) at 30ºC. *Top-left:* **PC$_{Ir}$^{H}** (40 µM) and DIPEA (10 µL). *Top-right:* **PC$_{Ir}$^{H}** (40 µM), DIPEA (10 µL) and **CH$_2$Cl$_2$** (10 equiv.). *Bottom-left:* **(^{CO2Et}PDP)NiCl$_2$** (40 µM), **PC$_{Ir}$^{H}** (40 µM) and DIPEA (10 µL). *Bottom-right:* **(^{CO2Et}PDP)NiCl$_2$** (40 µM), **PC$_{Ir}$^{H}** (40 µM), DIPEA (10 µL) and **CH$_2$Cl$_2$** (10 equiv.).

5.2.5.3. Study of the radical/polar crossover reactivity

The benzylic radical reduction by SET is pivotal for the development of the cyclopropanation, and corresponds with the boundary of the protocol. Thus, the redox potential of the benzylic radical and $PC_{Ir}{}^{H}$ (-1.42 V *vs* SCE) should match to undergo the radical/polar crossover reactivity. We estimated the redox potential for some examples of the radical formed after the first addition of 1-chloromethyl unit to the alkene (Table 5.16). Based on this finding, introducing aromatic substituents into the benzylic position was required to reach redox potentials below -1.4 V *vs* SCE.

Table 5. 16. Calculated redox potentials of substituted benzyl radical intermediates.

R·	theoretical $E^{0/-I}$ (V *vs* SCE)	R·	theoretical $E^{0/-I}$ (V *vs* SCE)
Ph ● CI	-1.56	Cl–⟨⟩–(Ph)● CI	-1.21
Ph ● CI	-1.36	pinacol-B–● CI	-1.00
F–⟨⟩–(Ph)● CI	-1.36	F_3C ● CI	-0.69
furyl–(Ph)● CI	-1.34	NC ● CI	-0.56
thienyl–(Ph)● CI	-1.33	EtOOC ● CI	-0.44
Cl–⟨⟩–(Ph)● CI	-1.3	O_2N ● CI	0.08

Theoretical redox potentials calculated at MNL15/6-31+g* level including solvent effects (SMD).

The preliminary results obtained with styrene were in concordance with this consideration. Its redox potential (-1.56 vs SCE) does not match with the reduction from PC_{Ir}^H, obtaining the insertion of another 1-chloromethyl radical (**v.I2**) and a mixture of homocoupling products (**v.I4**), instead of the radical/polar crossover reaction (Scheme 5.11).
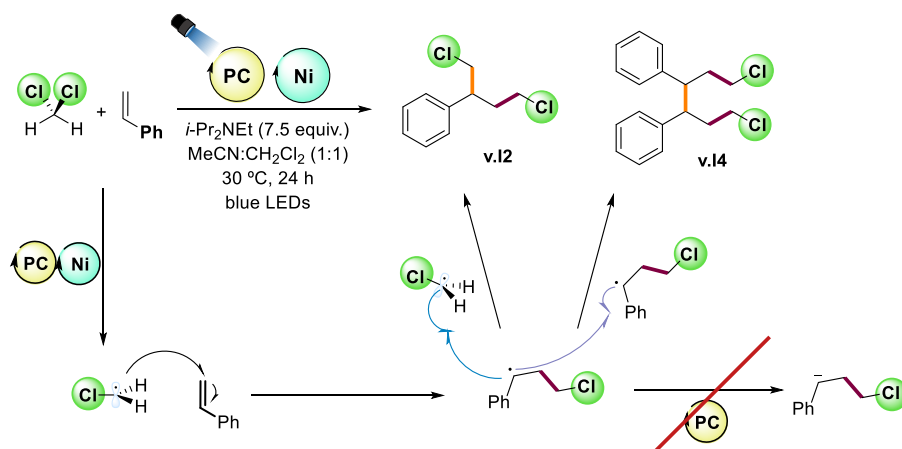
Scheme 5.11. Reactivity of styrene under photoredox radical conditions.

The correlation between the redox potential of diaryl substituted olefins and their reactivity towards cyclopropanation agrees with the radical/polar crossover process. In this sense, the control of the reaction selectivity by adding a protic source shows that we are in front of this pathway, and deuterium labelling experiment confirmed this hypothesis (Scheme 5.12).
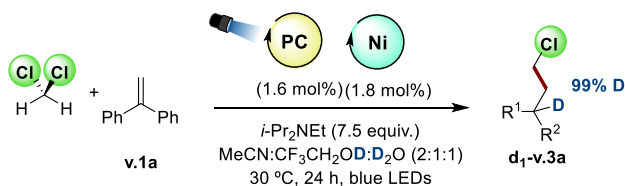
Scheme 5.12. Deuterium labelling experiments of dichloromethane approach.

Regarding the use of chloroform in a radical/polar crossover cyclopropanation, we previously identified its acidic proton (pKa~ 15.7) as possible barrier for the development of the methodology, due to the protonation of the benzylic radical anion. Although D_2O is the main source of protons for the benzylic radical anion (Scheme 5.13a), the loss of 60% of protons into the carbon from chloroform revealed an acidic equilibrium from the solvent $CHCl_3$. The incorporation of 50% of protons into this position when using deuterated chloroform confirmed this hypothesis (Scheme 5.13b).
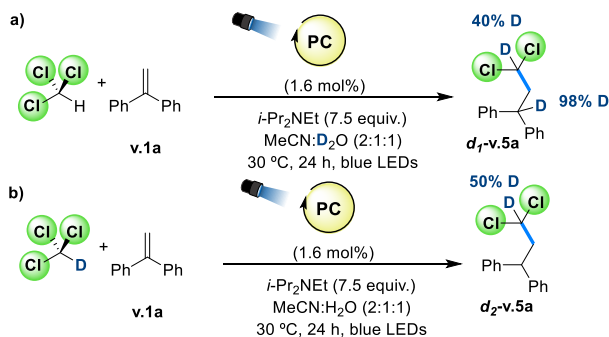
Scheme 5. 13. Deuterium labelling experiments of chloroform approach.

Coming back to the concept of radical/polar crossover reactivity, the understanding of a non-working example serves as an evidence. (3,3,3-trifluoroprop-1-en-2-yl)benzene presents a feasible redox potential (-0.69 vs SCE) to undergo the formation of the benzylic radical anion. However, the cyclopropanation was not formed, finding as major product **v.7b**. The formation of **v.7b** implies a radical/polar crossover step (Scheme 5.14): after the addition of a chloromethyl radical to the olefin, the benzylic radical is reduced, and the corresponding radical anion undergoes an anion-mediated fluoride elimination. The energy barriers for a radical-mediated version of this fluoride elimination are not feasible under experimental conditions,[17] limiting the practicability of this route through the radical anion generation.
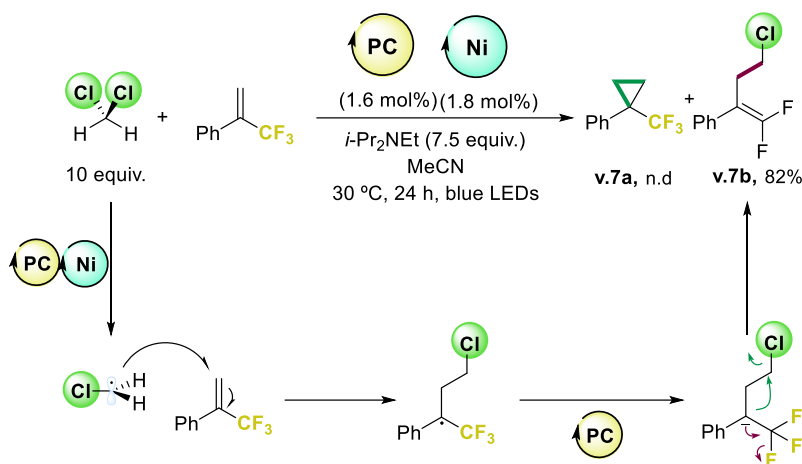
Scheme 5. 14. Fluoride elimination pathway.

5.2.5.4. Mechanistic proposal

Based on these results, we have proposed a plausible catalytic pathway for the photoredox activation of dichloromethane for the cyclopropanation of alkenes using $\textbf{PC}_{\textbf{Ir}}^{\textbf{H}}/(^{\textbf{CO2Et}}\textbf{PDP})\textbf{NiCl}_2$ as dual catalytic system (Scheme 5. 15). We have stablished an analogy with the mechanistic hypothesis of the previous cross-coupling reaction developed in *Chapter IV*. Under catalytic conditions, the $\textbf{[PC}_{\textbf{Ir}}^{\textbf{H}}\textbf{]}*$ excited state could be reductively quenched by the DIPEA [24] to form the reduced $\textbf{[PC}_{\textbf{Ir}}^{\textbf{H}}\textbf{]}^0$. Then, $\textbf{[PC}_{\textbf{Ir}}^{\textbf{H}}\textbf{]}^0$ ($E^o(PC^{+/0})$ = -1.42 V vs SCE) reduces $(^{\textbf{CO2Et}}\textbf{PDP})\textbf{NiCl}_2$ ($E^o(Ni^{II/I})$ = -1.32 V vs SCE) by one electron forming the key $\textbf{Ni}^\textbf{I}$ intermediate. UV-Vis spectroelectrochemistry and cyclic voltammetry suggest that the *in situ* generated $\textbf{Ni}^\textbf{I}$ species reacts with dichloromethane, recovering the initial $(^{\textbf{CO2Et}}\textbf{PDP})\textbf{NiCl}_2$ complex. Then, the activation of the Csp^3-Cl bond generates a free radical, which engages the alkene. The presence of this radical species has been confirmed by trapping it with TEMPO and by the

study of well-known secondary reactions with DIPEA by UV-Vis spectroscopy. The final benzylic radical is reduced by the photocatalyst to the corresponding radical anion. We can control the reactivity of the radical anion by tuning the solvent system. In one hand, the addition of protic solvents undergoes the final protonation of the radical anion. In the other, and as a main reaction of this chapter, the removal of any protic source from the system undergoes an intramolecular nucleophilic attack to the Csp^3−Cl, formalizing the cyclopropanation through a radical/polar crossover reactivity.
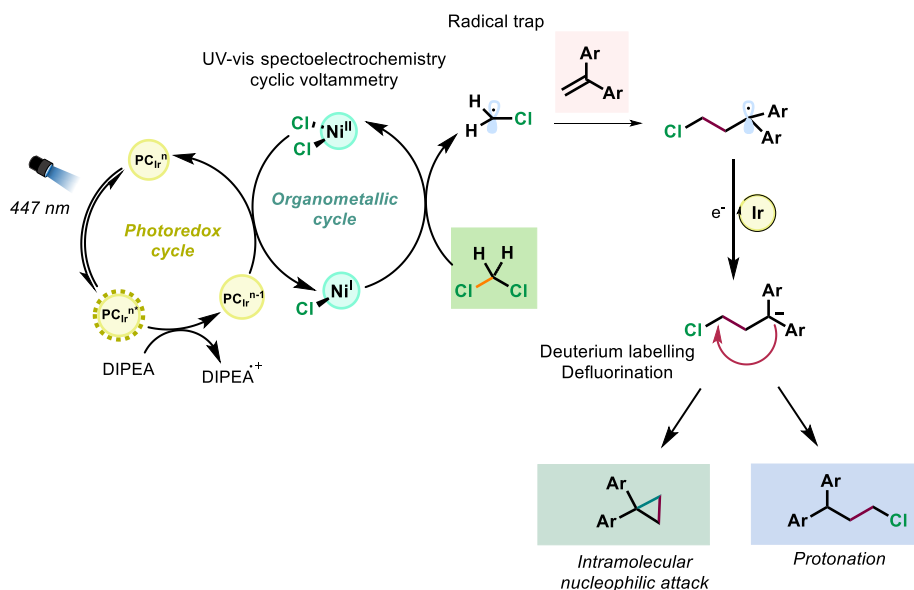
Scheme 5. 15. Hypothetical catalytic cycle for the visible-light cyclopropanation of alkenes *via* dichloromethane activation.

5.3. Conclusions

In this chapter, we expand our background in dual photocatalytic system based on iridium photocatalysts and multidentated N-based nickel complexes, developing a new strategy for the use of dichloromethane as C_1 synthon in cyclopropanation of aromatic alkenes. We explored tetradentated N-based aminopyridine nickel complexes as preferential candidates for the aforementioned reactivity, setting as the best system the combination of **CO2EtPDP)NiCl$_2$** as catalyst and [Ir(bpy)(ppy)$_2$](PF$_6$) (**PC$_{Ir}^H$)** as photocatalyst using iPr$_2$NEt as electron donor. Blank experiments revealed that the presence of all components (photocatalyst, catalyst, electron-donor and light) is totally required for the reaction to manifest. Once we established the optimal conditions for the cyclopropanation strategy, a broad substrate scope was tested reaching up to 89% yield for 34 different aromatic alkenes, exhibiting an excellent group tolerance. We consider this methodology as one of the first strategies for a general use of dichloromethane as C_1 synthon under mild conditions.

Regarding the mechanism, we proposed an analogue activation of Csp^3−Cl from previous chapters, where the *in situ* photogenerated **Ni^I** intermediate from (**CO2EtPDP)NiCl$_2$** is the active species in front of dichloromethane, based on spectroelectrochemical techniques. The activation results in the generation of free chloromethyl radicals, which are engaged by the alkene. A radical/polar crossover reactivity is reached by the reduction of the final benzylic radical, undergoing an intramolecular nucleophilic attack to the terminal Csp^3−Cl, achieving the final cyclopropanation.

The rationalization of the radical/polar crossover event allow us to tune the system for the development of a new synthesis of chloroalkanes, by adding protic source to the previous system. In parallel, we expand this protocol to the synthesis

of geminal 1,1-dichloroalkanes by using chloroform instead of dichloromethane, showing the potential and versatility of this system for the discovery of new reactivity through the activation of chlorinated compounds.

5.4. Experimental section

5.4.1. Materials and reagents

Reagents and solvents were used as received from the commercial supplier unless otherwise stated. Triethylamine and diisopropylethylamine were distilled over potassium hydroxide and were stored under argon. Photocatalysts [Ir(dmabpy)(ppy)$_2$](PF$_6$) (**PC$_{Ir}^{NMe2}$**),[25, 26] [Cu(bathocuproine)(xantphos)](PF$_6$) (**PC$_{Cu}$**)[27] and complexes (Py$_2^{Ts}$tacn)Ni(OTf)$_2$,[21] (Py$_2^{Ts}$tacn)Co(OTf)$_2$[28] were synthesized according to the literature procedures. Tetradentate aminopyridine complexes were synthetized according to *Chapter III* procedures.

For the synthesis of reagents, the solvents (DMF, hexane, Et$_2$O, CH$_2$Cl$_2$, MeCN and toluene) were used from a SPS-400, Innovative Technology solvent purification system and stored under argon with activated 4 Å molecular sieves. Anhydrous acetonitrile was purchased from Sigma-Aldrich® and water was purified with a Milli-Q Millipore Gradient AIS system. Water, methanol, ethanol, trifluoroethanol, acetonitrile, dimethylformamide, dimethylacetamide and tetrahydrofurane used for photoreactions were degassed by freeze-pump-thaw method (repeated 3 cycles) and were stored under argon. All the alkeness were filtered by a pad of Celite (Hyflo Super Cel from Sigma-Aldrich, CAS: 68855-54-9) before running the photoreactions.

The synthesis of air sensitive reagents as well as the preparation of visible light photocatalytic reactions were conducted inside a nitrogen-filled glove box (mBraun Unilab) with concentrations of O_2 and H_2O lower than 0.5 ppm and using Schlenk techniques under argon atmosphere.

5.4.2. Instruments

Nuclear magnetic resonance (NMR). NMR spectra were recorded on Bruker Fourier300, AV400, AV500 and AVIII500 spectrometers using standard conditions (300 K). All ^1H chemical shifts are reported in ppm and have been internally calibrated to the residual protons of the deuterated solvent. The ^{13}C chemical shifts have been internally calibrated to the carbon atoms of the deuterated solvent. The coupling constants were measured in Hz.

Mass Spectrometry. High resolution Mass Spectrometry (HRMS) data was collected on a HPLC-QqTOF (Maxis Impact, Bruker Daltonics) or HPLC-TOF (MicroTOF Focus, Bruker Daltonics) mass spectrometer using 1 mM solution of the analyzed compound.

Electrochemistry. All the electrochemical experiments were performed with a VSP potentiostat from BioLogic, equipped of the EC-Lab software. CV measurements were carried out under Ar atmosphere by using 1 mM solutions of nickel complex or Ir photoredox catalysts in MeCN, with tetrabutylammonium hexafluorophosphate (TBAPF$_6$) as supporting electrolyte (0.1 M). A single-compartment cell was employed, with glassy carbon (GC) working electrodes (3 mm and 1 mm diameter). Additionally, a Pt wire was used as a counter electrode and a Ag/AgCl wire as pseudo-reference, immersed in a bridge tube containing the same electrolyte solution (0.1 M TBAPF$_6$/MeCN) and separated from the working solution by a porous tip. Ferrocene (Fc) was added to the solution as an internal standard and all the potentials are first referenced vs. the Fc+/0 redox

couple and then vs. SCE. The working electrodes were polished by using 0.05 µm alumina powder (CHInstruments) on a polishing pad wet with distilled H_2O, followed by rinsing with distilled water/acetone and sonication to remove the residues of alumina over the electrode.

UV-Vis spectroscopy. UV-Vis spectra were recorded on an Agilent 8453 diode array spectrophotometer (190-1100 nm range) in 1 cm quartz cells. A cryostat from Unisoku Scientific Instruments was used for the temperature control.

Fluorescence spectroscopy. Fluorescence measurements were carried out on a Fluorolog Horiba Jobin Yvon spectrofluorimeter equipped with photomultiplier [or InGaAs if using the nitrogen cooled detector] detector, double monochromator and Xenon light source. Sample preparation was same as that of absorption experiments in 1 cm quartz cells.

Gas chromatography analysis. The analysis and quantification of the starting materials and products were carried out on an Agilent 7820A gas chromatograph (HP5 column, 30m or Cyclosil-B column, 30m) and a flame ionization detector. GC-MS spectral analyses were performed on an Agilent 7890A gas chromatograph interfaced with an Agilent 5975c MS mass spectrometer.

5.4.3. In-house developed parallel photoreactor
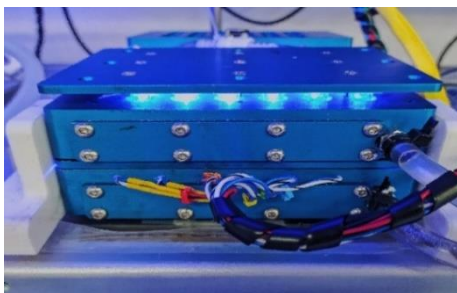
Figure 5. 7. In-house developed parallel photoreactors with 48 positions for vials of 1 mL.
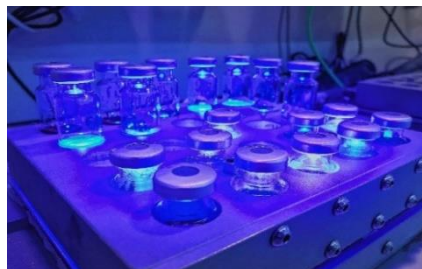
Figure 5. 8. In-house developed parallel photoreactors with 25 positions for vials of 10 or 21 mL.

Light source: The reactions were performed using Royal-Blue ($\lambda = 447\pm20$ nm) LUXEON Rebel ES LED, mounted on a 20 mm Square Saber - 1030 mW @ 700mA as a light source.

Temperature Control: Reaction temperature was controlled by a high precision thermoregulation Hubber K6 cryostat. Likewise, aiming at ensuring a stable irradiation the temperature of the LEDs was controlled and set at 22 ºC.

5.4.4. Experimental procedures

General procedure A for optimization screening: Inside an anaerobic box, aliquots from stock solutions of 1,1 diphenylethylene in MeCN, metal catalyst in MeCN, photocatalyst (30 µL, 0.06-0.12 µmol, 2 mol %) in MeCN were equally distributed into vial (1 mL of headspace) that contained glass beads. Then, a known amount of dichloromethane was added. If needed, degassed protic solvents were added to the vial to reach a total volume of 300 µL. Electron donor (in general *i*-Pr$_2$NEt) (7.5 equiv.). These vials were located in the small scale in house parallel photoreactor (Figure 5.6). All the photoreactor was sealed with a septum and removed from the anaerobic box, which was placed in the photoreactor at the indicated temperature (30 ºC). After irradiating for 24 h with blue LEDs ($\lambda = 447$ nm), each sample was diluted with ethyl acetate (0.2 mL) and a solution of biphenyl in ethyl acetate was added as internal standard (1.4×10^{-3} mmol in 0.20 mL). The organic phase was passed through a plug of MgSO$_4$ + SiO$_2$ and eluted with EtOAc. The resulting solution was analyzed by gas chromatography. The yield reported for each reaction is given as an average of at least two runs.

General procedure for cyclopropanation reaction: Inside an anaerobic box, aliquots from stock solutions of alkene (200 µL, 0.048 mmol, 1.0 equiv.) in MeCN, (**^{CO2Et}PDP)NiCl$_2$** (200 µL, 0.9 µmol, 1.8 mol %) in MeCN, **PC$_{Ir}^H$** (200 µL, 0.8 µmol, 1.6 mol %) in MeCN were equally distributed into 8 vials (10 mL of headspace) that contained glass beads. Then MeCN were added to each vial to reach a total volume of 2 mL total (concentration of substrate 24 mM).CH$_2$Cl$_2$ (100 µL, 0.48 mmol, 10 equiv.) *i*-Pr$_2$NEt (60 µL, 0.36 mmol, 7.5 equiv.) were added to these vials and they were placed in the photoreactor (Figure 5.6) at the indicated temperature (30 ºC) under orbital stirring. After irradiating the vials for 24 h with visible light (blue LED, 447 nm), they were opened and the content was combined in a separatory funnel. H$_2$O (15 mL) and Et$_2$O (15 mL) was added and

the organic layer was separated. The aqueous layer was extracted with Et_2O (3 x 15 mL), and the combined organic extracts were washed with HCl 10% (15 mL) and dried over $MgSO_4$. The solvent was removed under reduced pressure and the crude material was purified *via* column chromatography.

General procedure for chloromethyl insertion reaction: Inside an anaerobic box, aliquots from stock solutions of alkene (200 µL, 0.048 mmol, 1.0 equiv.) in MeCN, **(^{CO2Et}PDP)NiCl$_2$** (200 µL, 0.9 µmol, 1.8 mol %) in MeCN, **PC$_{Ir}$^{H}** (200 µL, 0.8 µmol, 1.6 mol %) in MeCN were equally distributed into 8 vials (10 mL of headspace) that contained glass beads. Then degassed H_2O and CF_3CH_2OH were added to each vial to reach a total volume of 2 mL total (concentration of substrate 24 Mm, MeCN:H_2O:CF_3CH_2OH, 3:1:1). CH_2Cl_2 (100 µL, 0.48 mmol, 10 equiv.) *i*-Pr$_2$NEt (60 µL, 0.36 mmol, 7.5 equiv.) were added to these vials and they were placed in the photoreactor (Figure 5.6) at the indicated temperature (30 ºC) under orbital stirring. After irradiating the vials for 24 h with visible light (blue LED, 447 nm), they were opened and the content was combined in a separatory funnel. H_2O (15 mL) and Et_2O (15 mL) was added and the organic layer was separated. The aqueous layer was extracted with Et_2O (3 x 15 mL), and the combined organic extracts were washed with HCl 10% (15 mL) and dried over $MgSO_4$. The solvent was removed under reduced pressure and the crude material was purified *via* column chromatography.

General procedure for dichloromethyl insertion reaction: Inside an anaerobic box, aliquots from stock solutions of alkene (200 µL, 0.020 mmol, 1.0 equiv.) in MeCN, **(^{CO2Et}PDP)NiCl$_2$** (200 µL, 0.45 µmol, 1.8 mol %) in MeCN, **PC$_{Ir}$^{H}** (200 µL, 0.4 µmol, 1.6 mol %) in MeCN were equally distributed into 8 vials (10 mL of headspace) that contained glass beads. Then degassed H_2O was added to each vial to reach a total volume of 2 mL total (concentration of substrate 210 mM, MeCN:H_2O, 3:2). CHCl$_3$ (10 equiv.) *i*-Pr$_2$NEt (30 µL, 0.18 mmol, 7.5

equiv.) were added to these vials and they were placed in the photoreactor (Figure 5.6) at the indicated temperature (30 ºC) under orbital stirring. After irradiating the vials for 24 h with visible light (blue LED, 447 nm), they were opened and the content was combined in a separatory funnel. H_2O (15 mL) and Et_2O (15 mL) was added and the organic layer was separated. The aqueous layer was extracted with Et_2O (3 x 15 mL), and the combined organic extracts were washed with HCl 10% (15 mL) and dried over $MgSO_4$. The solvent was removed under reduced pressure and the crude material was purified *via* column chromatography.

Procedure for the gram scale version of photoredox cyclopropanation reaction: Inside an anaerobic box, 1.2 g of diphenylethylene, **(^{CO2Et}PDP)NiCl$_2$** catalyst (1.8 mol %), **PC$_{Ir}$^{H}** (1.6 mol %) and acetonitrile were distributed into into a 1 L 2-necked round bottom flask. 10 equiv. of CH_2Cl_2 was added to the flask together with 7.5 equiv. of *i*-Pr$_2$Net. The final mixture was irradiated by a KESSIL lamp (λ = 467 nm), separated 7 cm (to maintain a temperature close to 30 ºC). After irradiating for 24 h, H_2O (150 mL) and Et_2O (150 mL) were added and the organic layer was separated. The aqueous layer was extracted with Et_2O (3 x 100 mL), and the combined organic extracts were washed with brine (150 mL) and dried over $MgSO_4$. The solvent was removed under reduced pressure and the crude material was purified *via* column chromatography yielding 79% of the pure cyclopropane product.

Procedure for reaction monitoring: Inside an anaerobic box, aliquots from stock solutions of alkene (200 µL, 0.048 mmol, 1.0 equiv.) in MeCN, **(^{CO2Et}PDP)NiCl$_2$** (200 µL, 0.9 µmol, 1.8 mol %) in MeCN, **PC$_{Ir}$^{H}** (200 µL, 0.8 µmol, 1.6 mol %) in MeCN were equally distributed into 8 vials (10 mL of headspace) that contained glass beads. Then MeCN were added to each vial to reach a total volume of 2 mL total (concentration of substrate 24 mM).CH_2Cl_2 (100 µL, 0.48 mmol, 10 equiv.) *i*-Pr$_2$NEt (60 µL, 0.36 mmol, 7.5 equiv.) were added to these vials and they were placed in the photoreactor (Figure 5.6) at the

indicated temperature (30 ℃) under orbital stirring. At specific points of time (see plot), aliquots of 100 μL were taken from the sealed vials and mixed with 29 μL of solution of biphenyl in EtOAc (34.8 mM) and the resulting mixture was analyzed by GC-FID. Light irradiation was switched off and on at specific points of the single-point monitoring experiment, which indicates that the reaction stops when the vial is not irradiated with visible light.
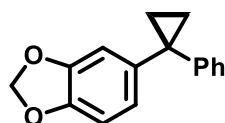
5.4.5. Characterization of products
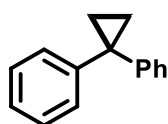
Product (**v.2a**): Cyclopropanation according to general procedure: scale 0.32 mmol, flash chromatography (SiO$_2$, 100% hexane) yielded 46 mg (84 %) of the title compound as a colorless liquid. **^{1}H NMR** (500 MHz, Chloroform-*d*) δ 7.35 – 7.16 (m, 10H), 1.35 (s, 4H). **^{13}C NMR** (126 MHz, Chloroform-*d*) δ 145.83, 128.55, 128.29, 126.07, 30.10, 16.58. **GC-MS** (m/z) : 194.1.
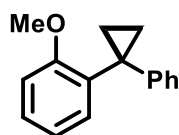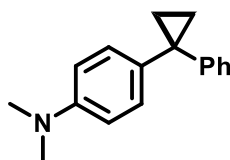

Product (**v.2b**): Cyclopropanation according to general procedure: scale 0.32 mmol, flash chromatography (SiO$_2$, 100% hexane) yielded 55 mg (87 %) of the title compound as a colorless liquid. **^{1}H NMR** (500 MHz, CDCl$_3$) δ 7.29 – 7.26 (m, 1H), 7.25 – 7.22 (m, 3H), 7.21 – 7.15 (m, 2H), 6.83 (ddd, *J* = 7.6, 1.7, 0.9 Hz, 1H), 6.78 (dd, *J* = 2.6, 1.7 Hz, 1H), 6.73 (ddd, *J* = 8.3, 2.6, 1.0 Hz, 1H), 3.76 (s, 3H), 1.30 (qd, *J* = 2.1, 1.0 Hz, 4H). **^{13}C NMR** (101 MHz, CDCl$_3$) δ 146.21, 133.25, 131.63, 128.13, 128.02, 128.00, 126.89, 125.31, 120.48, 111.03, 77.48, 77.16, 76.84, 55.48, 26.22, 16.37. **GC-MS** (m/z) : 224.1.
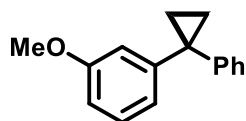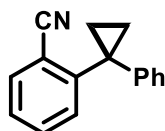
Product (**v.2c**): Cyclopropanation according to general procedure: scale 0.32 mmol, flash chromatography (SiO$_2$, 100% hexane) yielded 45 mg (79 %) of the title compound as a colorless liquid. **^{1}H NMR** (500 MHz, CDCl$_3$) δ 7.42 (dd, J = 7.5, 1.8 Hz, 1H), 7.28 – 7.18 (m, 4H), 7.16 – 7.13 (m, 2H), 7.12 – 7.07 (m, 1H), 6.94 (td, J = 7.4, 1.2 Hz, 1H), 6.86 (dd, J = 8.2, 1.2 Hz, 1H), 3.77 (s, 3H), 1.30 – 1.26 (m, 2H), 1.25 – 1.21 (m, 2H). **^{13}C NMR** (101 MHz, CDCl$_3$) δ 159.67, 147.58, 145.72, 129.33, 128.53, 128.39, 126.11, 120.98, 114.69, 111.20, 77.48, 77.16, 76.84, 55.29, 30.07, 16.64. **GC-MS** (m/z) : 224.1.
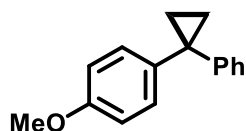
Product (**v.2d**): Cyclopropanation according to general procedure: scale 0.32 mmol, flash chromatography (SiO$_2$, 100% hexane) yielded 32 mg (85 %) of the title compound as a colorless liquid. **^{1}H NMR** (500 MHz, CDCl$_3$) δ 7.25 (tt, J = 7.1, 1.2 Hz, 2H), 7.22 – 7.13 (m, 5H), 6.84 – 6.80 (m, 2H), 3.78 (s, 3H), 1.26 (qd, J = 2.1, 1.0 Hz, 4H). **^{13}C NMR** (126 MHz, CDCl$_3$) δ 158.02, 146.41, 137.92, 129.98, 128.34, 128.04, 125.85, 113.79, 77.41, 77.16, 76.90, 55.41, 29.30, 16.45. **GC-MS** (m/z) : 224.1.
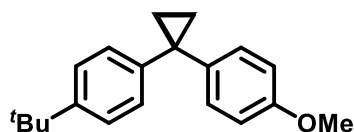
Product (**v.2e**): Cyclopropanation according to general procedure: scale 0.32 mmol, flash chromatography (SiO$_2$, 100% hexane) yielded 0.32 mg (81 %) of the title compound as a colorless liquid. **^{1}H NMR** (500 MHz, CDCl$_3$) δ 7.23 – 7.19 (m, 2H), 7.11 – 7.07 (m, 2H), 6.84 – 6.80 (m, 2H), 3.78 (s, 3H), 1.29 (s, 9H), 1.24 (dd, J = 6.1, 1.8 Hz, 4H). **^{13}C NMR** (126 MHz, CDCl$_3$) δ 158.01, 148.57, 143.43, 138.09, 130.18, 127.42, 125.22, 113.77, 55.41, 34.45, 31.51, 28.84, 16.46. **GC-MS** (m/z) : 280.2.
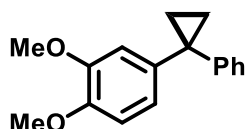
Product (**v.2f**): Cyclopropanation according to general procedure: scale 0.32 mmol, flash chromatography (SiO$_2$, 100% hexane) yielded 0.32 mg (89 %) of the title compound as a colorless liquid. **^{1}H NMR** (500 MHz, CDCl$_3$) δ 7.29 – 7.25 (m, 2H), 7.21 – 7.16 (m, 3H), 6.88 – 6.84 (m, 2H), 6.81 (d, J = 8.2 Hz, 1H), 3.88 (s, 3H), 3.85 (s, 3H), 1.30 (dq, J = 5.2, 2.2, 1.6 Hz, 4H).

^{13}C NMR (101 MHz, CDCl$_3$) δ 148.79, 147.54, 146.29, 138.23, 128.29, 127.66, 125.79, 121.09, 112.57, 111.04, 55.98, 55.91, 29.66, 16.66. **GC-MS** (m/z) : 254.1.
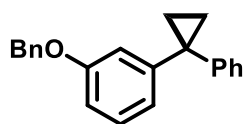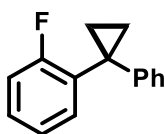
Product (**v.2g**): Cyclopropanation according to general procedure: scale 0.32 mmol, flash chromatography (SiO$_2$, 100% hexane) yielded 78.5 mg (52 %) of the title compound as a colorless liquid. **^{1}H NMR** (500 MHz, Chloroform-d) δ 7.45 – 7.38 (m, 4H), 7.37 – 7.32 (m, 1H), 7.32 – 7.27 (m, 3H), 7.26 – 7.24 (m, 1H), 7.23 – 7.18 (m, 2H), 6.90 – 6.80 (m, 3H), 5.04 (s, 2H), 1.32 (s, 4H). **^{13}C NMR** (126 MHz, Chloroform-d) δ 158.74, 147.50, 145.51, 137.02, 129.21, 128.56, 128.50, 128.27, 127.94, 127.61, 126.00, 120.96, 115.41, 111.98, 69.96, 29.93, 16.52. **GC-MS** (m/z) : 300.2.
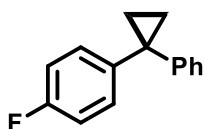
Product (**v.2h**): Cyclopropanation according to general procedure: scale 0.32 mmol, flash chromatography (SiO$_2$, 100% hexane) yielded 66 mg (76 %) of the title compound as a colorless liquid. **^{1}H ^{1}H NMR** (500 MHz, CDCl$_3$) δ 7.27 – 7.23 (m, 2H), 7.20 – 7.18 (m, 2H), 7.17 – 7.13 (m, 1H), 6.78 –

6.69 (m, 3H), 5.91 (s, 2H), 1.24 (qd, J = 2.0, 0.9 Hz, 4H). **^{13}C NMR** (126 MHz, CDCl$_3$) δ 147.61, 146.17, 145.94, 139.80, 128.38, 128.01, 125.98, 122.02, 109.75, 108.09, 101.03, 77.42, 77.16, 76.91, 29.96, 16.46. **GC-MS** (m/z) : 238.1.
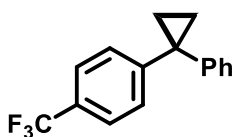
Product (**v.2i**): Cyclopropanation according to general procedure: scale 0.32 mmol, flash chromatography (SiO$_2$, 100% hexane) yielded 58 mg (69 %) of the title compound as as a colorless liquid. **^{1}H NMR** (500 MHz, CDCl$_3$) δ 7.27 (d, J = 4.6 Hz, 1H), 7.25 – 7.23 (m, 2H), 7.22 – 7.12 (m, 5H), 6.71 – 6.67 (m, 2H), 2.92 (s, 6H), 1.26 – 1.23 (m, 4H). **^{13}C NMR** (101 MHz, CDCl$_3$) δ 149.20, 146.92, 133.74, 129.72, 128.24, 127.94, 125.62, 112.76, 40.90, 29.12, 16.40. **GC-MS** (m/z) : 237.2.

Product (**v.3j**): Cyclopropanation according to general procedure: scale 0.32 mmol, flash chromatography (SiO$_2$, 100% hexane) yielded 66 mg (71 %) of the title compound as a colorless liquid. **^{1}H NMR** (500 MHz, CDCl$_3$) δ 7.48 – 7.41 (m, 3H), 7.37 – 7.29 (m, 3H), 7.24 (ddq, J = 6.9, 3.4, 1.8, 1.3 Hz, 3H), 1.40 – 1.37 (m, 2H), 1.31 – 1.29 (m, 2H). **^{13}C NMR** (126 MHz, CDCl$_3$) δ 147.61, 144.10, 132.55, 131.79, 129.66, 129.18, 128.88, 128.73, 126.79, 119.12, 112.42, 29.79, 16.68. **GC-MS** (m/z) : 219.1.
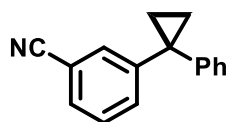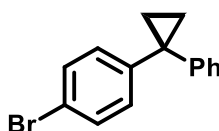
Product (**v.2k**): Cyclopropanation according to general procedure: scale 0.32 mmol, flash chromatography (SiO$_2$, 100% hexane) yielded 49 mg (7 %) of the title compound as a colorless liquid. **^{1}H NMR** (400 MHz, CDCl$_3$) δ 7.57 – 7.50 (m, 2H), 7.31 (dd, J = 7.6, 4.4 Hz, 3H), 7.25 – 7.16 (m, 4H), 1.44 – 1.31 (m, 4H). **^{13}C NMR** (126 MHz, CDCl$_3$) δ 143.91, 132.41, 132.20,

129.27, 128.76, 128.57, 128.37, 127.70, 126.90, 119.19, 109.54, 30.23, 17.39. **GC-MS** (m/z) : 219.1.
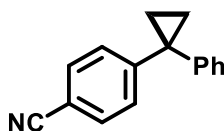
Product (**v.2l**): Cyclopropanation according to general procedure: scale 0.32 mmol, flash chromatography (SiO$_2$, 100% hexane) yielded 48 mg (70 %) of the title compound as a colorless liquid. **^{1}H NMR** (500 MHz, CDCl$_3$) δ 7.49 – 7.46 (m, 2H), 7.29 – 7.25 (m, 2H), 7.22 – 7.15 (m, 5H), 1.38 – 1.35 (m, 2H), 1.30 – 1.27 (m, 2H). **^{13}C NMR** (126 MHz, CDCl$_3$) δ 151.85, 143.88, 132.16, 129.25, 128.73, 128.34, 126.87, 119.16, 109.51, 77.41, 77.16, 76.90, 30.21, 17.36. **GC-MS** (m/z) : 219.1.
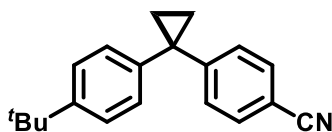
Product (**v.2m**): Cyclopropanation according to general procedure: scale 0.32 mmol, flash chromatography (SiO$_2$, 100% hexane) yielded 30 mg (5 %) of the title compound as a colorless liquid. **^{1}H NMR** (500 MHz, CDCl$_3$) δ 7.55 – 7.52 (m, 2H), 7.36 – 7.33 (m, 2H), 7.27 – 7.24 (m, 2H), 7.19 – 7.16 (m, 2H), 1.43 – 1.39 (m, 2H), 1.33 (s, 9H), 1.32 (d, J = 2.5 Hz, 2H). **^{13}C NMR** (126 MHz, CDCl$_3$) δ 152.04, 149.71, 140.83, 132.12, 128.71, 128.51, 125.59, 119.20, 109.45, 34.55, 31.46, 29.76, 17.29. **GC-MS** (m/z) : 275.2.
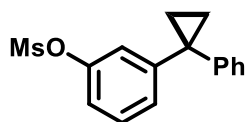
Product (**v.2n**): Cyclopropanation according to general procedure: scale 0.32 mmol, flash chromatography (SiO$_2$, 100% hexane) yielded 60 mg (79 %) of the title compound as a colorless liquid. **^{1}H NMR** (500 MHz, CDCl$_3$) δ 7.30 (dd, J

= 8.2, 6.9 Hz, 2H), 7.25 – 7.20 (m, 4H), 7.03 – 6.93 (m, 2H), 1.34 – 1.27 (m, 4H). ^{13}**C NMR** (101 MHz, CDCl$_3$) δ 162.60, 160.17, 145.78, 141.54, 141.50, 130.34, 130.26, 128.75, 128.45, 128.18, 126.12, 115.24, 115.03, 77.48, 77.16, 76.84, 29.45, 16.50. **GC-MS** (m/z) : 212.1.
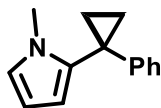

Product (**v.2o**): Cyclopropanation according to general procedure: scale 0.32 mmol, flash chromatography (SiO$_2$, 100% hexane) yielded 57 mg (75 %) of the title compound as a colorless liquid. ^{1}**H NMR** (400 MHz, CDCl$_3$) δ 7.45 (td, J = 7.6, 1.8 Hz, 1H), 7.26 – 7.17 (m, 5H), 7.16 – 7.07 (m, 2H), 7.01 (ddd, J = 10.3, 8.1, 1.3 Hz, 1H), 1.36 – 1.26 (m, 4H). ^{13}**C NMR** (101 MHz, CDCl$_3$) δ 163.71, 161.24, 145.15, 132.04, 132.00, 128.62, 128.54, 128.35, 127.05, 125.93, 124.14, 124.10, 115.92, 115.71, 77.48, 77.16, 76.84, 25.38, 15.58, 15.56. **GC-MS** (m/z) : 212.1.

Product (**v.2p**): Cyclopropanation according to general procedure: scale 0.32 mmol, flash chromatography (SiO$_2$, 100% hexane) yielded 58 mg (68 %) of the title compound as a colorless liquid. ^{1}**H NMR** (500 MHz, Chloroform-d) δ 7.56 – 7.51 (m, 2H), 7.35 – 7.28 (m, 5H), 7.27 – 7.23 (m, 2H), 1.43 – 1.38 (m, 2H), 1.38 – 1.33 (m, 2H). ^{13}**C NMR** (126 MHz, Chloroform-d) δ 150.02, 144.51, 128.77, 128.49, 128.24, 127.94, 126.45, 125.37, 125.22, 125.19, 125.16, 125.13, 123.21, 29.85, 16.78. **GC-MS** (m/z): 262.1.
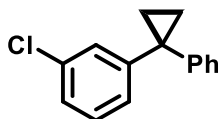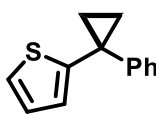
Product (**v.2q**): Cyclopropanation according to general procedure: scale 0.32 mmol, flash chromatography (SiO$_2$, 100% hexane) yielded 43 mg (75 %) of the title compound as a colorless liquid. **^{1}H NMR** (500 MHz, Chloroform-*d*) δ 7.55 (dd, *J* = 7.6, 1.8 Hz, 1H), 7.39 (dd, *J* = 7.8, 1.5 Hz, 1H), 7.30 (dd, *J* = 7.5, 1.4 Hz, 1H), 7.24 (dtd, *J* = 9.4, 4.5, 4.5, 2.3 Hz, 3H), 7.18 – 7.13 (m, 1H), 7.11 – 7.07 (m, 2H), 1.47 – 1.43 (m, 2H), 1.39 – 1.35 (m, 2H).**^{13}C NMR** (126 MHz, Chloroform-*d*) δ 144.43, 142.05, 136.63, 132.60, 129.91, 128.75, 128.16, 128.13, 128.10, 127.25, 127.17, 126.77, 126.10, 125.48, 28.57, 17.63. **GC-MS** (m/z) : 228.0.
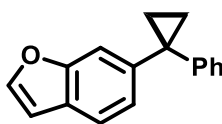
Product (**v.2r**): Cyclopropanation according to general procedure: scale 0.32 mmol, flash chromatography (SiO$_2$, 100% hexane) yielded 46 mg (74 %) of the title compound as a colorless liquid. **^{1}H NMR** (500 MHz, Chloroform-*d*) δ 7.44 – 7.38 (m, 2H), 7.33 – 7.27 (m, 2H), 7.25 – 7.20 (m, 3H), 7.14 – 7.11 (m, 2H), 1.36 – 1.32 (m, 2H), 1.31 – 1.27 (m, 2H). **^{13}C NMR** (126 MHz, Chloroform-*d*) δ 145.05, 144.86, 131.30, 130.16, 128.76, 128.41, 128.38, 128.35, 128.25, 127.17, 126.18, 119.75, 29.49, 16.47. **GC-MS** (m/z) : 272.0.
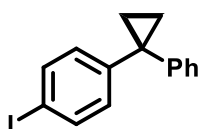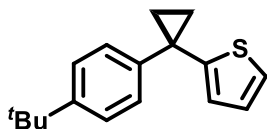
Product (**v.2s**): Cyclopropanation according to general procedure: scale 0.32 mmol, flash chromatography (SiO$_2$, 100% hexane) yielded 55 mg (82 %) of the title compound as a colorless liquid. **^{1}H NMR** (500 MHz, CDCl$_3$) δ 7.65 – 7.60 (m, 2H), 7.32 (dd, *J* = 8.2, 7.0 Hz, 2H), 7.25 – 7.20 (m, 2H), 7.04 – 6.98 (m, 2H), 1.36 (dt, *J* = 5.6, 2.9 Hz, 2H), 1.31 (dq, *J* = 5.4, 3.0, 2.5 Hz, 2H). **^{13}C NMR**

(126 MHz, CDCl₃) δ 145.75, 145.11, 137.43, 130.58, 128.55, 128.52, 126.34, 91.25, 29.72, 16.59. **GC-MS** (m/z) : 320.1.

Product (**v.2t**): Cyclopropanation according to general procedure: scale 0.32 mmol, flash chromatography (SiO₂, 100% hexane) yielded 72 mg (72 %) of the title compound as a colorless liquid. **¹H NMR** (500 MHz, Chloroform-d) δ 7.49 – 7.45 (m, 1H), 7.30 – 7.25 (m, 2H), 7.21 – 7.10 (m, 4H), 7.08 – 7.03 (m, 1H), 4.02 – 3.94 (m, 2H), 2.77 – 2.71 (m, 2H), 2.71 – 2.66 (m, 2H), 2.62 – 2.57 (m, 2H), 2.17 (d, J = 3.0 Hz, 1H), 1.97 – 1.90 (m, 2H), 1.90 – 1.83 (m, 2H), 1.80 – 1.72 (m, 2H), 1.65 (qd, J = 7.9, 7.9, 7.7, 4.2 Hz, 2H), 1.40 (qd, J = 8.7, 8.5, 8.5, 3.5 Hz, 2H). **¹H NMR** (400 MHz, CDCl₃) δ 7.32 – 7.27 (m, 3H), 7.26 – 7.18 (m, 3H), 7.17 – 7.14 (m, 1H), 7.13 – 7.07 (m, 2H), 3.09 (s, 3H), 1.38 – 1.29 (m, 4H). **¹³C NMR** (101 MHz, CDCl₃) δ 149.42, 148.82, 144.66, 129.80, 128.83, 128.61, 127.19, 126.57, 121.68, 119.45, 37.47, 29.88, 16.91. **GC-MS** (m/z) : 288.1.
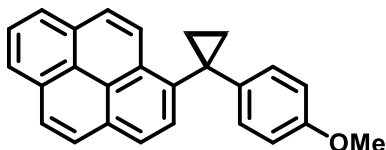
Product (**v.2u**): Cyclopropanation according to general procedure: scale 0.32 mmol, flash chromatography (SiO₂, 100% hexane) yielded 68 mg (86 %) of the title compound as a colorless liquid. **¹H NMR** (500 MHz, Chloroform-d) δ 7.27 – 7.21 (m, 2H), 7.14 (ddt, J = 7.9, 6.8, 1.2, 1.2 Hz, 1H), 7.01 – 6.92 (m, 2H), 6.60 (s, 1H), 6.12 (s, 2H), 3.46 (s, 3H), 1.35 (dd, J = 2.7, 0.8 Hz, 2H), 1.34 – 1.32 (m, 2H). **¹³C NMR** (126 MHz, Chloroform-d) δ 145.00, 128.27, 125.43, 125.33, 121.56, 108.26, 106.32, 34.14, 29.71, 17.22. **GC-MS** (m/z) : 197.1.
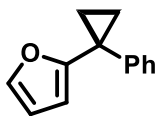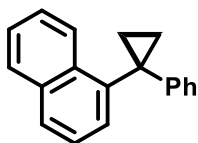
Product (**v.2v**): Cyclopropanation according to general procedure: scale 0.32 mmol, flash chromatography (SiO$_2$, 100% hexane) yielded 56 mg (74 %) of the title compound as a colorless liquid. **^{1}H NMR** (400 MHz, Chloroform-d) δ 7.39 – 7.34 (m, 3H), 7.34 – 7.32 (m, 1H), 7.31 – 7.23 (m, 2H), 6.28 (dd, J = 3.2, 1.9 Hz, 1H), 5.88 (dd, J = 3.2, 0.9 Hz, 1H), 1.46 – 1.42 (m, 2H), 1.29 – 1.25 (m, 2H). **^{13}C NMR** (101 MHz, Chloroform-d) δ 158.85, 142.81, 140.81, 128.86, 128.30, 126.59, 110.18, 105.60, 24.48, 15.02. **GC-MS** (m/z) : 184.1.
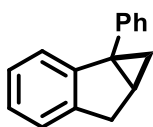
Product (**v.2w**): Cyclopropanation according to general procedure: scale 0.32 mmol, flash chromatography (SiO$_2$, 100% hexane) yielded 43 mg (62 %) of the title compound as a colorless liquid. **^{1}H NMR** (400 MHz, Chloroform-d) δ 7.40 – 7.30 (m, 4H), 7.27 – 7.22 (m, 1H), 7.11 (dd, J = 5.2, 1.2 Hz, 1H), 6.92 – 6.87 (m, 1H), 6.77 – 6.73 (m, 1H), 1.41 (s, 4H). **^{13}C NMR** (101 MHz, Chloroform-d) δ 151.66, 144.87, 128.59, 128.32, 126.54, 126.47, 124.28, 123.16, 26.10, 18.26. **GC-MS** (m/z) : 200.1.

Product (**v.2x**): Cyclopropanation according to general procedure: scale 0.32 mmol, flash chromatography (SiO$_2$, 100% hexane) yielded 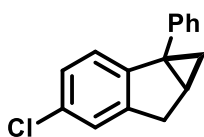24 mg (78 %) of the title compound as a colorless liquid. **^{1}H NMR** (500 MHz, Chloroform-d) δ 7.46 – 7.32 (m, 7H), 7.22 – 7.15 (m, 2H), 6.16 (t, J = 0.8, 0.8 Hz, 1H), 1.62 (td, J = 4.4, 4.4, 2.2 Hz, 2H), 1.38 – 1.34 (m, 2H). **^{13}C NMR** (126 MHz, Chloroform-d) δ 162.01, 154.39, 141.91, 129.54, 128.99, 128.75, 128.43, 127.17, 127.00, 123.18, 122.49, 120.05, 110.76, 102.73, 25.18, 15.28. **GC-MS** (m/z) : 234.1.

Product (**v.2y**): Cyclopropanation according to general procedure: scale 0.32 mmol, flash chromatography (SiO$_2$, 100% hexane) yielded 28 mg (83 %) of the title compound as a colorless liquid. **^{1}H NMR** (500 MHz, CDCl$_3$) δ 7.34 – 7.31 (m, 2H), 7.27 (d, J = 2.1 Hz, 1H), 7.25 (d, J = 2.0 Hz, 1H), 7.09 (dd, J = 5.2, 1.3 Hz, 1H), 6.88 (dd, J = 5.2, 3.5 Hz, 1H), 6.75 (dd, J = 3.5, 1.2 Hz, 1H), 1.37 (p, J = 2.2 Hz, 4H), 1.32 (s, 9H). **^{13}C NMR** (126 MHz, CDCl$_3$) δ 151.93, 149.36, 142.03, 128.12, 126.65, 125.33, 124.55, 123.27, 34.55, 31.52, 25.62, 18.40. **GC-MS** (m/z) : 256.1.
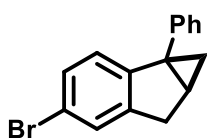

Product (**v.2z**): Cyclopropanation according to general procedure: scale 0.32 mmol, flash chromatography (SiO$_2$, 100% hexane) yielded 43 mg (39 %) of the title compound as a colorless liquid. **^{1}H NMR** (500 MHz, Chloroform-d) δ 8.48 (d, J = 9.2 Hz, 1H), 8.21 – 8.14 (m, 5H), 8.09 – 7.97 (m, 5H), 6.97 – 6.93 (m, 2H), 6.73 – 6.69 (m, 2H), 3.71 (s, 3H), 1.65 (q, J = 3.9, 3.9, 3.8 Hz, 2H), 1.58 – 1.56 (m, 2H). **^{13}C NMR** (126 MHz, Chloroform-d) δ 157.31, 138.70, 138.43, 131.31, 130.85, 130.55, 130.45, 128.83, 128.09, 127.74, 127.40, 127.34, 127.27, 127.13, 127.01, 126.74, 125.98, 125.90, 125.68, 125.16, 125.12, 125.09, 125.07, 125.00, 124.86, 124.81, 124.63, 115.03, 113.76, 113.59, 55.28, 55.23, 27.30, 18.31, 17.22. **GC-MS** (m/z) : 348.2.
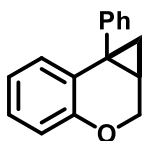
Product (**v.2aa**): Cyclopropanation according to general procedure: scale 0.32 mmol, flash chromatography (SiO$_2$, 100% hexane) yielded 62 mg (62 %) of the title compound as a white solid. **^{1}H NMR** (400 MHz, Chloroform-*d*) δ 8.23 – 8.09 (m, 1H), 7.87 (dd, *J* = 8.2, 1.5 Hz, 1H), 7.81 (d, *J* = 8.2 Hz, 1H), 7.64 (dd, *J* = 7.1, 1.2 Hz, 1H), 7.53 – 7.37 (m, 3H), 7.17 (dd, *J* = 8.2, 7.0 Hz, 2H), 7.11 – 7.04 (m, 1H), 7.01 – 6.96 (m, 2H), 1.56 (d, *J* = 2.4 Hz, 2H), 1.45 (t, *J* = 3.2, 3.2 Hz, 2H). ^{13}**C NMR** (126 MHz, Chloroform-*d*) δ 145.97, 140.62, 134.04, 133.04, 128.55, 128.30, 128.11, 127.64, 125.86, 125.78, 125.52, 125.15, 27.34, 18.32. **GC-MS** (m/z) : 244.1.

Product (**v.2ab**): Cyclopropanation according to general procedure: scale 0.32 mmol, flash chromatography (SiO$_2$, 100% hexane) yielded 33 mg (89 %) of the title compound as a white solid. **^{1}H NMR** (500 MHz, Chloroform-*d*) δ 7.42 – 7.38 (m, 2H), 7.35 – 7.31 (m, 2H), 7.28 – 7.23 (m, 1H), 7.22 – 7.19 (m, 1H), 7.15 – 7.05 (m, 3H), 3.40 (dd, *J* = 16.9, 6.5 Hz, 1H), 3.02 (d, *J* = 17.0 Hz, 1H), 2.02 – 1.93 (m, 1H), 1.73 (dd, *J* = 8.4, 4.5 Hz, 1H), 0.56 (t, *J* = 4.5, 4.5 Hz, 1H). ^{13}**C NMR** (126 MHz, Chloroform-*d*) δ 149.03, 141.90, 141.29, 129.13, 128.31, 126.37, 125.99, 125.72, 125.45, 123.80, 39.56, 35.56, 26.38, 21.74. **GC-MS** (m/z) : 206.1.

Product (**v.2ac**): Cyclopropanation according to general procedure: scale 0.32 mmol, flash chromatography (SiO$_2$, 100% hexane) yielded 82 mg (85 %) of the title compound as a colorless liquid. **^{1}H NMR** (500 MHz, Chloroform-*d*) δ 7.41 – 7.33 (m, 4H), 7.30 – 7.26 (m, 1H), 7.21 – 7.18 (m, 1H), 7.09 (ddt, *J* =

8.1, 1.8, 0.8, 0.8 Hz, 1H), 6.99 (d, J = 8.1 Hz, 1H), 3.44 – 3.32 (m, 1H), 3.02 (d, J = 17.2 Hz, 1H), 2.04 – 1.94 (m, 1H), 1.77 (dd, J = 8.4, 4.6 Hz, 1H), 0.57 (t, J = 4.6, 4.6 Hz, 1H). **^{13}C NMR** (126 MHz, Chloroform-d) δ 147.67, 143.86, 140.70, 131.30, 129.06, 128.75, 128.42, 127.25, 127.17, 126.59, 126.19, 125.99, 125.62, 124.79, 60.41, 39.09, 35.42, 26.61, 21.66, 21.07, 14.22. **GC-MS** (m/z) : 240.1.
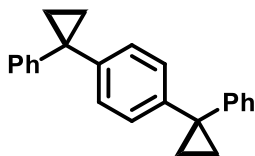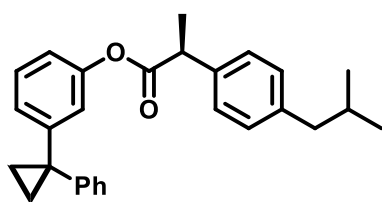

Product (**v.2ad**): Cyclopropanation according to general procedure: scale 0.32 mmol, flash chromatography (SiO$_2$, 100% hexane) yielded 48 mg (68 %) of the title compound as a colorless liquid. **^{1}H NMR** (500 MHz, Chloroform-d) δ 7.37 – 7.31 (m, 4H), 7.26 (ddt, J = 8.6, 4.7, 1.6, 1.6 Hz, 1H), 7.21 (ddt, J = 8.1, 1.8, 0.8, 0.8 Hz, 1H), 6.92 (d, J = 8.1 Hz, 1H), 3.37 (ddt, J = 17.1, 6.5, 1.1, 1.1 Hz, 1H), 3.00 (d, J = 17.2 Hz, 1H), 1.99 (dddd, J = 8.4, 6.6, 4.6, 0.8 Hz, 1H), 1.75 (dd, J = 8.4, 4.6 Hz, 1H), 0.55 (t, J = 4.6, 4.6 Hz, 1H). **^{13}C NMR** (126 MHz, Chloroform-d) δ 148.22, 144.27, 140.62, 129.07, 128.56, 128.42, 126.62, 125.29, 119.24, 39.18, 35.40, 26.53, 21.60. **GC-MS** (m/z) : 280.1.

Product (**v.2ae**): Cyclopropanation according to general procedure: scale 0.32 mmol, flash chromatography (SiO$_2$, 100% hexane) yielded 76 mg (79 %) of the title compound as a colorless liquid. **^{1}H NMR** (400 MHz, CDCl$_3$) δ 7.45 – 7.34 (m, 4H), 7.34 – 7.29 (m, 1H), 7.05 (td, J = 7.7, 7.3, 2.0 Hz, 1H), 6.86 (d, J = 7.9 Hz, 1H), 6.80 – 6.71 (m, 2H), 4.43 (d, J = 10.5 Hz, 1H), 4.12 (d, J = 10.6 Hz, 1H), 1.91 – 1.85 (m, 1H), 1.58 – 1.47 (m, 2H). **^{13}C NMR** (126 MHz, CDCl$_3$) δ 152.43, 142.82, 130.73, 130.43, 128.66, 128.50, 127.10, 126.37, 121.45, 117.20, 77.41, 77.16, 76.90, 62.74, 26.80, 26.23, 15.99. **GC-MS** (m/z) : 222.1.
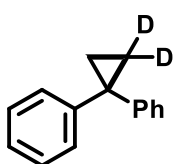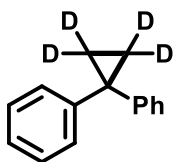
Product (**v.2af**): Cyclopropanation according to general procedure: scale 0.32 mmol, flash chromatography (SiO$_2$, 100% hexane) yielded 62 mg (81 %) of the title compound as a colorless liquid. **^{1}H NMR** (500 MHz, CDCl$_3$) δ 7.47 – 7.29 (m, 14H), 1.43 (dt, J = 3.8, 1.1 Hz, 8H). **^{13}C NMR** (126 MHz, CDCl$_3$) δ 145.87, 143.51, 128.75, 128.38, 128.18, 126.09, 29.67, 16.53. **GC-MS** (m/z) : 310.2.

Product (**v.2ag**): Cyclopropanation according to general procedure: scale 0.32 mmol, flash chromatography (SiO$_2$, 100% hexane) yielded 78 mg (73 %) of the title compound as a colorless liquid. **^{1}H NMR** (500 MHz, CDCl$_3$) δ 7.32 – 7.30 (m, 2H), 7.30 – 7.27 (m, 2H), 7.25 – 7.19 (m, 4H), 7.18 – 7.15 (m, 2H), 7.08 (dt, J = 7.8, 1.4 Hz, 1H), 6.88 (t, J = 2.1 Hz, 1H), 6.85 (ddd, J = 8.1, 2.3, 1.1 Hz, 1H), 3.94 (q, J = 7.2 Hz, 1H), 2.50 (d, J = 7.2 Hz, 2H), 1.90 (dt, J = 13.5, 6.8 Hz, 1H), 1.62 (d, J = 7.2 Hz, 3H), 1.31 (dt, J = 5.5, 2.0 Hz, 4H), 0.95 (d, J = 6.7 Hz, 6H). **^{13}C NMR** (126 MHz, CDCl$_3$) δ 173.33, 150.99, 147.56, 145.27, 140.91, 137.41, 129.63, 129.13, 128.53, 128.44, 127.36, 126.20, 126.02, 121.30, 119.14, 45.42, 45.20, 30.33, 29.82, 22.54, 18.70, 16.72. **GC-MS** (m/z) : 398.2.
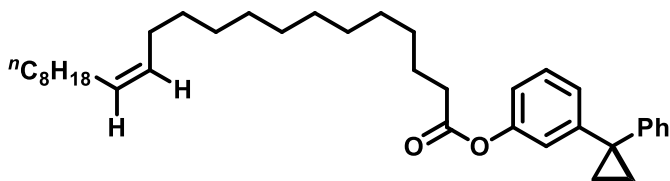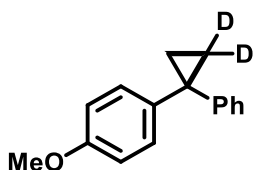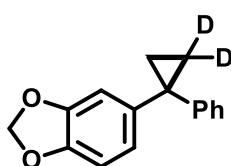
Product (**v.2ah**): Cyclopropanation according to general procedure: scale 0.32 mmol, flash chromatography (SiO$_2$, 100% hexane) yielded 31 mg (62 %) of the title compound as a colorless liquid. **^{1}H NMR** (500 MHz, Chloroform-d) δ 7.34 (d, *J* = 2.7 Hz, 6H), 7.20 (d, *J* = 7.7 Hz, 1H), 7.04 (q, *J* = 2.8, 2.6, 2.6 Hz, 2H), 5.48 (d, *J* = 2.4 Hz, 2H), 5.35 (t, *J* = 4.9, 4.9 Hz, 2H), 2.53 (td, *J* = 7.6, 7.5, 2.2 Hz, 2H), 2.02 (q, *J* = 6.7, 6.6, 6.6 Hz, 4H), 1.74 (p, *J* = 8.2, 8.2, 7.8, 7.8 Hz, 2H), 0.88 (td, *J* = 7.2, 6.9, 2.3 Hz, 4H). **^{13}C NMR** (126 MHz, Chloroform-d) δ 172.42, 150.81, 149.31, 143.15, 141.16, 130.06, 130.04, 129.19, 128.41, 128.38, 127.99, 125.79, 121.51, 121.07, 115.15, 34.55, 32.06, 29.93, 29.75, 29.74, 29.70, 29.68, 29.61, 29.47, 29.40, 29.27, 27.37, 25.06, 22.83, 14.26. **GC-MS** (m/z) : 419.2.
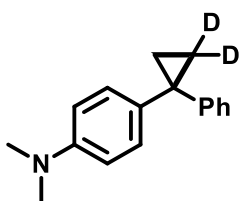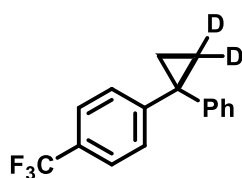

Product (**d-v.2a**): Cyclopropanation according to general procedure: scale 0.32 mmol, flash chromatography (SiO$_2$, 100% hexane) yielded 26 mg (80 %) of the title compound as a colorless liquid. **^{1}H NMR** (500 MHz, Chloroform-*d*) δ 7.34 – 7.29 (m, 5H), 7.29 – 7.26 (m, 3H), 7.25 – 7.20 (m, 2H), 1.34 (s, 2H). **^{13}C NMR** (126 MHz, Chloroform-*d*) δ 145.74, 128.66, 128.44, 128.27, 128.19, 127.89, 126.55, 125.95, 29.75, 16.28. **GC-MS** (m/z) : 196.0.

Product (**2d-v.2a**): Cyclopropanation according to general procedure: scale 0.32 mmol, flash chromatography (SiO$_2$, 100% hexane) yielded 33 mg (74 %) of the title compound as a colorless liquid. **^{1}H NMR** (500 MHz, CDCl$_3$) δ 7.33 – 7.19 (m, 10H). **^{13}C NMR** (126 MHz, CDCl$_3$) δ 145.84, 128.56, 128.39, 126.06, 30.35, 29.85, 29.69, 15.73. **GC-MS** (m/z) : 198.0.

Product (**d-v.2d**): Cyclopropanation according to general procedure: scale 0.32 mmol, flash chromatography (SiO$_2$, 100% hexane) yielded 23 mg (75 %) of the title compound as a colorless liquid. **^{1}H NMR** (500 MHz, Chloroform-*d*) δ 7.30 – 7.26 (m, 3H), 7.22 – 7.16 (m, 5H), 6.86 – 6.83 (m, 2H), 3.81 (s, 3H), 1.27 (s, 2H). **^{13}C NMR** (126 MHz, Chloroform-*d*) δ 157.87, 137.76, 129.84, 128.19, 127.89, 125.70, 113.66, 55.28, 55.25, 29.01, 16.12. **GC-MS** (m/z) : 226.1.
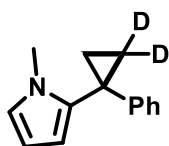
Product (**d-v.2h**): Cyclopropanation according to general procedure: scale 0.32 mmol, flash chromatography (SiO$_2$, 100% hexane) yielded 45 mg (68 %) of the title compound as a colorless liquid. **^{1}H NMR** (500 MHz, Chloroform-*d*) δ 7.32 – 7.12 (m, 5H), 6.90 – 6.61 (m, 3H), 5.94 (d, *J* = 1.1 Hz, 2H), 1.26 (d, *J* = 2.4 Hz, 2H). **^{13}C NMR** (126 MHz, Chloroform-*d*) δ 147.47, 146.01, 145.80, 139.64, 128.23, 127.87, 125.83, 121.88, 109.62, 107.95, 100.89, 29.67, 16.13. **GC-MS** (m/z) : 240.1.
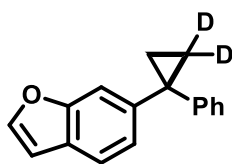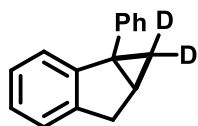
Product (**d-v.2i**): Cyclopropanation according to general procedure: scale 0.32 mmol, flash chromatography (SiO$_2$, 100% hexane) yielded 33 mg (60 %) of the title compound as a colorless liquid. **^{1}H NMR** (500 MHz, CDCl$_3$) δ 7.28 (d, *J* = 4.6 Hz, 1H), 7.25 – 7.22 (m, 2H), 7.20 – 7.12 (m, 5H), 6.81 – 6.69 (m, 2H), 2.94 (s, 6H), 1.28 – 1.24 (m, 2H). **^{13}C NMR** (101 MHz, CDCl$_3$) δ 150.01, 146.90, 132.74, 130.02, 129.34, 127.44, 125.68, 113.66, 41.10, 30.33, 16.55. **GC-MS** (m/z) : 239.2.

Product (**d-v.2p**): Cyclopropanation according to general procedure: scale 0.32 mmol, flash chromatography (SiO$_2$, 100% hexane) yielded 34 mg (69 %) of the title compound as a colorless liquid. **^{1}H NMR** (500 MHz, Chloroform-*d*) δ 7.53 (d, *J* = 8.2 Hz, 2H), 7.33 (ddd, *J* = 8.2, 7.1, 5.5 Hz, 4H), 7.29 – 7.23 (m, 3H), 1.39 (d, *J* = 4.8 Hz, 1H), 1.34 (d, *J* = 4.8 Hz, 1H). **^{13}C NMR** (126 MHz, Chloroform-*d*) δ 150.01, 144.49, 128.77, 128.49, 128.24, 127.94, 126.44, 125.37, 125.22, 125.19, 125.16, 125.13, 123.21, 29.72, 29.68, 16.58. **GC-MS** (m/z) : 264.1.
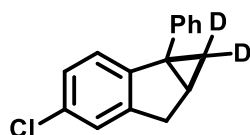
Product (**d-v.2u**): Cyclopropanation according to general procedure: scale 0.32 mmol, flash chromatography (SiO$_2$, 100% hexane) yielded 33 mg (79 %) of the title compound as a colorless liquid. **^{1}H NMR** (500 MHz, Chloroform-*d*) δ 7.27 – 7.22 (m, 2H), 7.17 – 7.11 (m, 2H), 7.00 – 6.95 (m, 2H), 6.60 (t, *J* = 2.3, 2.3 Hz, 1H), 6.16 – 6.09 (m, 2H), 3.46 (s, 3H), 1.31 (s, 3H). **^{13}C NMR** (126 MHz, Chloroform-*d*) δ 125.43, 125.32, 122.00, 121.56, 108.27, 106.41, 106.32, 34.13, 31.45, 30.21, 29.71, 29.67, 29.38, 29.17, 28.97, 17.01. **GC-MS** (m/z) : 199.1.
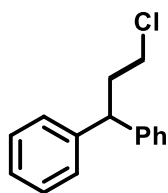
Product (**d-v.2x**): Cyclopropanation according to general procedure: scale 0.32 mmol, flash chromatography (SiO$_2$, 100% hexane) yielded 41 mg (75 %) of the title compound as a colorless liquid. **^{1}H NMR** ^{1}H NMR (500 MHz, Chloroform-*d*) δ 7.47 – 7.35 (m, 6H), 7.33 – 7.29 (m, 2H), 7.22 – 7.16 (m, 4H), 6.17 (d, *J* = 0.9 Hz, 1H), 1.61 (d, *J* = 4.4 Hz, 1H), 1.36 (d, *J* = 4.4 Hz, 1H). **^{13}C NMR** (126 MHz, Chloroform-*d*) δ 129.55, 129.05, 129.00, 128.43, 128.24, 127.00, 125.31, 123.18, 122.49, 120.06, 110.77, 102.73, 25.03, 21.47, 15.10. **GC-MS** (m/z) : 236.1.
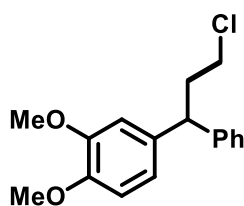
Product (**d-v.2ab**): Cyclopropanation according to general procedure: scale 0.32 mmol, flash chromatography (SiO$_2$, 100% hexane) yielded 69 mg (83 %) of the title compound as a colorless liquid. **^{1}H NMR** (500 MHz, Chloroform-*d*) δ 7.45 – 7.40 (m, 2H), 7.38 – 7.32 (m, 2H), 7.27 – 7.19 (m, 2H), 7.17 – 7.07 (m, 3H), 3.41 (ddt, *J* = 16.9, 6.6, 0.8, 0.8 Hz, 1H), 3.09 – 2.99 (m, 1H), 1.99 (d, *J* = 6.5 Hz, 1H). **^{13}C NMR** (126 MHz, Chloroform-*d*) δ 148.99, 141.90, 141.27, 130.95, 129.11, 128.56, 128.30, 127.71, 127.56, 126.35, 126.14, 125.98, 125.70, 125.44, 124.85, 124.11, 123.80, 120.31, 39.38, 38.20, 35.50, 26.20, 21.06. **GC-MS** (m/z) : 208.1.
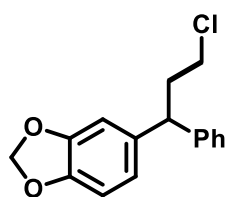

Product (**d-v.2ac**): Cyclopropanation according to general procedure: scale 0.32 mmol, flash chromatography (SiO$_2$, 100% hexane) yielded 13 mg (18 %) of the title compound as a colorless liquid. **^{1}H NMR** (400 MHz, Chloroform-*d*) δ 7.41 – 7.32 (m, 4H), 7.19 (q, *J* = 1.3, 1.2, 1.2 Hz, 1H), 7.08 (ddd, *J* = 8.1, 1.9, 0.9 Hz, 1H), 6.99 (d, *J* = 8.1 Hz, 1H), 3.38 (ddt, *J* = 17.2, 6.6, 1.1, 1.1 Hz, 1H), 3.01 (d, *J* = 17.2 Hz, 1H), 2.00 (d, *J* = 6.5 Hz, 1H). **^{13}C NMR** (101 MHz, Chloroform-*d*) δ 147.62, 143.86, 140.68, 131.28, 129.04, 128.74, 128.66, 128.41, 127.79, 127.60, 127.16, 126.58, 126.18, 125.61, 124.79, 38.92, 35.36, 26.43. **GC-MS** (m/z) : 242.1.

Product (**v.3a**): Chloromethyl insertion reaction according to general procedure: scale 0.32 mmol, flash chromatography (SiO$_2$, 100% hexane) yielded 0.32 mg (78 %) of the title compound as a colorless liquid. **^{1}H NMR** (500 MHz, Chloroform-d) δ 7.33 – 7.28 (m, 4H), 7.24 – 7.16 (m, 6H), 5.33 (t, *J* = 6.7 Hz, 2H), 4.52 (t, *J* = 7.9 Hz, 1H), 3.12 – 3.00 (m, 2H). **^{13}C NMR** (101 MHz, Chloroform-d) δ 142.78, 128.40, 128.26, 125.61, 35.91, 31.40, 28.99. **GC-MS** (m/z) : 230.3.
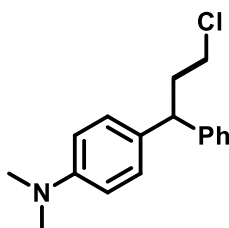
Product (**v.3b**): Chloromethyl insertion reaction according to general procedure: scale 0.32 mmol, flash chromatography (SiO$_2$, 100% hexane) yielded 55 mg (48 %) of the title compound as a colorless liquid. **^{1}H NMR** (500 MHz, Chloroform-*d*) δ 7.37 – 7.29 (m, 3H), 7.27 – 7.18 (m, 3H), 6.83 (d, *J* = 1.1 Hz, 2H), 6.75 (s, 1H), 4.17 (d, *J* = 7.1 Hz, 1H), 3.87 (s, 3H), 3.86 (s, 3H), 3.51 – 3.46 (m, 2H), 2.52 – 2.46 (m, 2H). **^{13}C NMR** (126 MHz, Chloroform-*d*) δ 128.61, 127.73, 126.49, 119.60, 111.42, 111.24, 55.89, 47.44, 43.27, 38.32. **GC-MS** (m/z) : 290.1.
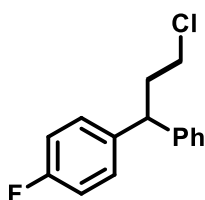
Product (**v.3c**): Chloromethyl insertion reaction according to general procedure: scale 0.32 mmol, flash chromatography (SiO$_2$, 100% hexane) yielded 45 mg (70 %) of the title compound as a colorless liquid. **^{1}H NMR** ^{1}H NMR (400 MHz, Chloroform-*d*) δ 7.36 – 7.29 (m, 2H), 7.27 – 7.20 (m, 3H), 6.78 – 6.74 (m, 2H), 6.73 (t, *J* = 1.1, 1.1 Hz, 1H), 5.93 (p, *J* = 1.5, 1.5, 1.5, 1.5 Hz, 2H), 4.16 (t, *J* = 7.8, 7.8 Hz, 1H), 3.48 (t, *J* = 6.6, 6.6 Hz, 2H), 2.46 (dtd, *J* = 8.2, 6.6, 6.6, 1.5 Hz, 2H). **^{13}C NMR** ^{13}C NMR (101 MHz, Chloroform-*d*) δ 147.86, 146.12, 143.64, 137.48,
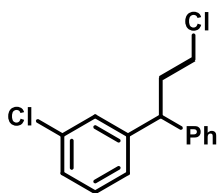
128.64, 127.67, 126.54, 120.84, 108.24, 100.94, 47.52, 43.15, 38.21. **GC-MS** (m/z) : 274.2.
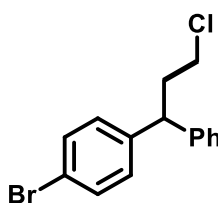
Product (**v.3d**): Chloromethyl insertion reaction according to general procedure: scale 0.32 mmol, flash chromatography (SiO$_2$, 100% hexane) yielded 32 mg (71 %) of the title compound as a colorless liquid. **^{1}H NMR** (500 MHz, Chloroform-d) δ 7.54 – 7.50 (m, 1H), 7.45 – 7.41 (m, 1H), 7.37 – 7.35 (m, 2H), 7.32 – 7.27 (m, 2H), 7.27 – 7.19 (m, 3H), 6.52 (t, J = 0.9, 0.9 Hz, 1H), 4.43 (dd, J = 8.2, 7.1 Hz, 1H), 3.58 (dt, J = 10.9, 6.2, 6.2 Hz, 1H), 3.49 (ddd, J = 10.9, 5.4, 1.5 Hz, 1H), 2.78 – 2.65 (m, 1H), 2.52 – 2.40 (m, 1H). **^{13}C NMR** (126 MHz, Chloroform-d) δ 159.51, 140.36, 128.79, 128.43, 128.04, 127.25, 123.66, 122.64, 120.58, 111.05, 103.06, 42.67, 42.54, 36.97.

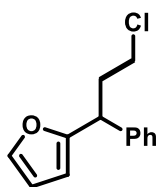Product (**v.3e**): Chloromethyl insertion reaction according to general procedure: scale 0.32 mmol, flash chromatography (SiO$_2$, 100% hexane) yielded 0.32 mg (71 %) of the title compound as a colorless liquid. **^{1}H NMR** (500 MHz, Chloroform-d) δ 7.33 (td, J = 7.2, 7.0, 1.6 Hz, 2H), 7.26 – 7.20 (m, 5H), 7.03 – 6.98 (m, 2H), 4.24 (t, J = 7.8, 7.8 Hz, 1H), 3.47 (td, J = 6.5, 6.5, 1.2 Hz, 2H), 2.55 – 2.44 (m, 2H). **^{13}C NMR** (126 MHz, Chloroform-d) δ 129.30, 129.24, 128.71, 127.77, 126.66, 115.50, 115.33, 47.05, 43.04, 38.21. **GC-MS** (m/z) : 248.1.

Product (**v.3f**): Chloromethyl insertion reaction according to general procedure: scale 0.32 mmol, flash chromatography (SiO$_2$, 100% hexane) yielded 0.32 mg (69 %) of the title compound as a colorless liquid. **^{1}H NMR** (400 MHz, Chloroform-*d*) δ 7.41 – 7.28 (m, 6H), 7.27 – 7.15 (m, 3H), 4.75 (t, *J* = 7.7, 7.7 Hz, 1H), 3.59 – 3.40 (m, 2H), 2.53 (qd, *J* = 7.4, 7.4, 7.0, 1.4 Hz, 2H).**^{13}C NMR** (101 MHz, Chloroform-*d*) δ 141.98, 140.94, 134.37, 129.97, 128.59, 128.26, 128.15, 127.74, 127.04, 126.68, 43.99, 42.78, 38.00. **GC-MS** (m/z) : 263.9.
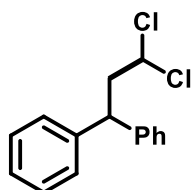
Product (**v.3g**): Chloromethyl insertion reaction according to general procedure: scale 0.32 mmol, flash chromatography (SiO$_2$, 100% hexane) yielded 78.5 mg (51 %) of the title compound as a colorless liquid. **^{1}H NMR** (500 MHz, Chloroform-*d*) δ 7.45 – 7.42 (m, 2H), 7.35 – 7.30 (m, 3H), 7.27 – 7.22 (m, 3H), 7.16 – 7.13 (m, 2H), 4.22 (t, *J* = 7.8, 7.8 Hz, 1H), 3.46 (td, *J* = 6.6, 6.6, 0.8 Hz, 2H), 2.53 – 2.46 (m, 2H). **^{13}C NMR** (126 MHz, Chloroform-*d*) δ 131.71, 129.61, 128.76, 128.62, 127.86, 127.78, 126.77, 47.23, 42.94, 37.90. **GC-MS** (m/z) : 310.0.
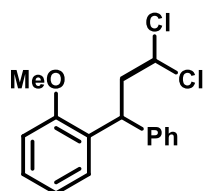
Product (**v.3h**): Chloromethyl insertion reaction according to general procedure: scale 0.32 mmol, flash chromatography (SiO$_2$, 100% hexane) yielded 66 mg (72 %) of the title compound as a colorless liquid. **^{1}H NMR** (500 MHz, Chloroform-*d*) δ 7.37 – 7.32 (m, 3H), 7.29 (d, *J* = 1.7 Hz, 1H), 7.28 – 7.24 (m, 1H), 6.32 (dd, *J* = 3.2, 1.9 Hz, 1H), 6.12 (dt, *J* = 3.2, 0.9, 0.9 Hz, 1H), 4.28 (t, *J* = 7.7, 7.7 Hz, 1H), 3.51 (dt, *J* = 10.9, 6.3, 6.3 Hz, 1H), 3.44 (ddd, *J* = 10.9, 7.6, 5.9 Hz, 1H), 2.66 – 2.49 (m, 1H), 2.40 – 2.27 (m, 1H). **^{13}C NMR**

(126 MHz, Chloroform-*d*) δ 141.69, 128.68, 127.87, 126.99, 110.07, 105.88, 42.76, 42.12, 37.32. **GC-MS** (m/z) : 220.1.

Product (**v.5a**): 1,1-dichloromethyl insertion reaction according to general procedure: scale 0.32 mmol, flash chromatography (SiO$_2$, 100% hexane) yielded 0.32 mg (77 %) of the title compound as a colorless liquid. **¹H NMR** (500 MHz, Chloroform-*d*) δ 7.33 – 7.28 (m, 4H), 7.24 – 7.16 (m, 6H), 5.33 (t, *J* = 6.7 Hz, 2H), 4.52 (t, *J* = 7.9 Hz, 1H), 3.12 – 3.00 (m, 2H). **¹³C NMR** (101 MHz, Chloroform-d) δ 142.78, 128.40, 128.26, 125.61, 35.91, 31.40, 28.99. **GC-MS** (m/z) : 264.1.
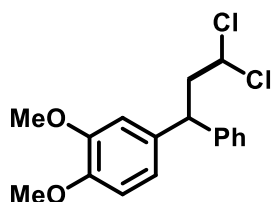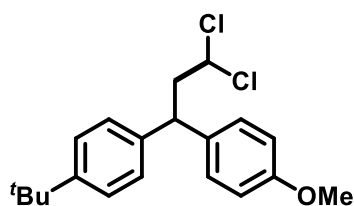
Product (**v.5b**): 1,1-dichloromethyl insertion reaction according to general procedure: scale 0.32 mmol, flash chromatography (SiO$_2$, 100% hexane) yielded 55 mg (52 %) of the title compound as a colorless liquid. **¹H NMR** (500 MHz, CDCl$_3$) δ 7.32 – 7.25 (m, 5H), 7.21 (dtd, *J* = 9.5, 7.8, 1.7 Hz, 3H), 6.94 (td, *J* = 7.5, 1.2 Hz, 1H), 6.87 (dd, *J* = 8.2, 1.2 Hz, 1H), 5.45 (dd, *J* = 7.2, 6.2 Hz, 1H), 4.70 (t, *J* = 7.8 Hz, 1H), 3.80 (s, 3H), 3.00 – 2.86 (m, 2H). **¹³C NMR** (126 MHz, CDCl$_3$) δ 157.20, 142.29, 130.89, 128.68, 128.21, 128.09, 127.87, 126.71, 120.83, 111.23, 72.46, 55.62, 48.52. **GC-MS** (m/z) : 294.1.
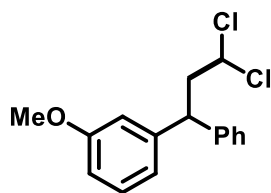
Product (**v.5c**): 1,1-dichloromethyl insertion reaction according to general procedure: scale 0.32 mmol, flash chromatography (SiO$_2$, 100% hexane) yielded 45 mg (47 %) of the title compound as a colorless liquid. **^{1}H NMR** (500 MHz, CDCl$_3$) δ 7.34 – 7.29 (m, 2H), 7.26 – 7.21 (m, 3H), 6.85 (dt, J = 7.6, 1.2 Hz, 1H), 6.80 – 6.75 (m, 2H), 5.41 (t, J = 6.7 Hz, 1H), 4.25 (t, J = 7.9 Hz, 1H), 3.78 (s, 3H), 2.95 – 2.89 (m, 2H). **^{13}C NMR** (126 MHz, CDCl$_3$) δ 160.03, 144.02, 142.30, 129.98, 128.98, 127.84, 127.07, 120.17, 114.20, 111.89, 72.13, 55.32, 49.30, 48.35. **GC-MS** (m/z) : 294.1.

Product (**v.5d**): 1,1-dichloromethyl insertion reaction according to general procedure: scale 0.32 mmol, flash chromatography (SiO$_2$, 100% hexane) yielded 32 mg (58 %) of the title compound as a colorless liquid. **^{1}H NMR** (500 MHz, CDCl$_3$) δ 7.39 – 7.17 (m, 8H), 6.84 – 6.81 (m, 2H), 6.73 (d, J = 1.7 Hz, 1H), 5.41 (t, J = 6.7 Hz, 1H), 4.23 (t, J = 7.9 Hz, 1H), 3.86 (s, 3H), 3.85 (s, 3H), 2.91 (dd, J = 7.9, 6.7 Hz, 2H). **^{13}C NMR** (126 MHz, CDCl$_3$) δ 149.27, 148.08, 142.65, 134.90, 128.94, 127.71, 126.99, 119.59, 111.48, 111.38, 72.19, 56.01, 49.52, 47.88. **GC-MS** (m/z) : 324.1.
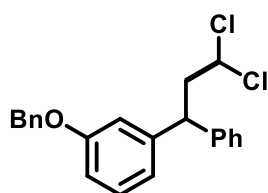
Product (**v.5e**): 1,1-dichloromethyl insertion reaction according to general procedure: scale 0.32 mmol, flash chromatography (SiO$_2$, 100% hexane) yielded 0.32 mg (49 %) of the title compound as a colorless liquid. **^{1}H NMR** (400 MHz, CDCl$_3$) δ 7.34 – 7.29 (m,

2H), 7.19 – 7.12 (m, 4H), 6.88 – 6.81 (m, 2H), 5.38 (t, J = 6.7 Hz, 1H), 4.19 (t, J = 7.9 Hz, 1H), 3.78 (s, 3H), 2.88 (ddd, J = 8.3, 6.7, 1.7 Hz, 2H), 1.29 (s, 9H). **^{13}C NMR** (126 MHz, CDCl$_3$) δ 158.55, 149.73, 139.74, 134.72, 128.88, 127.33, 125.83, 114.33, 72.37, 55.40, 49.68, 47.11, 34.55, 31.47. **GC-MS** (m/z) : 350.1.
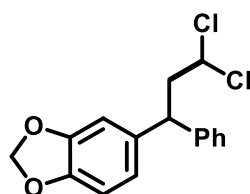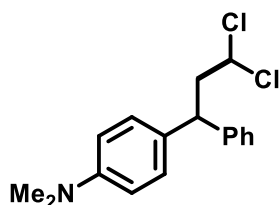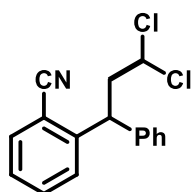

Product (**v.5f**): 1,1-dichloromethyl insertion reaction according to general procedure: scale 0.32 mmol, flash chromatography (SiO$_2$, 100% hexane) yielded 0.32 mg (43 %) of the title compound as a colorless liquid. **^{1}H NMR** (500 MHz, Chloroform-d) δ 7.45 – 7.38 (m, 4H), 7.37 – 7.31 (m, 3H), 7.27 – 7.22 (m, 4H), 6.92 – 6.81 (m, 3H), 5.40 (t, J = 6.7, 6.7 Hz, 1H), 4.26 (t, J = 7.8, 7.8 Hz, 1H), 2.92 (dd, J = 7.7, 6.6 Hz, 2H). **^{13}C NMR** (126 MHz, Chloroform-d) δ 159.22, 144.05, 142.27, 136.91, 130.00, 128.99, 128.75, 128.19, 127.84, 127.75, 127.08, 120.53, 115.04, 112.89, 72.12, 70.18, 49.29, 48.34. **GC-MS** (m/z) : 370.1.

Product (**v.5g**): 1,1-dichloromethyl insertion reaction according to general procedure: scale 0.32 mmol, flash chromatography (SiO$_2$, 100% hexane) yielded 78.5 mg (58 %) of the title compound as a colorless liquid. **^{1}H NMR** (500 MHz, Chloroform-d) δ 7.36 – 7.32 (m, 2H), 7.27 – 7.23 (m, 3H), 6.80 – 6.71 (m, 3H), 5.95 (q, J = 1.4, 1.4, 1.4 Hz, 2H), 5.42 (t, J = 6.7, 6.7 Hz, 1H), 4.22 (t, J = 7.9, 7.9 Hz, 1H), 2.89 (ddd, J = 8.2, 6.7, 1.5 Hz, 2H). **^{13}C NMR** (126 MHz, Chloroform-d) δ 148.06, 146.47, 142.42, 136.16, 130.22, 128.86, 128.61, 128.28, 127.56, 126.93, 126.67, 120.77, 111.09, 108.42, 108.15, 108.09, 101.08, 71.96, 49.30, 47.85, 39.55, 24.10. **GC-MS** (m/z) : 308.0.
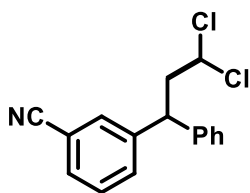
Product (**v.5h**): 1,1-dichloromethyl insertion reaction according to general procedure: scale 0.32 mmol, flash chromatography (SiO$_2$, 100% hexane) yielded 66 mg (65 %) of the title compound as a colorless liquid[1]**H NMR** (500 MHz, CDCl$_3$) δ 7.34 – 7.30 (m, 2H), 7.27 – 7.20 (m, 3H), 7.16 – 7.11 (m, 2H), 6.73 (d, J = 8.4 Hz, 2H), 5.43 (t, J = 6.7 Hz, 1H), 4.21 (t, J = 7.9 Hz, 1H), 2.95 (s, 6H), 2.93 – 2.89 (m, 2H). **¹³C NMR** (126 MHz, CDCl$_3$) δ 143.36, 131.38, 128.86, 128.62, 128.56, 127.77, 126.74, 113.15, 72.47, 49.65, 47.42, 40.84. **GC-MS** (m/z) : 307.1.

Product (**v.5i**): 1,1-dichloromethyl insertion reaction according to general procedure: scale 0.32 mmol, flash chromatography (SiO$_2$, 100% hexane) yielded 58 mg (69 %) of the title compound as as a colorless liquid. **¹H NMR** colorless liquid. **¹H NMR** (500 MHz, CDCl$_3$) δ 7.55 – 7.48 (m, 3H), 7.45 – 7.41 (m, 1H), 7.38 – 7.34 (m, 2H), 7.30 – 7.26 (m, 1H), 7.23 – 7.20 (m, 2H), 5.36 (dd, J = 7.5, 5.9 Hz, 1H), 4.32 (dd, J = 8.7, 7.0 Hz, 1H), 2.98 – 2.86 (m, 2H). **¹³C NMR** (126 MHz, CDCl$_3$) δ 144.28, 140.70, 132.38, 131.40, 130.80, 129.81, 129.40, 127.88, 127.75, 118.75, 113.15, 77.16, 71.43, 48.87, 47.96. **GC-MS** (m/z) : 289.1.
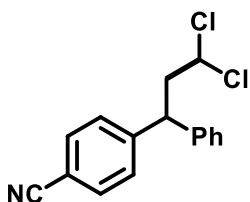
Product (**v.5j**): 1,1-dichloromethyl insertion reaction according to general procedure: scale 0.32 mmol, flash chromatography (SiO$_2$, 100% hexane) yielded 66 mg (70 %) of the title compound as a colorless liquid. **¹H NMR** (500 MHz, CDCl$_3$) δ 7.62 – 7.58 (m, 2H), 7.37 – 7.32 (m, 4H), 7.29 – 7.25 (m, 1H), 7.23 – 7.20 (m, 2H), 5.36 (dd, J = 7.5, 5.9 Hz, 1H), 4.37 – 4.31 (m, 1H), 2.99 – 2.86 (m, 2H). **¹³C NMR** (126 MHz, CDCl$_3$) δ 148.01, 140.65, 132.74, 129.31, 128.62, 127.85, 127.67, 118.68, 111.00, 71.43, 48.68, 48.34. **GC-MS** (m/z) : 289.1.

Product (**v.5k**): 1,1-dichloromethyl insertion reaction according to general procedure: scale 0.32 mmol, flash chromatography (SiO$_2$, 100% hexane) yielded 49 mg (56 %) of the title compound as a colorless liquid. **¹H NMR** (500 MHz, CDCl$_3$) δ 5.35 (dd, J = 7.5, 6.0 Hz, 1H), 4.33 (dd, J = 8.6, 7.1 Hz, 1H), 2.98 – 2.86 (m, 2H). **¹³C NMR** (126 MHz, CDCl$_3$) δ 148.06, 140.68, 132.79, 129.36, 128.66, 127.89, 127.72, 118.72, 111.07, 71.44, 48.74, 48.38. **GC-MS** (m/z) : 289.1.
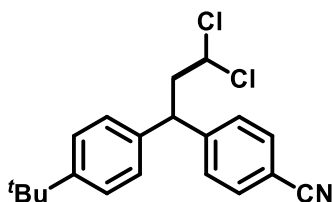
Product (**v.5l**): 1,1-dichloromethyl insertion reaction according to general procedure: scale 0.32 mmol, flash chromatography (SiO$_2$, 100% hexane) yielded 48 mg (52 %) of the title compound as a colorless liquid. **¹H NMR** (500 MHz, CDCl$_3$) δ 7.62 – 7.59 (m, 2H), 7.38 – 7.34 (m, 4H), 7.14 – 7.12 (m, 2H), 5.36 (dd, J = 7.5, 5.9 Hz, 1H), 4.30 (dd, J =

8.6, 7.0 Hz, 1H), 2.98 – 2.84 (m, 2H), 1.30 (s, 9H). **^{13}C NMR** (126 MHz, CDCl$_3$) δ 150.66, 148.34, 137.53, 132.76, 128.68, 127.48, 126.24, 118.78, 110.95, 71.59, 48.88, 48.00, 34.64, 31.42. **GC-MS** (m/z) : 345.1.
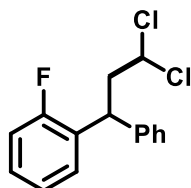
Product (**v.5m**): 1,1-dichloromethyl insertion reaction according to general procedure: scale 0.32 mmol, flash chromatography (SiO$_2$, 100% hexane) yielded 30 mg (70 %) of the title compound as a colorless liquid. **^{1}H NMR** (500 MHz, CDCl$_3$) δ 7.36 – 7.21 (m, 7H), 7.14 (td, J = 7.5, 1.3 Hz, 1H), 7.05 (ddd, J = 10.5, 8.1, 1.3 Hz, 1H), 5.46 (t, J = 6.7 Hz, 1H), 4.61 (t, J = 7.9 Hz, 1H), 3.02 – 2.94 (m, 2H). **^{13}C NMR** (126 MHz, CDCl$_3$) δ 161.77, 159.80, 141.17, 129.03, 128.72, 127.96, 127.25, 124.57, 116.23, 116.06, 71.86, 48.23,   41.84. **^{19}F NMR** (376 MHz, CDCl$_3$) δ -116.55. **GC-MS** (m/z) : 282.1.
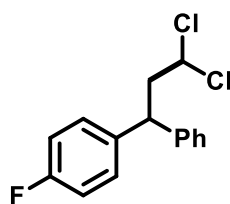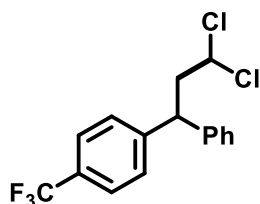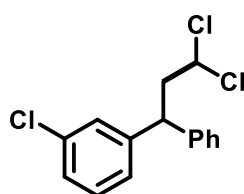
Product (**v.5n**): 1,1-dichloromethyl insertion reaction according to general procedure: scale 0.32 mmol, flash chromatography (SiO$_2$, 100% hexane) yielded 60 mg (68 %) of the title compound as a colorless liquid. **^{1}H NMR** (500 MHz, CDCl$_3$) δ 7.38 – 7.33 (m, 2H), 7.30 – 7.26 (m, 2H), 7.26 – 7.22 (m, 3H), 7.07 – 7.01 (m, 2H), 5.40 (t, J = 6.7 Hz, 1H), 4.30 (t, J = 7.9 Hz, 1H), 3.00 – 2.87 (m, 2H). **^{13}C NMR** (75 MHz, CDCl$_3$) δ 142.16, 138.24, 129.40, 129.29, 129.08, 127.78, 127.21, 115.96, 115.68, 71.93, 49.41, 47.57. **^{19}F NMR** (471 MHz, CDCl$_3$) δ -115.81. **GC-MS** (m/z) : 282.1.

Product (**v.5o**): 1,1-dichloromethyl insertion reaction according to general procedure: scale 0.32 mmol, flash chromatography (SiO$_2$, 100% hexane) yielded 57 mg (65 %) of the title compound as a colorless liquid. **¹H NMR** (500 MHz, CDCl$_3$) δ 7.58 (d, J = 8.2 Hz, 2H), 7.39 – 7.32 (m, 4H), 7.29 – 7.26 (m, 1H), 7.24 (dt, J = 8.0, 1.1 Hz, 2H), 5.38 (dd, J = 7.1, 6.4 Hz, 1H), 4.36 (t, J = 7.8 Hz, 1H), 3.00 – 2.88 (m, 2H). **¹³C NMR** (101 MHz, CDCl$_3$) δ 146.62, 141.32, 129.25, 128.24, 127.89, 127.52, 126.02, 125.98, 125.95, 125.91, 71.67, 49.02, 48.21. **¹⁹F NMR** (376 MHz, CDCl$_3$) δ -62.62. **GC-MS** (m/z) : 332.1.
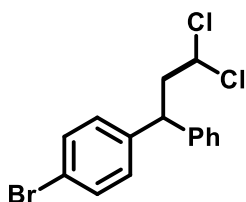
Product (**v.5p**): 1,1-dichloromethyl insertion reaction according to general procedure: scale 0.32 mmol, flash chromatography (SiO$_2$, 100% hexane) yielded 58 mg (67 %) of the title compound as a colorless liquid. **¹H NMR** (500 MHz, Chloroform-d) δ 7.61 (ddd, J = 7.7, 5.8, 1.5 Hz, 1H), 7.43 (ddd, J = 16.9, 7.9, 1.4 Hz, 2H), 7.38 – 7.31 (m, 6H), 7.31 – 7.26 (m, 5H), 7.24 – 7.19 (m, 2H), 7.19 – 7.15 (m, 1H), 5.50 (t, J = 6.7, 6.7 Hz, 1H), 4.87 (t, J = 7.8, 7.8 Hz, 1H), 2.96 (dd, J = 8.0, 6.5 Hz, 2H). **¹³C NMR** (126 MHz, Chloroform-d) δ 140.70, 139.75, 130.29, 130.25, 128.86, 128.82, 128.42, 128.12, 128.10, 127.18, 127.12, 126.83, 126.56, 71.61, 48.71, 44.26, 26.48. **GC-MS** (m/z) : 299.0.
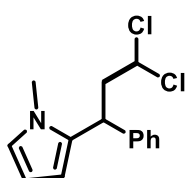
Product (**v.5q**): 1,1-dichloromethyl insertion reaction according to general procedure: scale 0.32 mmol, flash chromatography (SiO$_2$, 100% hexane) yielded 43 mg (78 %) of the title compound as a colorless liquid. **^{1}H** (500 MHz, Chloroform-*d*) δ 7.51 – 7.48 (m, 1H), 7.39 – 7.30 (m, 2H), 7.28 – 7.17 (m, 2H), 7.05 – 7.01 (m, 2H), 6.98 (d, *J* = 8.1 Hz, 1H), 5.12 (d, *J* = 10.1 Hz, 1H), 4.52 (d, *J* = 7.8 Hz, 1H), 3.49 (ddt, *J* = 11.1, 10.1, 7.8, 7.8 Hz, 1H), 3.32 – 3.24 (m, 1H). **^{13}C NMR** (126 MHz, Chloroform-*d*) δ 145.11, 143.45, 143.34, 138.16, 130.60, 130.18, 129.29, 128.97, 128.55, 128.40, 127.77, 127.65, 127.41, 126.69, 126.53, 121.19, 121.03, 74.78, 74.58, 60.26, 56.69, 54.02, 52.74, 36.20, 32.93, 29.71. **GC-MS** (m/z) : 342.1.
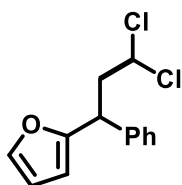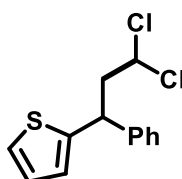

Product (**v.5r**): 1,1-dichloromethyl insertion reaction according to general procedure: scale 0.32 mmol, flash chromatography (SiO$_2$, 100% hexane) yielded 46 mg (52 %) of the title compound as a colorless liquid. **^{1}H NMR** (400 MHz, Chloroform-*d*) δ 7.35 – 7.29 (m, 2H), 7.27 – 7.21 (m, 1H), 7.20 – 7.15 (m, 2H), 6.57 (s, 1H), 6.15 (d, *J* = 2.1 Hz, 2H), 5.57 (dd, *J* = 7.2, 6.3 Hz, 1H), 4.24 (t, *J* = 7.7, 7.7 Hz, 1H), 3.34 (s, 3H), 2.94 (dt, *J* = 14.4, 7.2, 7.2 Hz, 1H), 2.75 (ddd, *J* = 14.3, 8.0, 6.3 Hz, 1H). **^{13}C NMR** (101 MHz, Chloroform-*d*) δ 132.54, 128.94, 127.77, 127.05, 122.37, 106.64, 105.78, 71.90, 49.96, 40.73, 33.84. **^{13}C NMR** (101 MHz, Chloroform-*d*) δ 132.54, 128.94, 127.77, 127.05, 122.37, 106.64, 105.78, 71.90, 49.96, 40.73, 33.84. **GC-MS** (m/z) : 267.1.

Product (**v.5s**): 1,1-dichloromethyl insertion reaction according to general procedure: scale 0.32 mmol, flash chromatography (SiO$_2$, 100% hexane) yielded 55 mg (46 %) of the title compound as a colorless liquid. **^{1}H NMR** (400 MHz, Chloroform-*d*) δ 7.39 – 7.34 (m, 3H), 7.30 (p, *J* = 2.2, 2.2, 2.0, 2.0 Hz, 2H), 6.33 (dd, *J* = 3.2, 1.9 Hz, 1H), 6.13 – 6.11 (m, 1H), 5.44 (dd, *J* = 7.4, 6.2 Hz, 1H), 4.32 (t, *J* = 7.8, 7.8 Hz, 1H), 3.00 (dt, *J* = 14.5, 7.3, 7.3 Hz, 1H), 2.79 (ddd, *J* = 14.4, 8.4, 6.2 Hz, 1H). **^{13}C NMR** (101 MHz, Chloroform-*d*) δ 142.01, 128.91, 127.79, 127.39, 110.20, 106.27, 71.46, 48.28, 42.64. **GC-MS** (m/z) : 254.1.
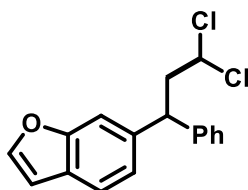
Product (**v.5t**): 1,1-dichloromethyl insertion reaction according to general procedure: scale 0.32 mmol, flash chromatography (SiO$_2$, 100% hexane) yielded 72 mg (57 %) of the title compound as a colorless liquid. **^{1}H NMR** ^{1}H NMR (500 MHz, Chloroform-*d*) δ 7.39 – 7.33 (m, 2H), 7.33 – 7.29 (m, 3H), 7.21 (dd, *J* = 5.1, 1.2 Hz, 1H), 6.97 (dd, *J* = 5.1, 3.5 Hz, 1H), 6.92 (dt, *J* = 3.5, 1.1, 1.1 Hz, 1H), 5.43 (dd, *J* = 7.3, 6.2 Hz, 1H), 4.53 (t, *J* = 7.8, 7.8 Hz, 1H), 2.99 (d, *J* = 7.2 Hz, 1H), 2.92 (s, 1H). **^{13}C NMR** (126 MHz, Chloroform-*d*) δ 146.28, 141.78, 128.97, 127.59, 127.40, 126.82, 124.41, 124.39, 71.53, 50.56, 44.05. **GC-MS** (m/z) : 272.1.

Product (**v.5u**): 1,1-dichloromethyl insertion reaction according to general procedure: scale 0.32 mmol, flash chromatography (SiO$_2$, 100% hexane) yielded 68 mg (37 %) of the title compound as a colorless liquid. **^{1}H NMR** (400 MHz, CDCl$_3$) δ 7.52 – 7.48 (m, 1H),

7.43 (dt, J = 8.3, 1.0 Hz, 1H), 7.39 – 7.26 (m, 6H), 7.25 – 7.18 (m, 2H), 6.49 (t, J = 0.9 Hz, 1H), 5.49 (dd, J = 7.5, 6.0 Hz, 1H), 4.45 (ddd, J = 8.3, 7.1, 0.9 Hz, 1H), 3.12 (dt, J = 14.4, 7.3 Hz, 1H), 2.93 – 2.82 (m, 1H). **^{13}C NMR** (126 MHz, CDCl$_3$) δ 158.32, 155.04, 139.32, 129.17, 128.10, 127.81, 124.09, 122.95, 120.86, 111.27, 103.56, 71.47, 48.02, 43.24. **GC-MS** (m/z) : 306.1.
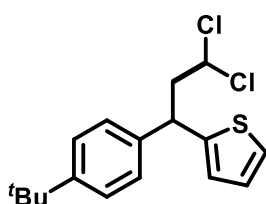

Product (**v.5v**): 1,1-dichloromethyl insertion reaction according to general procedure: scale 0.32 mmol, flash chromatography (SiO$_2$, 100% hexane) yielded 56 mg (72 %) of the title compound as a colorless liquid. **^{1}H NMR** (500 MHz, CDCl$_3$) δ 7.39 – 7.34 (m, 2H), 7.27 – 7.19 (m, 3H), 6.99 – 6.89 (m, 2H), 5.44 (dd, J = 7.2, 6.2 Hz, 1H), 4.51 (t, J = 7.8 Hz, 1H), 3.01 – 2.87 (m, 2H), 1.33 (s, 9H).

^{13}C NMR (126 MHz, CDCl$_3$) δ 150.37, 146.68, 138.82, 127.30, 126.94, 125.99, 124.50, 124.37, 71.83, 50.86, 43.74, 34.62, 31.47. **GC-MS** (m/z) : 328.0.
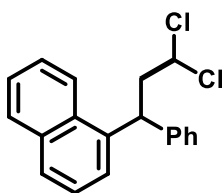

Product (**v.5w**): 1,1-dichloromethyl insertion reaction according to general procedure: scale 0.32 mmol, flash chromatography (SiO$_2$, 100% hexane) yielded 43 mg (38 %) of the title compound as a colorless liquid. **^{1}H NMR** (400 MHz, Chloroform-d) δ 8.24 – 8.12 (m, 1H), 7.90 – 7.84 (m, 1H), 7.80 (dt, J = 8.1, 1.1, 1.1 Hz, 1H), 7.57 – 7.41 (m, 4H), 7.37 – 7.29 (m, 4H), 7.25 – 7.20 (m, 1H), 5.57 (dd, J = 7.4, 6.0 Hz, 1H), 5.14 (dd, J = 8.4, 6.9 Hz, 1H), 3.16 – 2.98 (m, 2H). **^{13}C NMR** (101 MHz, Chloroform-d) δ 142.01, 137.91, 134.20, 131.54, 128.95, 128.91, 127.95, 127.78, 126.98, 126.39, 125.72, 125.32, 124.18, 123.42, 72.11, 49.61, 43.48. **GC-MS** (m/z) : 314.1.
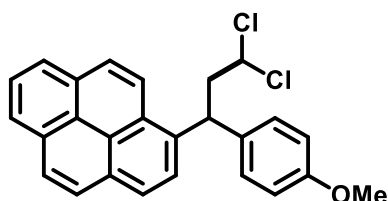
Product (**v.5x**): 1,1-dichloromethyl insertion reaction according to general procedure: scale 0.32 mmol, flash chromatography (SiO$_2$, 100% hexane) yielded 24 mg (39 %) of the title compound as a colorless liquid. **^{1}H NMR** (500 MHz, Chloroform-*d*) δ 8.47 (d, *J* = 9.4 Hz, 1H), 8.20 (dd, *J* = 7.7, 2.1 Hz, 3H), 8.15 (d, *J* = 9.4 Hz, 1H), 8.07 (d, *J* = 3.3 Hz, 2H), 8.03 (t, *J* = 7.6, 7.6 Hz, 1H), 7.96 (d, *J* = 8.0 Hz, 1H), 7.33 – 7.30 (m, 2H), 6.89 – 6.86 (m, 2H), 5.58 (t, *J* = 6.6, 6.6 Hz, 1H), 5.43 (t, *J* = 7.7, 7.7 Hz, 1H), 3.79 (s, 3H), 3.25 – 3.18 (m, 2H). **^{13}C NMR** δ 158.42, 136.01, 134.46, 131.39, 130.70, 130.27, 128.95, 128.73, 128.04, 127.34, 126.06, 125.33, 125.08, 125.04, 124.84, 124.40, 122.70, 114.32, 72.20, 55.26, 49.96, 42.77. **GC-MS** (m/z) : 416.1.
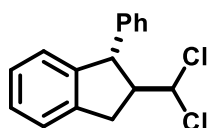

Product (**v.5y**): 1,1-dichloromethyl insertion reaction according to general procedure: scale 0.32 mmol, flash chromatography (SiO$_2$, 100% hexane) yielded 28 mg (58 %) of the title compound as a colorless liquid. **^{1}H NMR** (500 MHz, Chloroform-*d*) δ 7.38 – 7.31 (m, 2H), 7.27 – 7.19 (m, 4H), 7.12 – 7.09 (m, 1H), 7.08 – 7.03 (m, 2H), 5.15 (d, *J* = 10.3 Hz, 1H), 4.58 (d, *J* = 7.8 Hz, 1H), 3.49 (ddt, *J* = 11.2, 10.2, 7.8, 7.8 Hz, 1H), 3.28 (dd, *J* = 15.9, 7.9 Hz, 1H), 3.12 (dd, *J* = 15.9, 11.2 Hz, 1H). **^{13}C NMR** (126 MHz, Chloroform-*d*) δ 146.22, 141.12, 138.88, 129.37, 128.85, 128.52, 128.42, 127.43, 125.15, 124.60, 75.18, 75.09, 56.74, 53.27, 36.49. **GC-MS** (m/z) : 276.1.
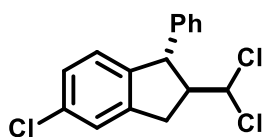
Product (**v.5z**): 1,1-dichloromethyl insertion reaction according to general procedure: scale 0.32 mmol, flash chromatography (SiO$_2$, 100% hexane) yielded 43 mg (74 %) of the title compound as a colorless liquid. **^{1}H**

^{1}H NMR (500 MHz, Chloroform-*d*) δ 7.40 – 7.29 (m, 3H), 7.27 – 7.26 (m, 1H), 7.21 – 7.14 (m, 2H), 7.05 – 7.01 (m, 3H), 5.13 (d, *J* = 10.1 Hz, 1H), 4.54 (d, *J* = 7.8 Hz, 1H), 3.49 (ddt, *J* = 11.1, 10.1, 7.8, 7.8 Hz, 1H), 3.31 – 3.25 (m, 1H). **^{13}C NMR** (126 MHz, Chloroform-*d*) δ 144.59, 143.41, 143.05, 142.93, 142.16, 138.28, 133.14, 133.00, 129.29, 128.97, 128.54, 128.40, 127.73, 127.40, 127.31, 126.28, 126.10, 124.81, 124.69, 74.82, 74.64, 60.35, 56.78, 53.95, 52.67, 36.26, 32.98. **GC-MS** (m/z) : 310.1.
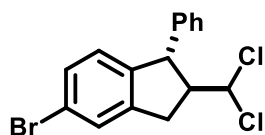

Product (**v.5ç**): 1,1-dichloromethyl insertion reaction according to general procedure: scale 0.32 mmol, flash chromatography (SiO$_2$, 100% hexane) yielded 62 mg (60 %) of the title compound as a white solid.

^{1}H NMR (400 MHz, Chloroform-d) δ 7.34 – 7.27 (m, 2H), 7.25 – 7.19 (m, 3H), 7.19 – 7.16 (m, 2H), 7.14 – 7.09 (m, 2H), 4.08 (q, *J* = 6.1, 6.1, 5.6 Hz, 2H), 3.70 (q, *J* = 7.2, 7.1, 7.1 Hz, 1H), 2.62 – 2.56 (m, 2H), 2.48 (d, *J* = 7.2 Hz, 2H), 1.91 – 1.83 (m, 1H), 1.67 – 1.56 (m, 5H), 1.51 (d, *J* = 7.2 Hz, 3H), 1.37 – 1.28 (m, 2H), 0.93 (d, *J* = 6.6 Hz, 6H). **^{13}C NMR** (126 MHz, Chloroform-d) δ 174.79, 142.43, 140.44, 137.89, 129.26, 128.36, 128.26, 127.15, 125.68, 64.60, 45.21, 45.05, 35.76, 30.96, 30.19, 28.41, 25.44, 22.39, 18.45. **GC-MS** (m/z) : 356.1.

5.5. References

1. Qiao, J. X.; Cheney, D. L.; Alexander, R. S.; Smallwood, A. M.; King, S. R.; He, K.; Rendina, A. R.; Luettgen, J. M.; Knabb, R. M.; Wexler, R. R.; Lam, P. Y. S., Achieving structural diversity using the perpendicular conformation of alpha-substituted phenylcyclopropanes to mimic the bioactive conformation of ortho-substituted biphenyl P4 moieties: Discovery of novel, highly potent inhibitors of Factor Xa. *Bioorganic & Medicinal Chemistry Letters* **2008,** *18* (14), 4118-4123.

2. Abe, H.; Kikuchi, S.; Hayakawa, K.; Iida, T.; Nagahashi, N.; Maeda, K.; Sakamoto, J.; Matsumoto, N.; Miura, T.; Matsumura, K.; Seki, N.; Inaba, T.; Kawasaki, H.; Yamaguchi, T.; Kakefuda, R.; Nanayama, T.; Kurachi, H.; Hori, Y.; Yoshida, T.; Kakegawa, J.; Watanabe, Y.; Gilmartin, A. G.; Richter, M. C.; Moss, K. G.; Laquerre, S. G., Discovery of a Highly Potent and Selective MEK Inhibitor: GSK1120212 (JTP-74057 DMSO Solvate). *ACS Medicinal Chemistry Letters* **2011,** *2* (4), 320-324.

3. Talele, T. T., The "Cyclopropyl Fragment" is a Versatile Player that Frequently Appears in Preclinical/Clinical Drug Molecules. *Journal of Medicinal Chemistry* **2016,** *59* (19), 8712-8756.

4. Yadav, R. N.; Srivastava, A. K.; Banik, B. K., 10 - One-pot strategy: A highly economical tool in organic synthesis and medicinal chemistry. In *Green Approaches in Medicinal Chemistry for Sustainable Drug Design*, Banik, B. K., Ed. Elsevier: 2020; pp 353-425.

5. Freund, A., Ueber Trimethylen. *Journal für Praktische Chemie* **1882,** *26* (1), 367-377.

6. Simmons, H. E.; Smith, R. D., A new synthesis of cyclopropanes from olefins. *Journal of the American Chemical Society* **1958,** *80* (19), 5323-5324.

7. Simmons, H. E.; Smith, R. D., A New Synthesis of Cyclopropanes. *Journal of the American Chemical Society* **1959,** *81* (16), 4256-4264.

8. Cheng, D.; Huang, D.; Shi, Y., Synergistic effect of additives on cyclopropanation of olefins. *Organic & Biomolecular Chemistry* **2013,** *11* (34), 5588-5591.

9. Charette, A. B.; Beauchemin, A., Simmons-Smith Cyclopropanation Reaction. In *Organic Reactions*, pp 1-415.

10. Moser, W. R., Mechanism of the copper-catalyzed addition of diazoalkanes to olefins. II. Electronic effects. *Journal of the American Chemical Society* **1969,** *91* (5), 1141-1146.

11. Moßler, G., Über die Zersetzung von Chloroform durch alkoholische Lauge. *Monatshefte für Chemie und verwandte Teile anderer Wissenschaften* **1908,** *29* (6), 573-581.

12. Sheikh, Y. M.; Leclercq, J.; Djerassi, C., Addition of dichlorocarbene to steroidal olefins. Preparation of a stereoisomer of demethylgorgosterol, a cyclopropane-containing marine sterol. *Journal of the Chemical Society, Perkin Transactions 1* **1974,** (0), 909-914.

13. von E. Doering, W.; Hoffmann, A. K., The Addition of Dichlorocarbene to Olefins. *Journal of the American Chemical Society* **1954,** *76* (23), 6162-6165.

14. Gartia, Y.; Pulla, S.; Ramidi, P.; Farris, C. C.; Nima, Z.; Jones, D. E.; Biris, A. S.; Ghosh, A., A Novel Iron Complex for Cross-Coupling Reactions of Multiple C–Cl Bonds in Polychlorinated Solvents with Grignard Reagents. *Catalysis Letters* **2012,** *142* (11), 1397-1404.

15. Zhou, Y.-Y.; Uyeda, C., Reductive Cyclopropanations Catalyzed by Dinuclear Nickel Complexes. *Angewandte Chemie International Edition* **2016,** *55* (9), 3171-3175.

16. del Hoyo, A. M.; Herraiz, A. G.; Suero, M. G., A Stereoconvergent Cyclopropanation Reaction of Styrenes. *Angewandte Chemie International Edition* **2017,** *56* (6), 1610-1613.

17. Phelan, J. P.; Lang, S. B.; Compton, J. S.; Kelly, C. B.; Dykstra, R.; Gutierrez, O.; Molander, G. A., Redox-Neutral Photocatalytic Cyclopropanation via Radical/Polar Crossover. *Journal of the American Chemical Society* **2018,** *140* (25), 8037-8047.

18. Njue, C. K.; Nuthakki, B.; Vaze, A.; Bobbitt, J. M.; Rusling, J. F., Vitamin B12-mediated electrochemical cyclopropanation of styrene. *Electrochemistry Communications* **2001,** *3* (12), 733-736.

19. Giese, B., Formation of CC Bonds by Addition of Free Radicals to Alkenes. *Angewandte Chemie International Edition in English* **1983,** *22* (10), 753-764.

20. D.P. Curran, N. A. P. a. B. G., Radical Reactions in Organic Synthesis. In *Stereochemistry of Radical Reactions Concepts , Guidelines and Synthetic Applications*, Wiley: 1995; pp 1-22.

21. Claros, M.; Ungeheuer, F.; Franco, F.; Martin-Diaconescu, V.; Casitas, A.; Lloret-Fillol, J., Reductive Cyclization of Unactivated Alkyl Chlorides with Tethered Alkenes

under Visible-Light Photoredox Catalysis. *Angewandte Chemie International Edition* **2019,** *58* (15), 4869-4874.

22. Rountree, E. S.; McCarthy, B. D.; Eisenhart, T. T.; Dempsey, J. L., Evaluation of Homogeneous Electrocatalysts by Cyclic Voltammetry. *Inorganic Chemistry* **2014,** *53* (19), 9983-10002.

23. Böhm, A.; Bach, T., Radical Reactions Induced by Visible Light in Dichloromethane Solutions of Hünig's Base: Synthetic Applications and Mechanistic Observations. *Chemistry – A European Journal* **2016,** *22* (44), 15921-15928.

24. McTiernan, C. D.; Morin, M.; McCallum, T.; Scaiano, J. C.; Barriault, L., Polynuclear gold(i) complexes in photoredox catalysis: understanding their reactivity through characterization and kinetic analysis. *Catalysis Science & Technology* **2016,** *6* (1), 201-207.

25. Monos, T. M.; Sun, A. C.; McAtee, R. C.; Devery, J. J.; Stephenson, C. R. J., Microwave-Assisted Synthesis of Heteroleptic Ir(III)+ Polypyridyl Complexes. *The Journal of Organic Chemistry* **2016,** *81* (16), 6988-6994.

26. Pannwitz, A.; Prescimone, A.; Wenger, O. S., Ruthenium(II)–Pyridylimidazole Complexes as Photoreductants and PCET Reagents. *European Journal of Inorganic Chemistry* **2017,** *2017* (3), 609-615.

27. Luo, S.-P.; Mejía, E.; Friedrich, A.; Pazidis, A.; Junge, H.; Surkus, A.-E.; Jackstell, R.; Denurra, S.; Gladiali, S.; Lochbrunner, S.; Beller, M., Photocatalytic Water Reduction with Copper-Based Photosensitizers: A Noble-Metal-Free System. *Angewandte Chemie International Edition* **2013,** *52* (1), 419-423.

28. Call, A.; Codolà, Z.; Acuña-Parés, F.; Lloret-Fillol, J., Photo- and Electrocatalytic H2 Production by New First-Row Transition-Metal Complexes Based on an Aminopyridine Pentadentate Ligand. *Chemistry – A European Journal* **2014,** *20* (20), 6171-6183.

UNIVERSITAT ROVIRA I VIRGILI
VISIBLE-LIGHT METALLAPHOTOREDOX STRATEGIES FOR ORGANIC TRANSFORMATIONS THROUGH THE CLEAVAGE
OF CSP3-CL BONDS
Jordi Aragón Artigas

CHAPTER VI:

General Conclusions

UNIVERSITAT ROVIRA I VIRGILI
VISIBLE-LIGHT METALLAPHOTOREDOX STRATEGIES FOR ORGANIC TRANSFORMATIONS THROUGH THE CLEAVAGE
OF CSP3-CL BONDS
Jordi Aragón Artigas

In *Chapter III*, we synthesized and fully characterized a family of tetradentate N-based aminopyridine cobalt and nickel complexes. First, we designed and synthesized nine different ligands based on three different scaffolds: tris(2-pyridylmethyl)amine scaffold (**^{X}TPA**) and (S,S)-bis-pyridine ligands based on a (S,S)-cyclohexyldiamine (**^{X}MCP**) and bispyrrolidine backbone (**^{X}PDP**), where X referred to the substituents in the pyridine ring (X= H, CO$_2$Et or DMM). The complexes have been characterized by paramagnetic ^{1}H-NMR, elemental analysis, X-ray diffraction and UV-Vis spectroscopy. The study of ^{1}H-NMR at different temperatures allowed us to determine the electronic configuration of the metal center and the paramagnetic behavior of the complexes. Then, we have tested the efficiency of the library for the photoredox activation of inert alkyl chlorides in two different transformations: the reductive dechlorination of alkyl chlorides and the intramolecular cyclization of chloroalkanes with pendant alkenes. The library of complexes is depending on the type of substrate in the photoactivation of Csp^3−Cl bonds and very sensitive to temperature variation.

The effectiveness of the library decreased with challenging primary chloroalkanes, wherein only (**^{DMM}MCP)NiCl$_2$**, (**^{DMM}PDP)NiCl$_2$** and (**^{CO2Et}MCP)CoCl$_2$** showed an optimal catalytic response. Catalytic results together with the monitoring of the hydrogen formation and the kinetic monitoring revealed two different mechanisms for each metal in the cleavage of Csp^3−Cl bond where the different behavior of the metal related to their electronic properties plays a key role. These complexes showed a promising catalytic response against the activation of inert alkyl chlorides, and a further optimization of the conditions and more detailed mechanistic study would lead to their implementation in challenging methodologies.

In *Chapter IV*, we have developed a dual catalytic system for the reductive cross-coupling reaction of unactivated alkyl chlorides with aromatic alkenes. We determined as the best system for the reaction the combination of (**Py$_2$^{Ts}tacn)Ni(OTf)$_2$** as the catalyst and [Ir(dmabpy)(ppy)$_2$](PF$_6$) (**PC$_{Ir}$^{NMe2}**) as photocatalyst using *i*Pr$_2$NEt as an electron donor. Once we established the optimal conditions for the cross-coupling strategy, a broad substrate scope was tested, reaching up to 85% yield for 36 different alkyl chlorides and 14 different aromatic olefins, exhibiting an excellent group tolerance. We proposed the photogeneration of a **Ni^I** intermediate from (**Py$_2$^{Ts}tacn)Ni(OTf)$_2$**, as well as its role as active specie against alkyl chlorides, based on spectroscopic techniques. According to DFT studies, the most feasible pathway consists of an oxidative addition/S$_N$2 step in which the formation of a **Ni^{III}**–alkyl compound from the photogenerated **Ni^I**, is followed by the release of the carbon-centered radical. However, we cannot discard the concerted halogen atom abstraction by **Ni^I**, forming directly the free organic radical. Such a carbon-centered radical intermediate can attack a radical acceptor forming a new C−C bond. These results underline bio-inspired complexes as a potential playground for developing new intermolecular cross-coupling processes using inert alkyl chlorides or other inert bonds as an alternative to low index metal coordinated structures. In this regard, investigations are currently underway.

In *Chapter V*, we developed a new strategy for the use of dichloromethane as C$_1$ synthon in cyclopropanation of aromatic alkenes, expanding our background in dual photocatalytic system based on iridium photocatalysts and multidentated N-based nickel complexes. We determined as the best system for the reaction the combination of **^{CO2Et}PDP)NiCl$_2$** as catalyst and [Ir(bpy)(ppy)$_2$](PF$_6$) (**PC$_{Ir}$^{H}**) as photocatalyst using *i*Pr$_2$NEt as electron donor. Once we established the optimal conditions for the cyclopropanation strategy, a broad substrate scope was tested reaching up to 89% yield for 34 different aromatic alkenes, exhibiting an excellent group tolerance. We consider this methodology as one of the first strategies for a

general use of dichloromethane as C_1 synthon under mild conditions. We proposed an analogue activation of Csp^3−Cl from previous chapters, where the *in situ* photogenerated **Ni^I** intermediate from **(^{CO2Et}PDP)NiCl$_2$** is the active species in front of dichloromethane, based on spectroelectrochemical techniques. The activation results in the generation of free chloromethyl radicals, which are engaged by the alkene. A radical/polar crossover reactivity is reached by the reduction of the final benzylic radical, undergoing an intramolecular nucleophilic attack to the terminal Csp^3−Cl, achieving the final cyclopropanation. The rational tuning of the system afforded the development of a new synthesis of chloroalkanes, by adding protic source to the previous system. In parallel, we expanded this protocol to the synthesis of geminal 1,1-dichloroalkanes by using chloroform instead of dichloromethane, showing the potential and versatility of tetradentate aminopyridine complexes for the discovery of new reactivity through the activation of chlorinated inert compounds.

As a general conclusion, the combination of the exhaustive and precise high-throughput experimentation with the mechanistic understanding of catalytic reactions are essential to develop more robust and efficient catalysts but also to translate the catalytic activity to new methodologies. This thesis remarks the relevance of pentadentate and tetradentate aminopyridine ligands for affording low-valent nickel and cobalt intermediates capable of activate inert alkyl chlorides. This is a significant step forward in the general application of alkyl chlorides as C-centered radical precursors for the development of sustainable organic methodologies.

VISIBLE-LIGHT METALLAPHOTOREDOX STRATEGIES FOR ORGANIC TRANSFORMATIONS THROUGH THE CLEAVAGE OF CSP3-CL BONDS

Jordi Aragón Artigas

UNIVERSITAT ROVIRA I VIRGILI
VISIBLE-LIGHT METALLAPHOTOREDOX STRATEGIES FOR ORGANIC TRANSFORMATIONS THROUGH THE CLEAVAGE
OF CSP3-CL BONDS
Jordi Aragón Artigas

VISIBLE-LIGHT METALLAPHOTOREDOX STRATEGIES FOR ORGANIC TRANSFORMATIONS THROUGH THE CLEAVAGE OF CSP3-CL BONDS

Jordi Aragón Artigas

UNIVERSITAT ROVIRA I VIRGILI
VISIBLE-LIGHT METALLAPHOTOREDOX STRATEGIES FOR ORGANIC TRANSFORMATIONS THROUGH THE CLEAVAGE
OF CSP3-CL BONDS
Jordi Aragón Artigas